NASA Contractor Report 3201

Rotary Balance Data for a Typical Single-Engine General Aviation Design for an Angle-of-Attack Range of 8° to 90°

II - High-Wing Model C

Randy S. Hultberg, Julio Chu,
and Waldo L. Dickens

CONTRACT NAS1-14849
OCTOBER 1980

NASA

NASA Contractor Report 3201

Rotary Balance Data for a Typical Single-Engine General Aviation Design for an Angle-of-Attack Range of 8° to 90°

II - High-Wing Model C

Randy S. Hultberg, Julio Chu,
and Waldo L. Dickens
Bihrle Applied Research, Inc.
Jericho, New York

Prepared for
Langley Research Center
under Contract NAS1-14849

National Aeronautics
and Space Administration

**Scientific and Technical
Information Branch**

1980

SUMMARY

Aerodynamic characteristics obtained in a helical flow environment utilizing a rotary balance located in the Langley spin tunnel are presented in plotted form for a 1/6-scale, single-engine, high-wing, general aviation model (model C). The configurations tested included the basic airplane and control deflections, wing leading edge devices, tail designs and airplane components. Data are presented without analysis for an angle-of-attack range of 8° to 90° and clockwise and counter-clockwise rotations covering an $\frac{\Omega b}{2V}$ range from 0 to .9.

INTRODUCTION

The NASA Langley Research Center has a broad general aviation stall/spin research program underway which includes spin-tunnel and free-flight radio control model tests, as well as full-scale flight tests for a number of configurations typical of light, general aviation airplanes. To support this effort, rotary balance wind tunnel force tests covering these same configurations have been conducted to establish a data base for analysis of model and full-scale flight results, and to develop design charts for desirable stall/spin characteristics.

A 1/6-scale, single-engine, general aviation model, referred to as model C, having a high-wing location, was tested in a helical flow environment utilizing a rotary balance located in the Langley spin tunnel. This report presents the data obtained for the basic configuration and control settings, various wing leading-edge modifications, tail designs and airplane components. Data for model C having a low-wing location are presented in reference 1.

SYMBOLS

The units for physical quantities used herein are presented in the International System of Units (SI) and U.S. Customary Units. The measurements were made in the U.S. Customary Units; equivalent dimensions were determined by using the conversion factors given in reference 2.

b wing span, m (ft)

$\bar{c}$ mean aerodynamic chord, cm (in.)

C_N normal-force coefficient, $\frac{\text{Normal force}}{qS}$

C_A axial-force coefficient, $\frac{\text{Axial force}}{qS}$

C_Y side-force coefficient, $\frac{\text{Side force}}{qS}$

C_ℓ rolling-moment coefficient, $\frac{\text{Rolling moment}}{qSb}$

C_m pitching-moment coefficient, $\frac{\text{Pitching moment}}{qS\bar{c}}$

C_n yawing-moment coefficient, $\frac{\text{Yawing moment}}{qSb}$

q free-stream dynamic pressure, N/m^2 (lb/ft^2)

S wing area, m^2 (ft^2)

V free-stream velocity, m/sec (ft/sec)

α angle of attack, deg

β angle of sideslip, deg

Ω angular velocity about spin axis, rad/sec

$\frac{\Omega b}{2V}$ spin coefficient, positive for clockwise spin

δ_a aileron deflection, positive when right aileron is down $(\delta_{a_{right}} - \delta_{a_{left}})/2$, deg

δ_e all movable horizontal tail deflection, positive when trailing edge is down, deg

δ_r rudder deflection, positive when trailing edge is to left, deg

Abbreviations:

cg center of gravity
LE leading edge
SR spin radius
TE trailing edge

TEST EQUIPMENT

A rotary balance measures the forces and moments acting on an airplane while subjected to rotational flow conditions; the background for this apparatus is discussed in reference 3. A photograph and sketch of the rotary balance apparatus installed in the Langley spin tunnel are shown in figures 1 and 2, respectively. The rotating portion of the balance system, mounted on a horizontal supporting boom which is hinged at the wall, is moved from the wall to the center of the tunnel by cables. The rotary arm of the balance system, which rotates about a vertical axis, is attached to the outer end of the horizontal supporting boom and is driven by a drive shaft through couplings and gears.

A test model is mounted on a strain gauge balance which is affixed to the bottom of the rotary balance apparatus. Controls located outside the tunnel are used to activate motors on the rig which position the model to the desired attitude. The angle-of-attack range of the rig is 8 to 90 degrees and the sideslip angle range is ±15 degrees. The spin radius and the lateral displacement motors allow the operator to position the moment center of the balance longitudinally and laterally relative to the spin axis. This is done for each combination of angle of attack and sideslip angle. The general practice is to mount the moment center of the balance at the cg location about which the aerodynamic moments are desired. Electrical current from the balance, and to the motors on the rig, is conducted through the slip-rings located at the rig head. Examples

of how the rig is positioned for different angle of attack and sideslip angle are shown in figures 2a and 2b, respectively.

The model can be rotated up to 90 rpm in either direction. By using different rotational speeds and a specific airflow in the tunnel, the motions of a steady spinning airplane can be simulated. The aerodynamic forces and moments can then be measured for values of $\frac{\Omega b}{2V}$, including the case of $\frac{\Omega b}{2V} = 0$, where static aerodynamic forces and moments can be obtained.

A NASA six-component strain gauge balance is mounted inside the model and measures the normal, lateral and longitudinal forces and the yawing, rolling and pitching moments acting about the model body axis. The interactions that exist between the six components are available from balance calibration tests and are accounted for after the balance voltages are converted to forces and moments.

The data acquisition, reduction and presentation system for the rotary balance system is composed of a 12-channel scanner/voltmeter, a mini-computer, and a plotter. With this equipment, on-line digital print-out and/or graphical plots of data are possible.

TEST PROCEDURES

Rotary aerodynamic data are obtained in two steps. The first step is to record the inertial forces and moments (tares) acting on the model at different attitudes and rotational speeds. To accomplish this, a covered bird-cage like structure is mounted to the upper rig which encloses the model without touching it. In this manner, the air immediately surrounding the model is rotated with it. As the rig is rotated at the desired attitude and rate, the inertial forces and moments generated by the model are measured and stored on magnetic tape for later use.

The second step in the data-gathering process is to measure aerodynamic and inertial forces at different attitudes and rotational speeds for a selected tunnel velocity with, of course, the cage structure removed. The tares are subtracted from these values, and the remaining aerodynamic forces and moments are then converted to coefficient form and stored on magnetic tape.

MODEL

A 1/6-scale high-wing, single-engine, light general aviation model was constructed of fiberglass-epoxy, wood and aluminum. A three-view drawing of this model is shown in figure 3, dimensional characteristics of the basic model are listed in Table I, and a photograph of the model installed on the rotary balance located in the Langley spin tunnel is presented in figure 1.

The various airplane components were removable for component build-up tests, the testing of wing leading edge devices and tail configurations. The three tail configurations tested involved different vertical and horizontal locations of the horizontal tail as shown in figure 4. The wing leading edge modifications include a full-span leading edge droop of large nose radius and an outboard drooped section of large nose radius (figures 5 and 6).

The model control surfaces could be set at any position prior to the test. The maximum deflections for the control surfaces were:

Rudder, deg	25 right, 25 left
All movable horizontal tail, deg	15 up, 2 down
Aileron, deg	20 up, 10 down

TEST CONDITIONS

The tests were conducted in the spin tunnel at an airstream velocity of 7.62 m/sec (25 ft/sec) which corresponds to a Reynolds number of approximately 119,000 based on model wing chord. Unless noted otherwise in Table II, all the configurations were tested through an angle-of-attack range of 8 to 90° at a zero sideslip angle, with the spin axis passing through the full-scale airplane cg location for angles of attack above 30°. For angles of attack below 35°, the spin axis was set 182.9 cm (72 in.) forward of the cg location. Consequently, data was obtained for both 0 and 182.9 cm (72 in.) spin radius at angles of attack of 30 and 35°. For each angle of attack, data were obtained for nominal $\frac{\Omega b}{2V}$ values of .1, .2, .3, .4, .5, .6, .7, .8, and .9 in both clockwise and counter clockwise directions, as well as for $\frac{\Omega b}{2V} = 0$ (static value).

DATA PRESENTATION

Table II identifies the configurations tested and the corresponding appendix figure numbers which present the aerodynamic data. The aerodynamic coefficients vs. $\frac{\Omega b}{2V}$ are presented for each configuration in six sequentially numbered figures in the following order: C_n, C_ℓ, C_m, C_N, C_Y, C_A. Each figure in turn consists of four (seven for the basic configuration) pages which present the subject aerodynamic coefficient vs. $\frac{\Omega b}{2V}$ for the following angles of attack and spin radii, unless noted otherwise in Table II:

a) α = 8, 10, 12, 14, 16 deg SR = 182.9 cm (72 in.)

b) α = 18, 20, 25, 30, 35 deg SR = 182.9 cm (72 in.)

c) α = 30, 35, 40, 45, 50 deg SR = 0

d) α = 55, 60, 70, 80, 90 deg SR = 0

All the moment data are presented for a cg position of $.21\bar{c}$.

Lift coefficient vs, angle of attack for zero rotation rate is presented at the end of the Appendix for several configurations cited in Table II.

REFERENCES

1. Mulcay, William J.; Rose, Robert A.: Rotary Balance Data for a Typical Single-Engine General Aviation Design for an Angle-of-Attack Range of 8° to 90°. I - Low-Wing Model C. NASA CR-3200, 1980.

2. Mechtly, E.A.: The International System of Units - Physical Constants and Conversion Factors. NASA SP-7012, 1973.

3. Bihrle, William, Jr.; Hultberg, Randy S.; and Mulcay, William: Rotary Balance Data for a Typical Single-Engine Low-Wing General Aviation Design for an Angle-of-Attack Range of 30° to 90°. NASA CR-2972, 1978.

TABLE I.- DIMENSIONAL CHARACTERISTICS OF THE BASIC MODEL

Overall length, m (ft)	1.31 (4.29)
Wing:	
Span, m (ft)	1.66 (5.46)
Area, m^2 (ft^2)	.38 (4.06)
Root chord, cm (in.)	22.32 (8.79)
Tip chord, cm (in.)	22.32 (8.79)
Mean aerodynamic chord, cm (in.)	22.32 (8.79)
Leading edge of $\bar{c}$, distance rearward of leading edge of root chord, cm (in.)	0.0 (0.0)
Aspect ratio	7.4
Dihedral, deg	1.5
Incidence:	
Root, deg	+3.257
Tip, deg	+1.0
Airfoil section	NACA 63_2 A415
Horizontal tail:	
Span, m (ft)	0.54 (1.78)
Incidence, deg	0.0
Airfoil section	NACA $63A_1$ 012(modified)
Vertical tail:	
Airfoil section	NACA $63A_1$ 012
Sweep @ LE, deg	41.0

TABLE II.- CONFIGURATIONS TESTED AND FIGURE INDEX

(Unless noted otherwise, all configurations tested through α=8 to 90° at β=0°.)

FIGURE NO.	CONFIGURATION	δ_e deg	δ_a deg	δ_r deg	REMARKS
[a] A1-A6	Basic	0	0	0	also α=8-60°, SR=6"
A7-A12	↓	↓	↓	↓	β=10°
A13-A18	↓	-15	↓	-25	
A19-A24	↓	↓	+20up 10down	↓	
A25-A30	T tail	0	0	0	
A31-A36	↓	-15	↓	-25	
A37-A42	#1 Horiz. tail	0	↓	0	
A43-A48	↓	-15	↓	-25	
A49-A54	Horiz. tail off	off	↓	0	
A55-A60	Vert. tail off	0	↓	off	
A61-A66	Horiz. and vert. tail off	off	↓	↓	
[a] A67-A72	Full-span LE wing droop w/large nose radius	0	↓	0	
[a] A73-A78	Outboard LE wing droop w/large nose radius	↓	↓	↓	

[a] C_L vs. α presented in figure A79.

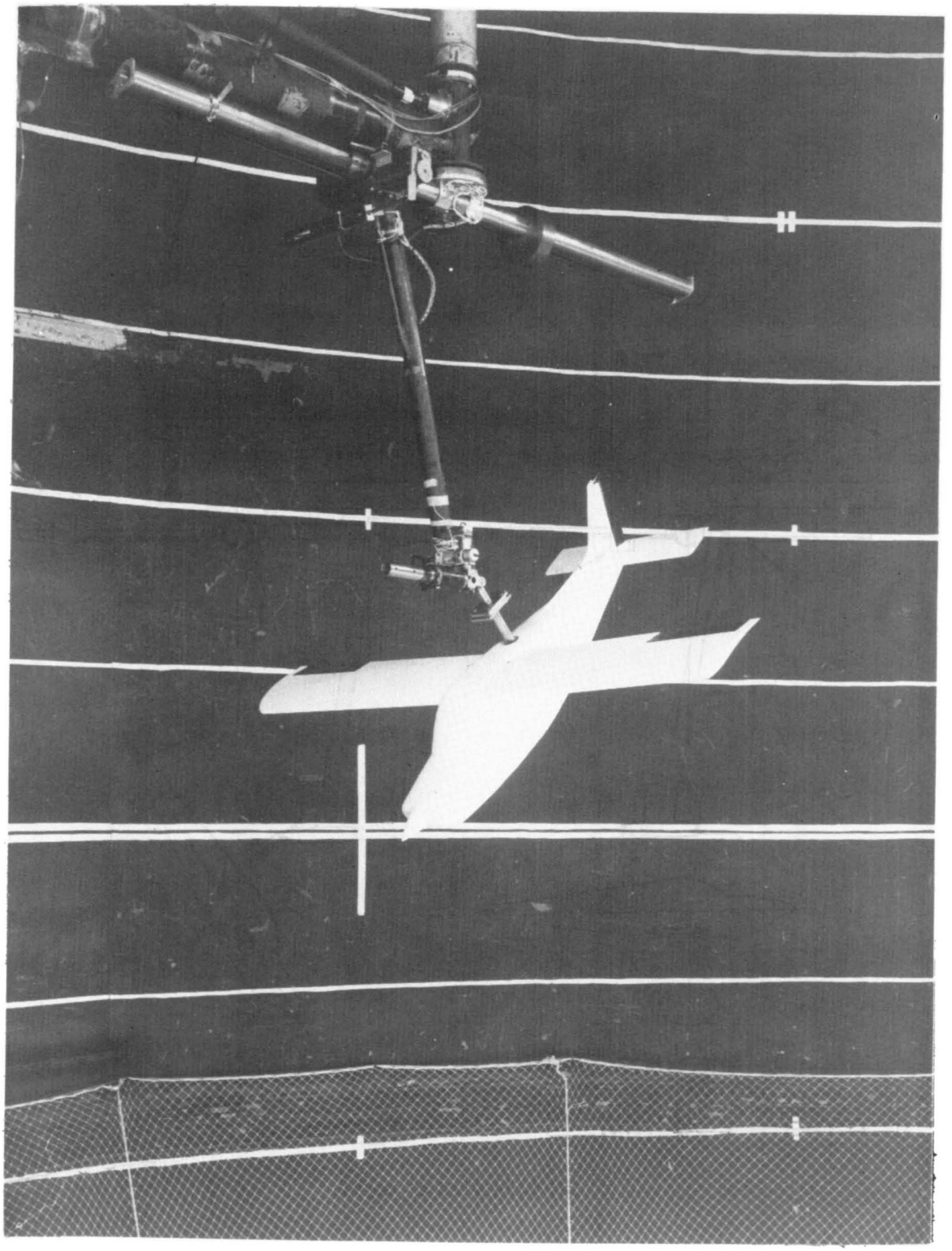

Figure 1. - Photograph of 1/6-scale model installed on rotary balance apparatus.

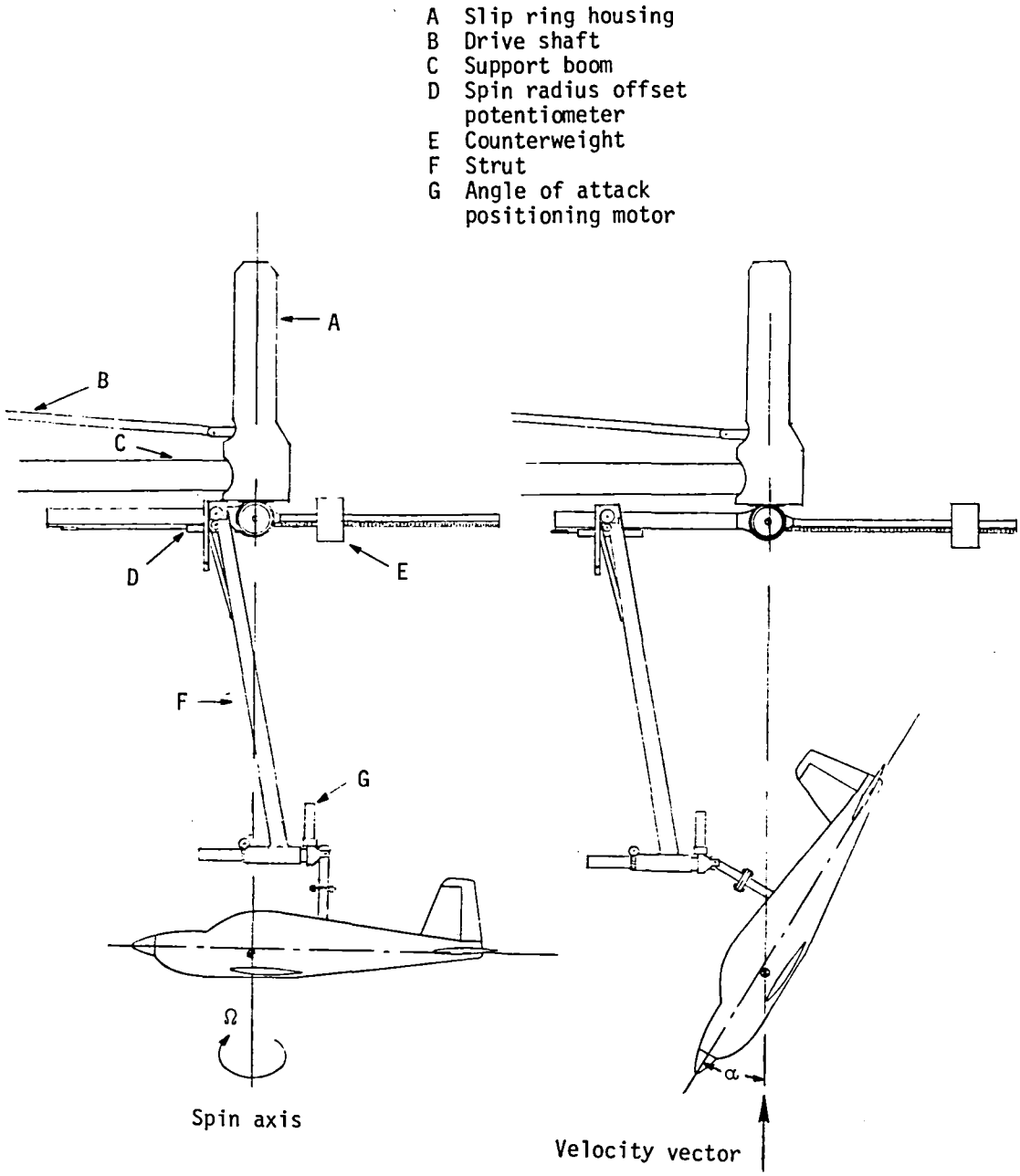

(a) Side view of model.

Figure 2.- Sketch of rotary balance apparatus.

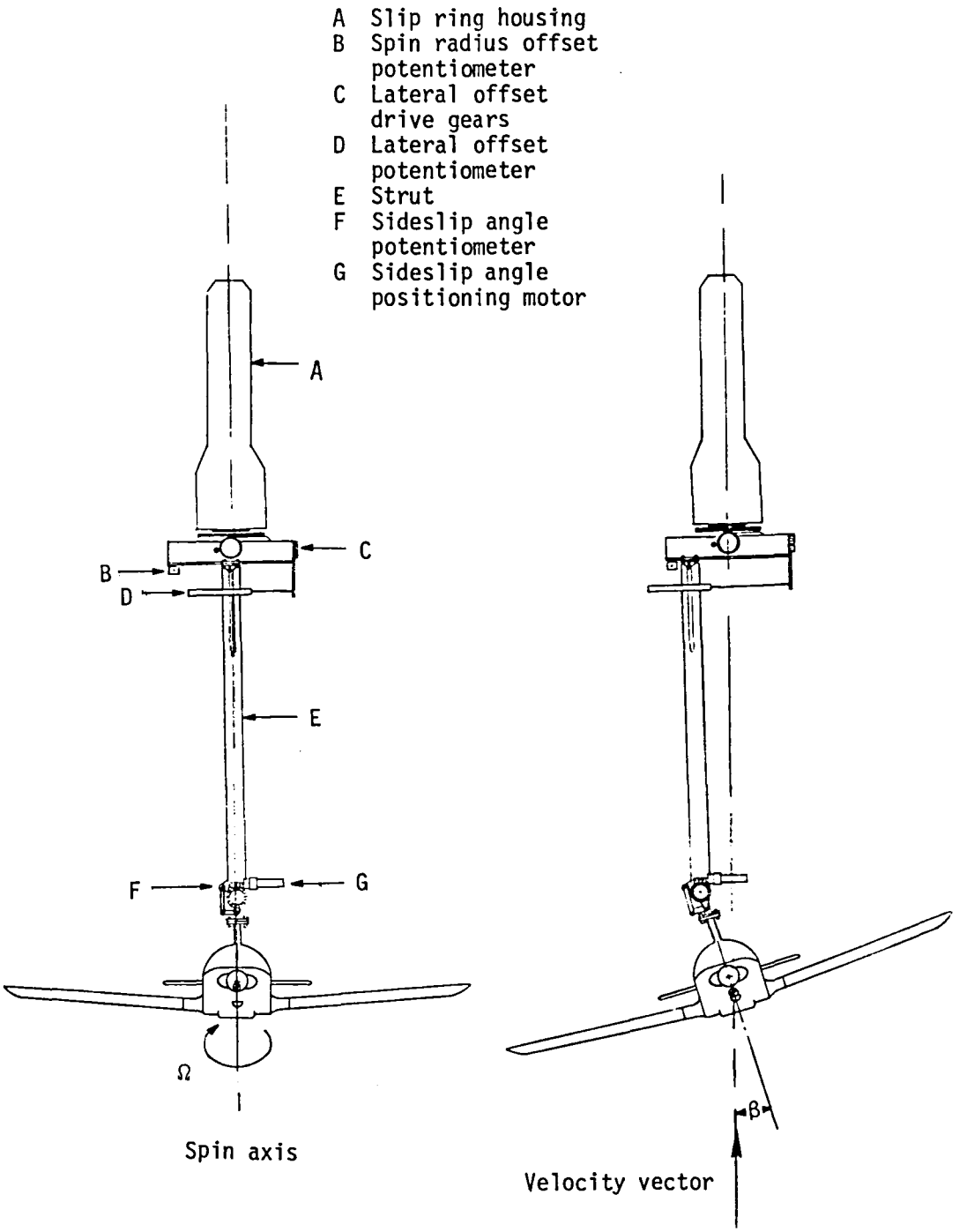

(b) Front view of model.

Figure 2.- Concluded.

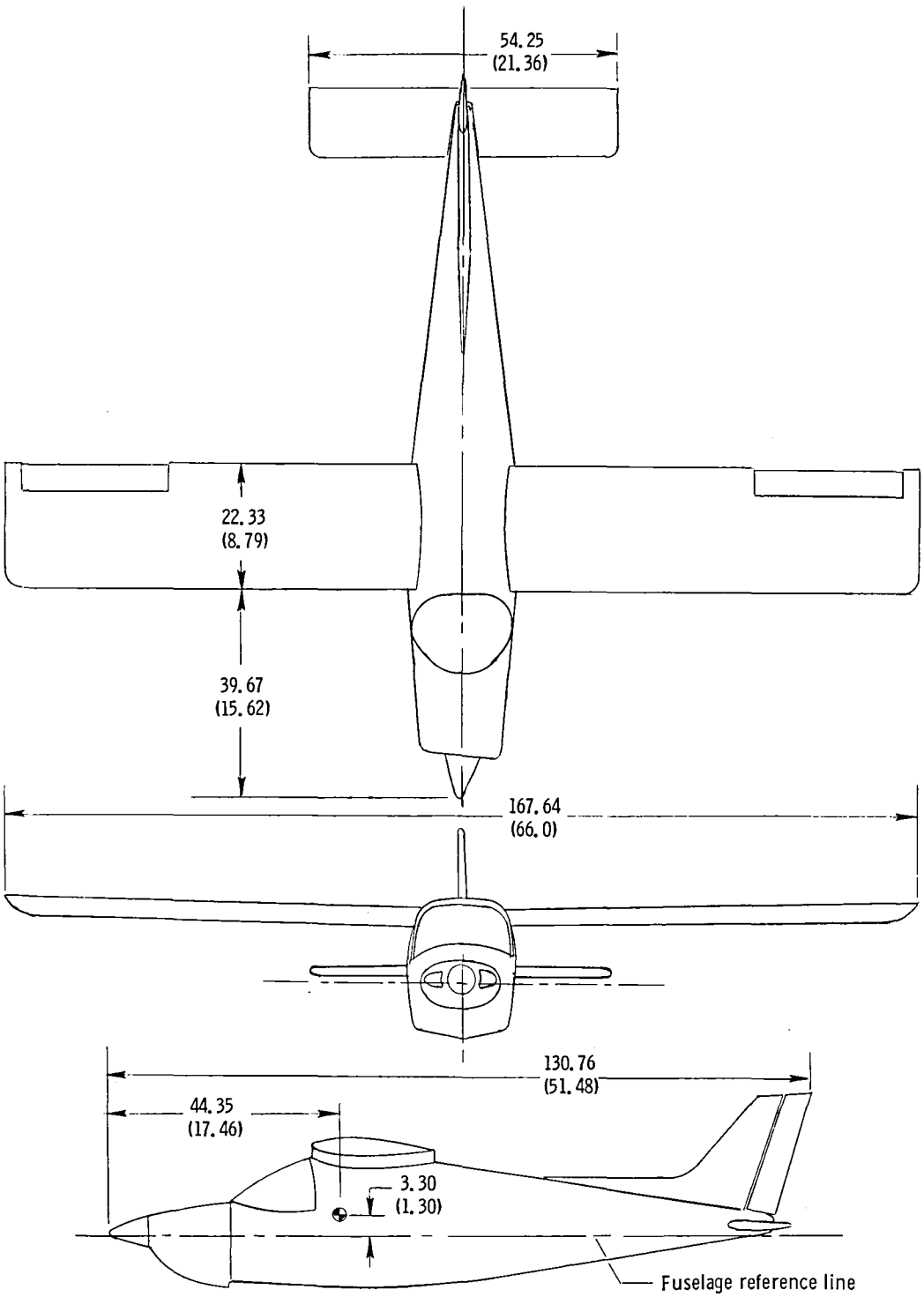

Figure 3. - Three-view drawing of 1/6-scale high-wing general aviation model C. Center-of-gravity positioned at 0.21 $\bar{c}$. Dimensions are given in centimeters(inches), model scale.

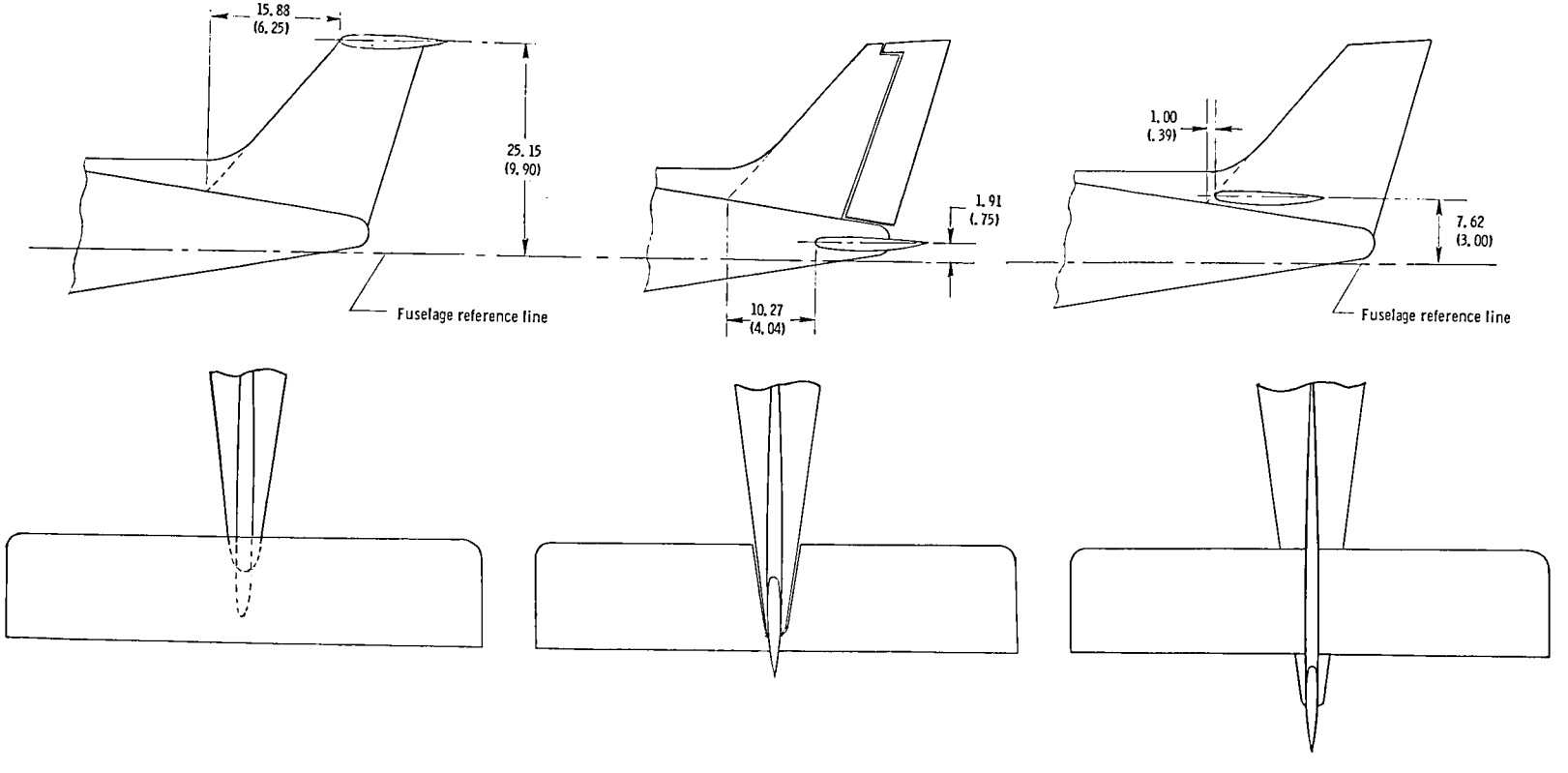

a) T-tail

b) Basic tail

c) Tail 1

Figure 4. - Tail configurations tested on the model. Dimensions are given in centimeters(inches), model scale.

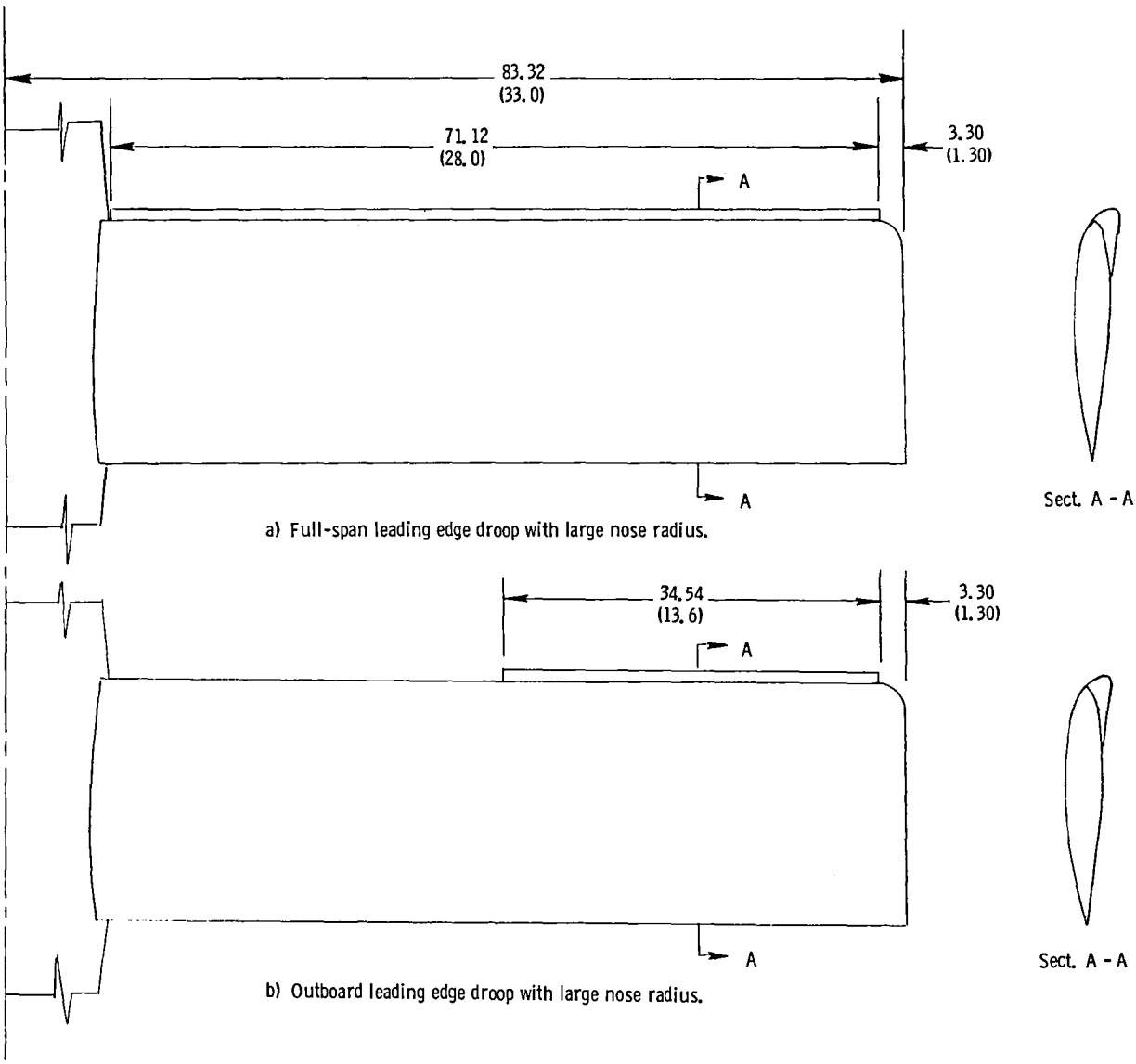

Figure 5. - Wing leading edge modifications tested on the model. Dimensions are given in centimeters(inches), model scale.

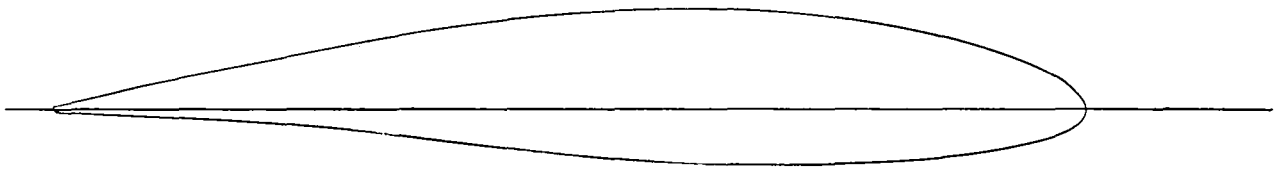

a) Basic airfoil.

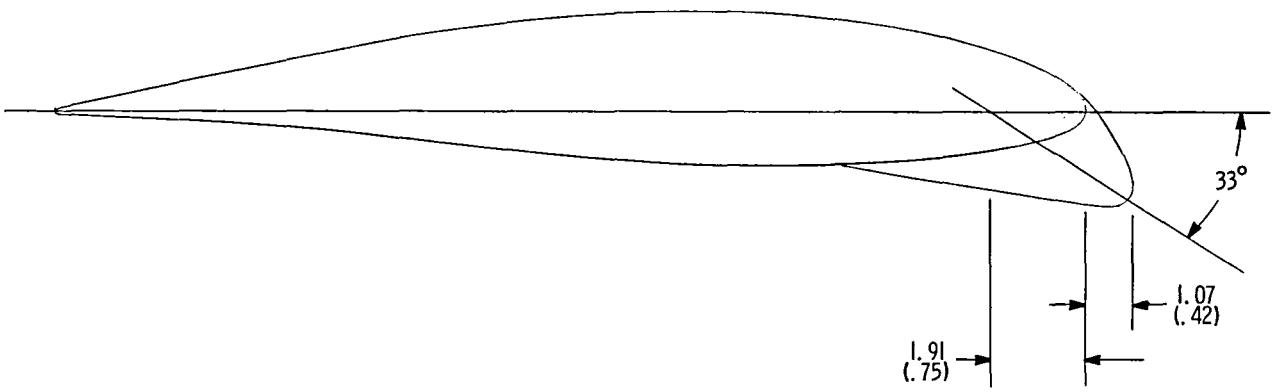

b) Basic airfoil with large nose radius.

Figure 6. - Airfoil sections tested on model. Dimensions are given in centimeters (inches) model scale.

APPENDIX

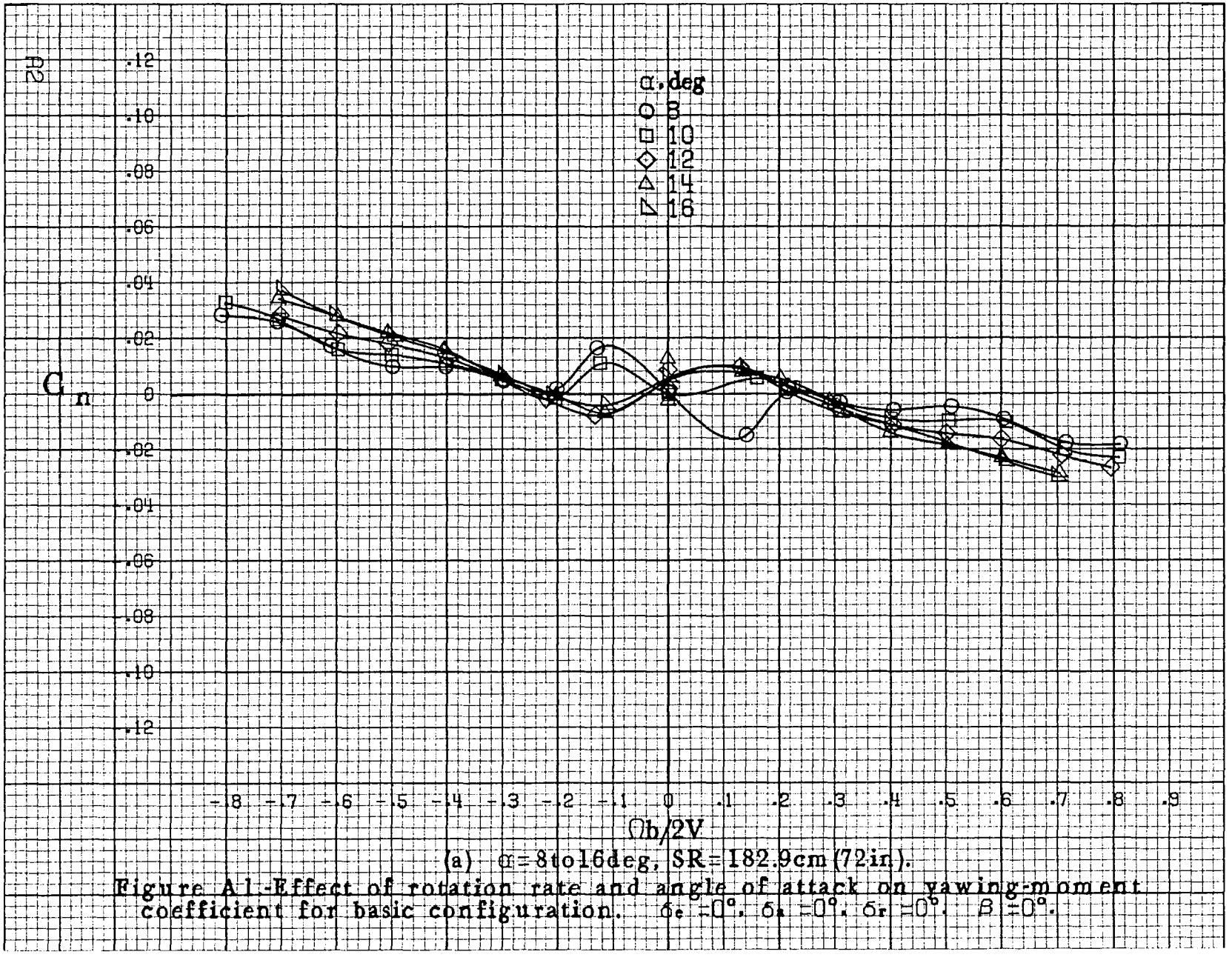

(a) α=8to16deg, SR=182.9cm(72in).

Figure A1.-Effect of rotation rate and angle of attack on yawing-moment coefficient for basic configuration. $\delta_e = 0°$, $\delta_a = 0°$, $\delta_r = 0°$, $\beta = 0°$.

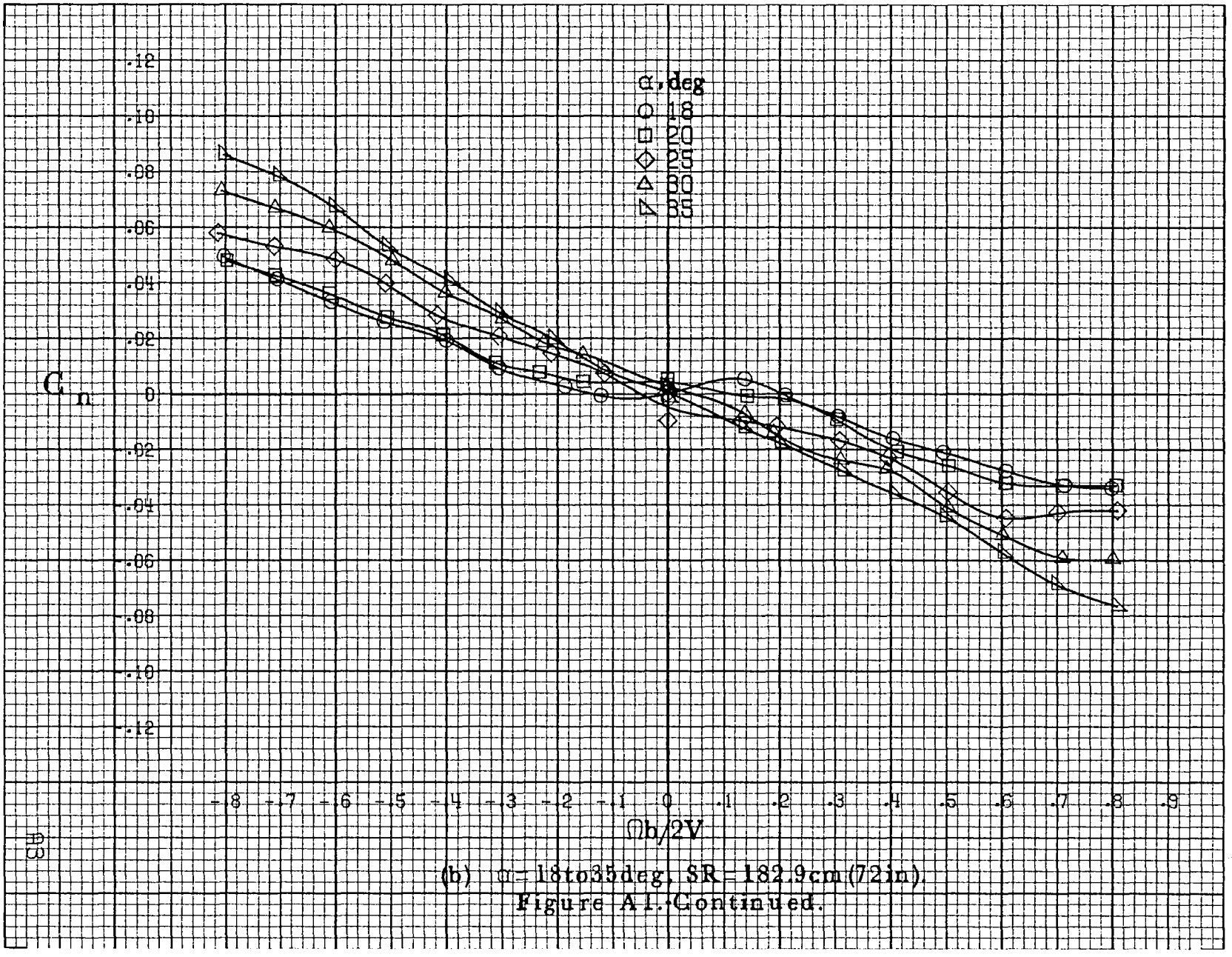

(b) α = 18 to 35 deg, SR = 182.9 cm (72 in).

Figure A1. Continued.

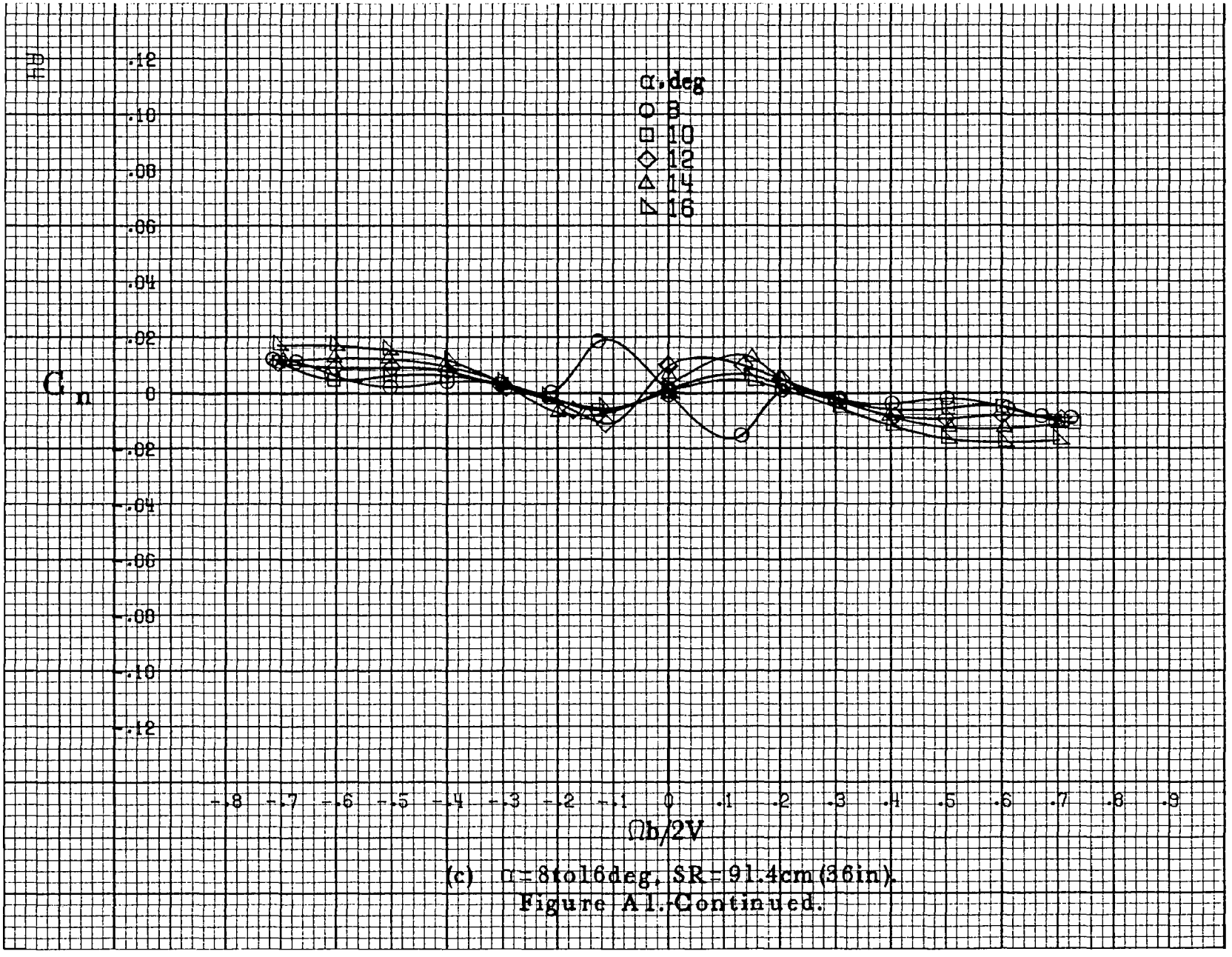

(c) α = 8 to 16 deg, SR = 91.4 cm (36 in).

Figure A1.-Continued.

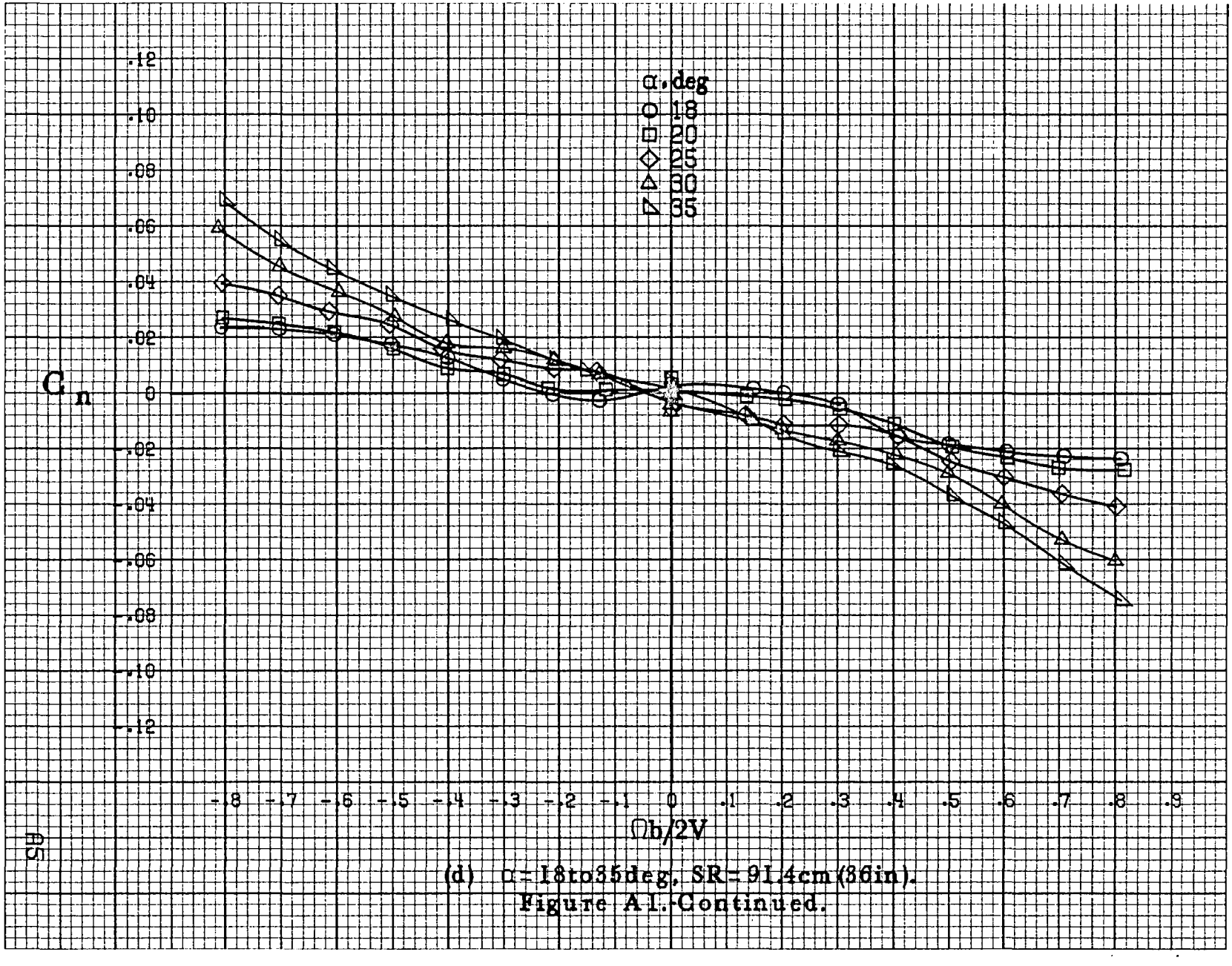

(d) α = 18 to 35 deg, SR = 91.4 cm (36 in).

Figure A1.-Continued.

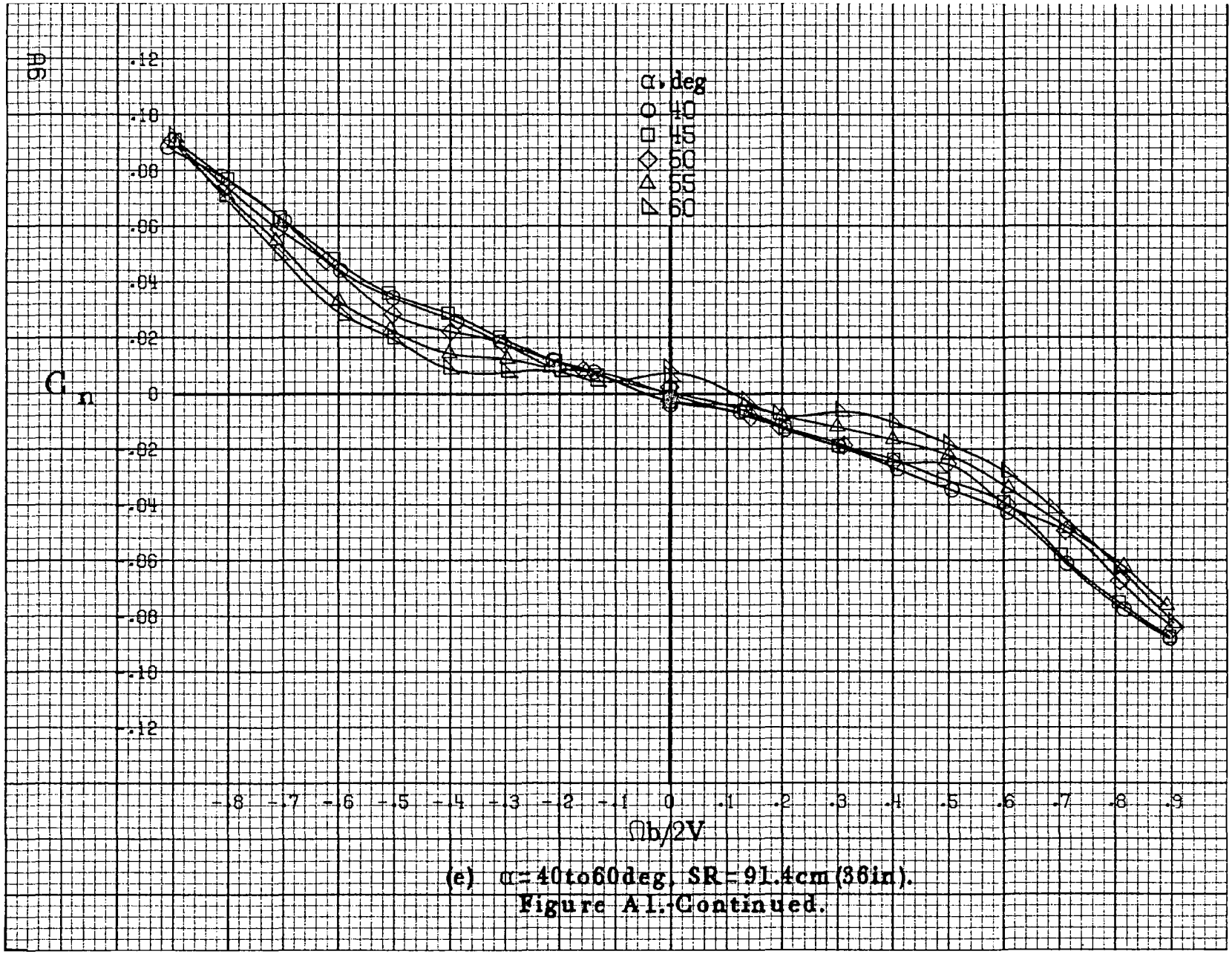

(e) α = 40 to 60 deg, SR = 91.4 cm (36 in).

Figure A1.-Continued.

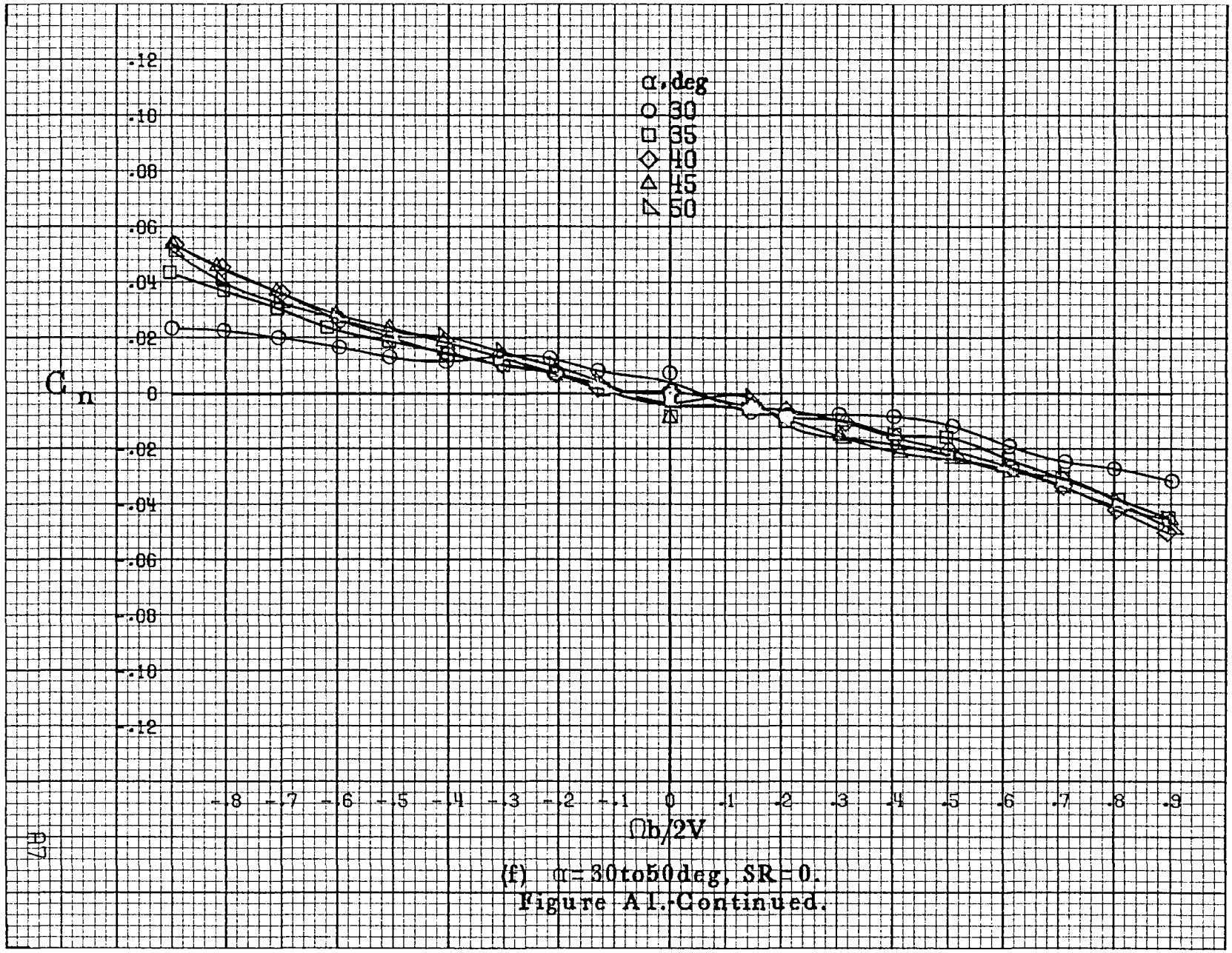

(f) $\alpha = 30$ to 50 deg, SR = 0.

Figure A1.-Continued.

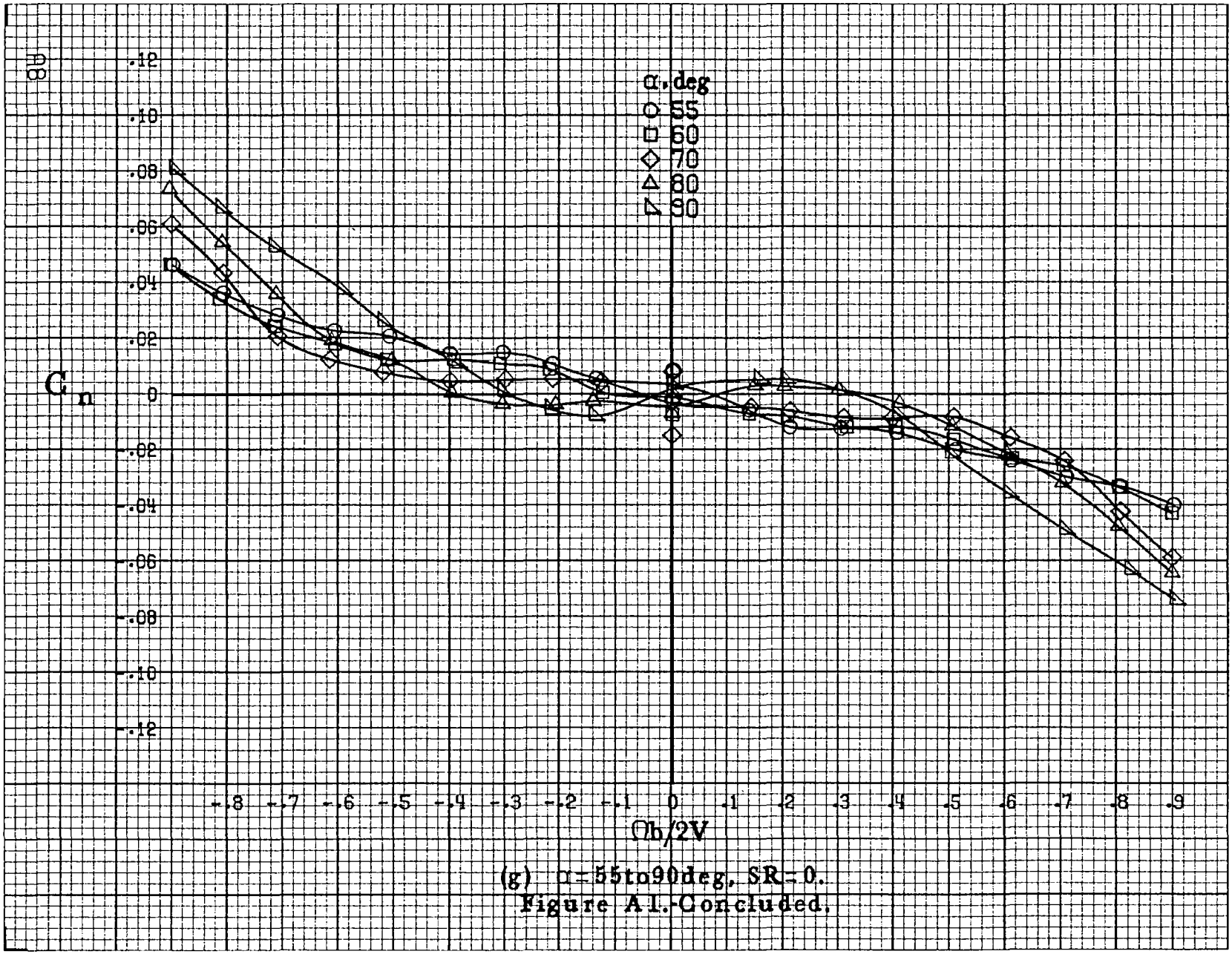

(g) α = 55 to 90 deg, SR = 0.

Figure A1.-Concluded.

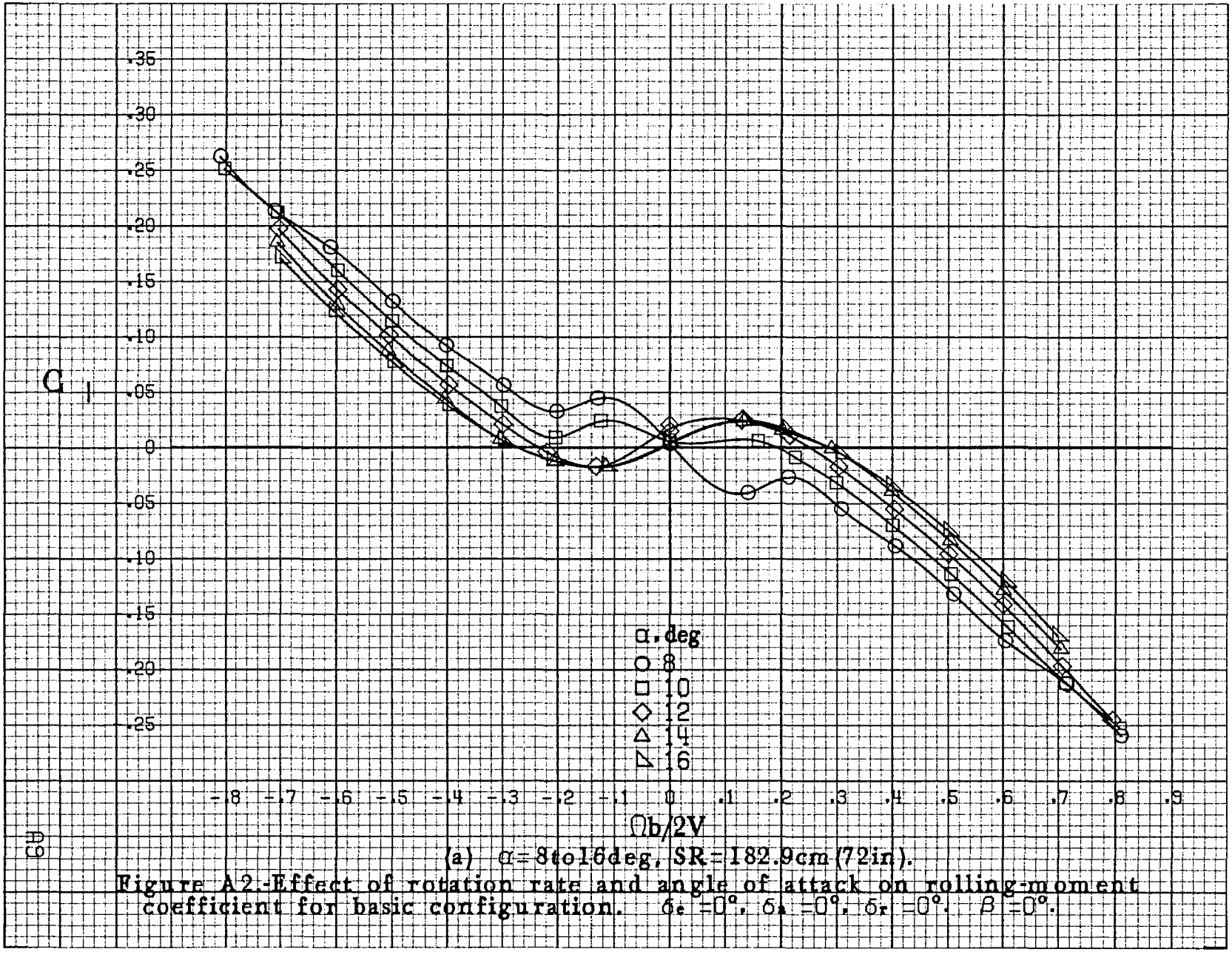

Figure A2.-Effect of rotation rate and angle of attack on rolling-moment coefficient for basic configuration. $\delta_e = 0°$, $\delta_a = 0°$, $\delta_r = 0°$, $\beta = 0°$.

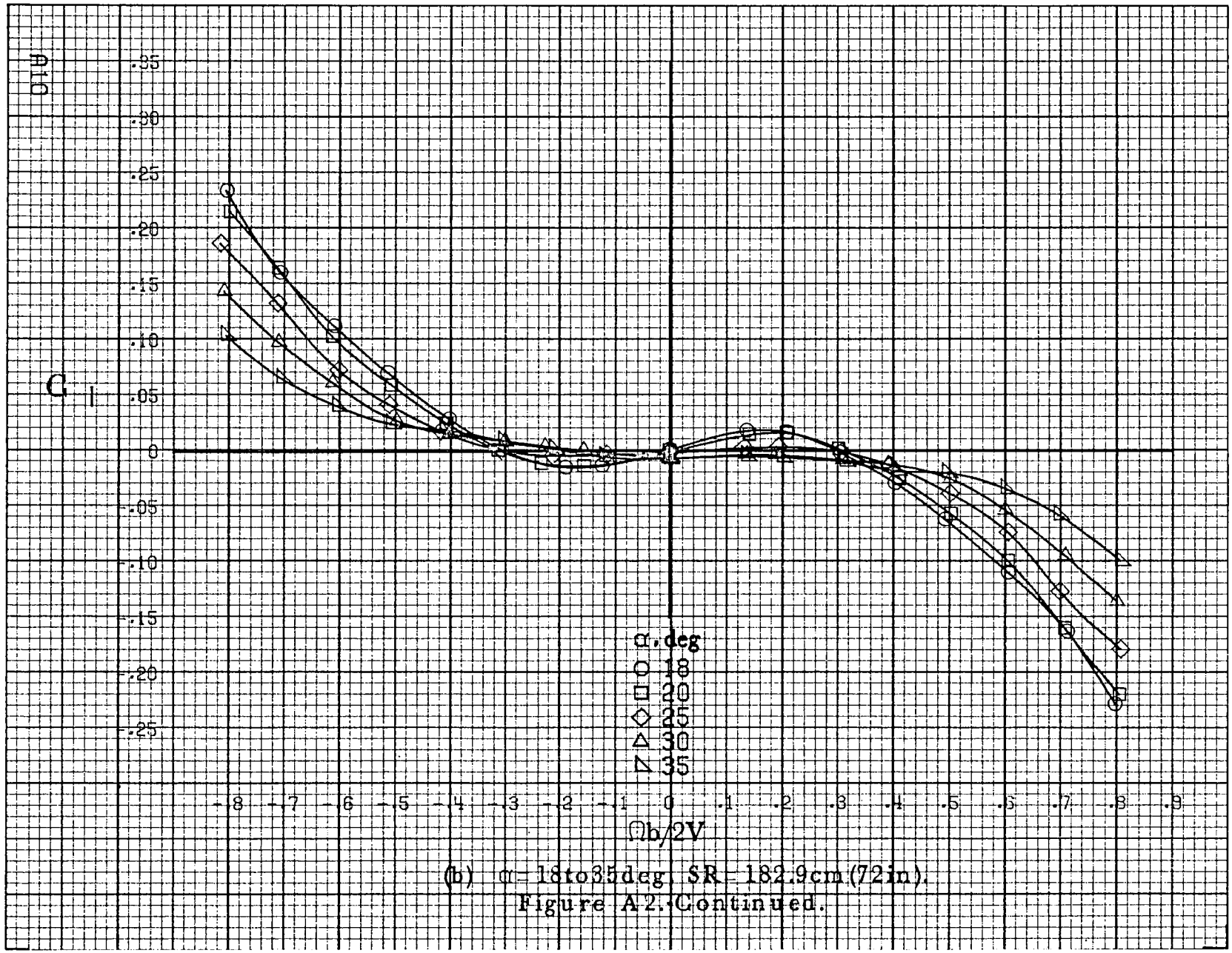

(b) α = 18 to 35 deg, R = 182.9 cm (72 in).

Figure A2. Continued.

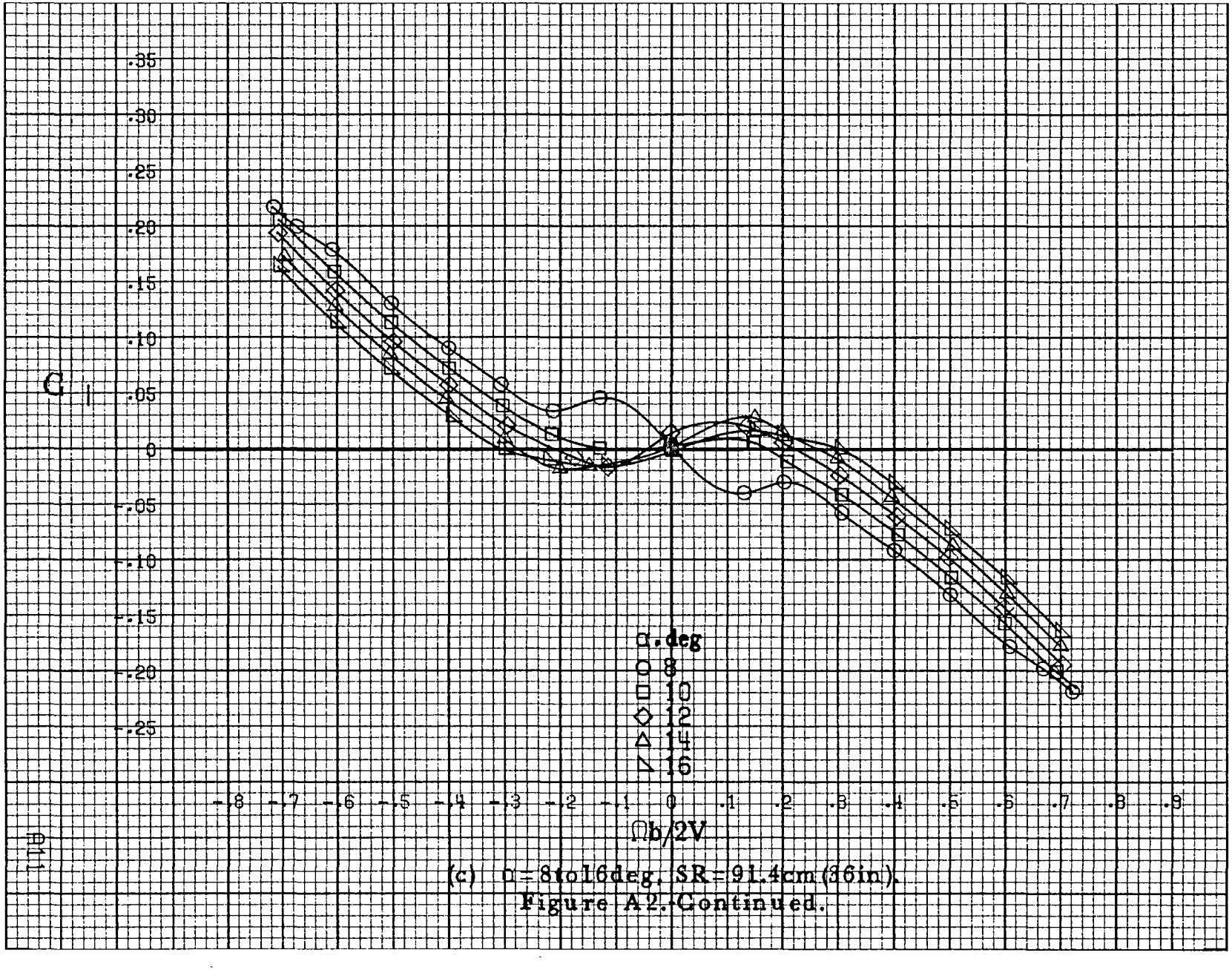

(c) α = 8 to 16 deg, SR = 91.4 cm (36 in).

Figure A2. Continued.

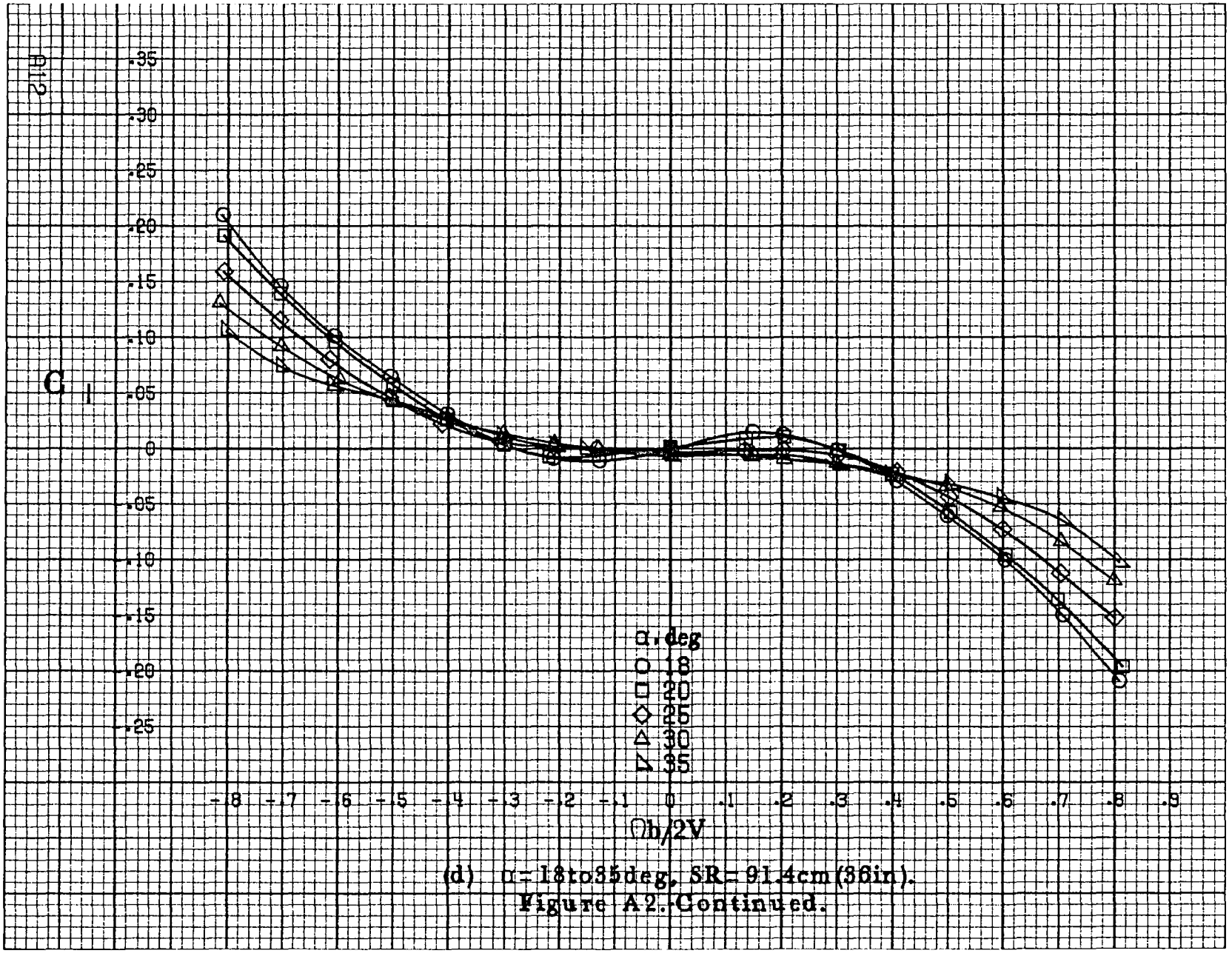

(d) α = 18 to 35 deg, SR = 91.4 cm (36 in).

Figure A2.-Continued.

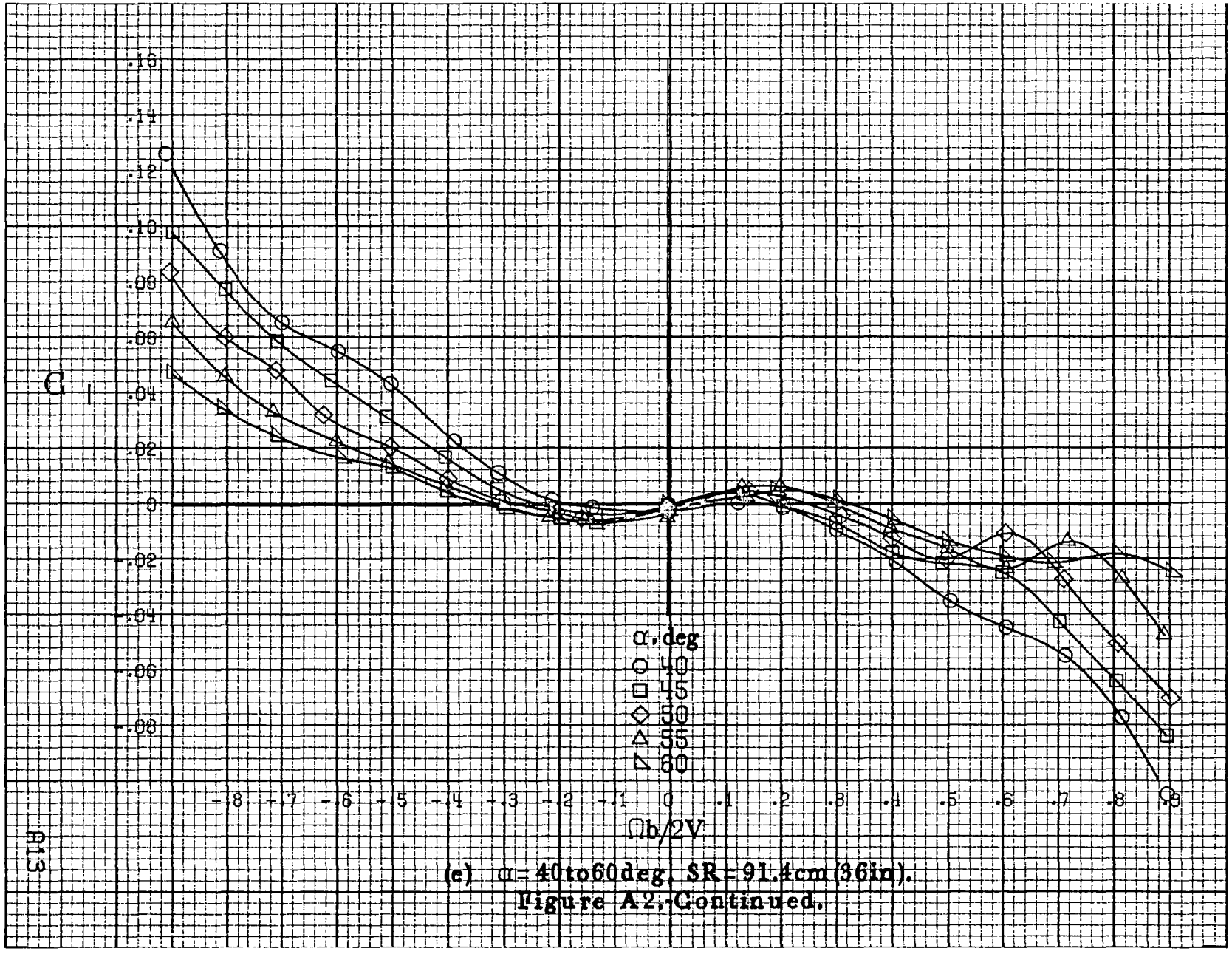

(e) $\alpha = 40$ to 60 deg, SR = 91.4 cm (36 in).

Figure A2.-Continued.

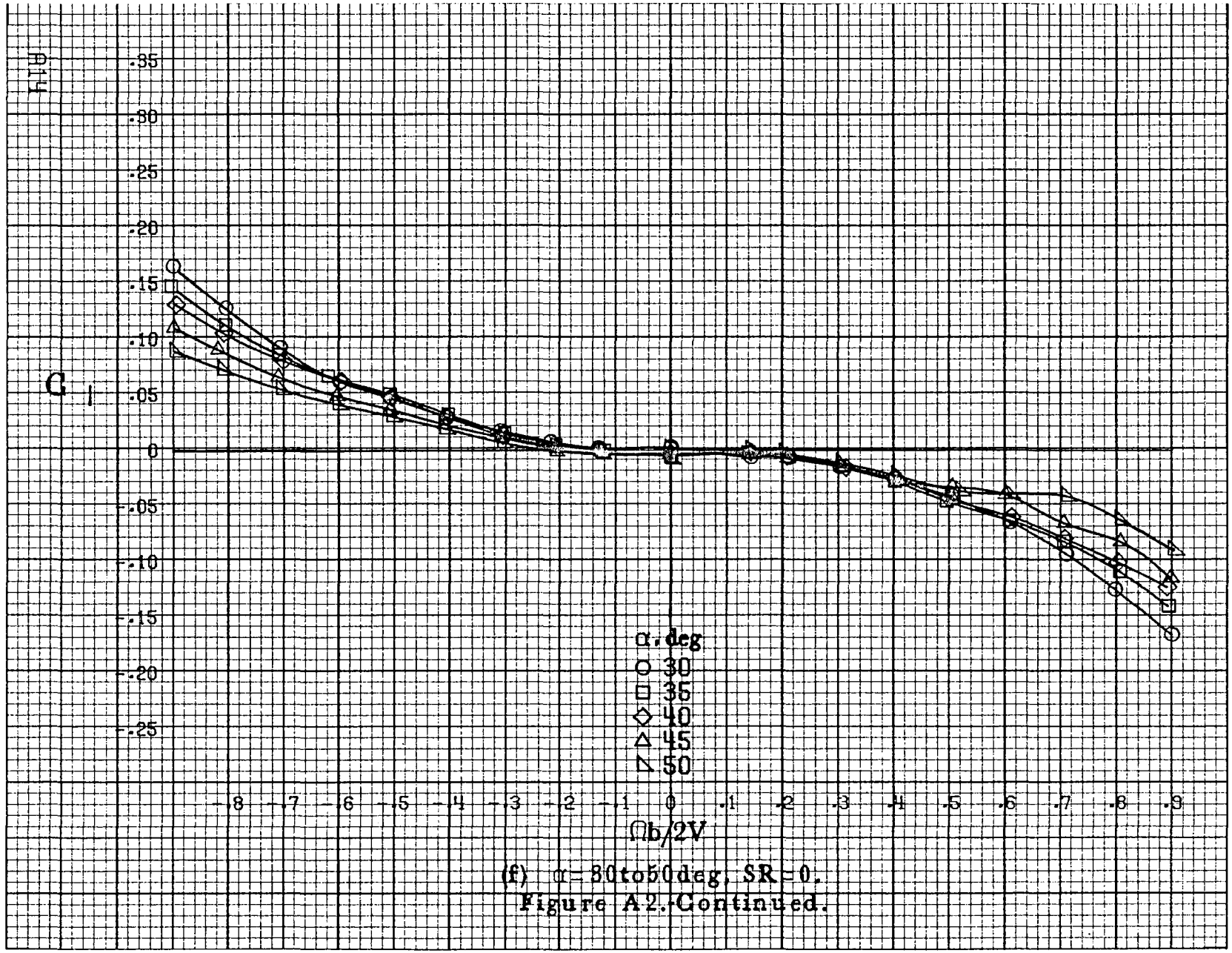

(f) $\alpha = 30$ to 50 deg, SR = 0.

Figure A2.-Continued.

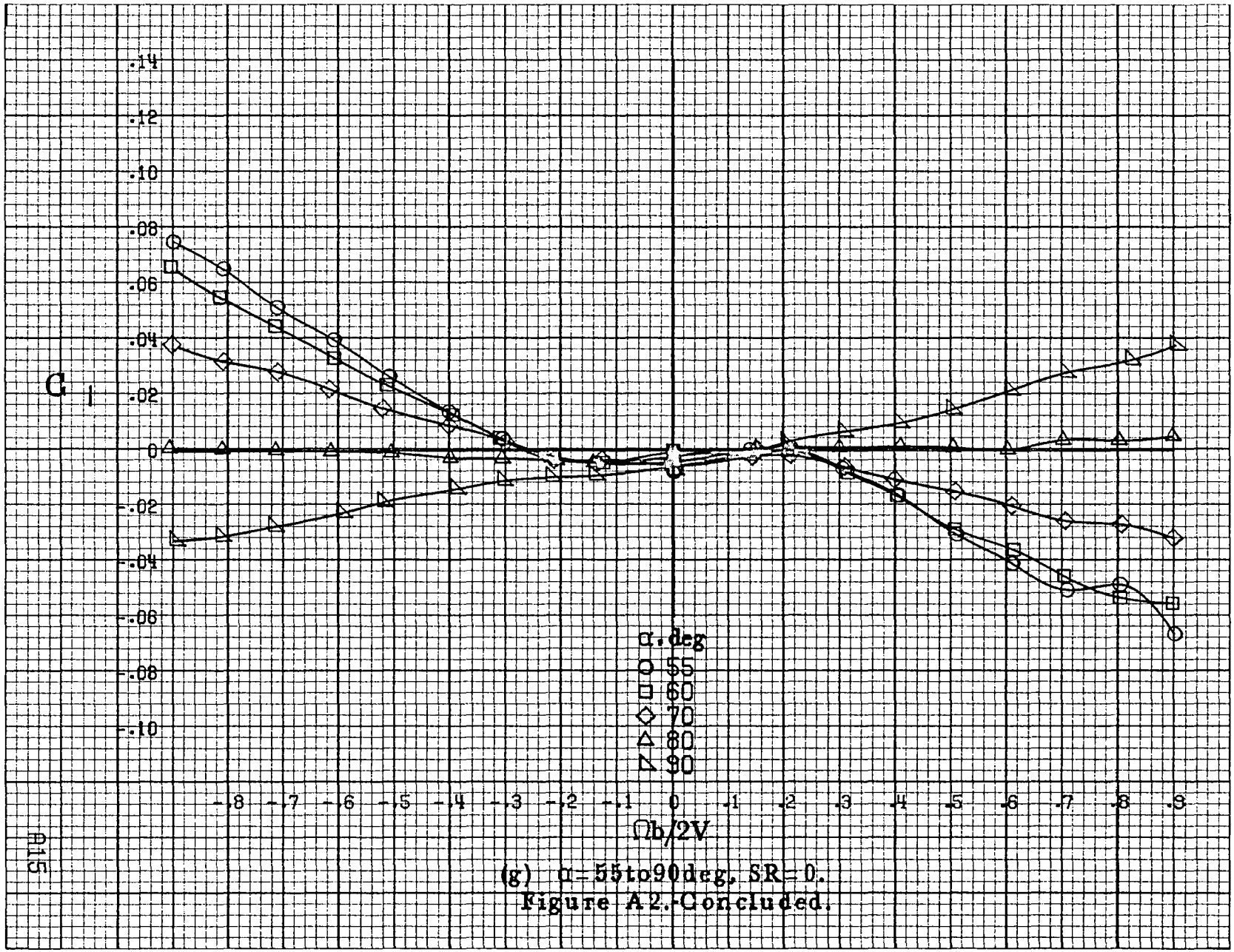

(g) α = 55 to 90 deg, SR = 0.

Figure A2.-Concluded.

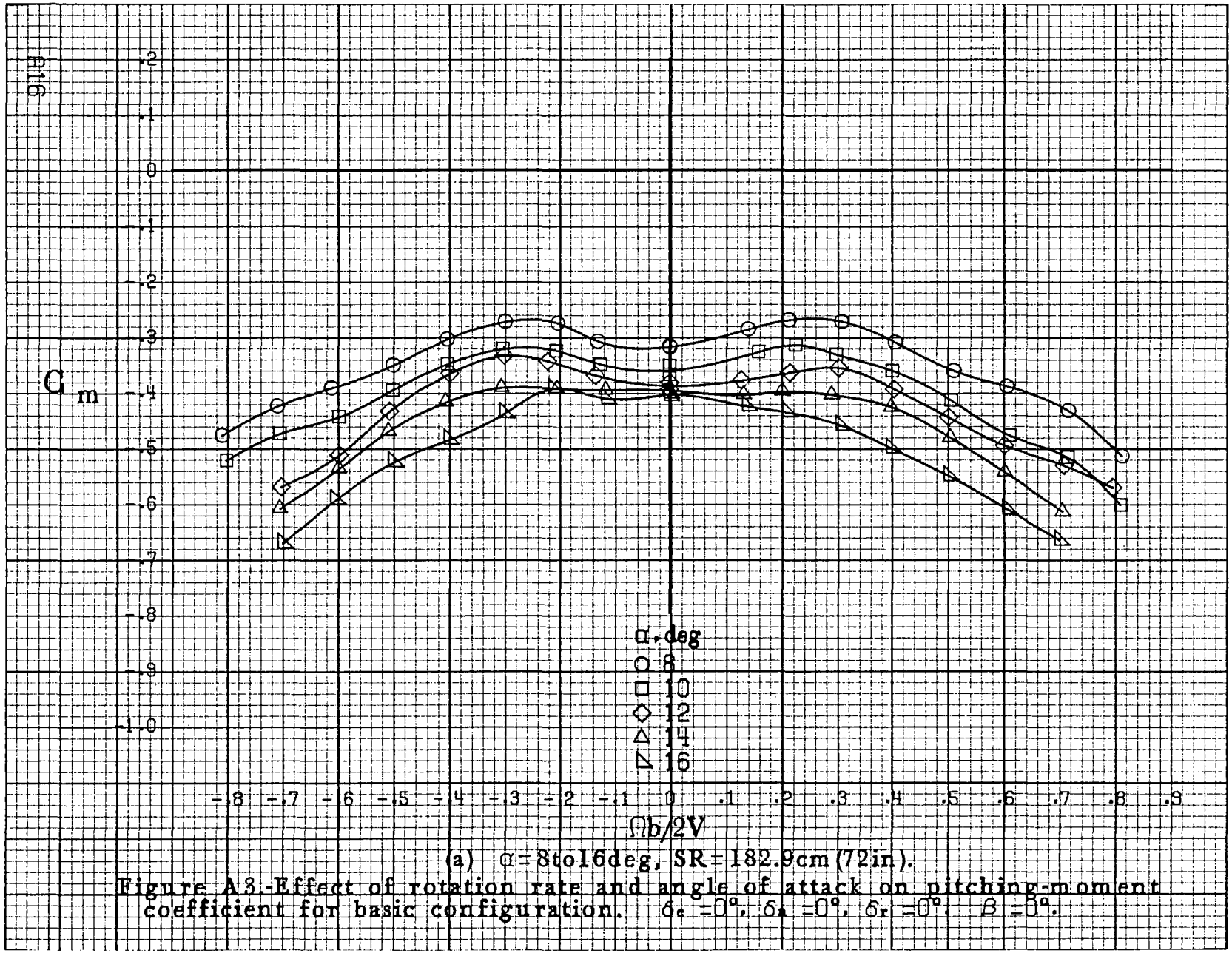

(a) $\alpha = 8$ to 16 deg, SR = 182.9 cm (72 in).

Figure A3.-Effect of rotation rate and angle of attack on pitching-moment coefficient for basic configuration. $\delta_e = 0°$, $\delta_a = 0°$, $\delta_r = 0°$, $\beta = 0°$.

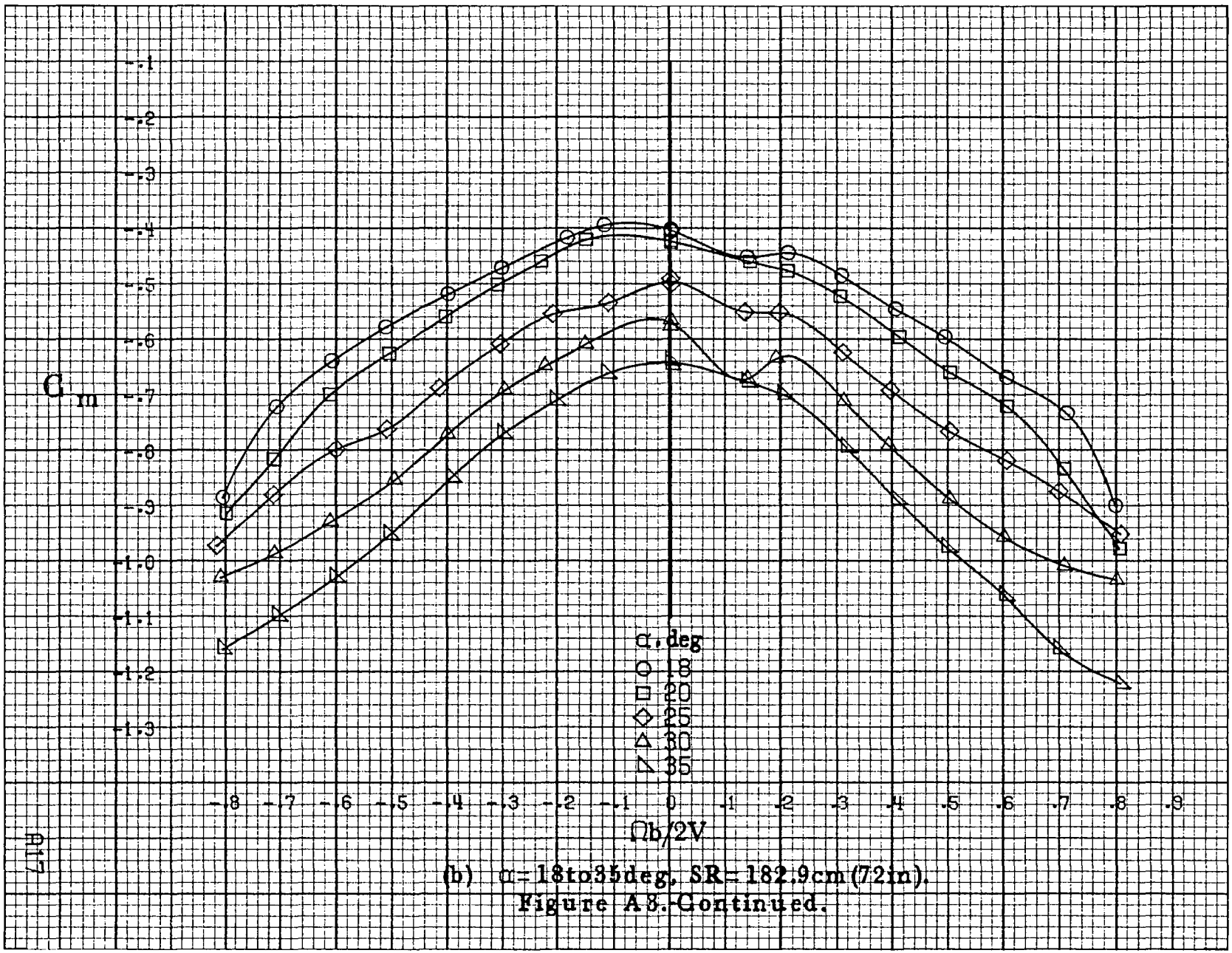

(b) α = 18 to 35 deg, SR = 182.9 cm (72 in).

Figure A8.-Continued.

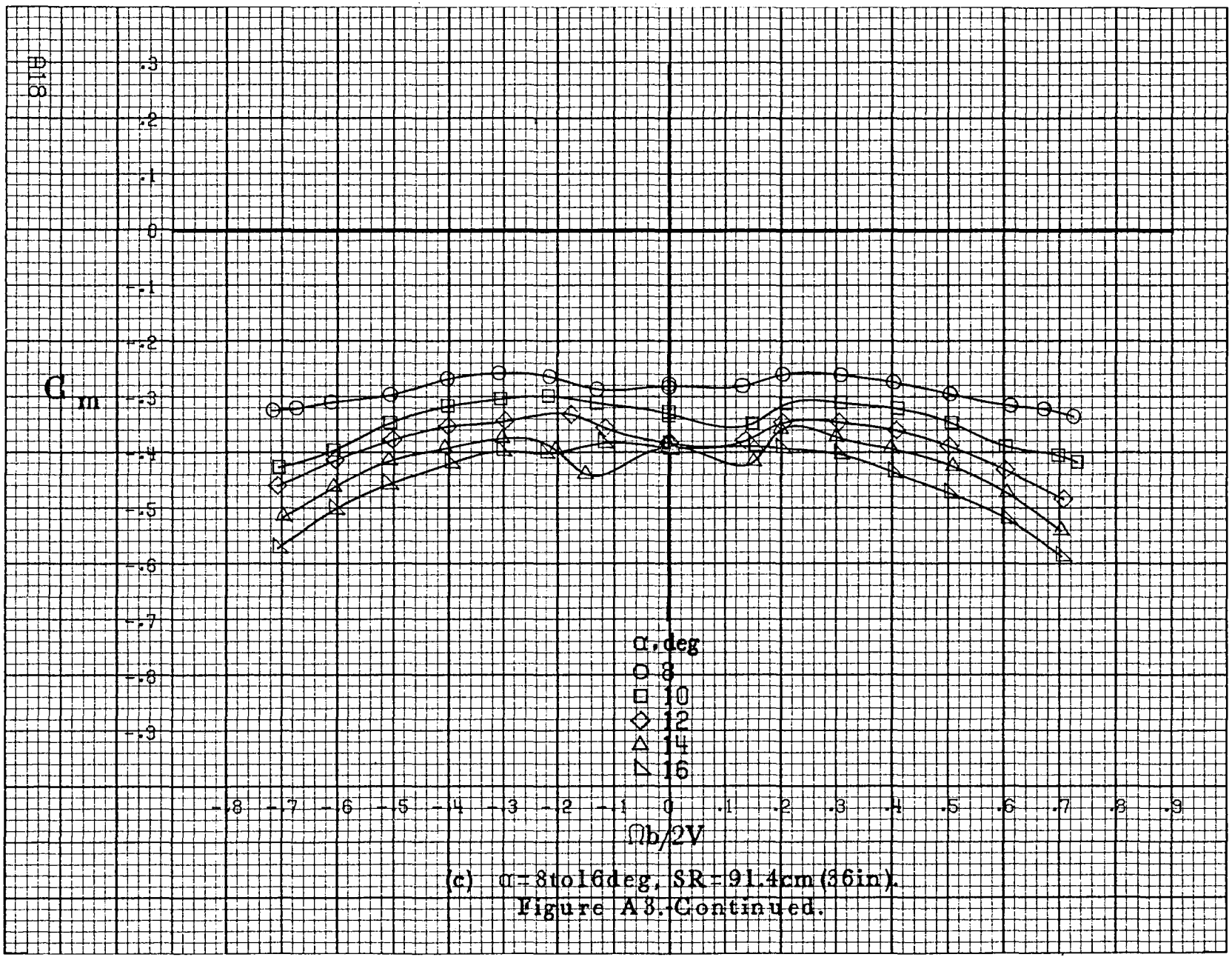

(c) α = 8 to 16 deg, SR = 91.4 cm (36 in).

Figure A8.-Continued.

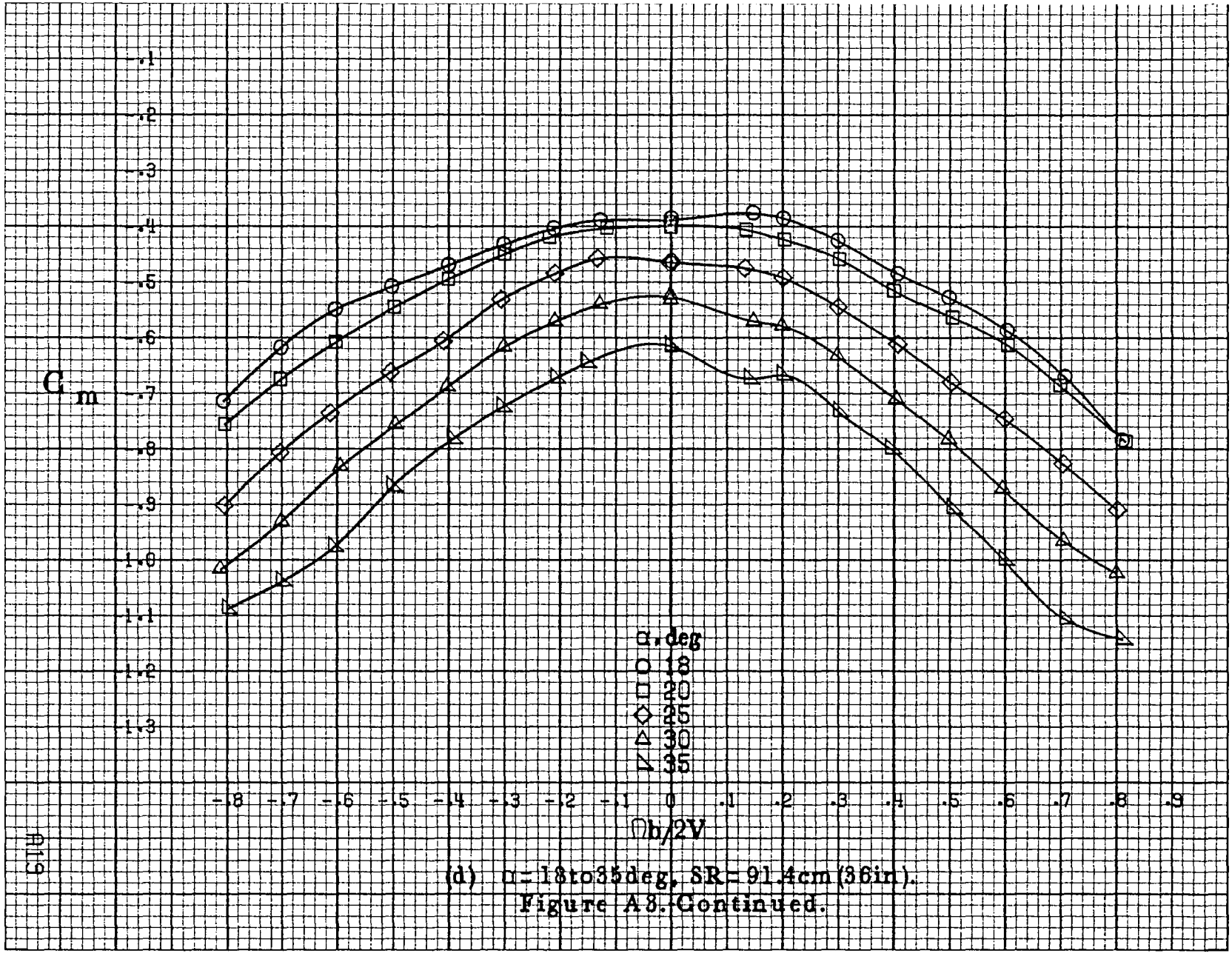

(d) α = 18 to 35 deg, SR = 91.4 cm (36 in).

Figure A8.-Continued.

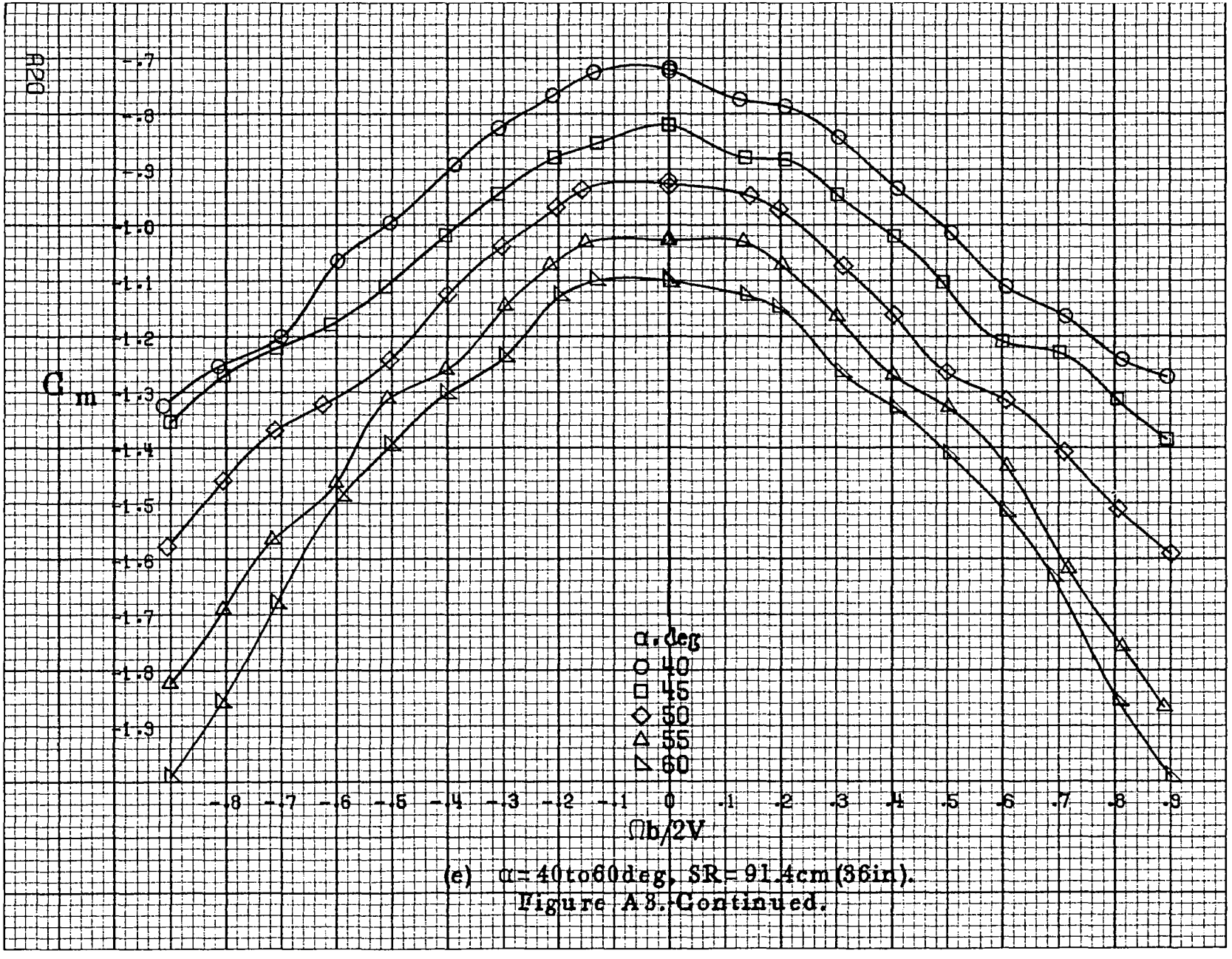

(e) $\alpha = 40$ to 60 deg, SR = 91.4 cm (36 in).

Figure A3.-Continued.

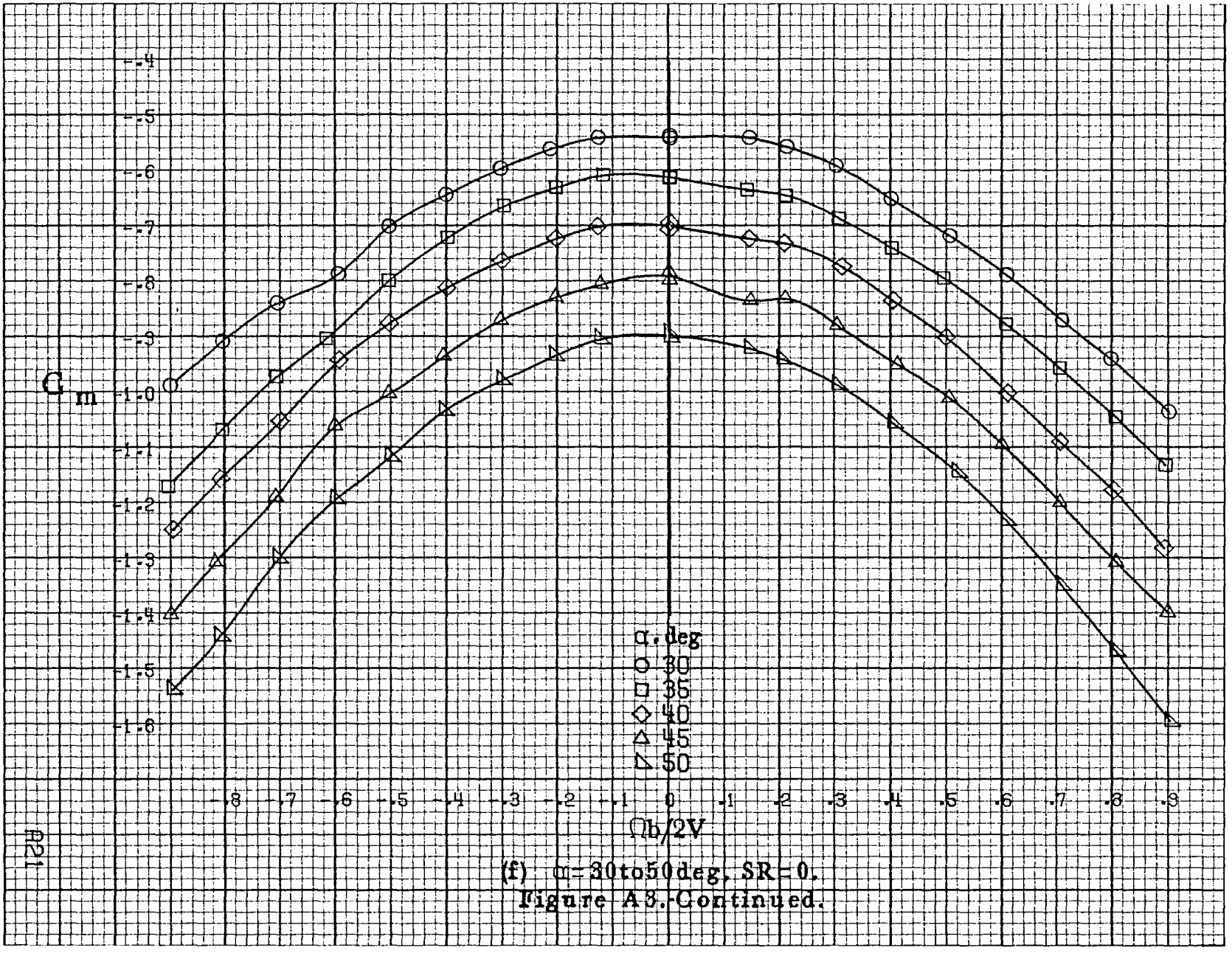

(f) $\alpha = 30$ to 50 deg, SR = 0.

Figure A3.-Continued.

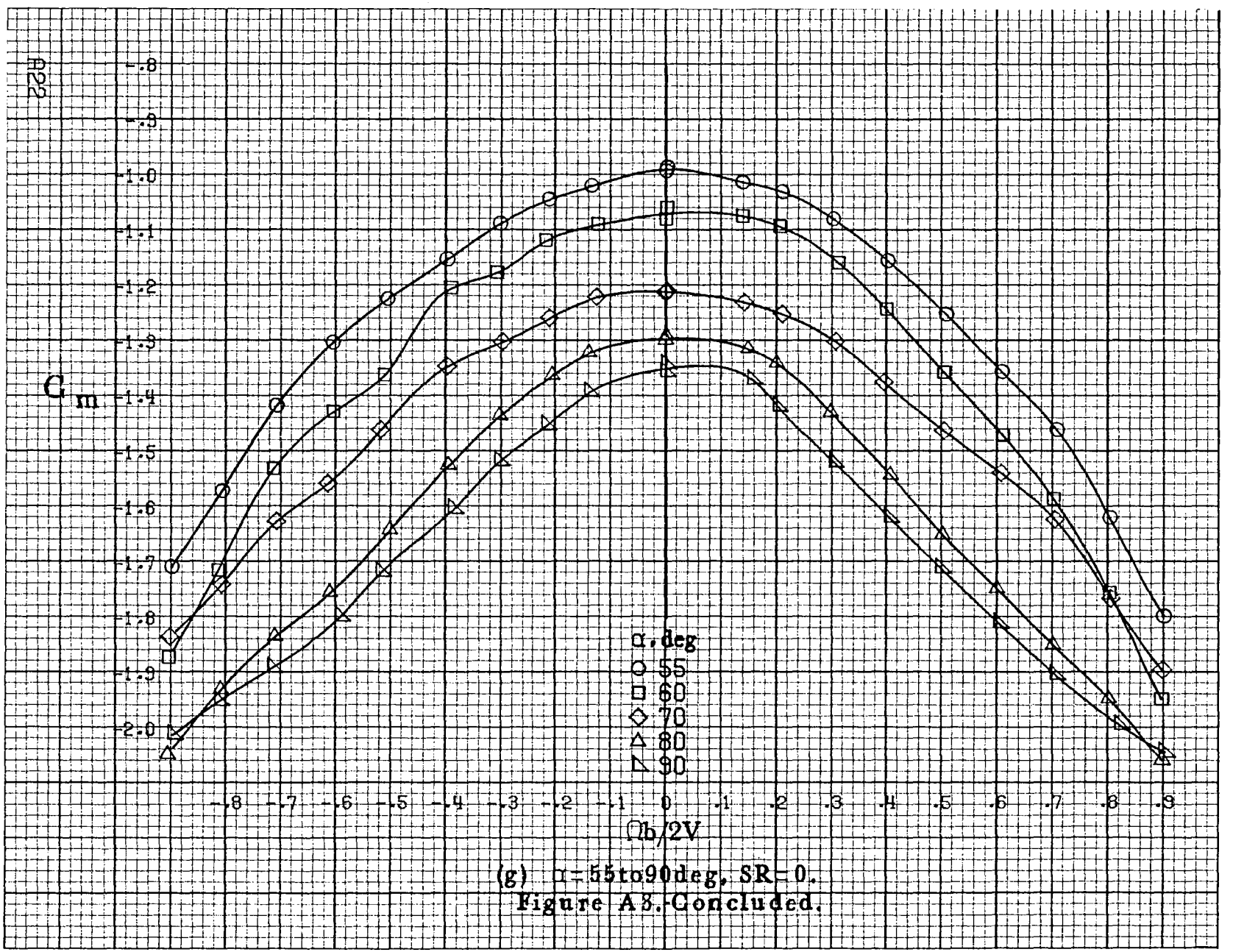

(g) α = 55 to 90 deg, SR = 0.

Figure A3.-Concluded.

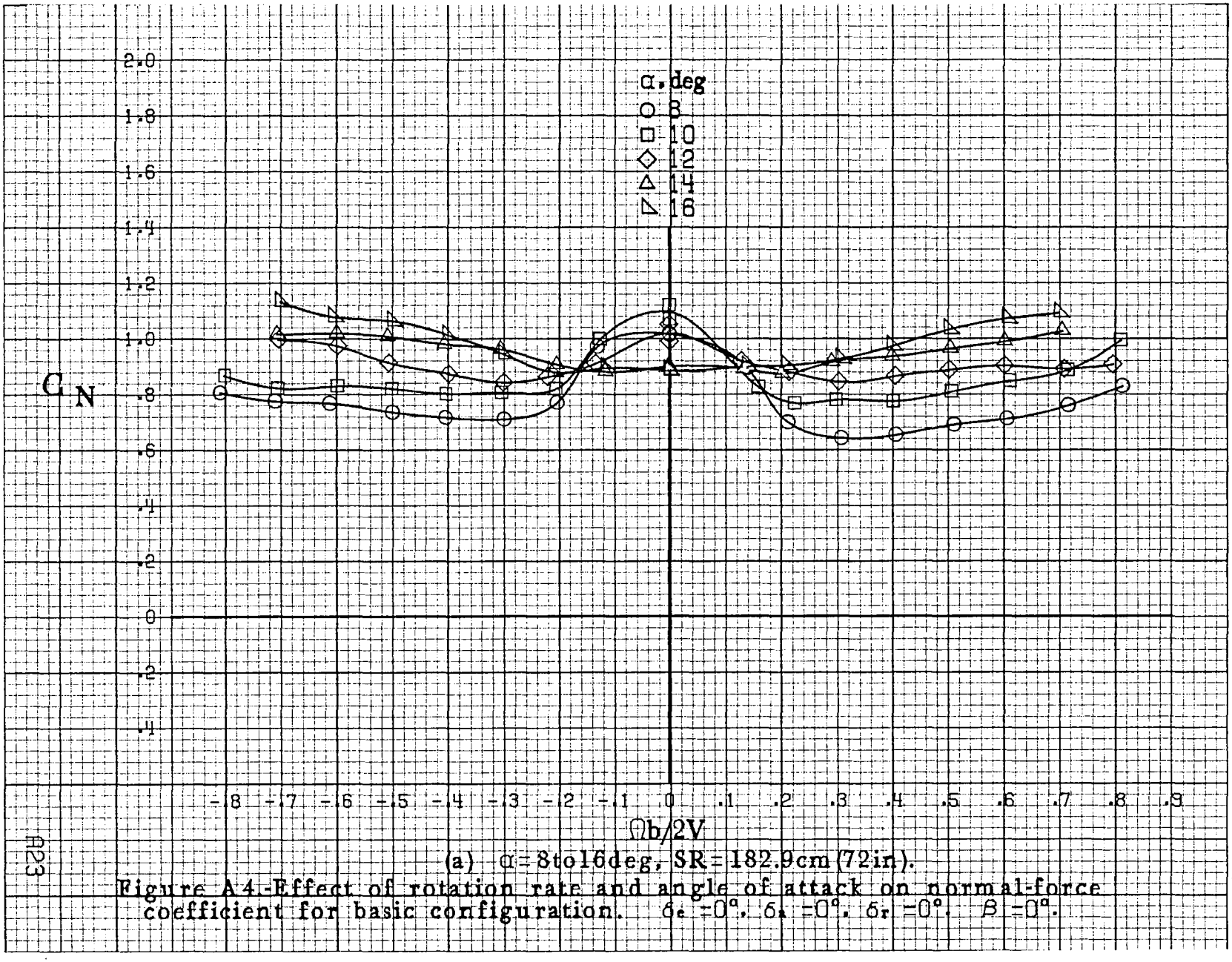

(a) $\alpha = 8$ to 16deg, SR = 182.9cm (72in).

Figure A4-Effect of rotation rate and angle of attack on normal-force coefficient for basic configuration. $\delta_e = 0°$, $\delta_a = 0°$, $\delta_r = 0°$, $\beta = 0°$.

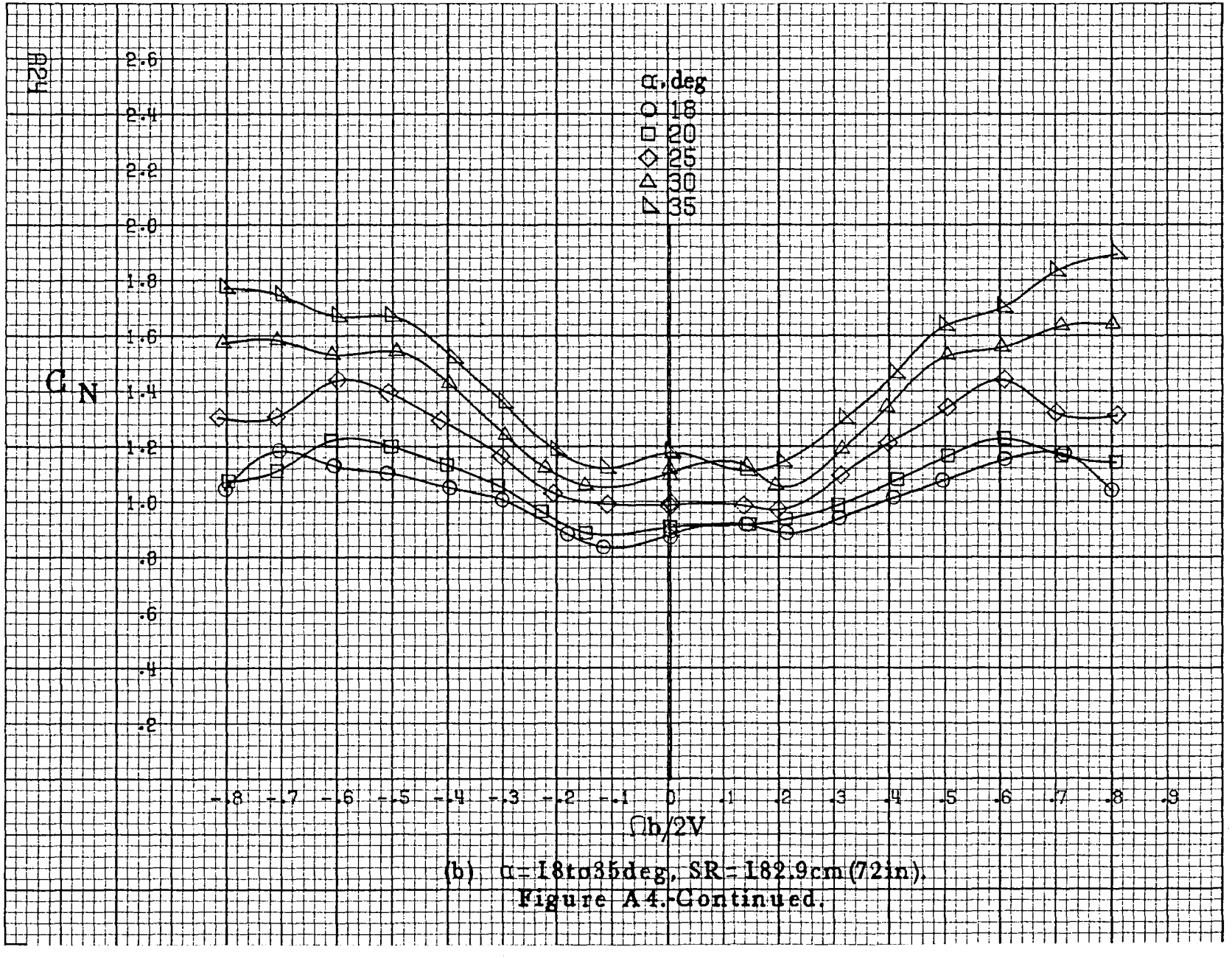

(b) α = 18 to 35 deg, SR = 182.9 cm (72 in).

Figure A4.-Continued.

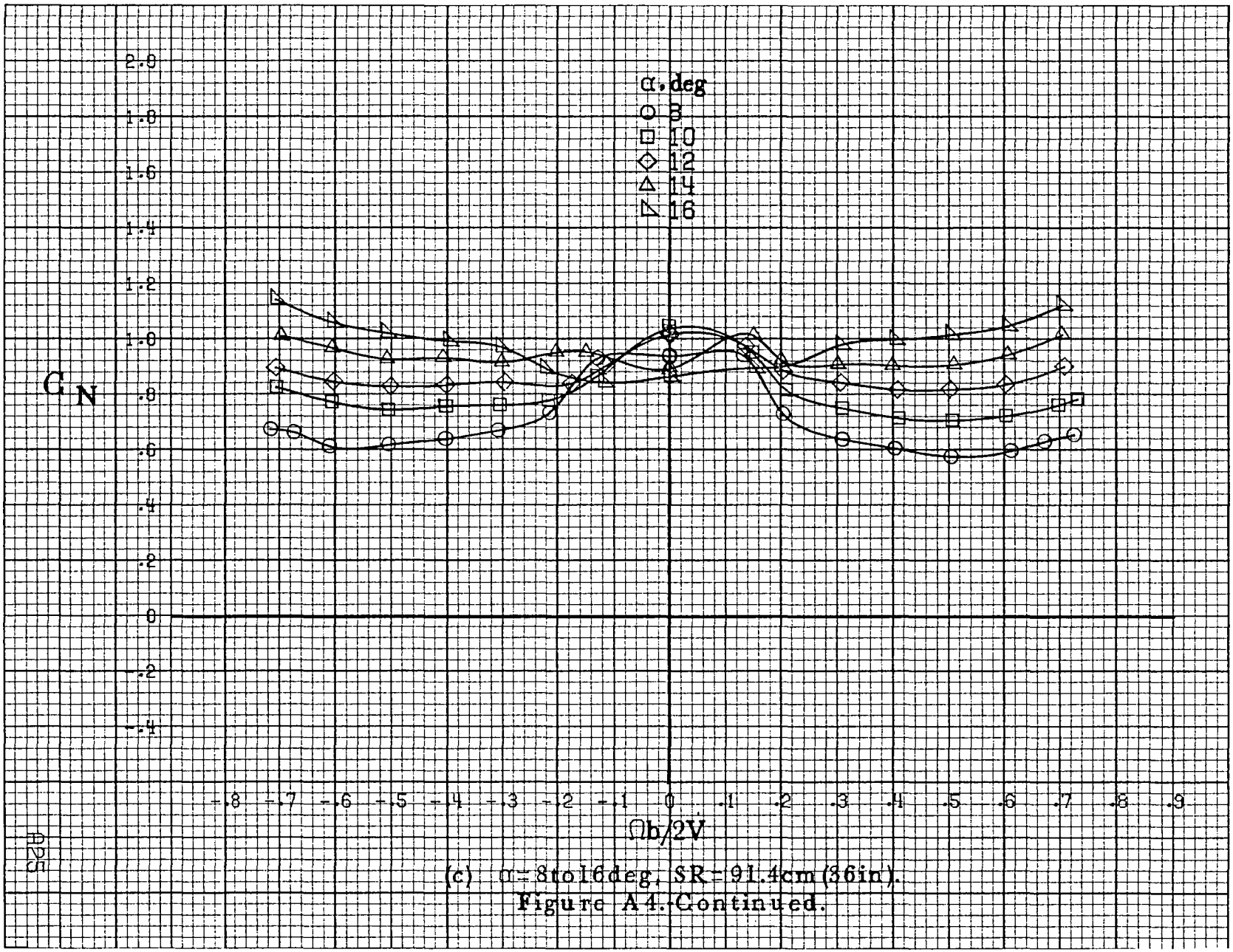

(c) α = 8 to 16 deg, SR = 91.4 cm (36 in).

Figure A4.-Continued.

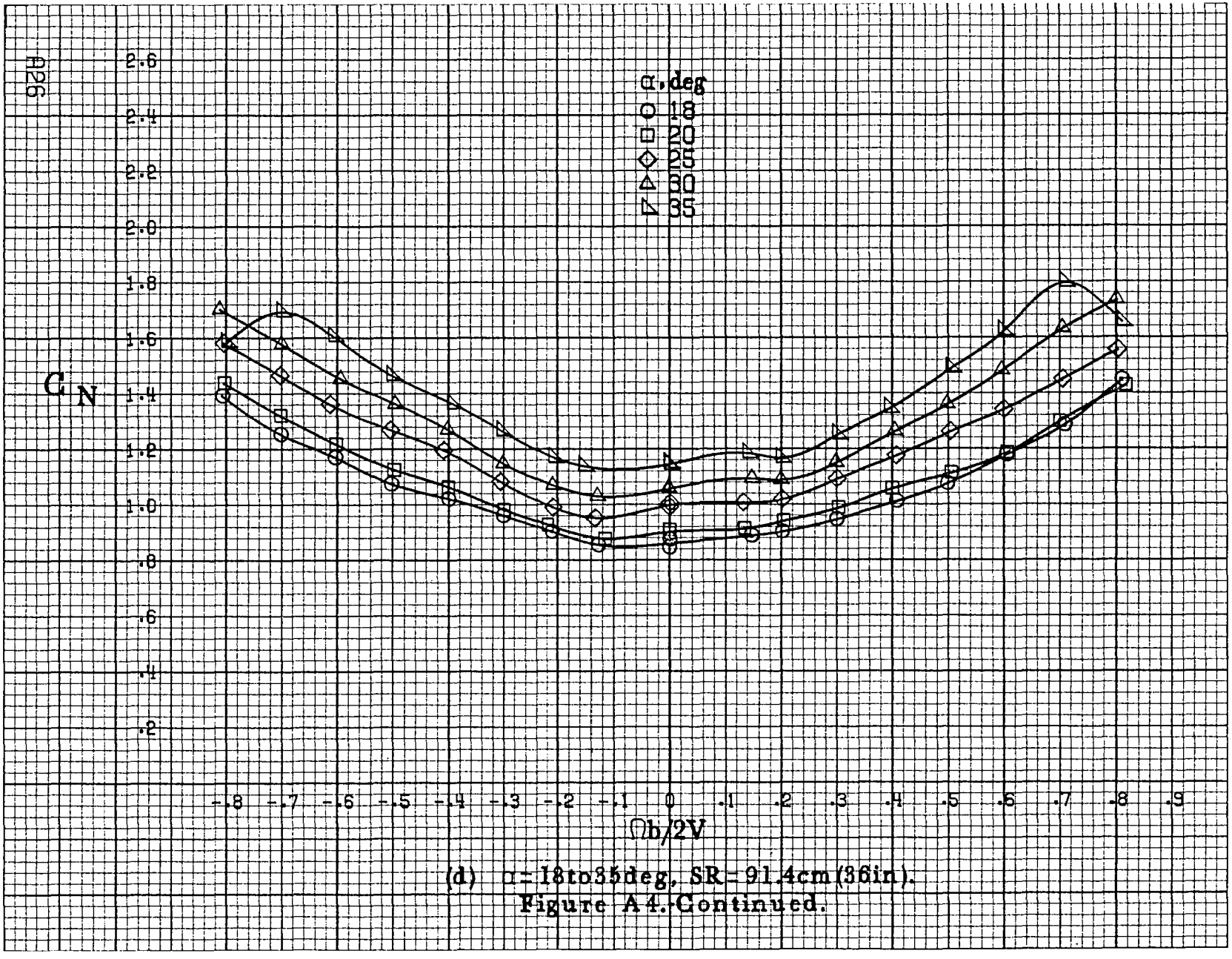

(d) α = 18 to 35 deg, SR = 91.4 cm (36 in).

Figure A4.-Continued.

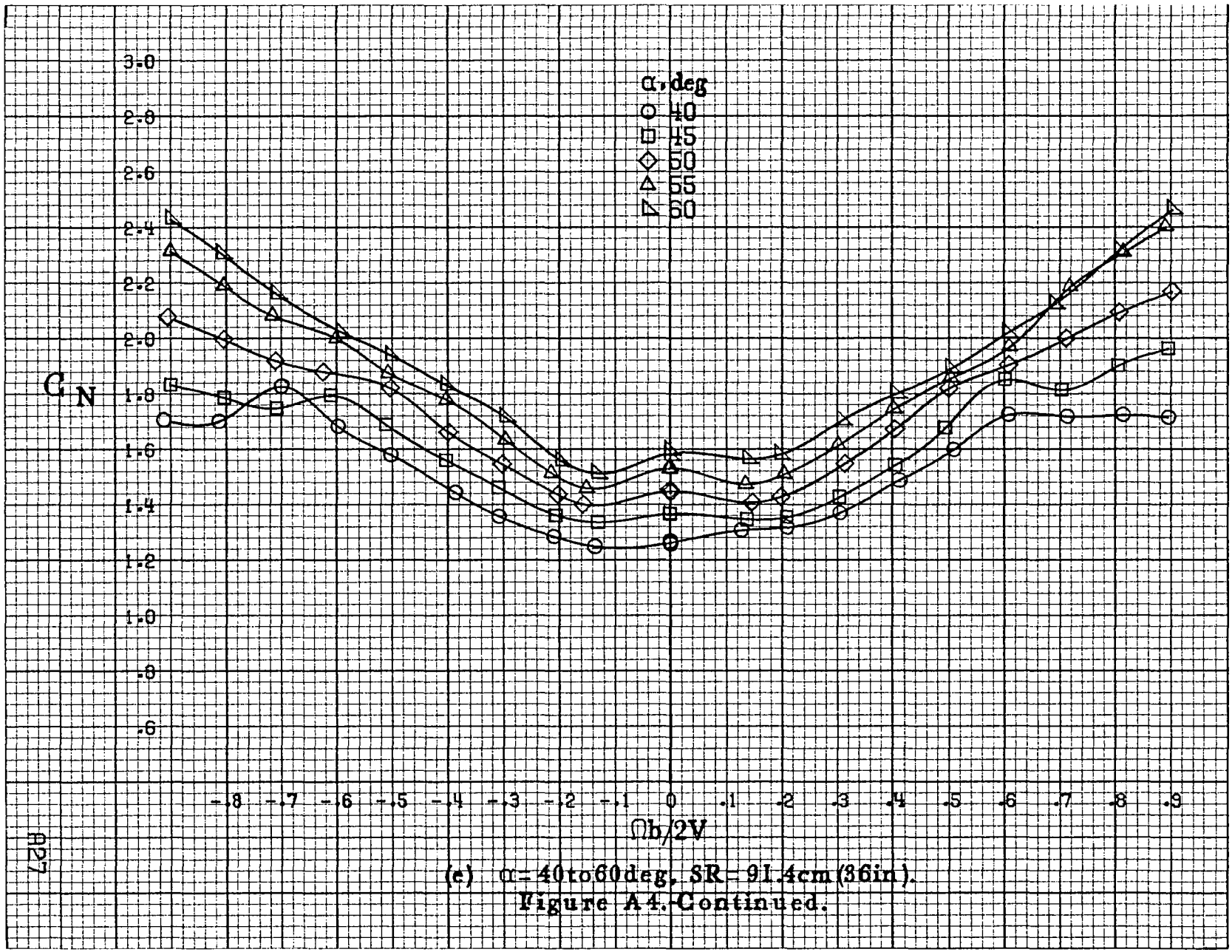

(c) α = 40 to 60 deg, SR = 91.4 cm (36 in.).

Figure A4.-Continued.

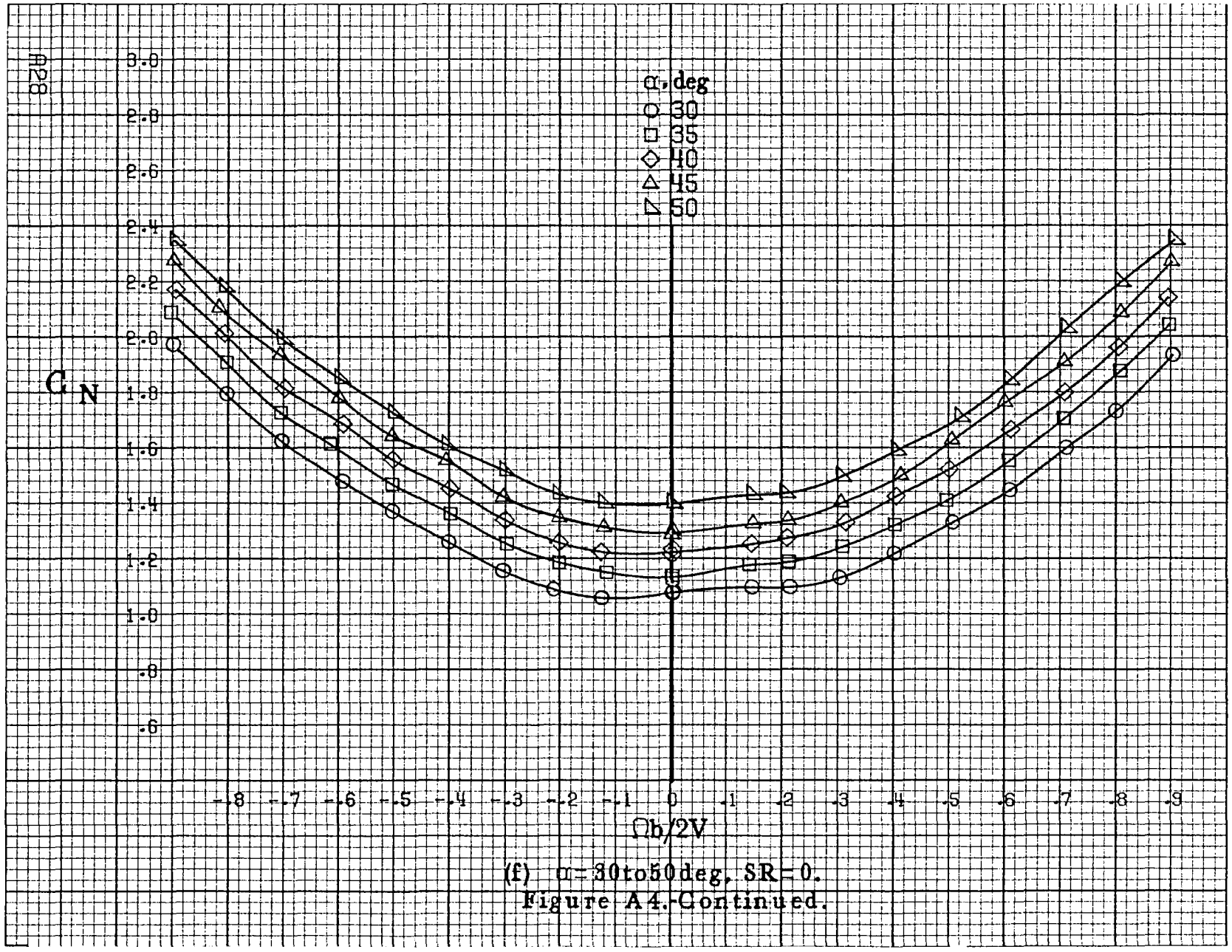

(f) α = 30 to 50 deg, SR = 0.

Figure A4.-Continued.

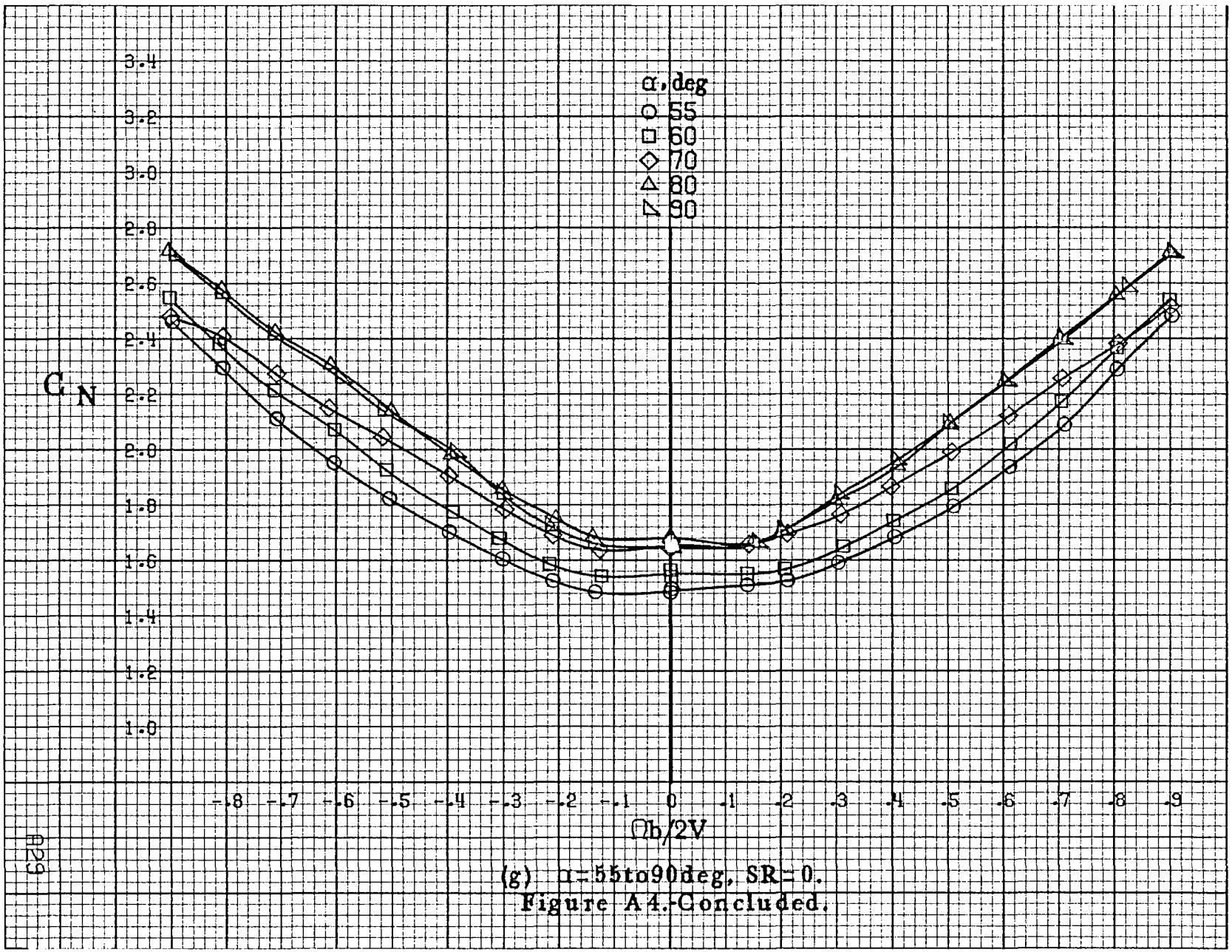

(g) α = 55 to 90 deg, SR = 0.

Figure A4.-Concluded.

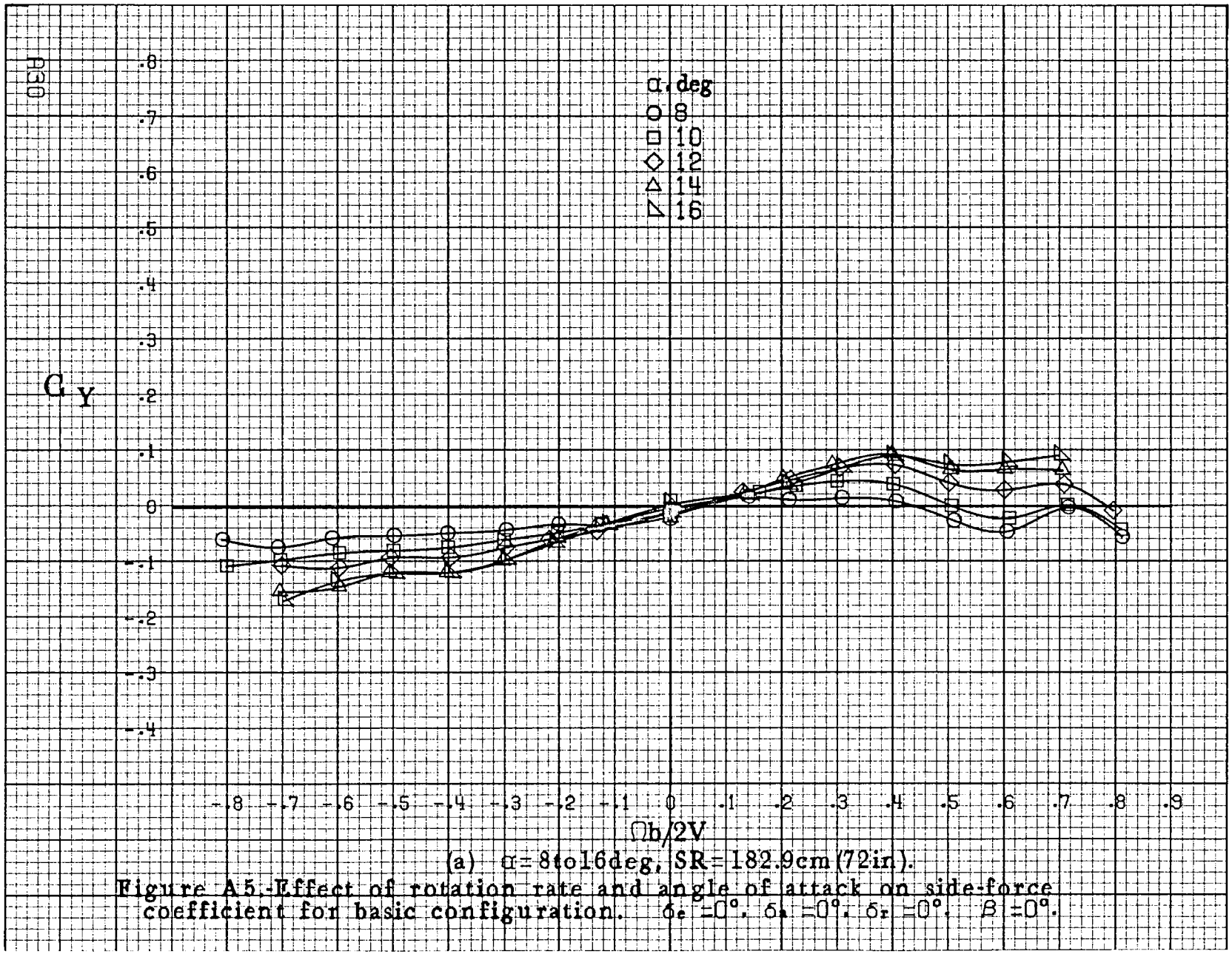

(a) $\alpha = 8$ to 16 deg, SR = 182.9 cm (72 in.).

Figure A5.-Effect of rotation rate and angle of attack on side-force coefficient for basic configuration. $\delta_e = 0°$, $\delta_a = 0°$, $\delta_r = 0°$, $\beta = 0°$.

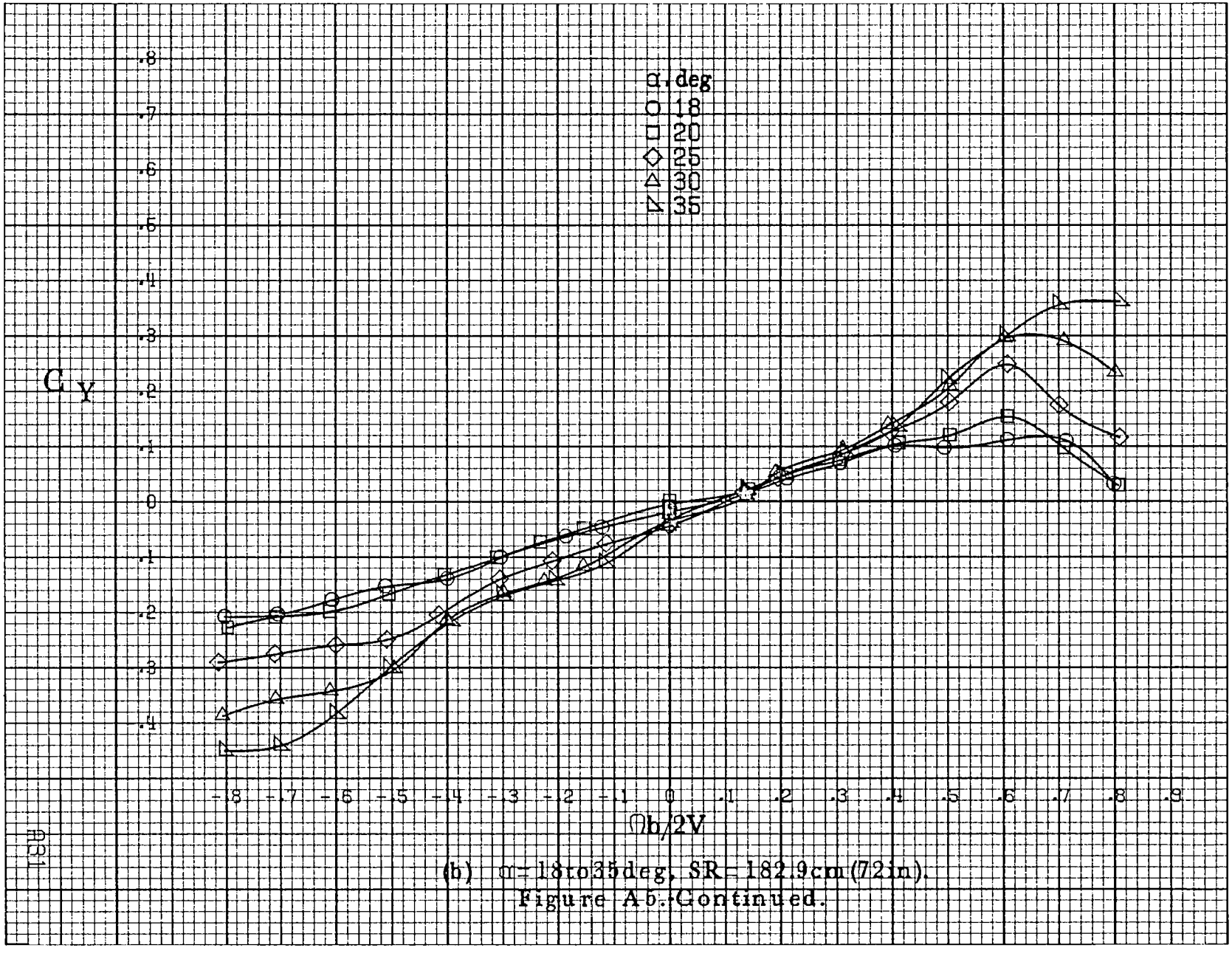

(b) α = 18 to 35 deg, SR = 182.9 cm (72 in).

Figure A5.-Continued.

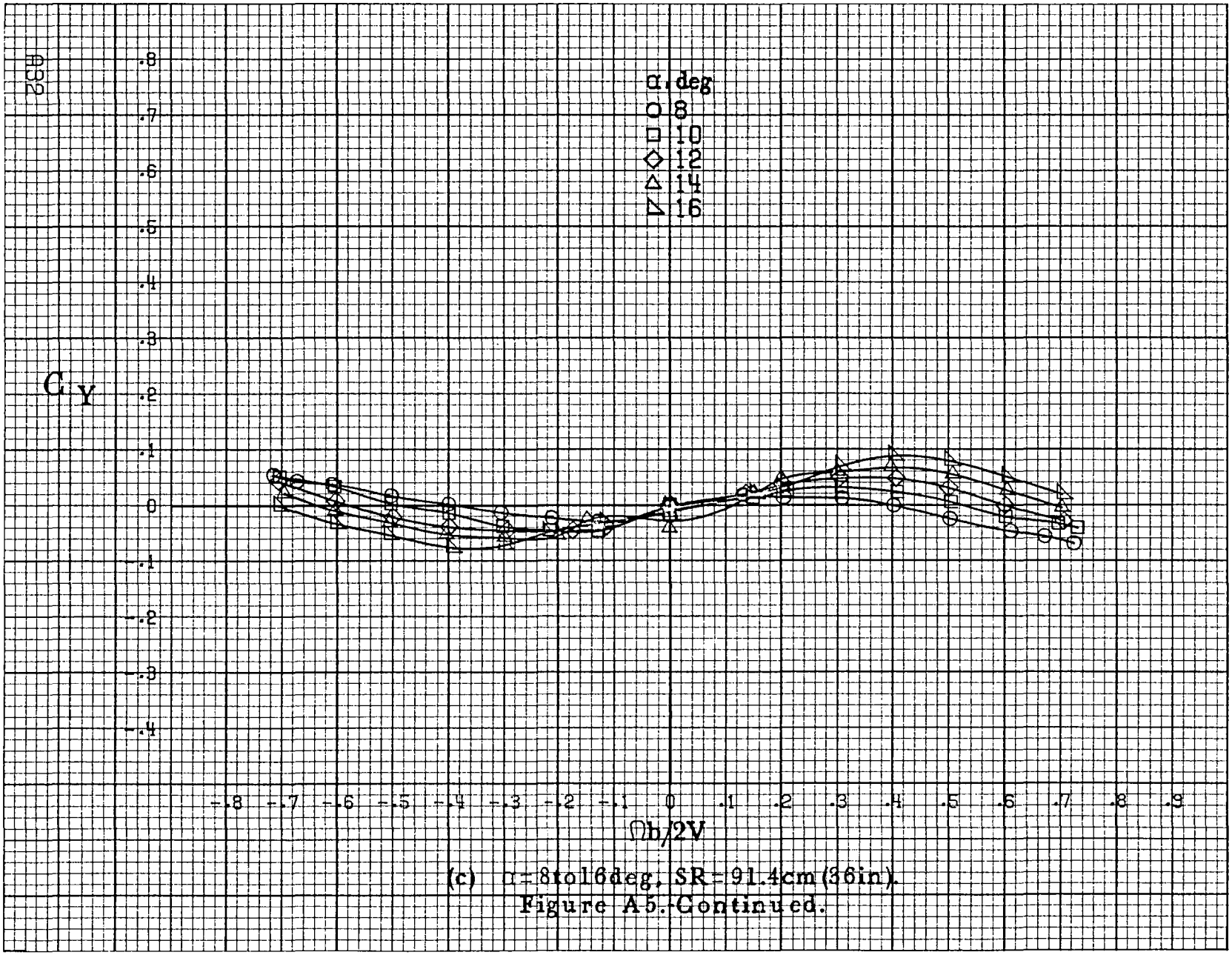

(c) α=8to16deg, SR=91.4cm(36in).

Figure A5.-Continued.

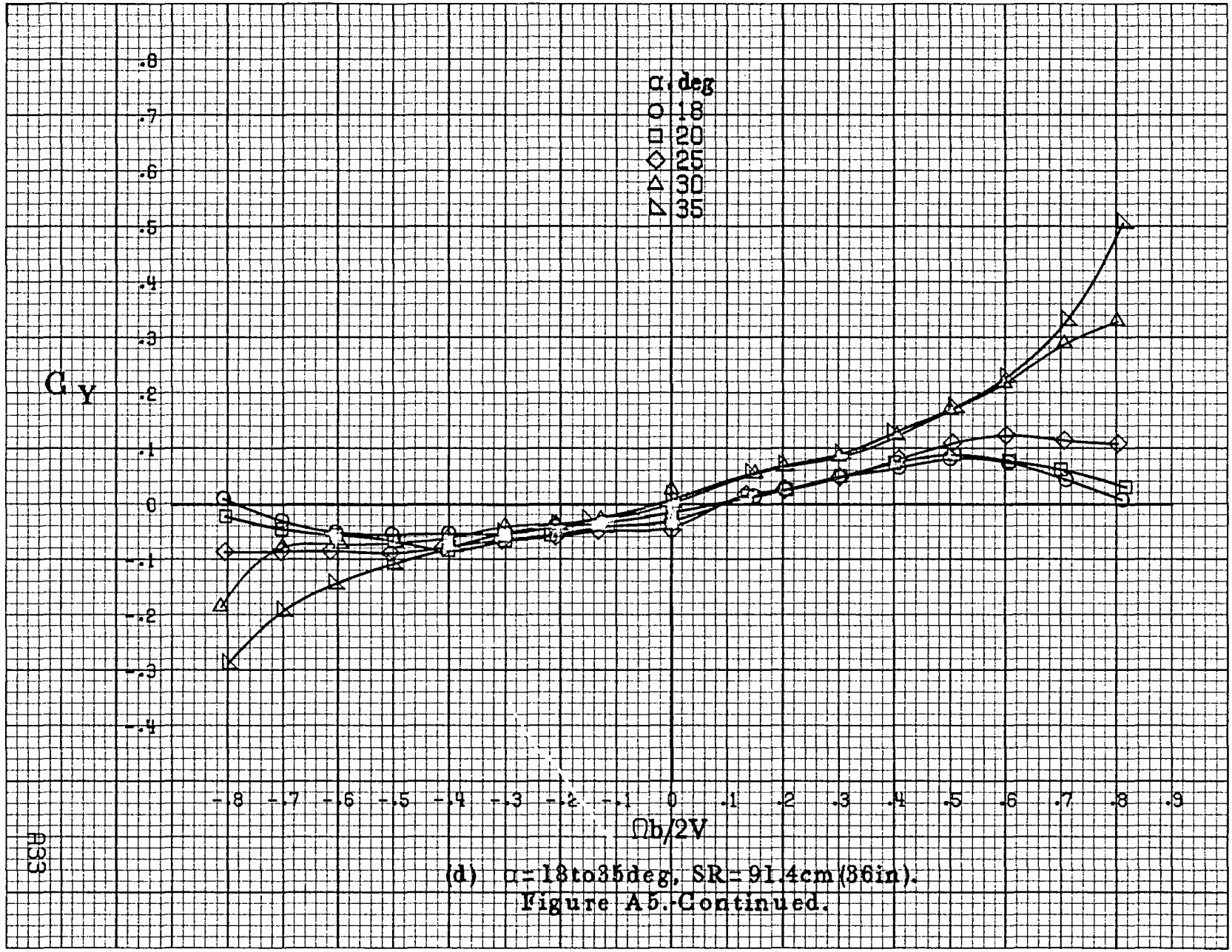

(d) α = 18 to 35 deg, SR = 91.4 cm (36 in).

Figure A5.-Continued.

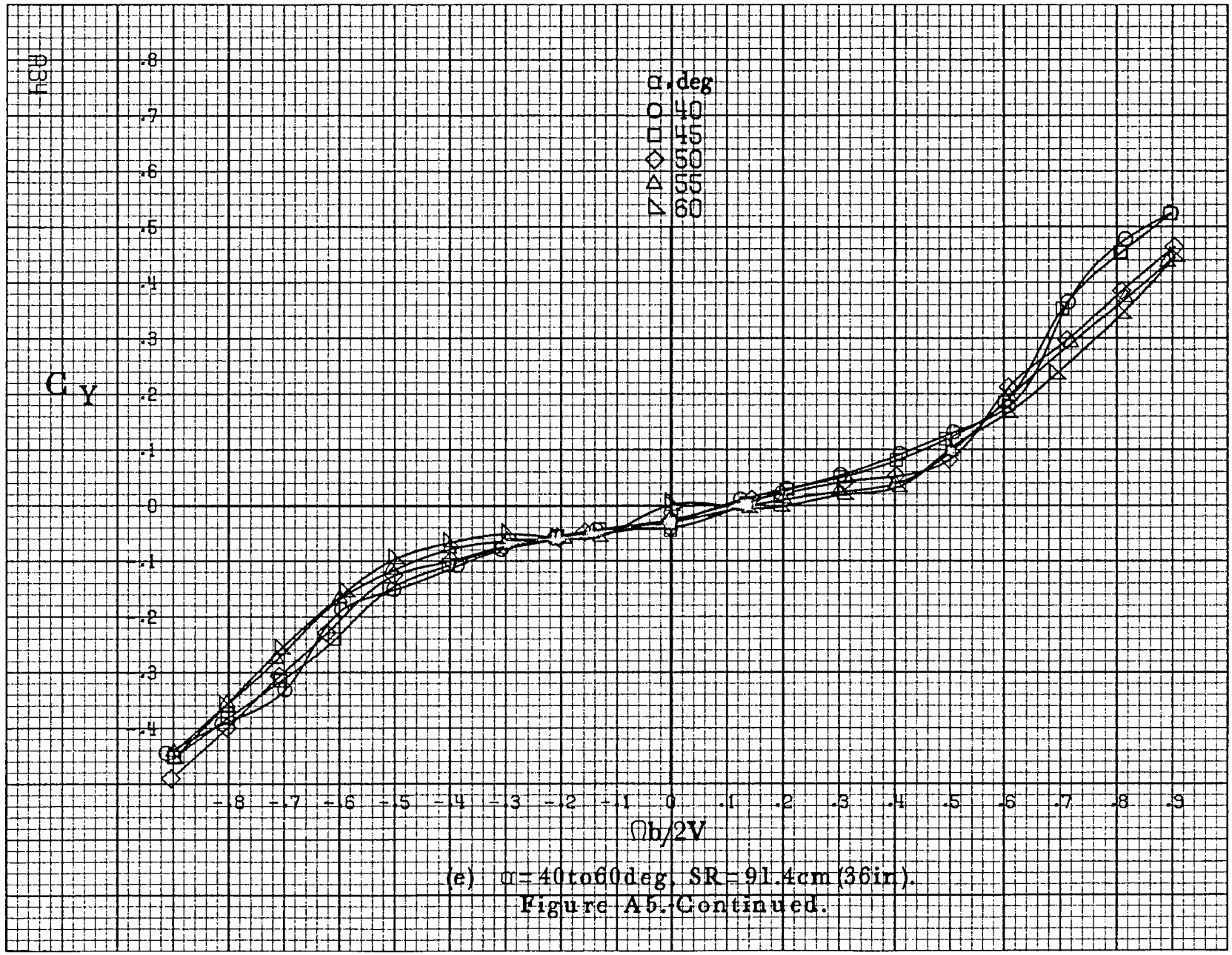

(e) α = 40 to 60 deg, SR = 91.4 cm (36 in).

Figure A5. Continued.

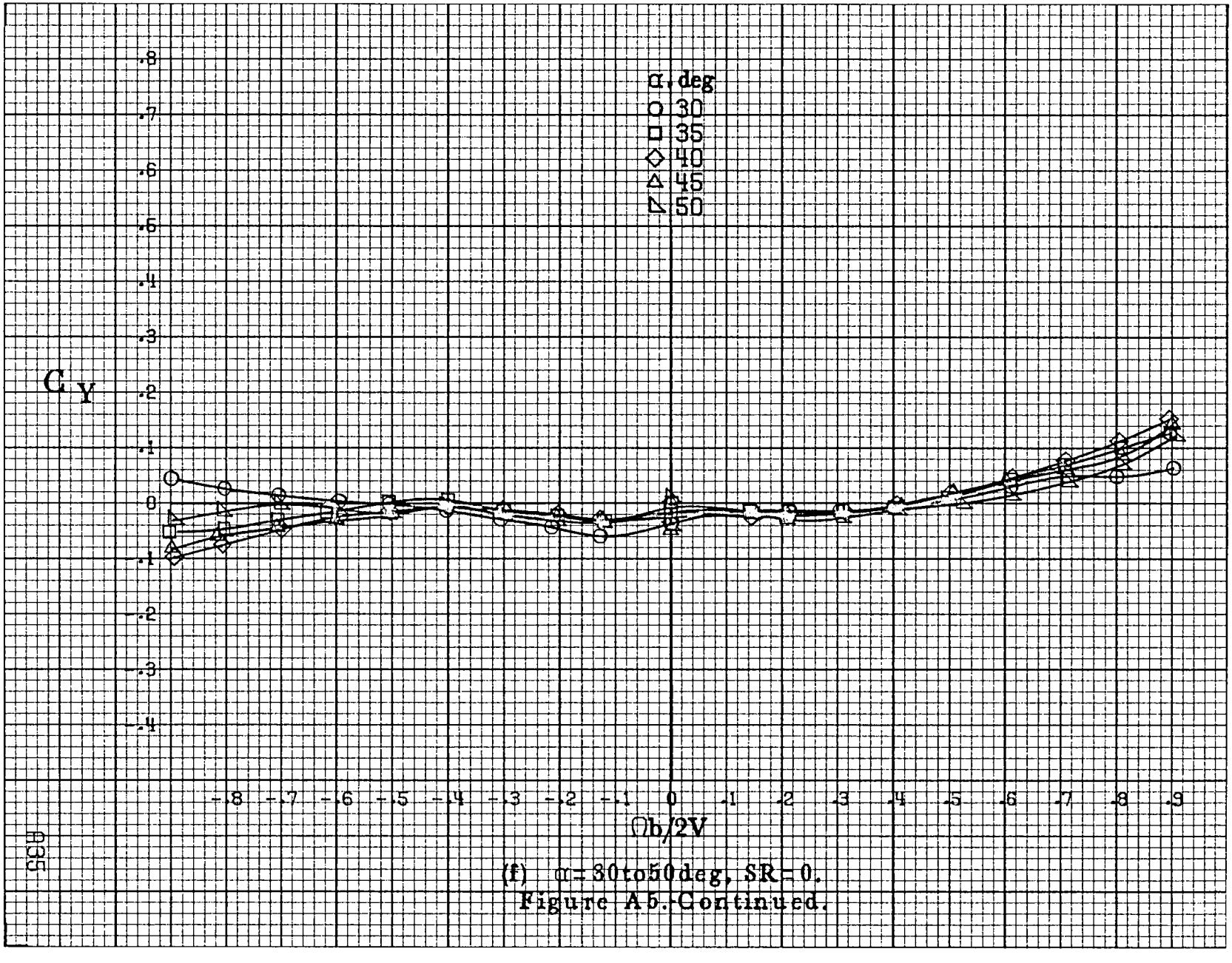

(f) $\alpha = 30$ to 50 deg, SR = 0.

Figure A5.-Continued.

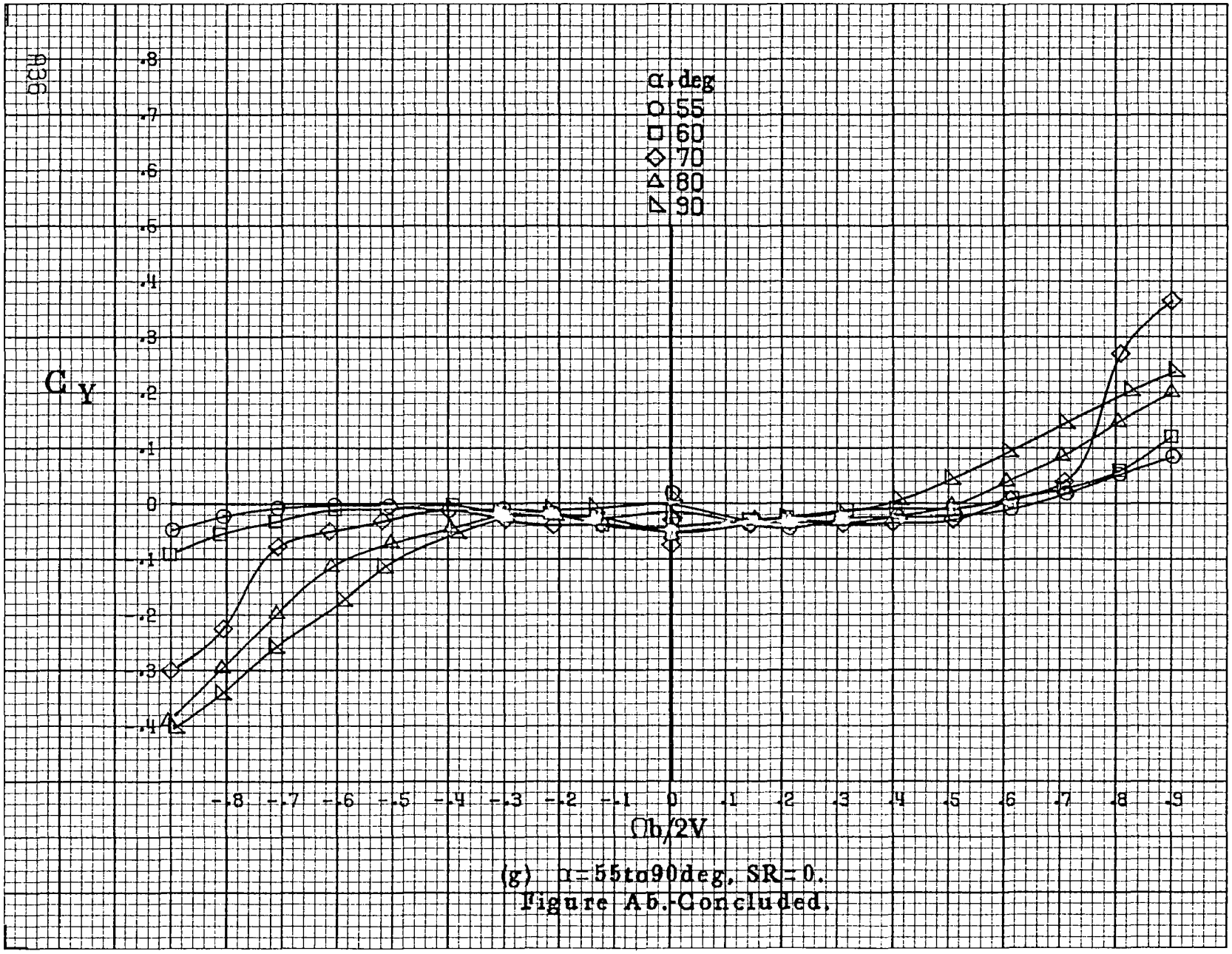

(g) α = 55 to 90 deg, SR = 0.

Figure A6.-Concluded.

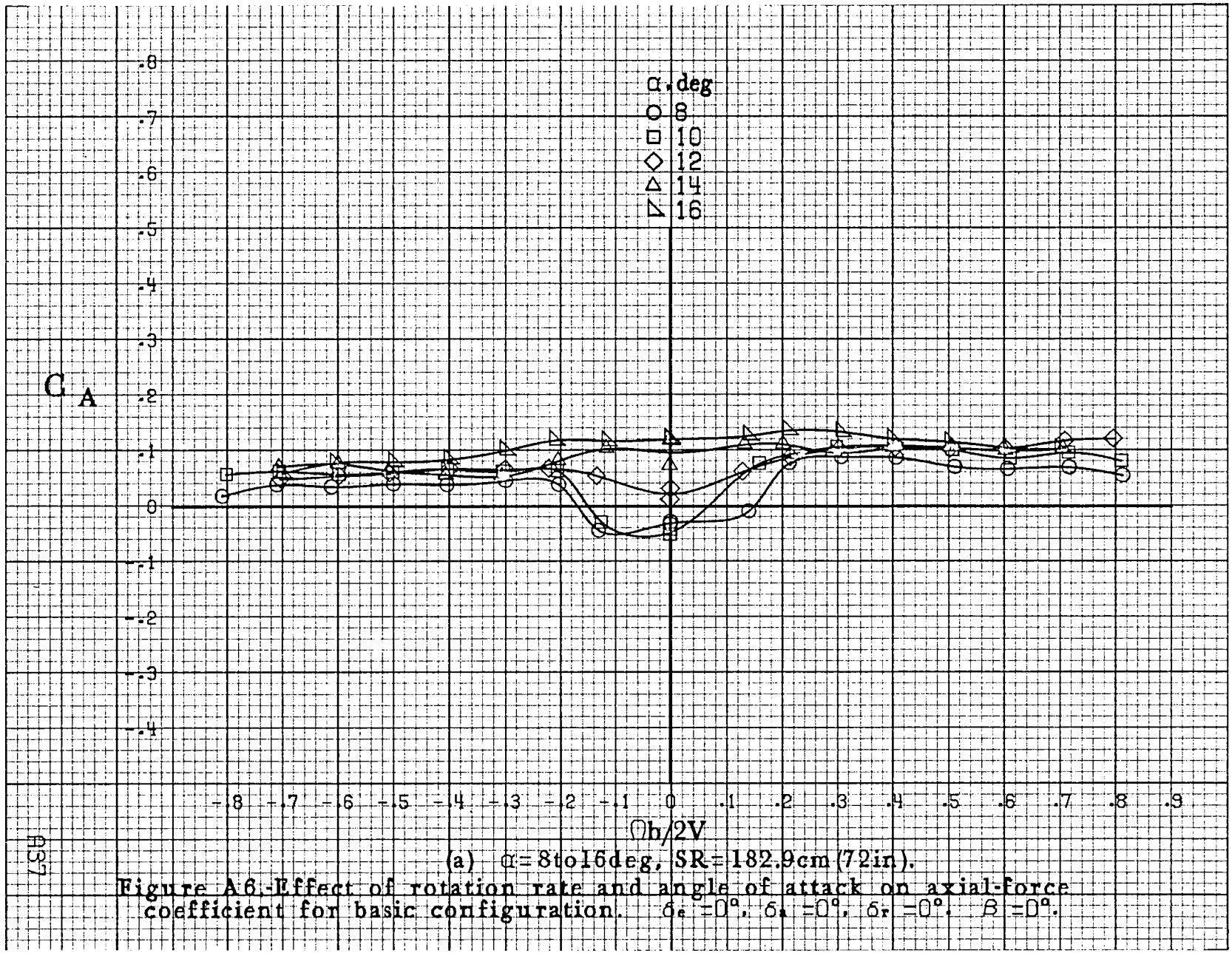

(a) $\alpha = 8$ to 16 deg, SR = 182.9 cm (72 in).

Figure A6.-Effect of rotation rate and angle of attack on axial-force coefficient for basic configuration. $\delta_e = 0°$, $\delta_a = 0°$, $\delta_r = 0°$, $\beta = 0°$.

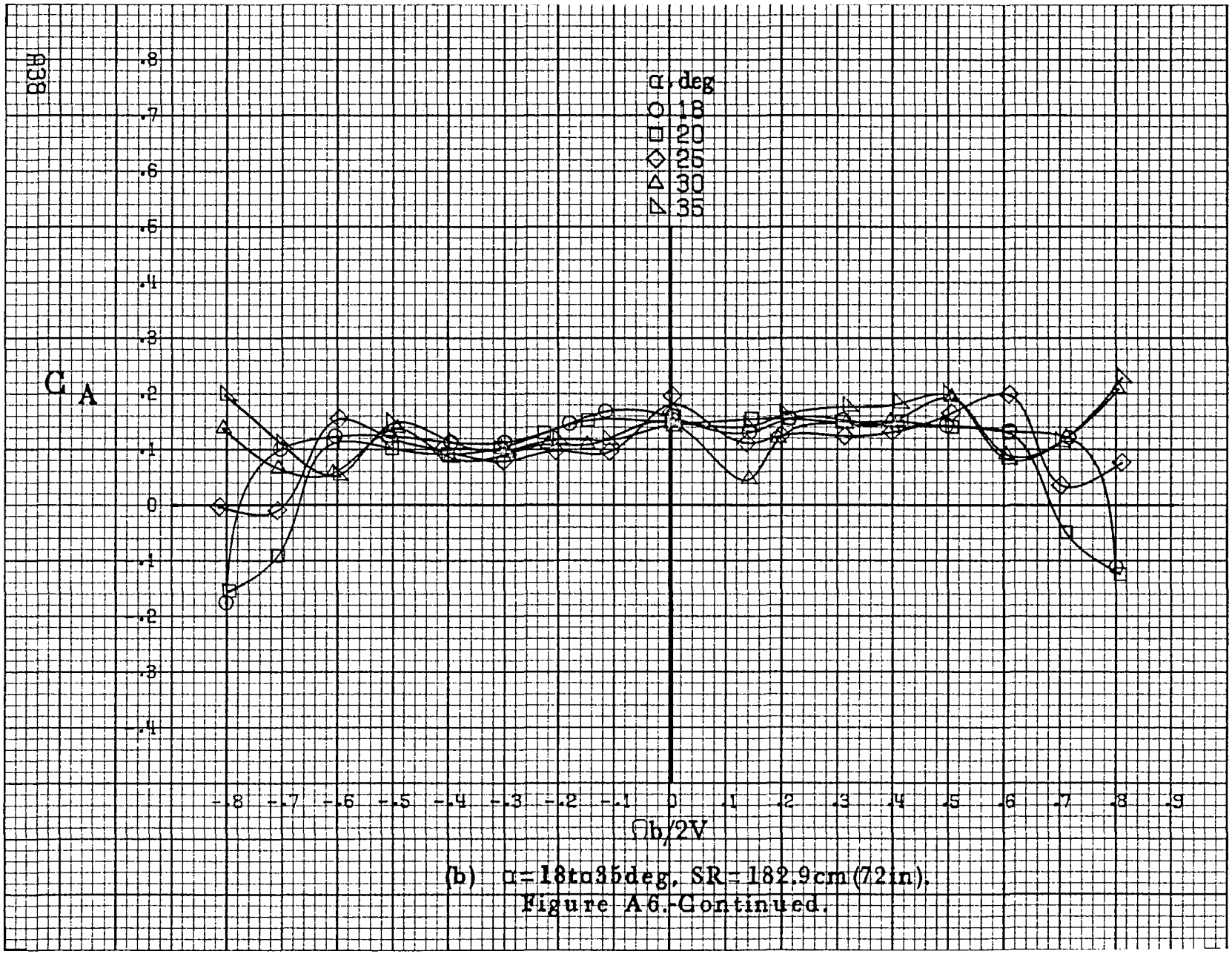

(b) α = 18 to 35 deg, SR = 182.9 cm (72 in).

Figure A6.-Continued.

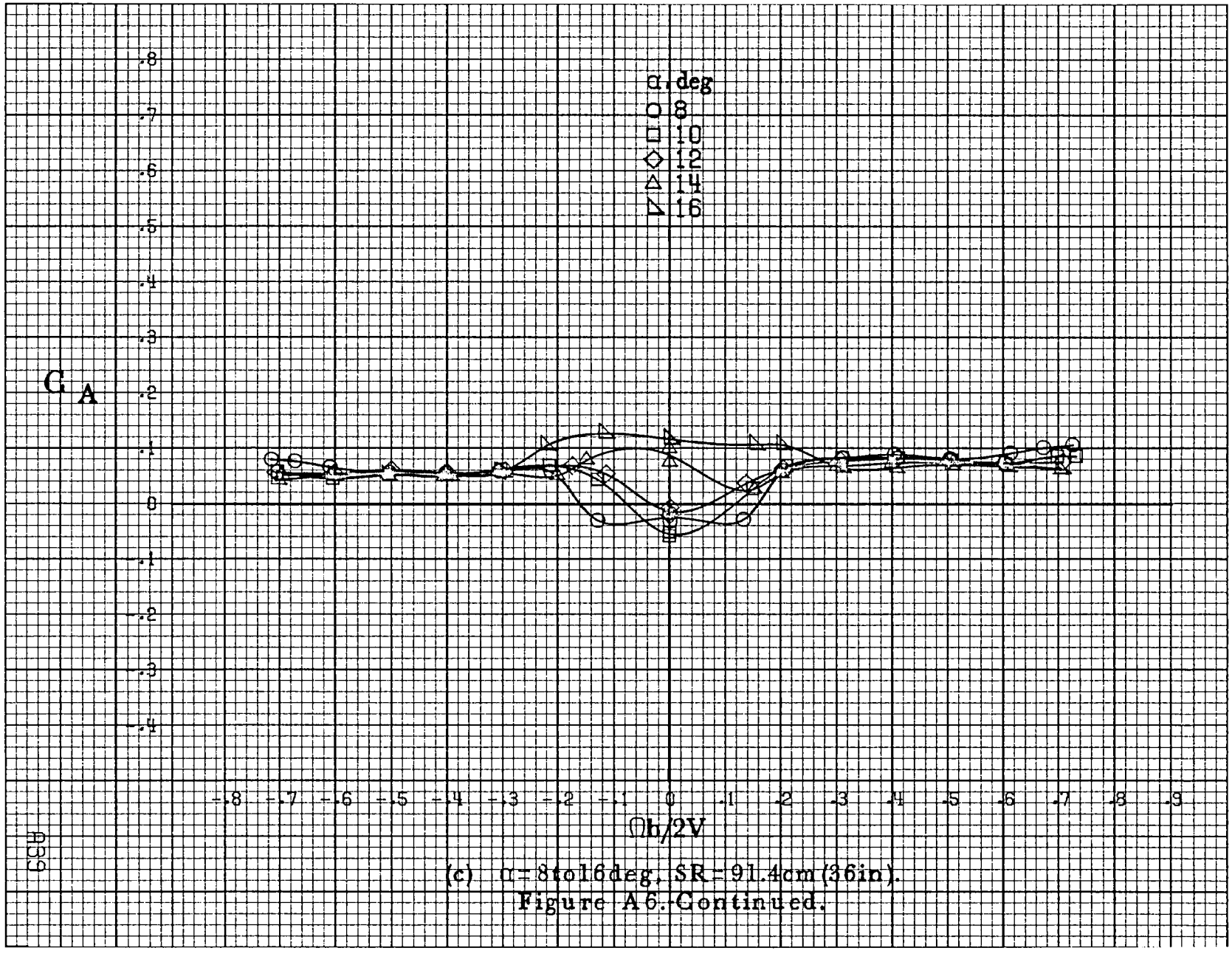

(c) α = 8 to 16 deg, SR = 91.4 cm (36 in).

Figure A6.-Continued.

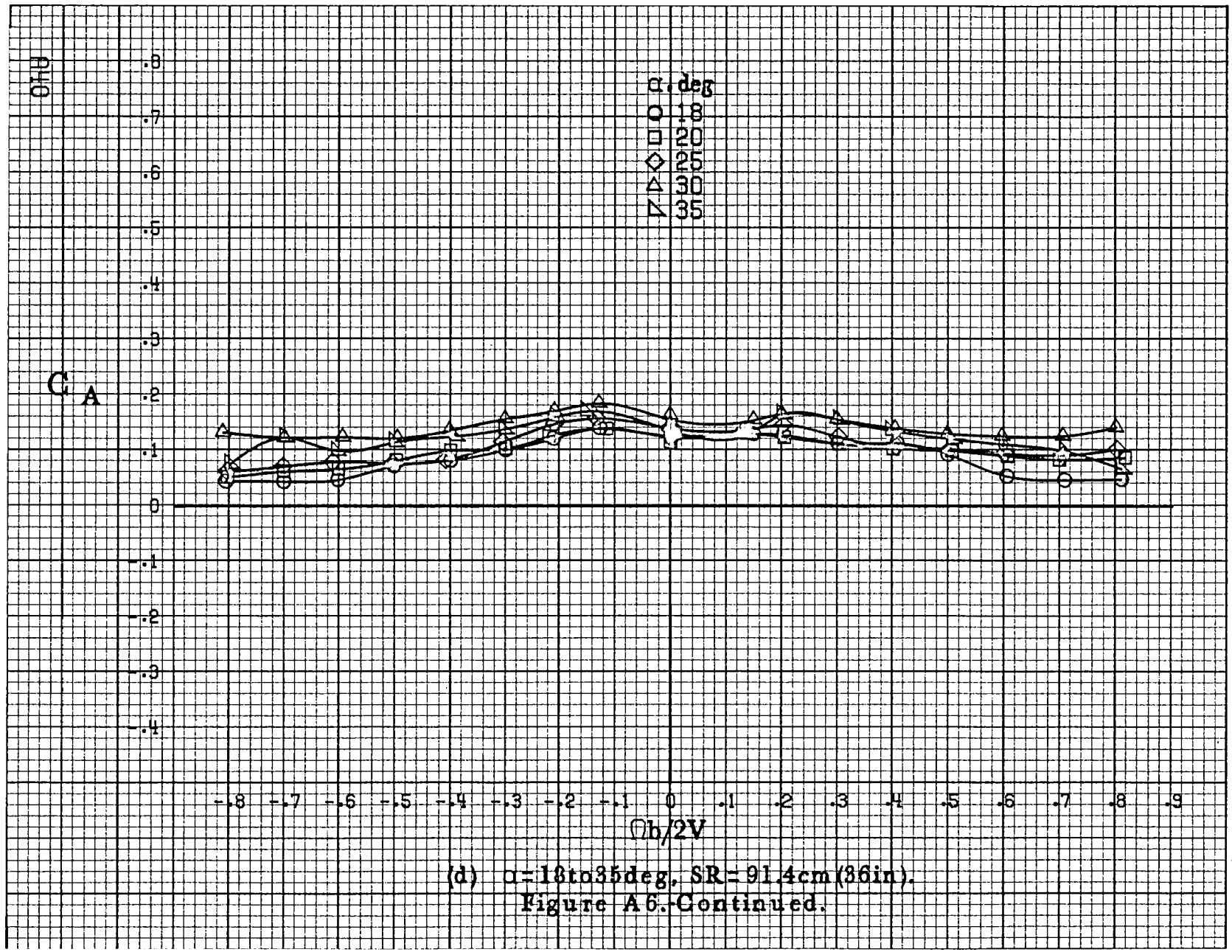

(d) α=18to35deg, SR=91.4cm(36in).

Figure A6.-Continued.

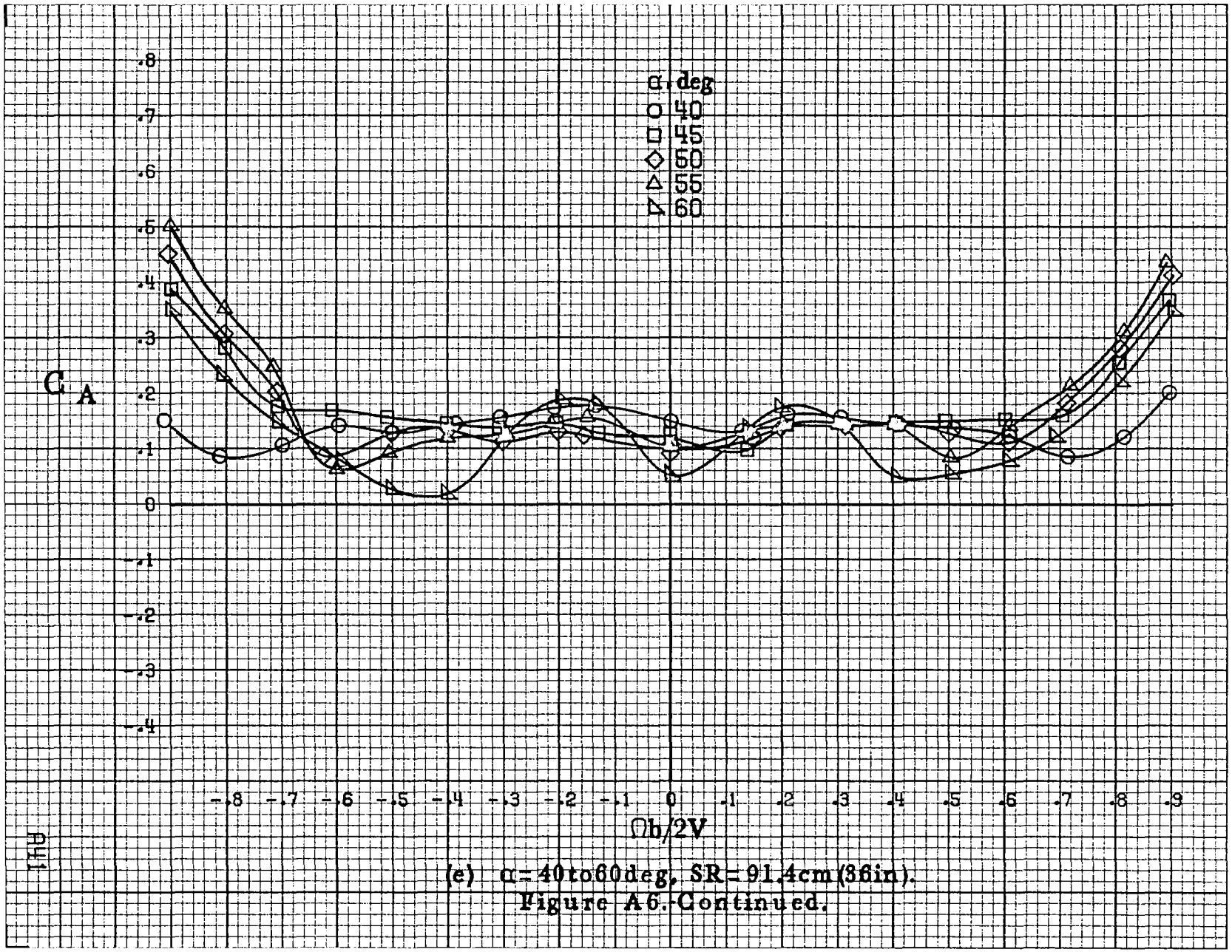

(e) α = 40 to 60 deg, SR = 91.4 cm (36 in).

Figure A6.-Continued.

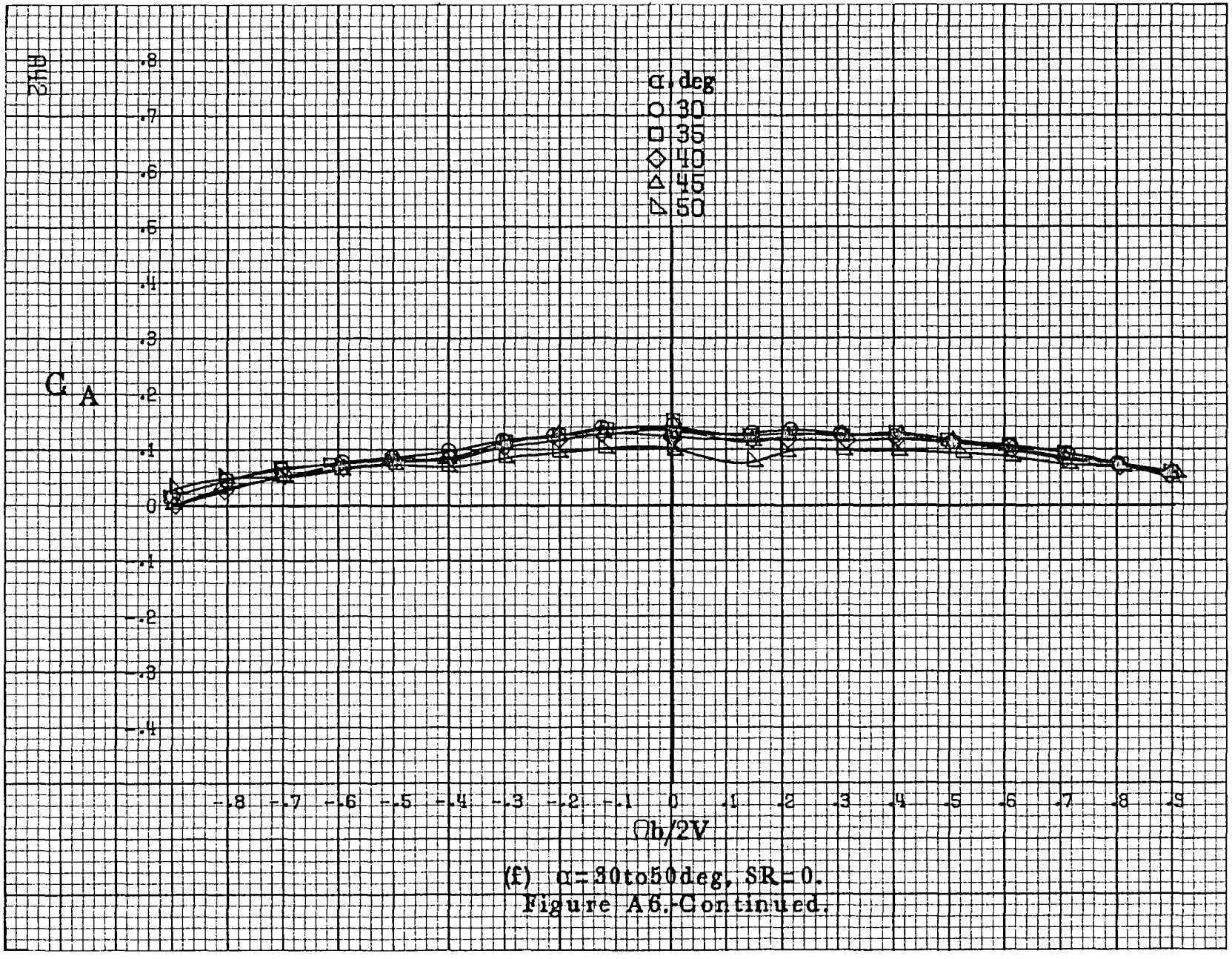

(f) $\alpha = 30$ to 50 deg, SR = 0.

Figure A6.-Continued.

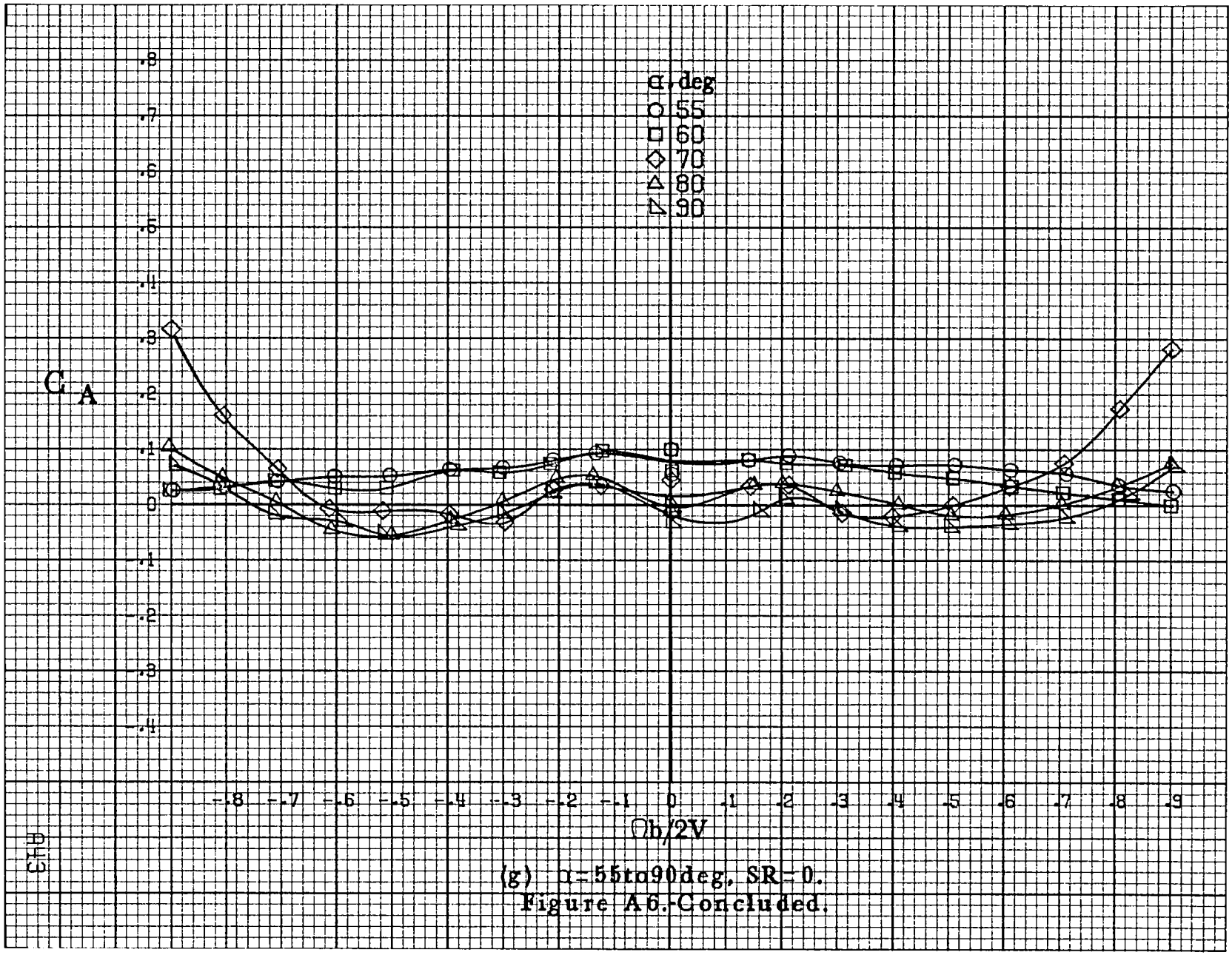

(g) $\alpha = 55$ to 90 deg, SR = 0.

Figure A6.-Concluded.

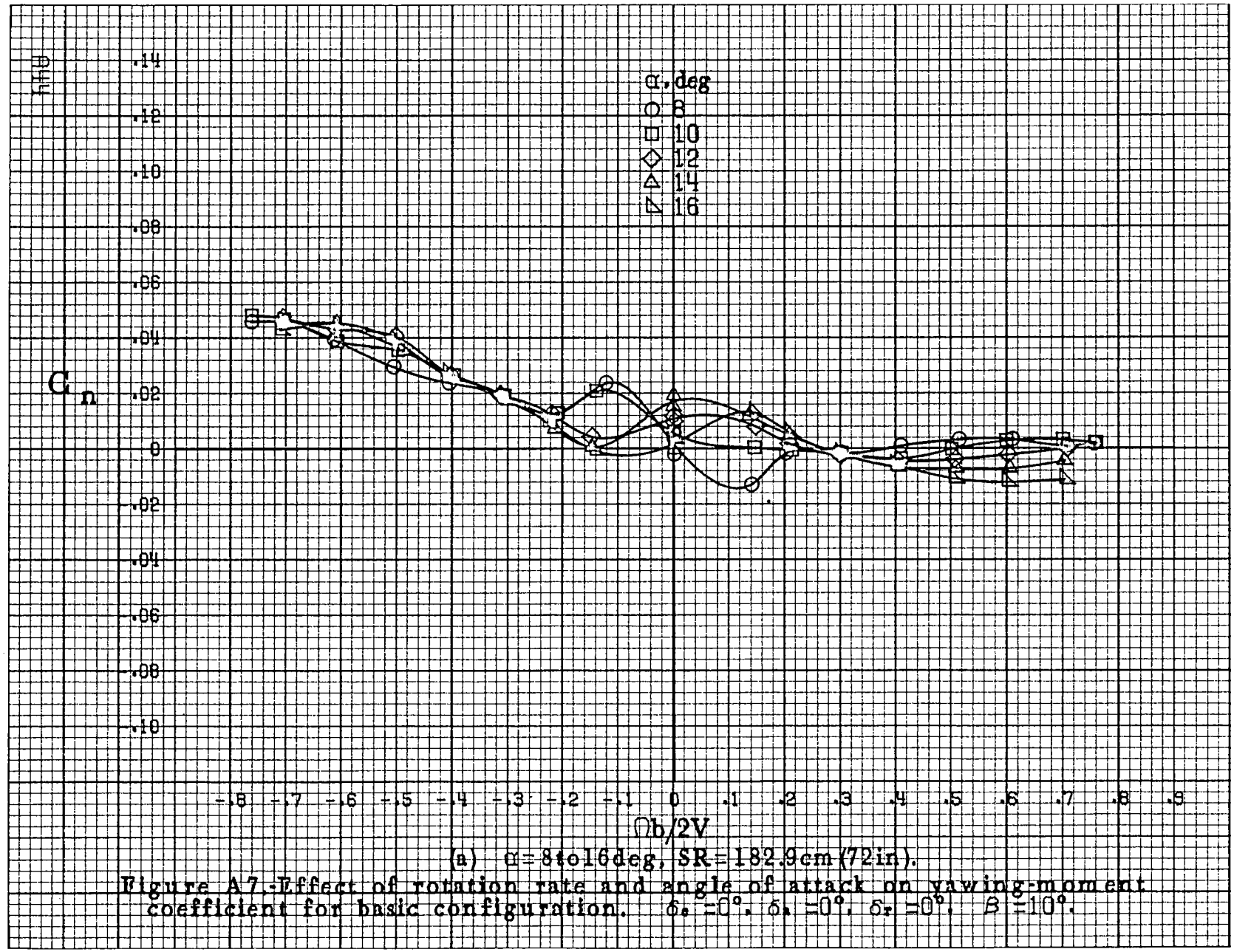

(a) $\alpha = 8$ to 16 deg, SR = 182.9 cm (72 in).

Figure A7.-Effect of rotation rate and angle of attack on yawing-moment coefficient for basic configuration. $\delta_e = 0°$, $\delta_a = 0°$, $\delta_r = 0°$, $\beta = 10°$.

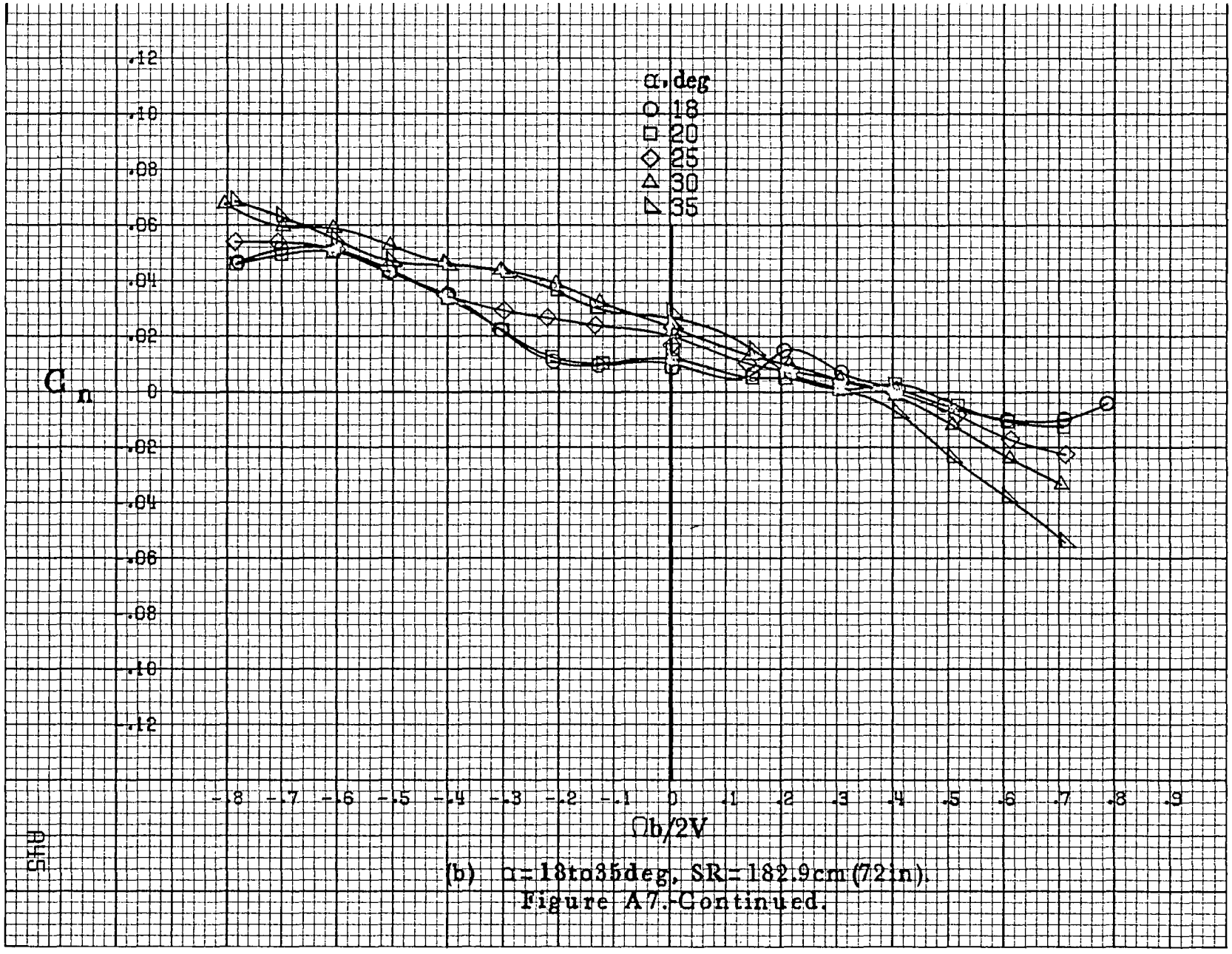

(b) α = 18 to 35 deg, SR = 182.9 cm (72 in).

Figure A7.-Continued.

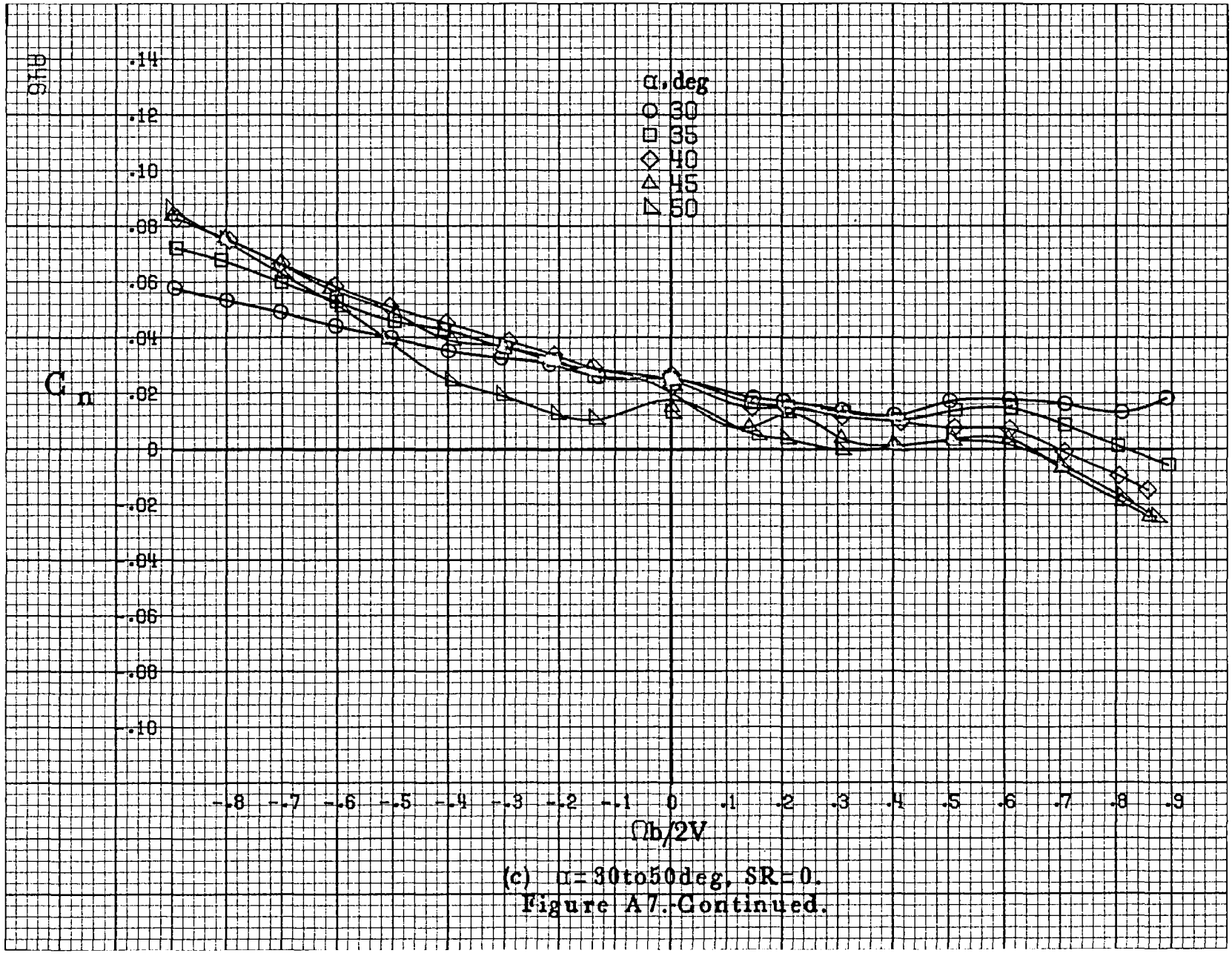

(c) α = 30 to 50 deg, SR = 0.

Figure A7.-Continued.

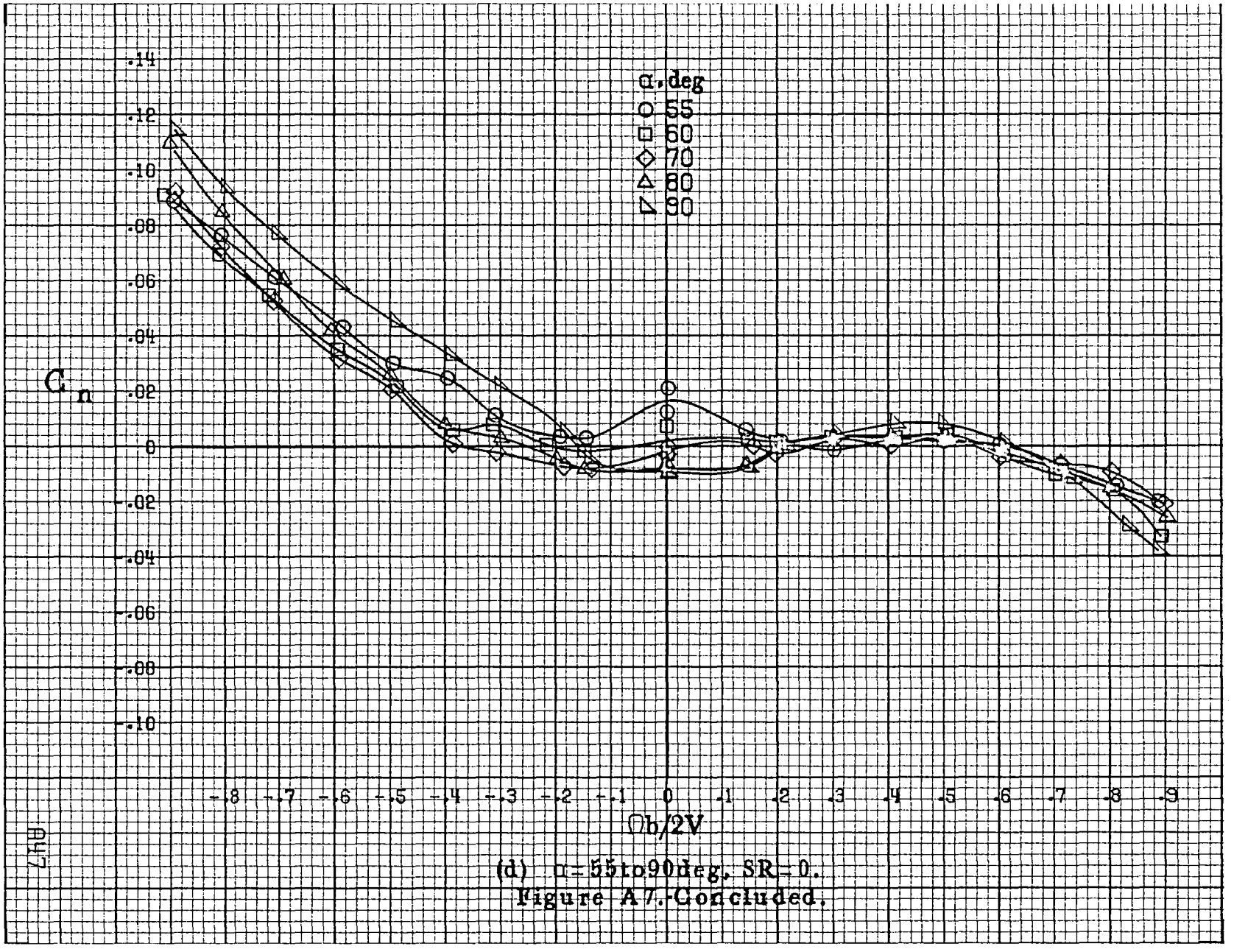

(d) α = 55 to 90 deg, SR = 0.

Figure A7.-Concluded.

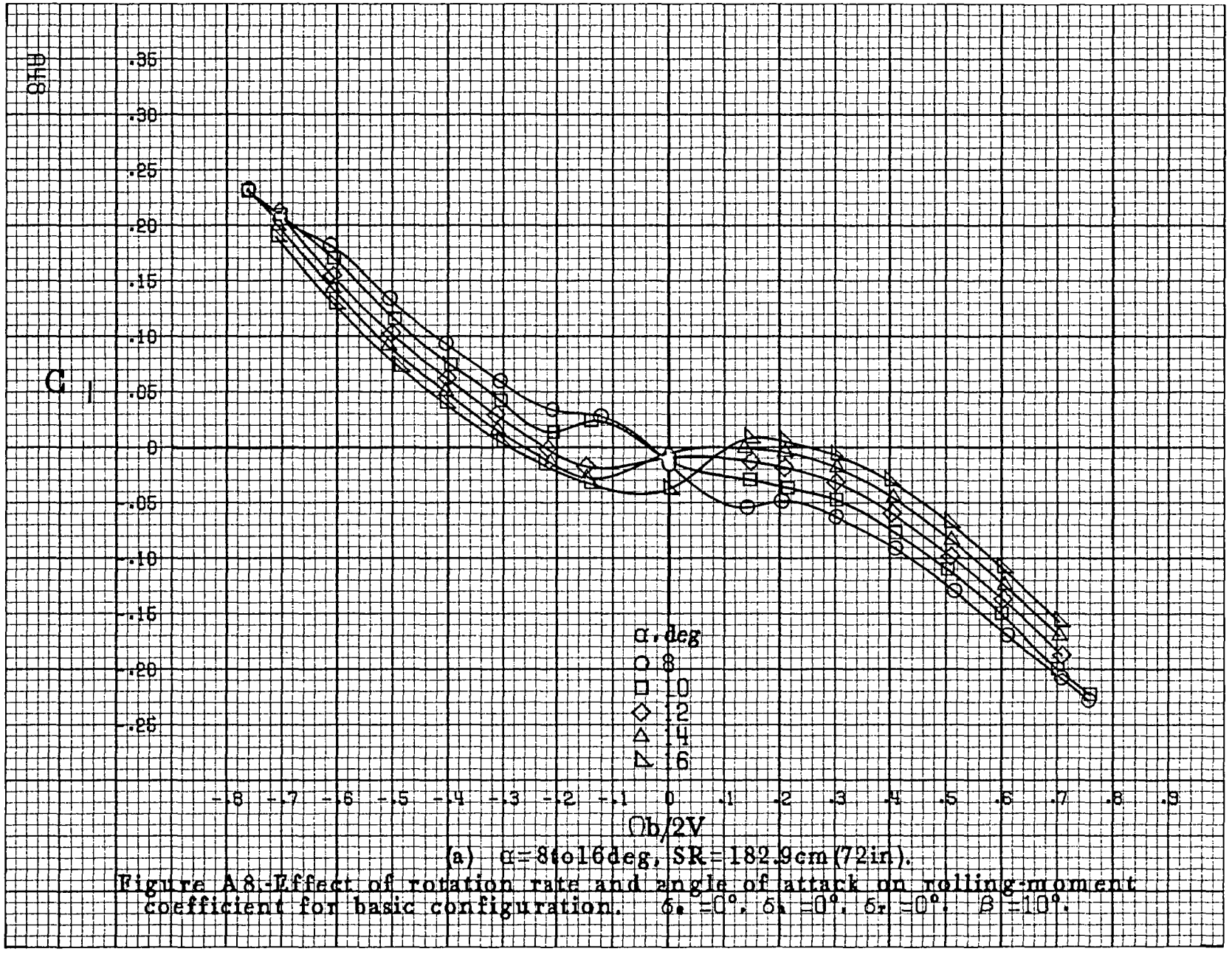

(a) $\alpha = 8$ to 16 deg, SR = 182.9 cm (72 in.).

Figure A8.-Effect of rotation rate and angle of attack on rolling-moment coefficient for basic configuration. $\delta_e = 0°$, $\delta_a = 0°$, $\delta_r = 0°$, $\beta = 10°$.

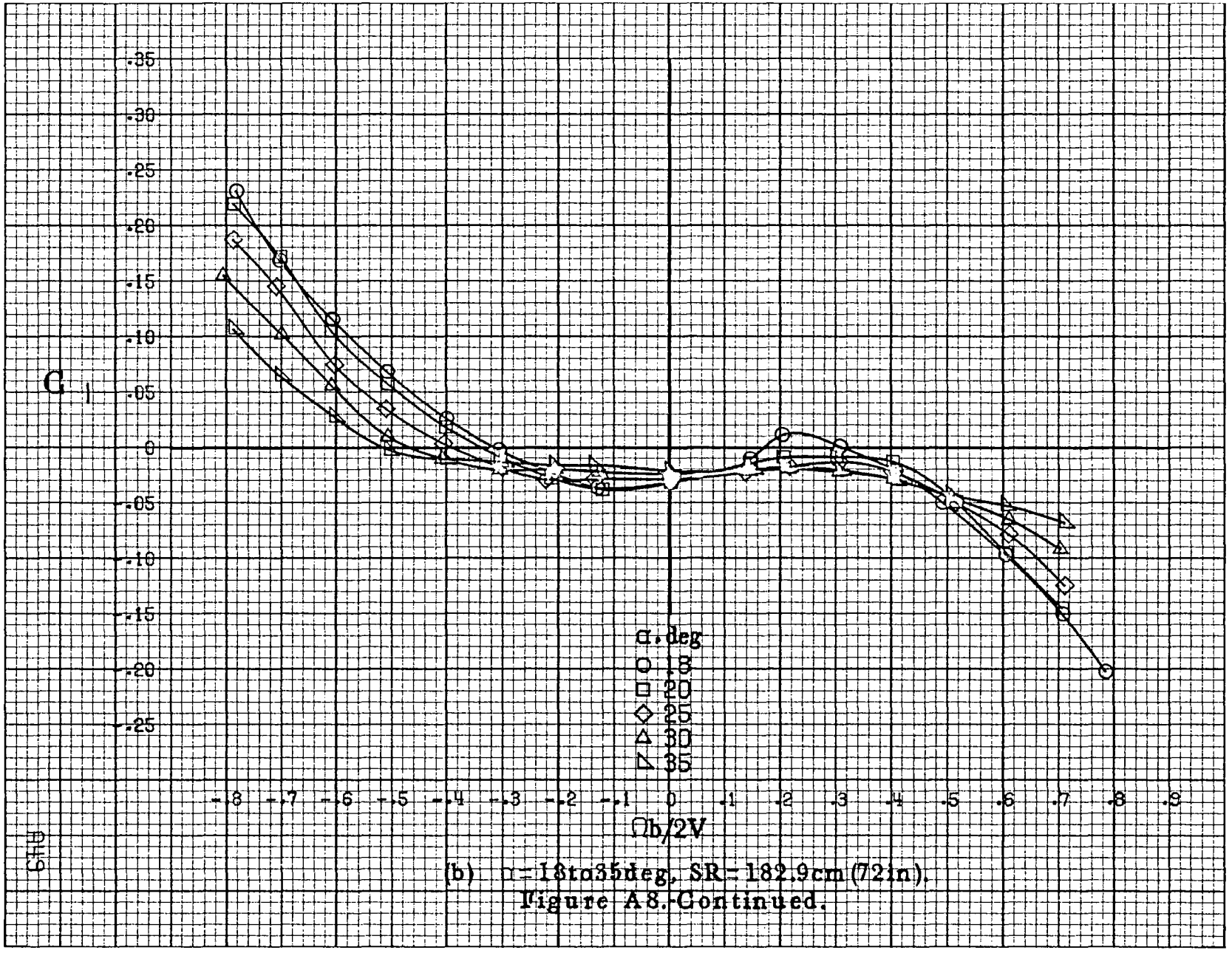

(b) $\alpha = 18$ to 35 deg, SR = 182.9 cm (72 in).

Figure A8.-Continued.

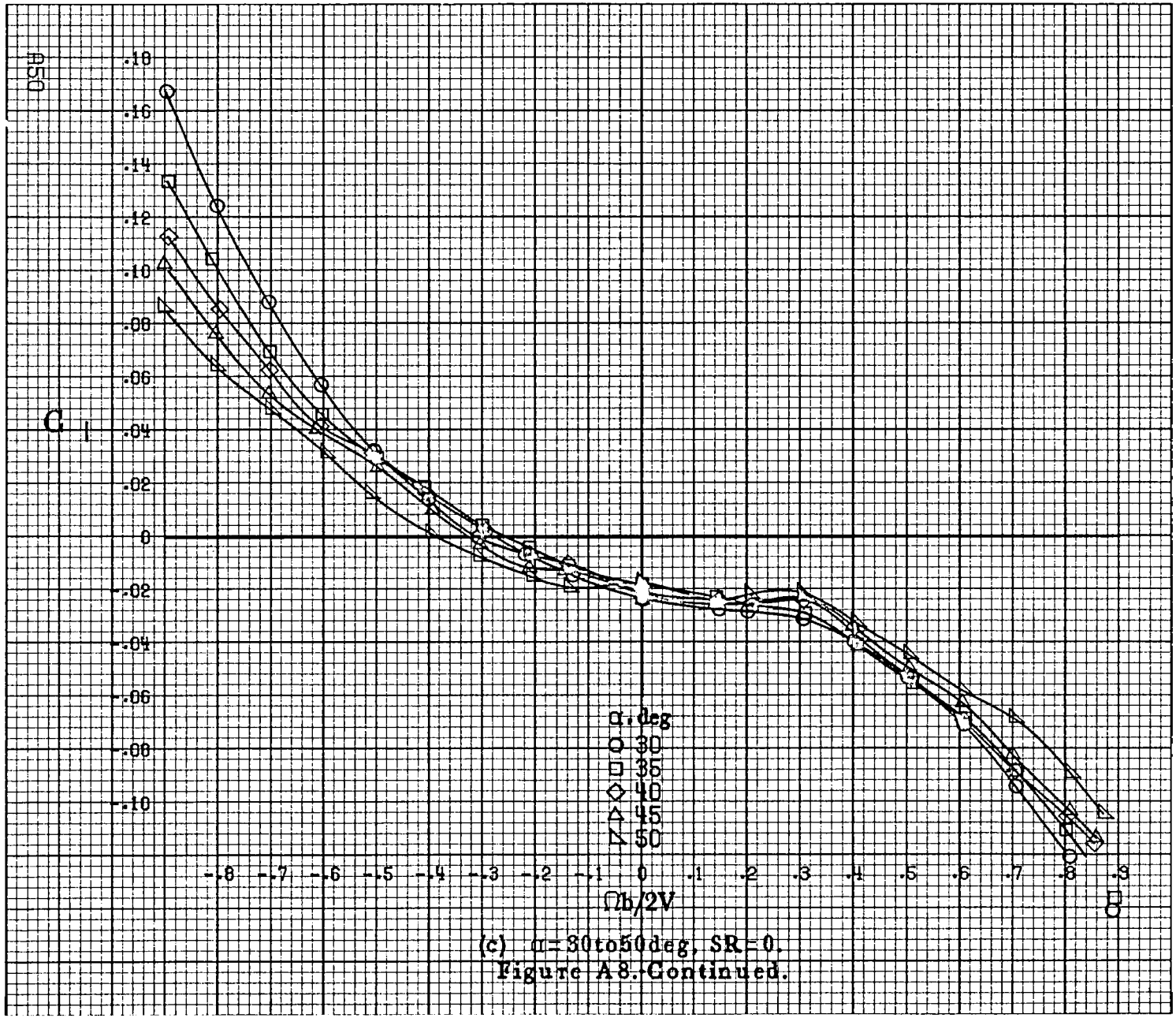

(c) α = 30 to 50 deg, SR = 0.

Figure A8.-Continued.

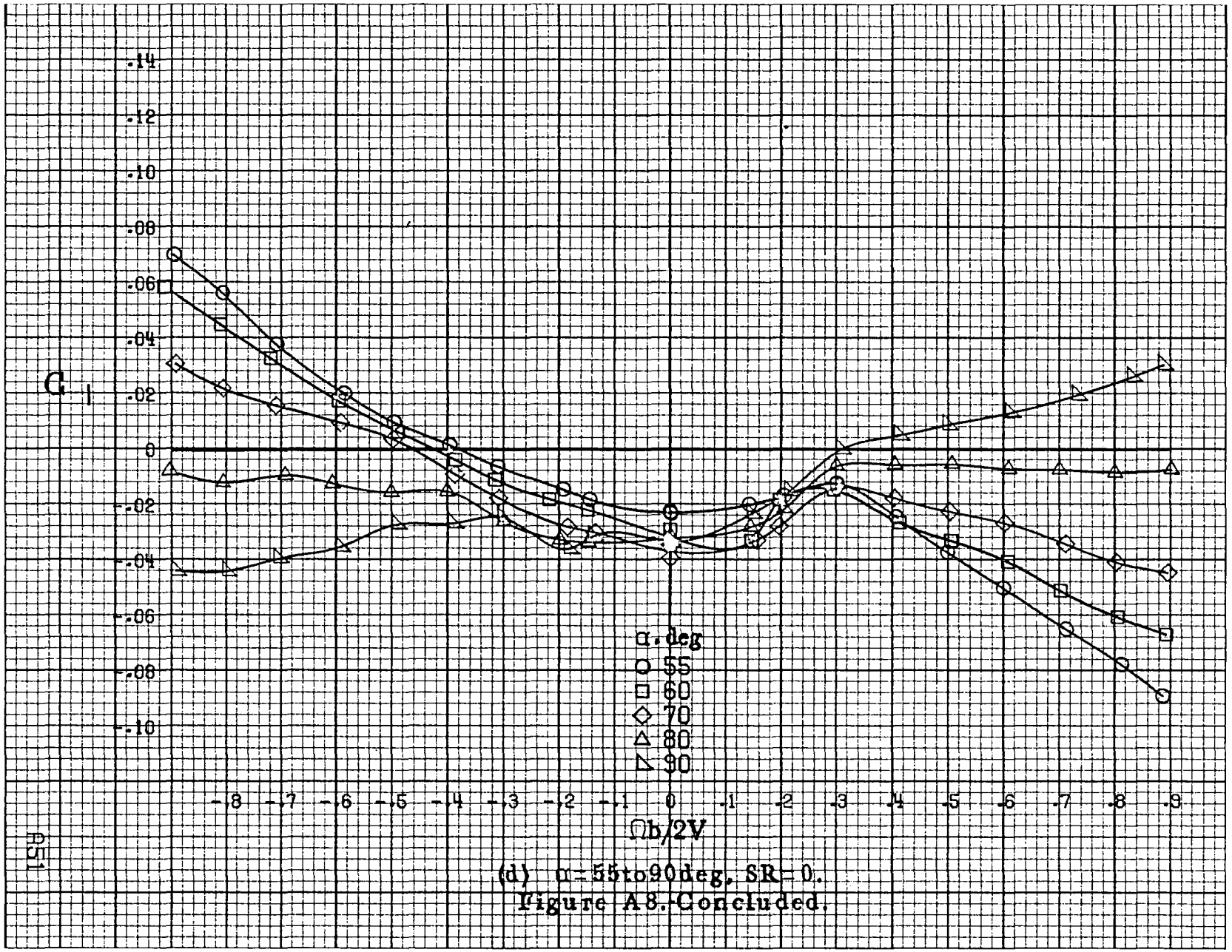

(d) α = 55 to 90 deg, SR = 0.

Figure A8.-Concluded.

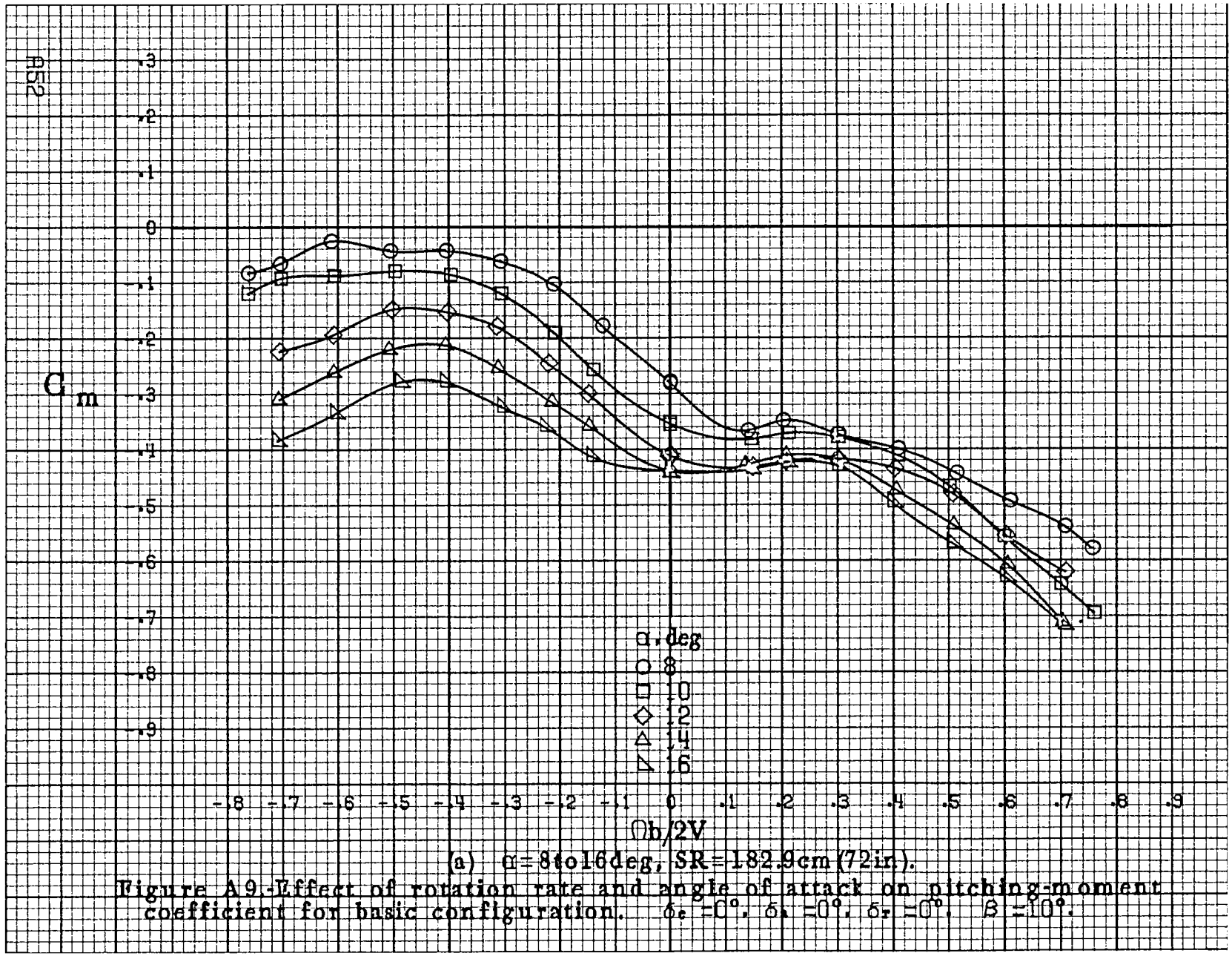

(a) $\alpha = 8$ to 16 deg, SR = 182.9 cm (72 in.).

Figure A9.-Effect of rotation rate and angle of attack on pitching-moment coefficient for basic configuration. $\delta_e = 0°$, $\delta_a = 0°$, $\delta_r = 0°$, $\beta = 0°$.

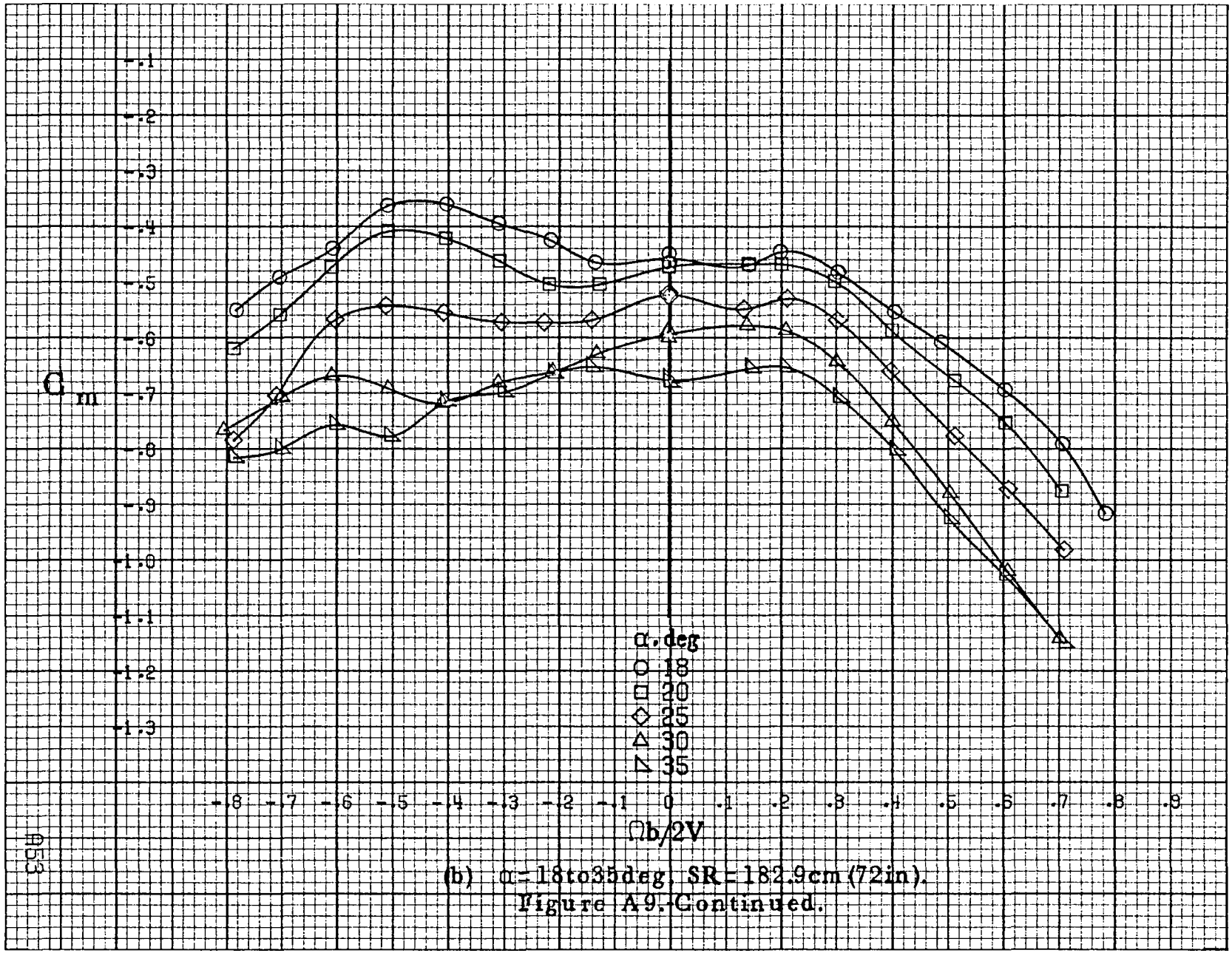

(b) α = 18 to 35 deg, SR = 182.9 cm (72 in).

Figure A9.- Continued.

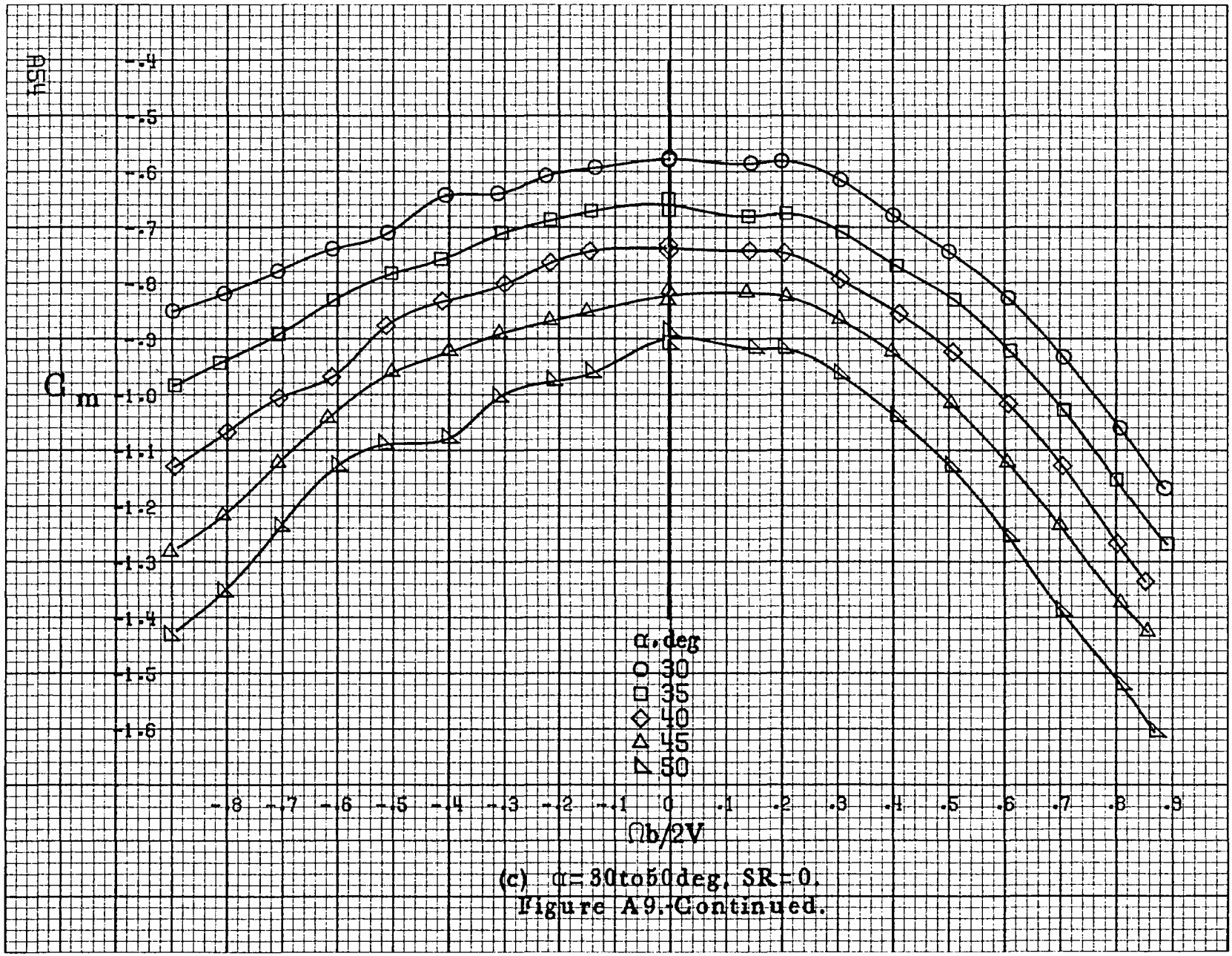

(c) α = 30 to 50 deg, SR = 0.

Figure A9.-Continued.

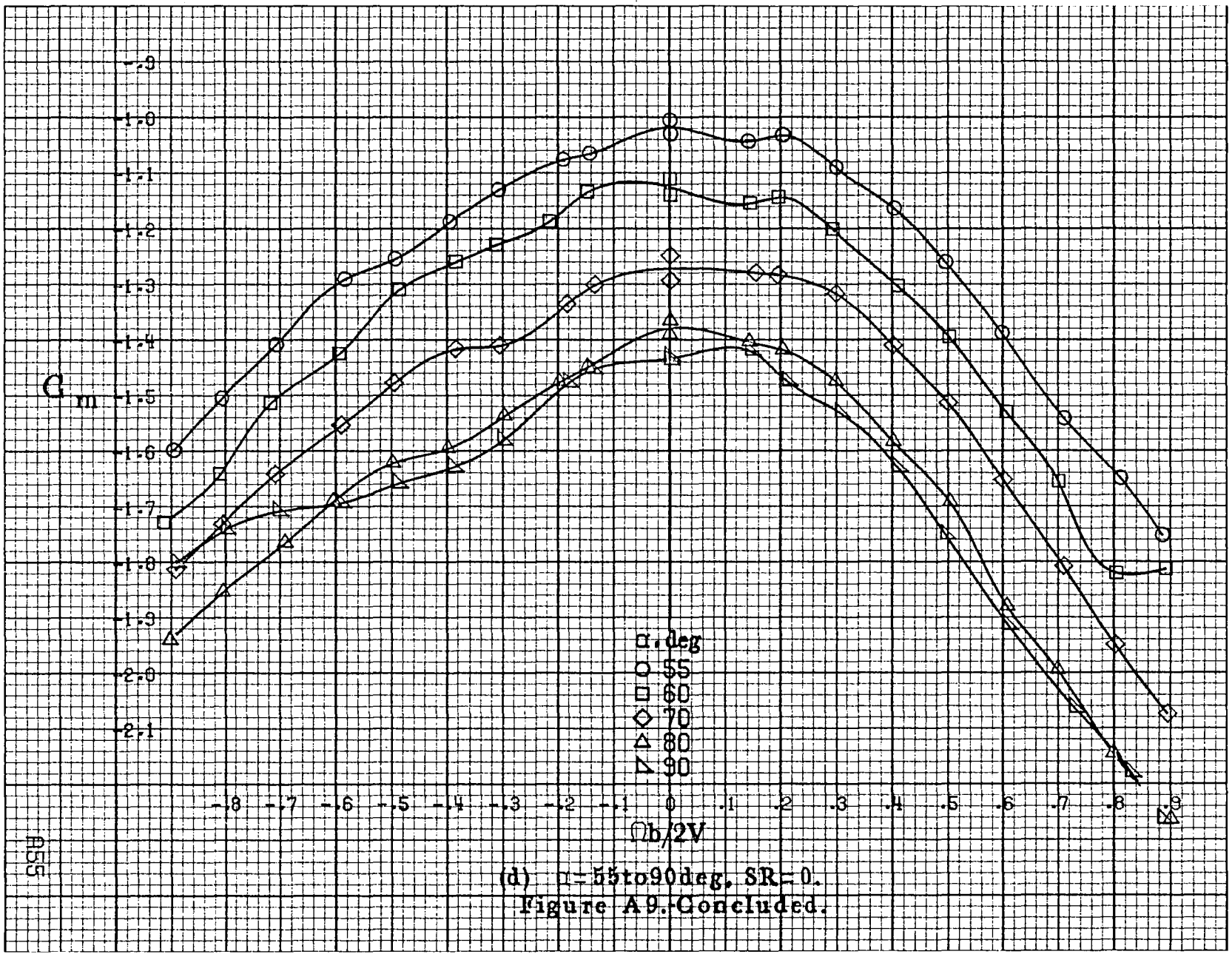

(d) α = 55 to 90 deg, SR = 0.

Figure A9.-Concluded.

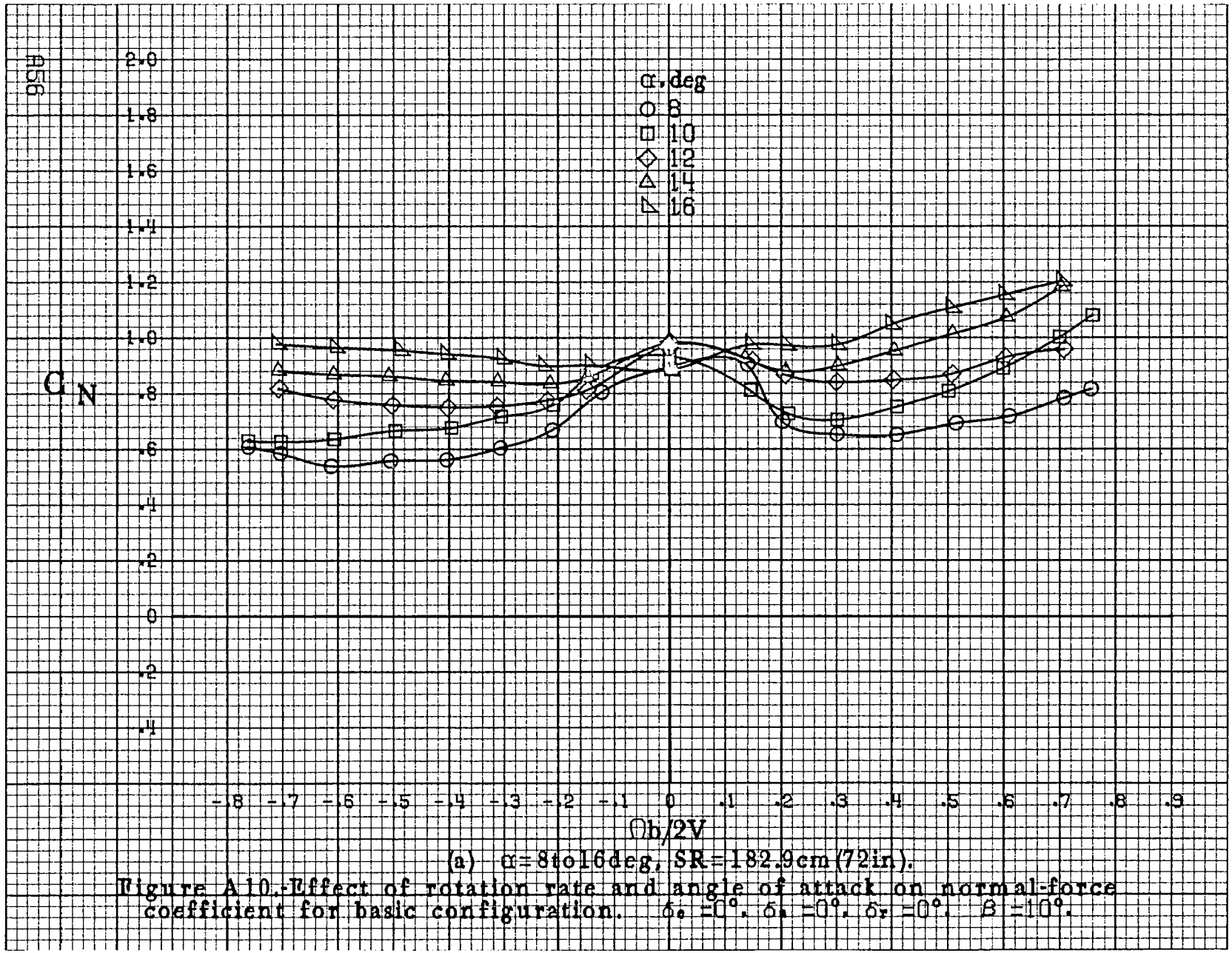

(a) α = 8 to 16 deg, SR = 182.9 cm (72 in.).

Figure A10.-Effect of rotation rate and angle of attack on normal-force coefficient for basic configuration. $\delta_e = 0°$, $\delta_a = 0°$, $\delta_r = 0°$, $\beta = 10°$.

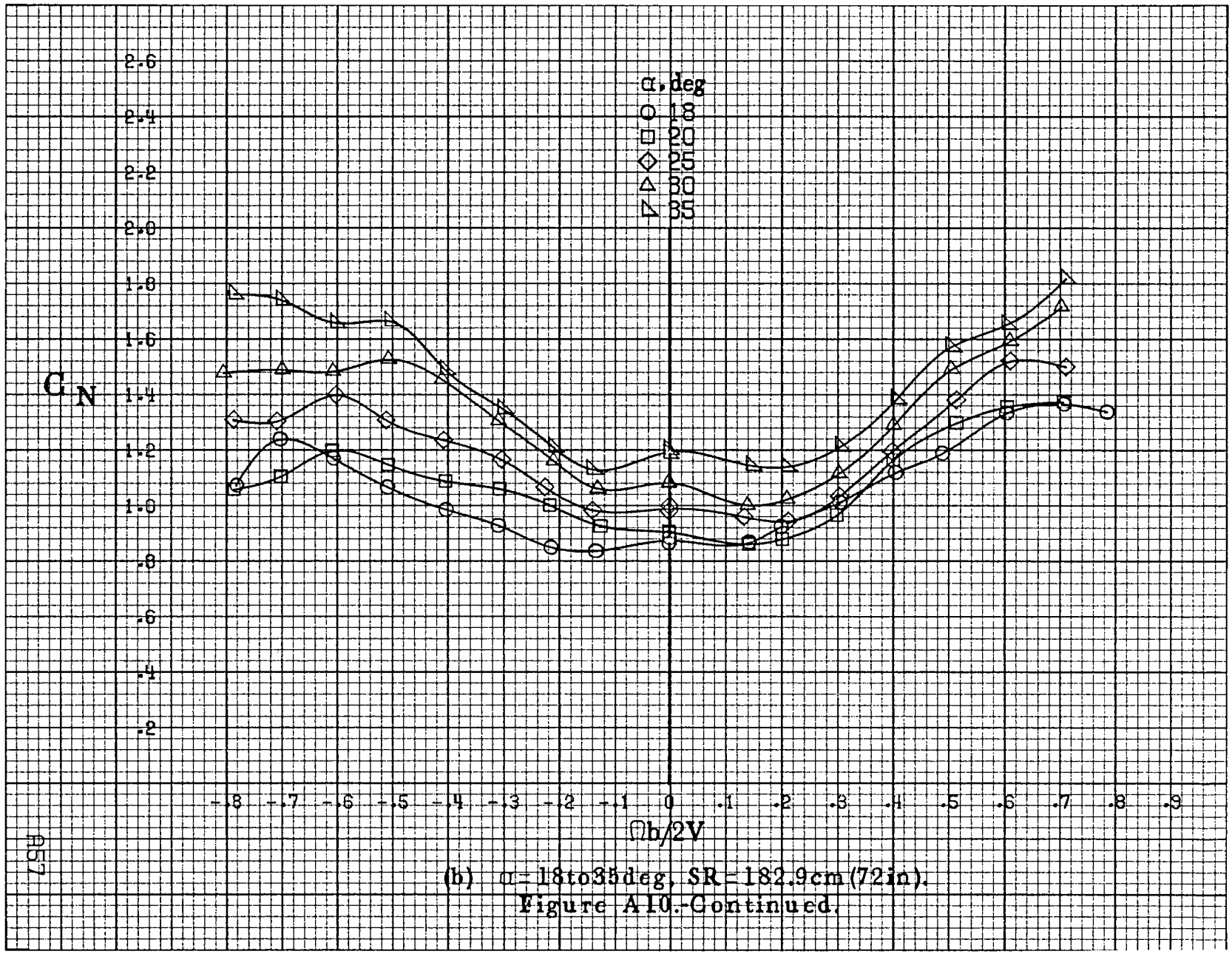

(b) $\alpha = 18$ to 35 deg, SR = 182.9 cm (72 in).

Figure A10.-Continued.

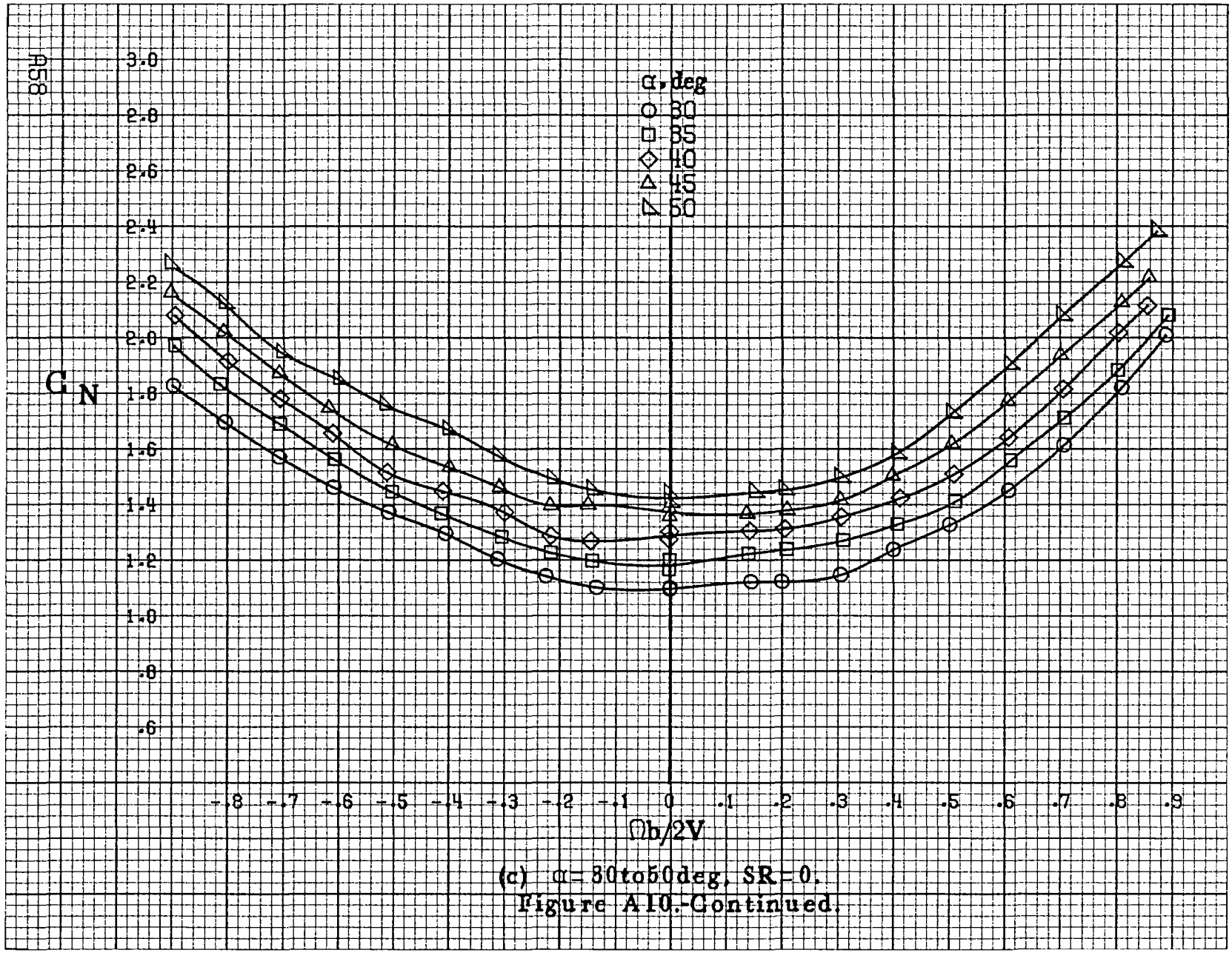

(c) α = 30 to 50 deg, SR = 0.

Figure A10.-Continued.

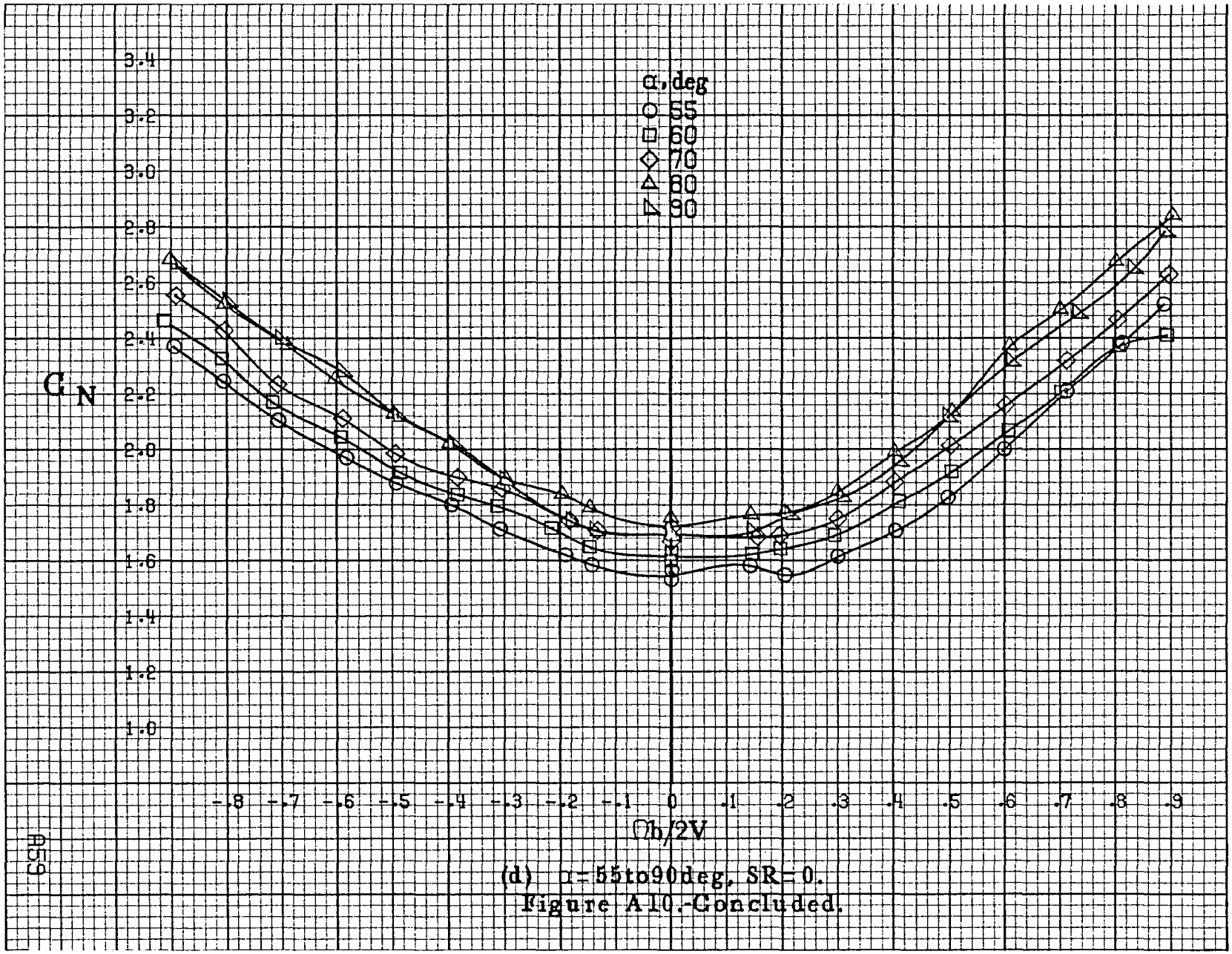

(d) α = 55 to 90 deg, SR = 0.

Figure A10.-Concluded.

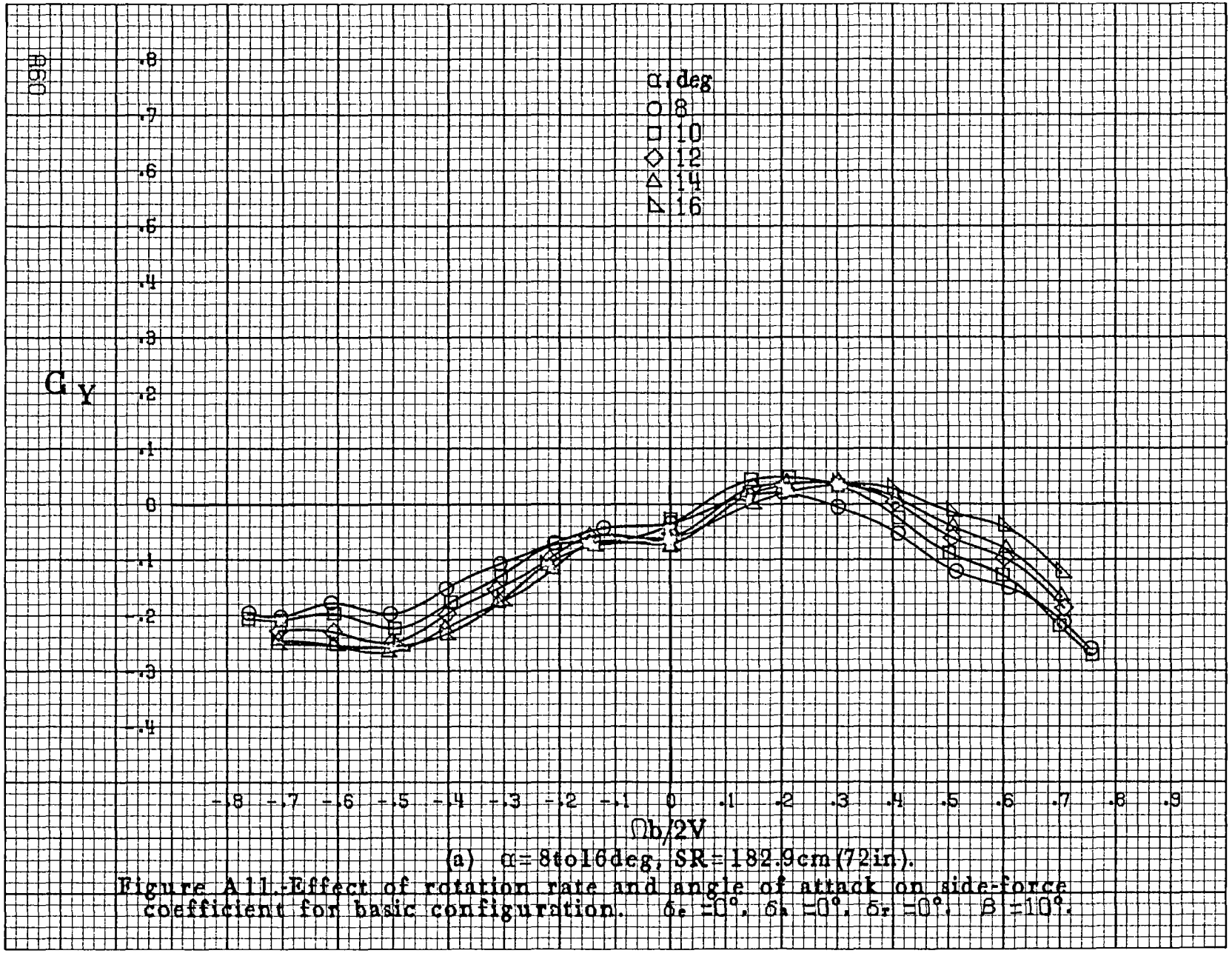

(a) α = 8 to 16 deg, SR = 182.9 cm (72 in.).

Figure A11.-Effect of rotation rate and angle of attack on side-force coefficient for basic configuration. $\delta_e = 0°$, $\delta_a = 0°$, $\delta_r = 0°$, $\beta = 10°$.

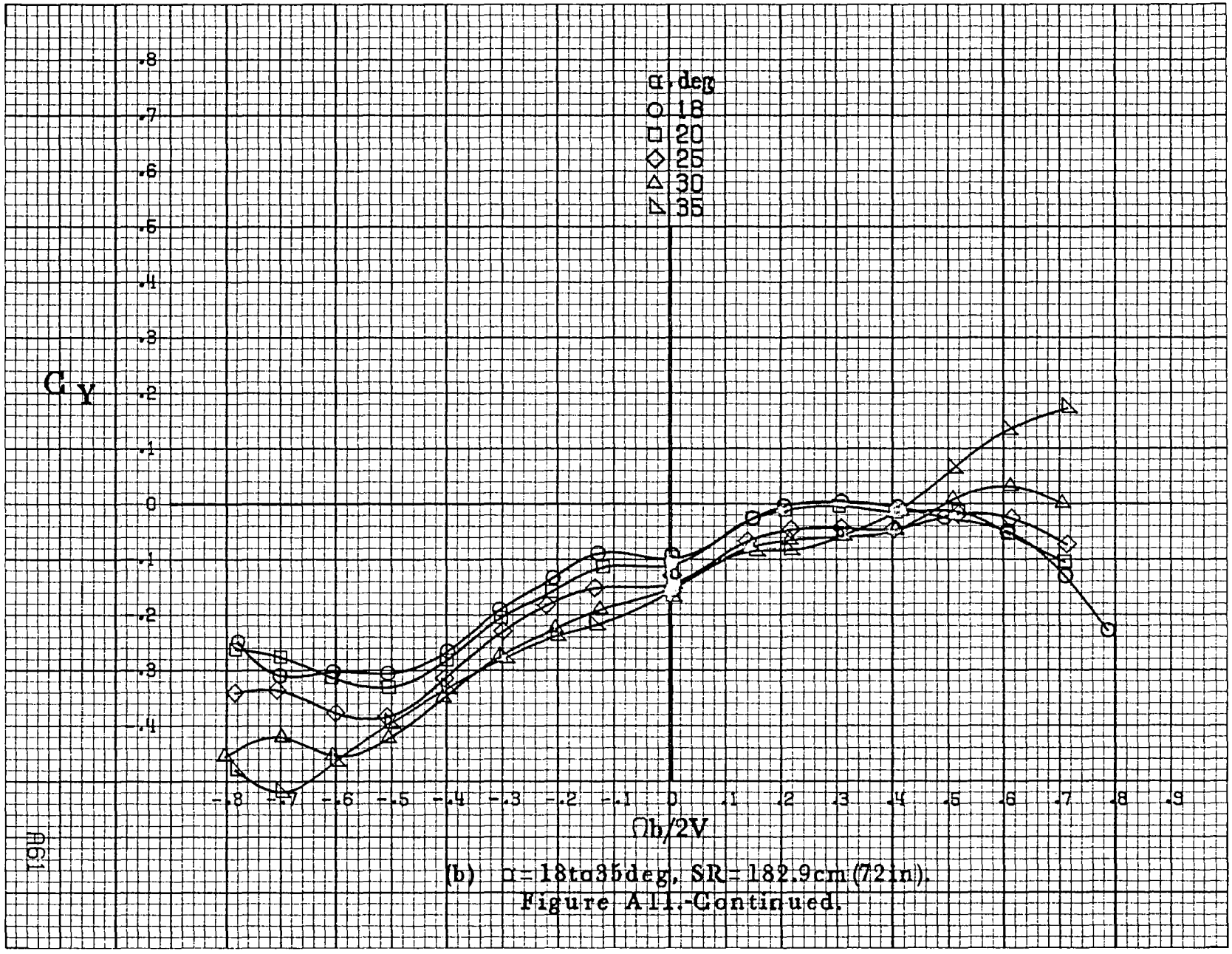

(b) α=18to35deg, SR=182.9cm(72in).

Figure A11.-Continued.

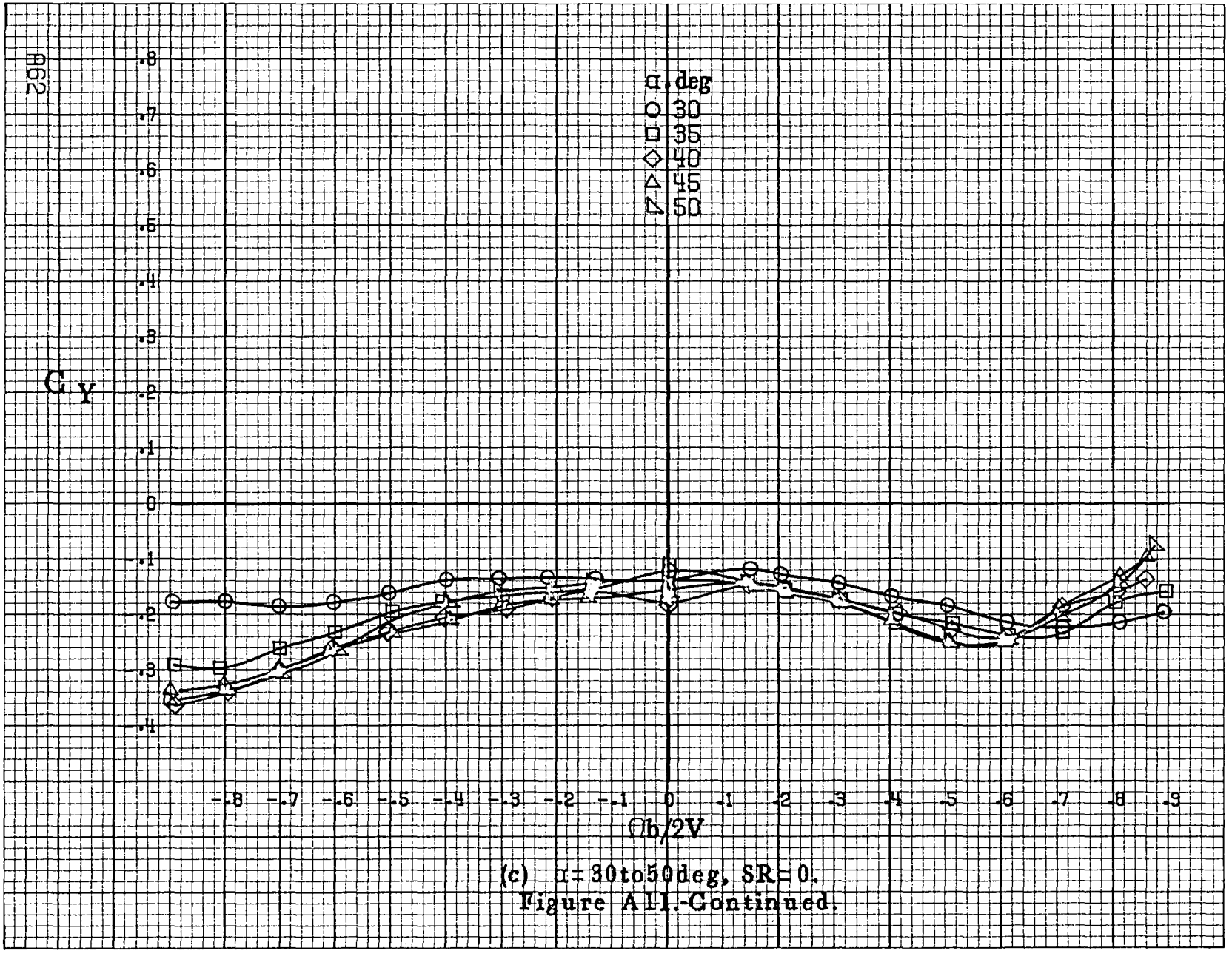

(c) α = 30 to 50 deg, SR = 0.

Figure A11.-Continued.

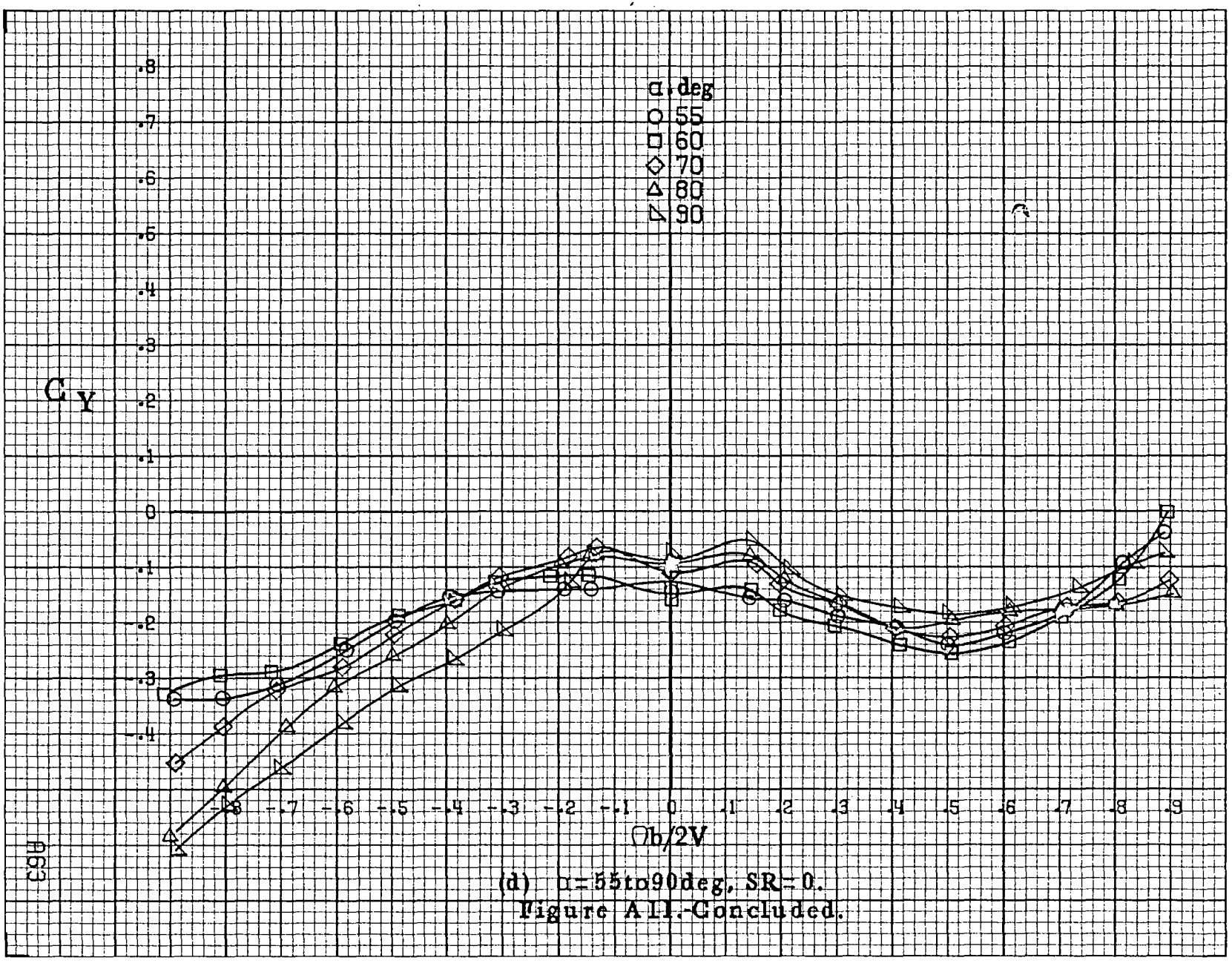

(d) $\alpha = 55$ to 90 deg, SR = 0.

Figure A11.-Concluded.

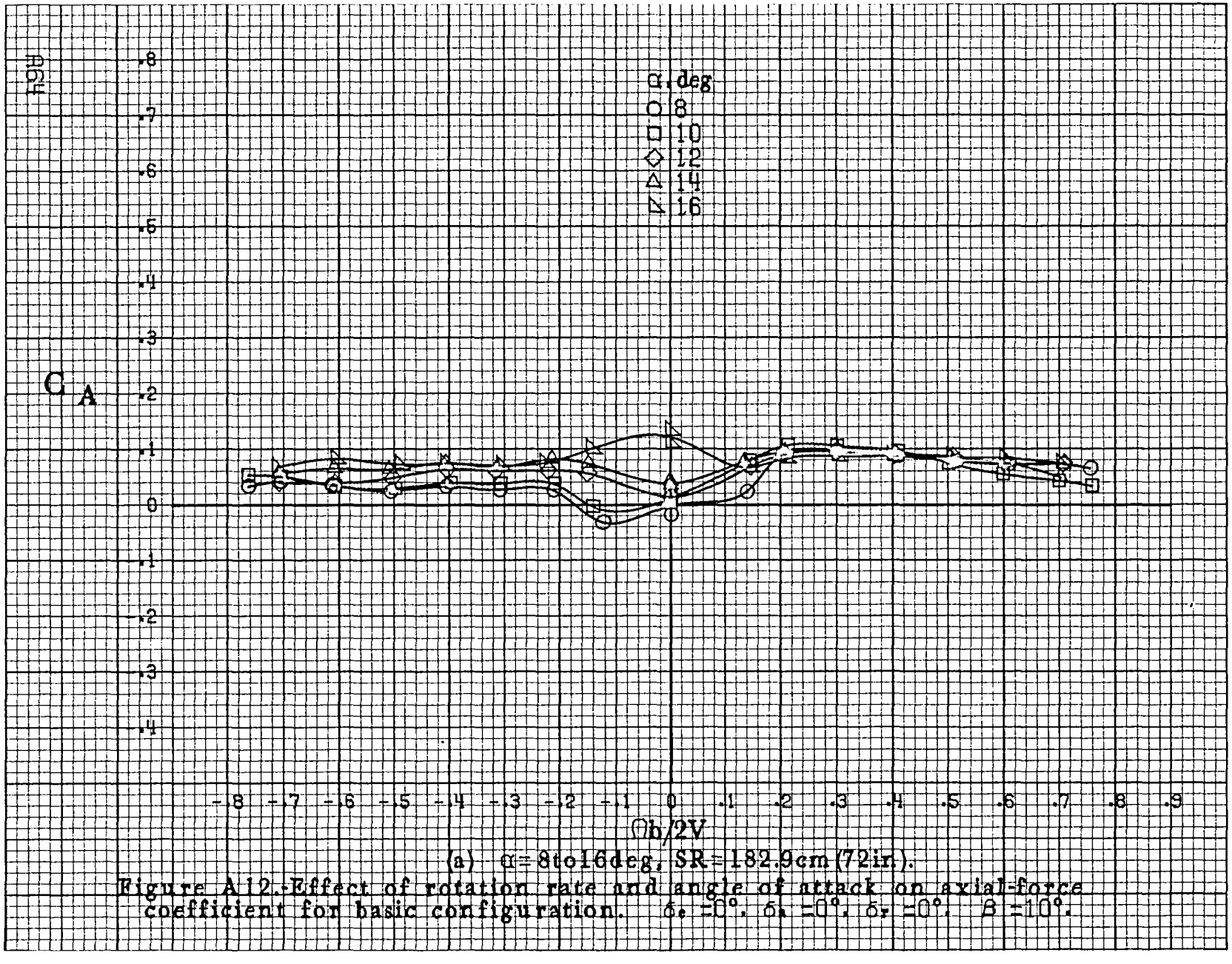

(a) $\alpha = 8$ to 16 deg, SR = 182.9 cm (72 in.).

Figure A12.-Effect of rotation rate and angle of attack on axial-force coefficient for basic configuration. $\delta_e = 0°$, $\delta_a = 0°$, $\delta_r = 0°$, $\beta = 10°$.

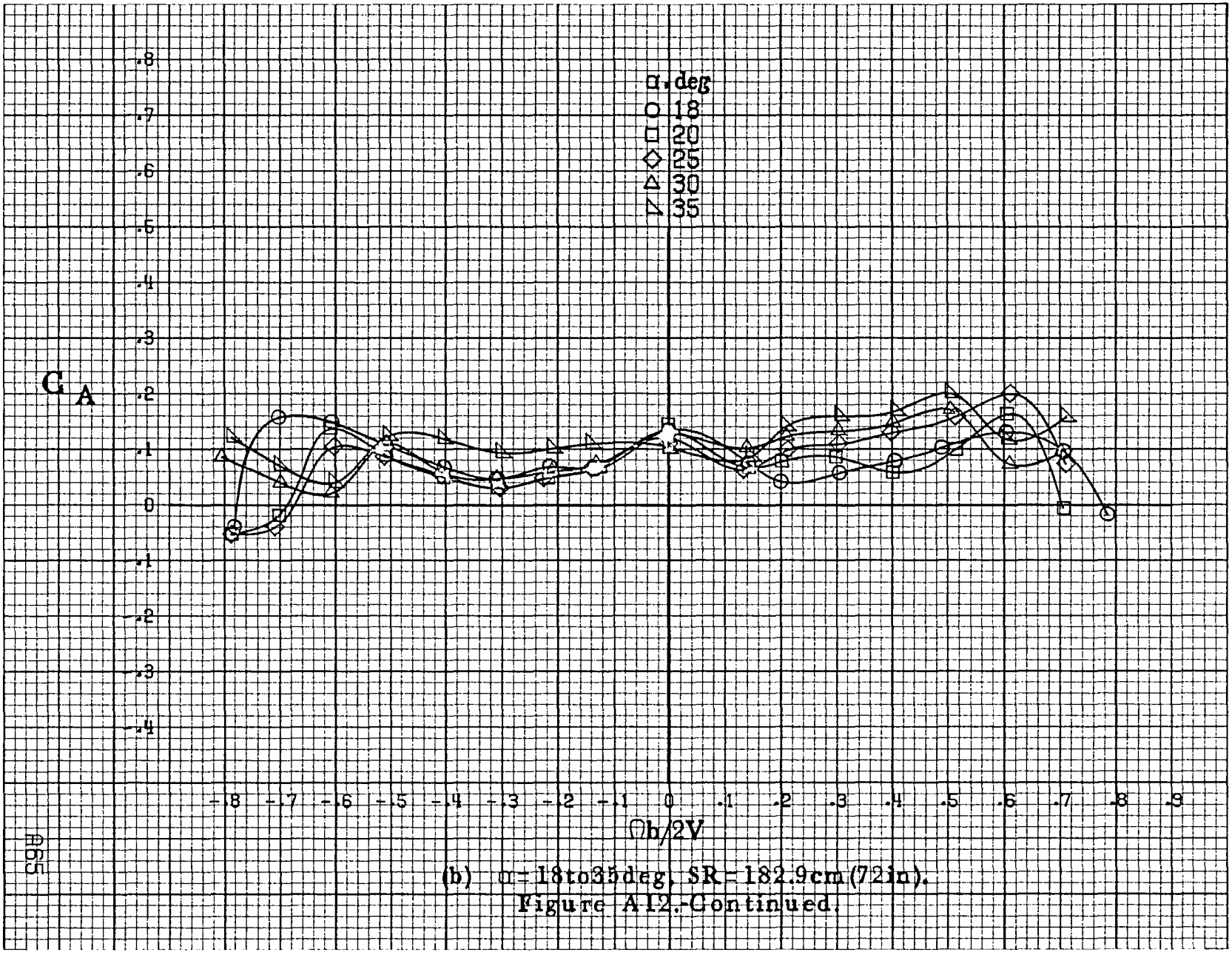

(b) α = 18 to 35 deg, SR = 182.9 cm (72 in).

Figure A12.-Continued.

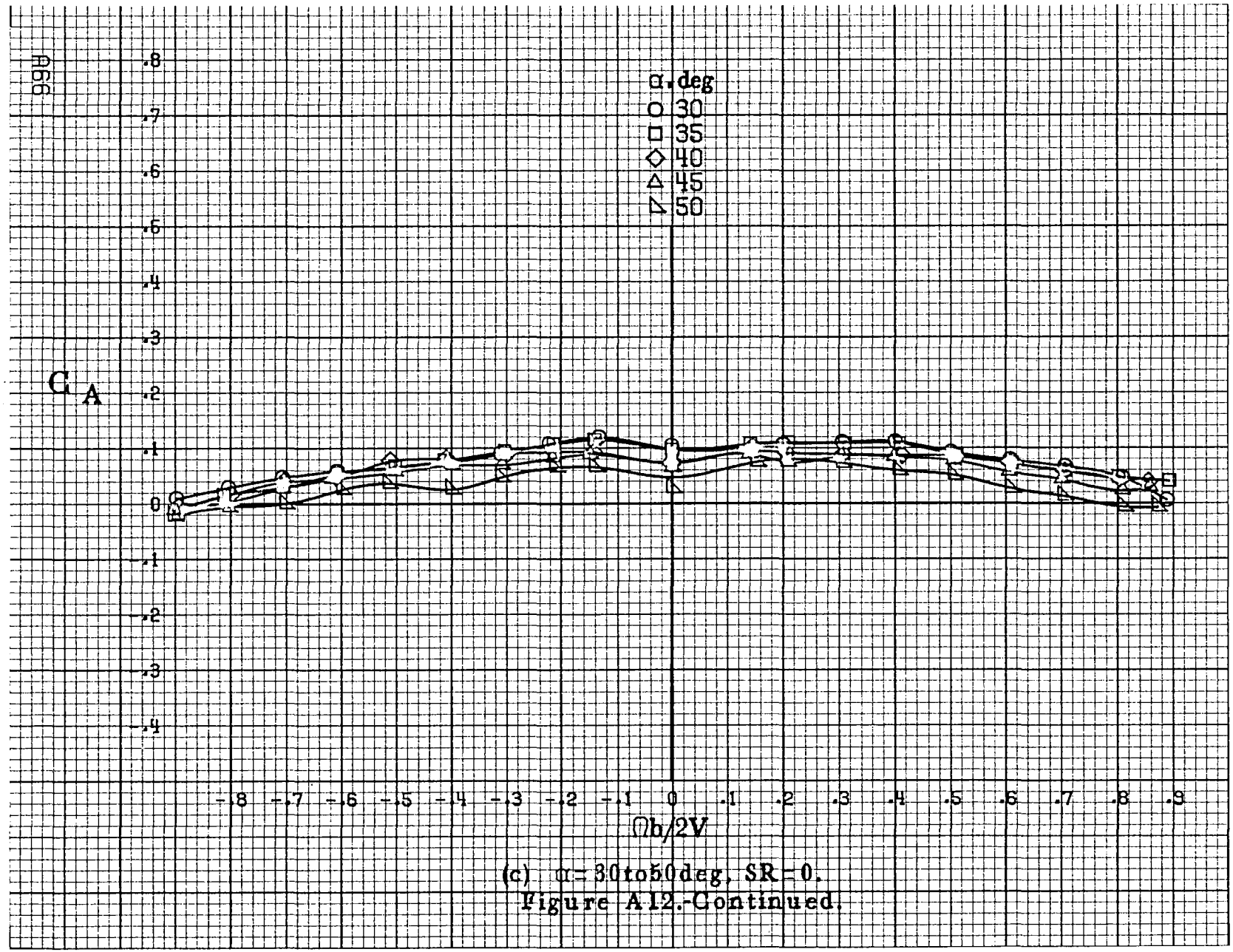

(c) α = 30 to 50 deg, SR = 0.

Figure A12.-Continued.

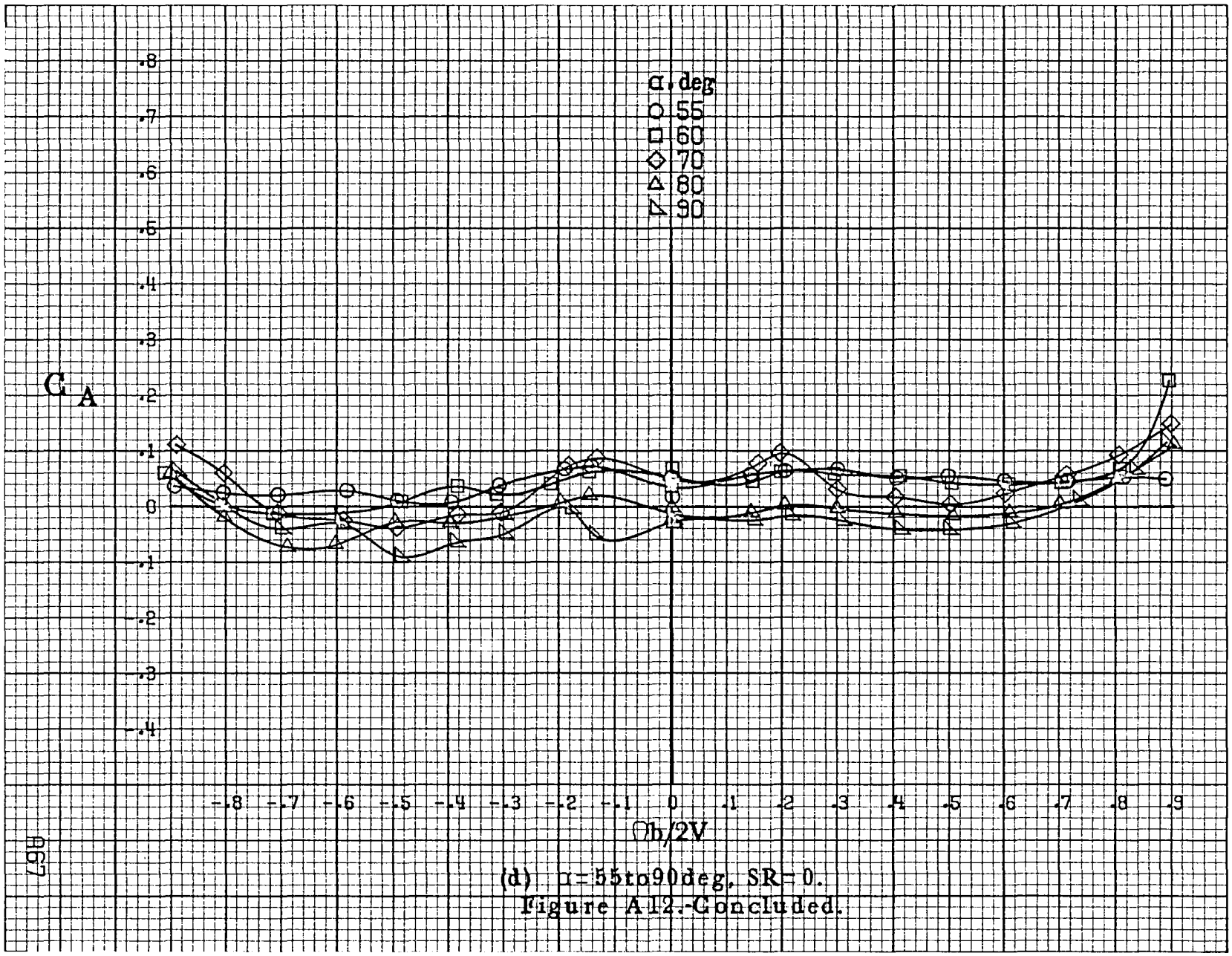

(d) $\alpha = 55$ to 90 deg, SR = 0.

Figure A12.-Concluded.

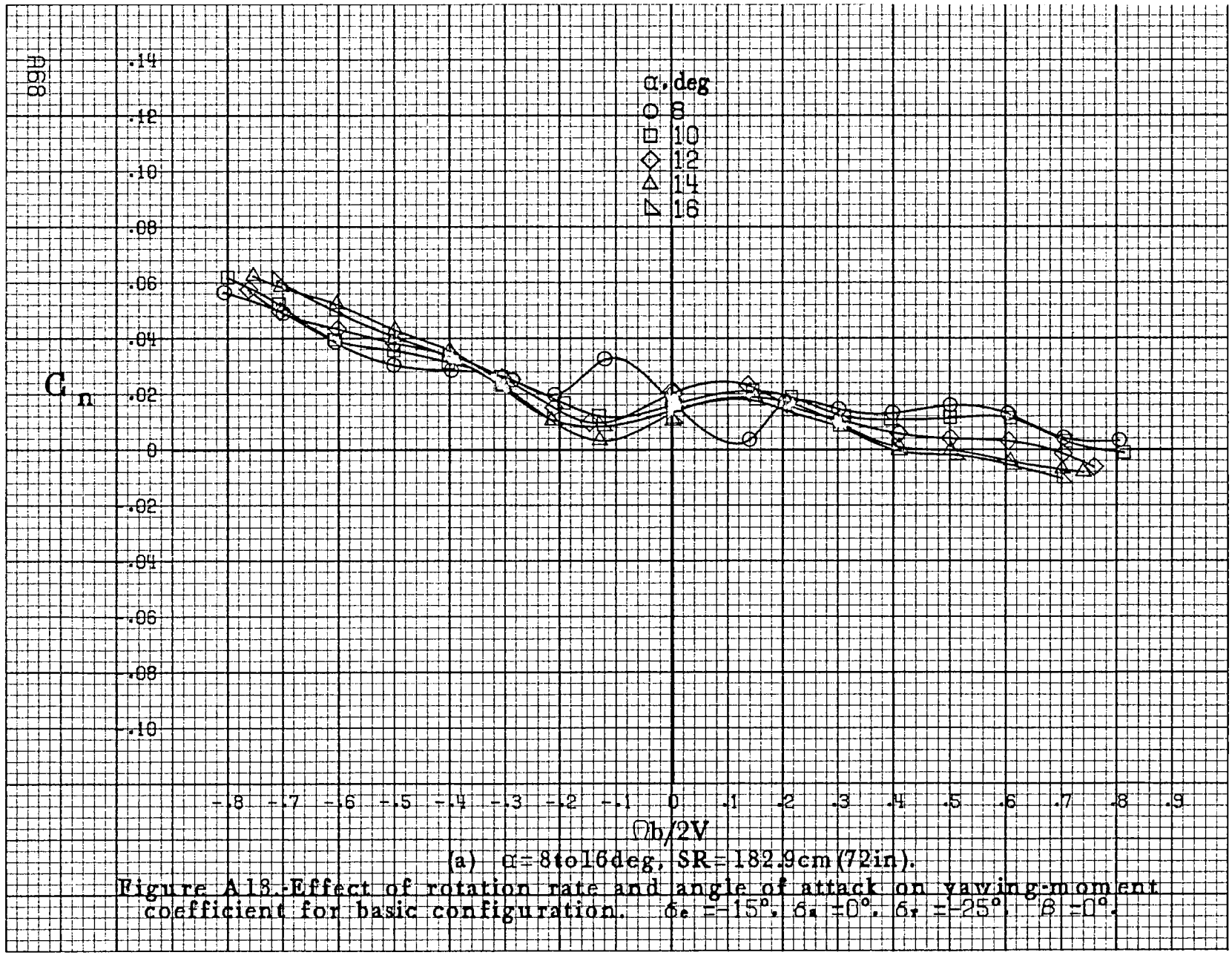

(a) $\alpha = 8$ to 16 deg, SR = 182.9 cm (72 in.).

Figure A18.-Effect of rotation rate and angle of attack on yawing-moment coefficient for basic configuration. $\delta_e = -15°$, $\delta_a = 0°$, $\delta_r = -25°$, $\beta = 0°$.

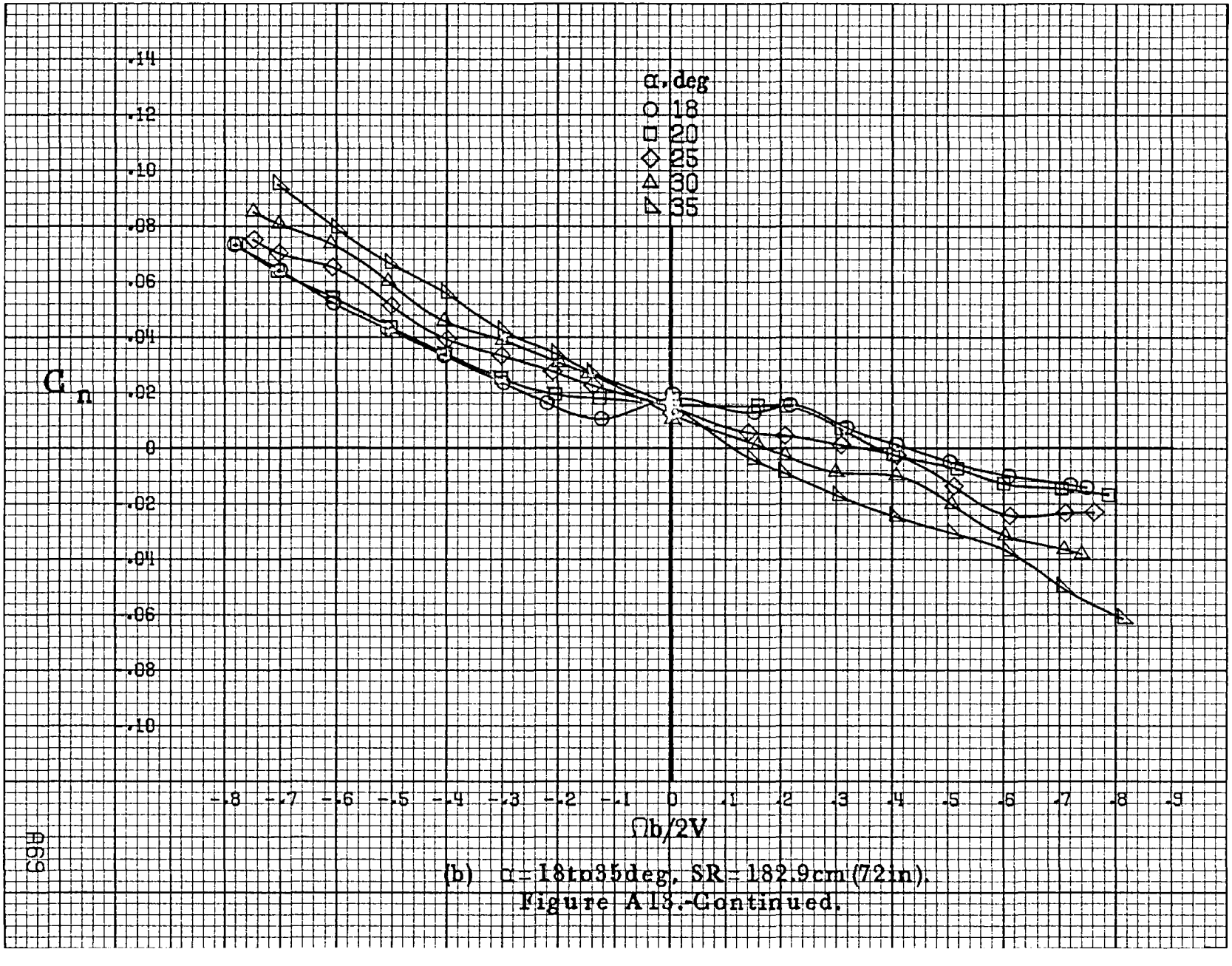

(b) α = 18 to 35 deg, SR = 182.9 cm (72 in).

Figure A18.-Continued.

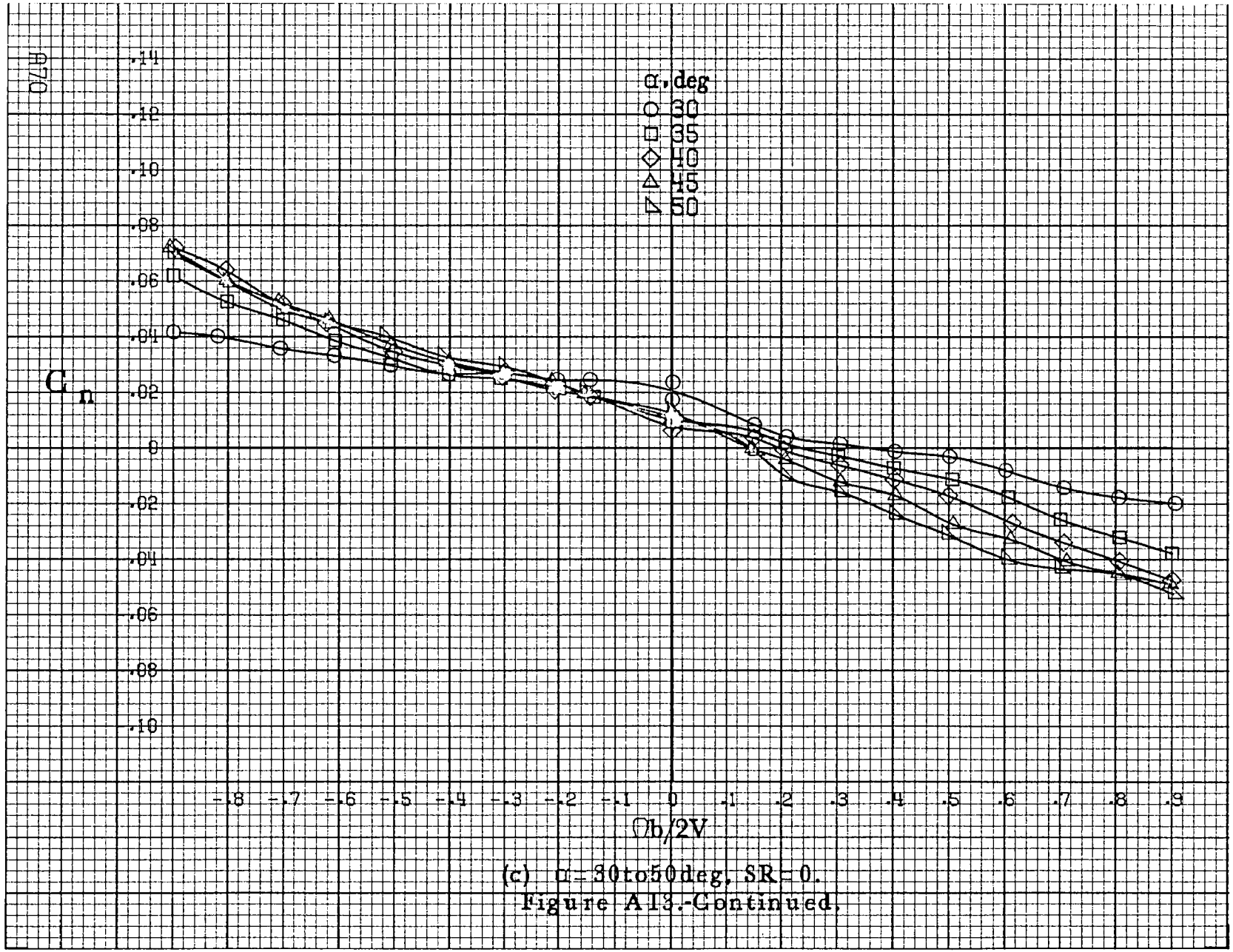

(c) $\alpha = 30$ to 50 deg, SR = 0.

Figure A13.-Continued.

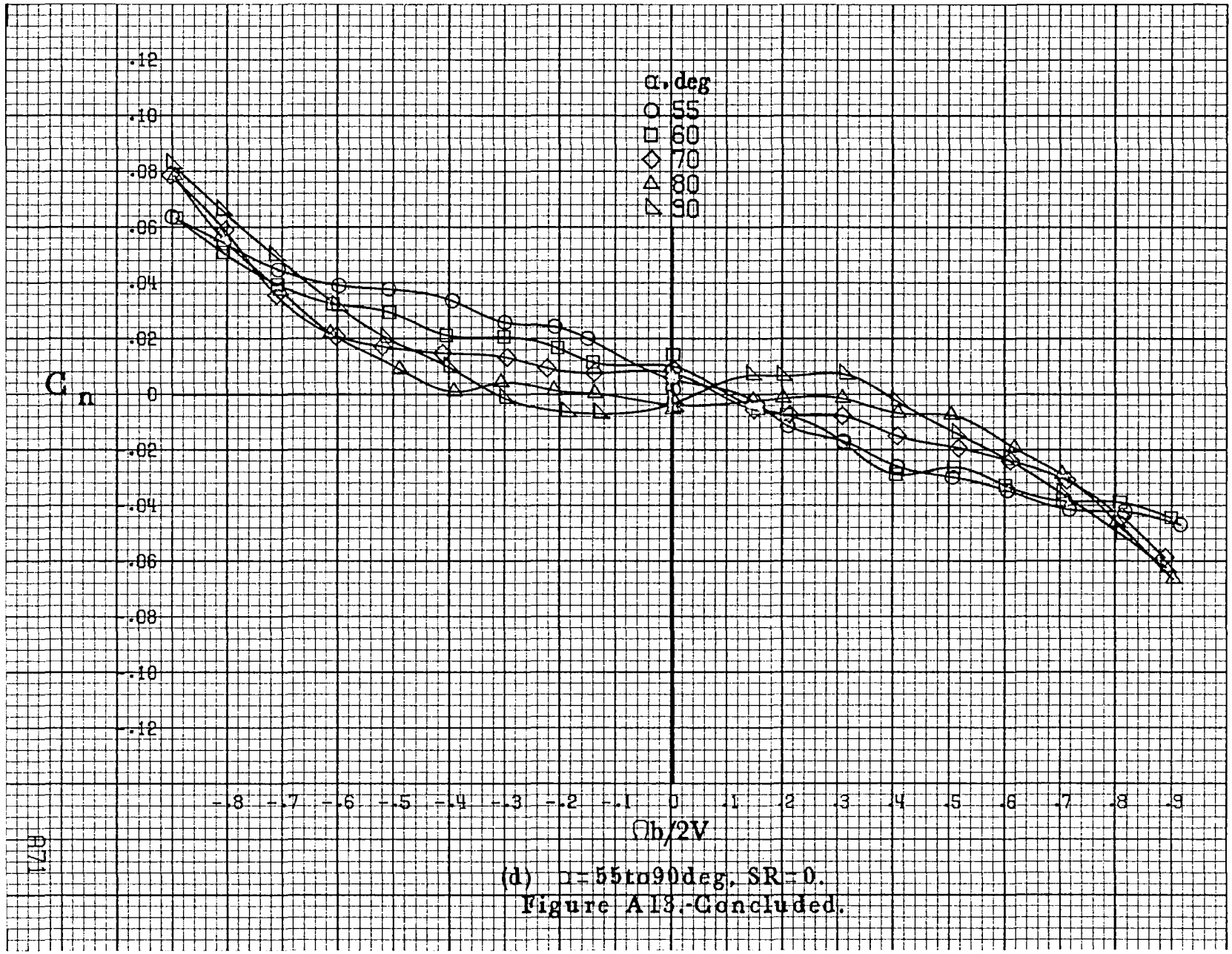

(d) $\alpha = 55$ to 90 deg, SR = 0.

Figure A13.-Concluded.

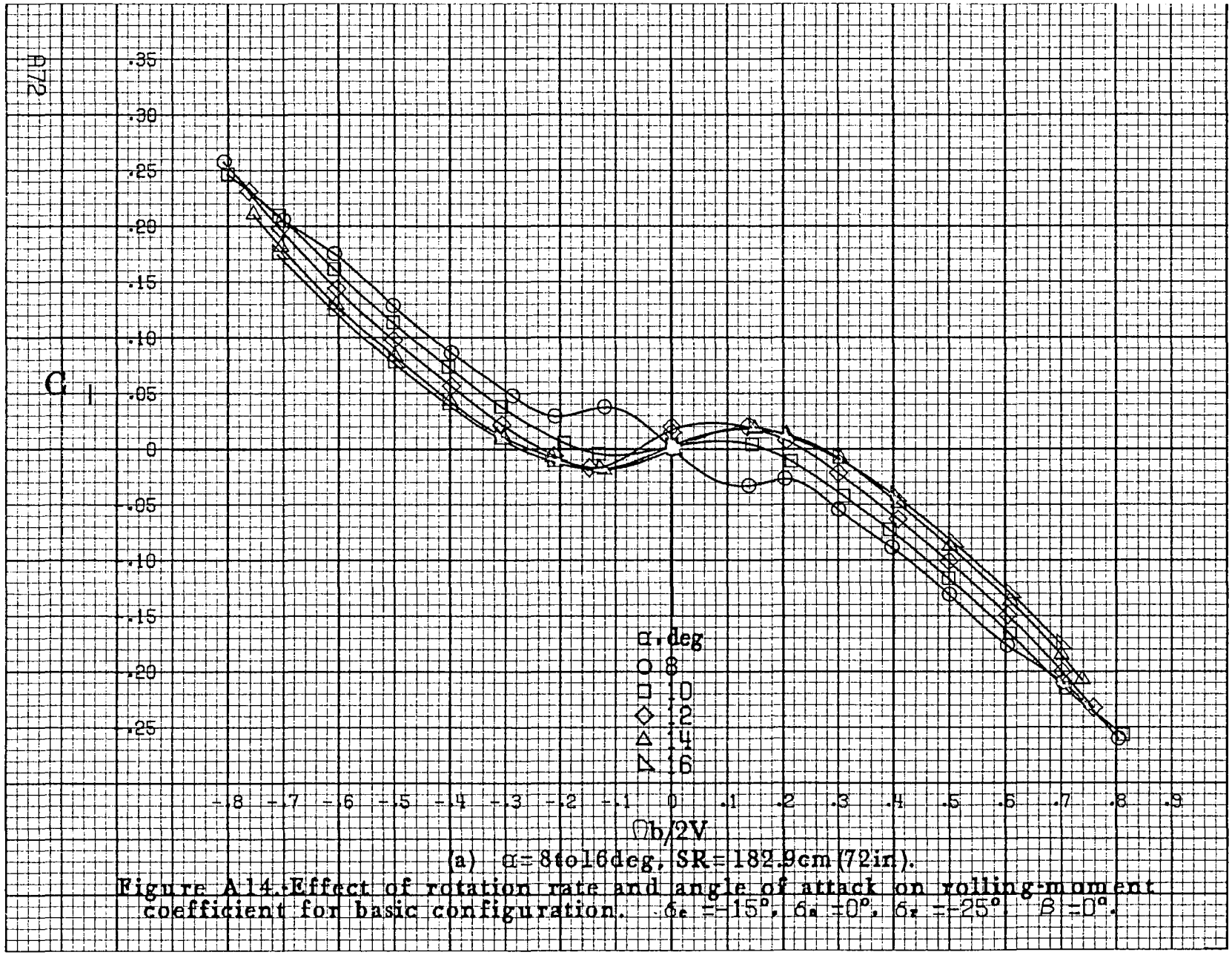

(a) α = 8 to 16 deg, SR = 182.9 cm (72 in.).

Figure A14.-Effect of rotation rate and angle of attack on rolling-moment coefficient for basic configuration. $\delta_e = -15°$, $\delta_a = 0°$, $\delta_r = -25°$, $\beta = 0°$.

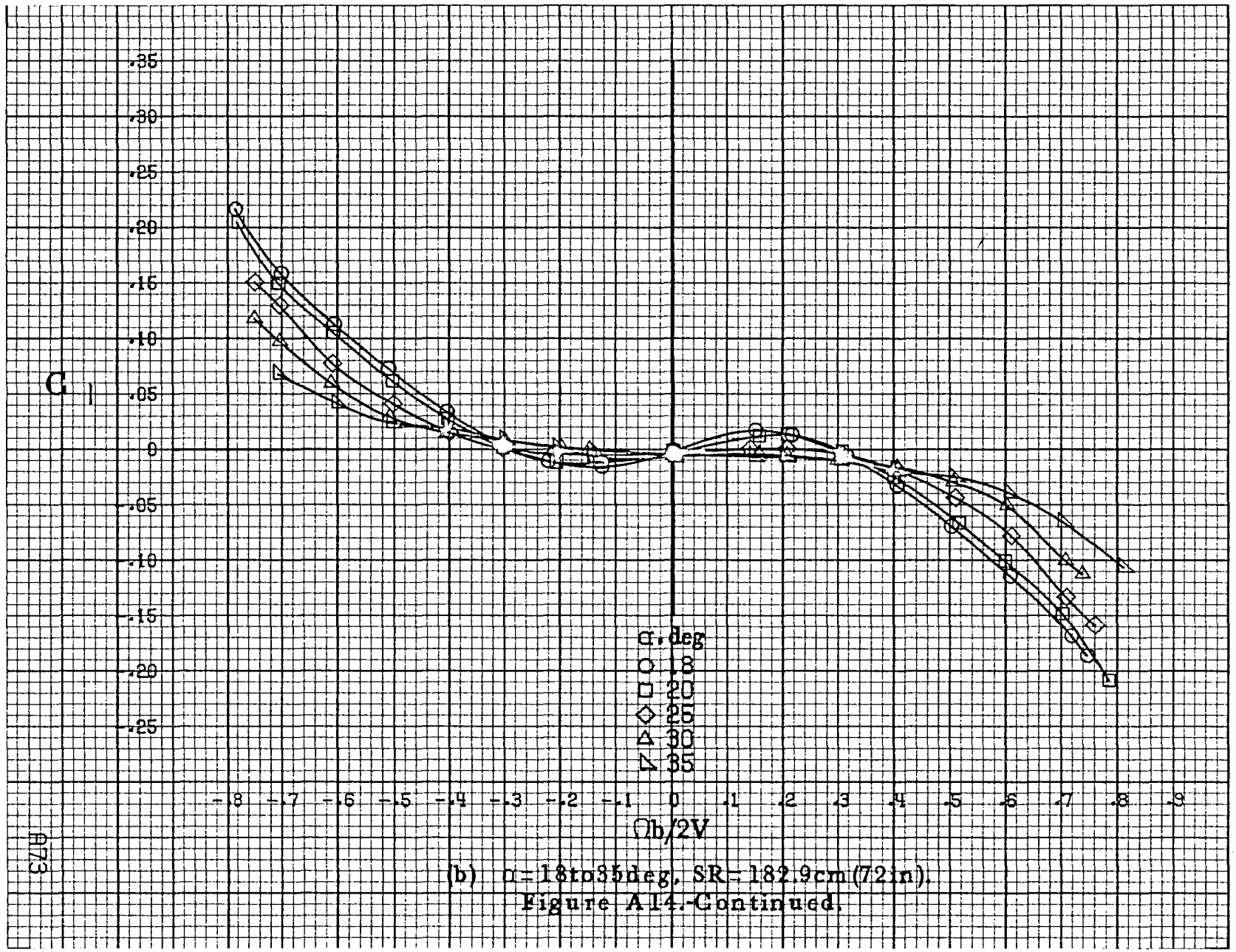

(b) α = 18 to 35 deg, SR = 182.9 cm (72 in).

Figure A14.-Continued.

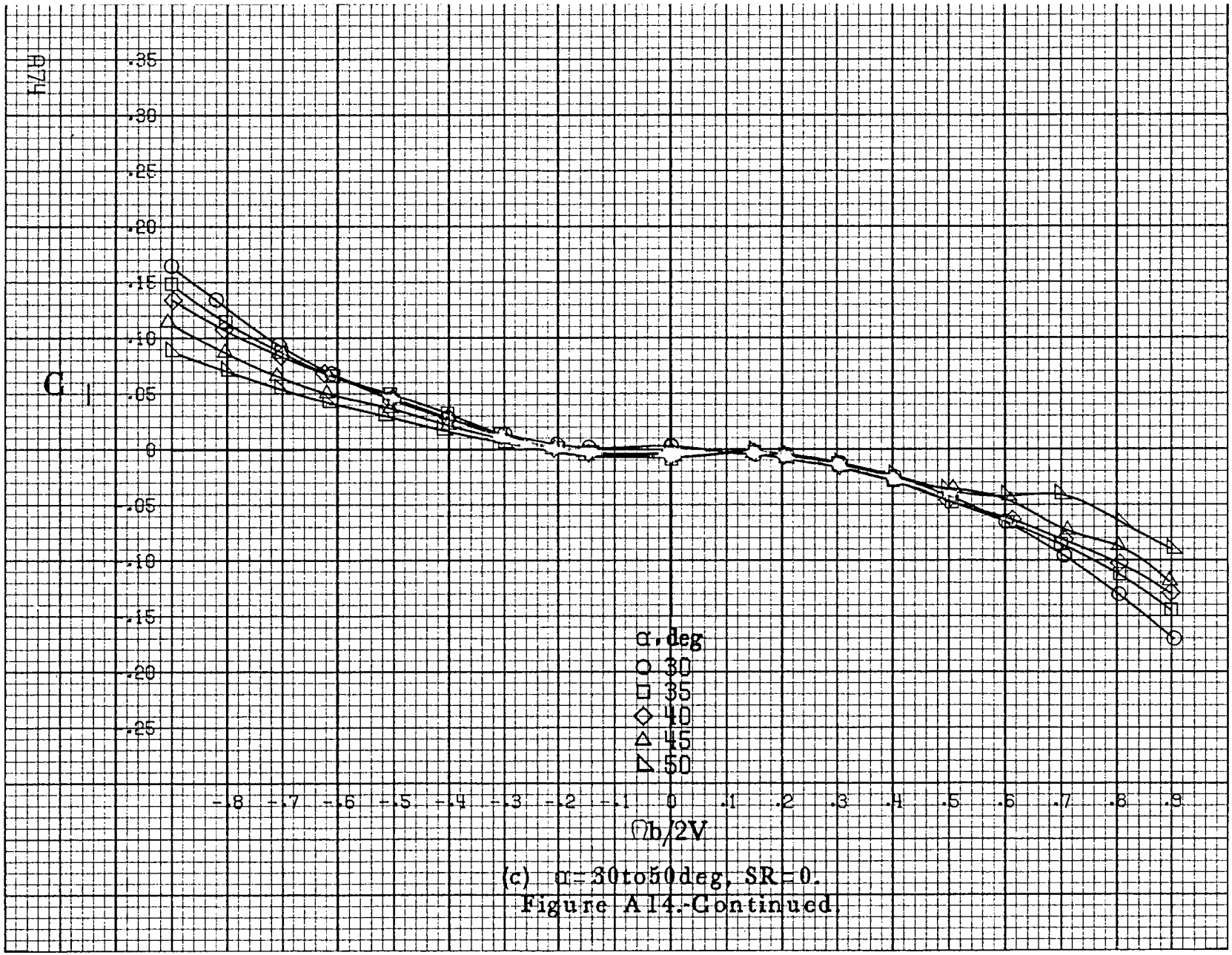

(c) α = 30 to 50 deg, SR = 0.

Figure A14.-Continued.

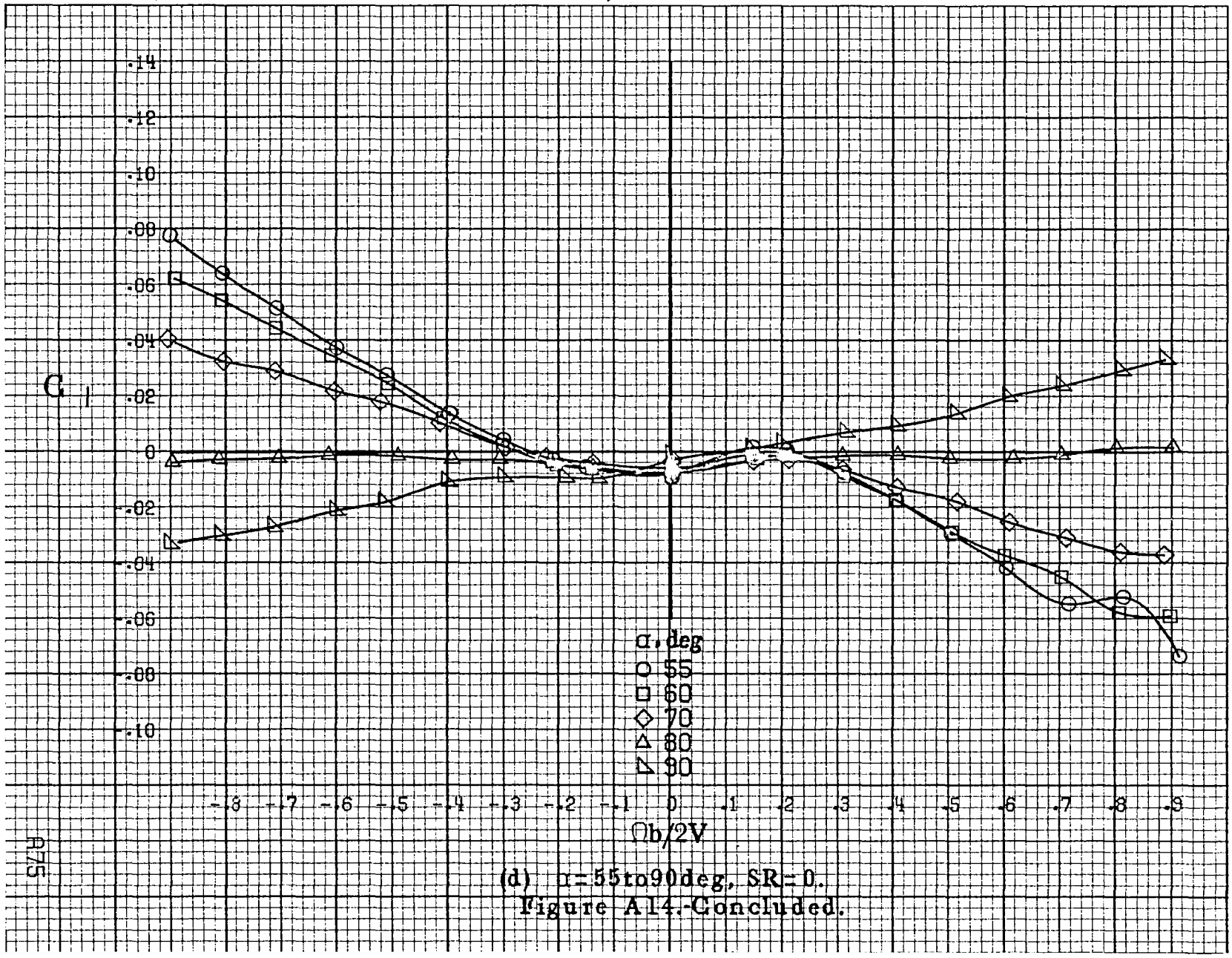

(d) α = 55 to 90 deg, SR = 0.

Figure A14.-Concluded.

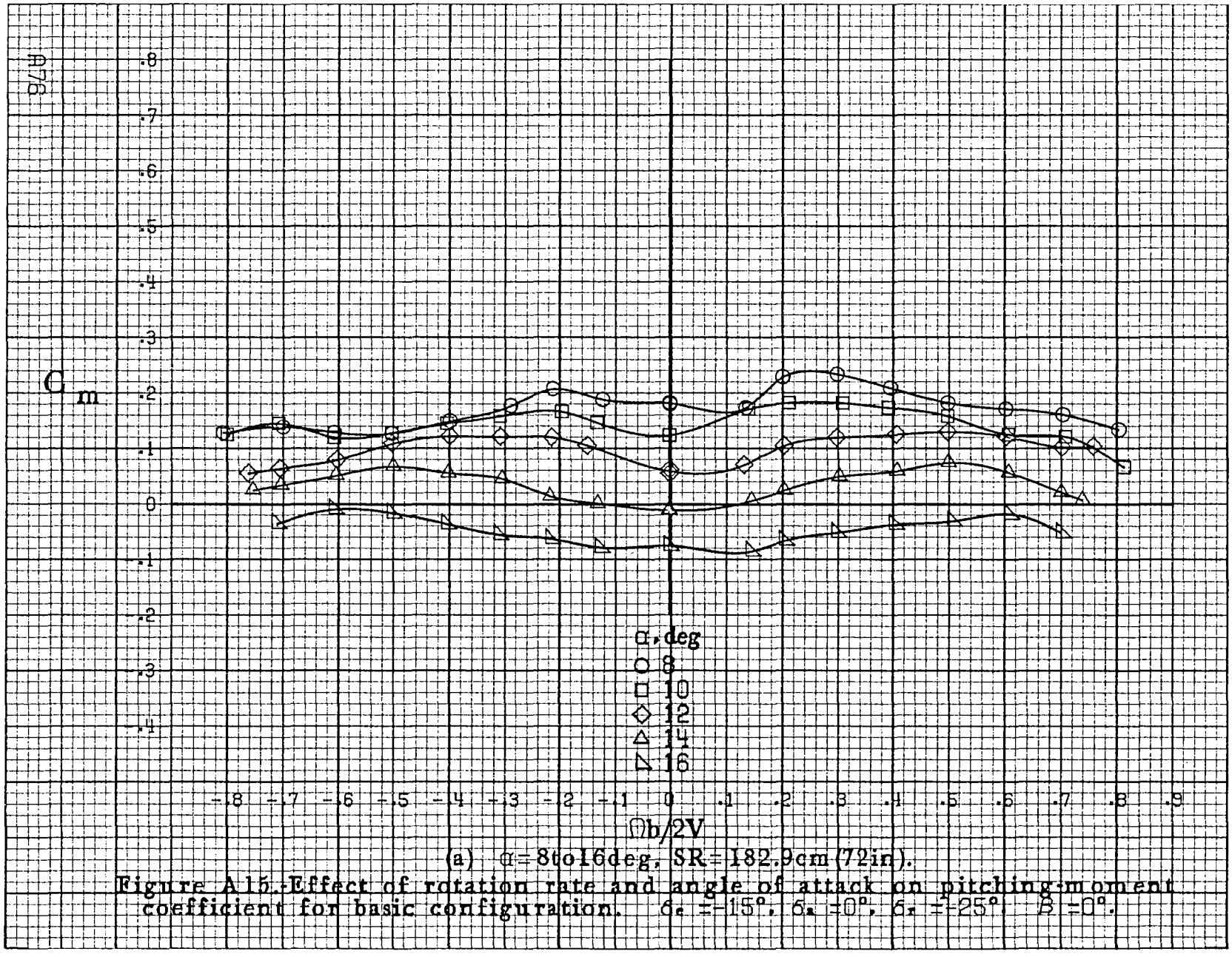

(a) $\alpha = 8$ to 16 deg, SR = 182.9 cm (72 in).

Figure A15.-Effect of rotation rate and angle of attack on pitching-moment coefficient for basic configuration. $\delta_e = -15°$, $\delta_a = 0°$, $\delta_r = -25°$, $\beta = 0°$.

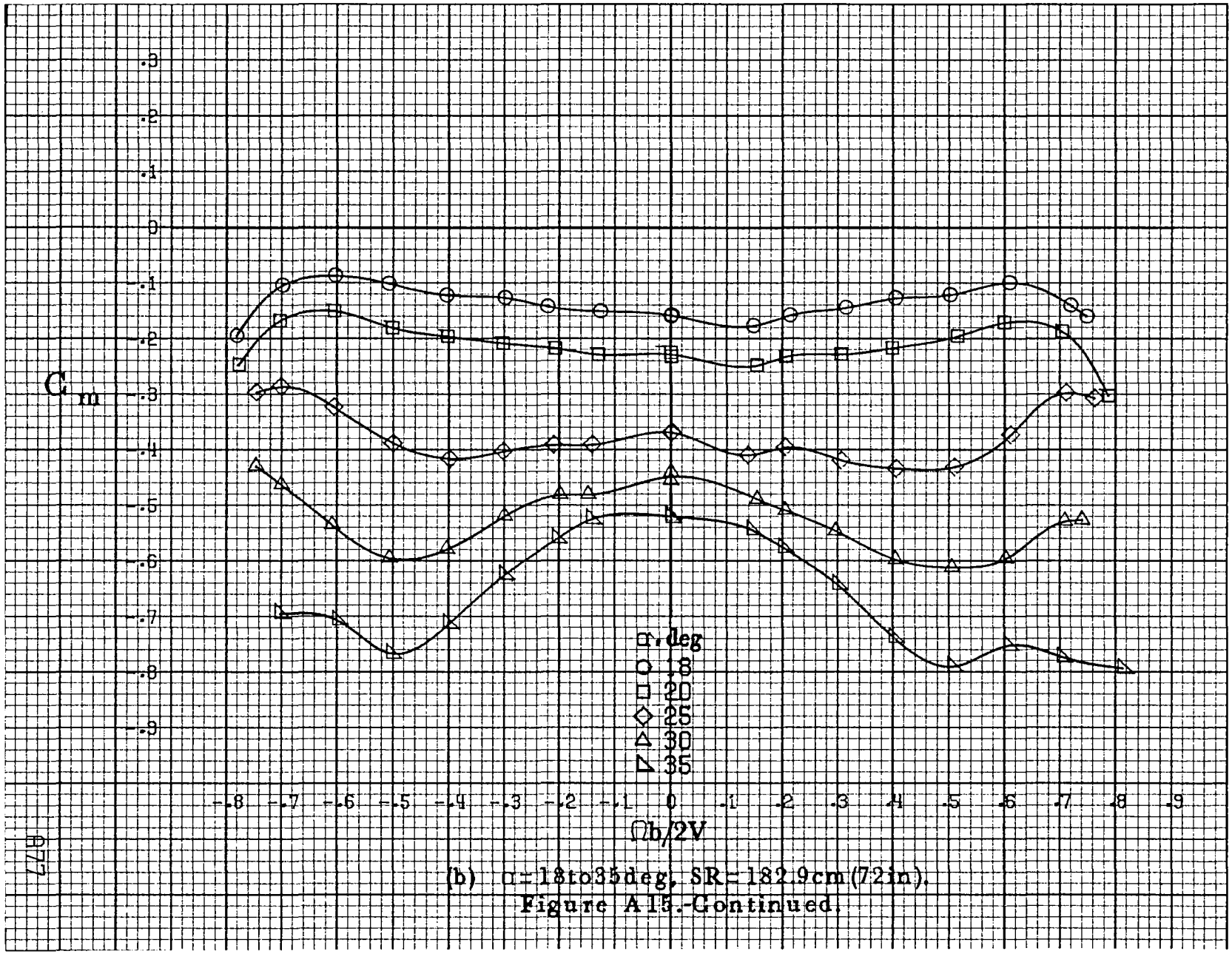

(b) α = 18 to 35 deg, SR = 182.9 cm (72 in).

Figure A15.-Continued.

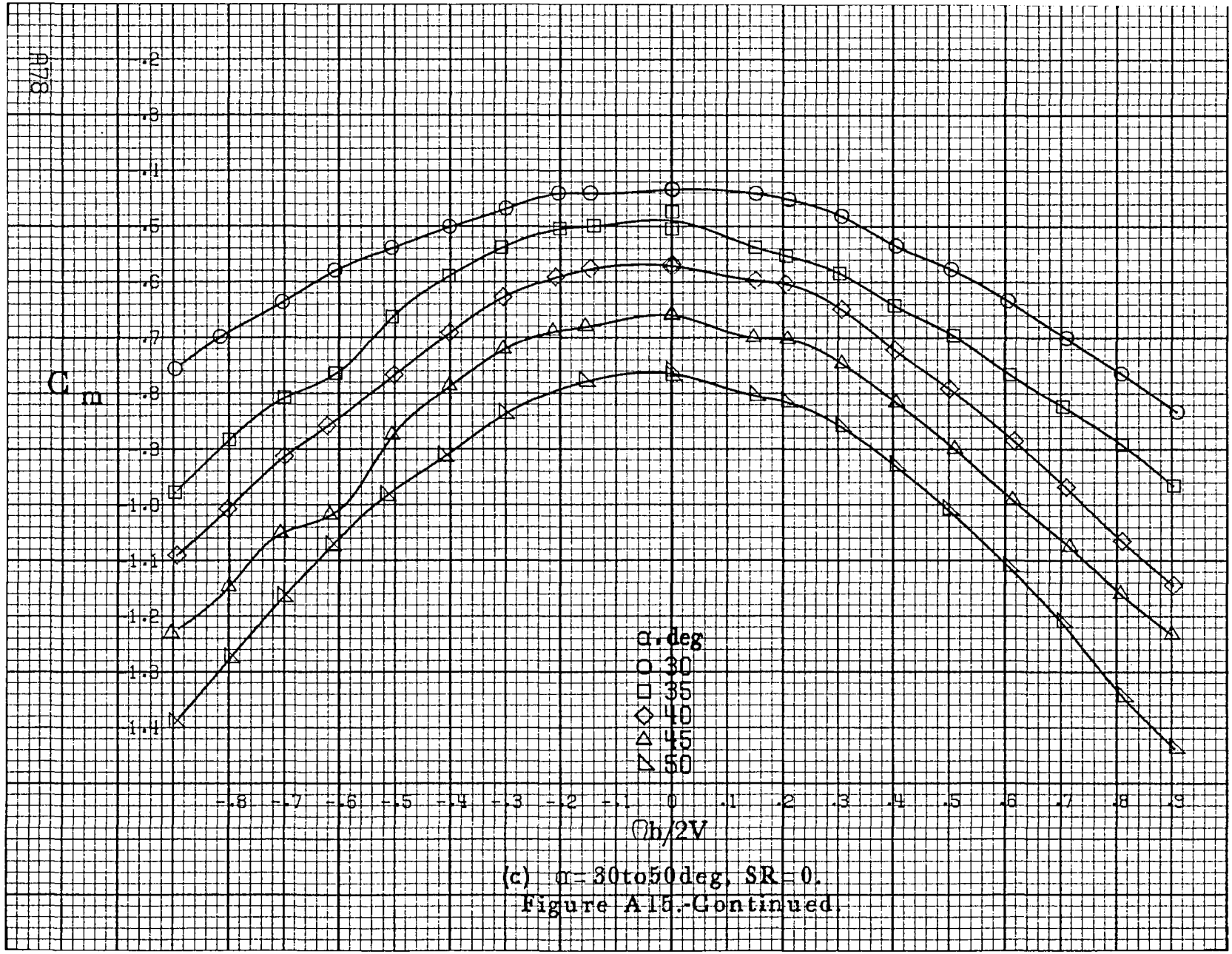

(c) $\alpha = 30$ to 50 deg, SR = 0.

Figure A15.-Continued.

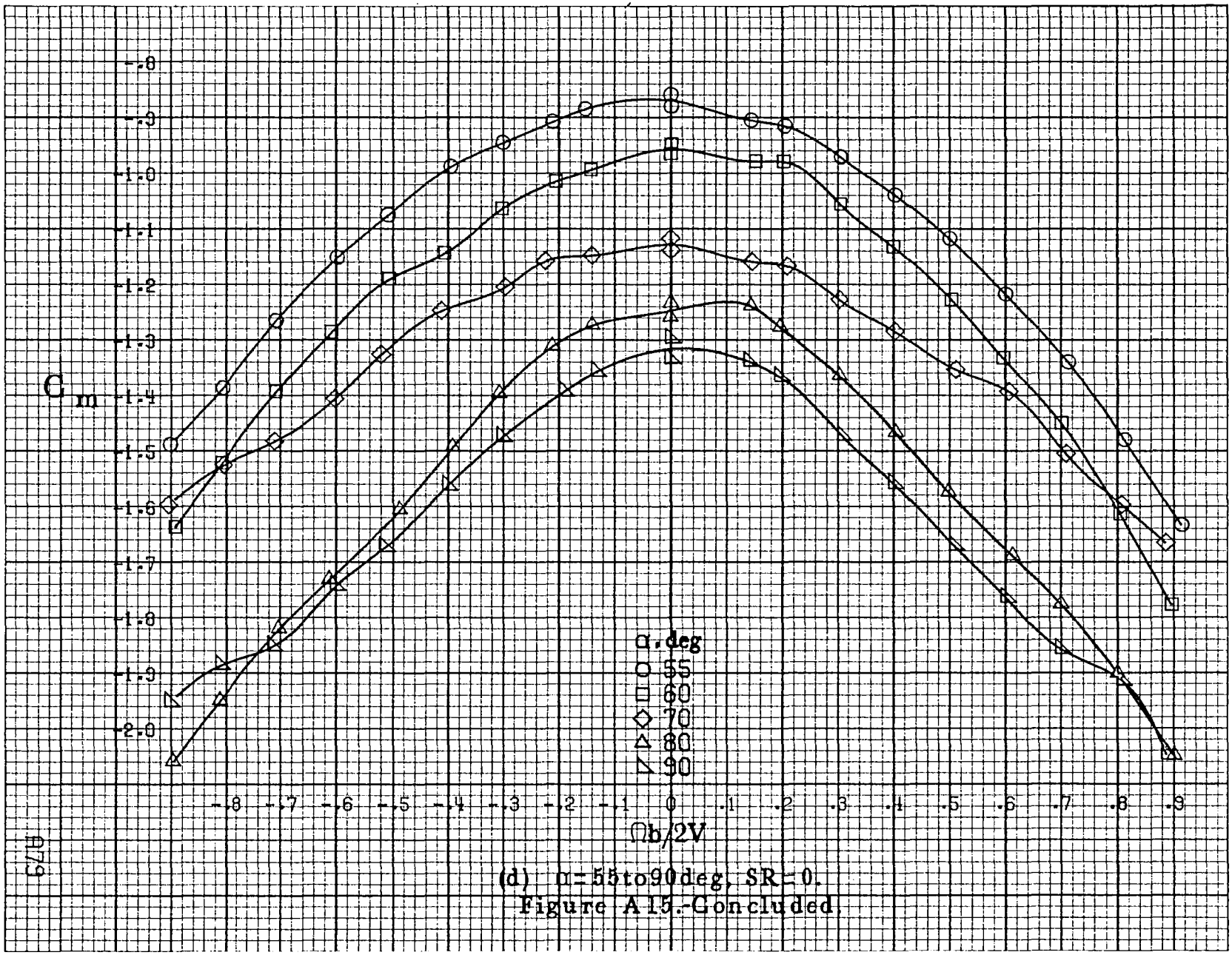

(d) α = 55 to 90 deg, SR = 0.

Figure A15.-Concluded.

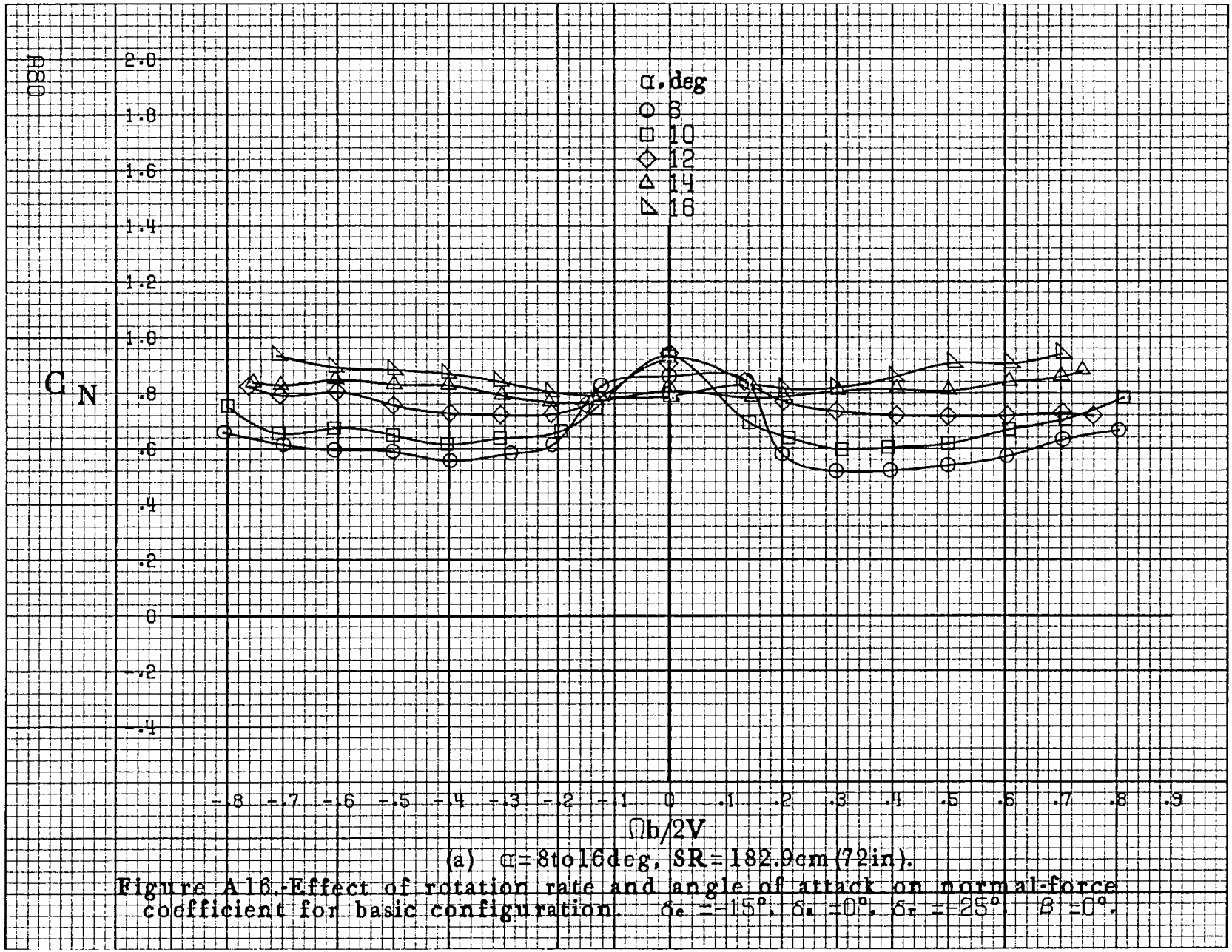

(a) $\alpha = 8$ to 16 deg, SR = 182.9 cm (72 in).

Figure A16.-Effect of rotation rate and angle of attack on normal-force coefficient for basic configuration. $\delta_e = -15°$, $\delta_a = 0°$, $\delta_r = -25°$, $\beta = 0°$.

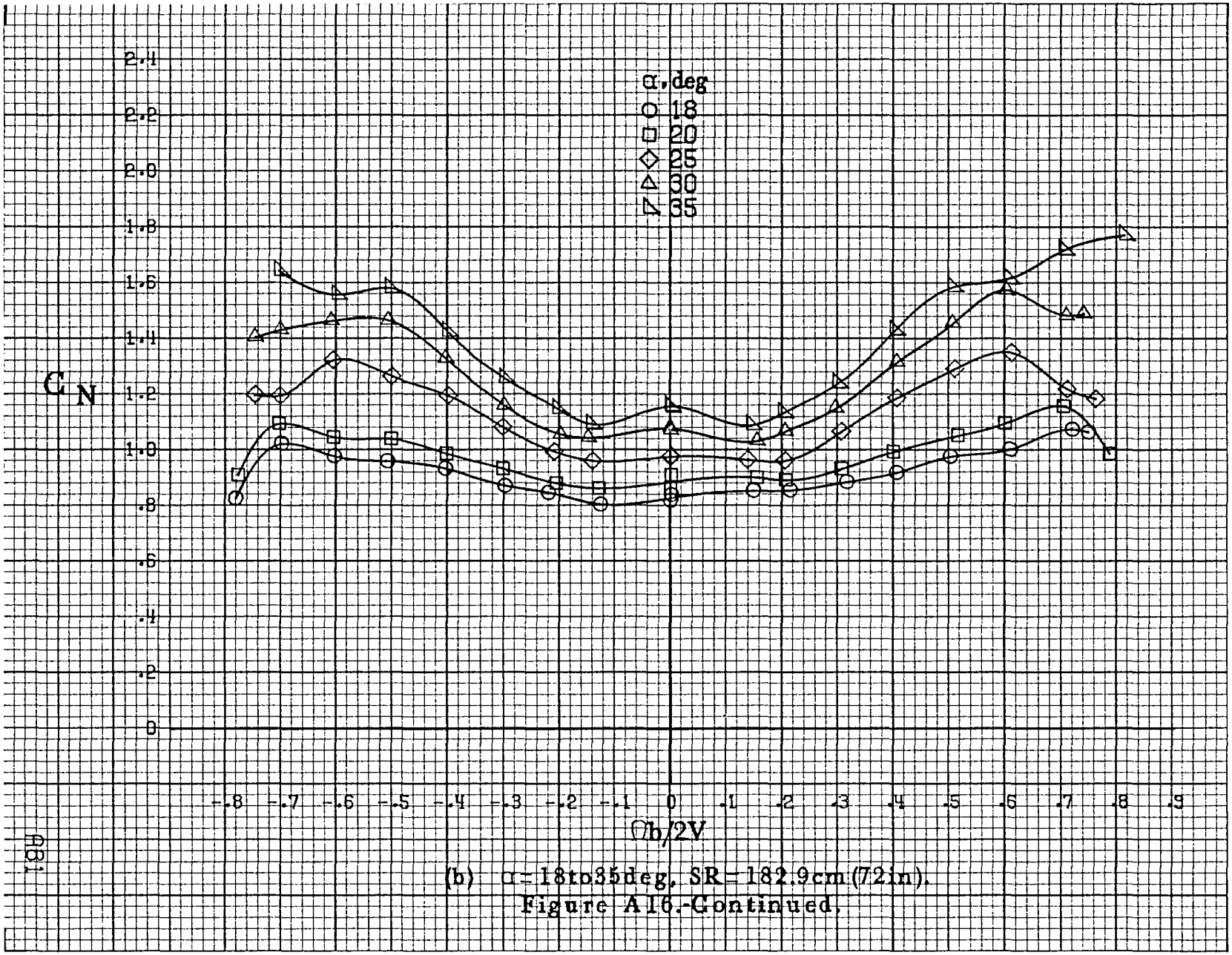

(b) α = 18 to 35 deg, SR = 182.9 cm (72 in).

Figure A16.-Continued.

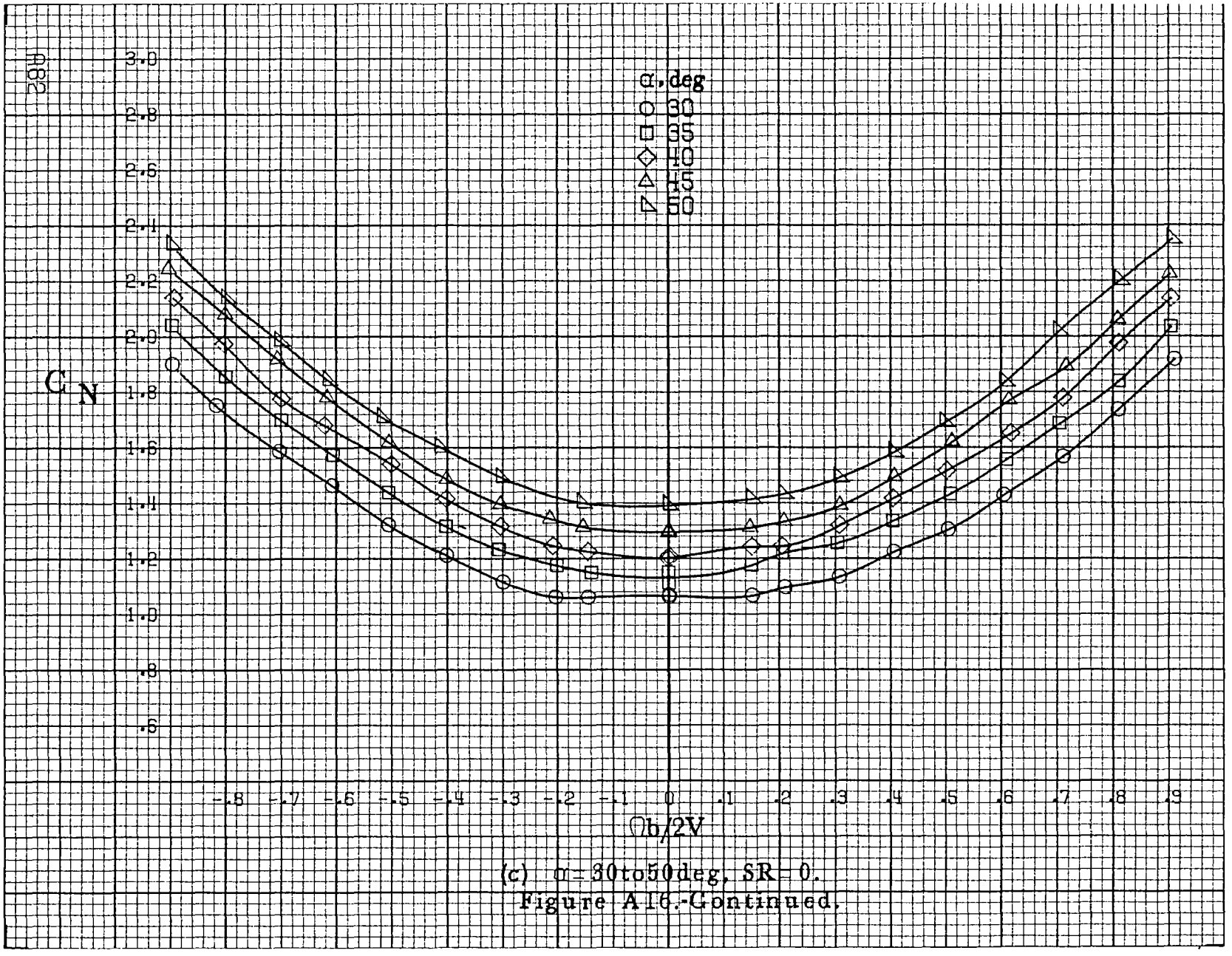

(c) $\alpha = 30$ to 50 deg, SR = 0.

Figure A16.-Continued.

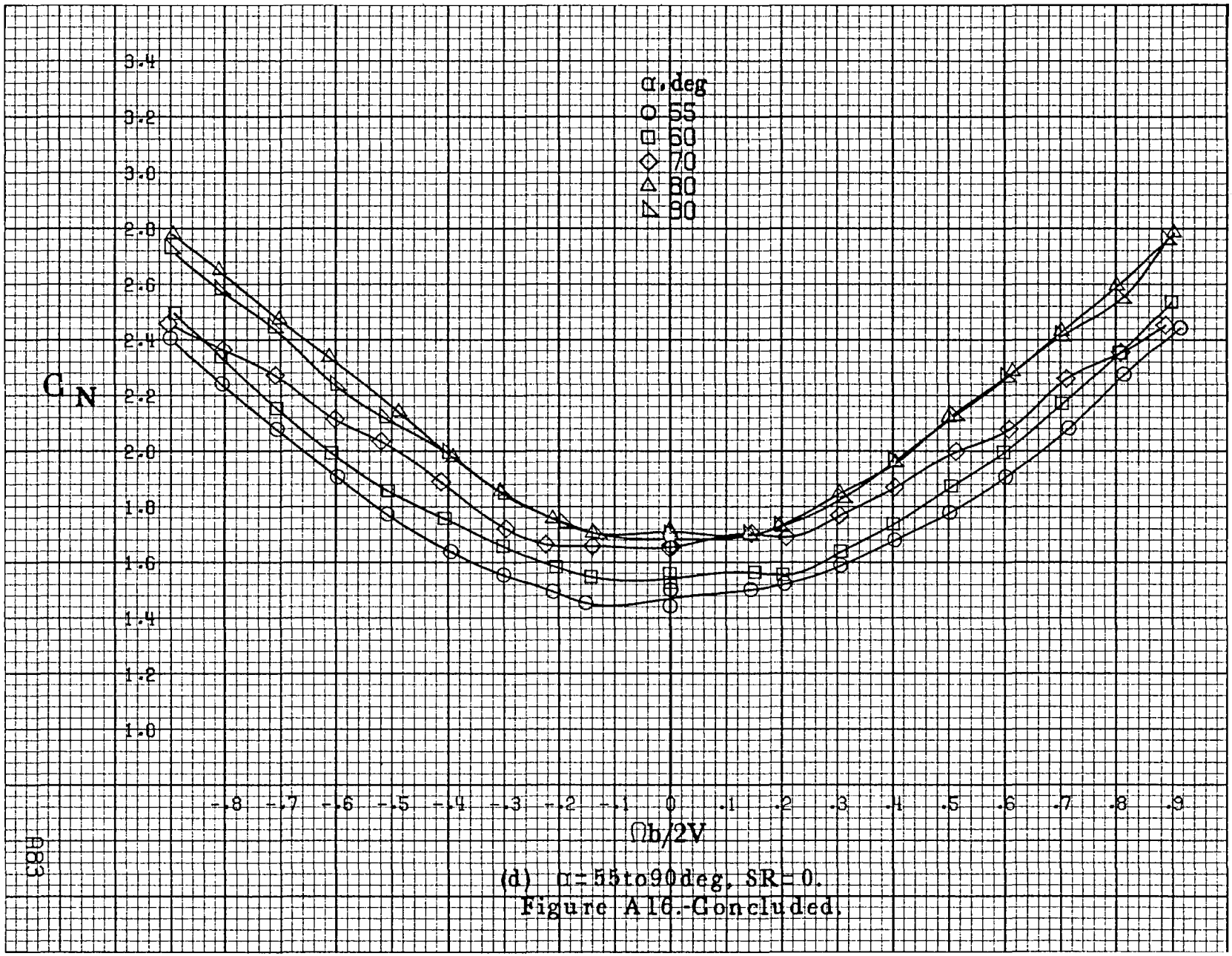

(d) $\alpha = 55$ to 90 deg, SR = 0.

Figure A16.-Concluded.

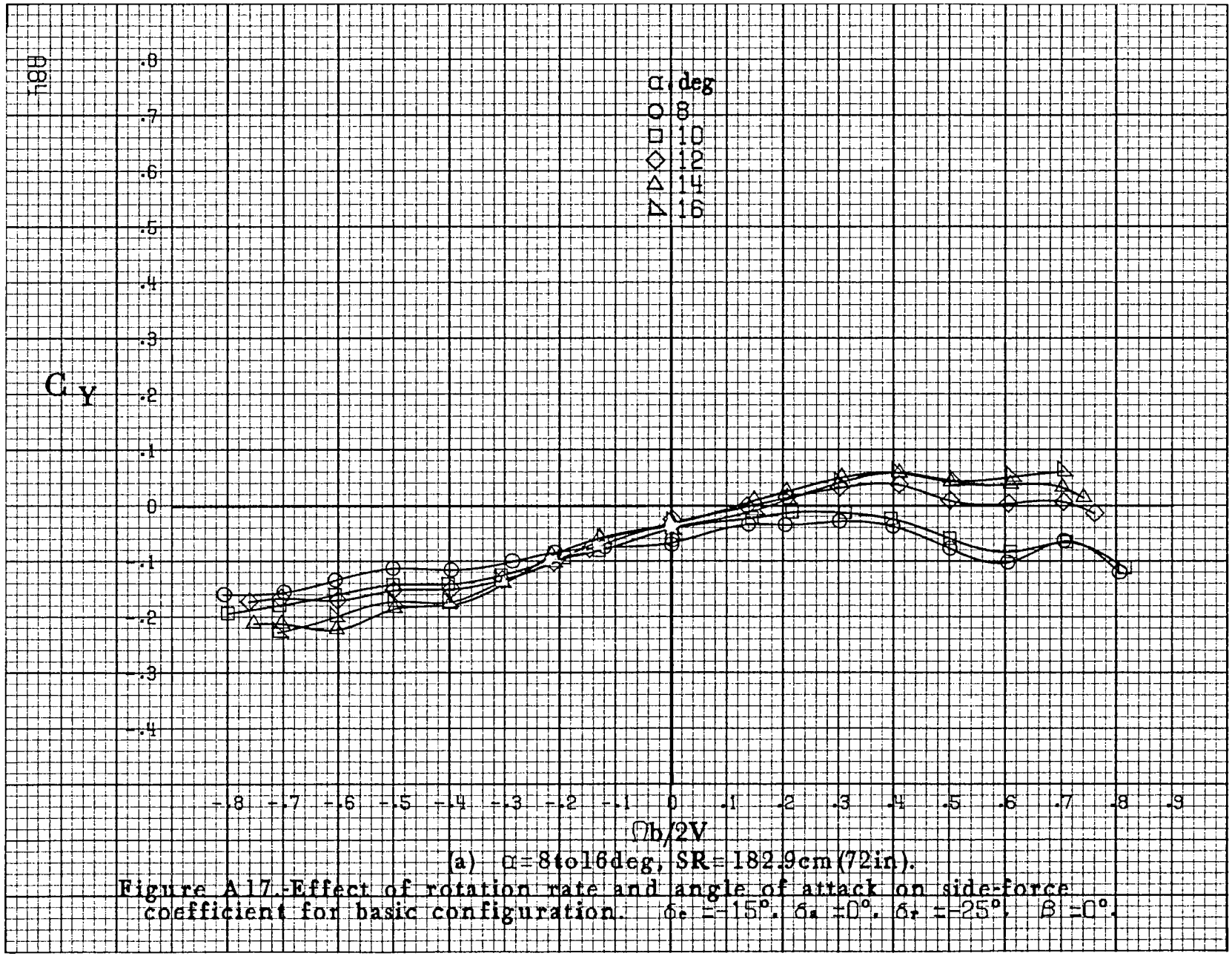

(a) α=8to16deg, SR=182.9cm(72in).

Figure A17.-Effect of rotation rate and angle of attack on side-force coefficient for basic configuration. $\delta_e = -15°$, $\delta_a = 0°$, $\delta_r = -25°$, $\beta = 0°$.

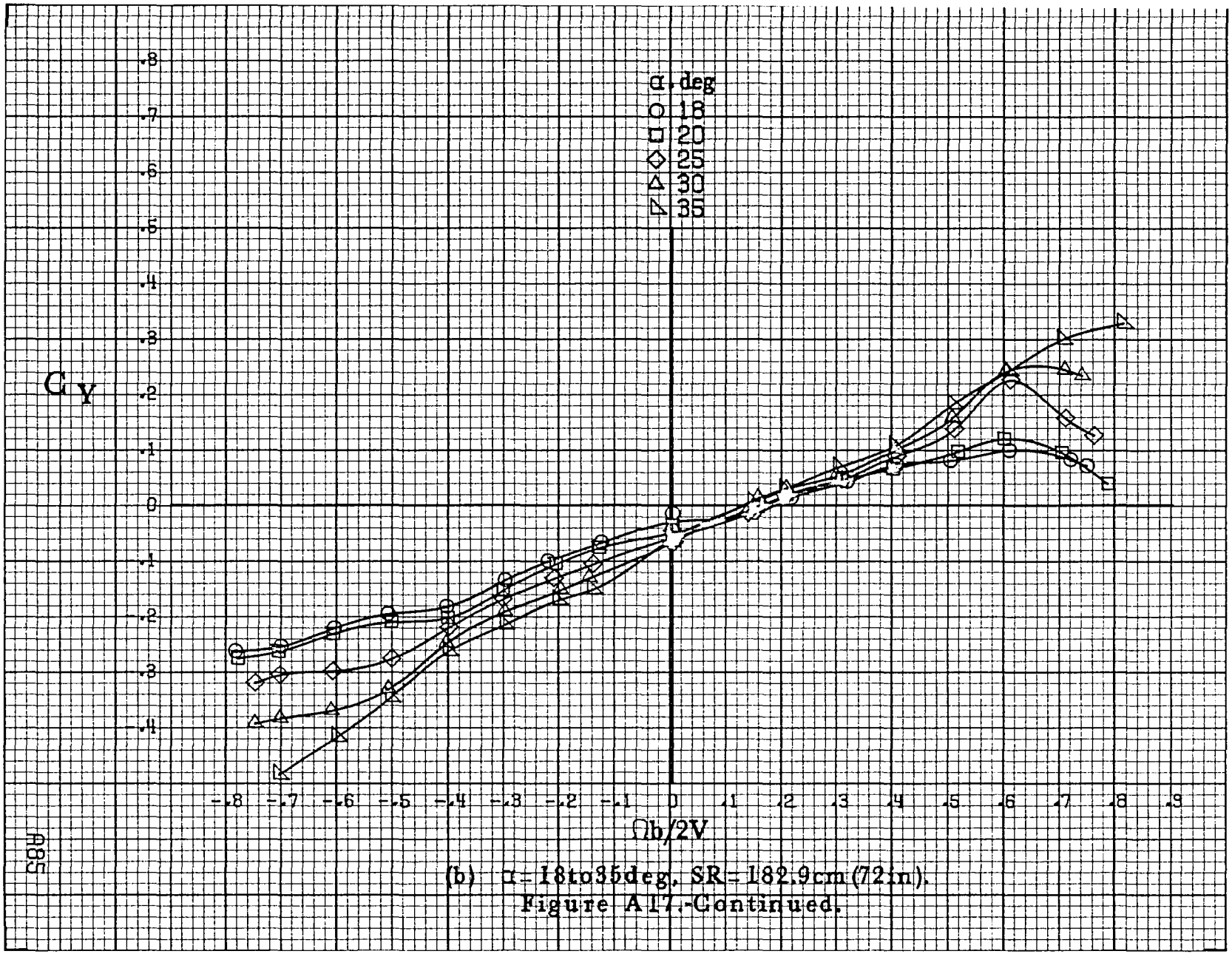

(b) α = 18 to 35 deg, SR = 182.9 cm (72 in).

Figure A17.-Continued.

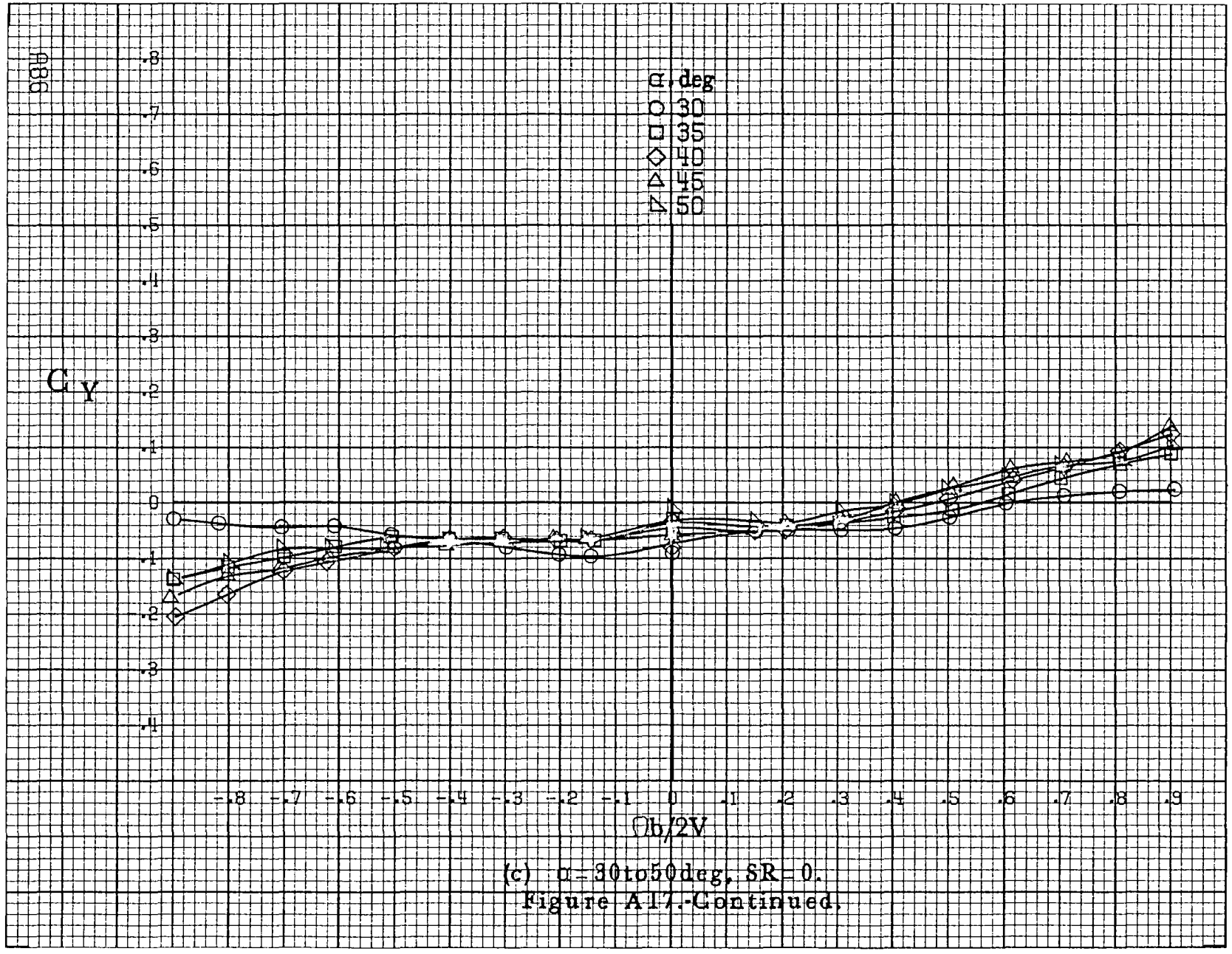

(c) α = 30 to 50 deg, SR = 0.

Figure A17.-Continued.

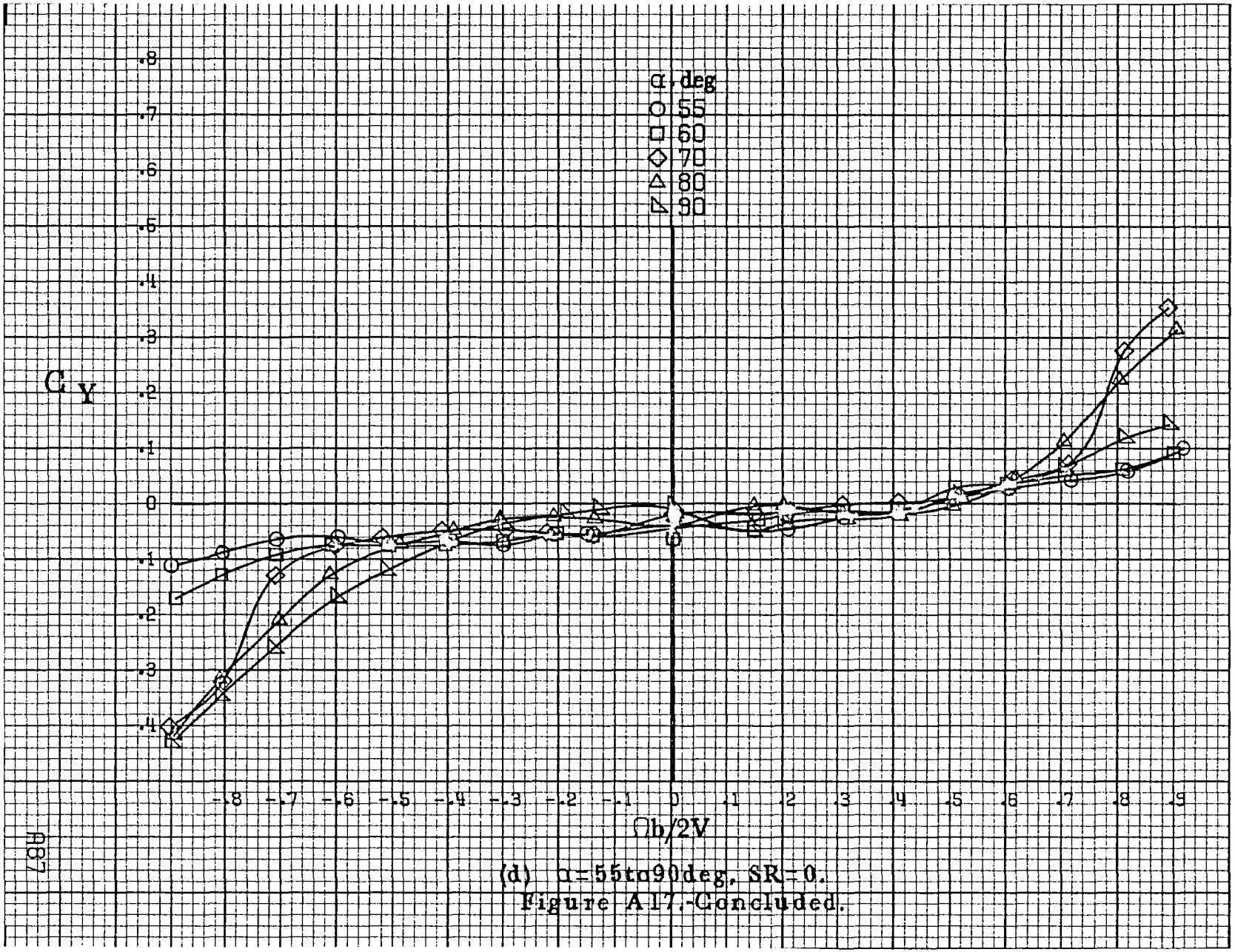

(d) α=55tα90deg, SR=0.

Figure A17.-Concluded.

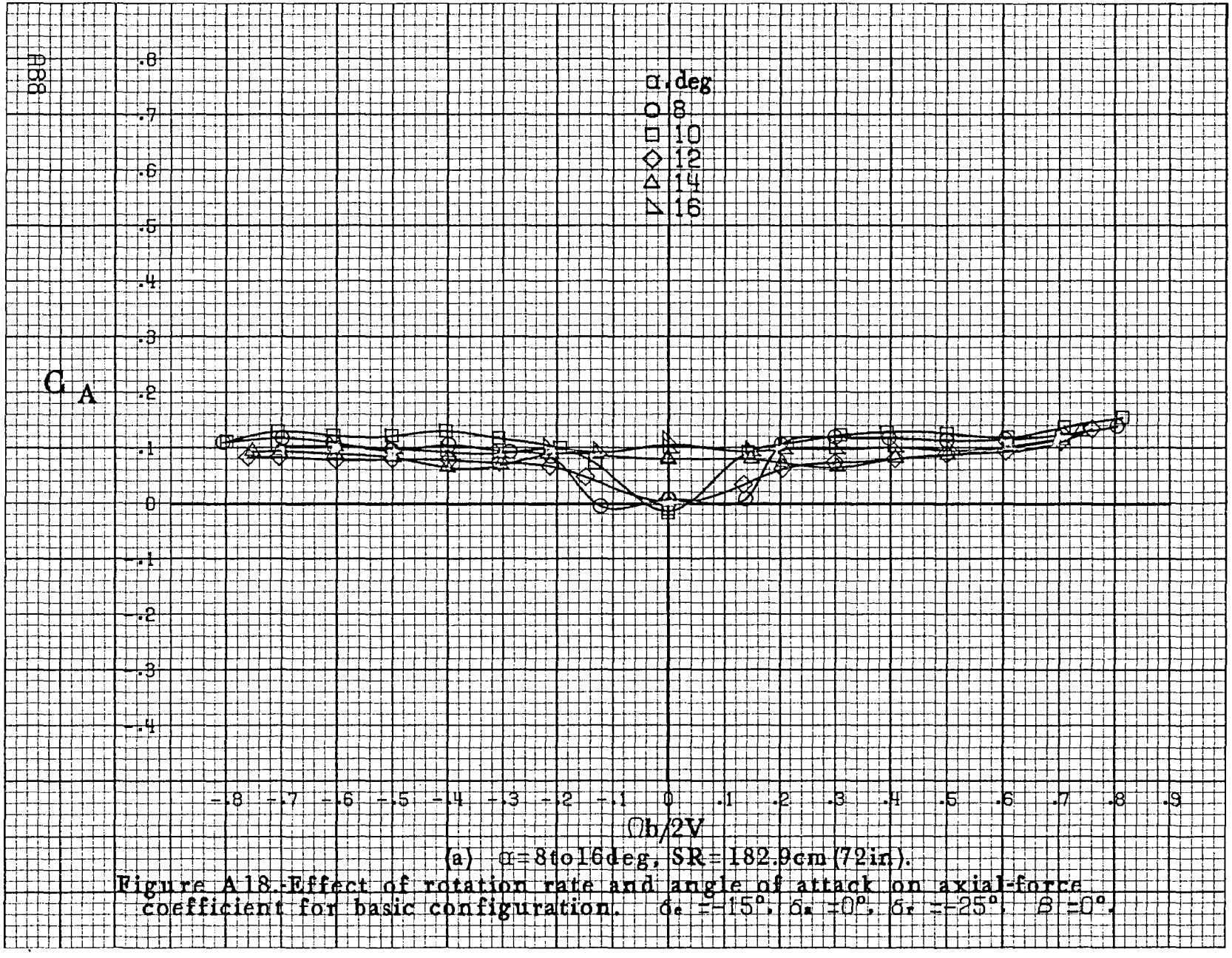

(a) α = 8 to 16 deg, SR = 182.9 cm (72 in.).

Figure A18.-Effect of rotation rate and angle of attack on axial-force coefficient for basic configuration. $\delta_a = -15°$, $\delta_e = 0°$, $\delta_r = -25°$, $\beta = 0°$.

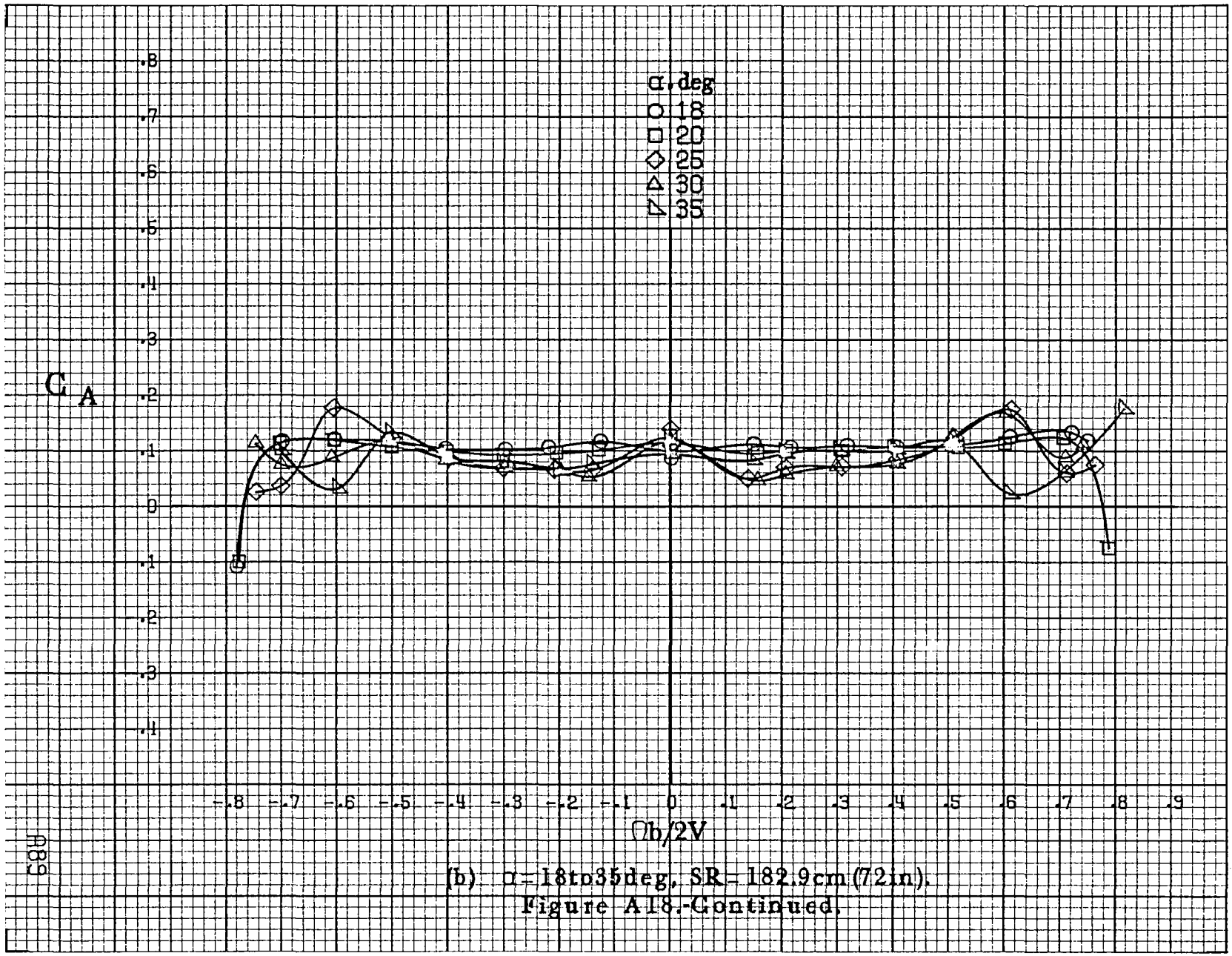

(b) α = 18 to 35 deg, SR = 182.9 cm (72 in).

Figure A18.-Continued.

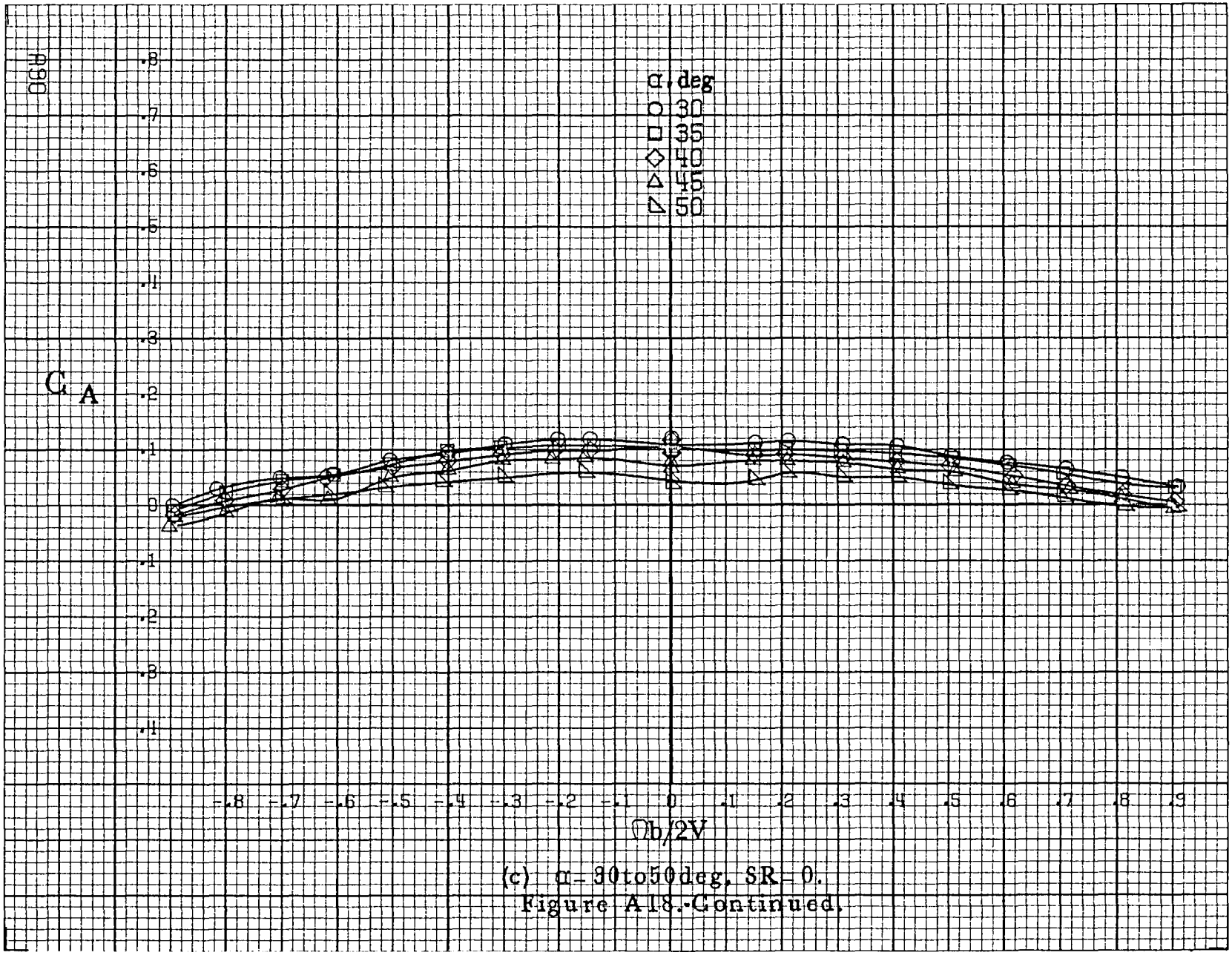

(c) α = 30 to 50 deg, SR = 0.

Figure A18.-Continued.

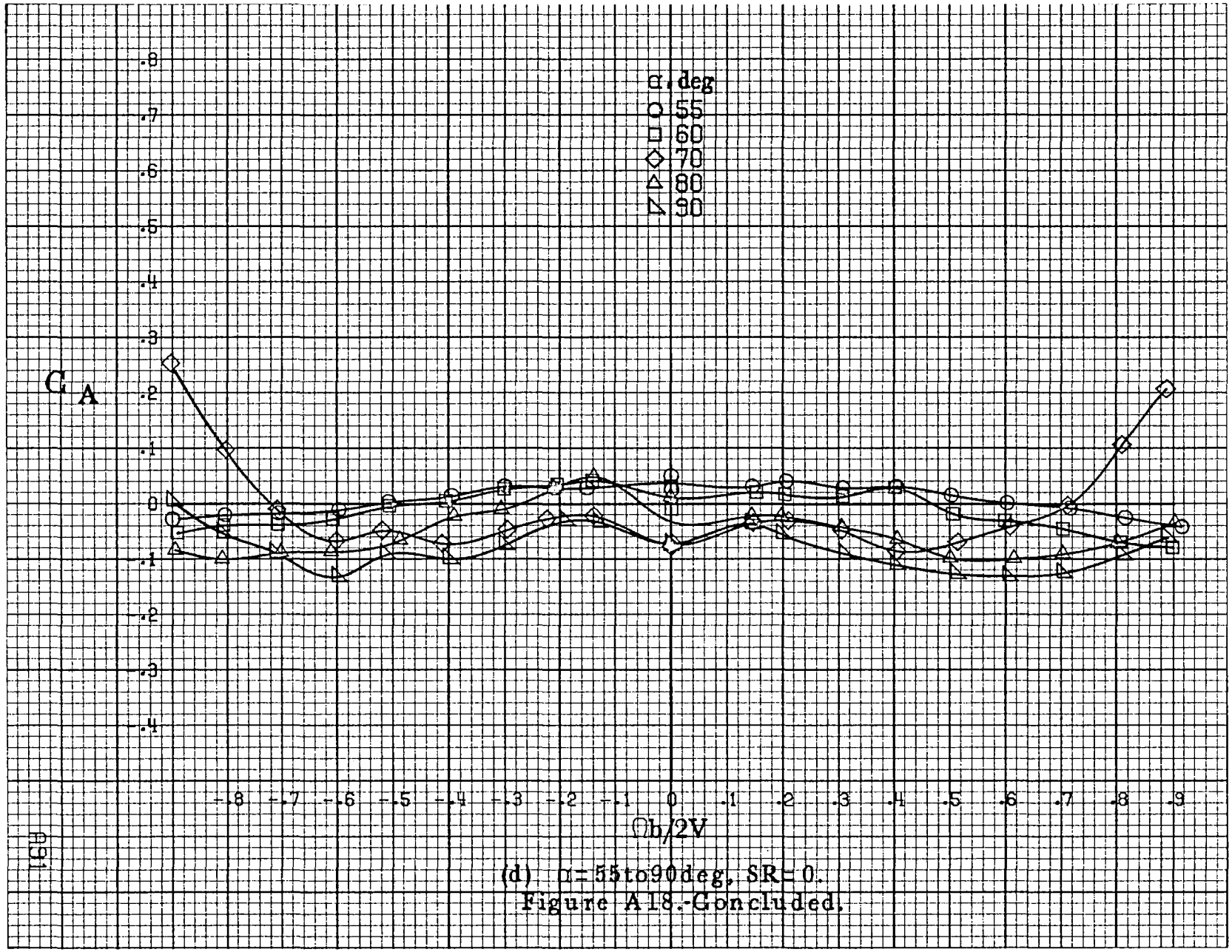

(d) $\alpha = 55$ to 90 deg, SR = 0.

Figure A18.-Concluded.

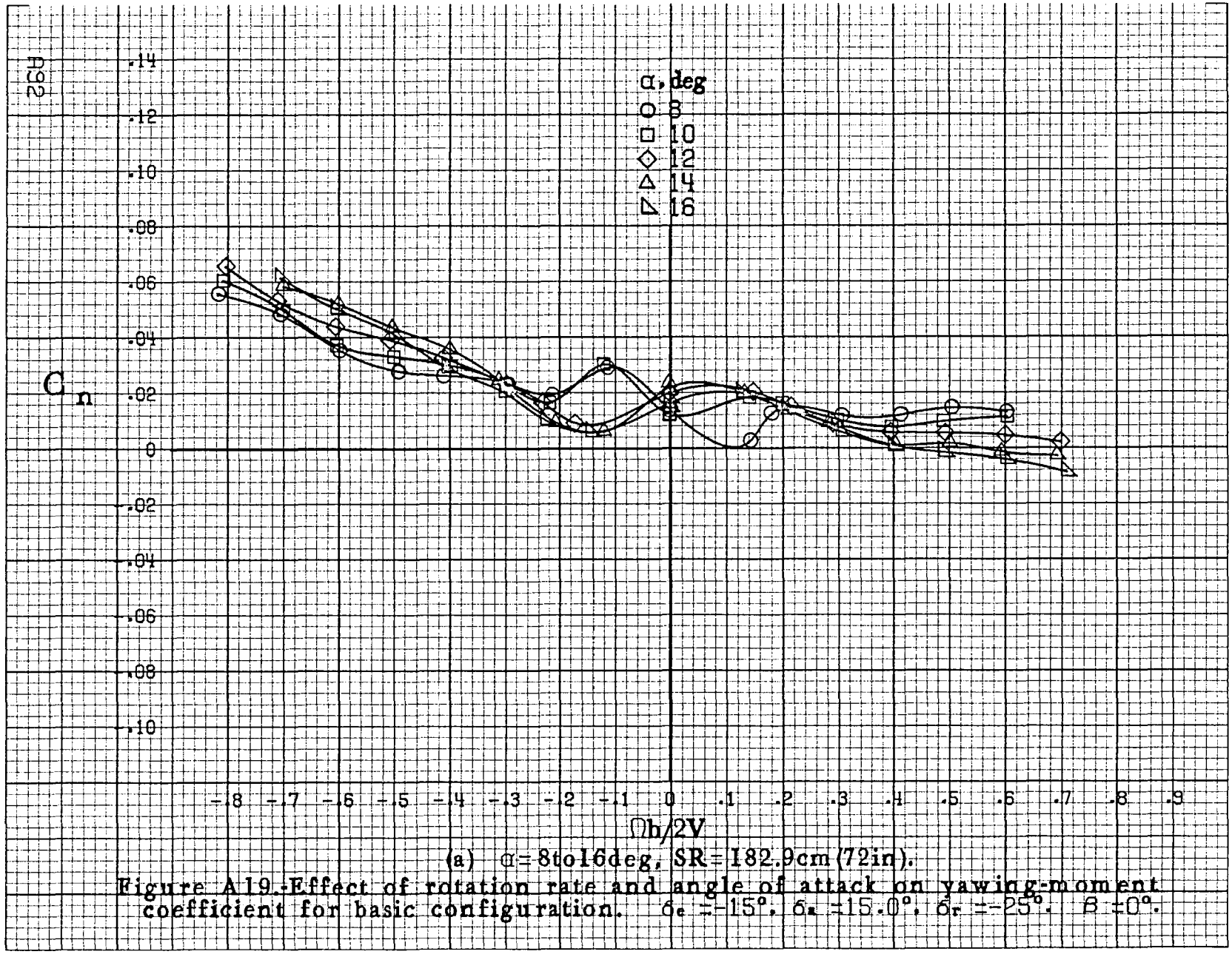

(a) $\alpha = 8$ to 16 deg, SR = 182.9 cm (72 in).

Figure A19.-Effect of rotation rate and angle of attack on yawing-moment coefficient for basic configuration. $\delta_e = -15°$, $\delta_a = 15.0°$, $\delta_r = -25°$, $\beta = 0°$.

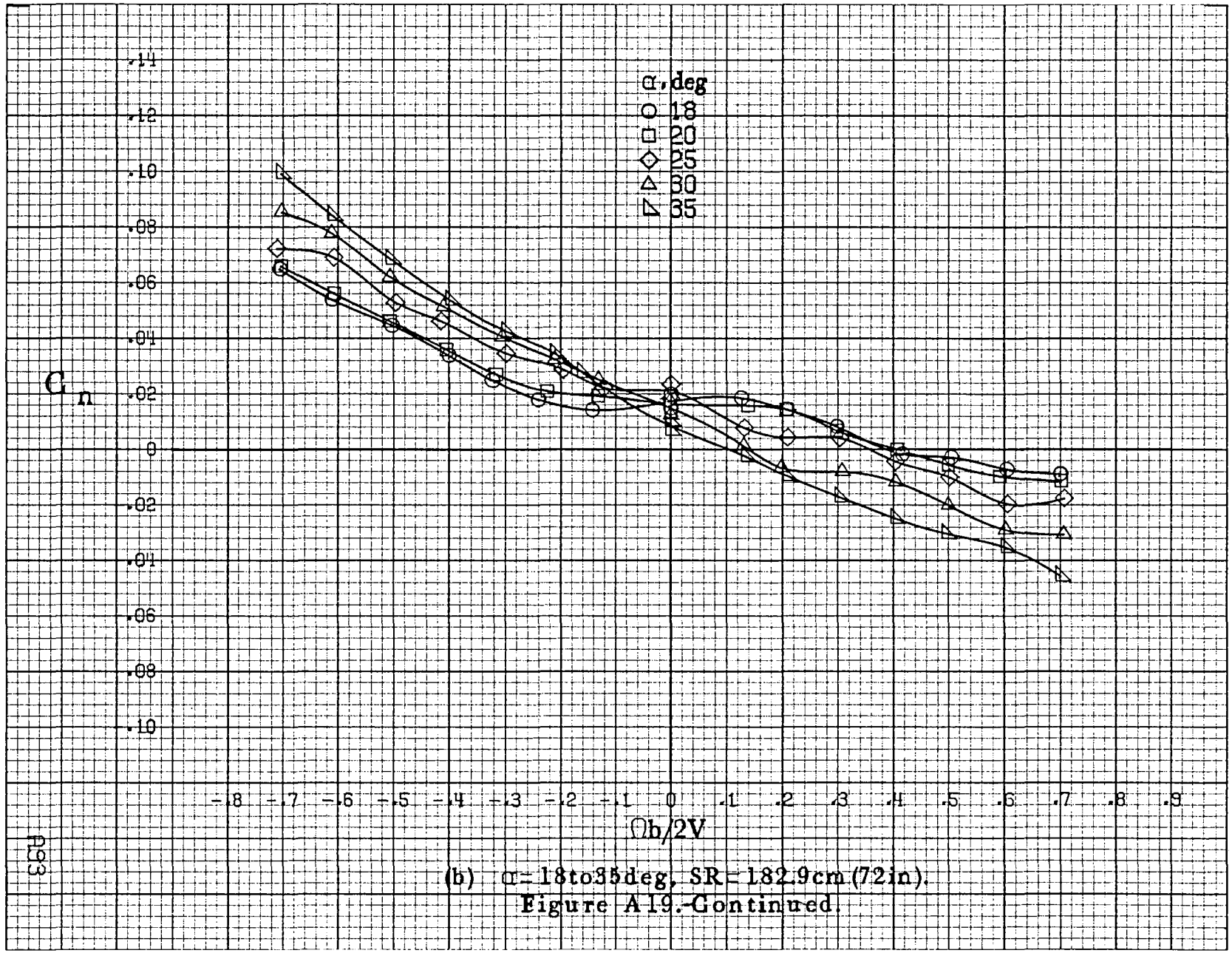

(b) α = 18 to 35 deg, SR = 182.9 cm (72 in).

Figure A19.-Continued.

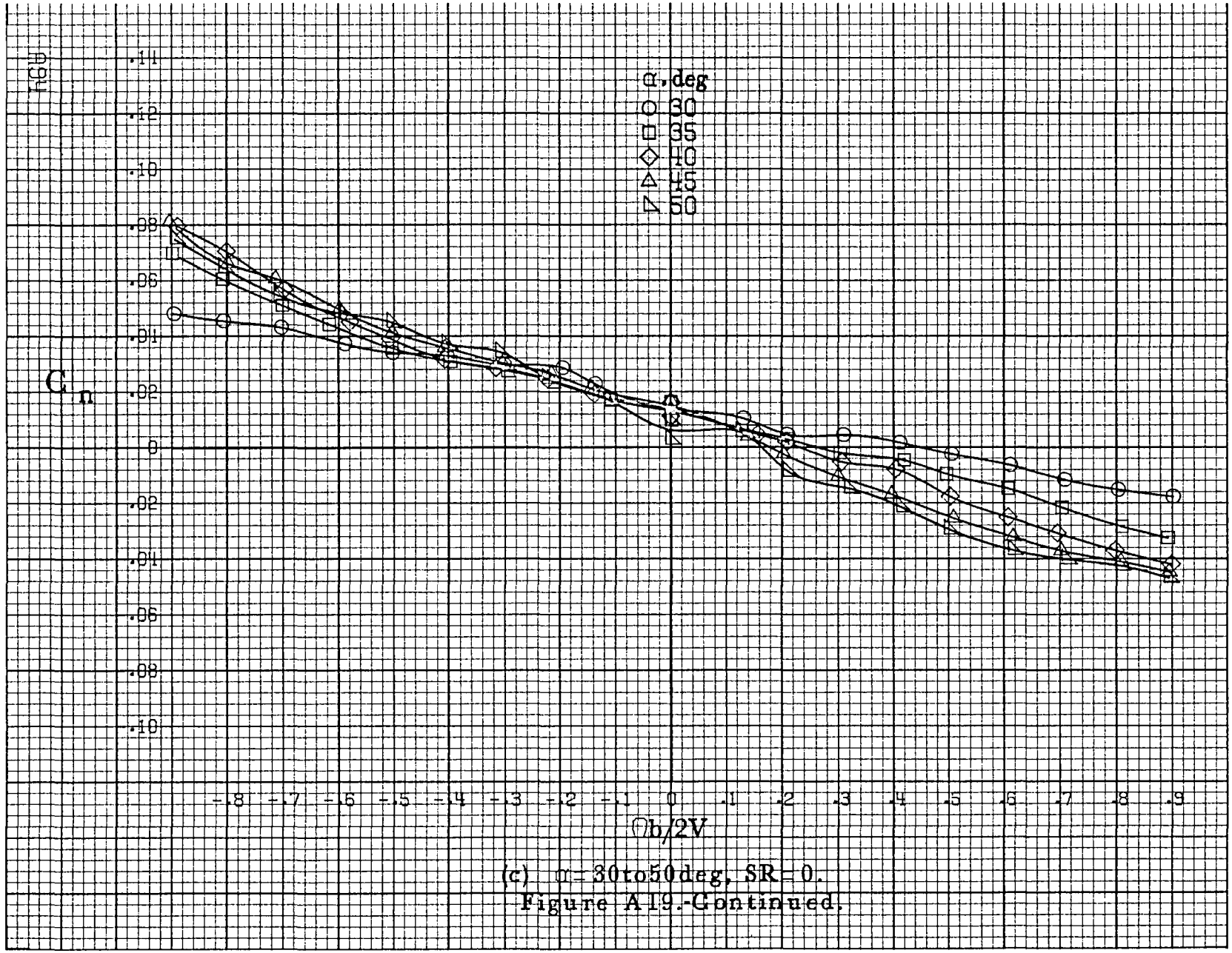

(c) α = 30 to 50 deg, SR = 0.

Figure A19.-Continued.

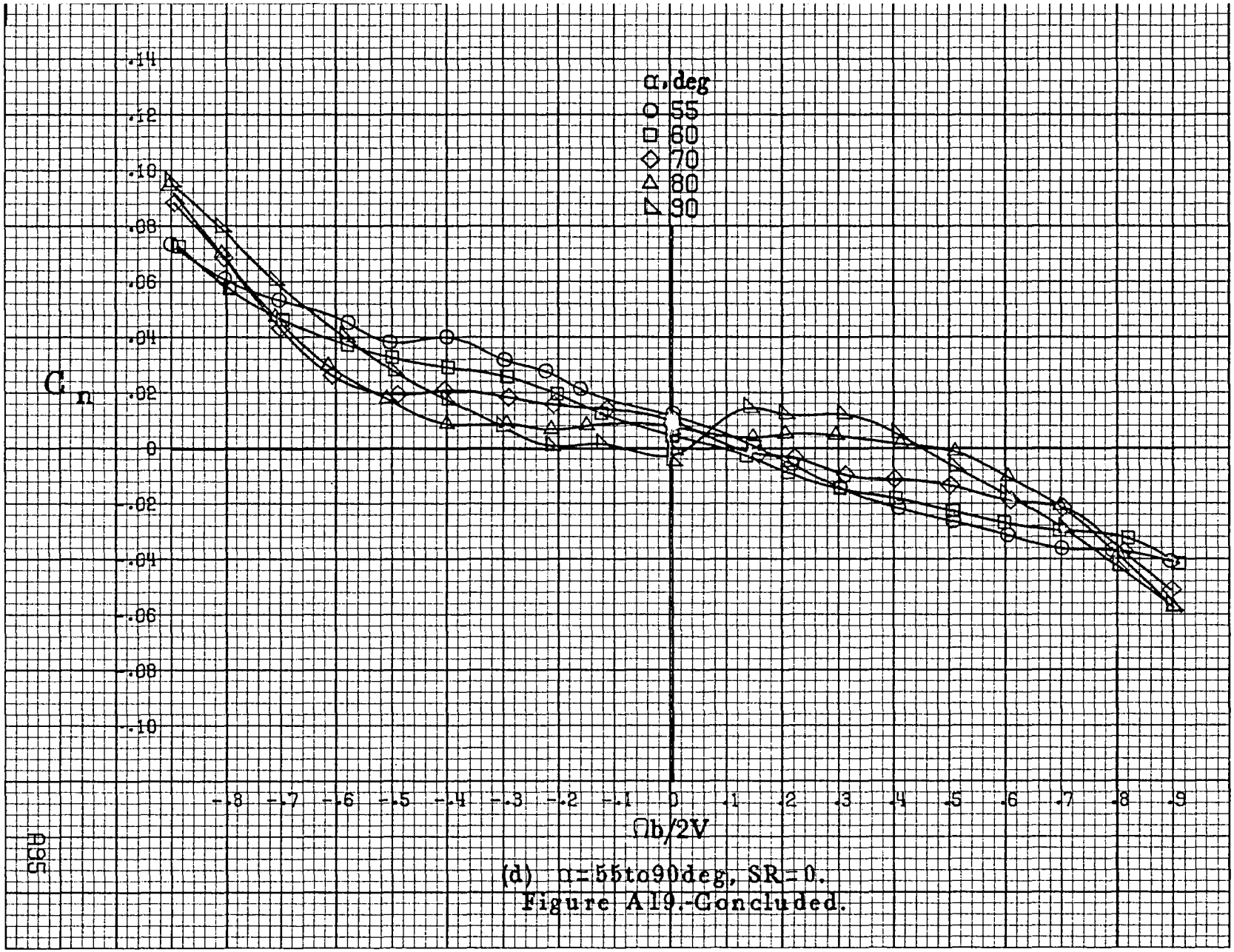

(d) α=55to90deg, SR=0.

Figure A19.-Concluded.

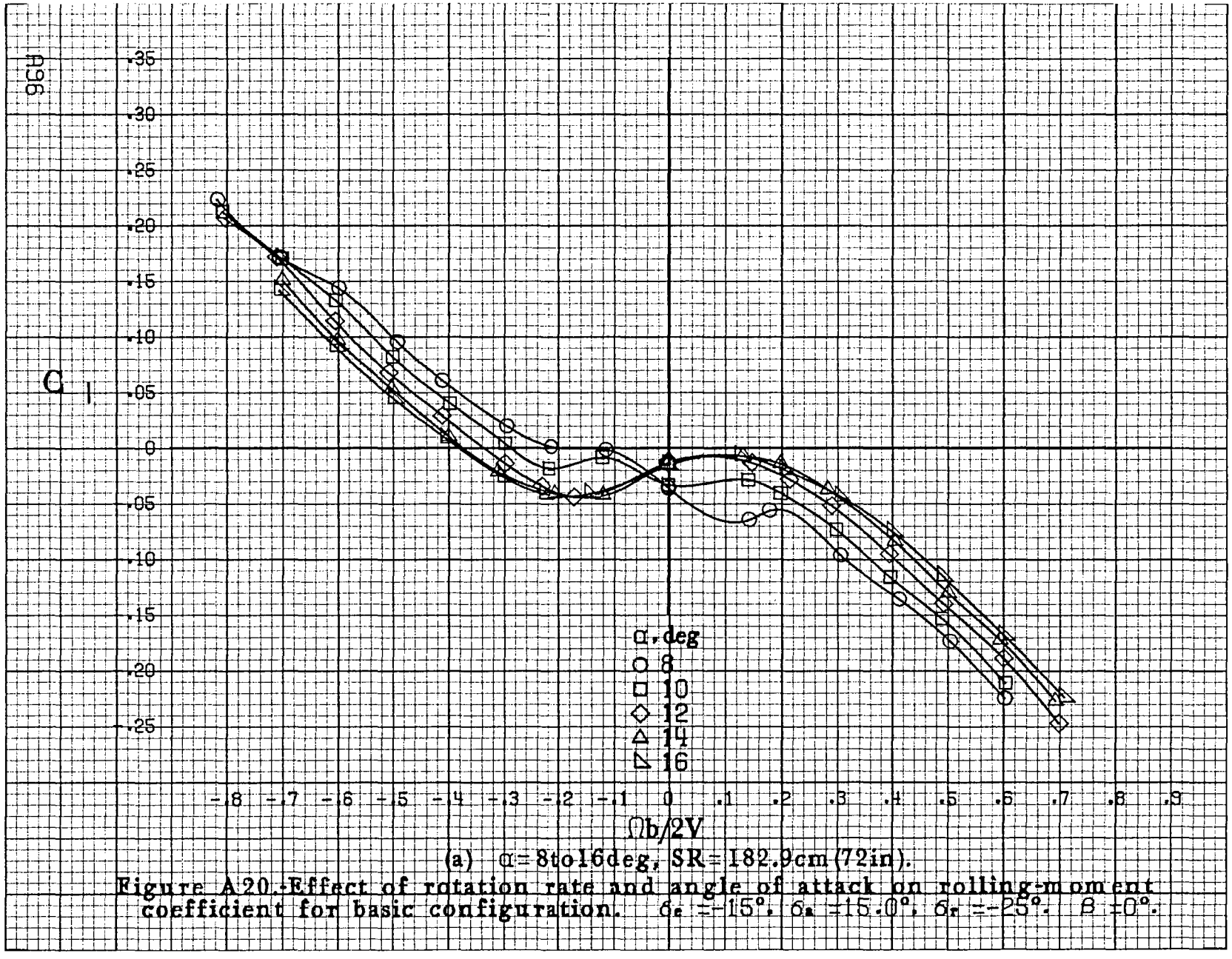

(a) $\alpha = 8$ to 16 deg, SR = 182.9 cm (72 in).

Figure A20.-Effect of rotation rate and angle of attack on rolling-moment coefficient for basic configuration. $\delta_e = -15°$, $\delta_a = 15.0°$, $\delta_r = -25°$, $\beta = 0°$.

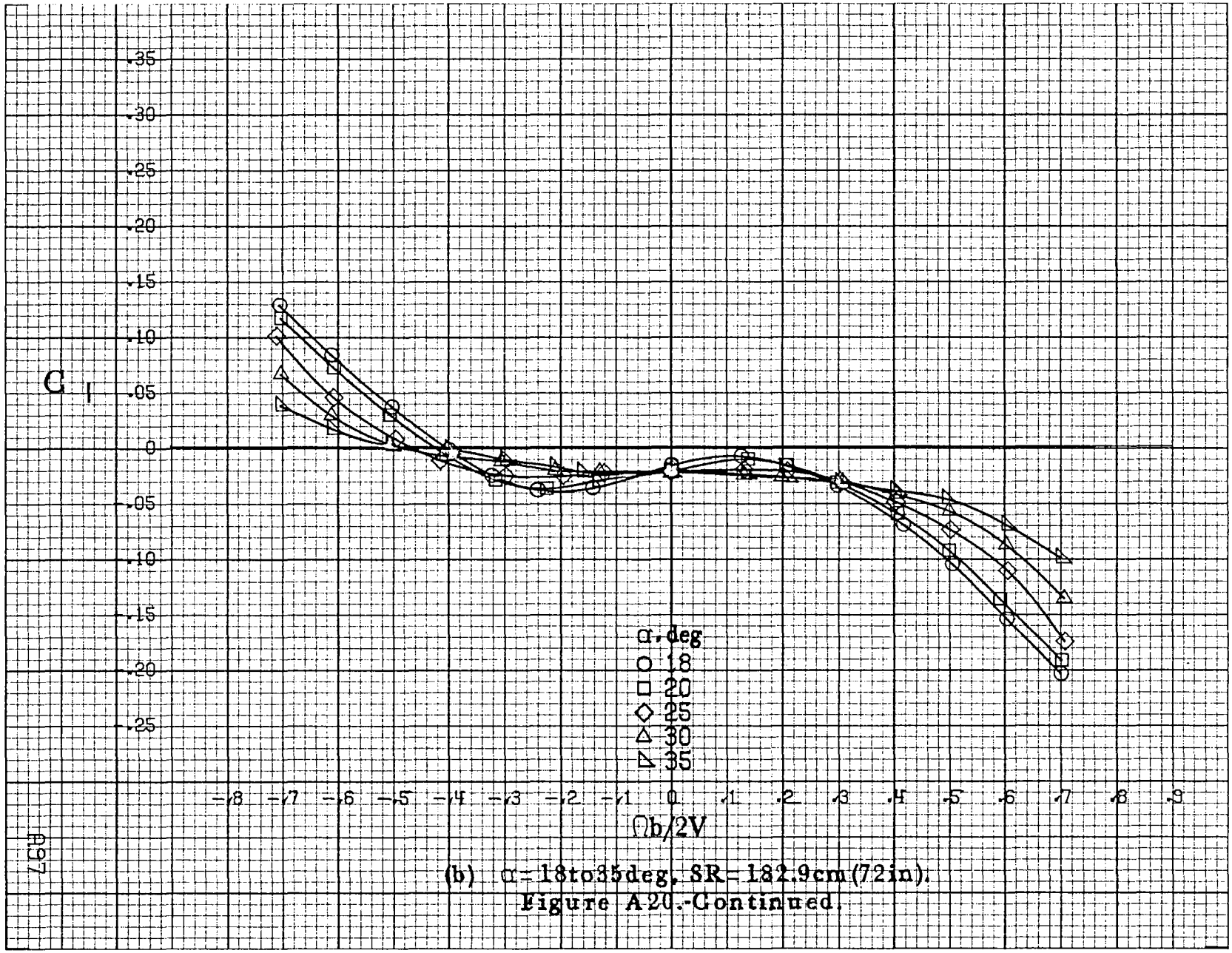

(b) α = 18 to 35 deg, SR = 182.9 cm (72 in).

Figure A20.-Continued.

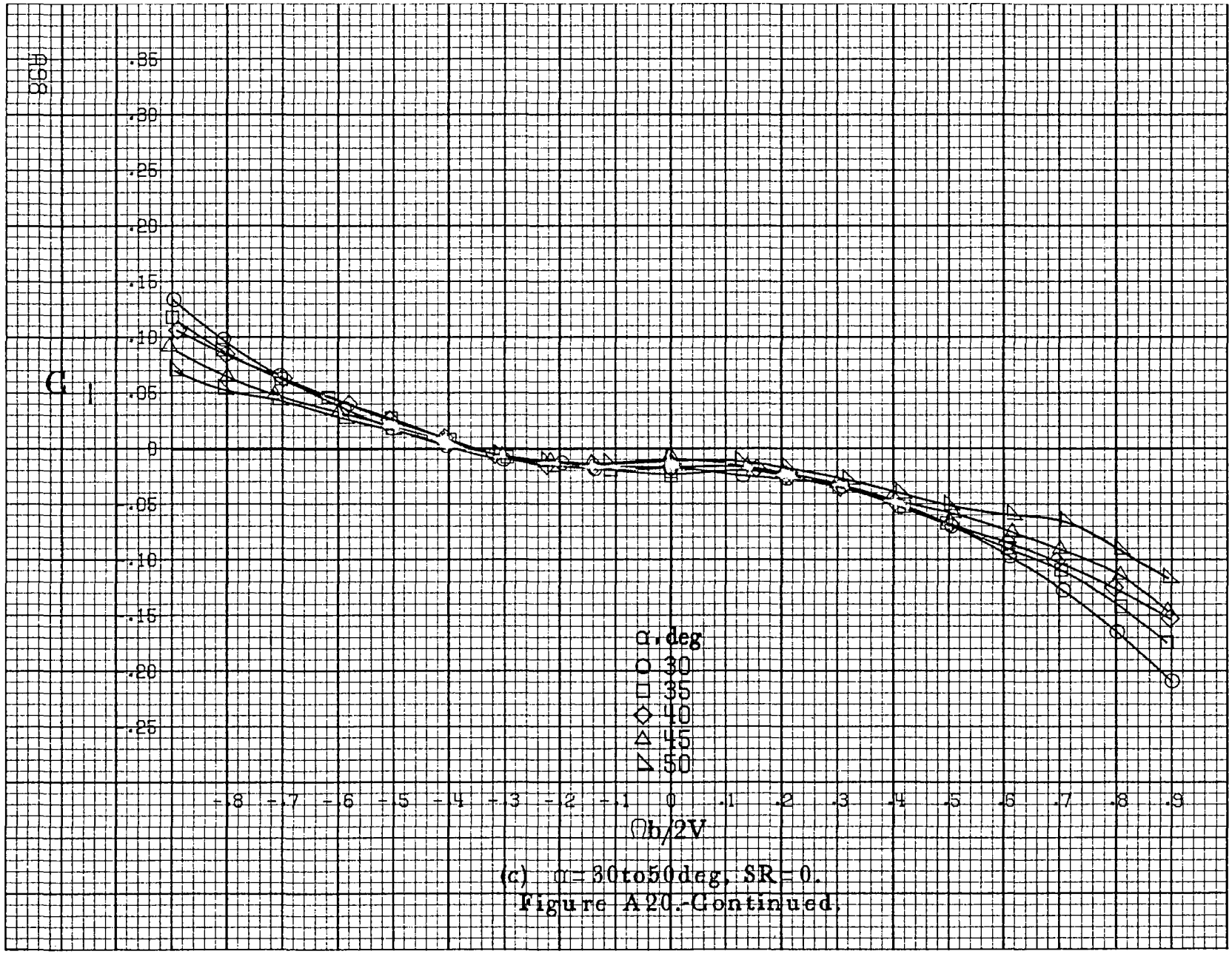

(c) $\alpha = 30$ to 50 deg, SR = 0.

Figure A20.-Continued.

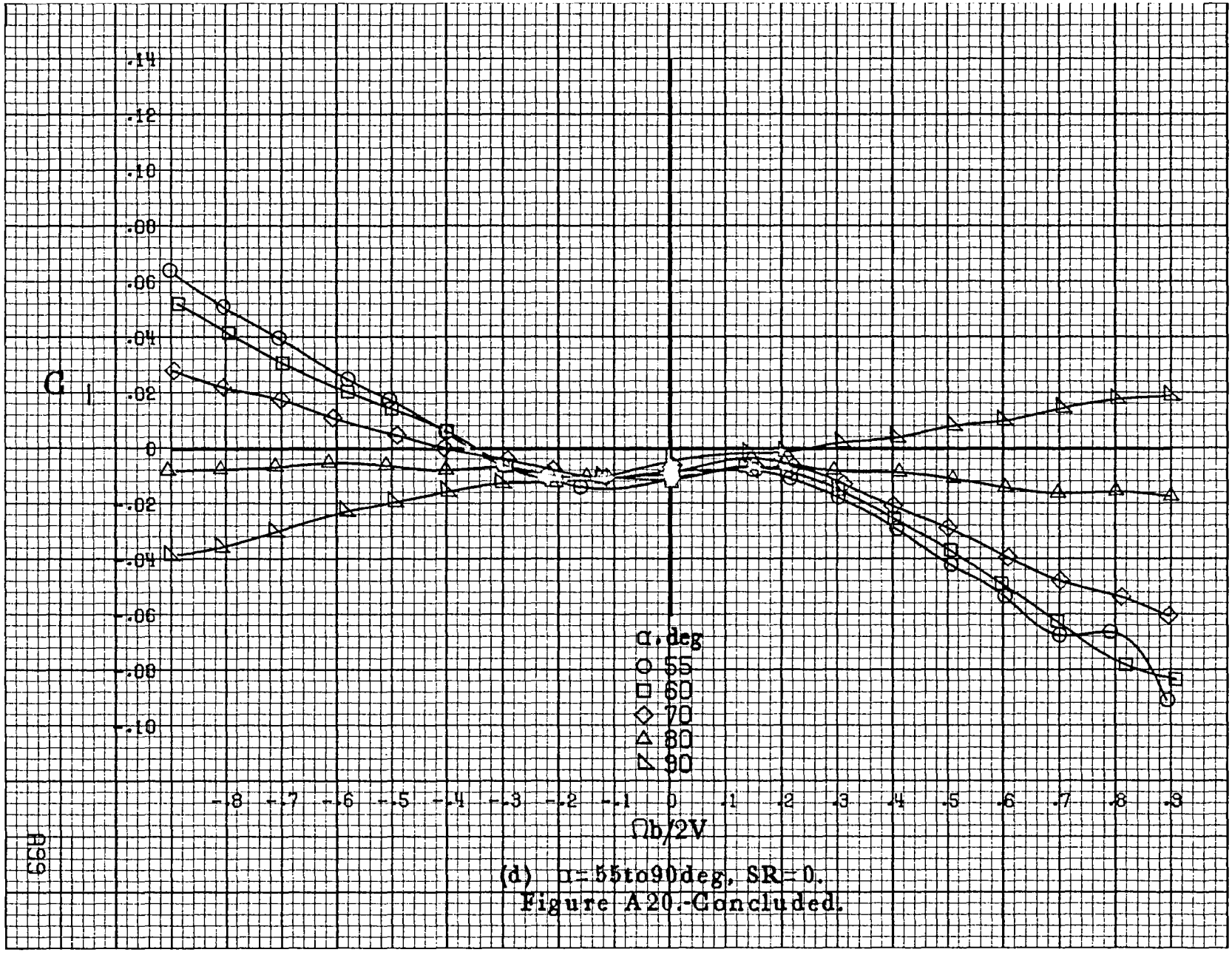

(d) $\alpha = 55$ to 90 deg, SR = 0.

Figure A20.-Concluded.

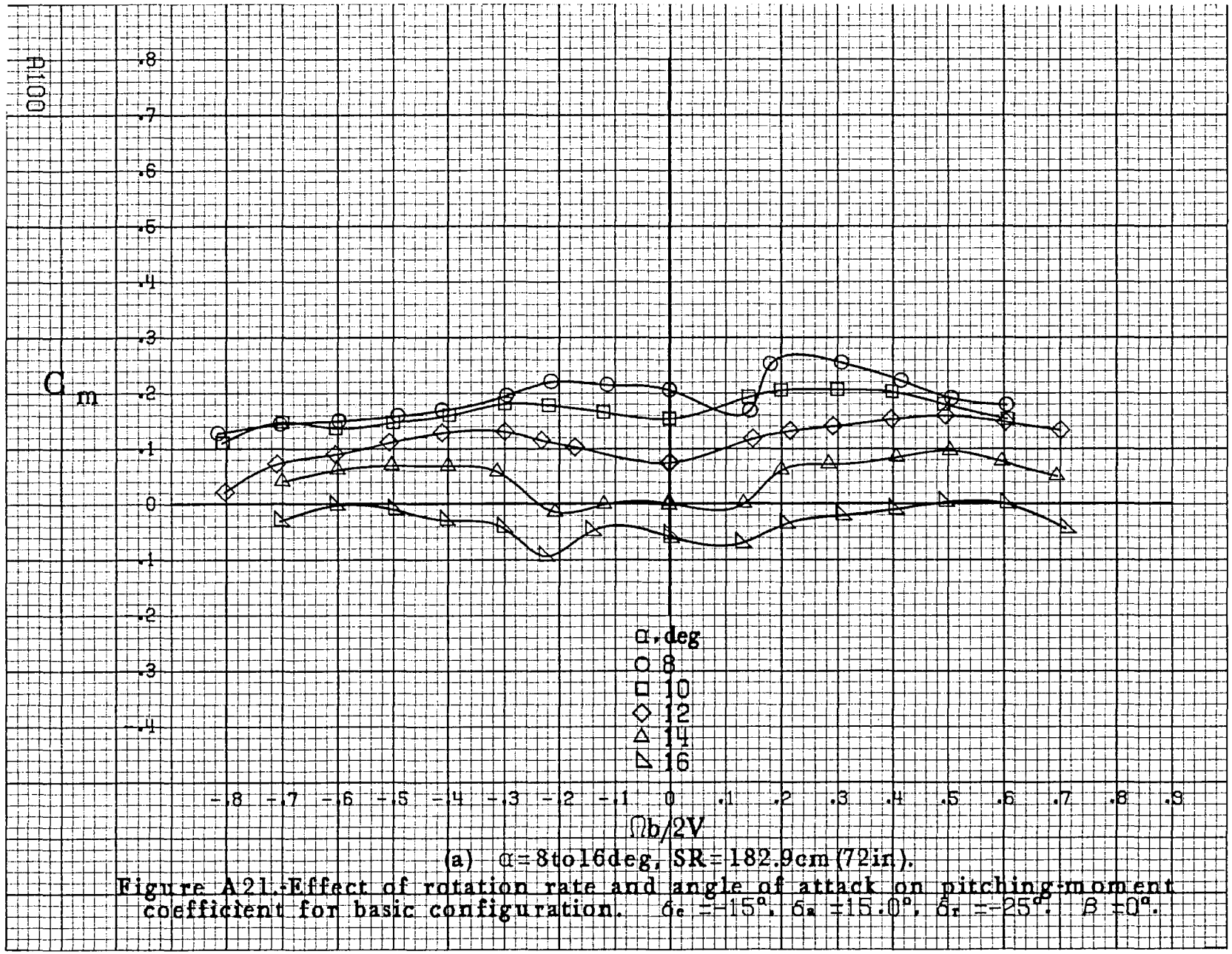

(a) α=8to16deg, SR=182.9cm(72in.).

Figure A21.-Effect of rotation rate and angle of attack on pitching-moment coefficient for basic configuration. $\delta_e = -15°$, $\delta_a = 15.0°$, $\delta_r = -25°$. $\beta = 0°$.

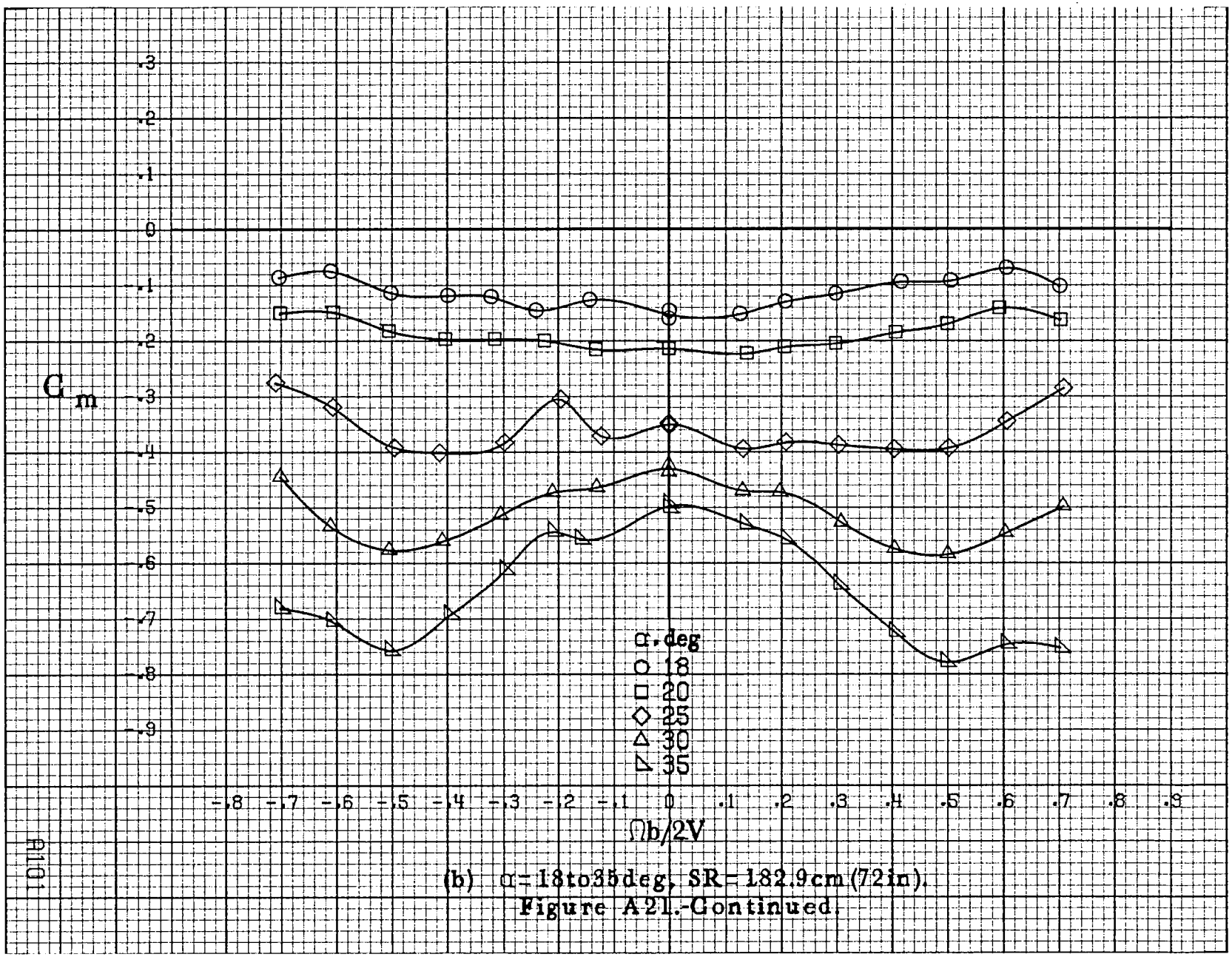

B10-1

(b) α = 18 to 35 deg, SR = 182.9 cm (72 in).

Figure A21.-Continued.

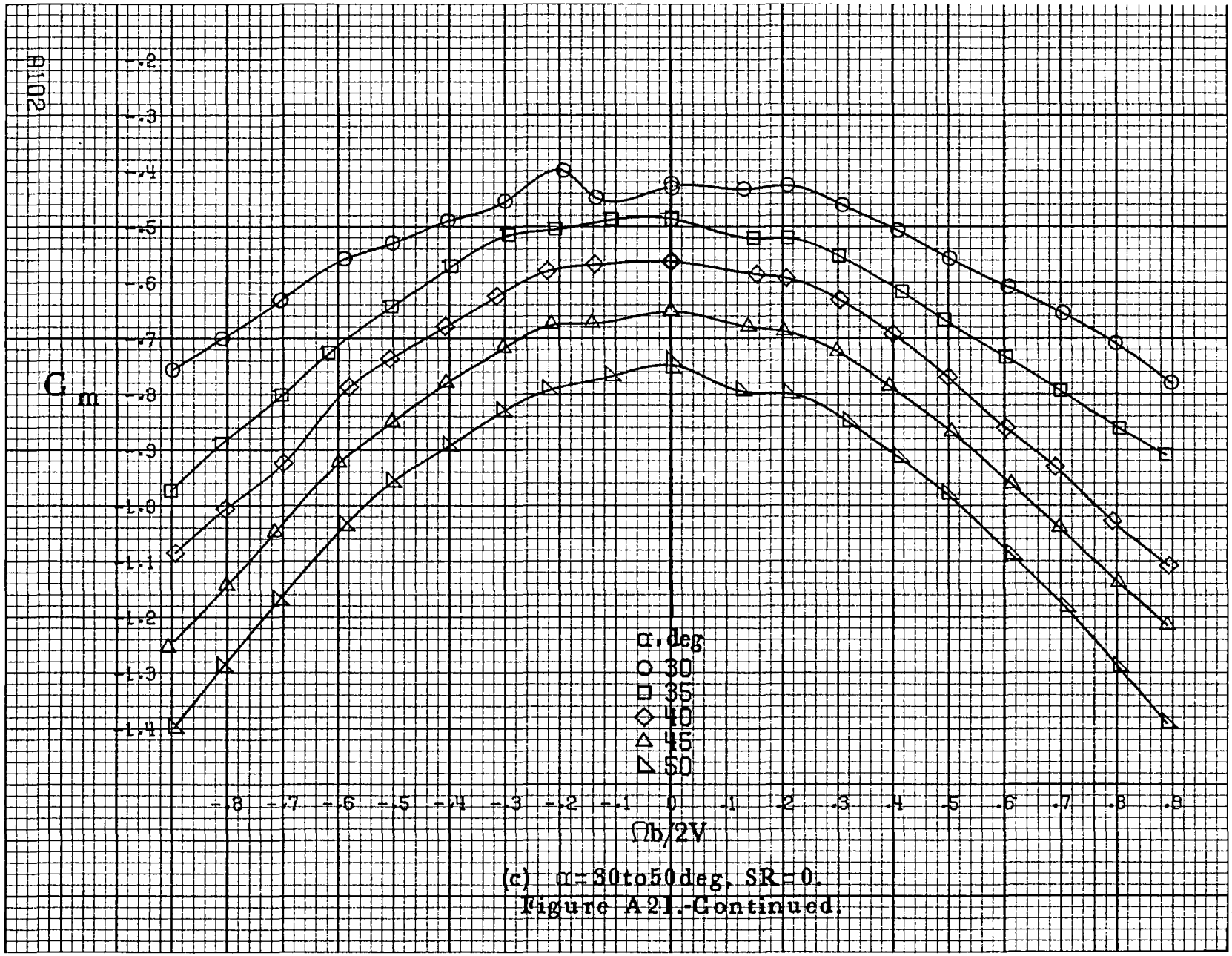

(c) α=30to50deg, SR=0.

Figure A21.-Continued.

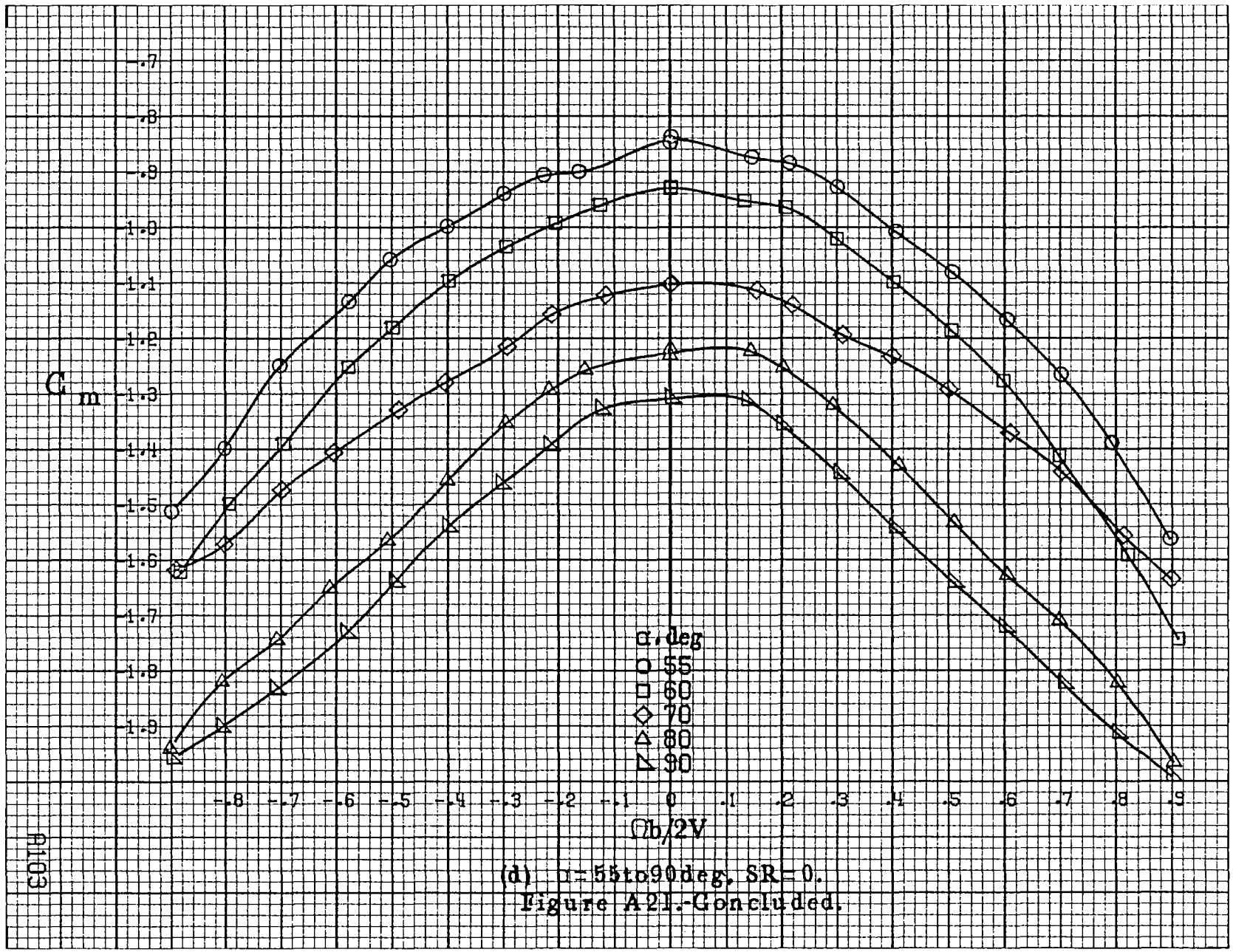

(d) α = 55 to 90 deg, SR = 0.

Figure A21.-Concluded.

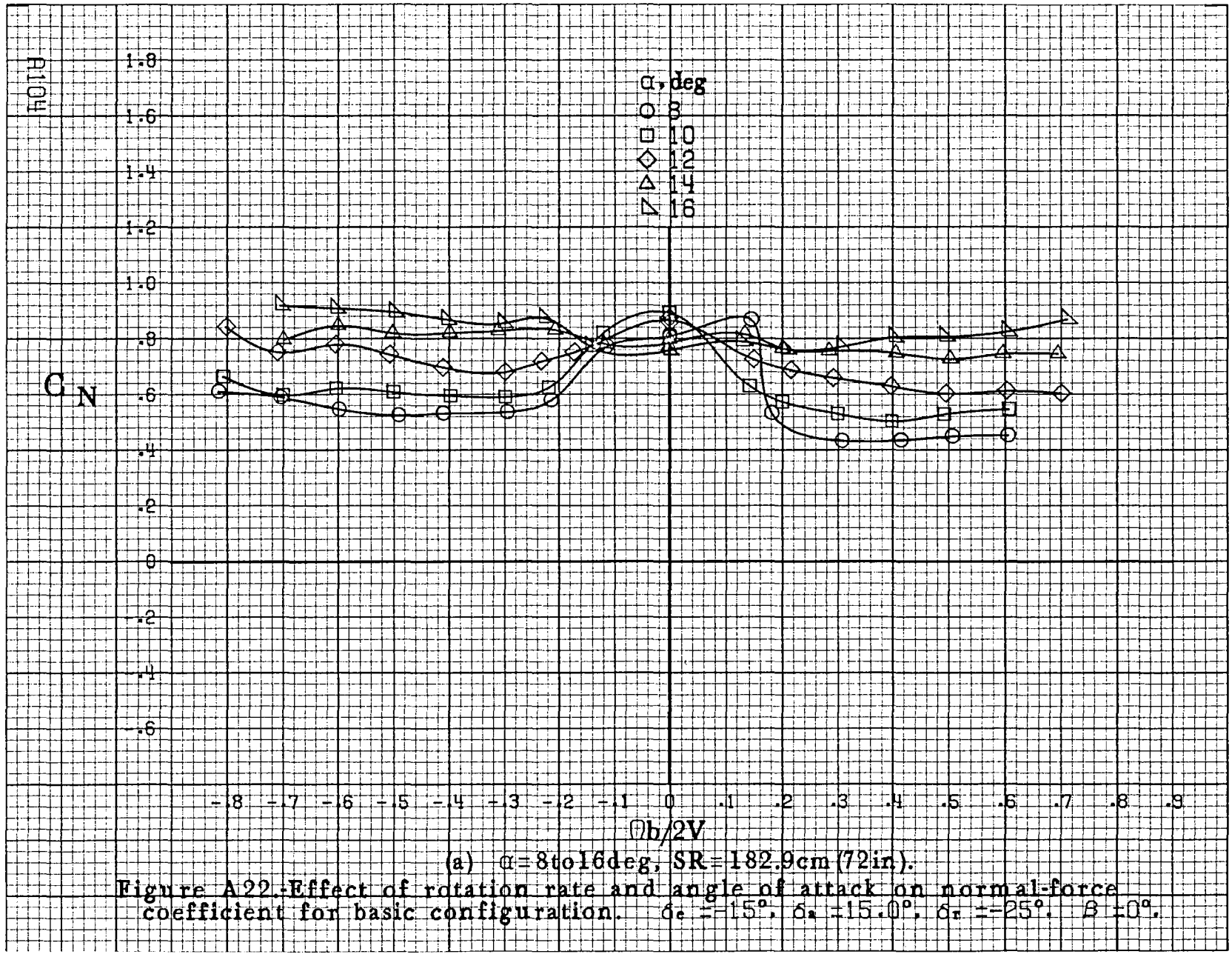

(a) α = 8 to 16 deg, SR = 182.9 cm (72 in.).

Figure A22.-Effect of rotation rate and angle of attack on normal-force coefficient for basic configuration. $\delta_e = -15°$, $\delta_a = 15.0°$, $\delta_r = -25°$, $\beta = 0°$.

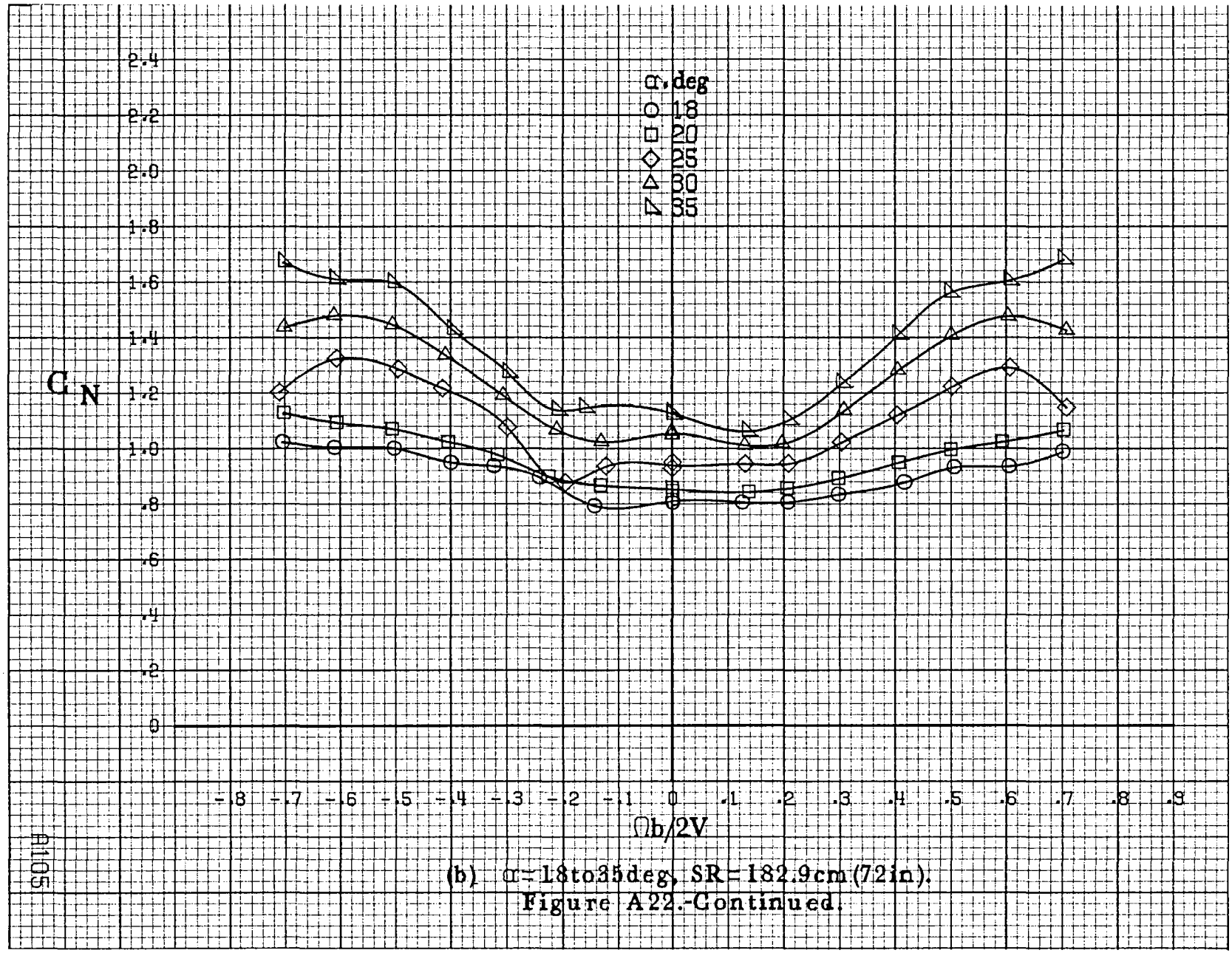

(b) α = 18 to 35 deg, SR = 182.9 cm (72 in).

Figure A22.-Continued.

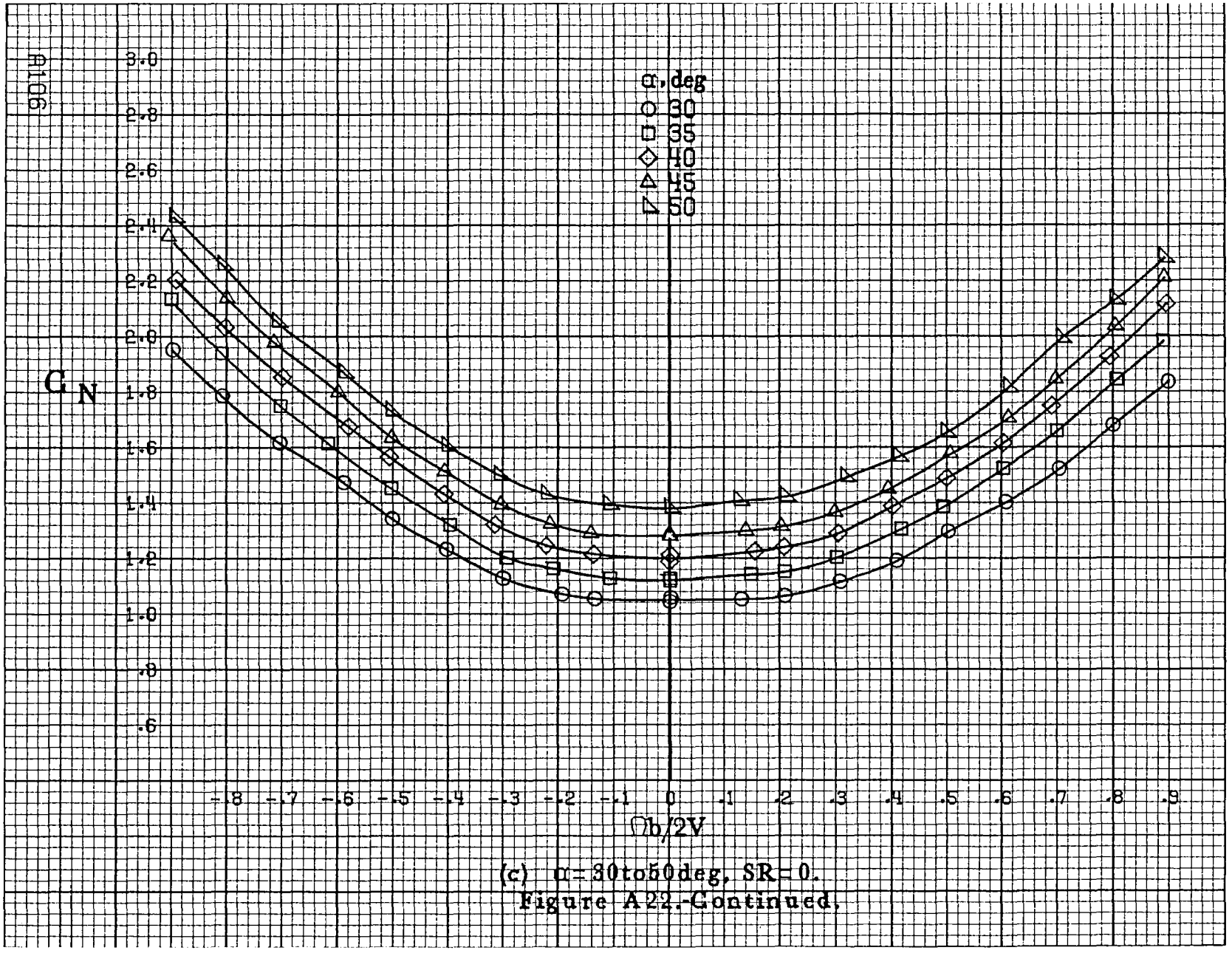

(c) α = 30 to 50 deg, SR = 0.

Figure A22.-Continued.

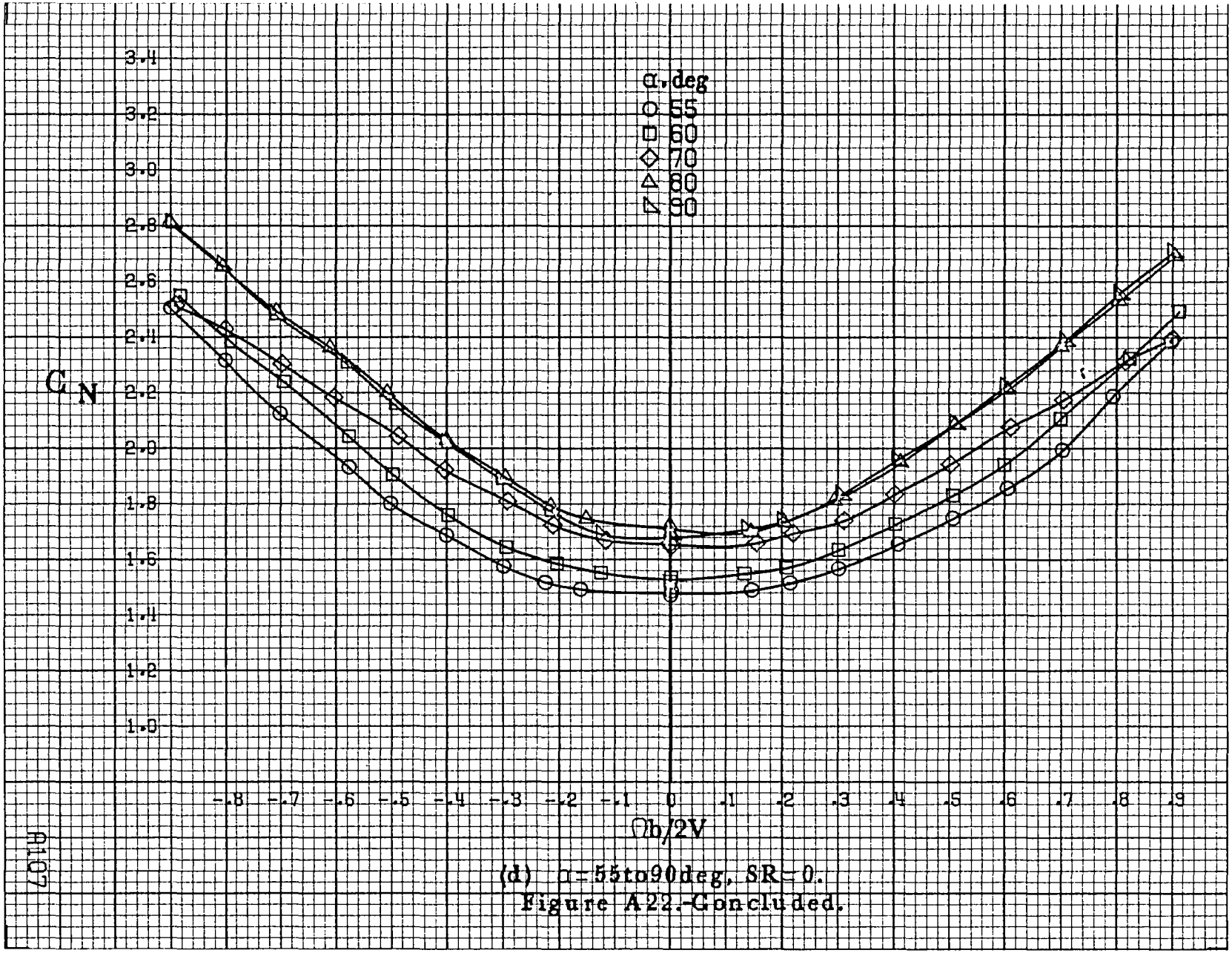

(d) $\alpha = 55$ to 90 deg, $SR = 0$.

Figure A22.-Concluded.

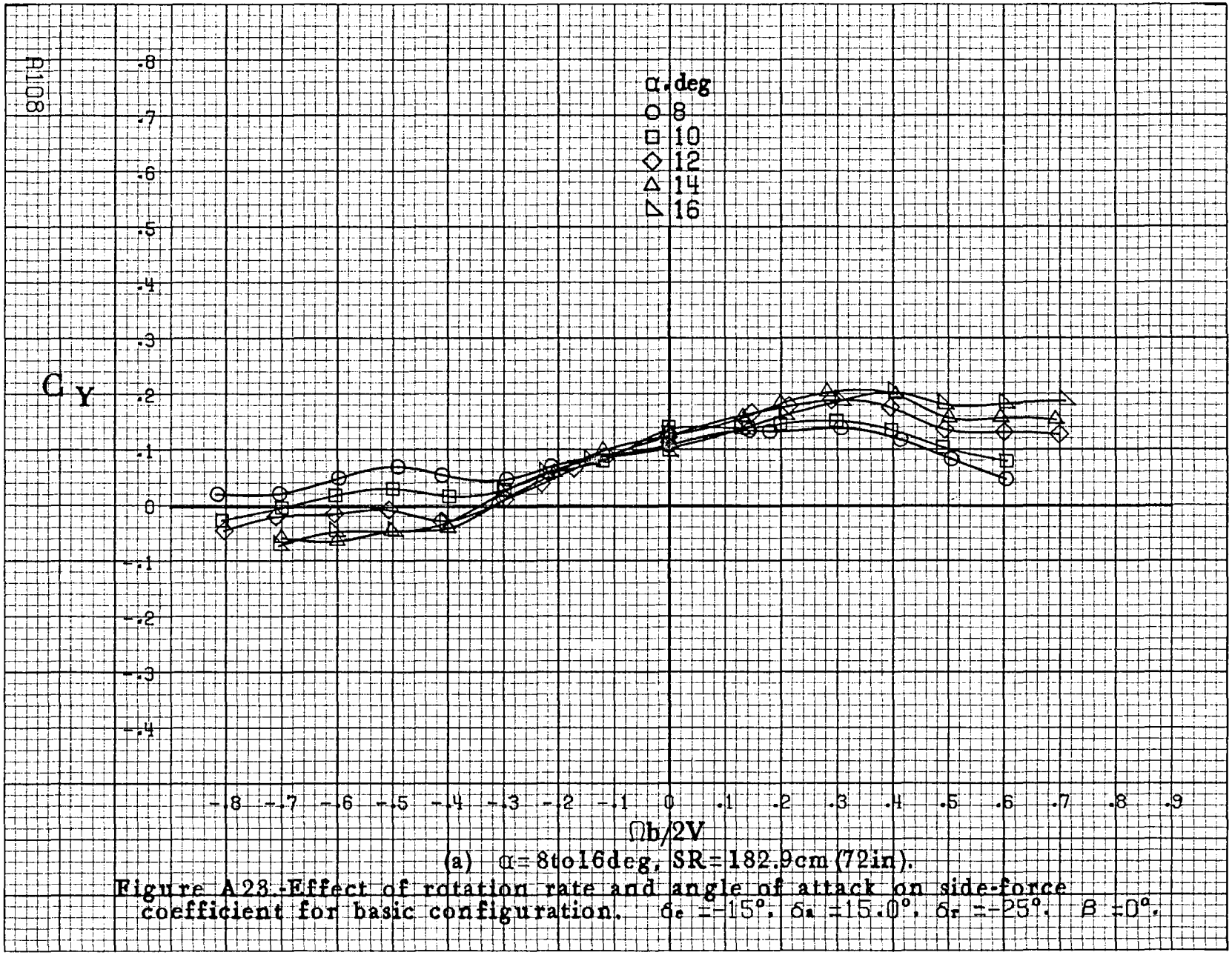

(a) $\alpha = 8$ to 16deg, SR = 182.9cm (72in).

Figure A23.-Effect of rotation rate and angle of attack on side-force coefficient for basic configuration. $\delta_e = -15°$, $\delta_a = 15.0°$, $\delta_r = -25°$, $\beta = 0°$.

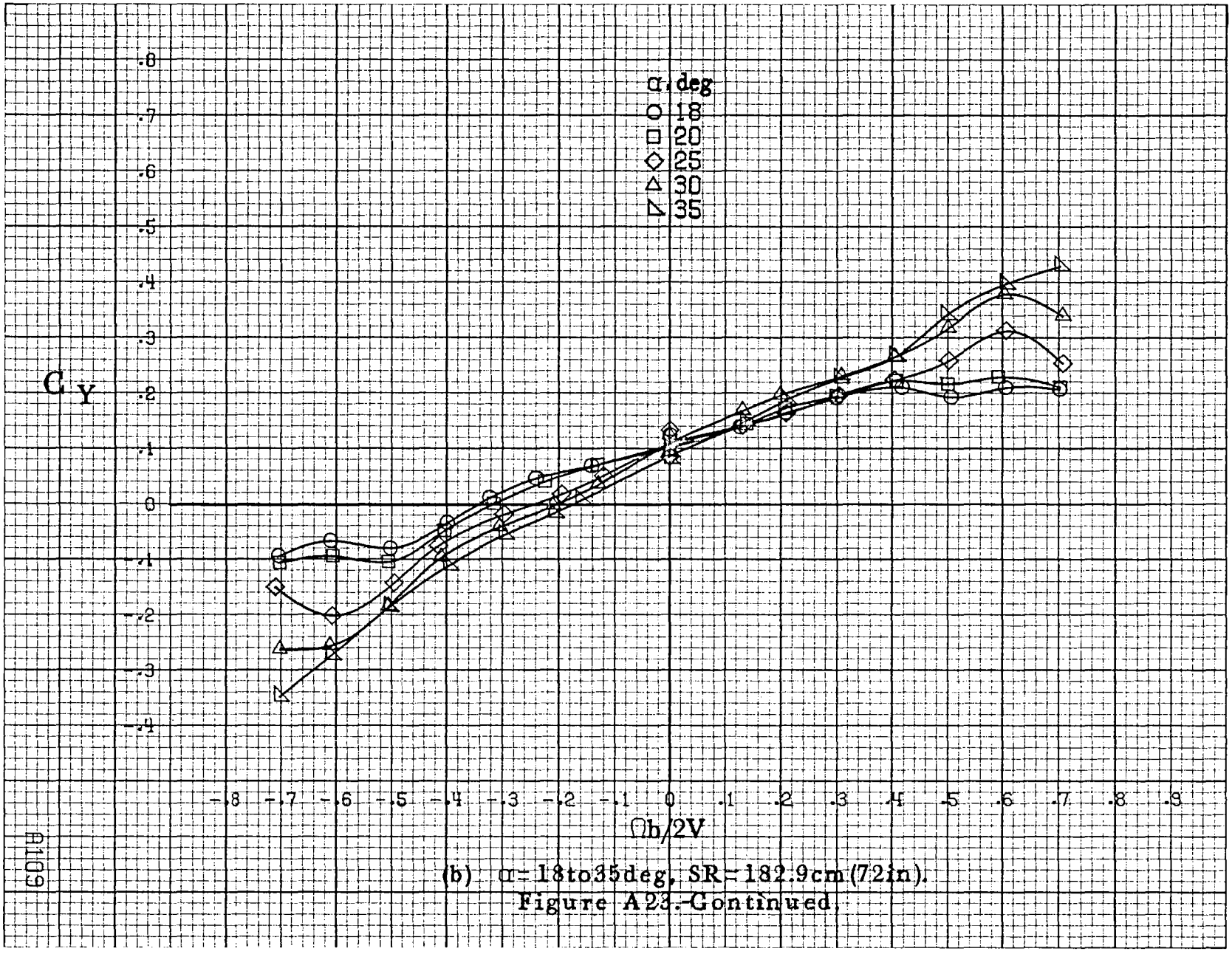

(b) α = 18 to 35 deg, SR = 182.9 cm (72 in).

Figure A23.-Continued.

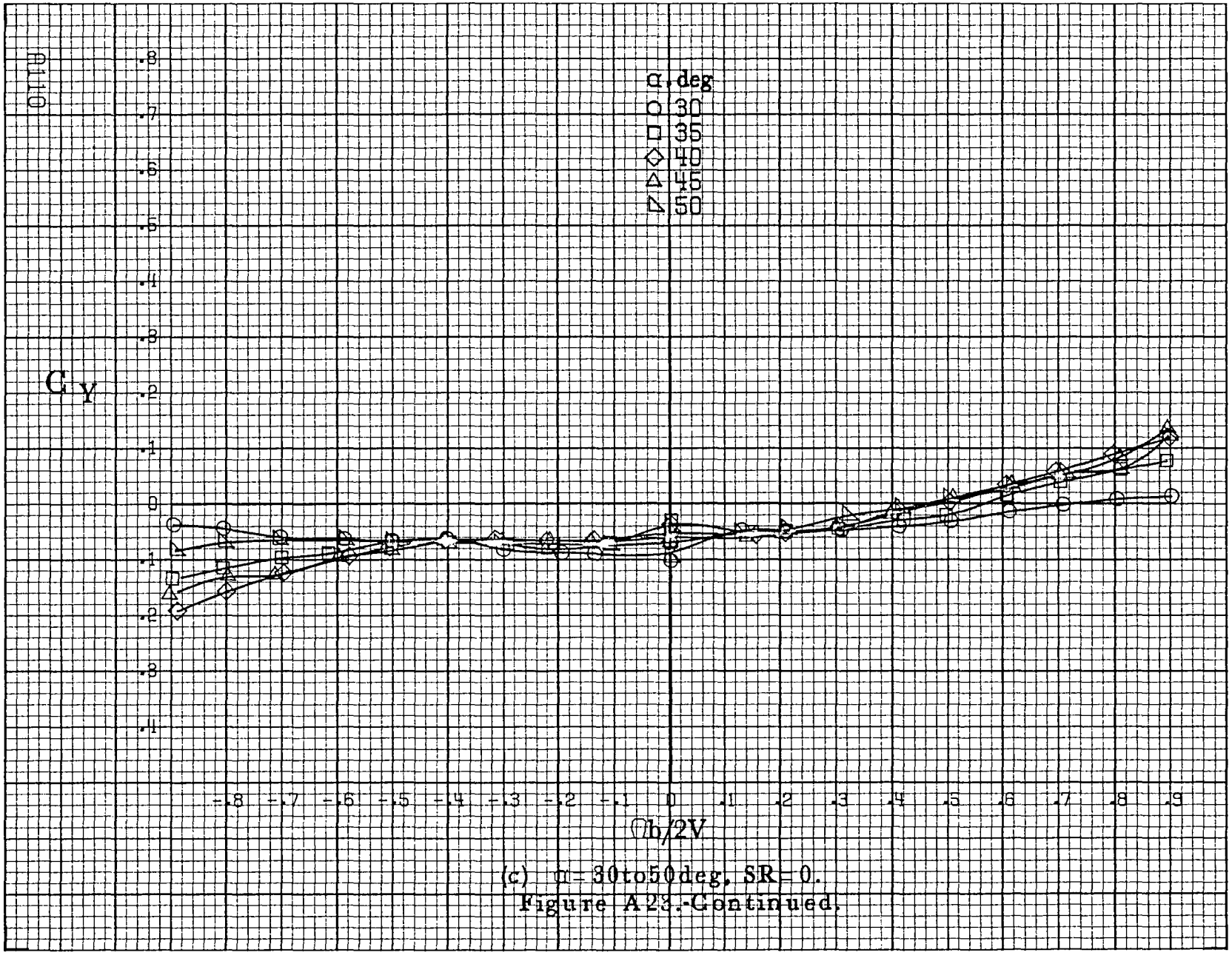

(c) $\alpha = 30$ to 50 deg, SR = 0.

Figure A23.-Continued.

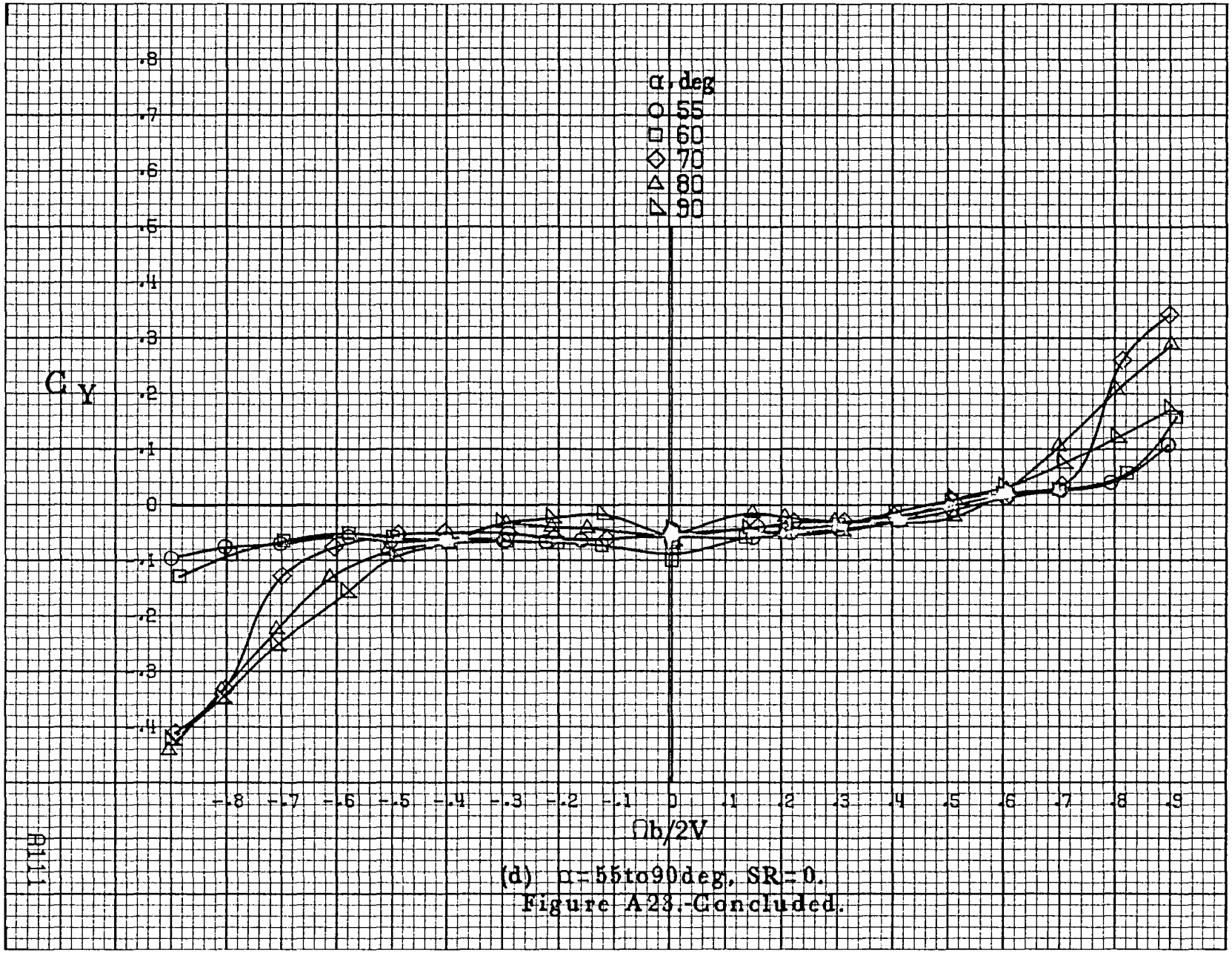

(d) α=55to90deg, SR=0.

Figure A23.-Concluded.

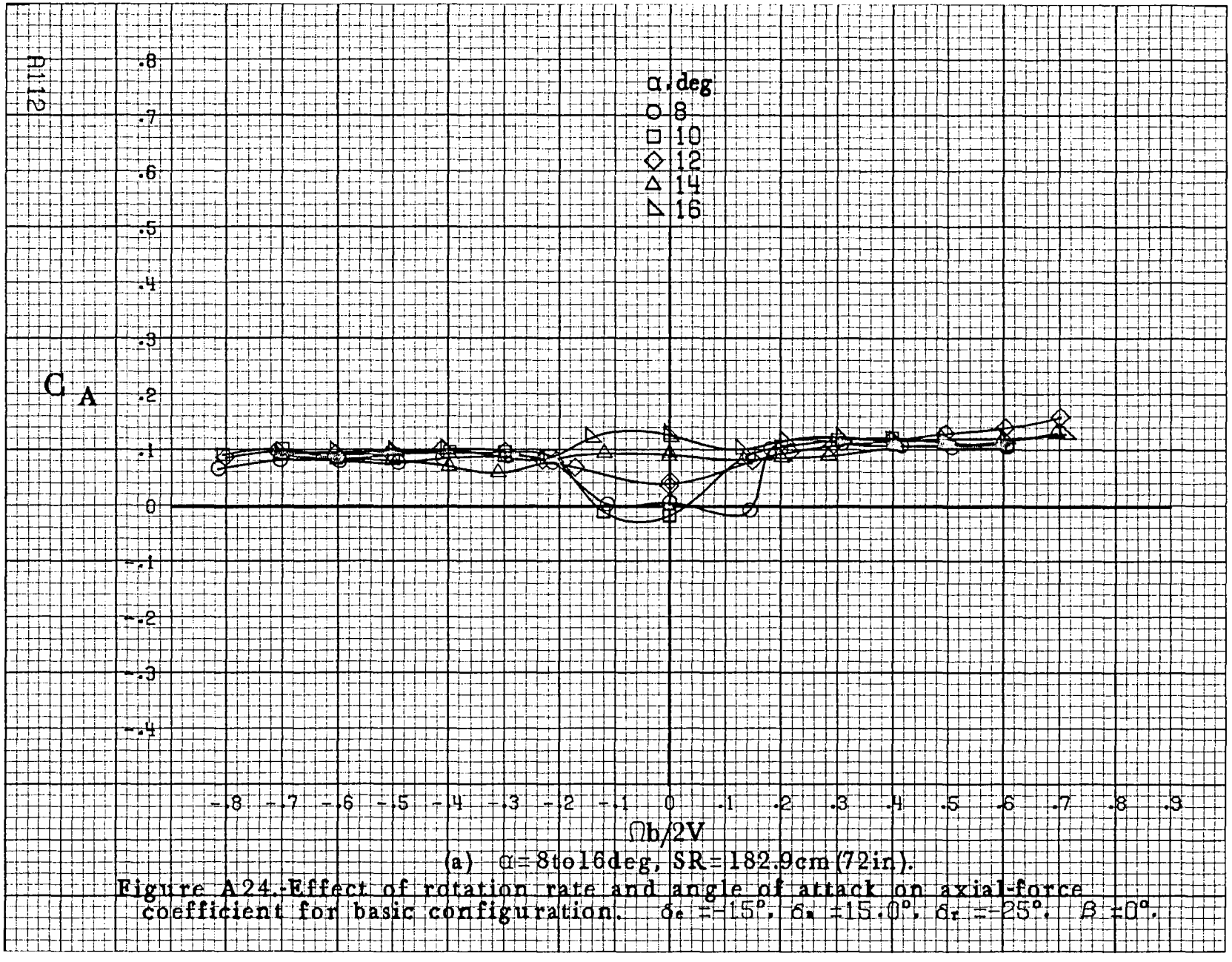

(a) α = 8 to 16 deg, SR = 182.9 cm (72 in.).

Figure A24.-Effect of rotation rate and angle of attack on axial-force coefficient for basic configuration. δ_e = -15°, δ_a = 15.0°, δ_r = 25°, β = 0°.

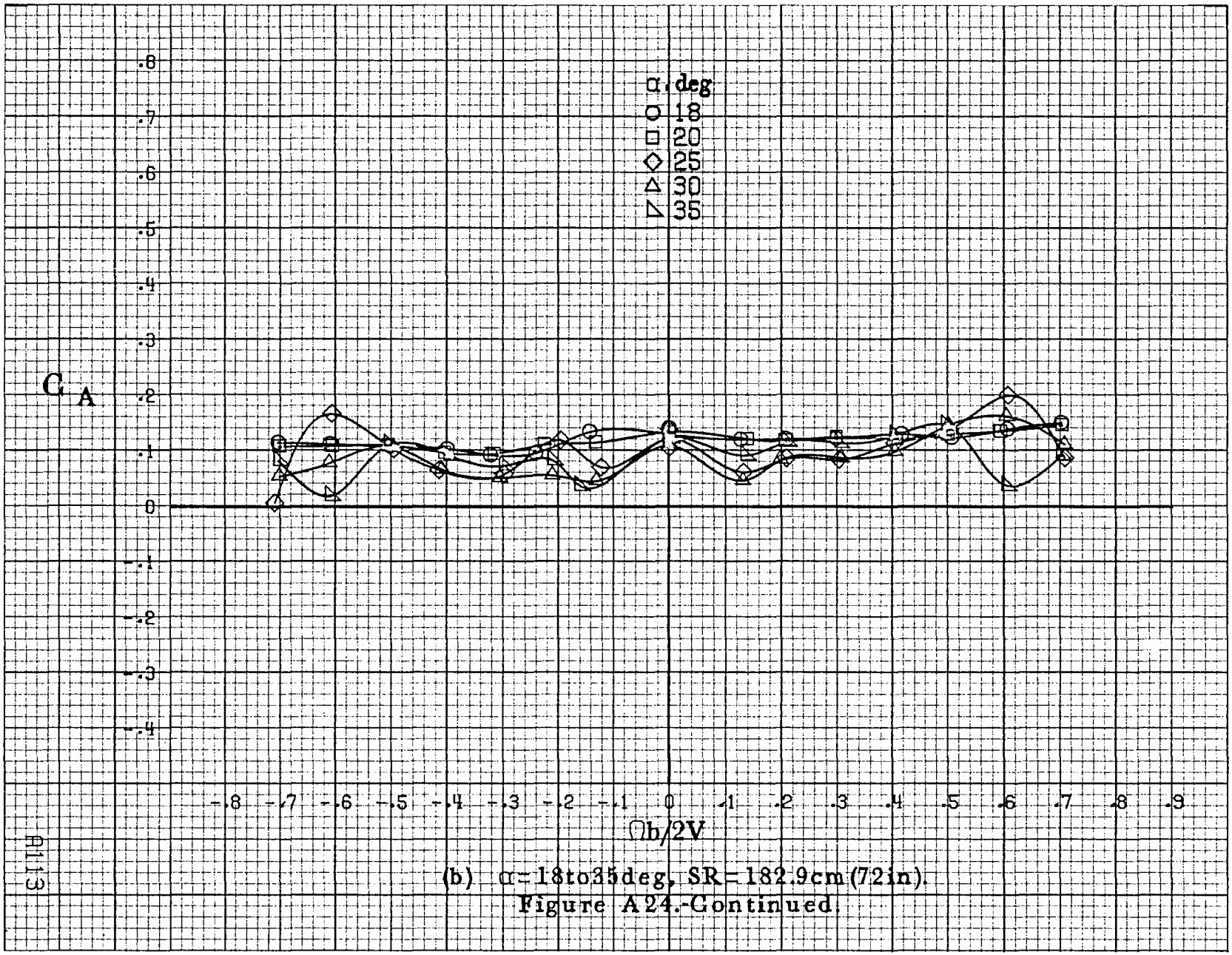

(b) α=18to35deg, SR=182.9cm(72in).

Figure A24.-Continued.

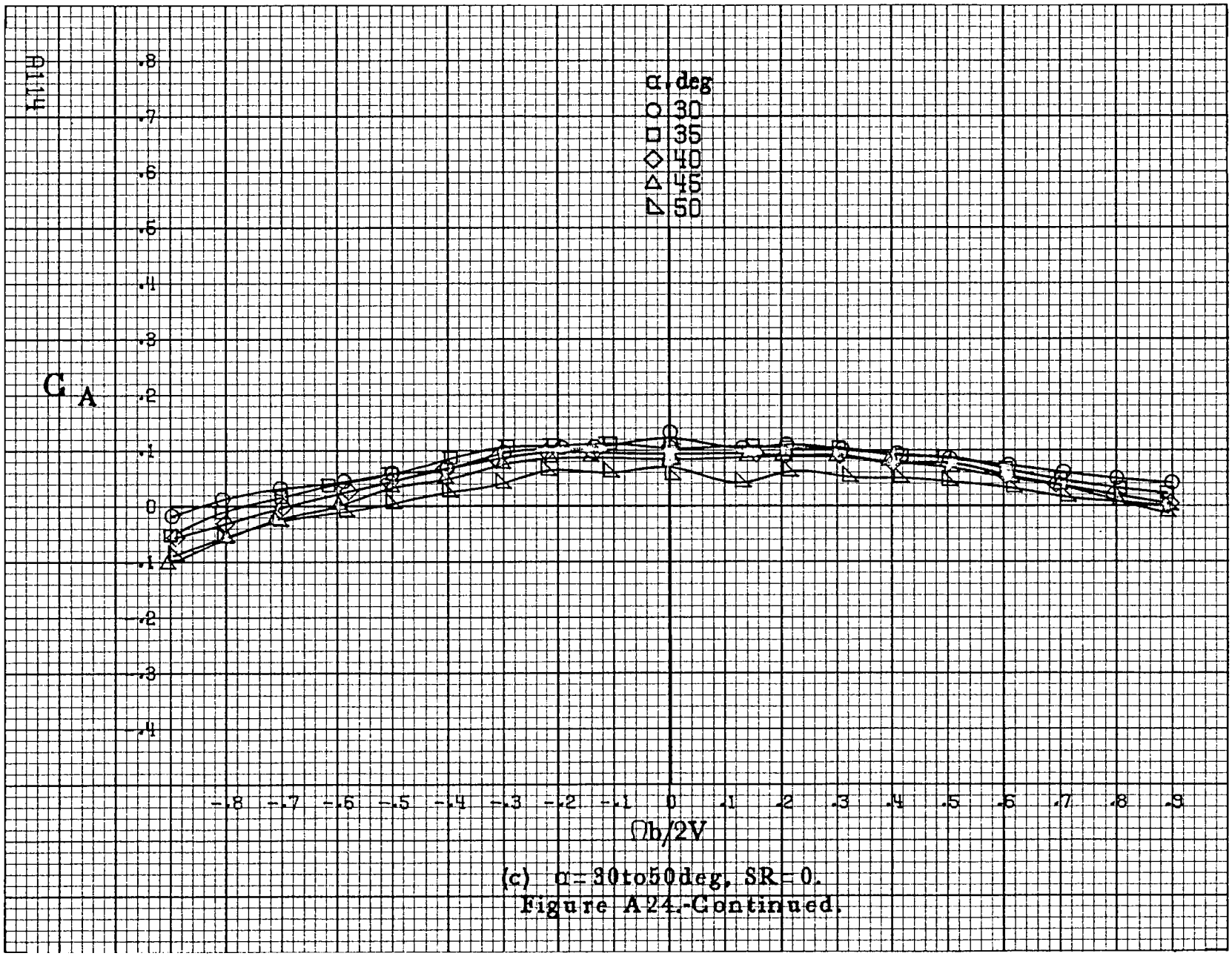

(c) α = 30 to 50 deg, SR = 0.

Figure A24.-Continued.

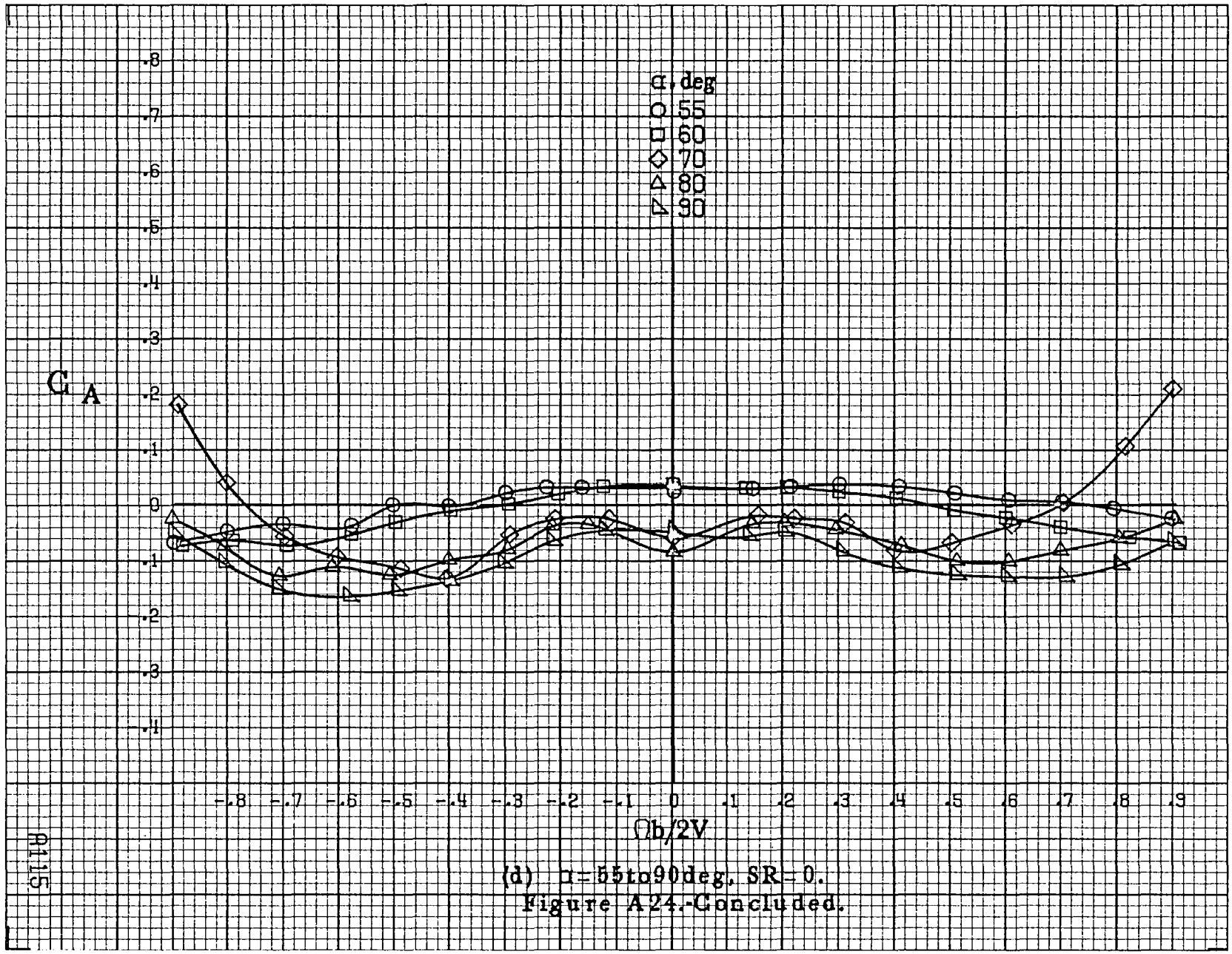

(d) $\alpha = 55$ to 90 deg, SR = 0.

Figure A24.-Concluded.

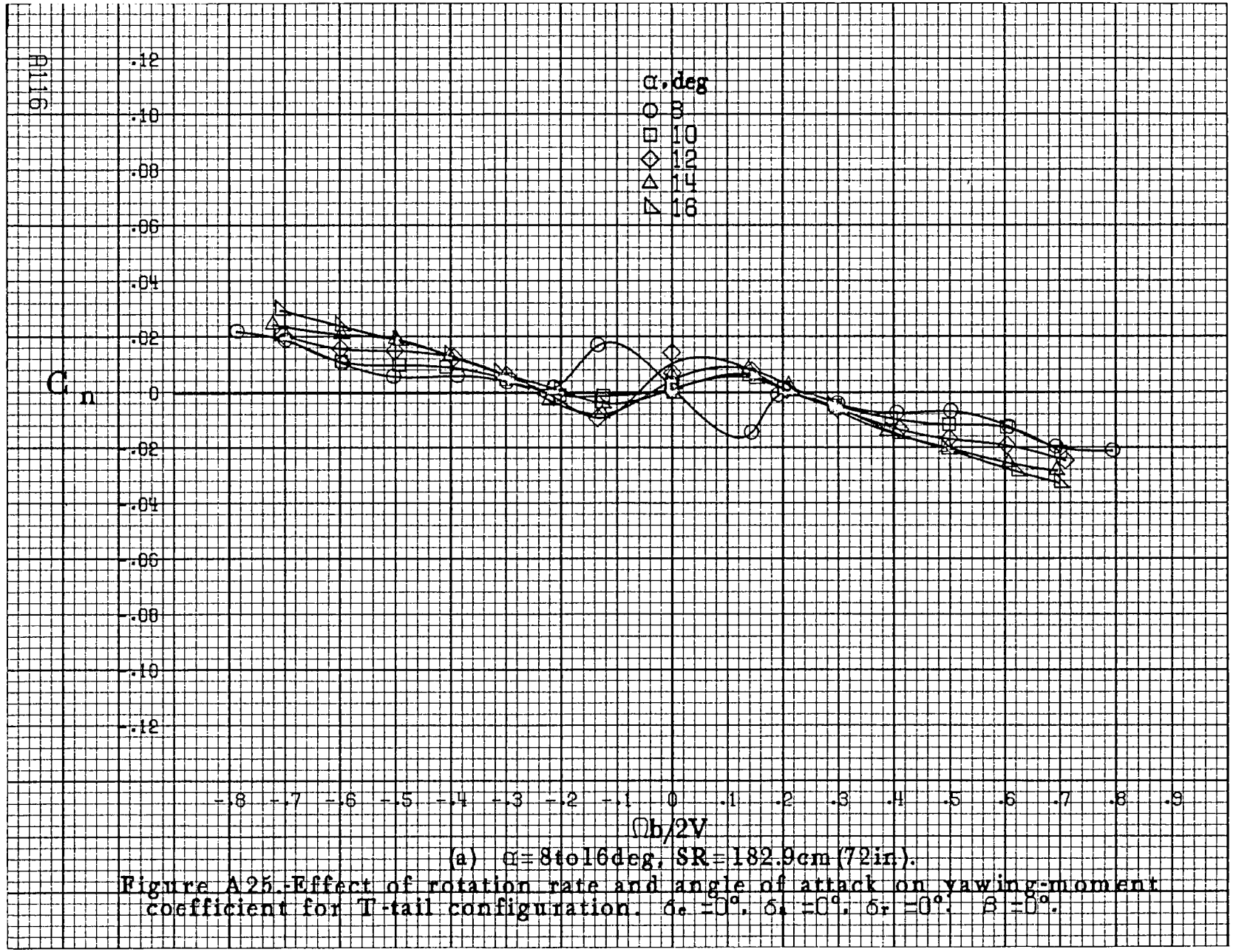

(a) α = 8 to 16 deg, SR = 182.9 cm (72 in.).

Figure A25.-Effect of rotation rate and angle of attack on yawing-moment coefficient for T-tail configuration. $\delta_e = 0°$, $\delta_a = 0°$, $\delta_r = 0°$, $\beta = 0°$.

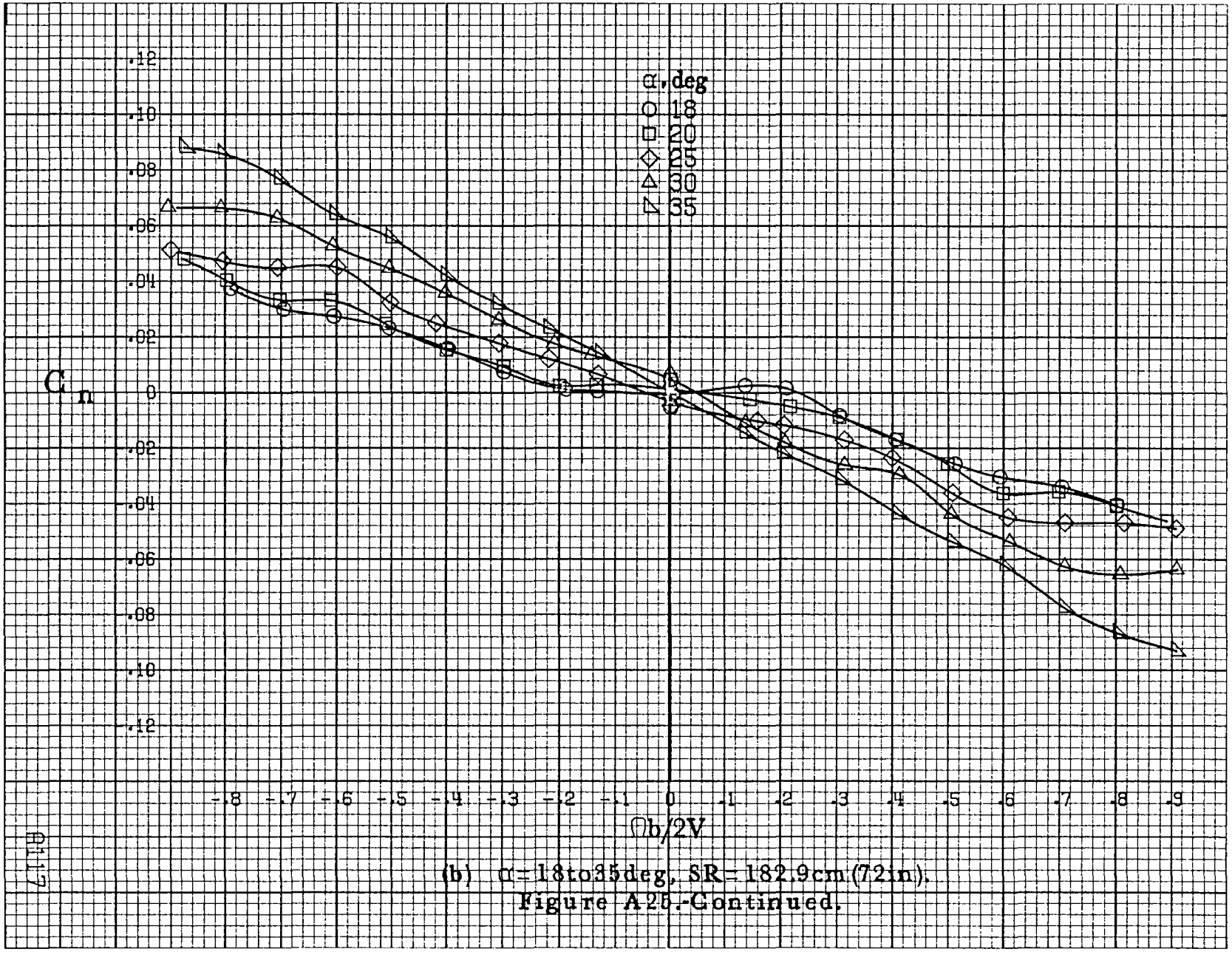

(b) α=18to35deg, SR=182.9cm(72in).

Figure A25.-Continued.

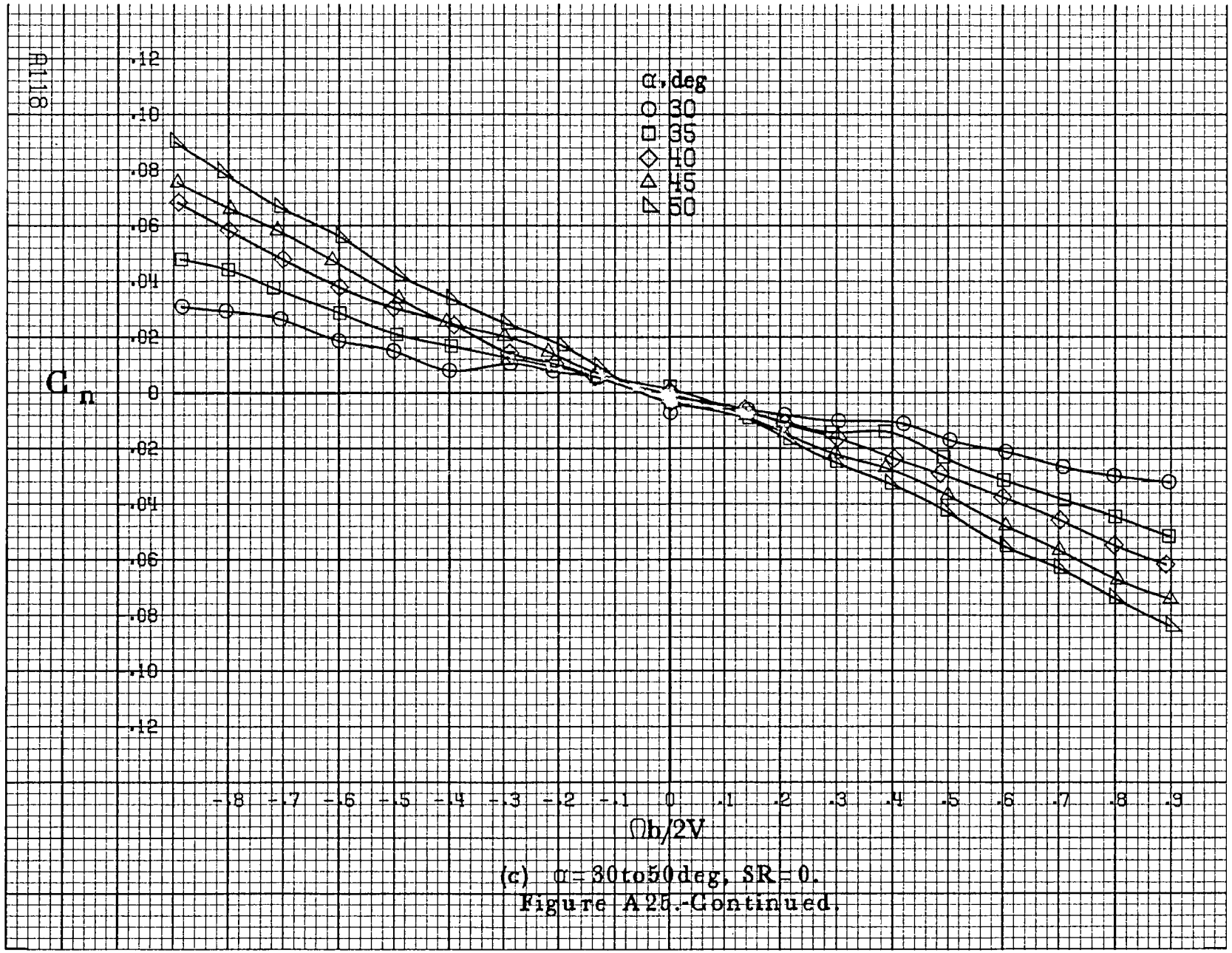

(c) α = 30 to 50 deg, SR = 0.

Figure A25.-Continued.

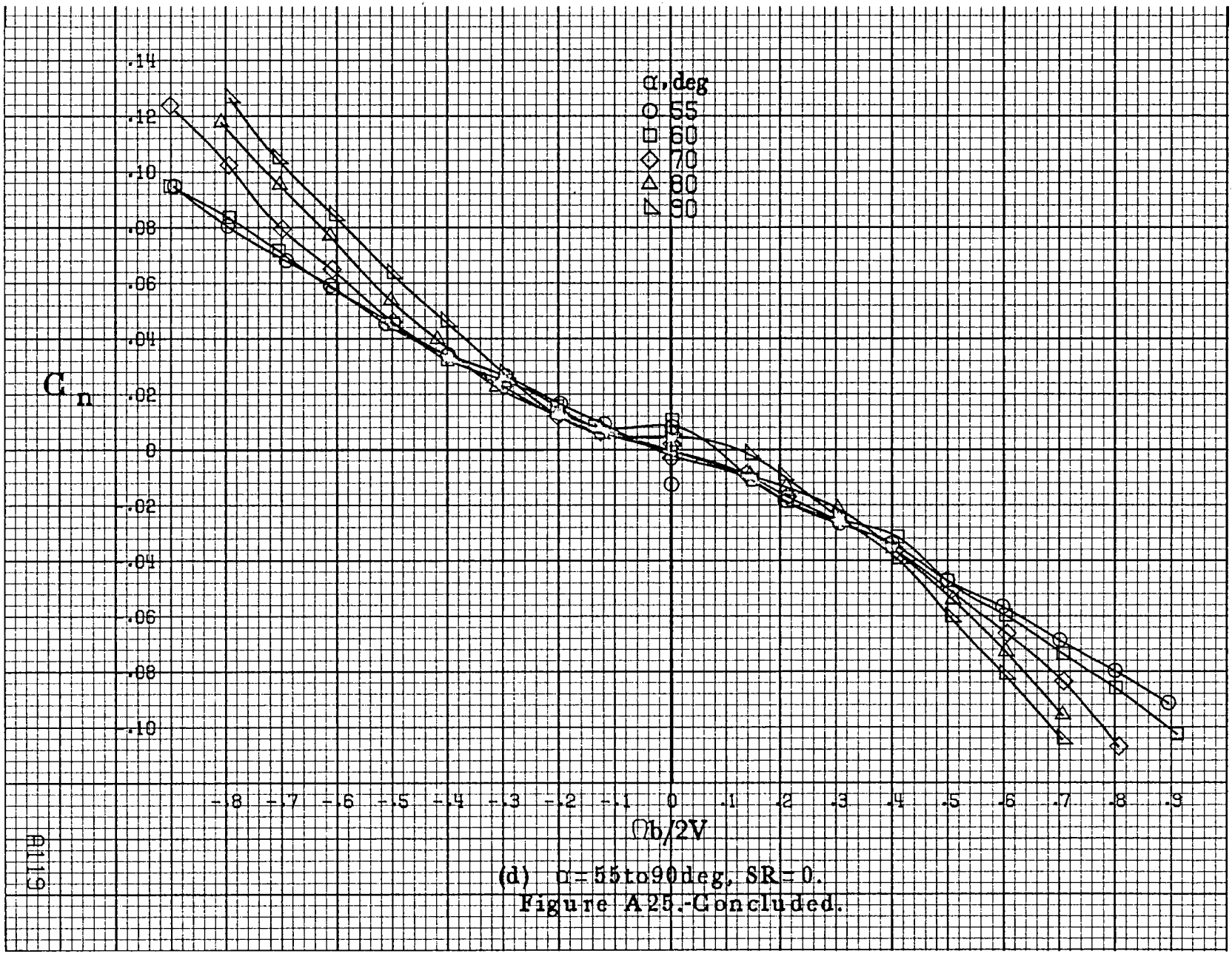

(d) α = 55 to 90 deg, SR = 0.

Figure A25.-Concluded.

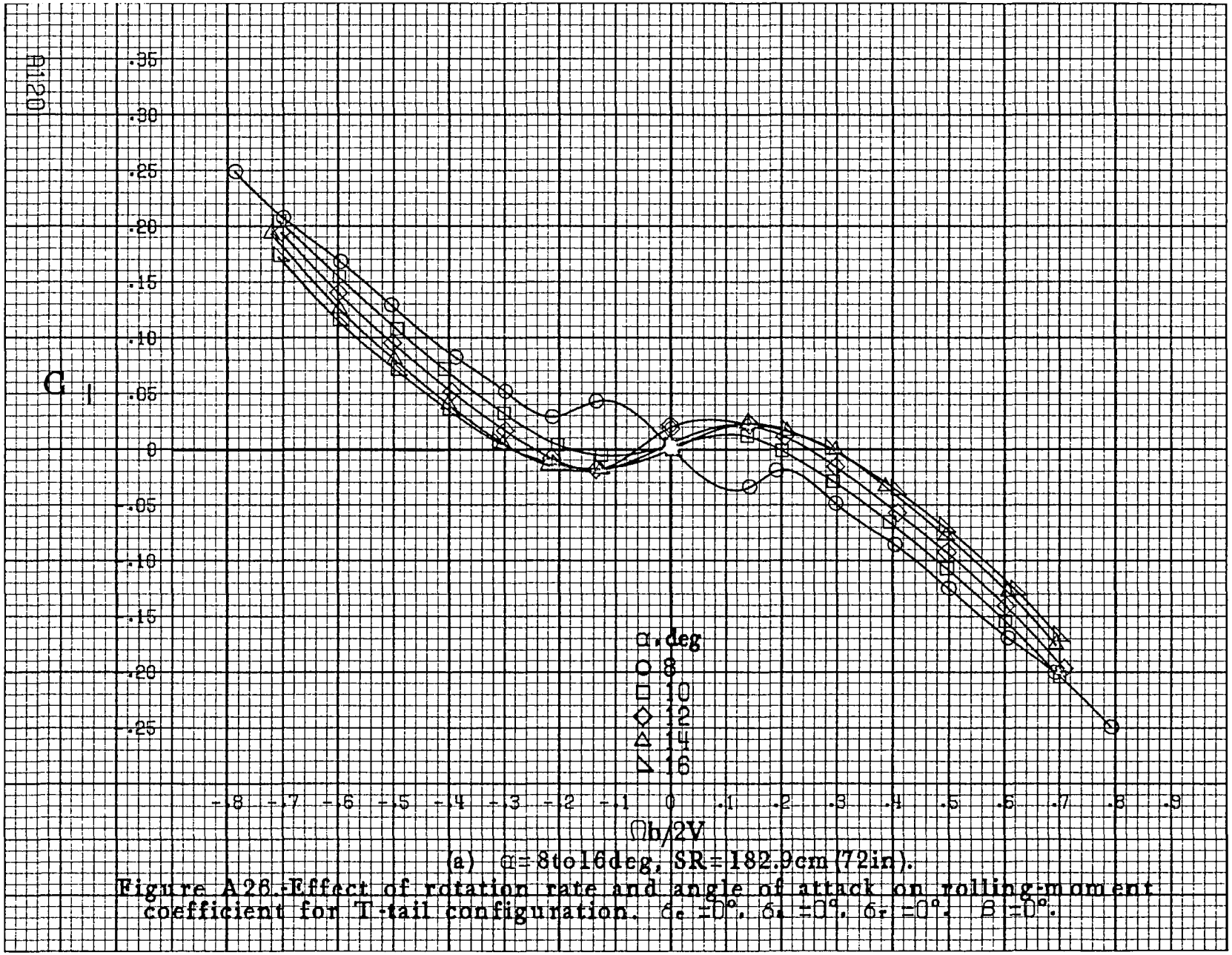

(a) α = 8 to 16 deg, SR = 182.9 cm (72 in).

Figure A26.-Effect of rotation rate and angle of attack on rolling-moment coefficient for T-tail configuration. $\delta_e = 0°$, $\delta_a = 0°$, $\delta_r = 0°$, $\beta = 0°$.

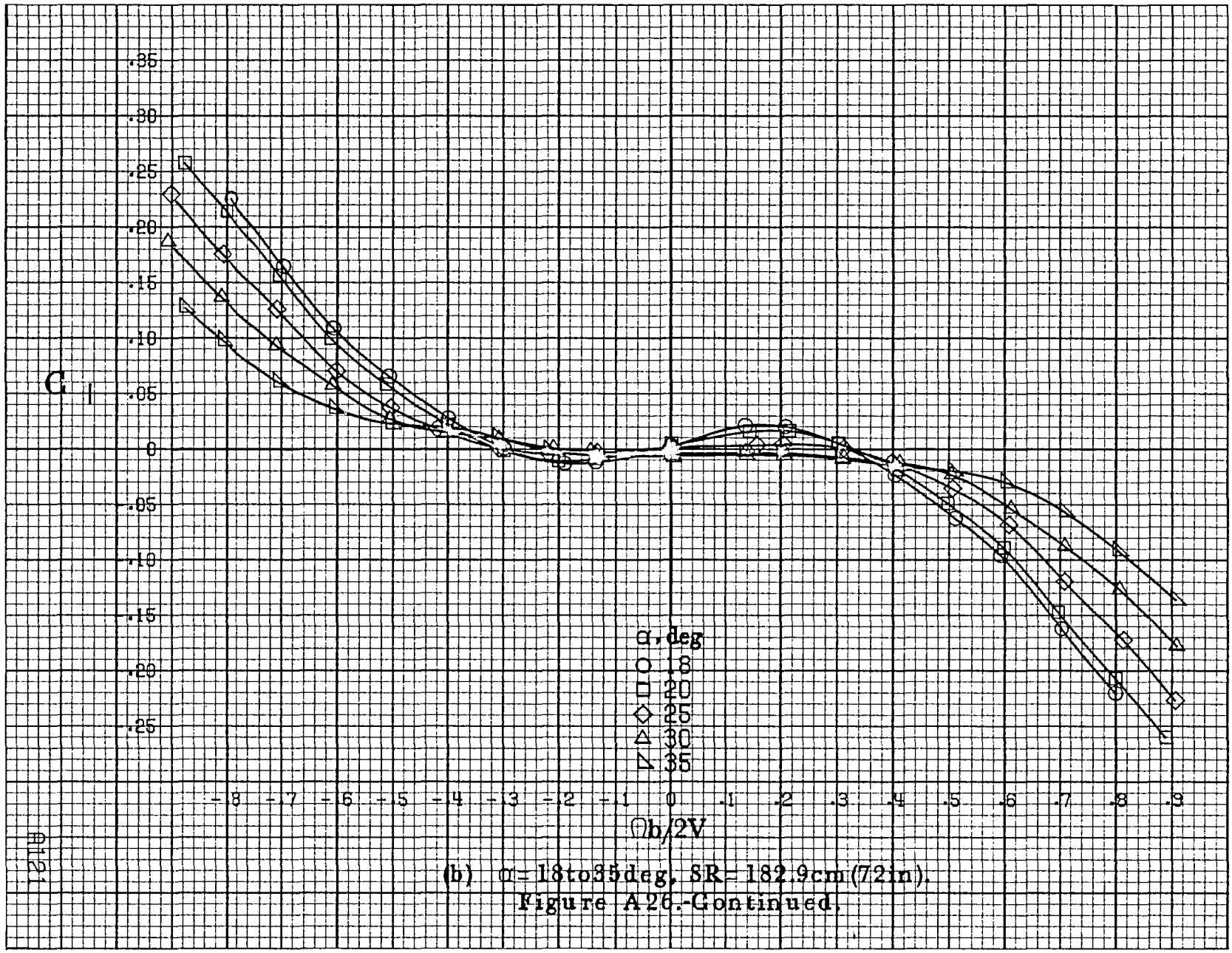

(b) α = 18 to 35 deg, SR = 182.9 cm (72 in).

Figure A26.-Continued.

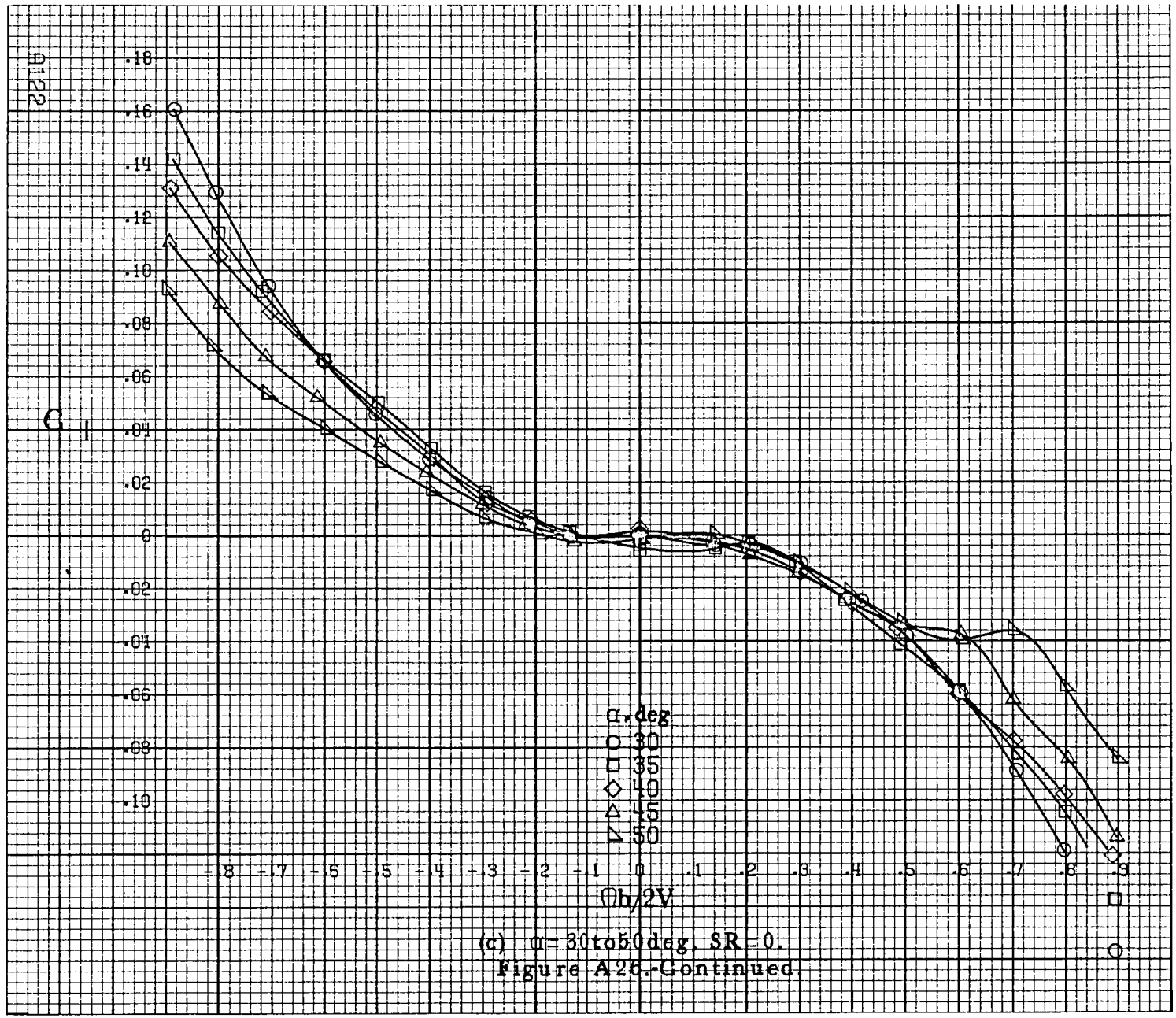

(c) α = 30 to 50 deg, SR = 0.

Figure A26.-Continued.

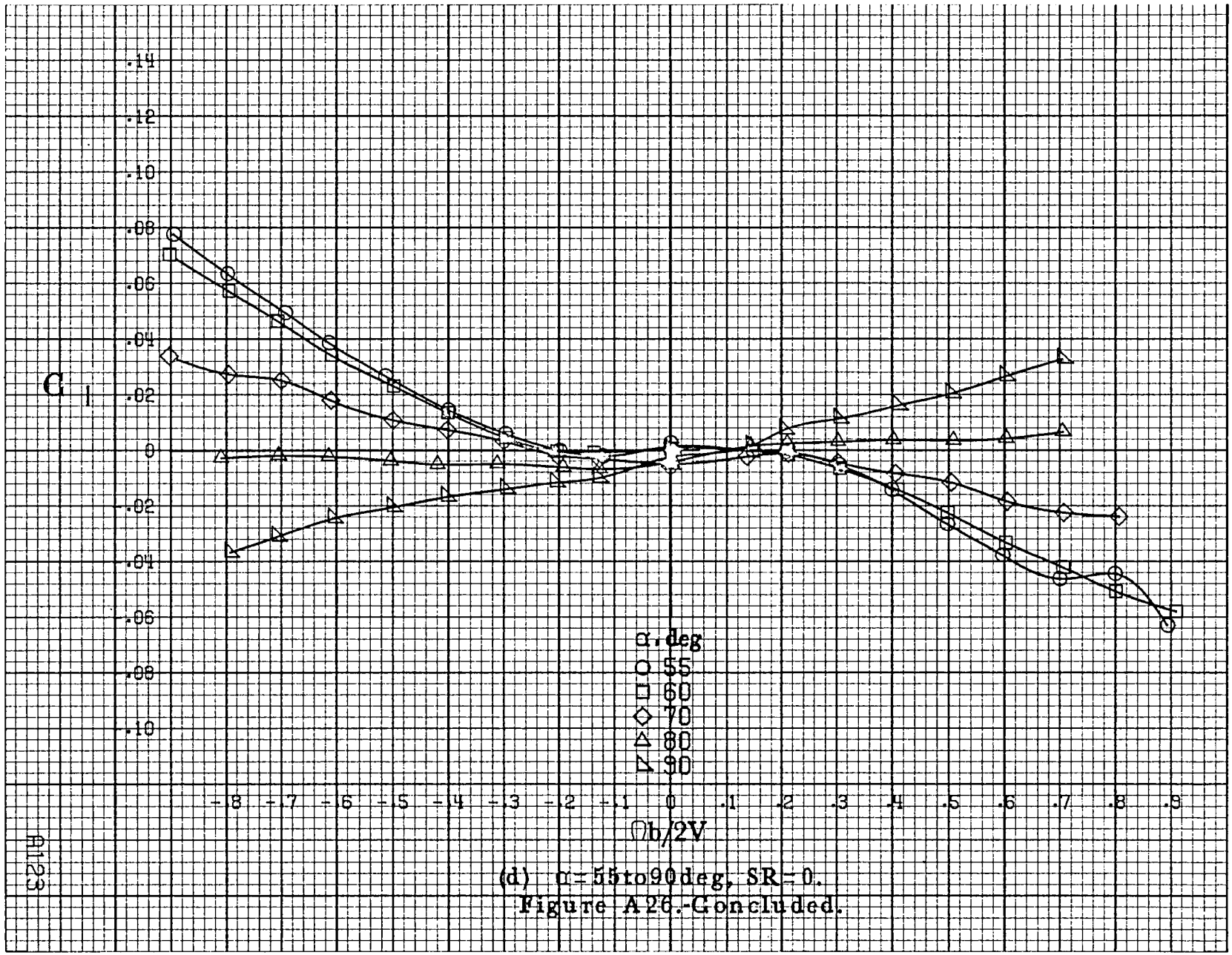

(d) α = 55 to 90 deg, SR = 0.

Figure A26.-Concluded.

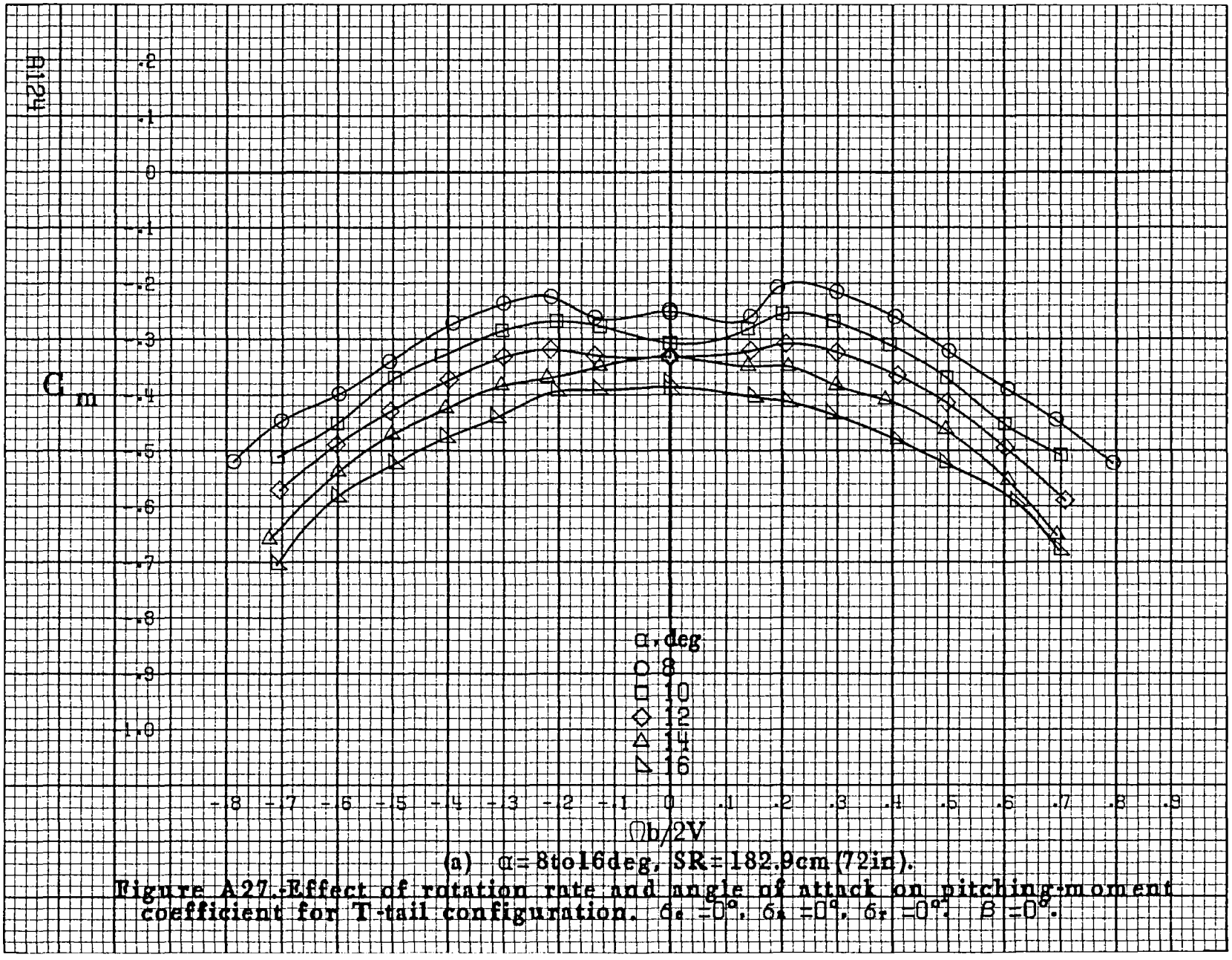

(a) $\alpha = 8$ to 16 deg, SR = 182.9 cm (72 in).

Figure A27.-Effect of rotation rate and angle of attack on pitching-moment coefficient for T-tail configuration. $\delta_e = 0°$, $\delta_a = 0°$, $\delta_r = 0°$, $\beta = 0°$.

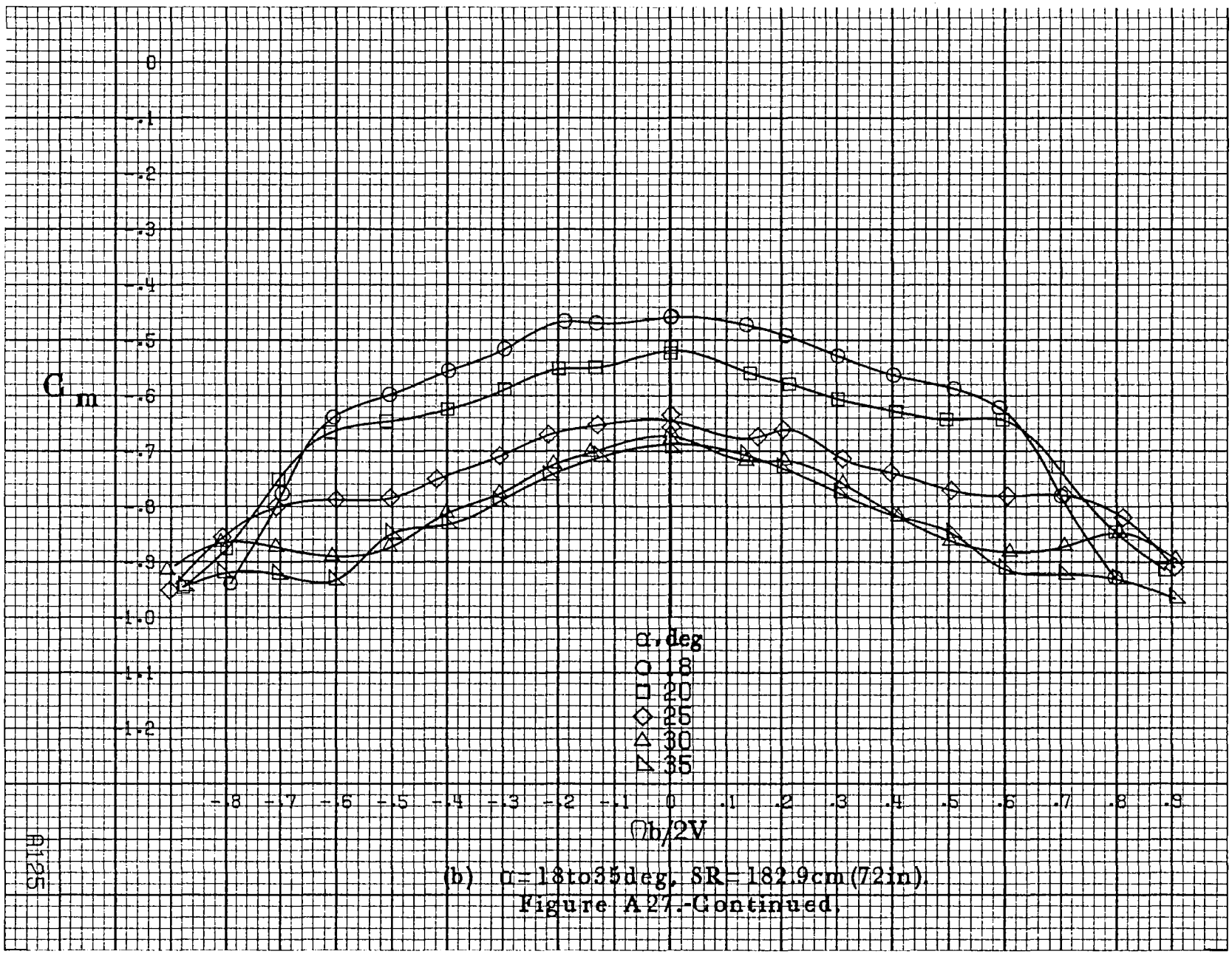

(b) α = 18 to 35 deg, δ_R = 182.9 cm (72 in).

Figure A27.-Continued.

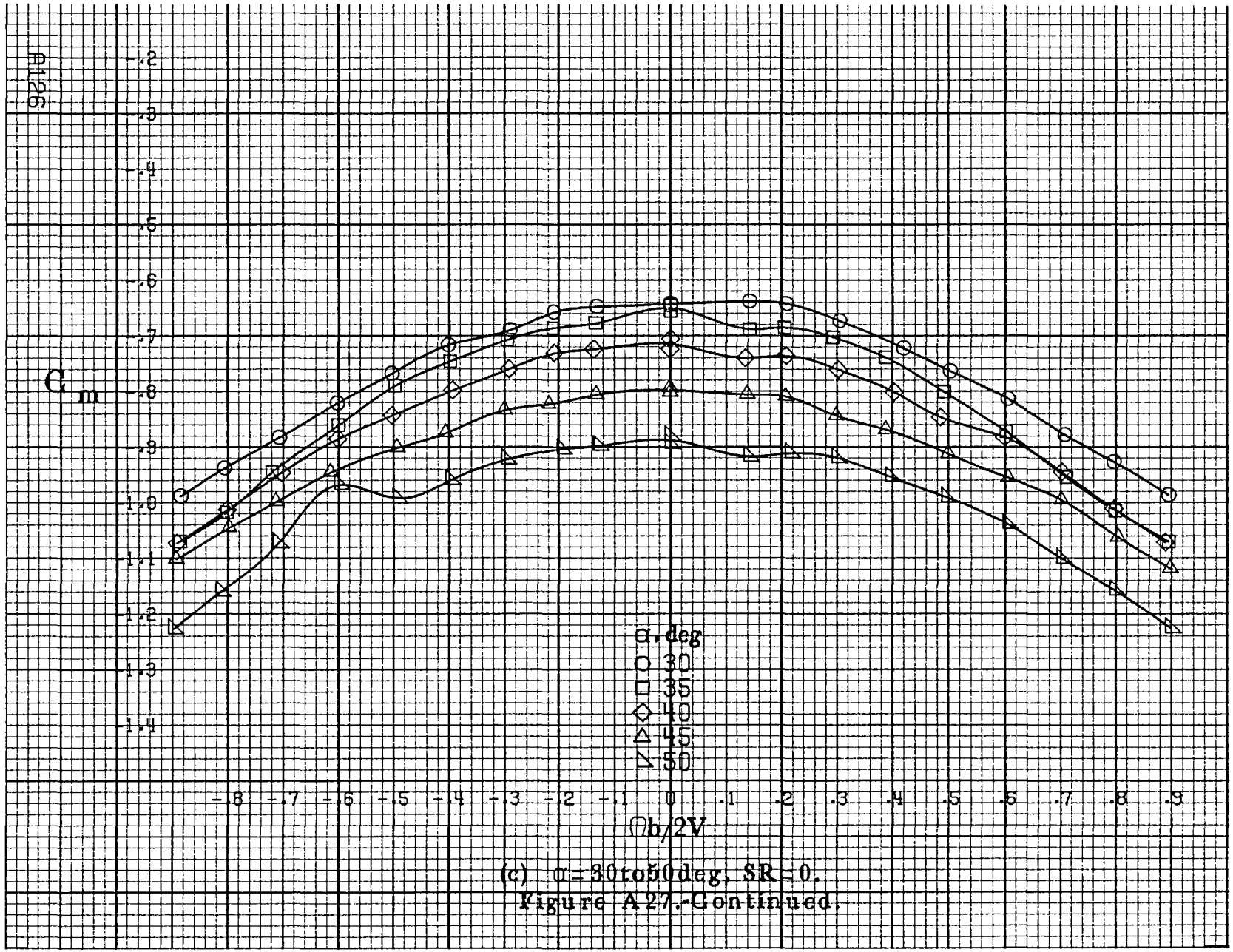

(c) $\alpha = 30$ to 50 deg, SR = 0.

Figure A27.-Continued.

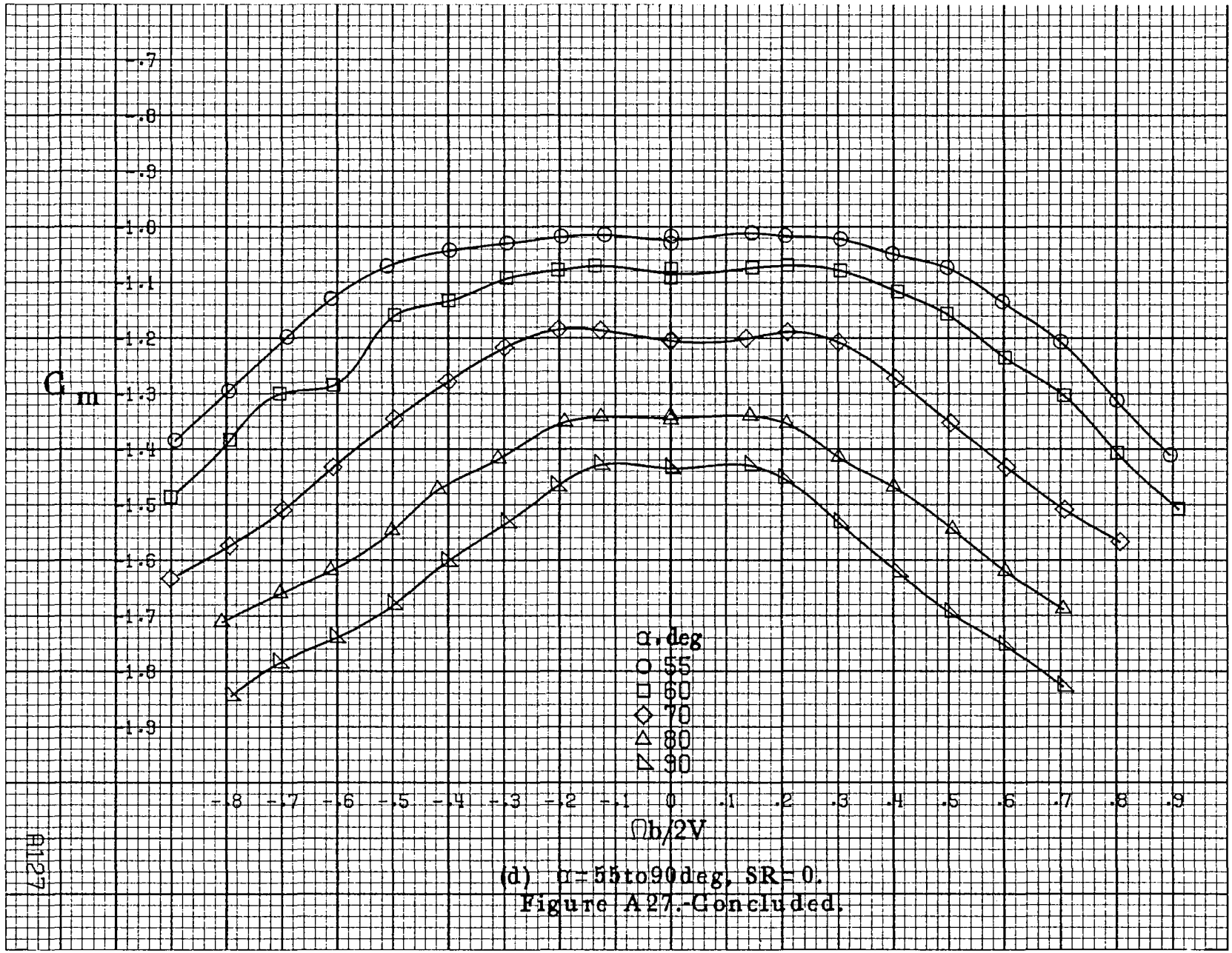

(d) α = 55 to 90 deg, SR = 0.

Figure A27.-Concluded.

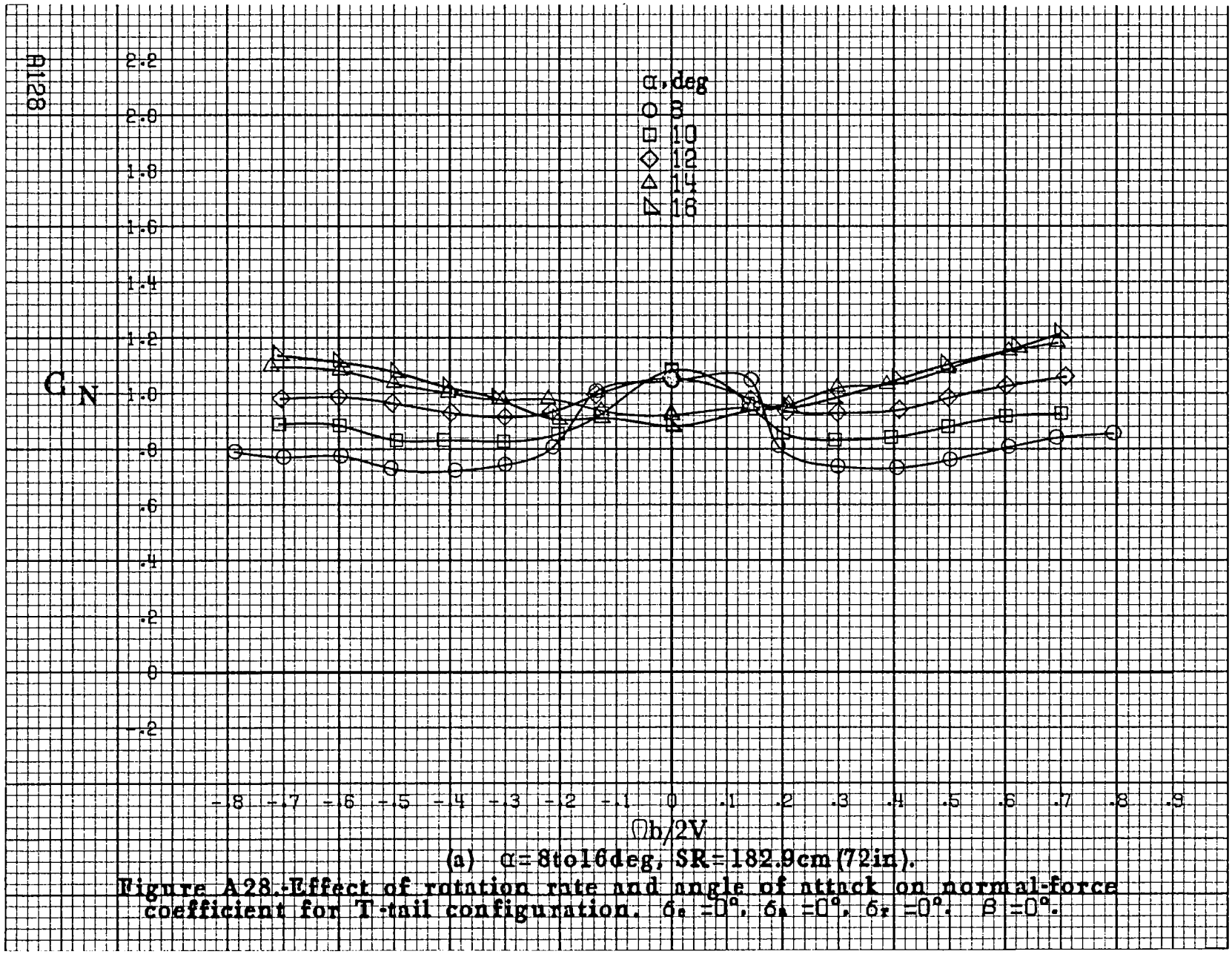

(a) α = 8 to 16 deg, SR = 182.9 cm (72 in.).

Figure A28.-Effect of rotation rate and angle of attack on normal-force coefficient for T-tail configuration. $\delta_e = 0°$, $\delta_a = 0°$, $\delta_r = 0°$, $\beta = 0°$.

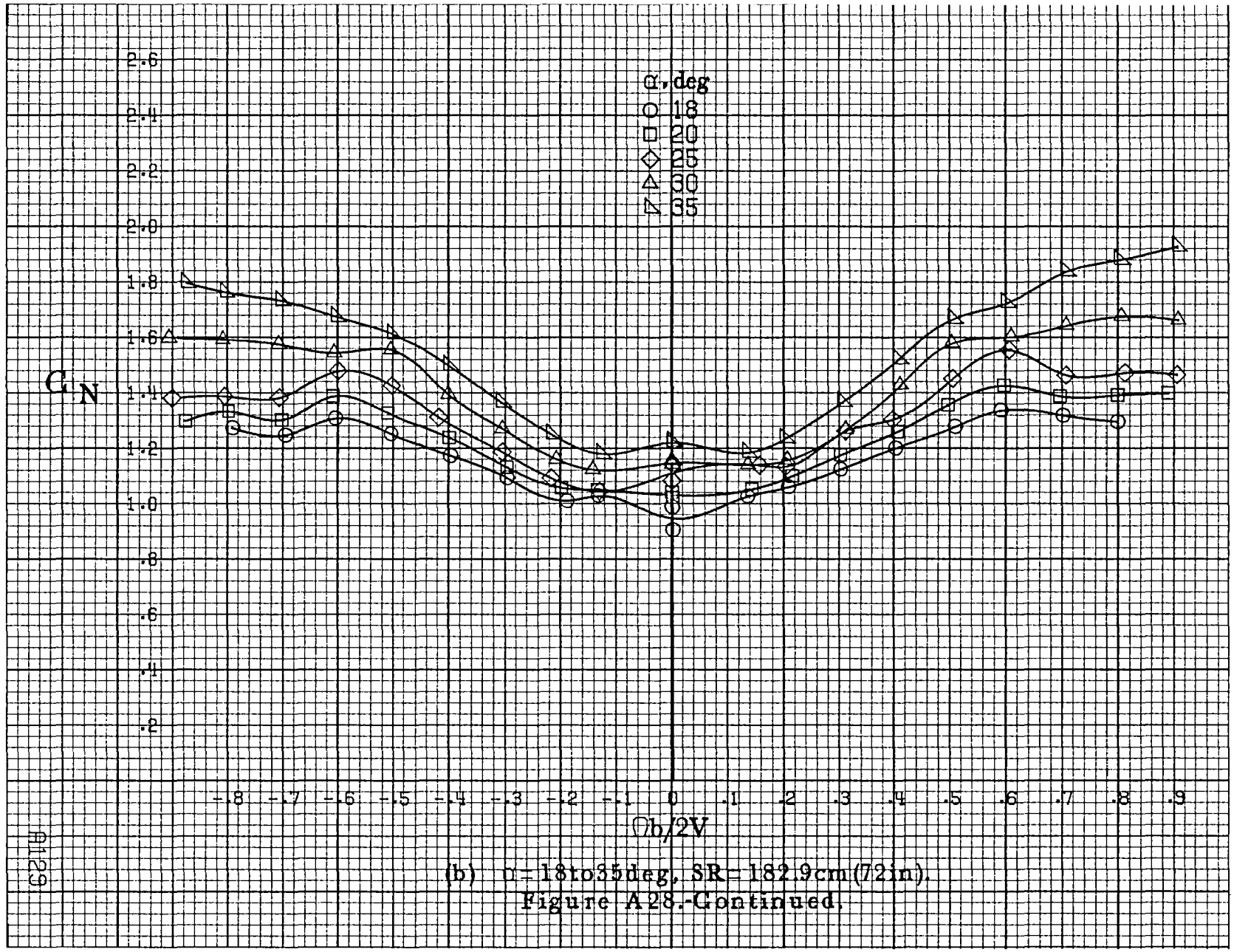

(b) $\alpha = 18$ to 35 deg, SR = 182.9 cm (72 in).

Figure A28.-Continued.

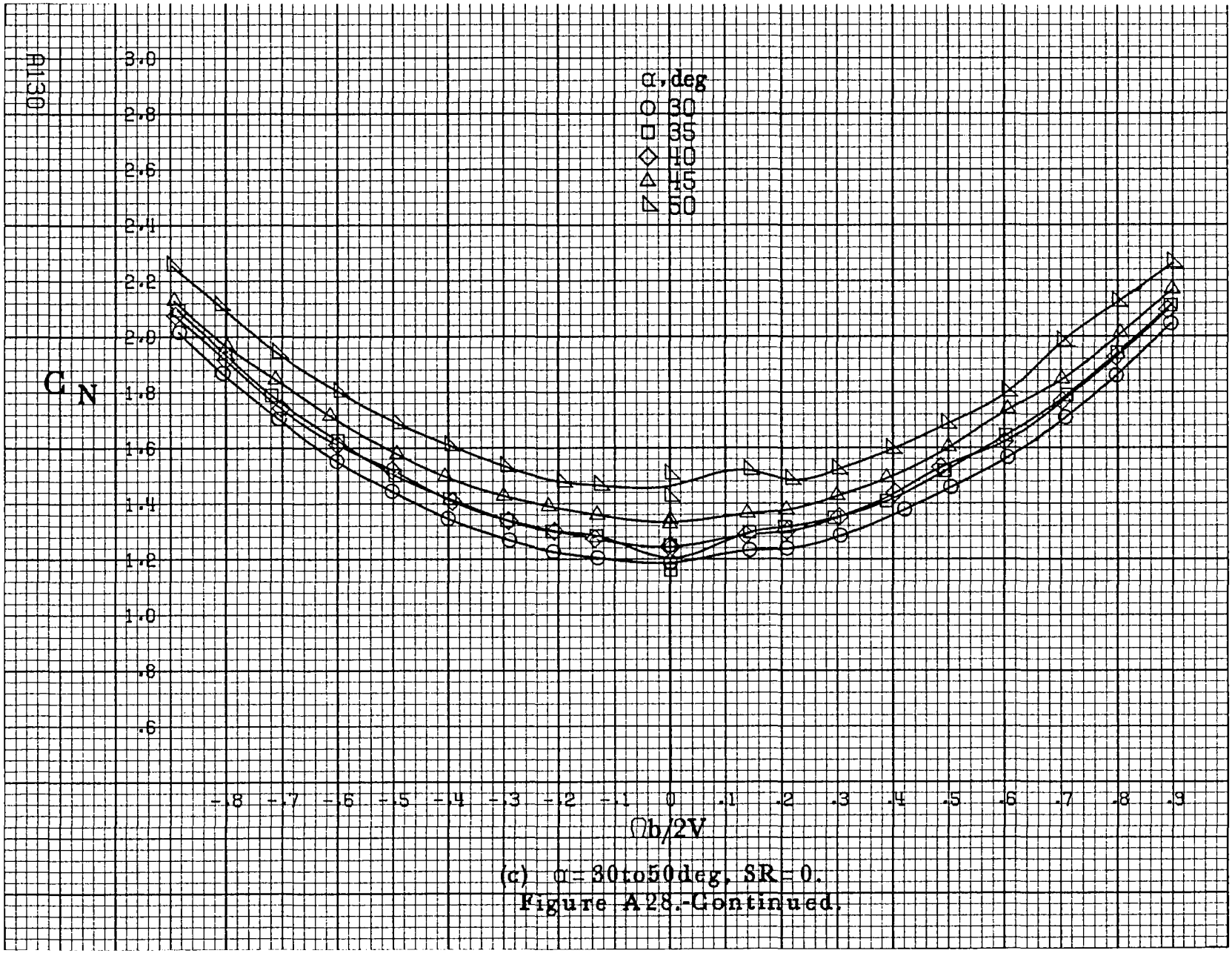

(c) $\alpha = 30$ to 50 deg, SR = 0.

Figure A28.-Continued.

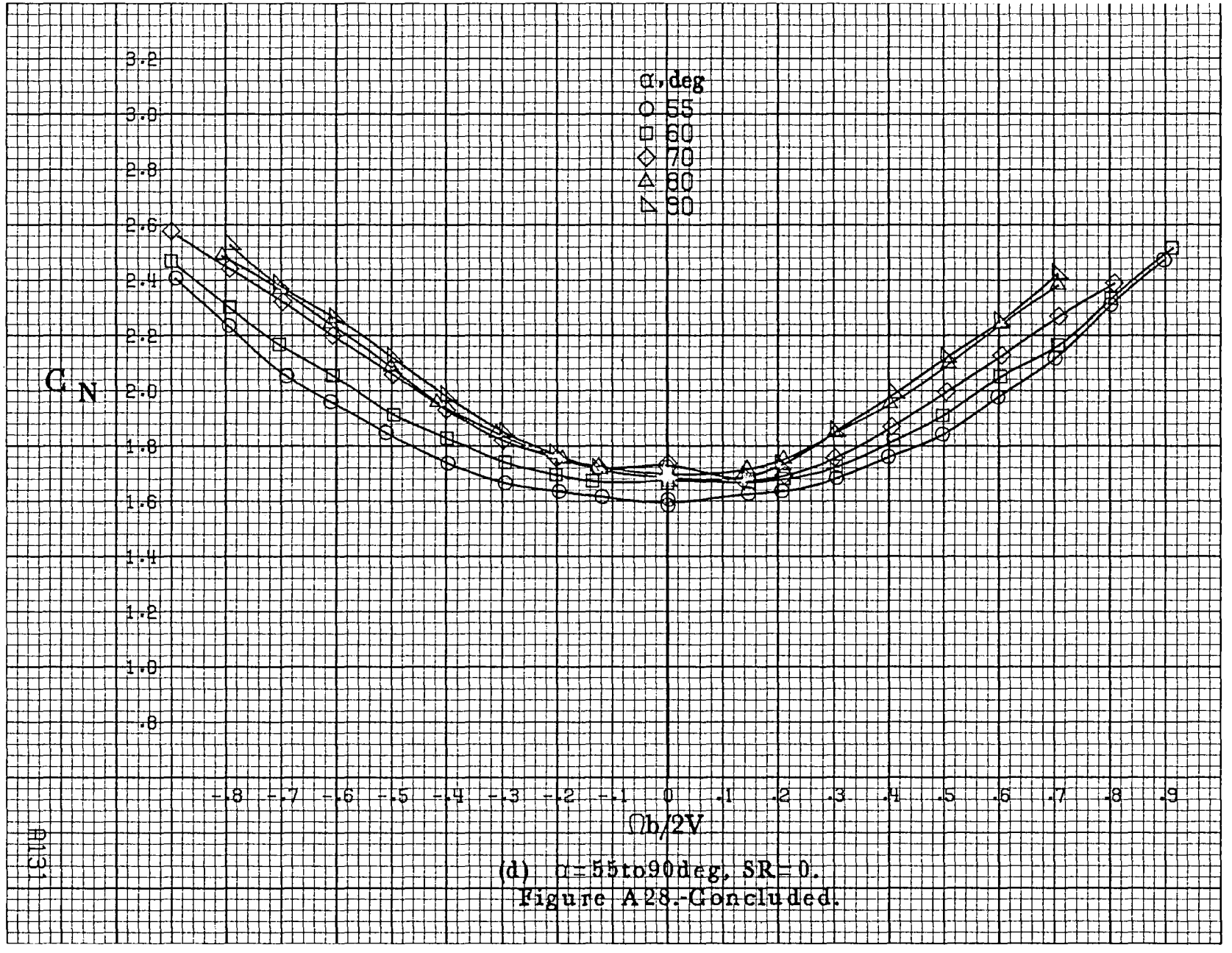

(d) α = 55 to 90 deg, SR = 0.

Figure A28.-Concluded.

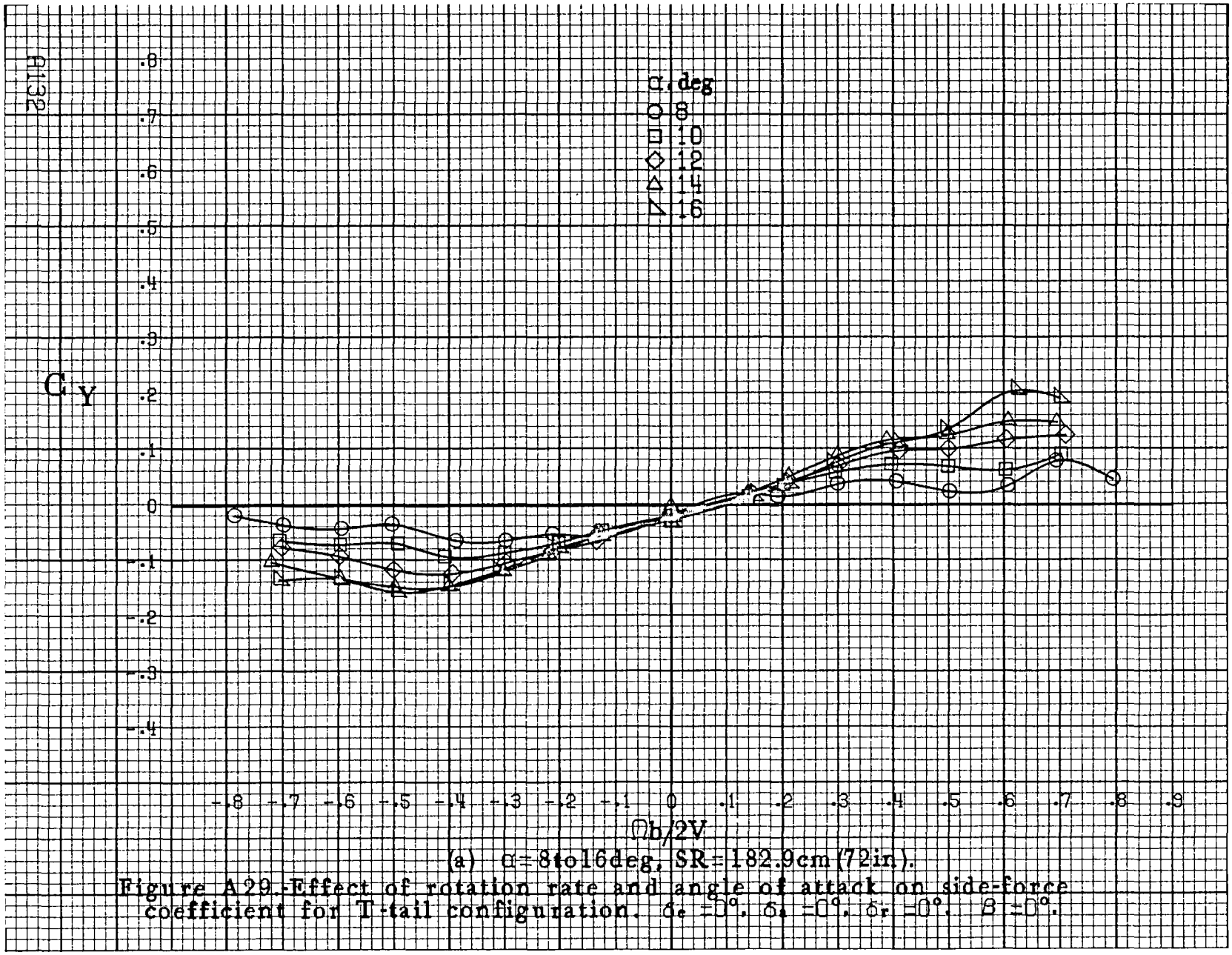

(a) α = 8 to 16 deg, SR = 182.9 cm (72 in.).

Figure A29.-Effect of rotation rate and angle of attack on side-force coefficient for T-tail configuration. $\delta_e = 0°$, $\delta_a = 0°$, $\delta_r = 0°$, $\beta = 0°$.

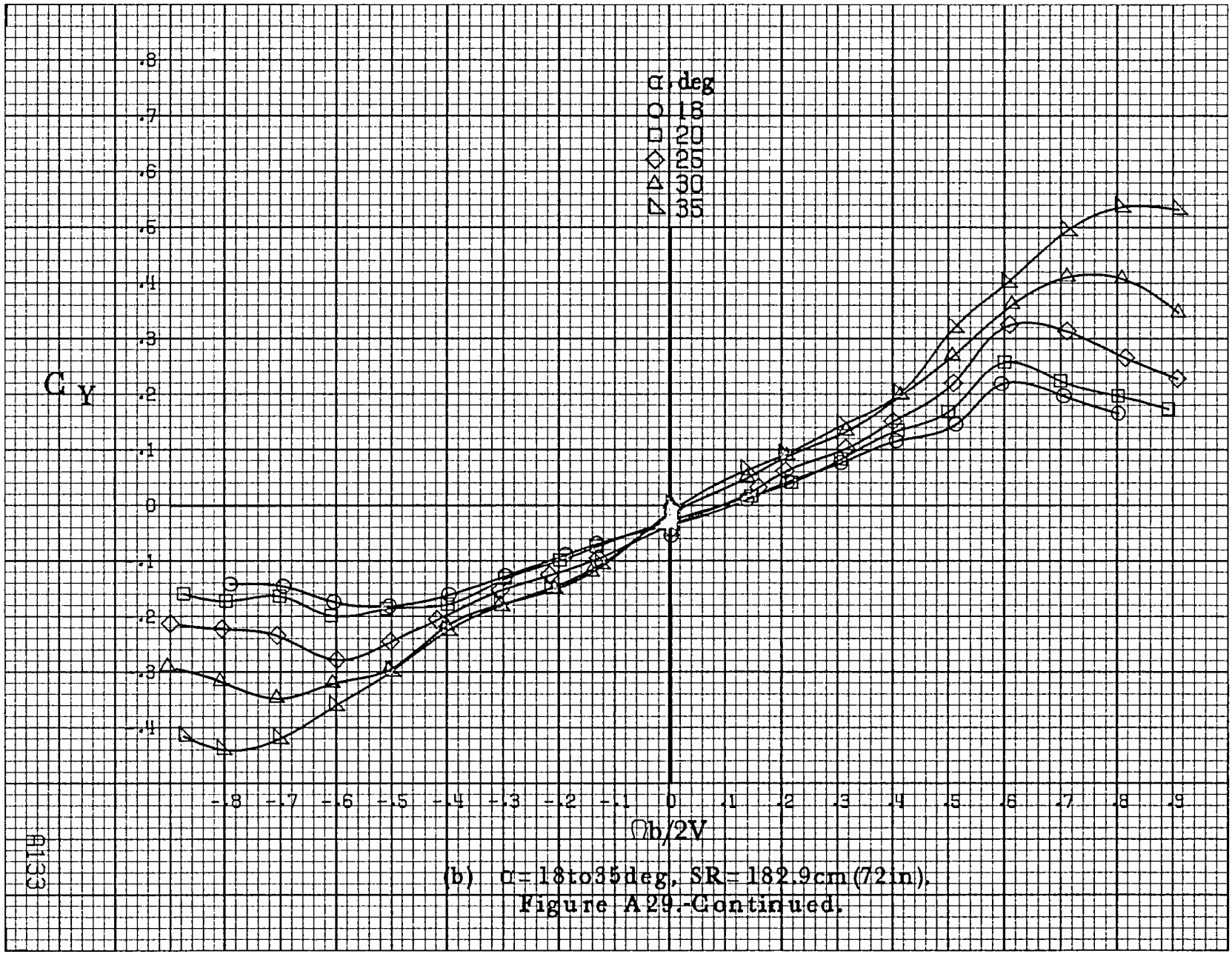

(b) α = 18 to 35 deg, SR = 182.9 cm (72 in).

Figure A29.-Continued.

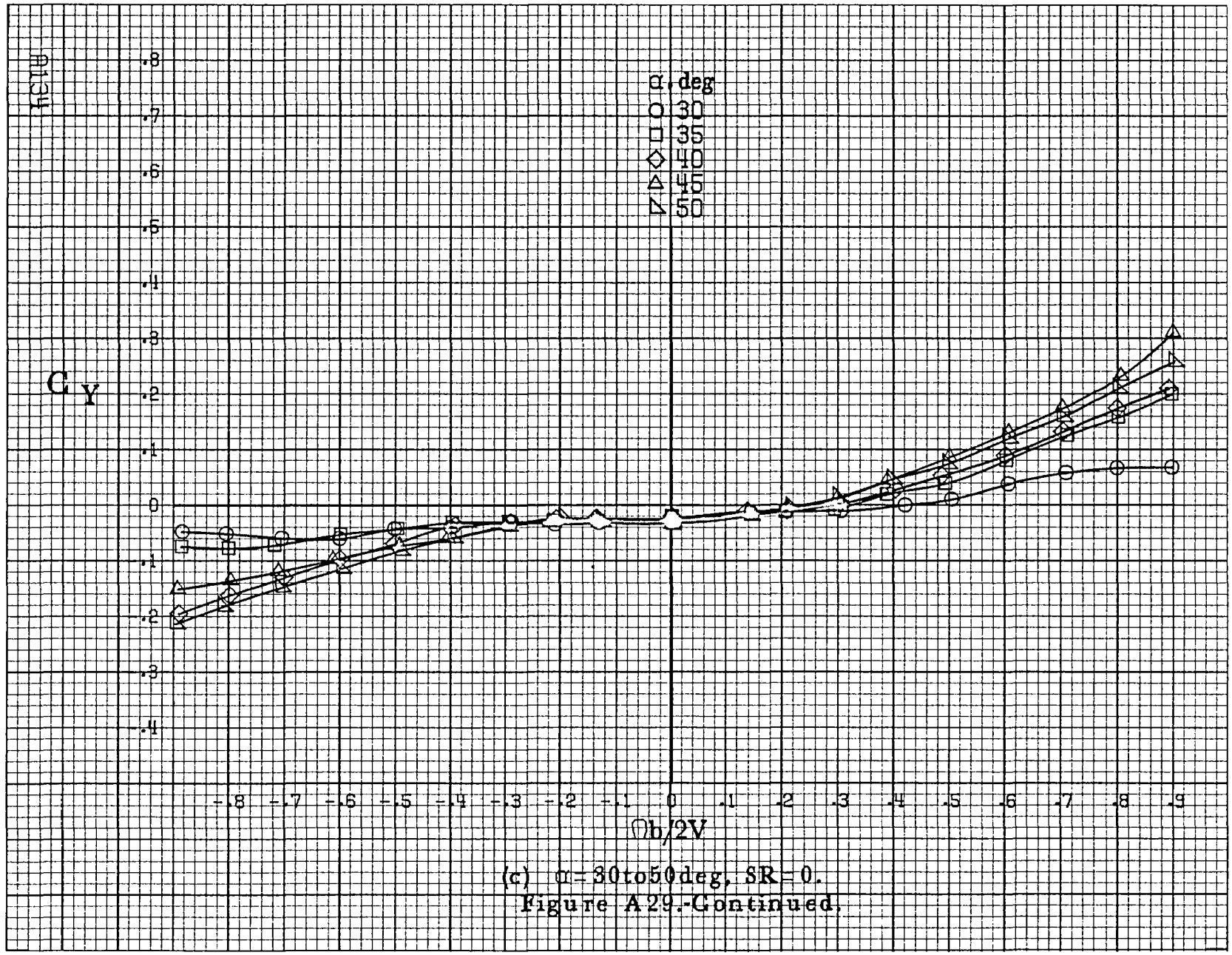

(c) $\alpha = 30$ to 50 deg, SR = 0.

Figure A29.-Continued.

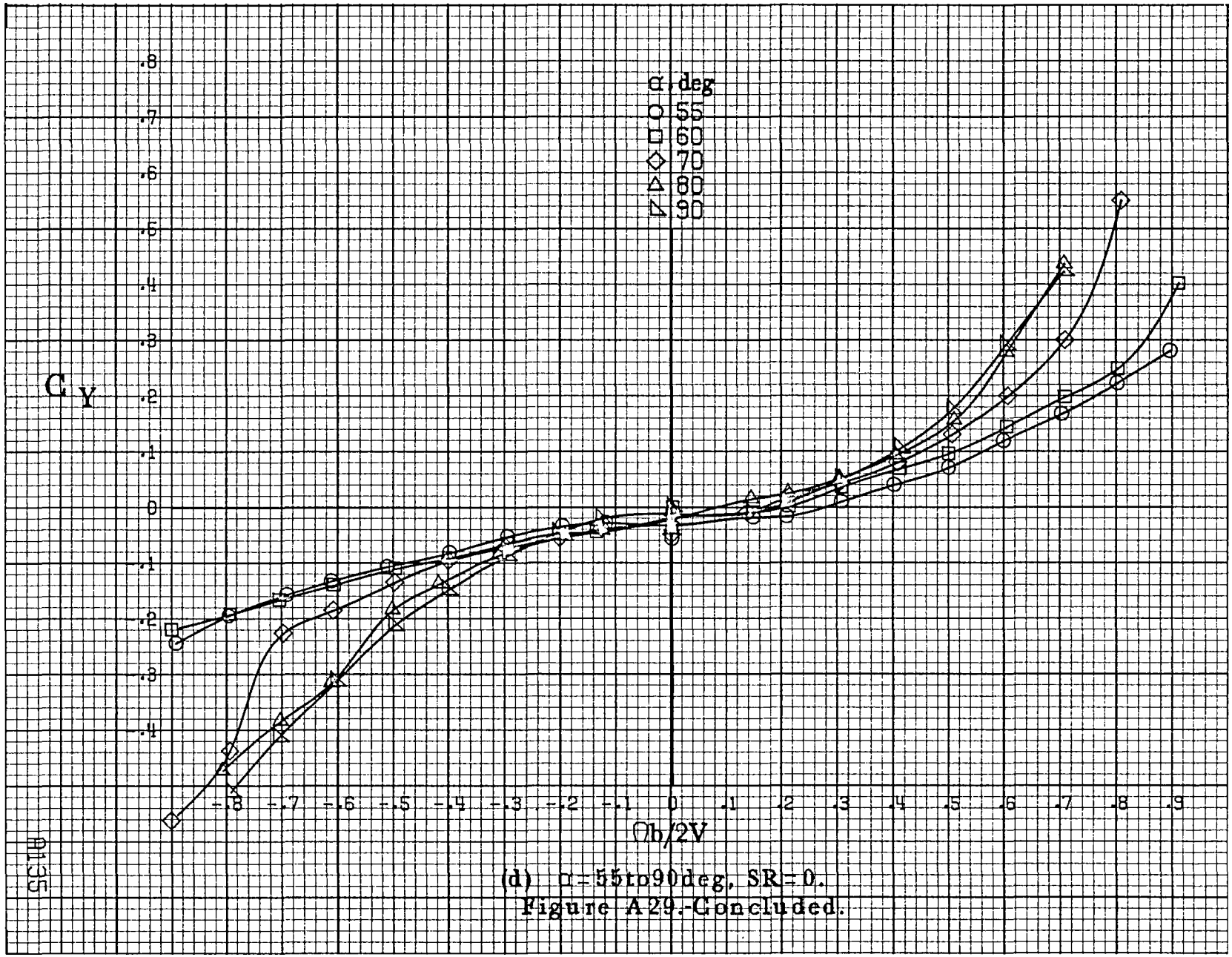

(d) $\alpha = 55$ to 90 deg, SR = 0.

Figure A29.-Concluded.

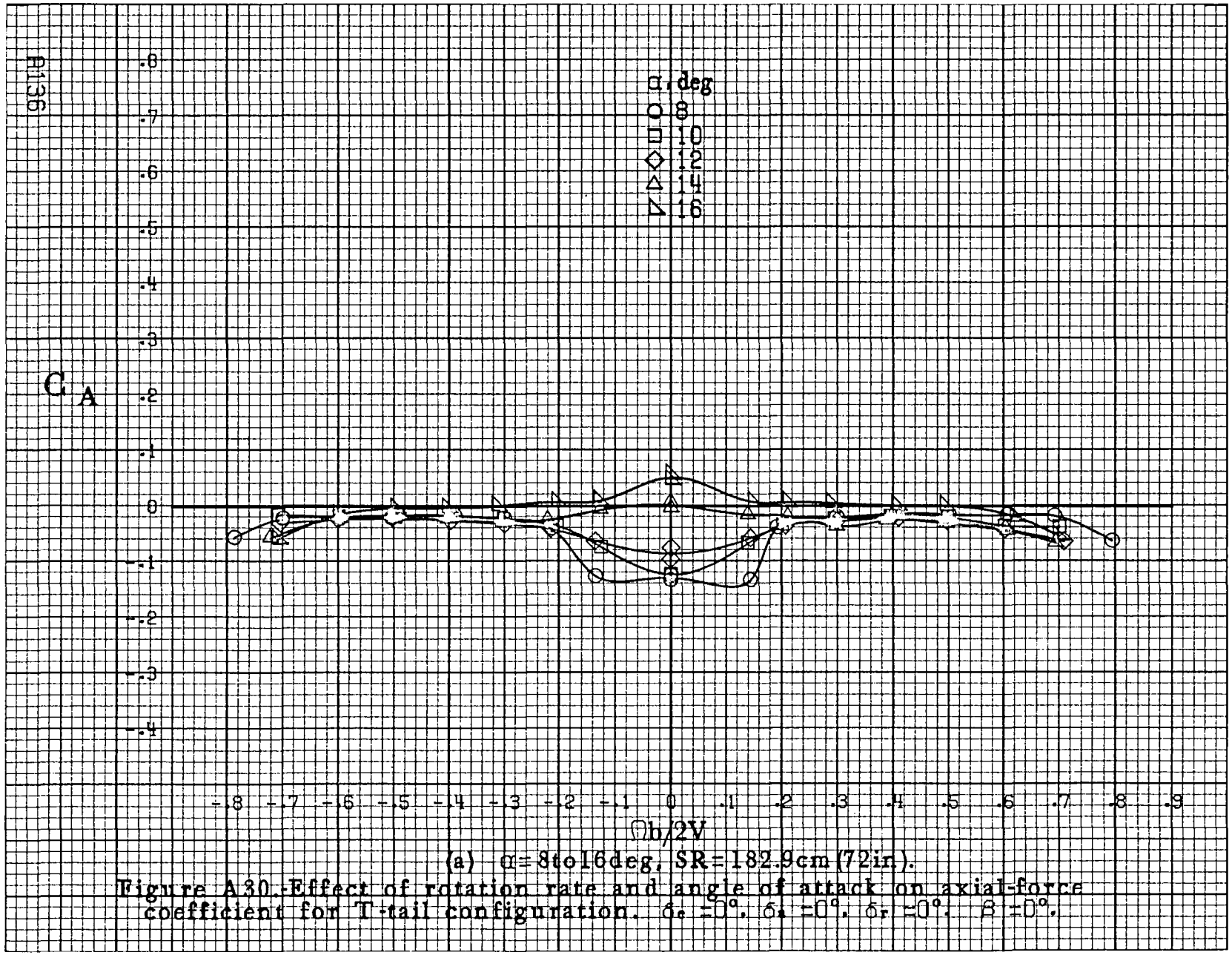

(a) $\alpha = 8$ to 16 deg, SR = 182.9 cm (72 in.).

Figure A30.- Effect of rotation rate and angle of attack on axial-force coefficient for T-tail configuration. $\delta_e = 0°$, $\delta_a = 0°$, $\delta_r = 0°$, $\beta = 0°$.

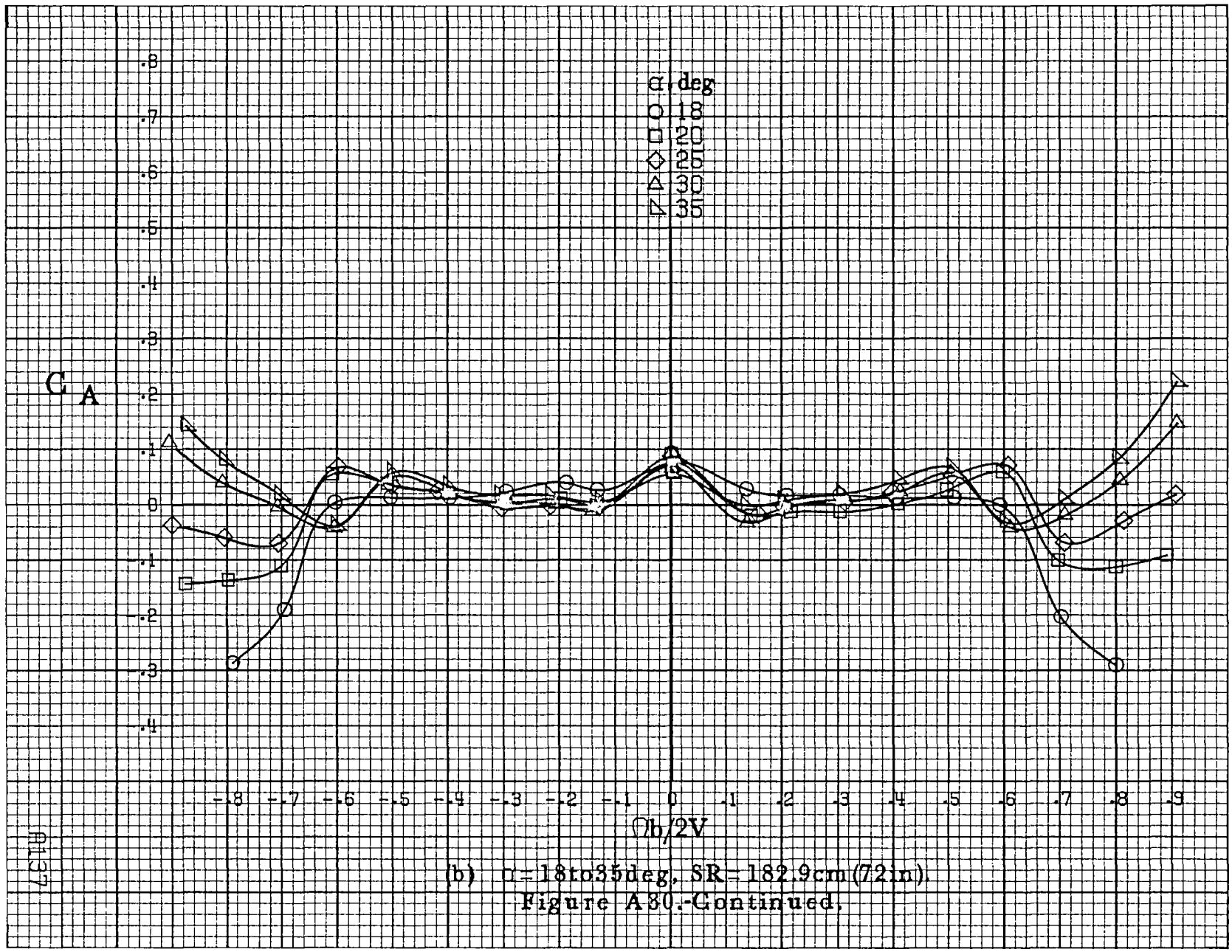

(b) α = 18 to 35 deg, SR = 182.9 cm (72 in).

Figure A30.-Continued.

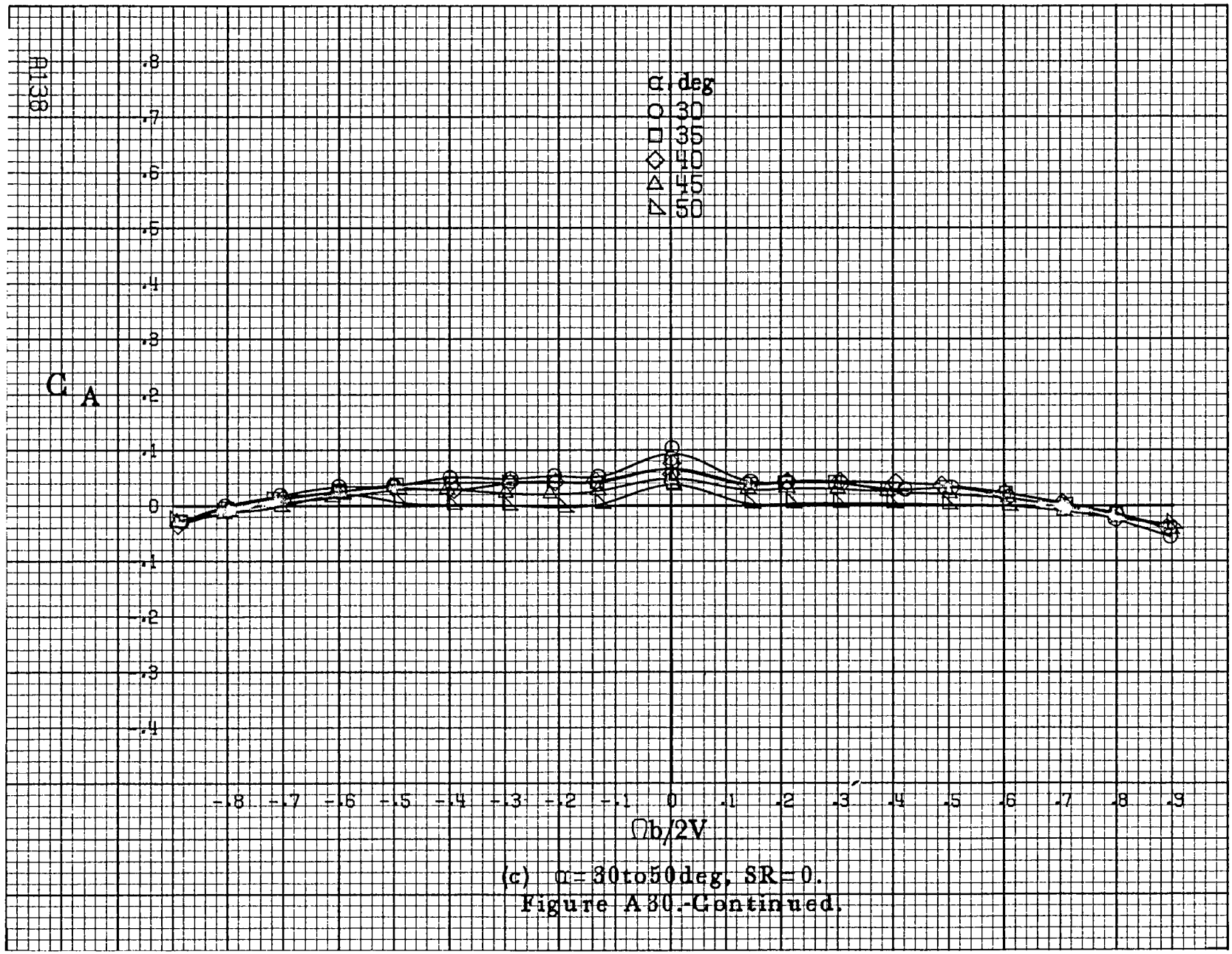

(c) $\alpha = 30$ to 50 deg, SR = 0.

Figure A30.-Continued.

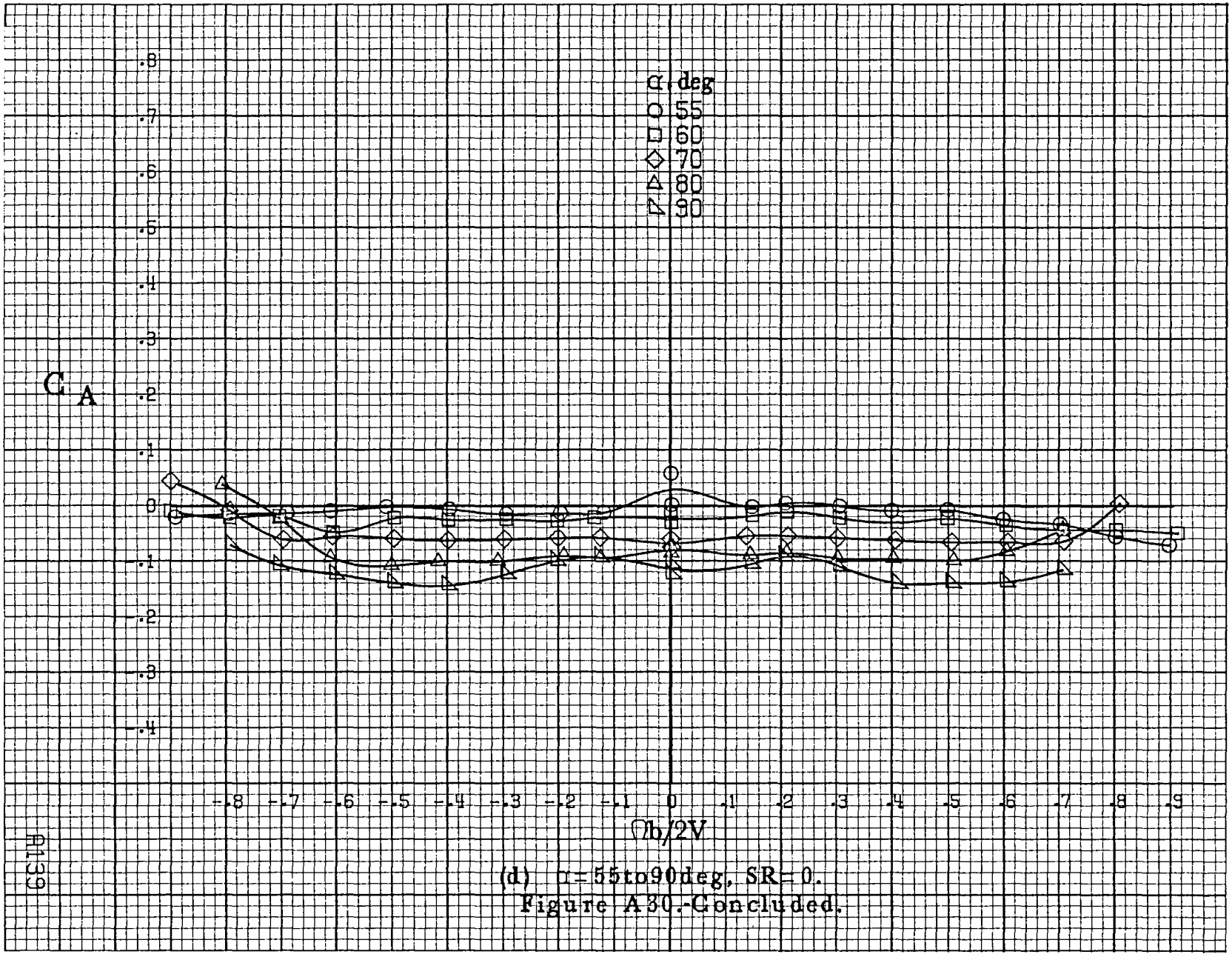

(d) $\alpha = 55$ to 90 deg, SR = 0.

Figure A30.-Concluded.

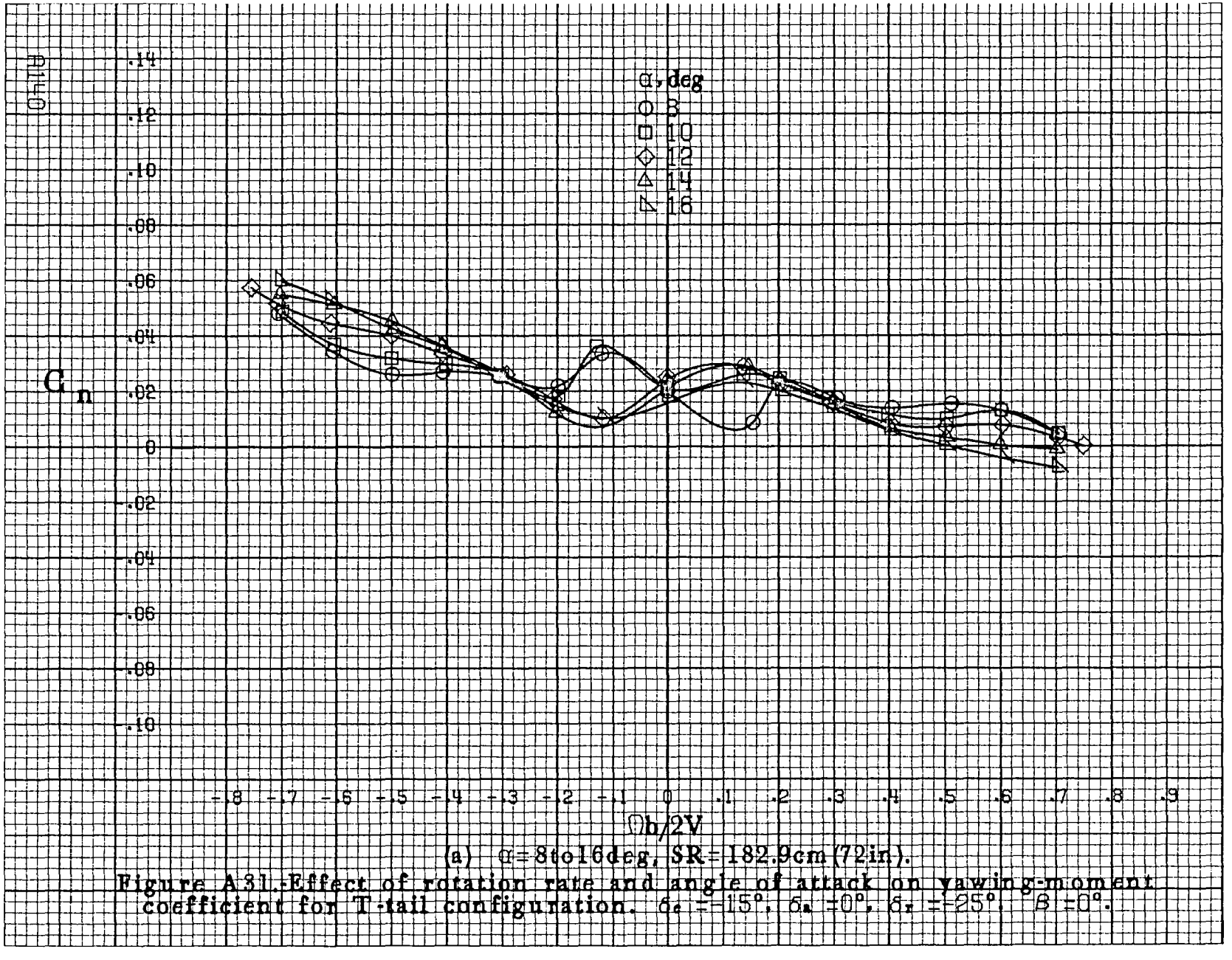

(a) $\alpha = 8$ to 16 deg, SR = 182.9 cm (72 in.).

Figure A31.-Effect of rotation rate and angle of attack on yawing-moment coefficient for T-tail configuration. $\delta_e = -15°$, $\delta_a = 0°$, $\delta_r = -25°$, $\beta = 0°$.

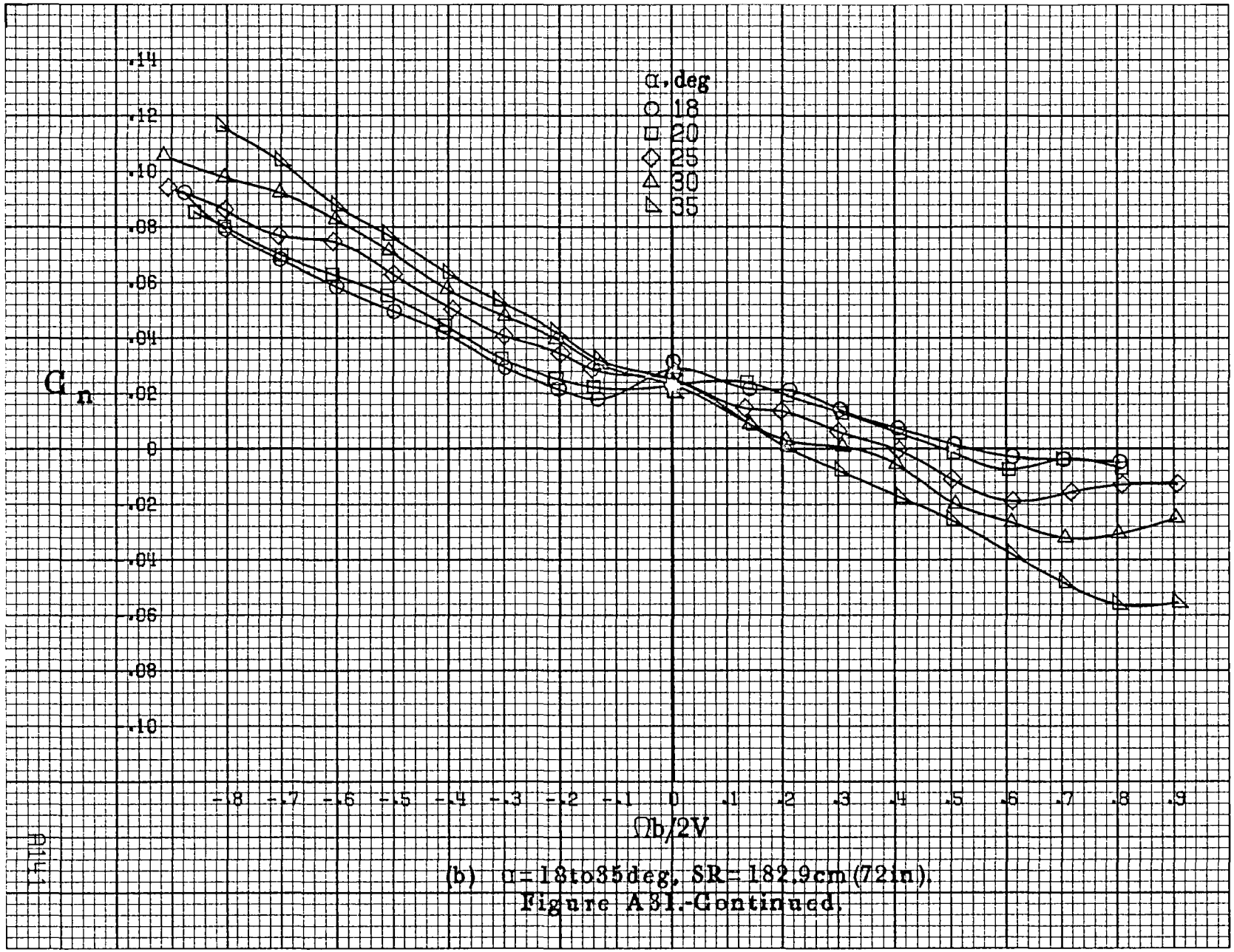

(b) α = 18 to 35 deg, SR = 182.9 cm (72 in).

Figure A31.-Continued.

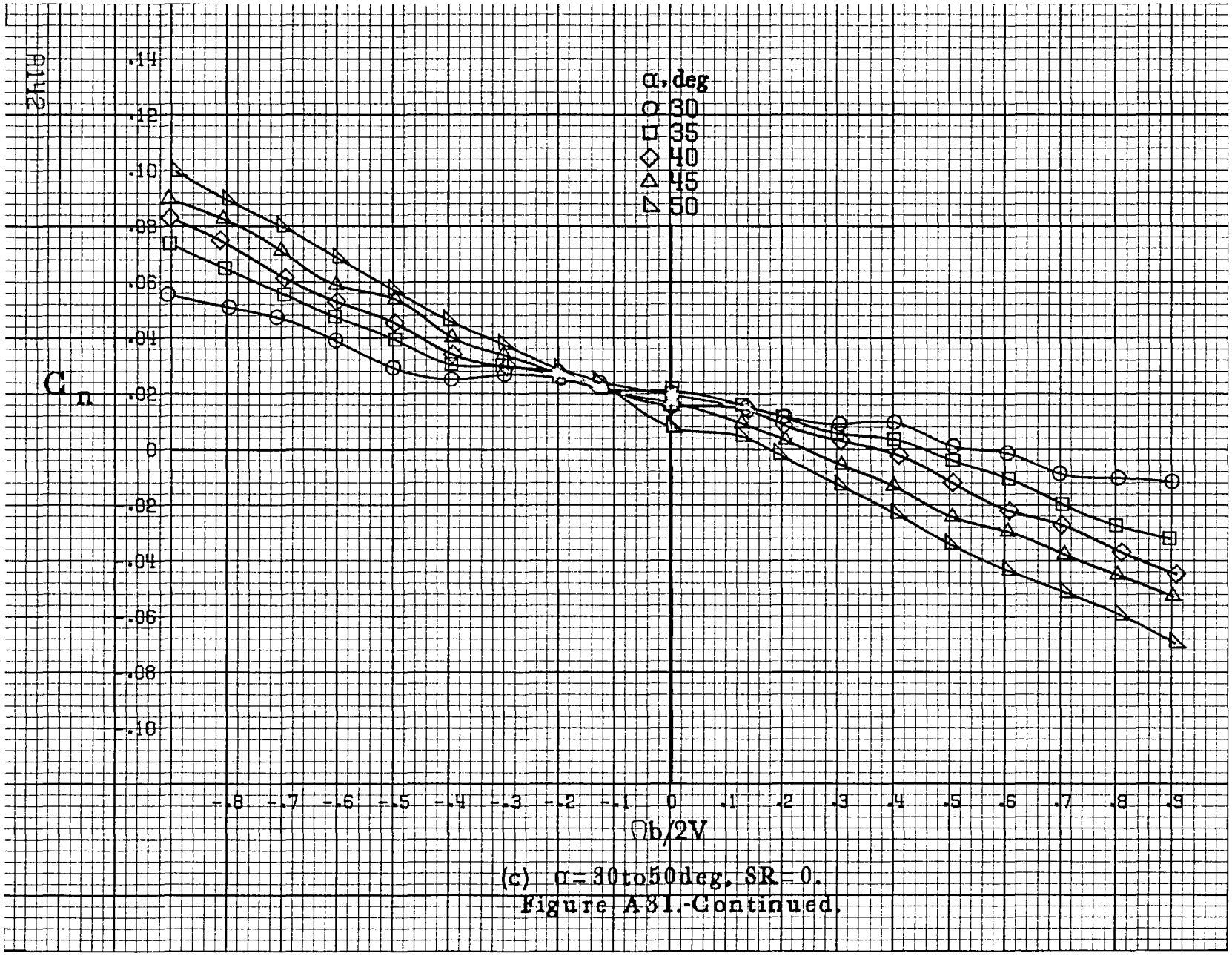

(c) α = 30 to 50 deg, SR = 0.

Figure A31.-Continued.

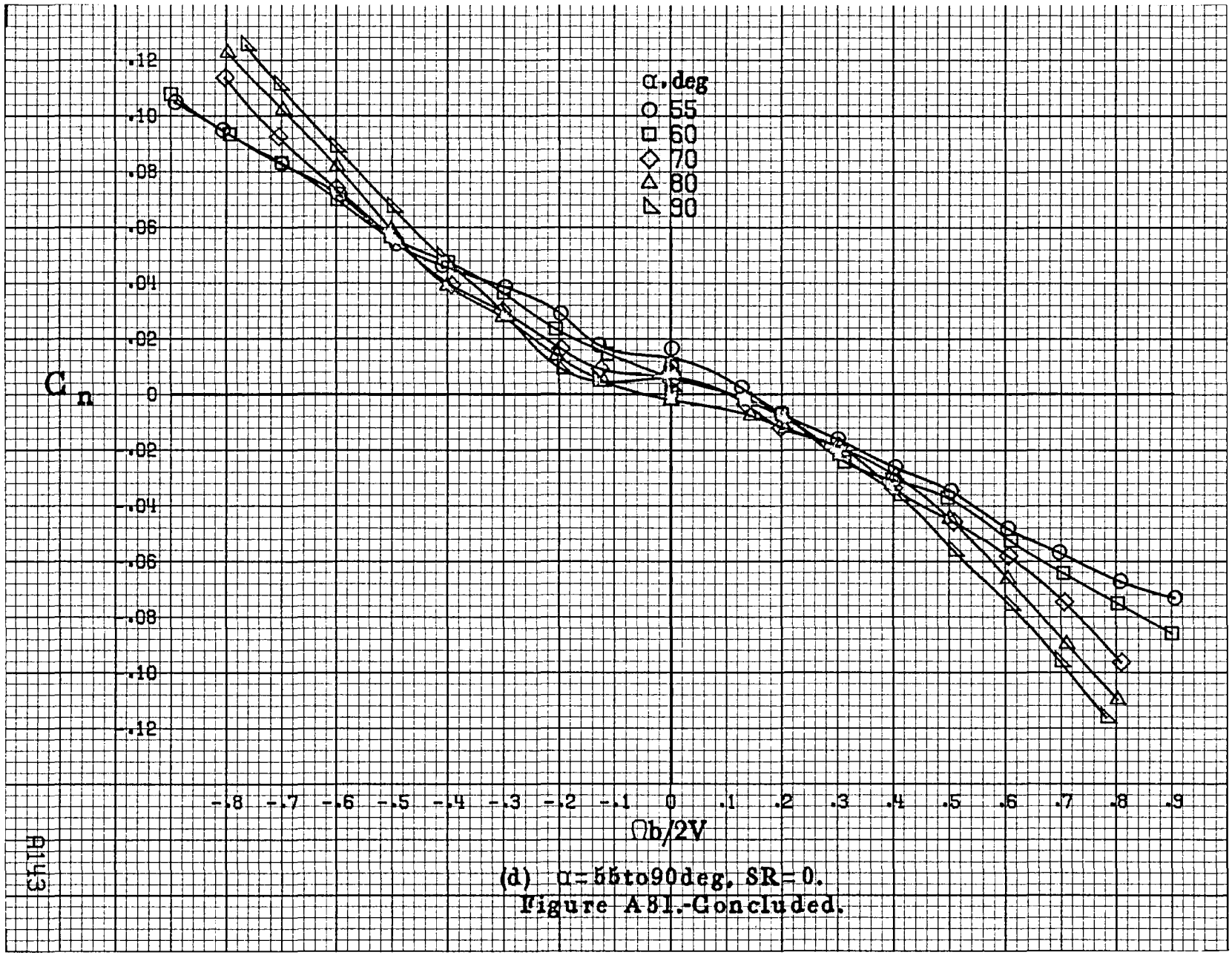

(d) α=55to90deg, SR=0.

Figure A31.-Concluded.

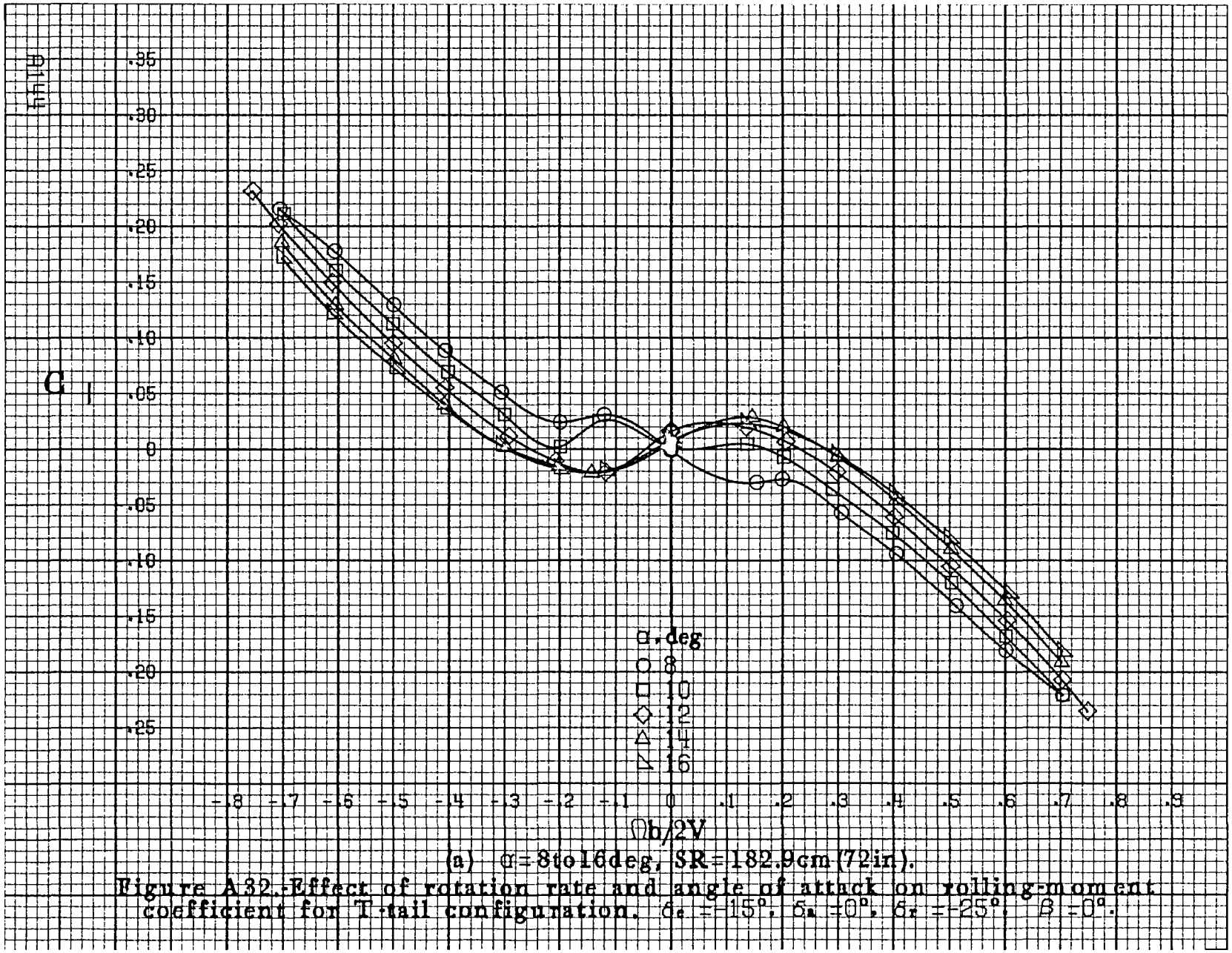

(a) α = 8 to 16 deg, SR = 182.9 cm (72 in.).

Figure A32.-Effect of rotation rate and angle of attack on rolling-moment coefficient for T-tail configuration. $\delta_e = -15°$, $\delta_a = 0°$, $\delta_r = -25°$, $\beta = 0°$.

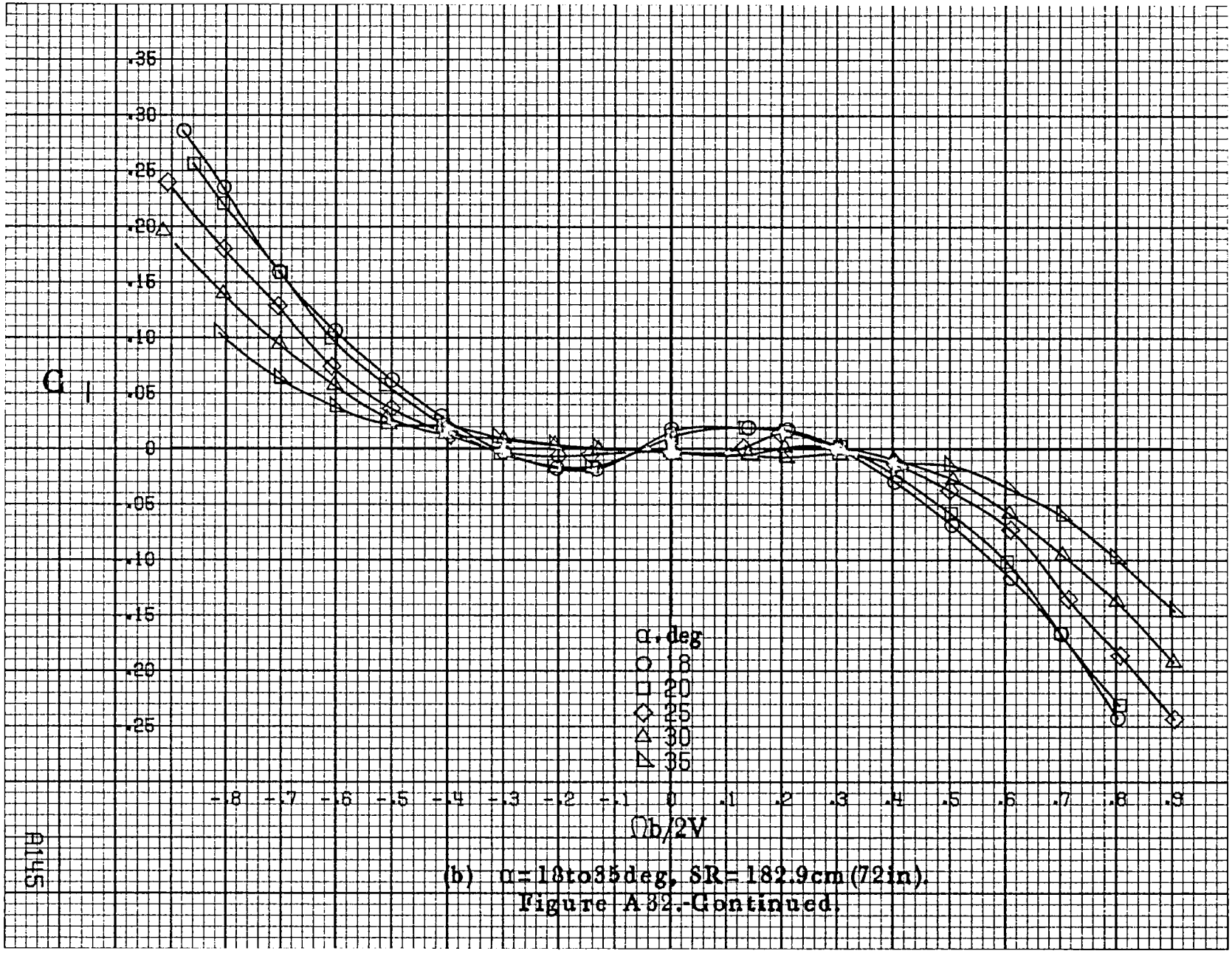

(b) α = 18 to 35 deg, SR = 182.9 cm (72 in).

Figure A32.-Continued.

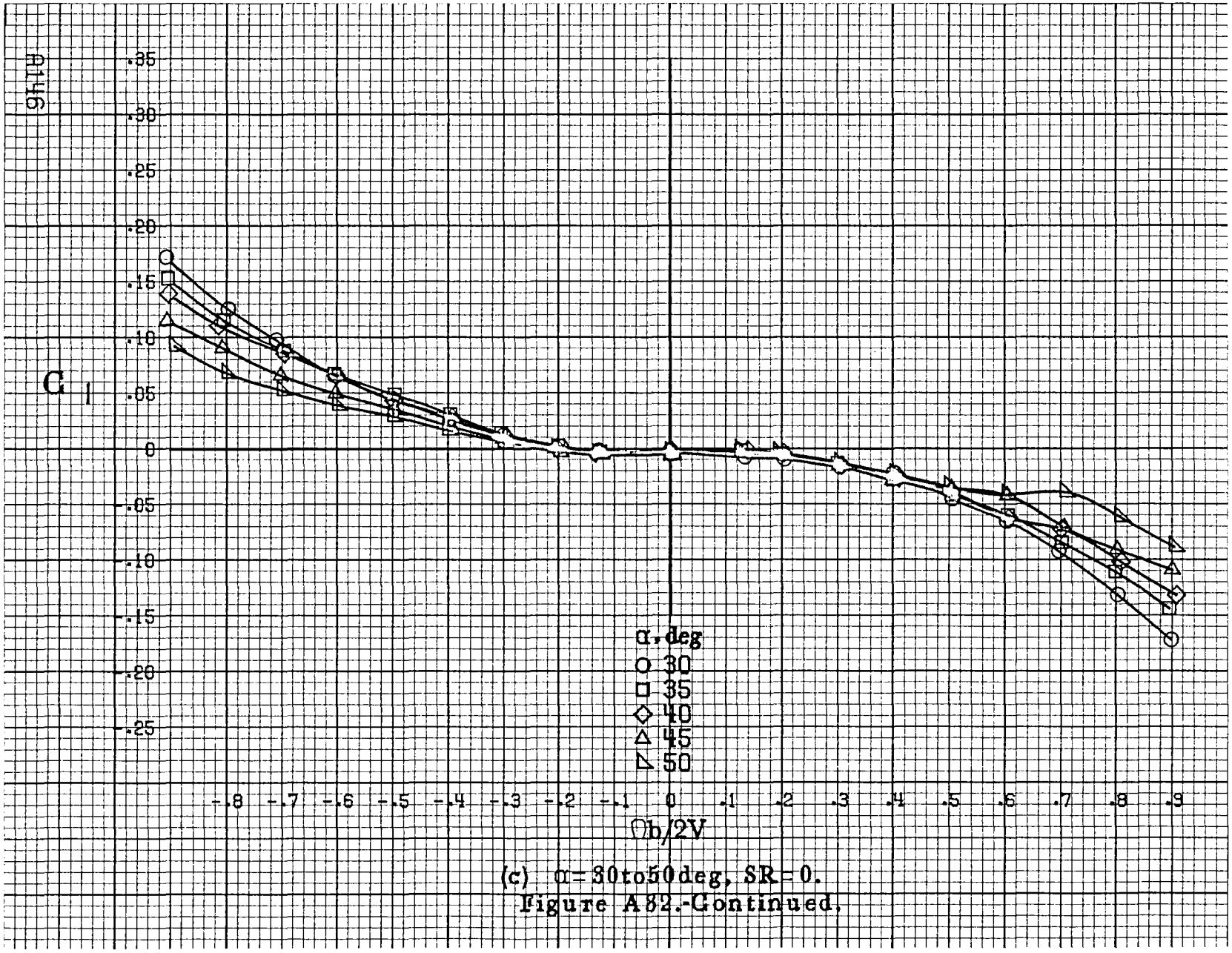

(c) $\alpha = 30$ to 50 deg, SR = 0.

Figure A82.-Continued.

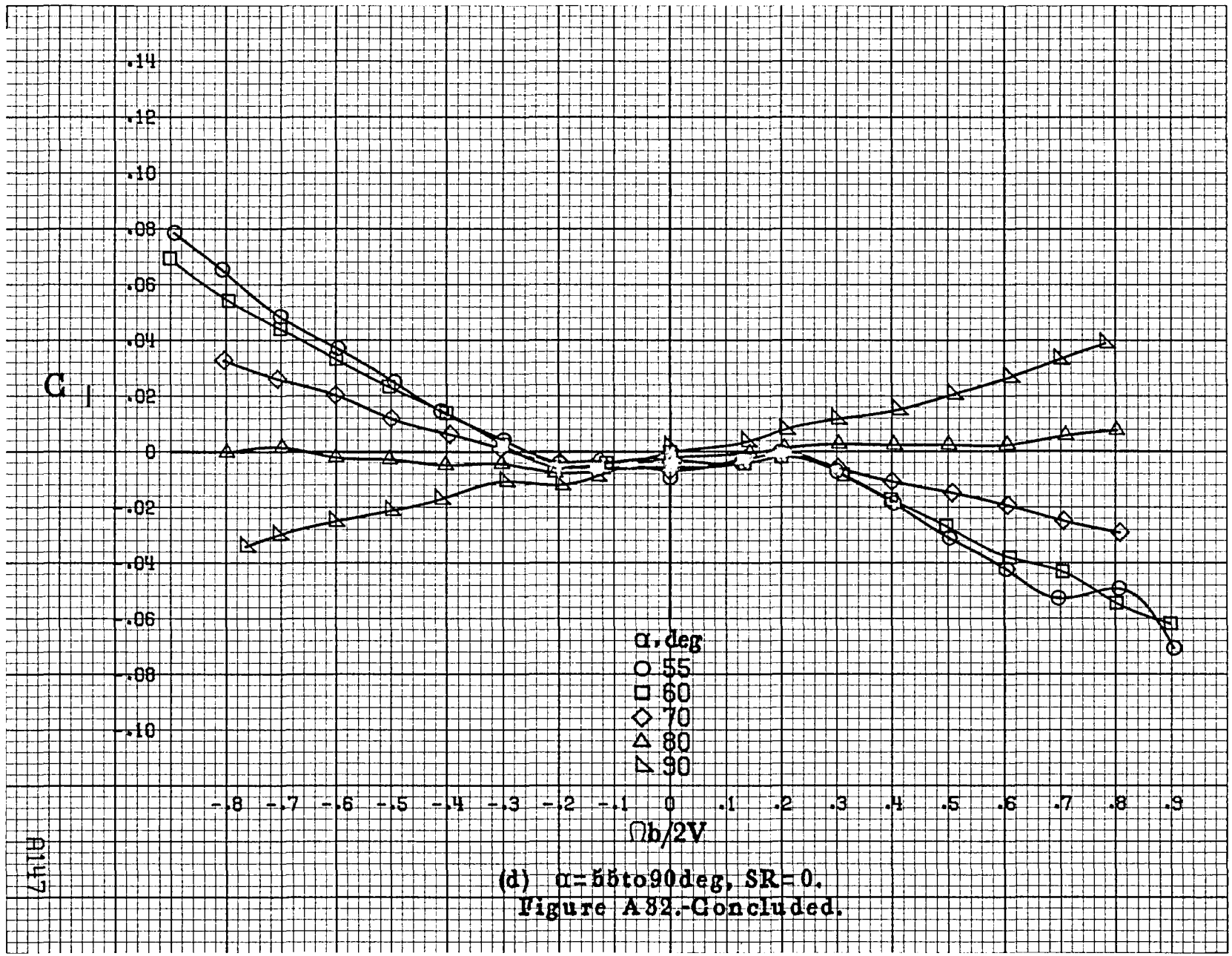

(d) α=55to90deg, SR=0.

Figure A82.-Concluded.

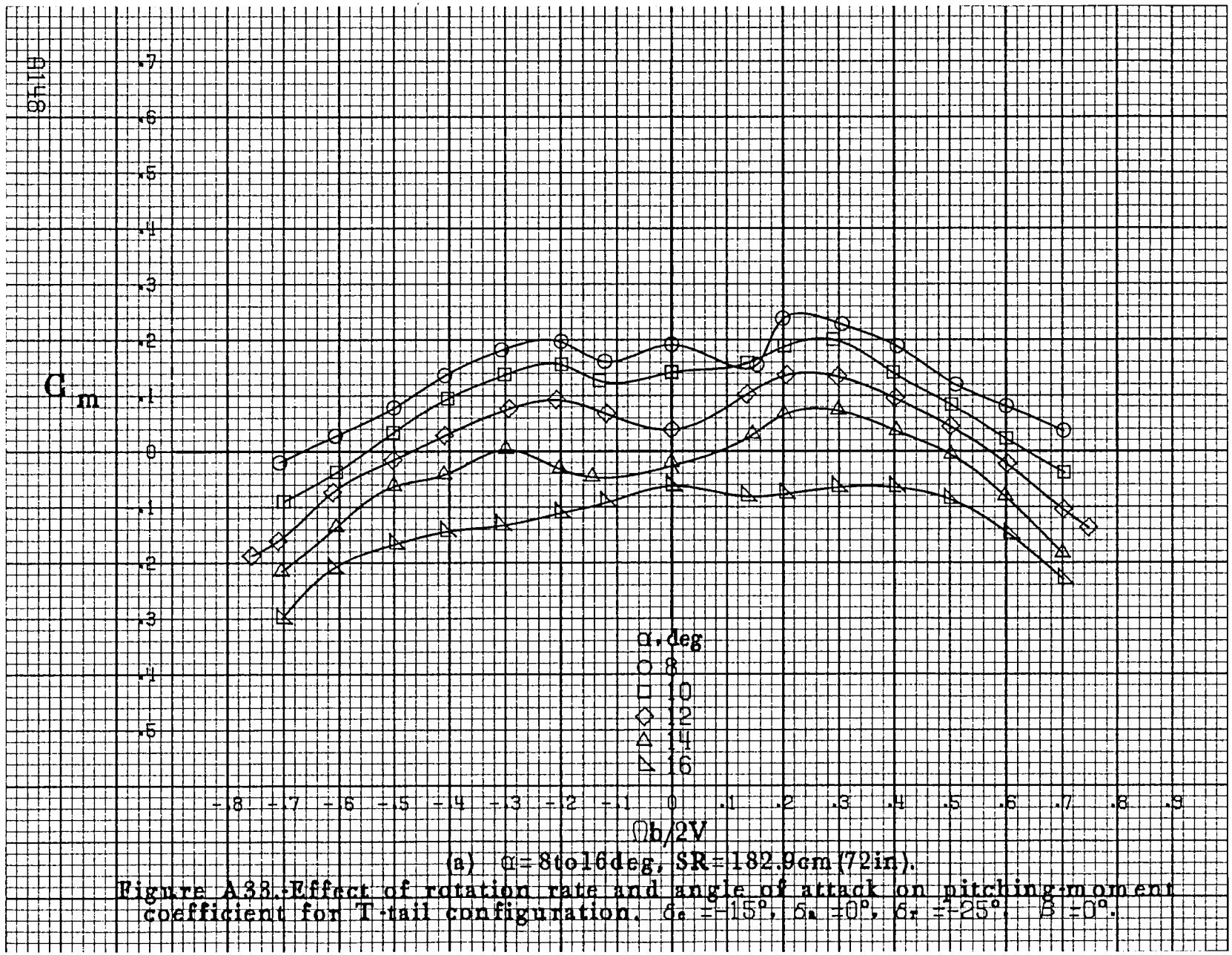

(a) α = 8 to 16 deg, SR = 182.9 cm (72 in.).

Figure A38.-Effect of rotation rate and angle of attack on pitching-moment coefficient for T-tail configuration. δ_e = -15°, δ_a = 0°, δ_r = -25°, β = 0°.

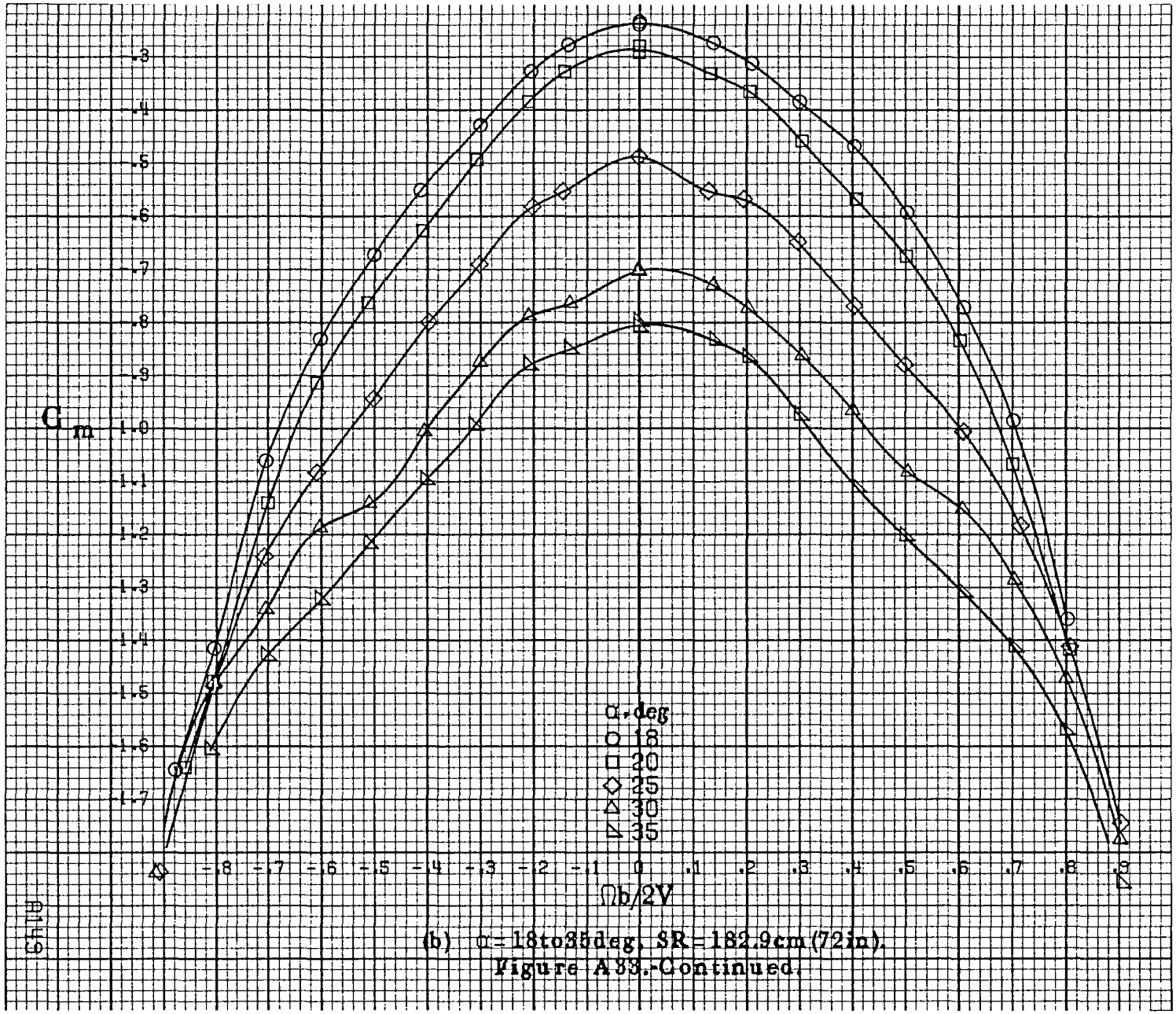

(b) α = 18 to 35 deg, SR = 182.9 cm (72 in).

Figure A33.-Continued.

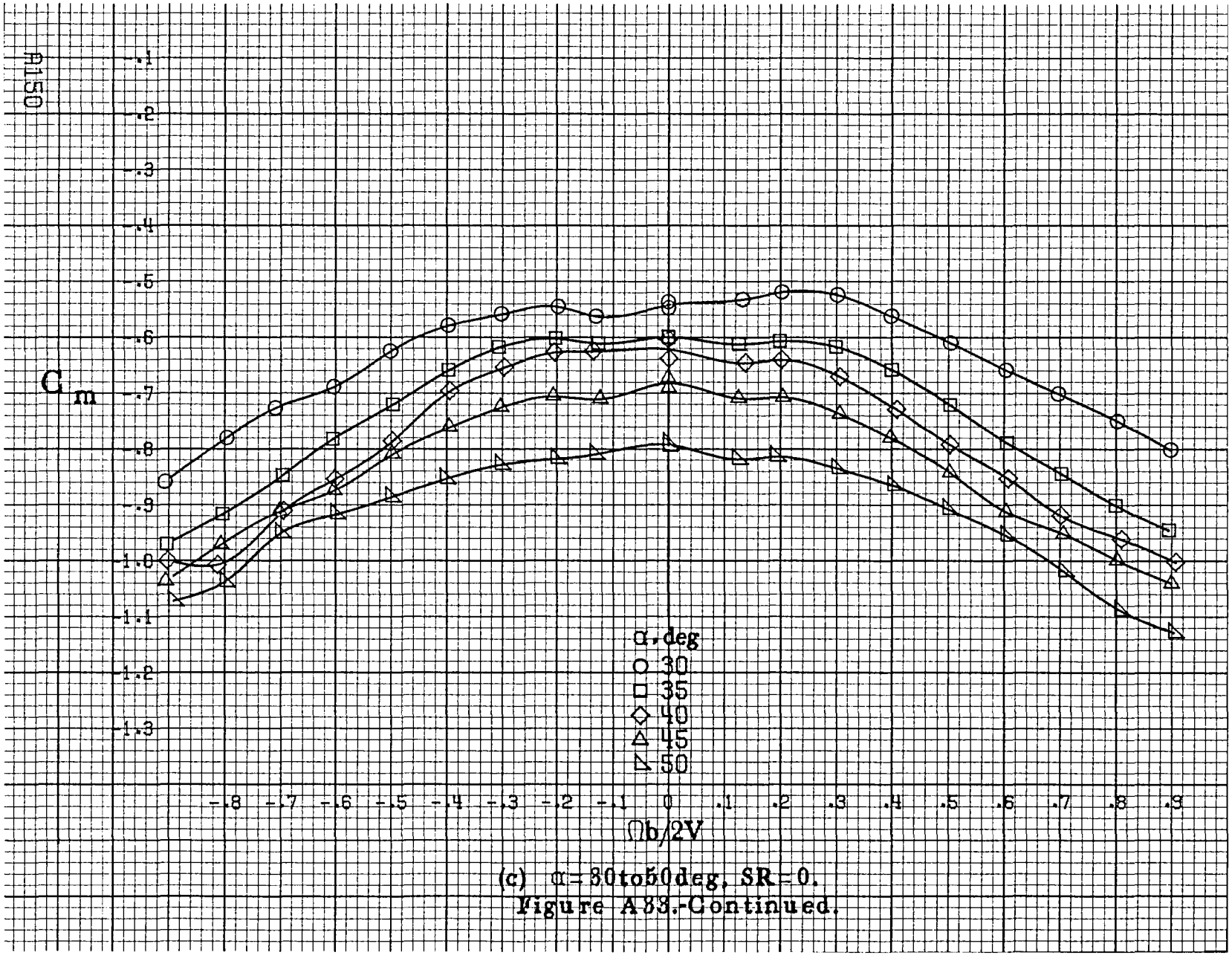

(c) α = 30 to 50 deg, SR = 0.

Figure A33.-Continued.

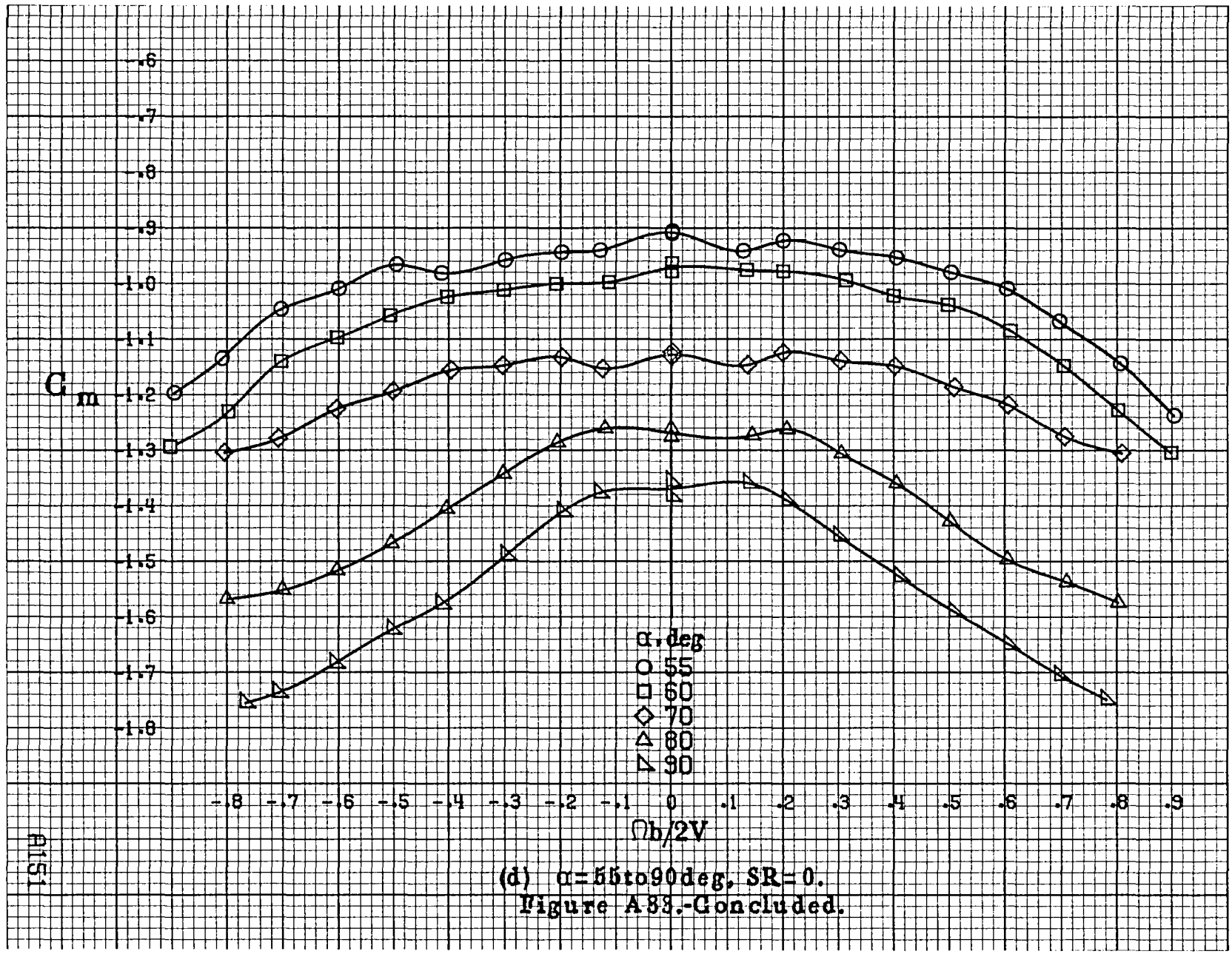

(d) α=55to90deg, SR=0.

Figure A33.-Concluded.

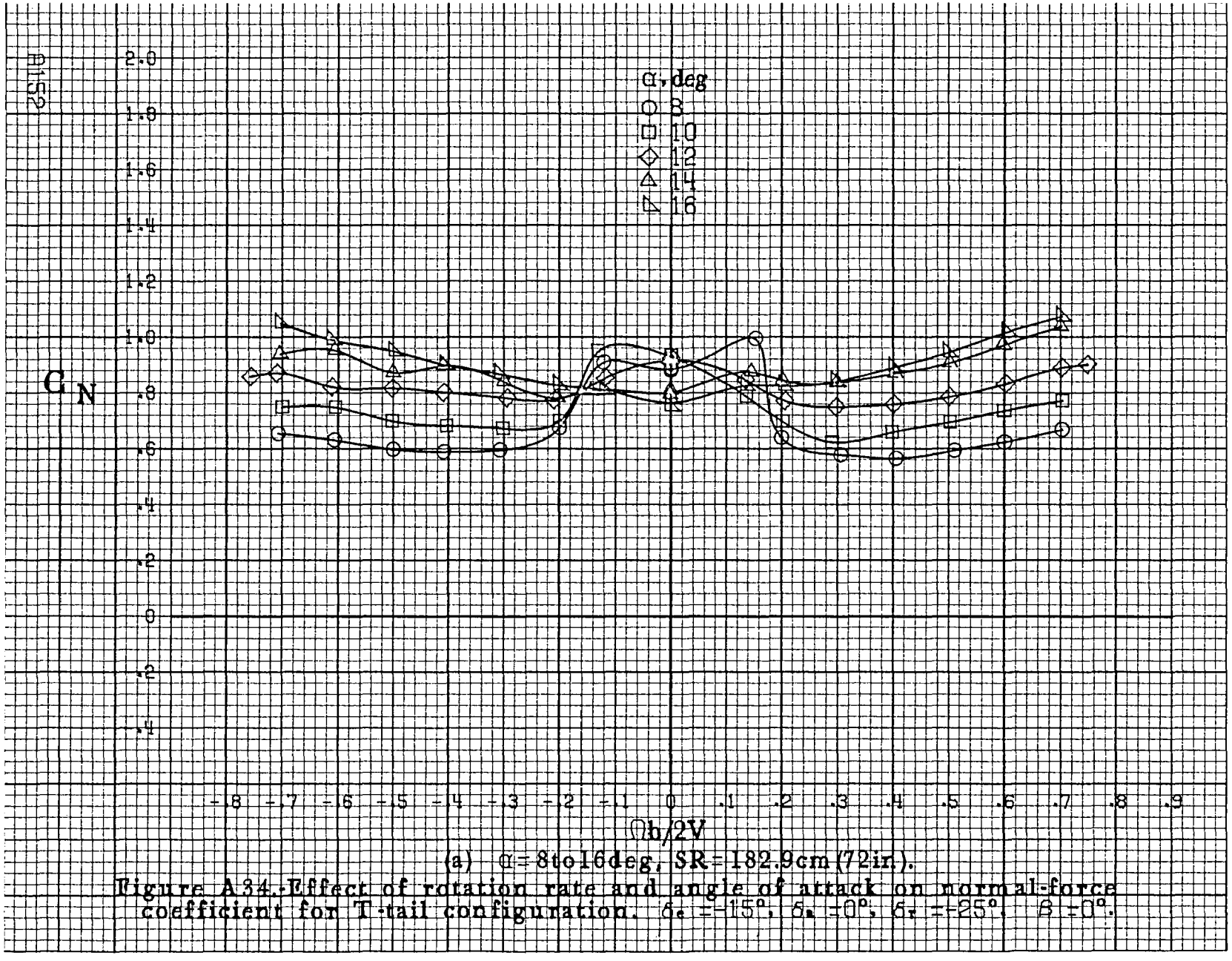

(a) α = 8 to 16 deg, SR = 182.9 cm (72 in.).

Figure A34.-Effect of rotation rate and angle of attack on normal-force coefficient for T-tail configuration. $\delta_e = -15°$, $\delta_a = 0°$, $\delta_r = +25°$, $\beta = 0°$.

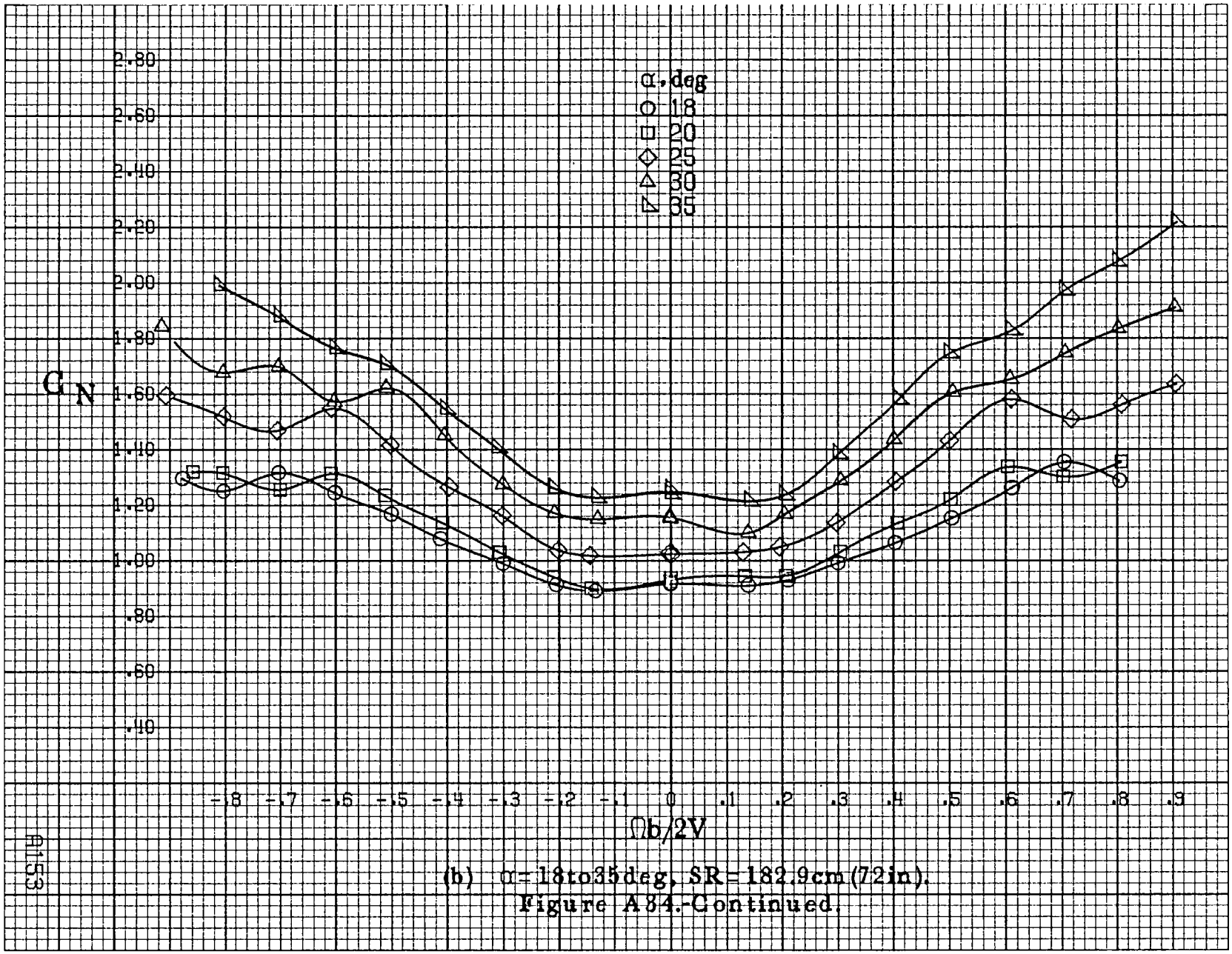

(b) α = 18 to 35 deg, SR = 182.9 cm (72 in).

Figure A84.-Continued.

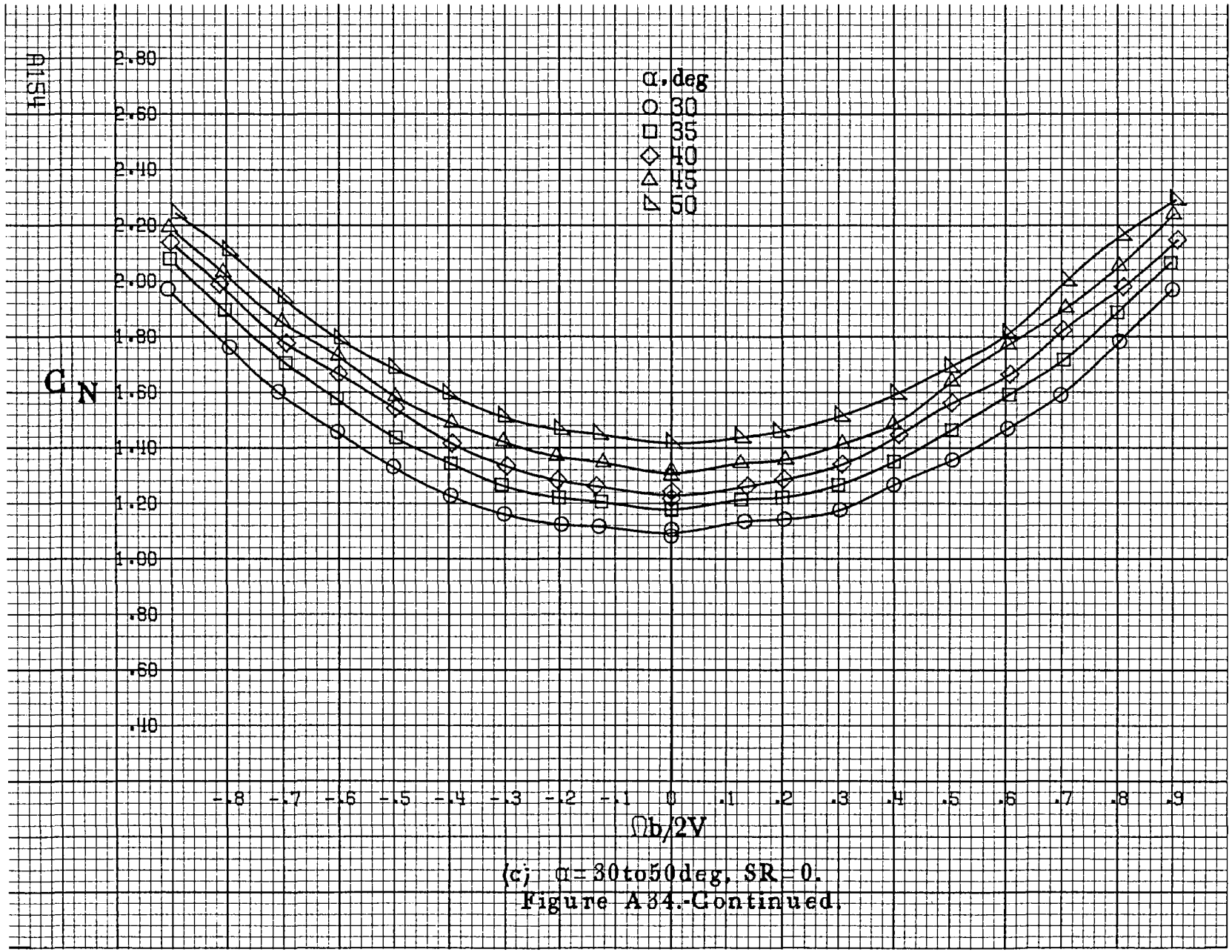

(c) $\alpha = 30$ to 50 deg, SR = 0.

Figure A34.-Continued.

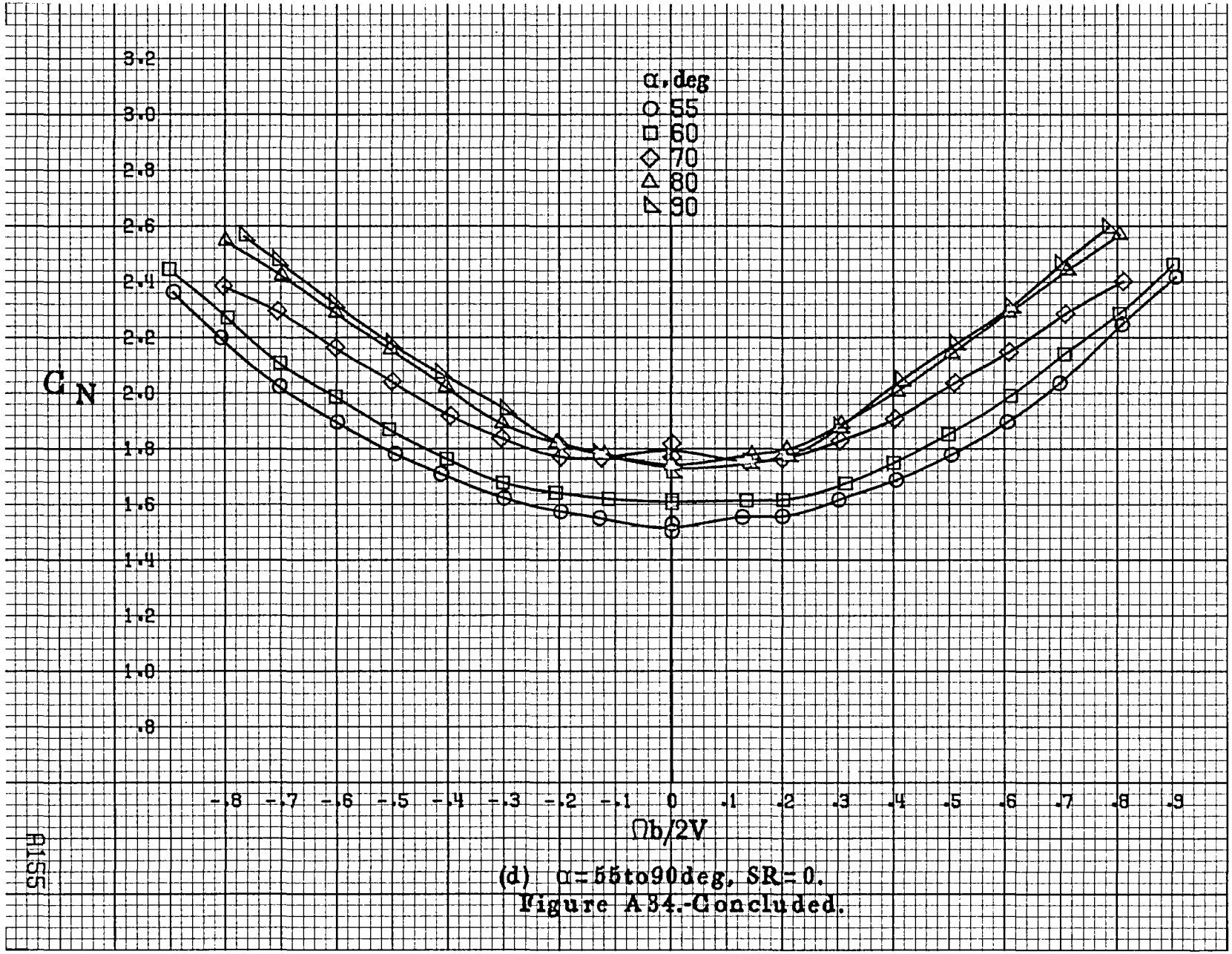

(d) α = 55 to 90 deg, SR = 0.

Figure A34.-Concluded.

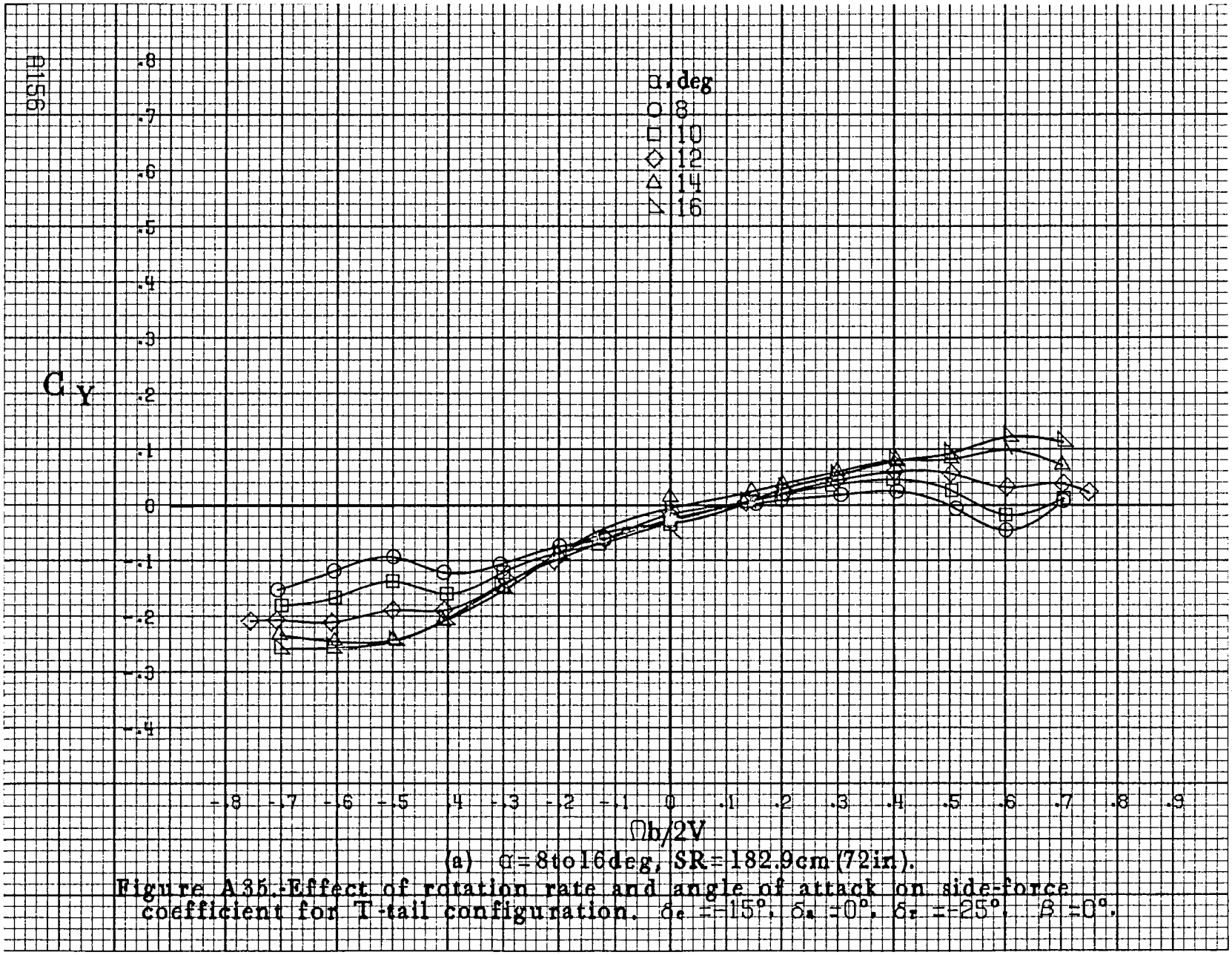

(a) α=8to16deg, SR=182.9cm(72in).

Figure A35.-Effect of rotation rate and angle of attack on side-force coefficient for T-tail configuration. δ_e =-15°, δ_a =0°, δ_r =-25°, β =0°.

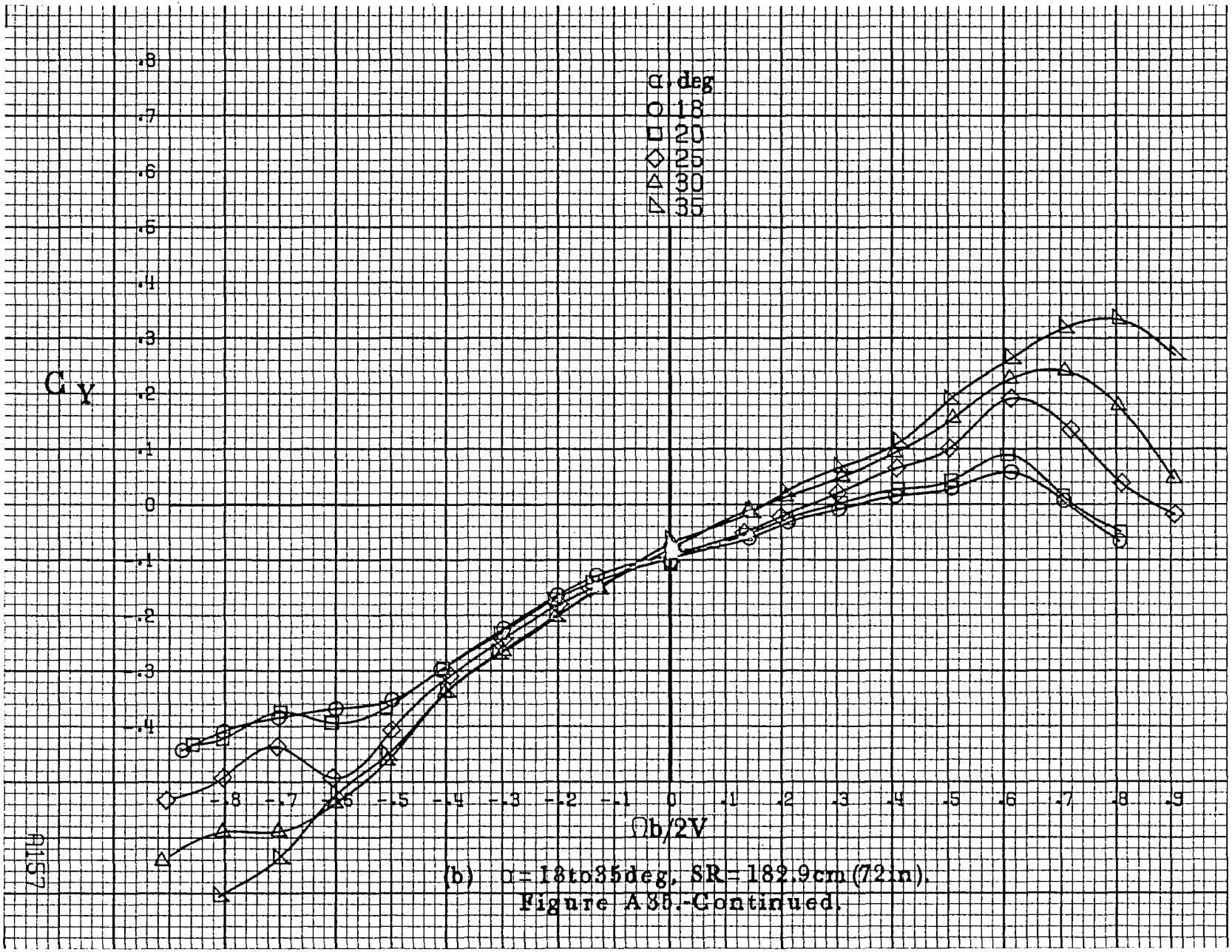

(b) α = 18 to 35 deg, SR = 182.9 cm (72 in).

Figure A35.-Continued.

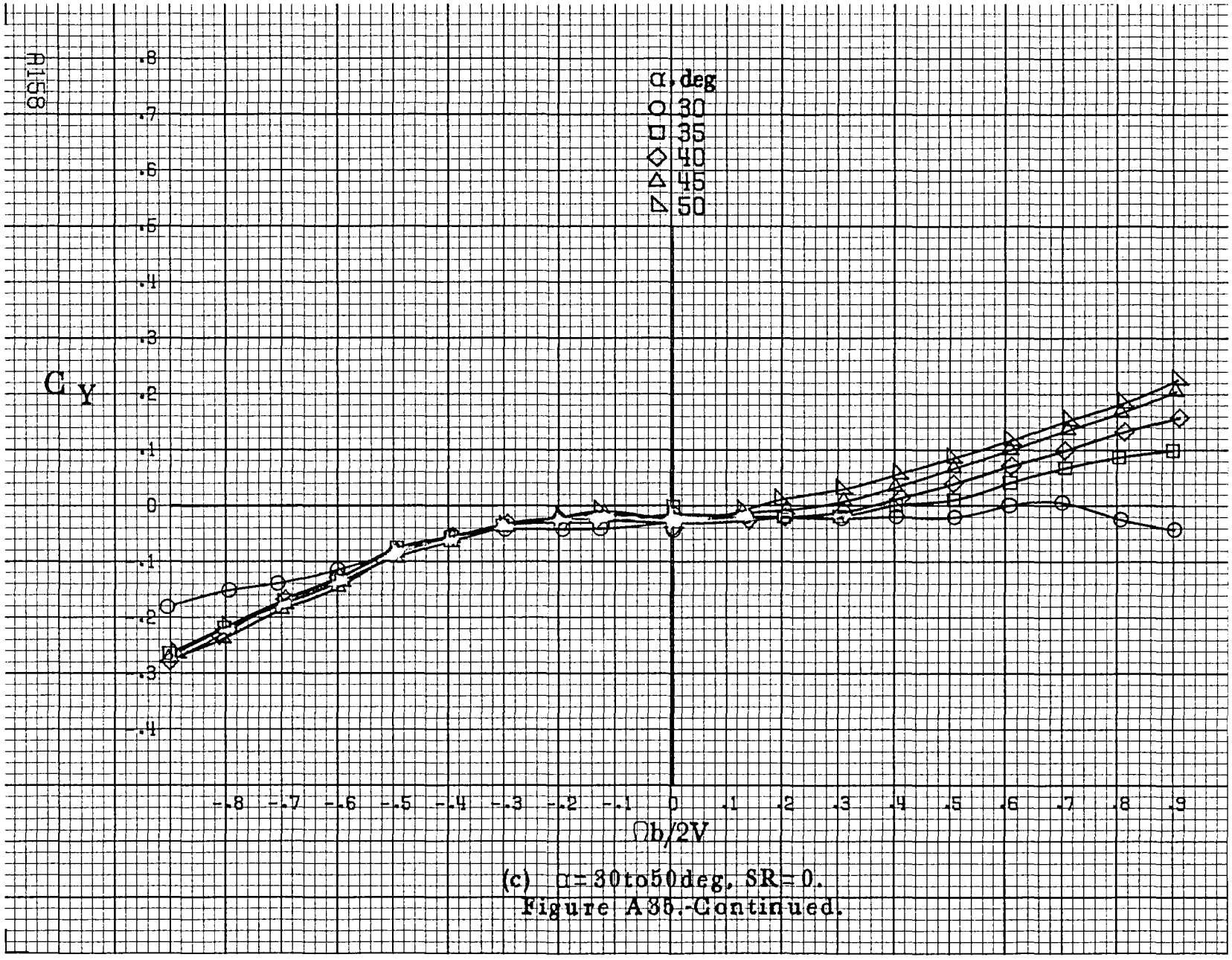

(c) α = 30 to 50 deg, SR = 0.

Figure A36.-Continued.

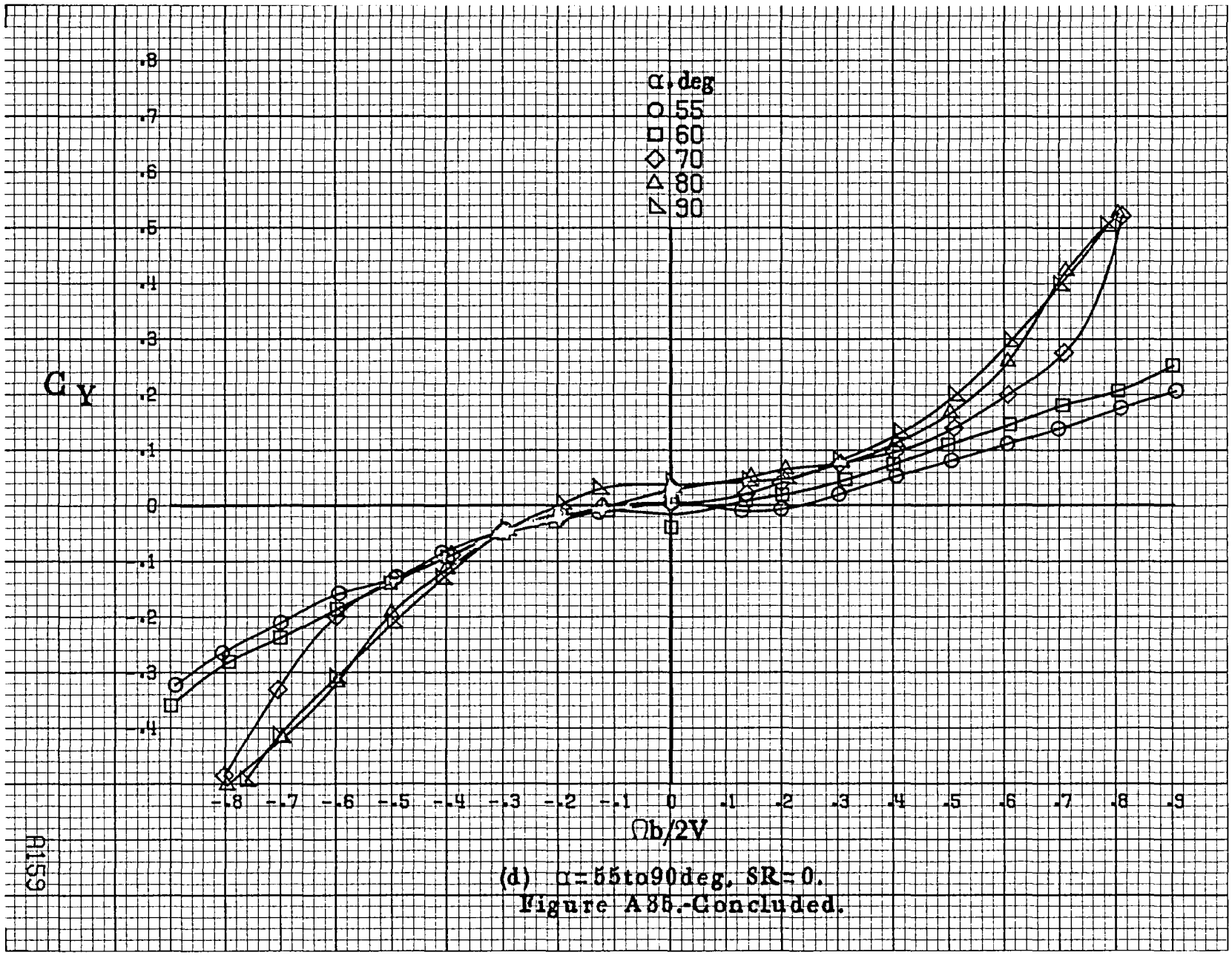

P-1559

(d) α = 55 to 90 deg, SR = 0.

Figure A35.- Concluded.

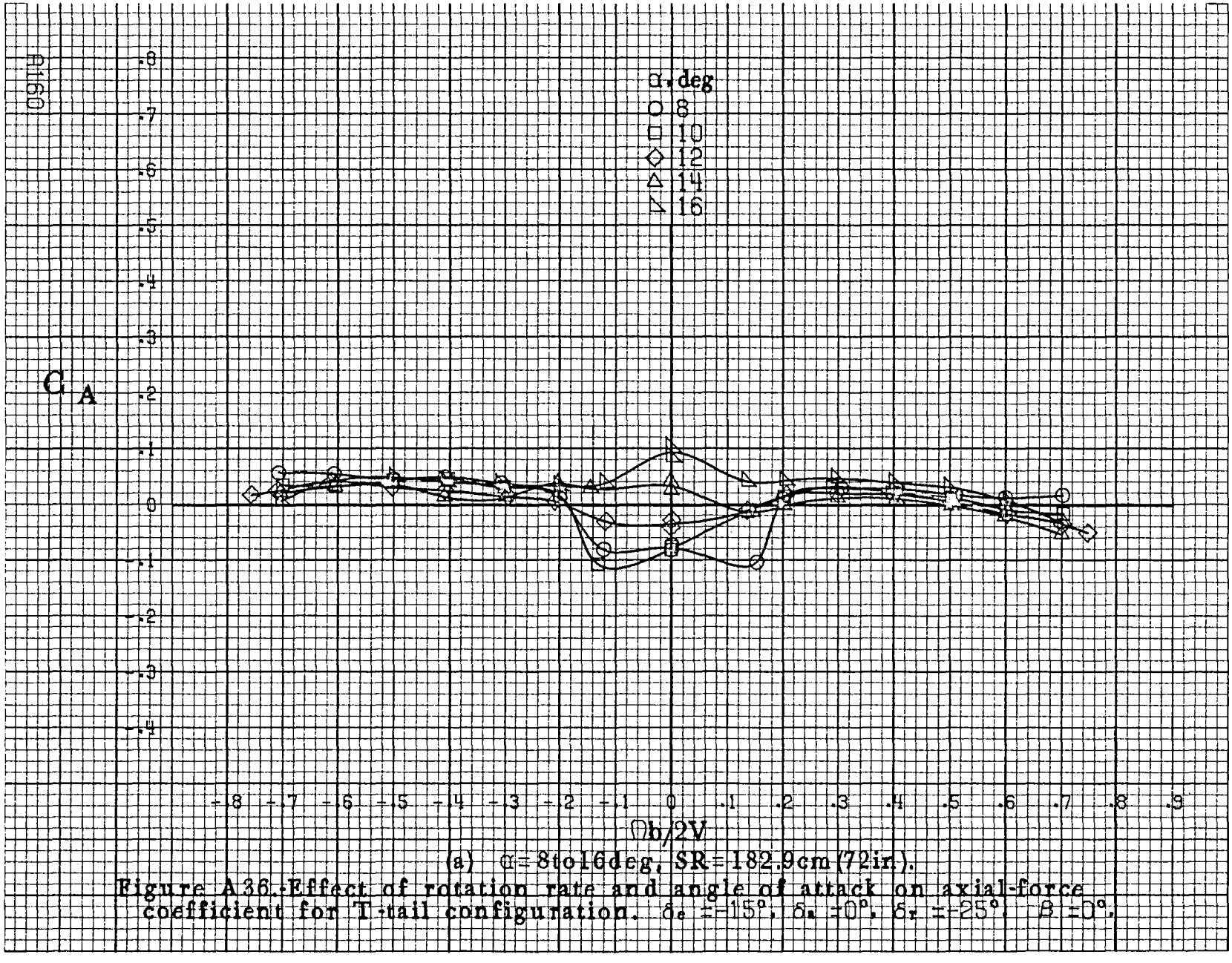

(a) $\alpha = 8$ to 16 deg, SR = 182.9 cm (72 in.).

Figure A36.-Effect of rotation rate and angle of attack on axial-force coefficient for T-tail configuration. $\delta_e = -15°$, $\delta_a = 0°$, $\delta_r = -25°$, $\beta = 0°$.

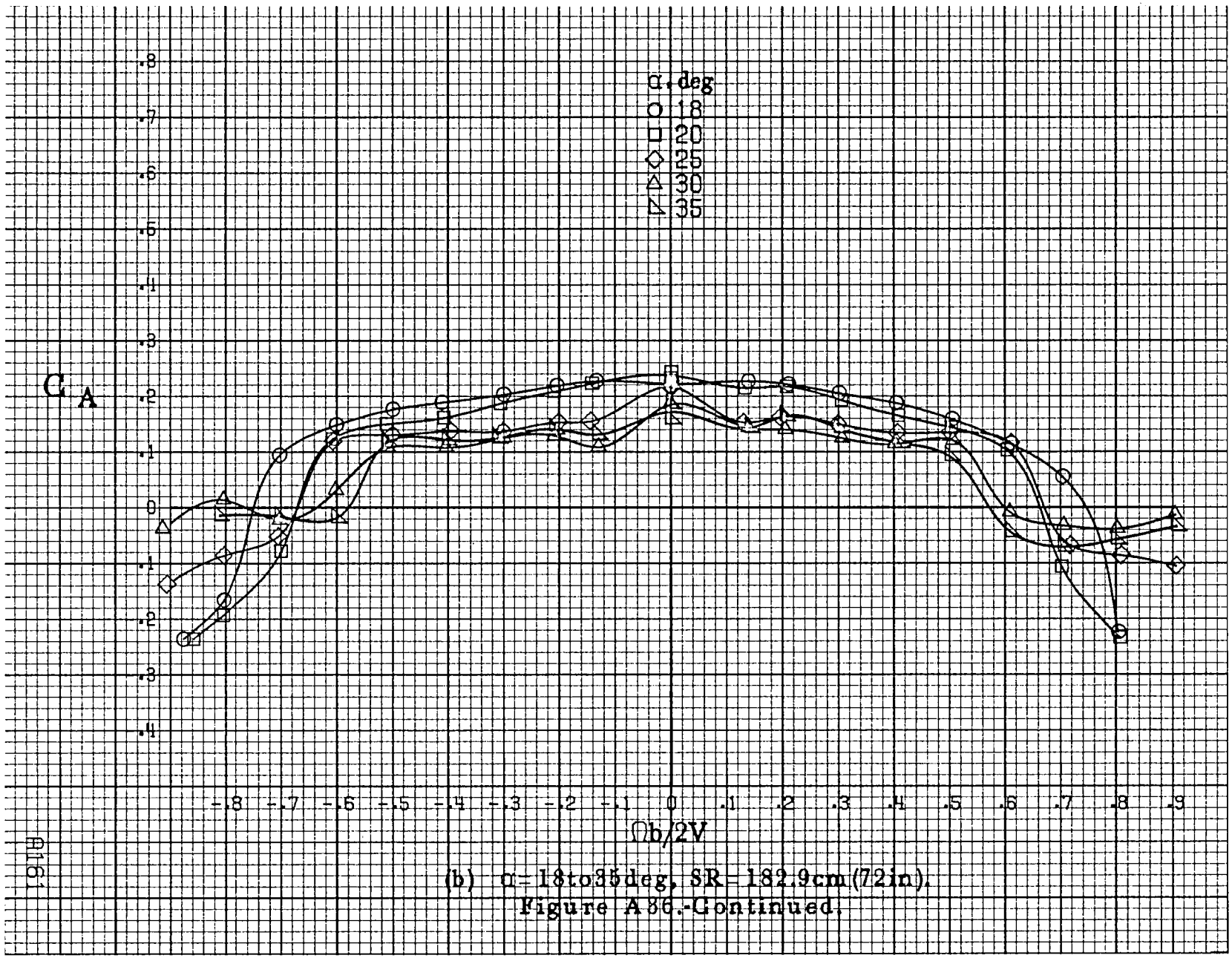

(b) α = 18 to 35 deg, SR = 182.9 cm (72 in).

Figure A36.-Continued.

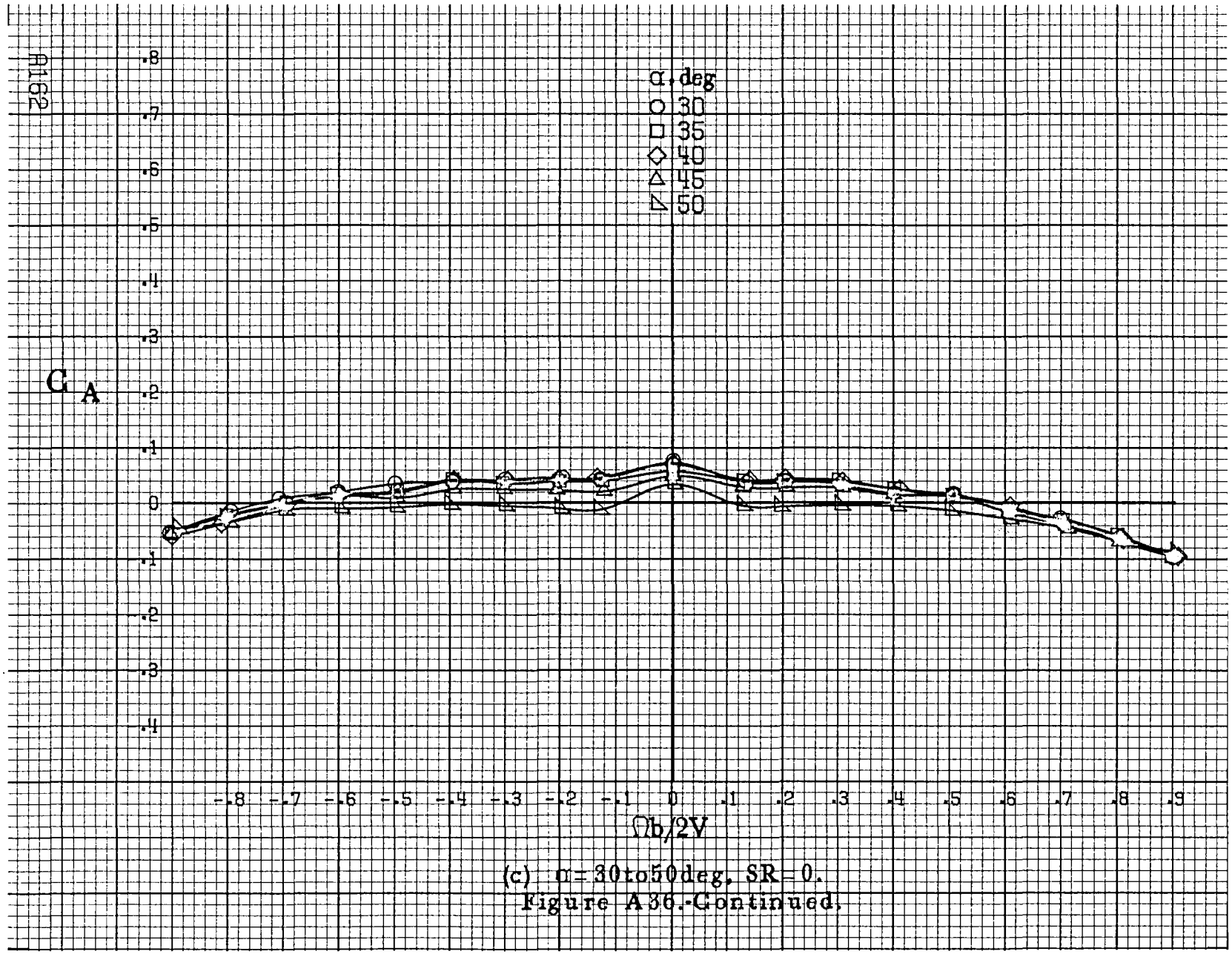

(c) $n = 30$ to 50 deg, $SR = 0$.

Figure A36.-Continued.

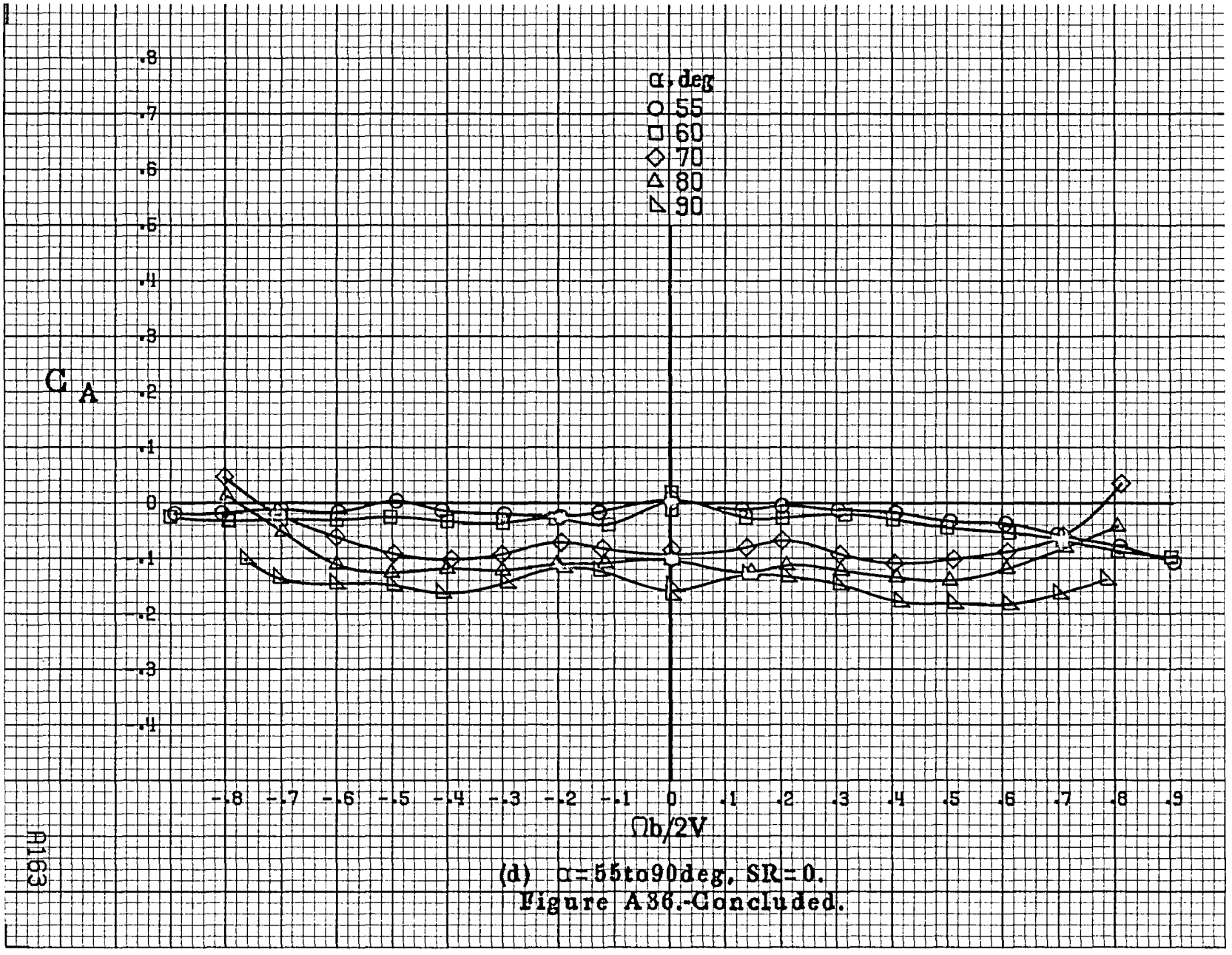

(d) α=55to90deg, SR=0.

Figure A36.-Concluded.

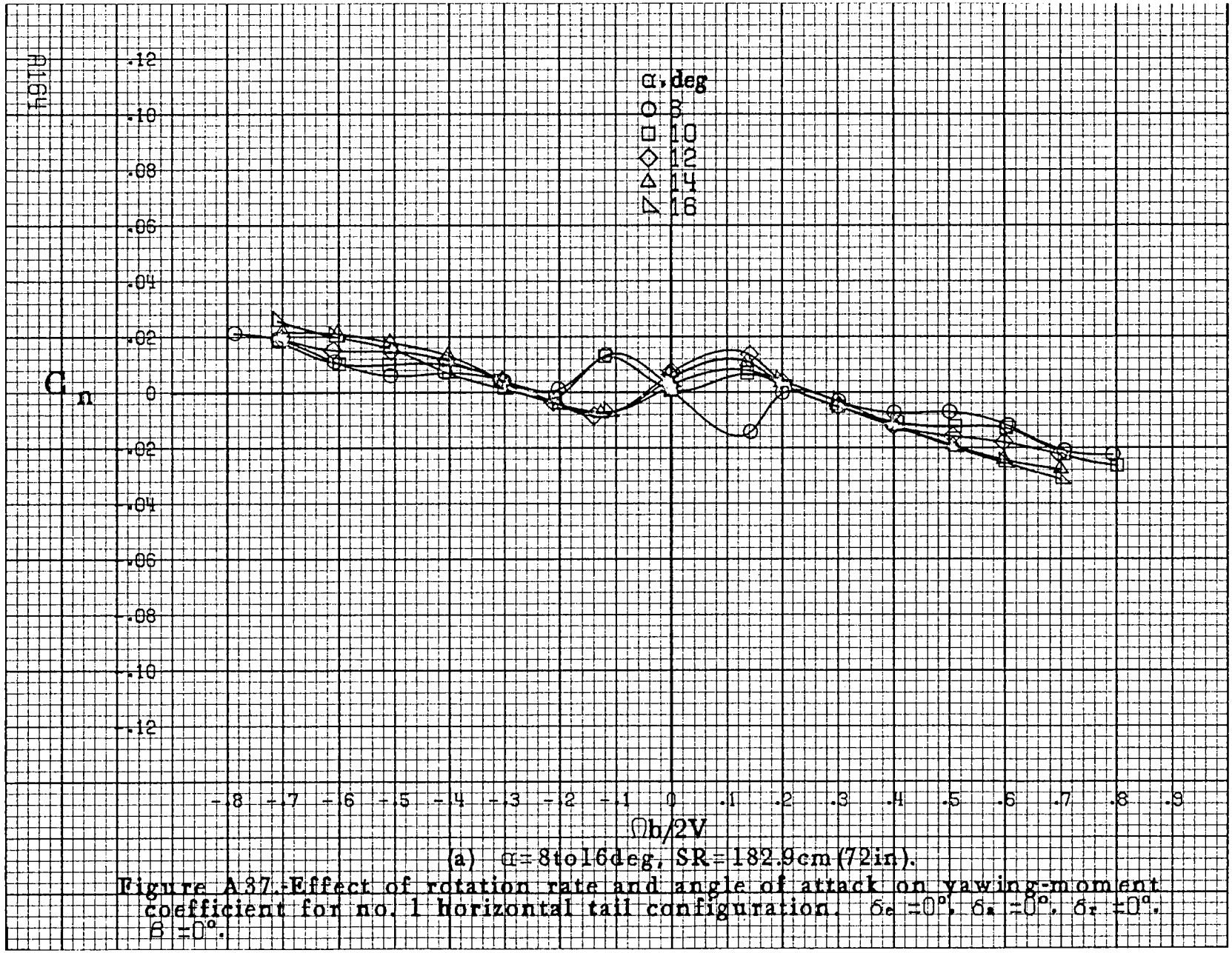

(a) α = 8 to 16 deg, SR = 182.9 cm (72 in).

Figure A37.-Effect of rotation rate and angle of attack on yawing-moment coefficient for no. 1 horizontal tail configuration. $\delta_e = 0°$, $\delta_a = 0°$, $\delta_r = 0°$, $\beta = 0°$.

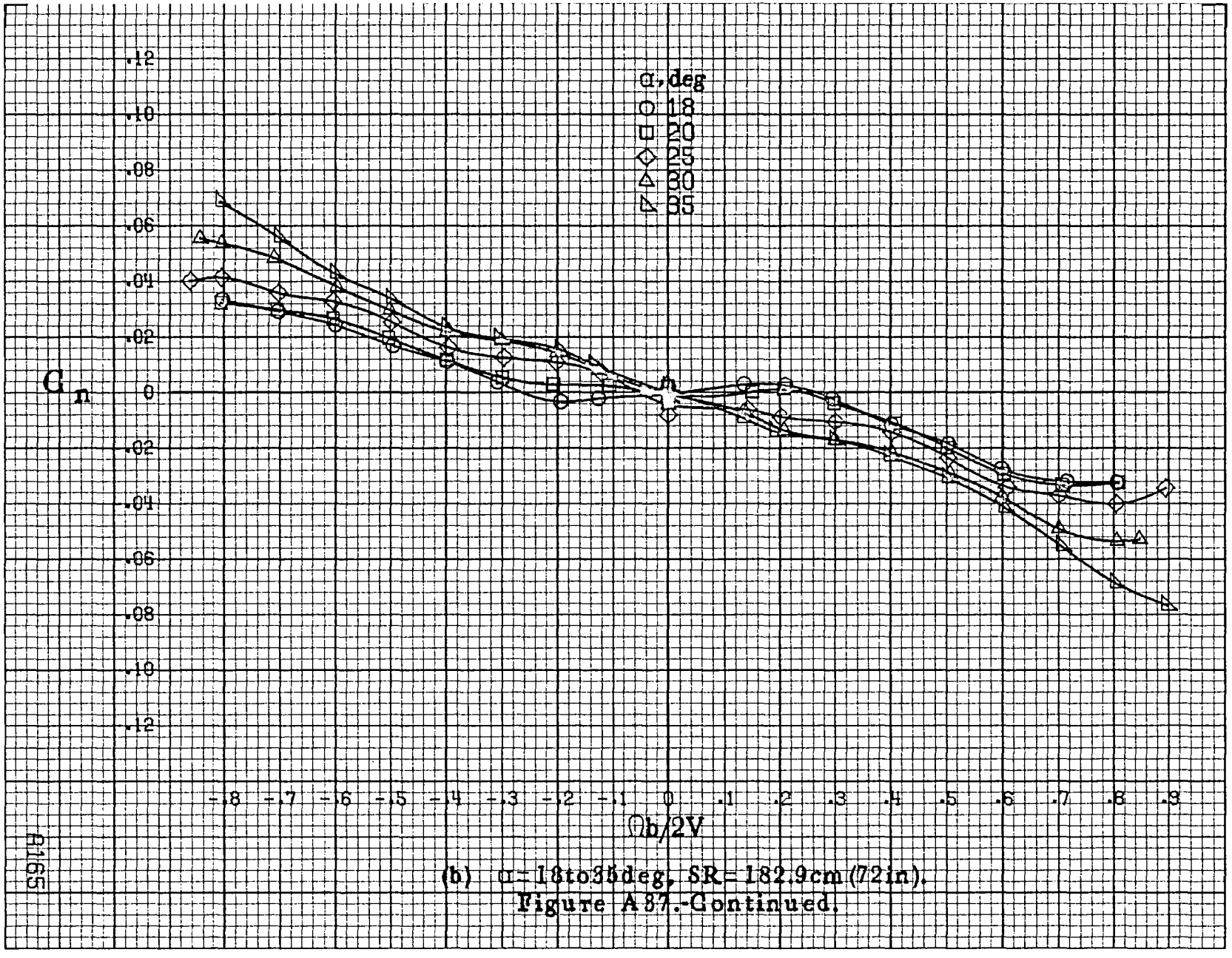

(b) α = 18 to 35 deg, SR = 182.9 cm (72 in).

Figure A87.-Continued.

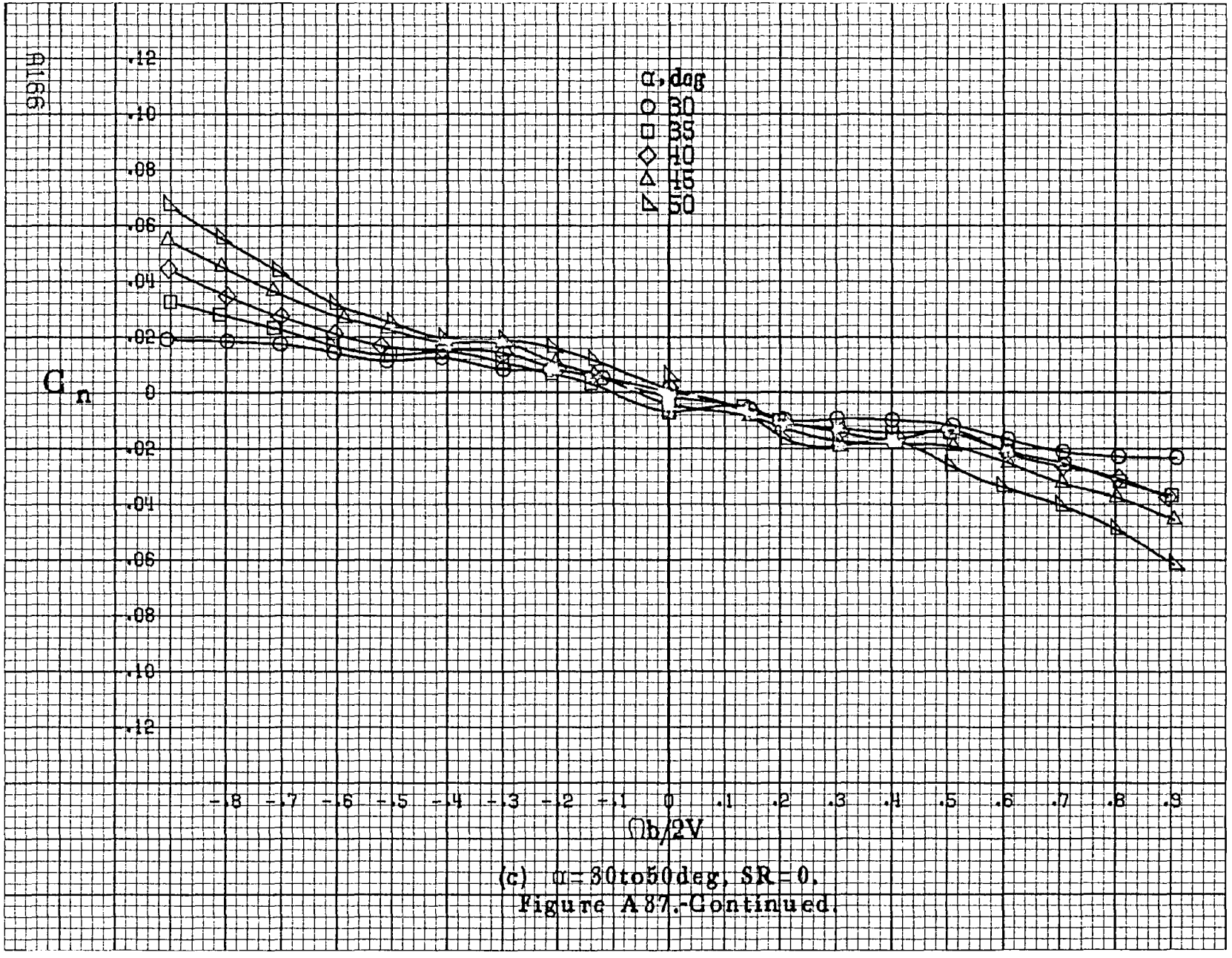

(c) α = 30 to 50 deg, SR = 0.

Figure A87.-Continued.

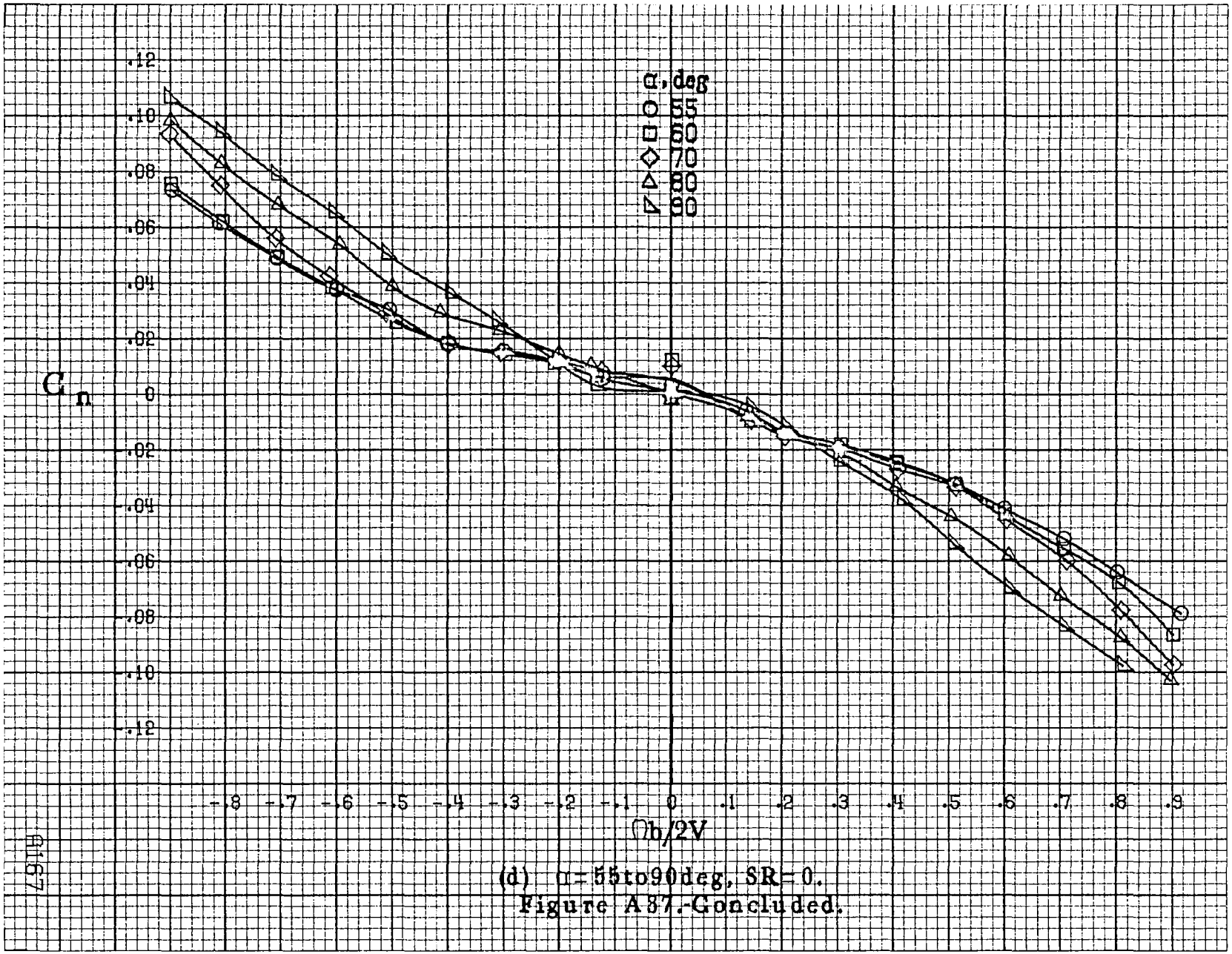

(d) α = 55 to 90 deg, SR = 0.

Figure A37.-Concluded.

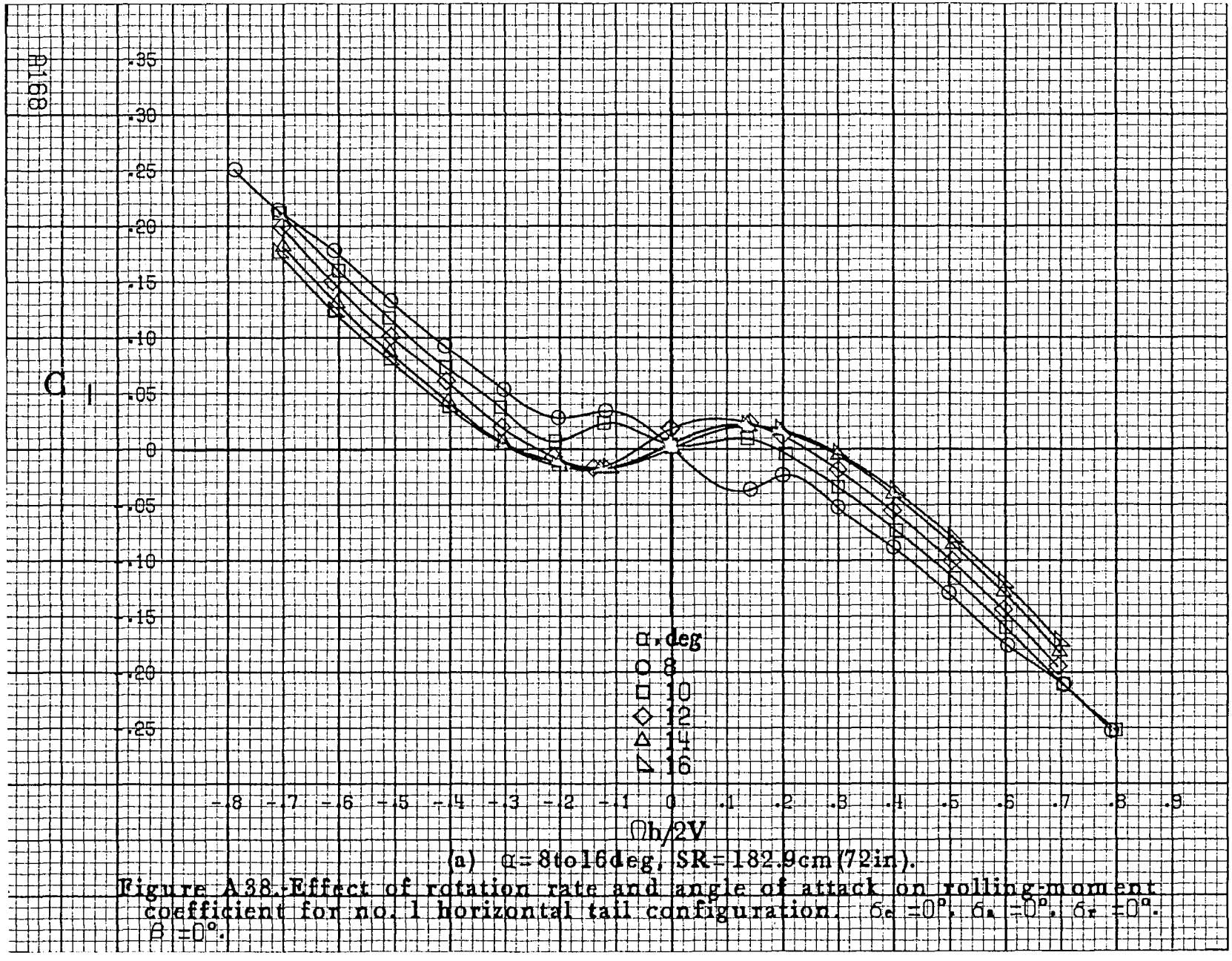

(a) α = 8 to 16 deg, SR = 182.9 cm (72 in.).

Figure A38.-Effect of rotation rate and angle of attack on rolling-moment coefficient for no. 1 horizontal tail configuration. $\delta_e = 0°$, $\delta_a = 0°$, $\delta_r = 0°$, $\beta = 0°$.

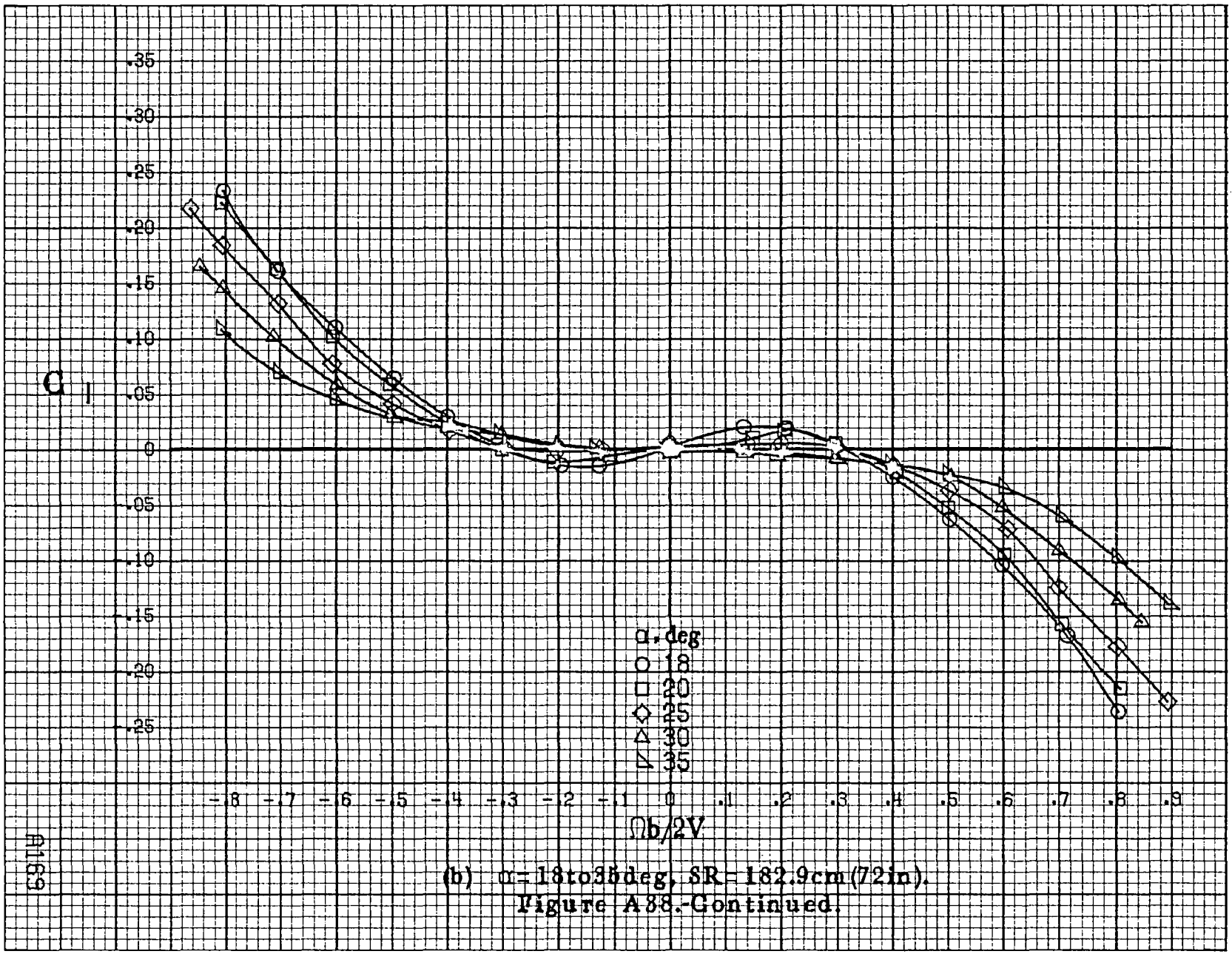

(b) $\alpha = 18$ to 35 deg, SR = 182.9 cm (72 in).

Figure A38.-Continued.

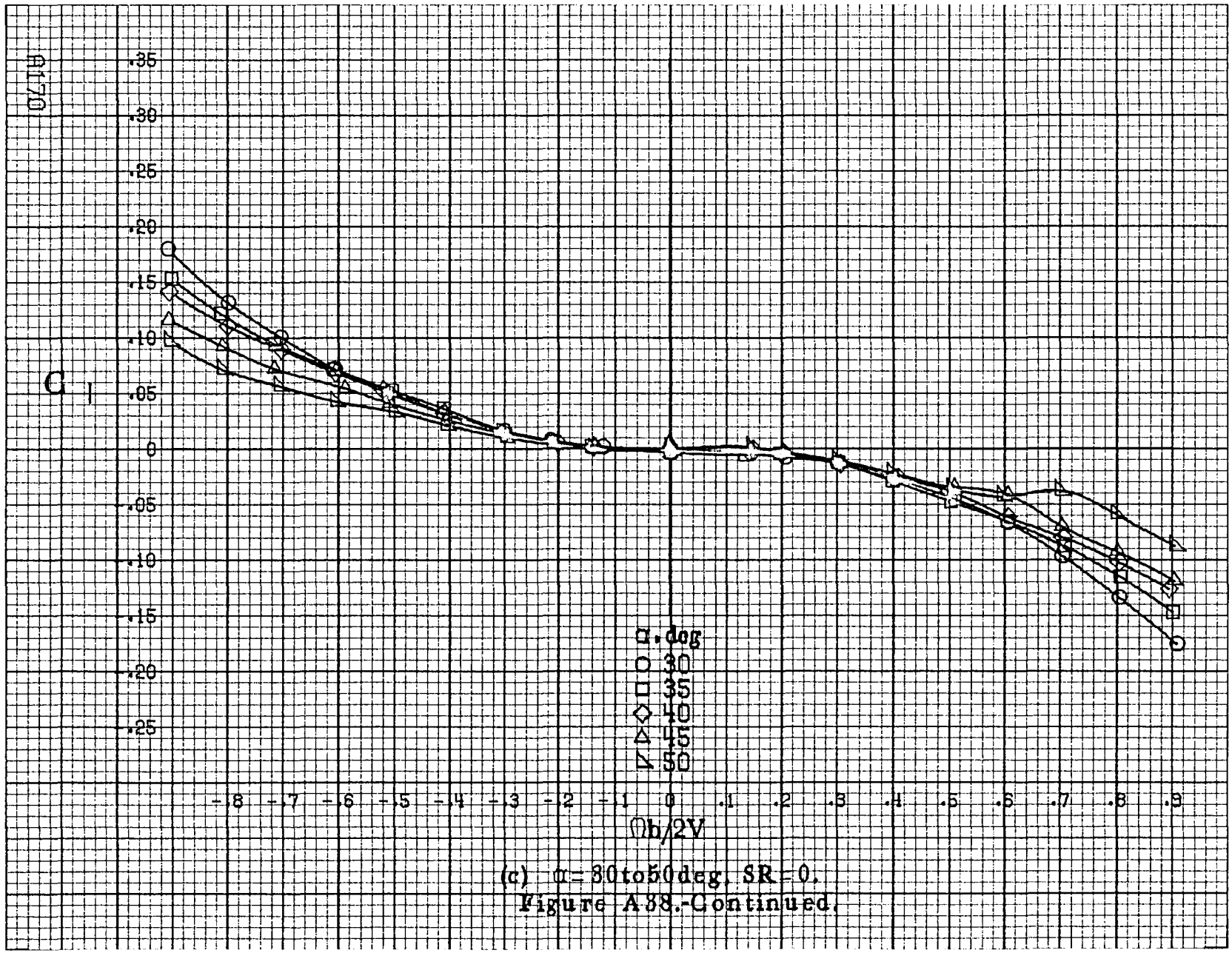

(c) $\alpha = 30$ to 50 deg, SR = 0.

Figure A38.-Continued.

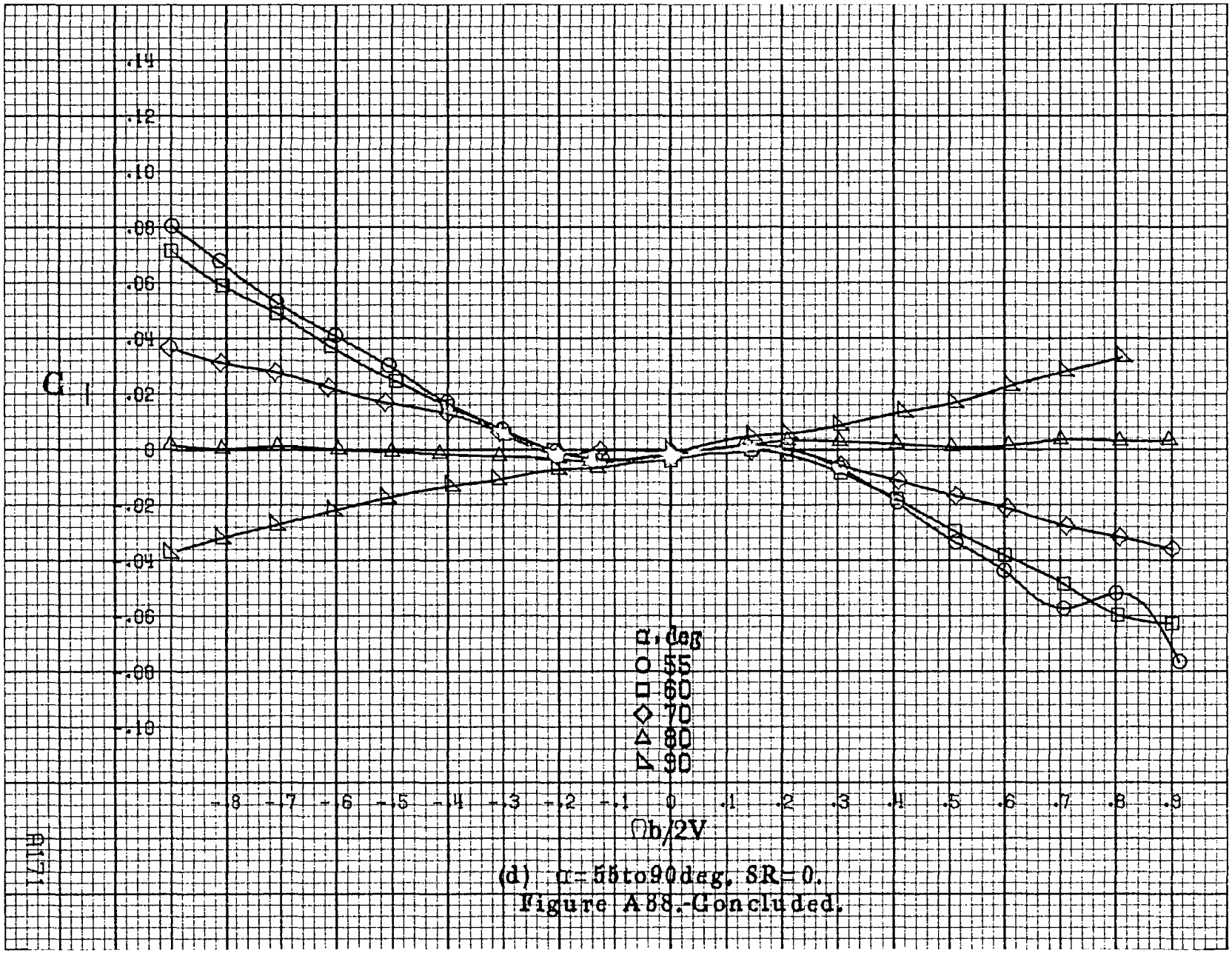

(d) $\alpha = 55$ to 90 deg, $SR = 0$.

Figure A88.-Concluded.

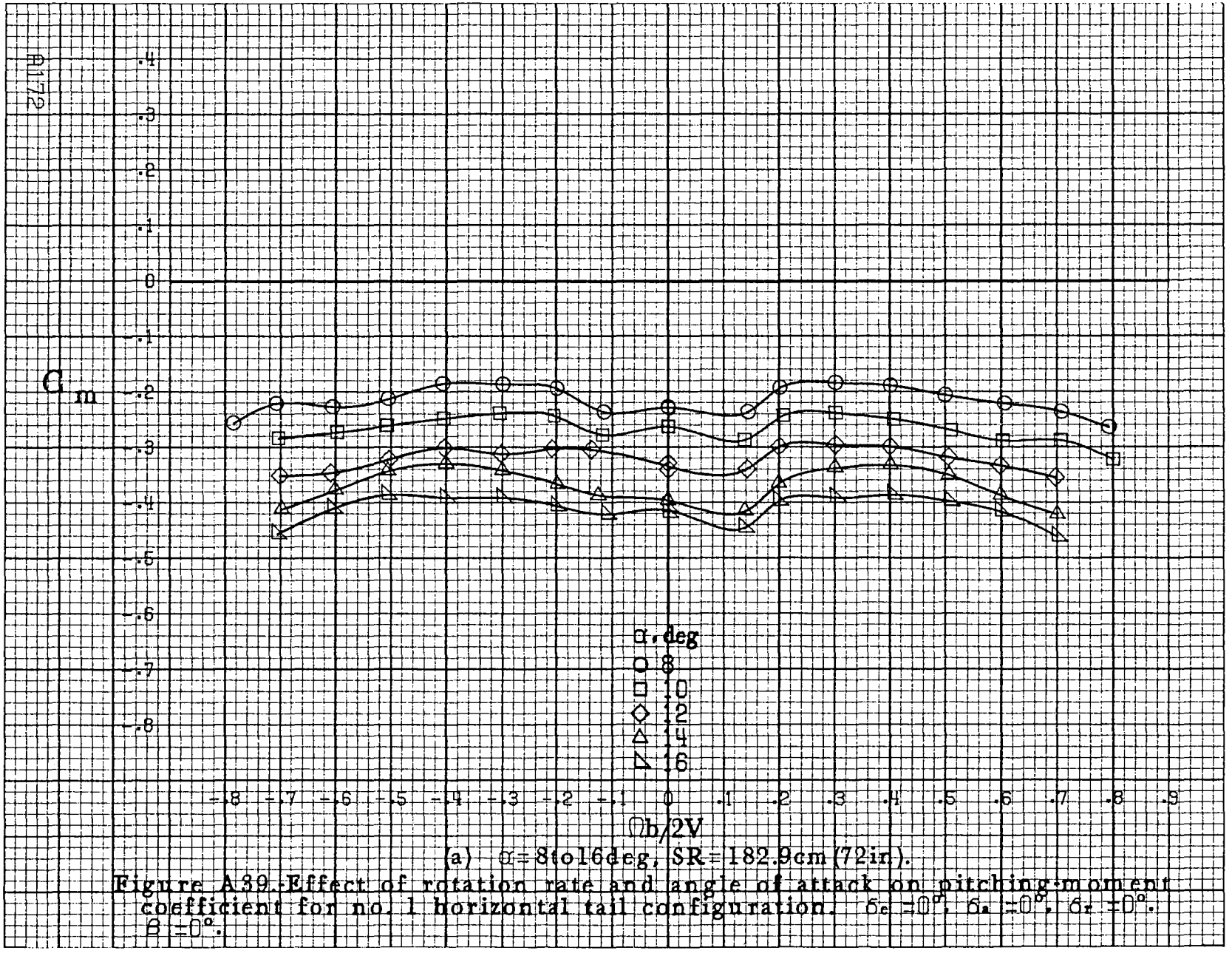

(a) $\alpha = 8$ to 16 deg, SR = 182.9 cm (72 in.).

Figure A39.-Effect of rotation rate and angle of attack on pitching-moment coefficient for no. 1 horizontal tail configuration. $\delta_e = 0°$, $\delta_a = 0°$, $\delta_r = 0°$. $\beta = 0°$.

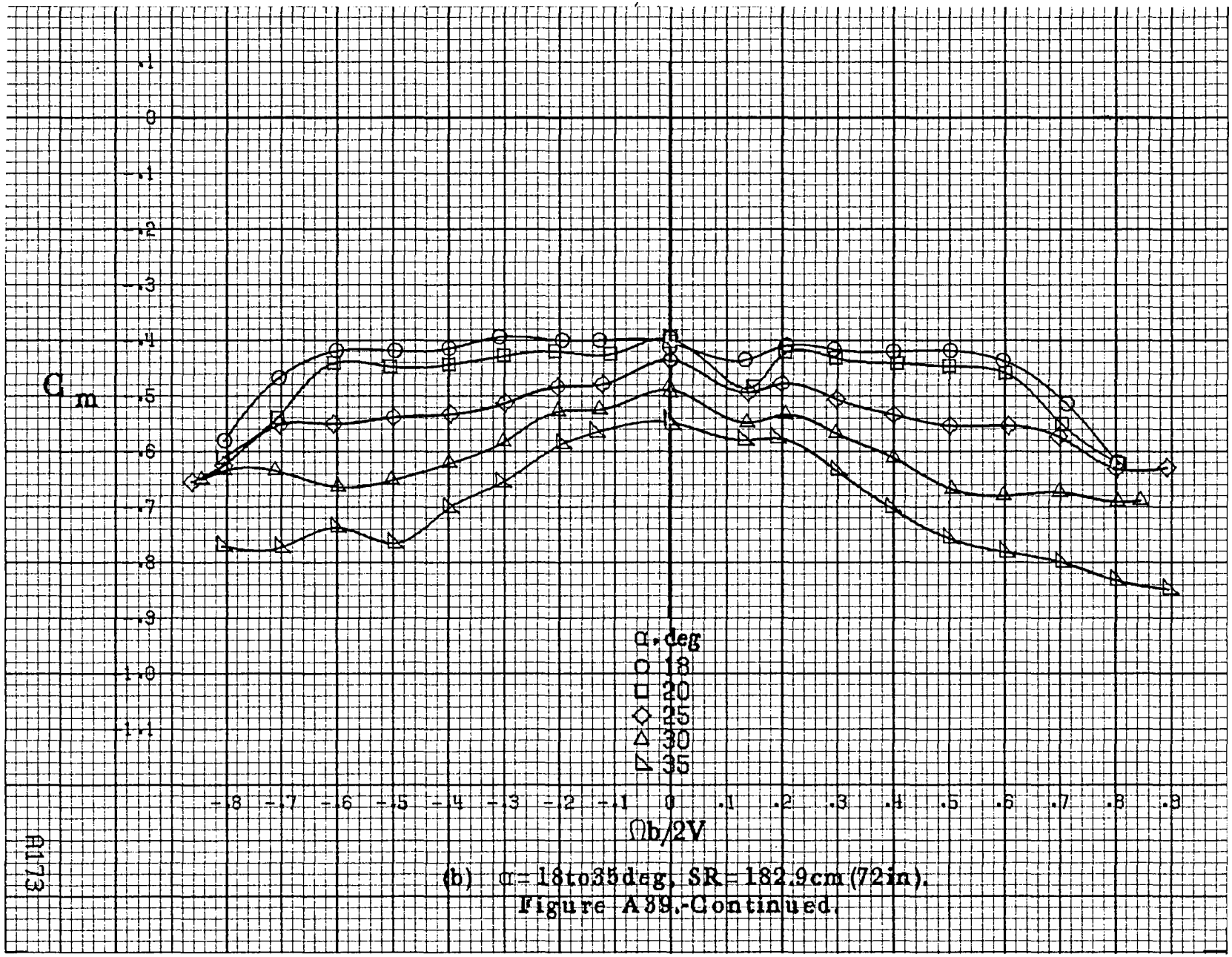

(b) $\alpha = 18$ to 35 deg, SR = 182.9 cm (72 in).

Figure A39.-Continued.

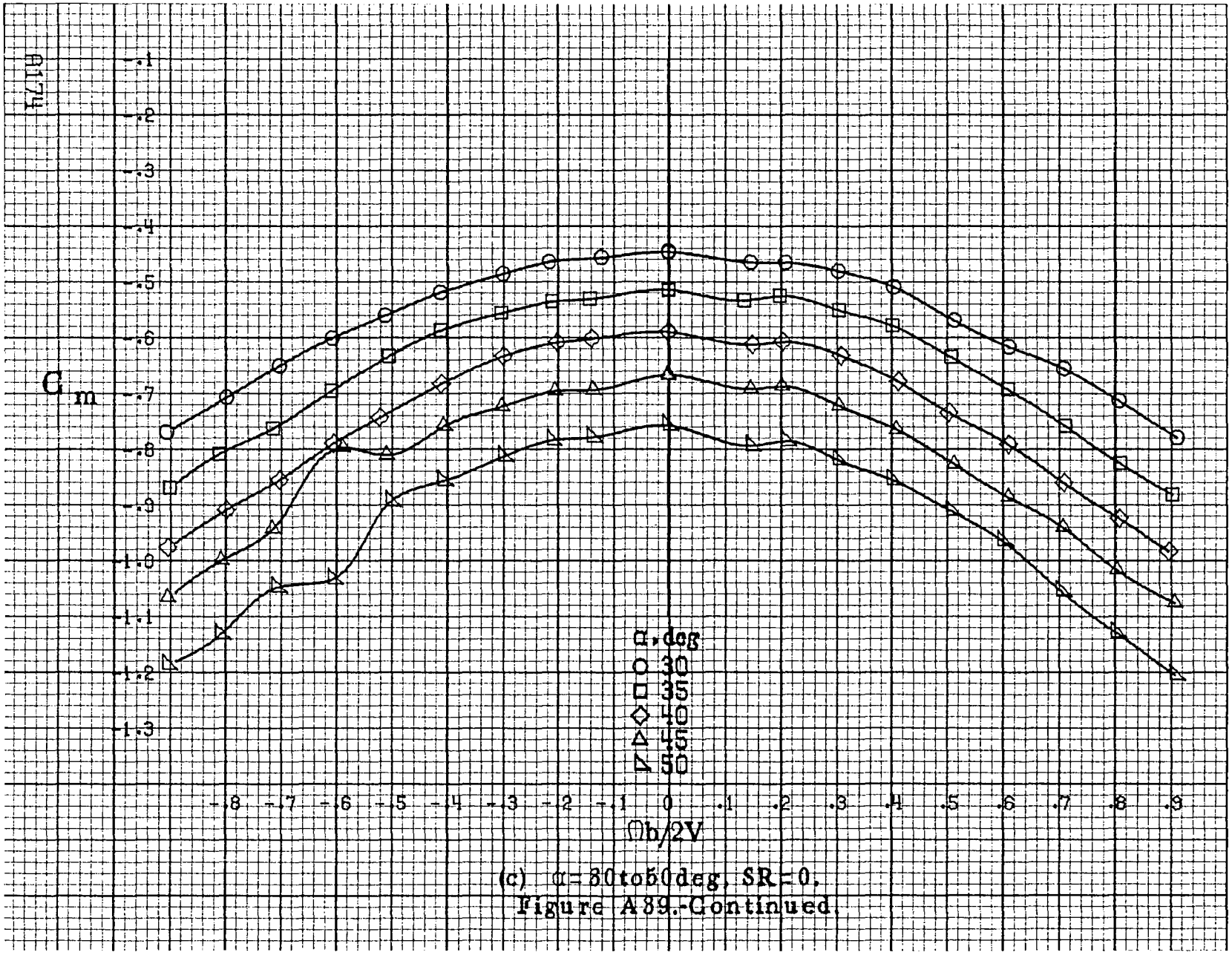

(c) $\alpha = 30$ to 50 deg, SR = 0.

Figure A39.-Continued.

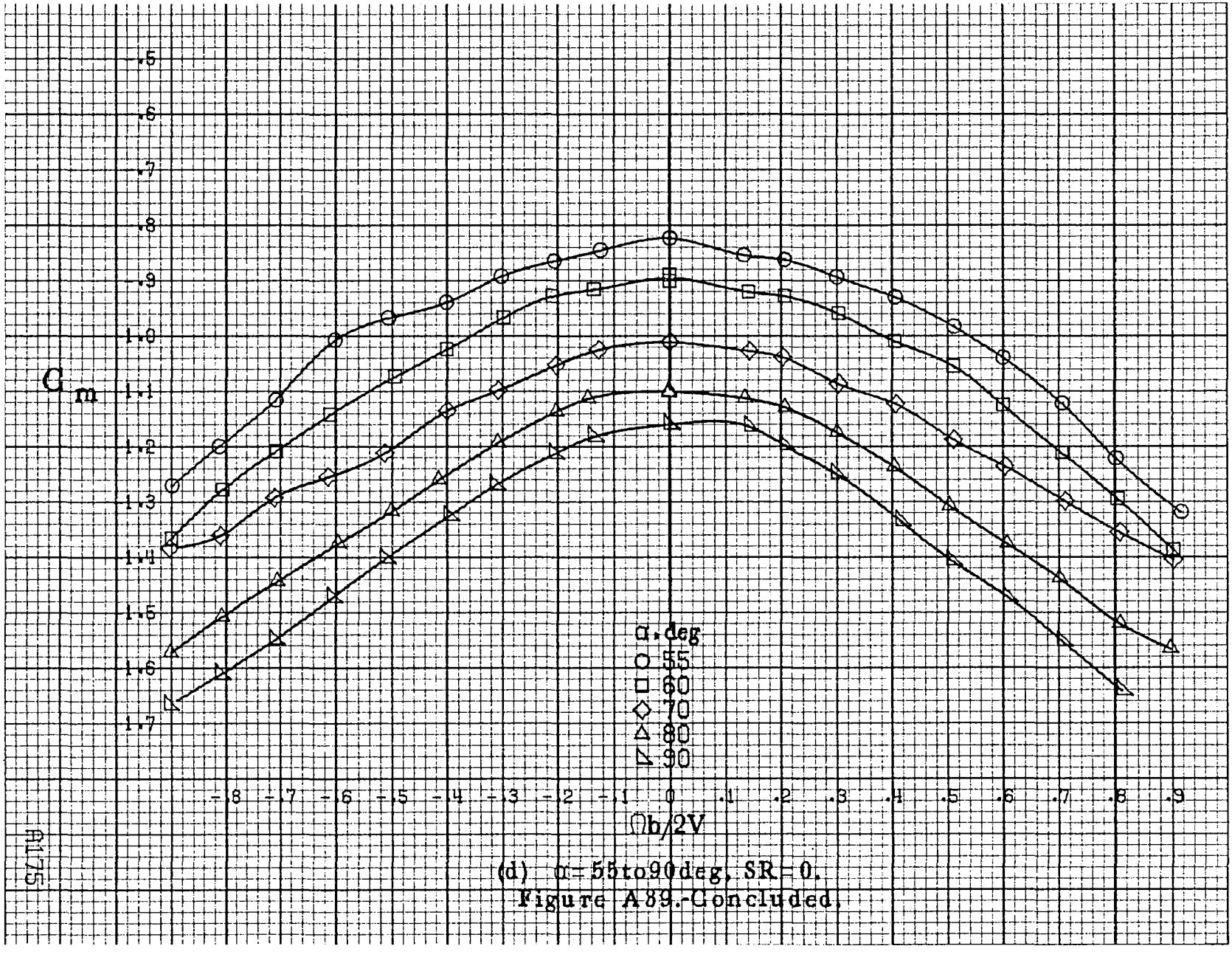

(d) $\alpha = 55$ to 90 deg, SR = 0.

Figure A89.-Concluded.

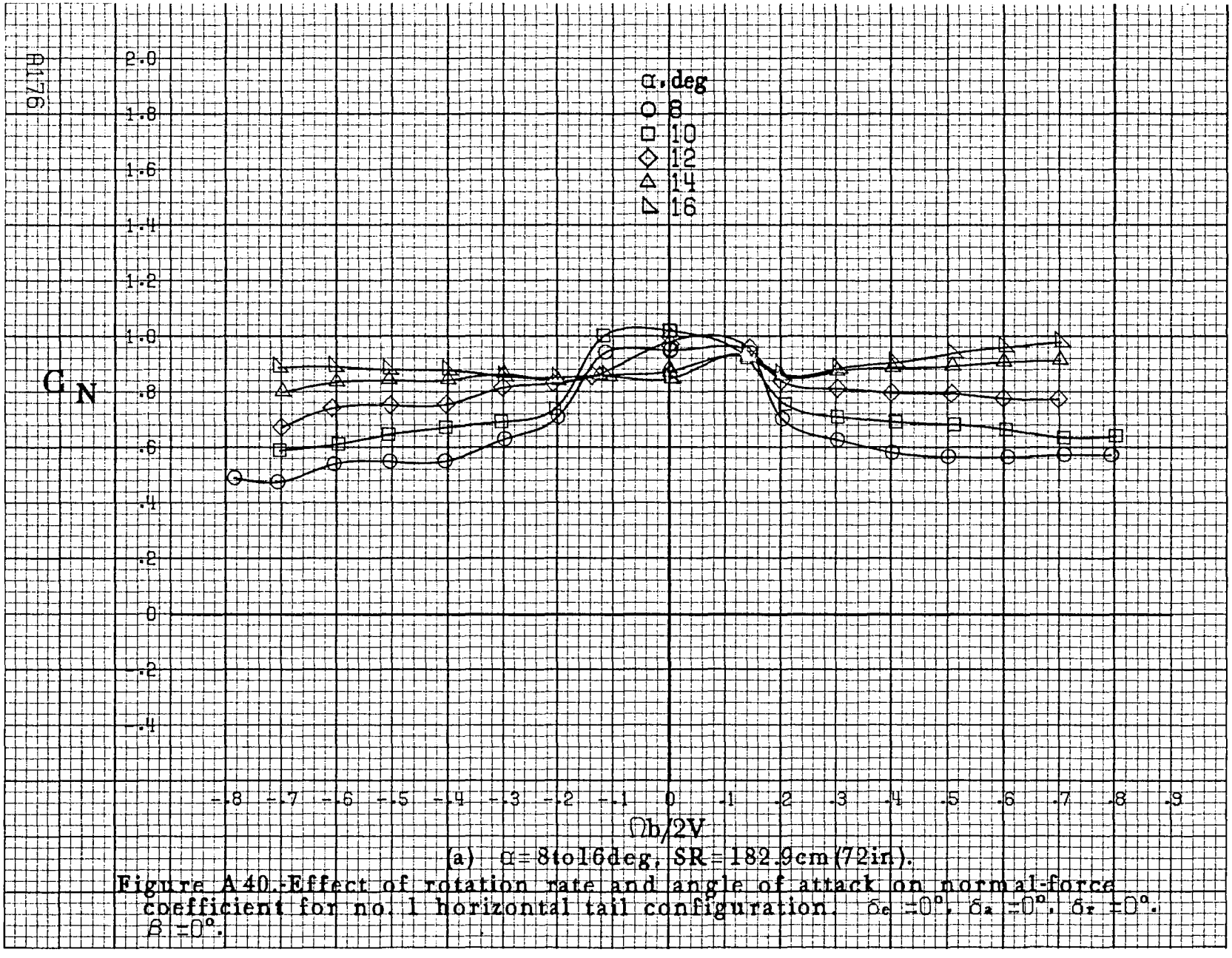

(a) $\alpha = 8$ to 16 deg, SR = 182.9 cm (72 in).

Figure A40. Effect of rotation rate and angle of attack on normal-force coefficient for no. 1 horizontal tail configuration. $\delta_e = 0°$, $\delta_a = 0°$, $\delta_r = 0°$, $\beta = 0°$.

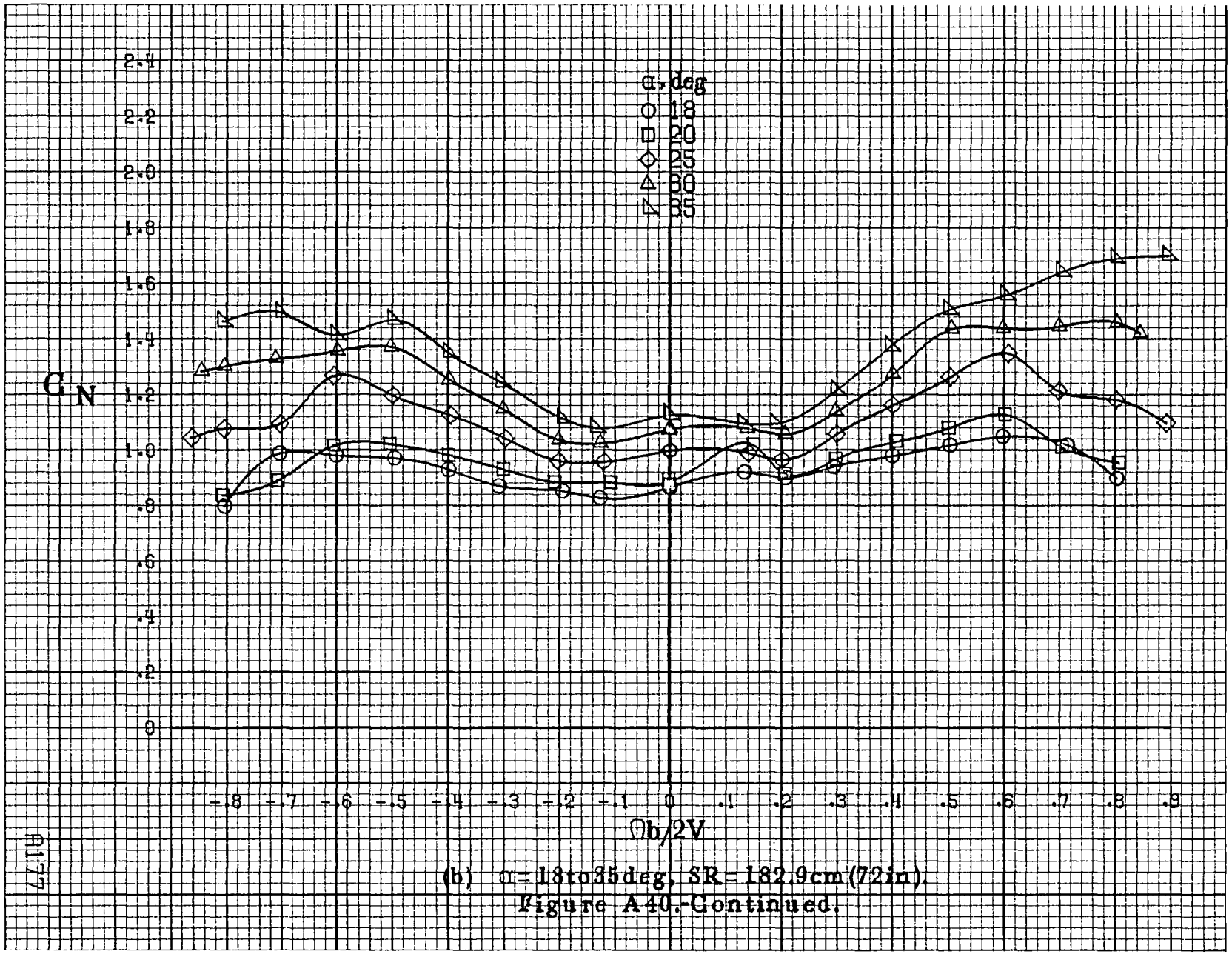

D-775

(b) α = 18 to 35 deg, SR = 182.9 cm (72 in).

Figure A40.-Continued.

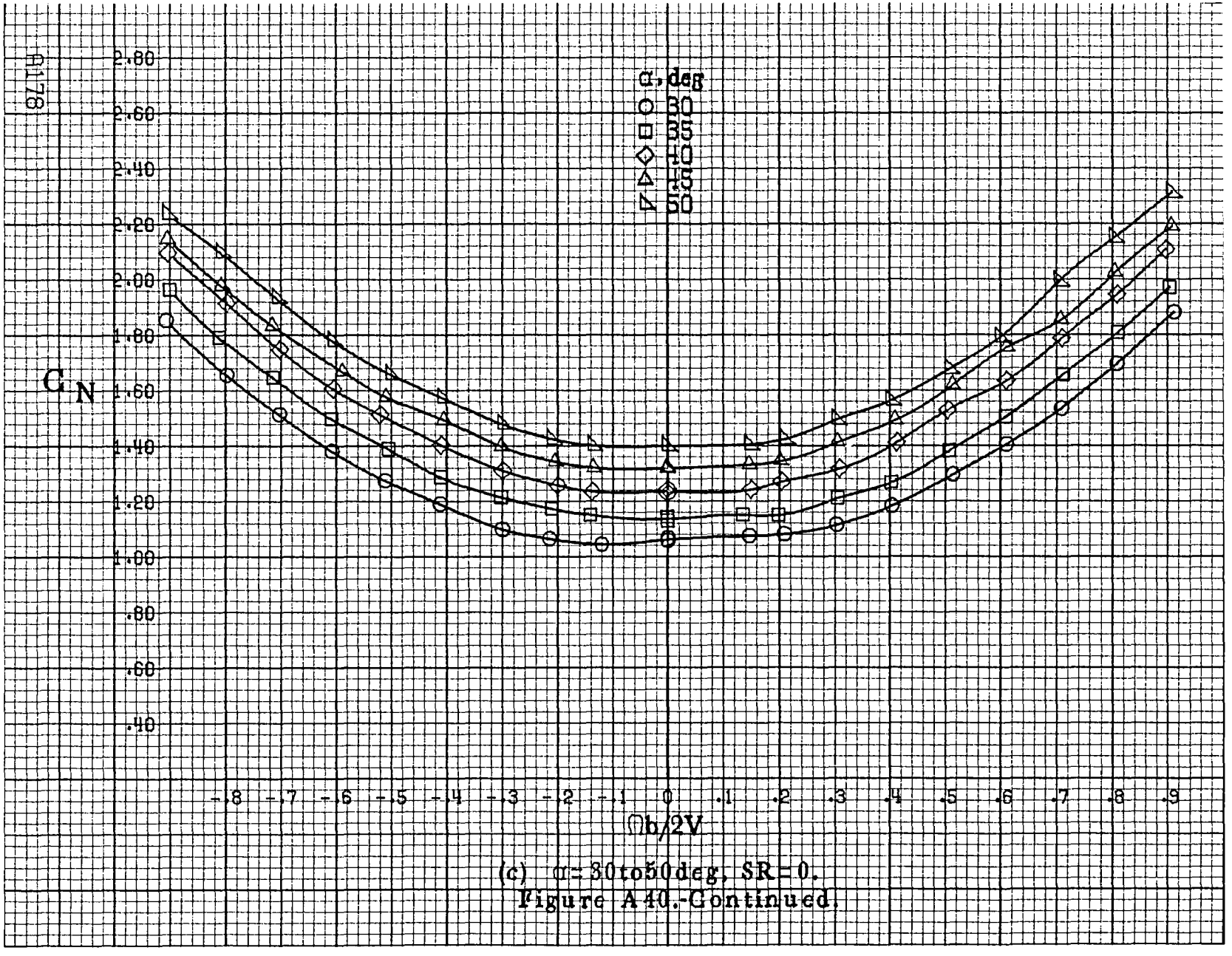

(c) $\alpha = 30$ to 50 deg, SR = 0.

Figure A40.-Continued.

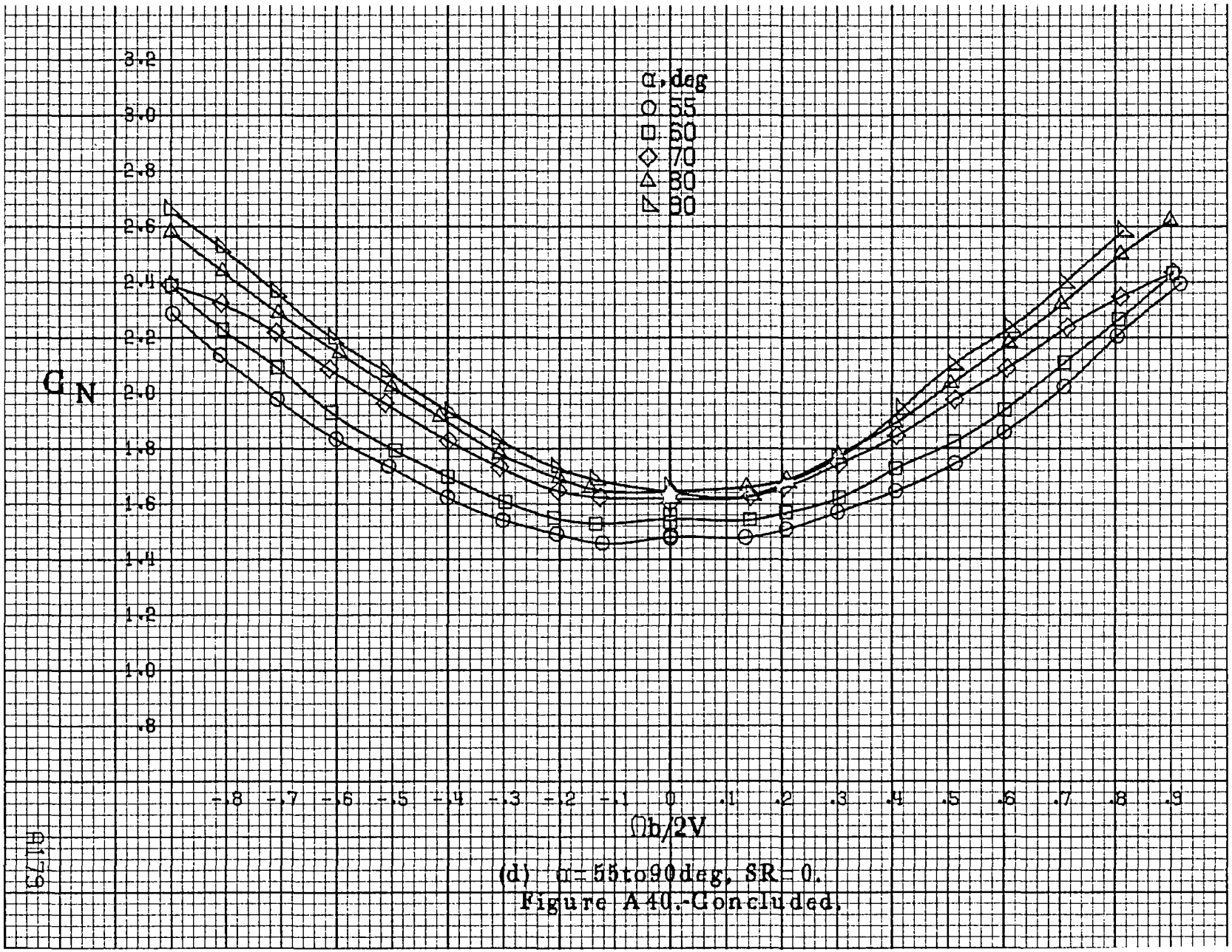

(d) α = 55 to 90 deg, SR = 0.

Figure A40.-Concluded.

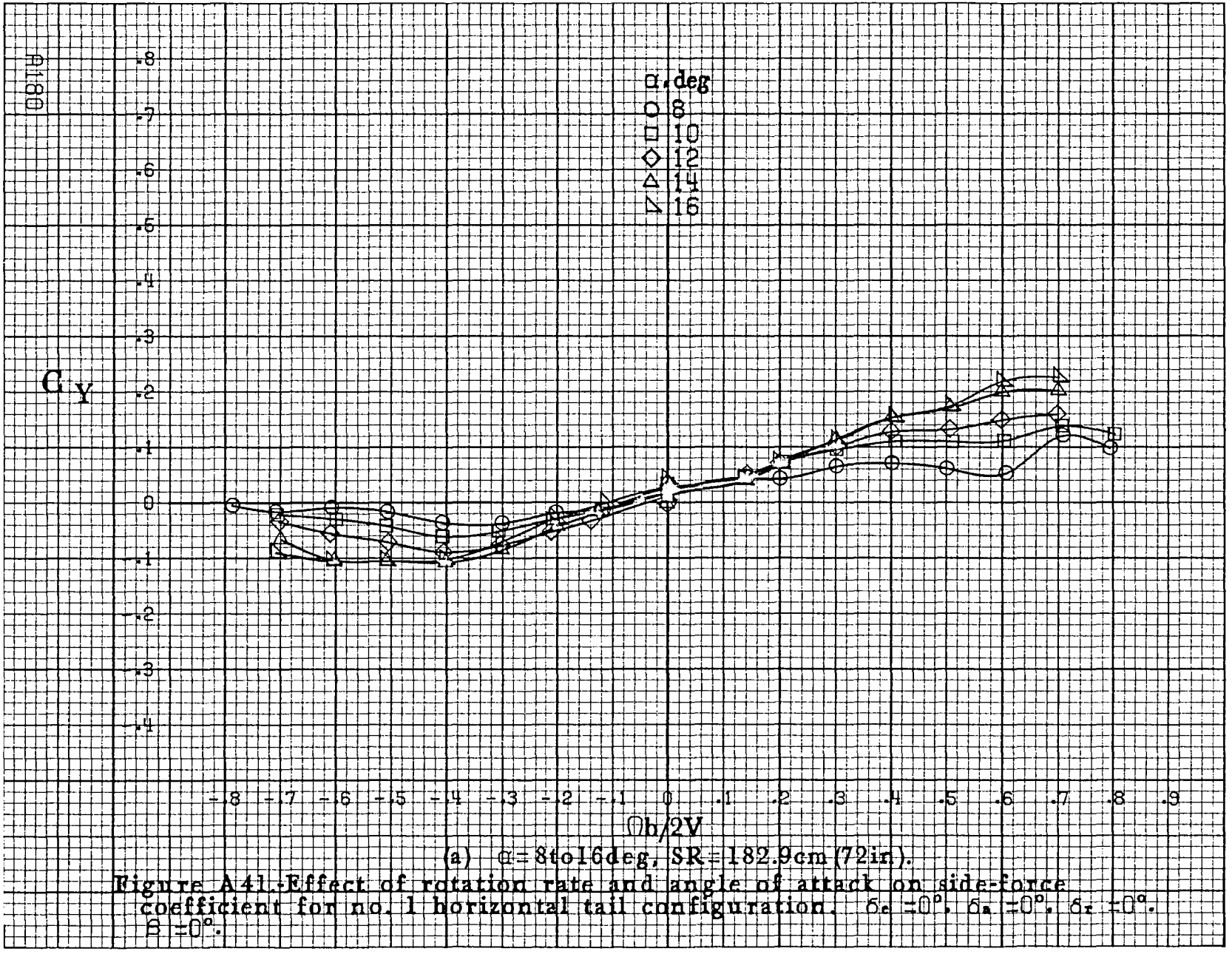

(a) $\alpha = 8$ to 16 deg, SR = 182.9 cm (72 in).

Figure A41.-Effect of rotation rate and angle of attack on side-force coefficient for no. 1 horizontal tail configuration. $\delta_e = 0°$, $\delta_a = 0°$, $\delta_r = 0°$, $\beta = 0°$.

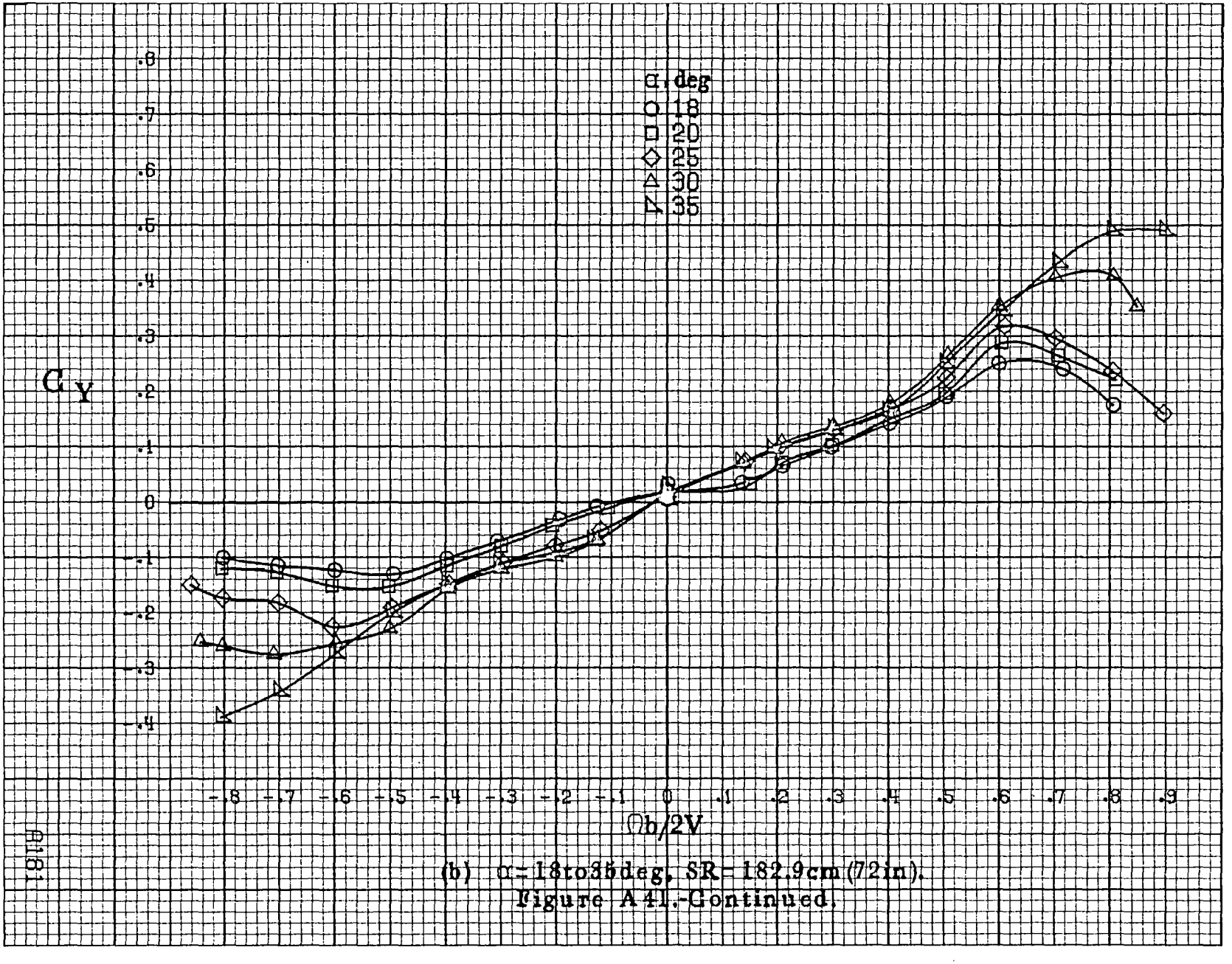

(b) $\alpha = 18$ to 35 deg, SR = 182.9 cm (72 in).

Figure A41.-Continued.

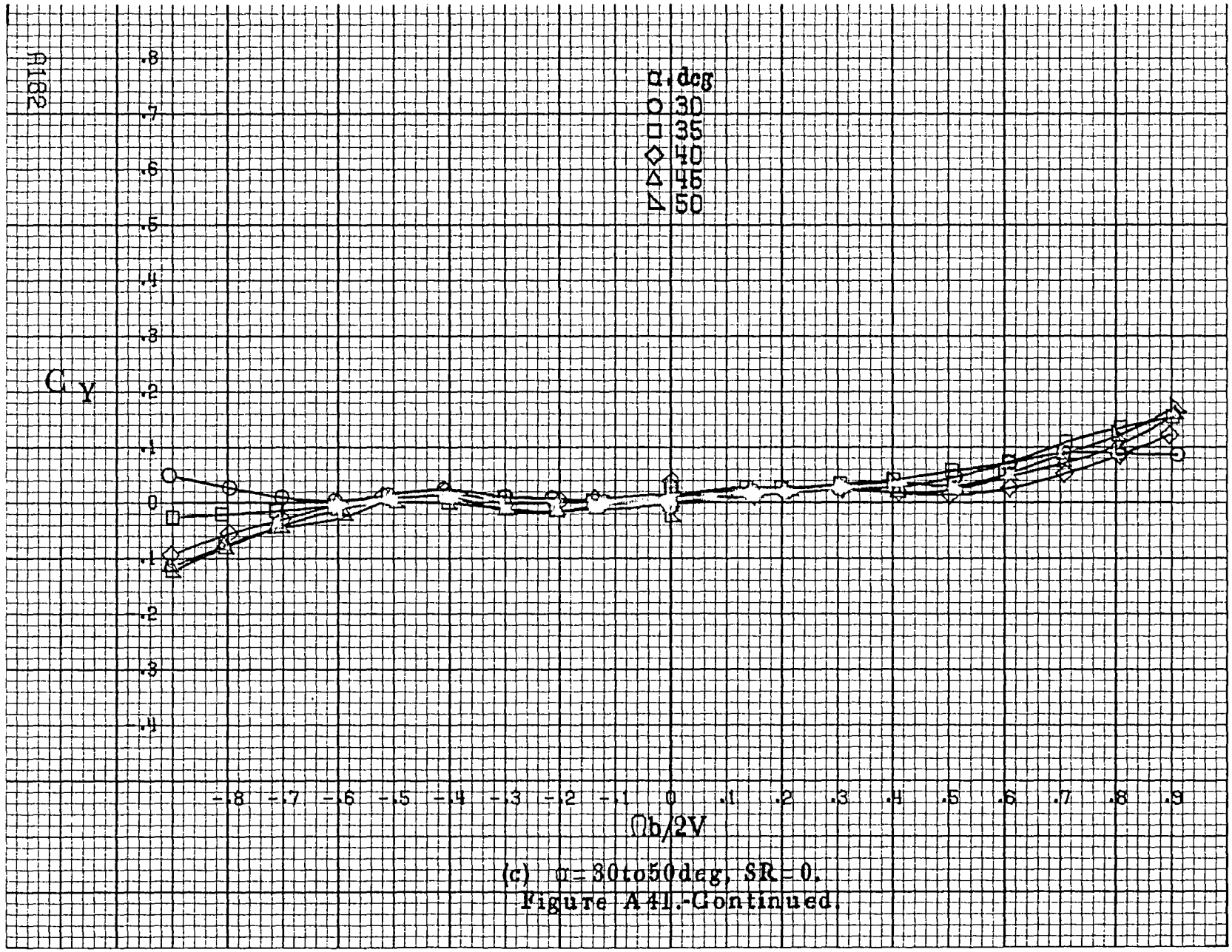

(c) α=30to50deg, SR=0.

Figure A41.-Continued.

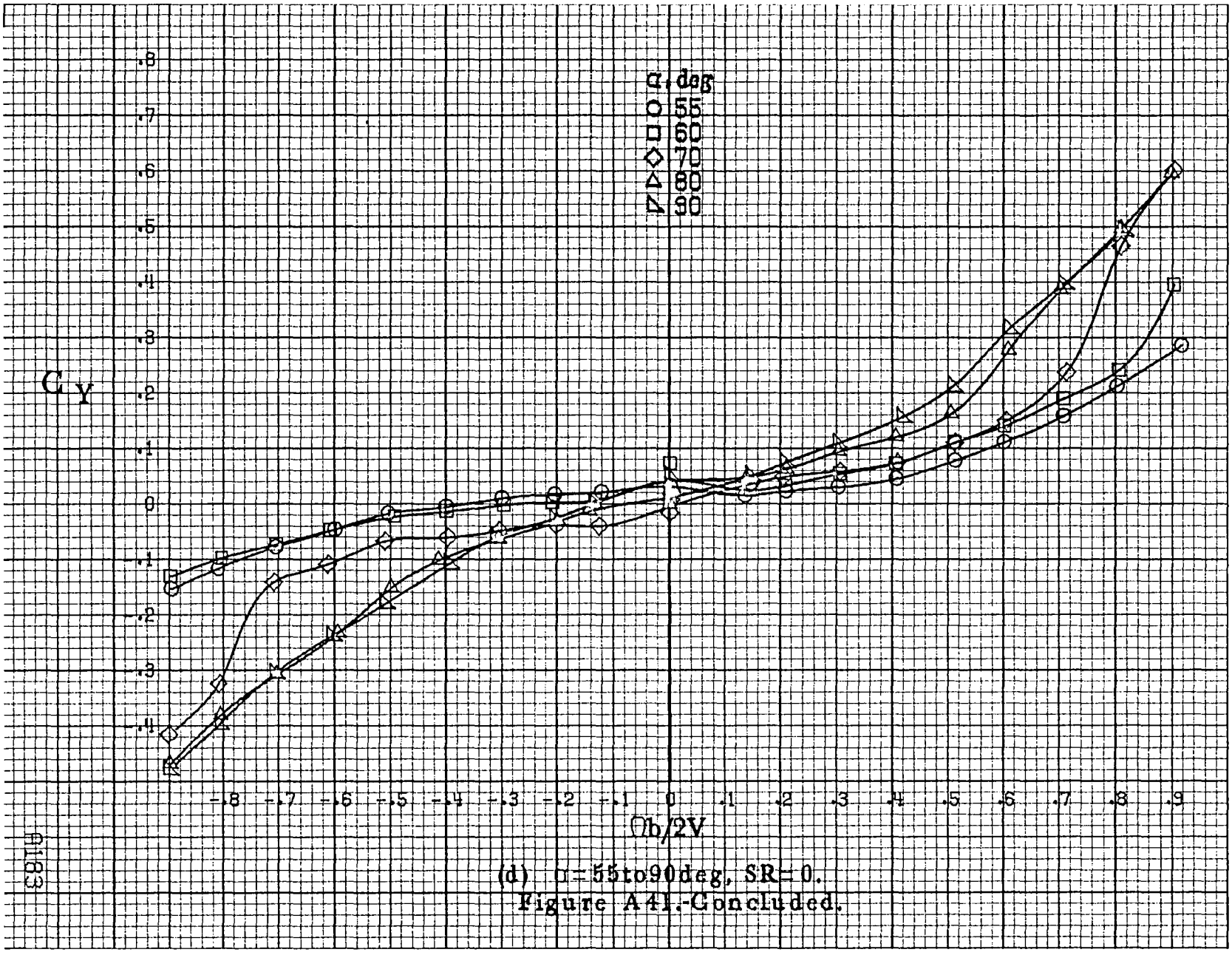

(d) α = 55 to 90 deg, SR = 0.

Figure A41.-Concluded.

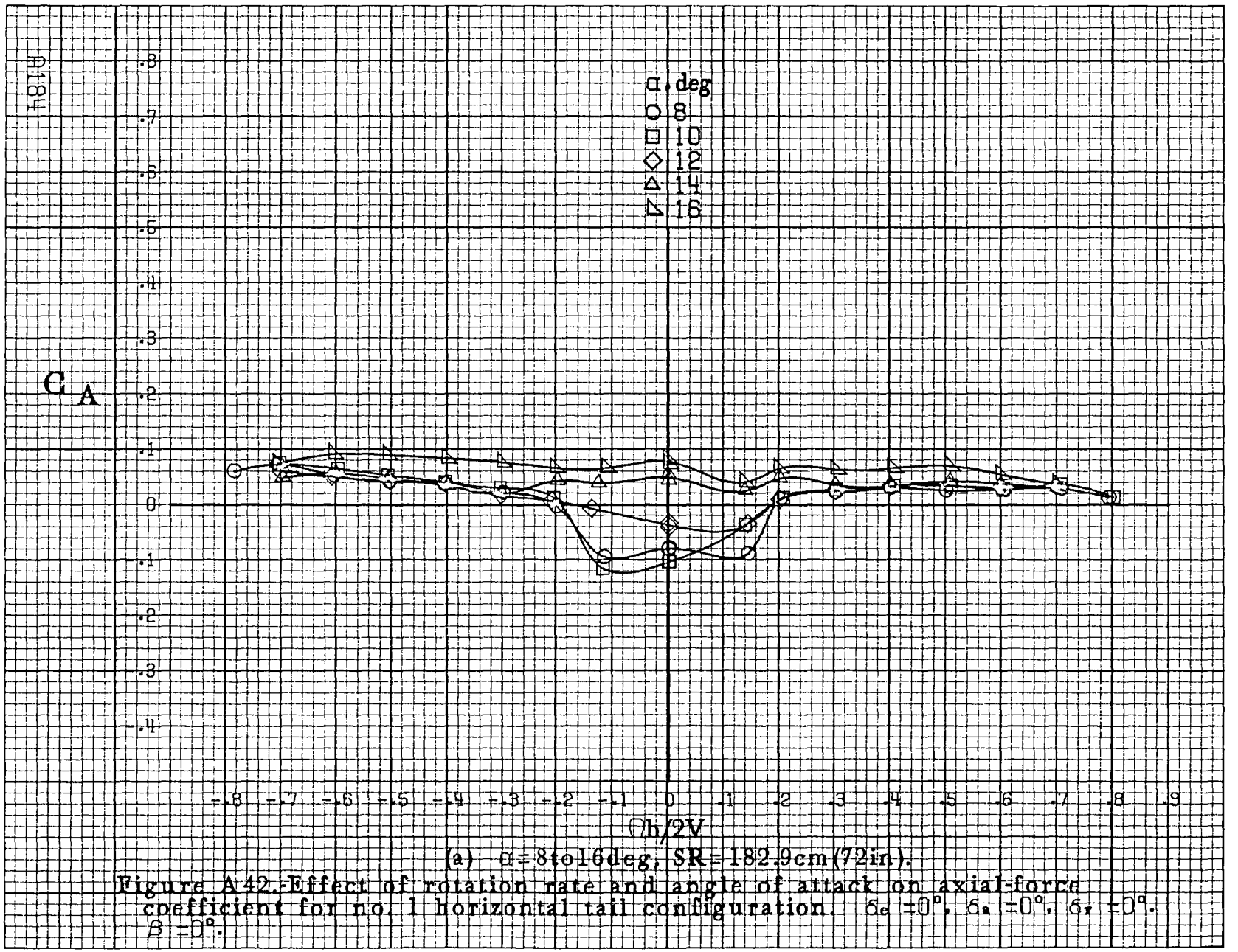

(a) $\alpha = 8$ to 16 deg, SR = 182.9 cm (72 in.).

Figure A42.-Effect of rotation rate and angle of attack on axial-force coefficient for no. 1 horizontal tail configuration. $\delta_e = 0°$, $\delta_a = 0°$, $\delta_r = 0°$, $\beta = 0°$.

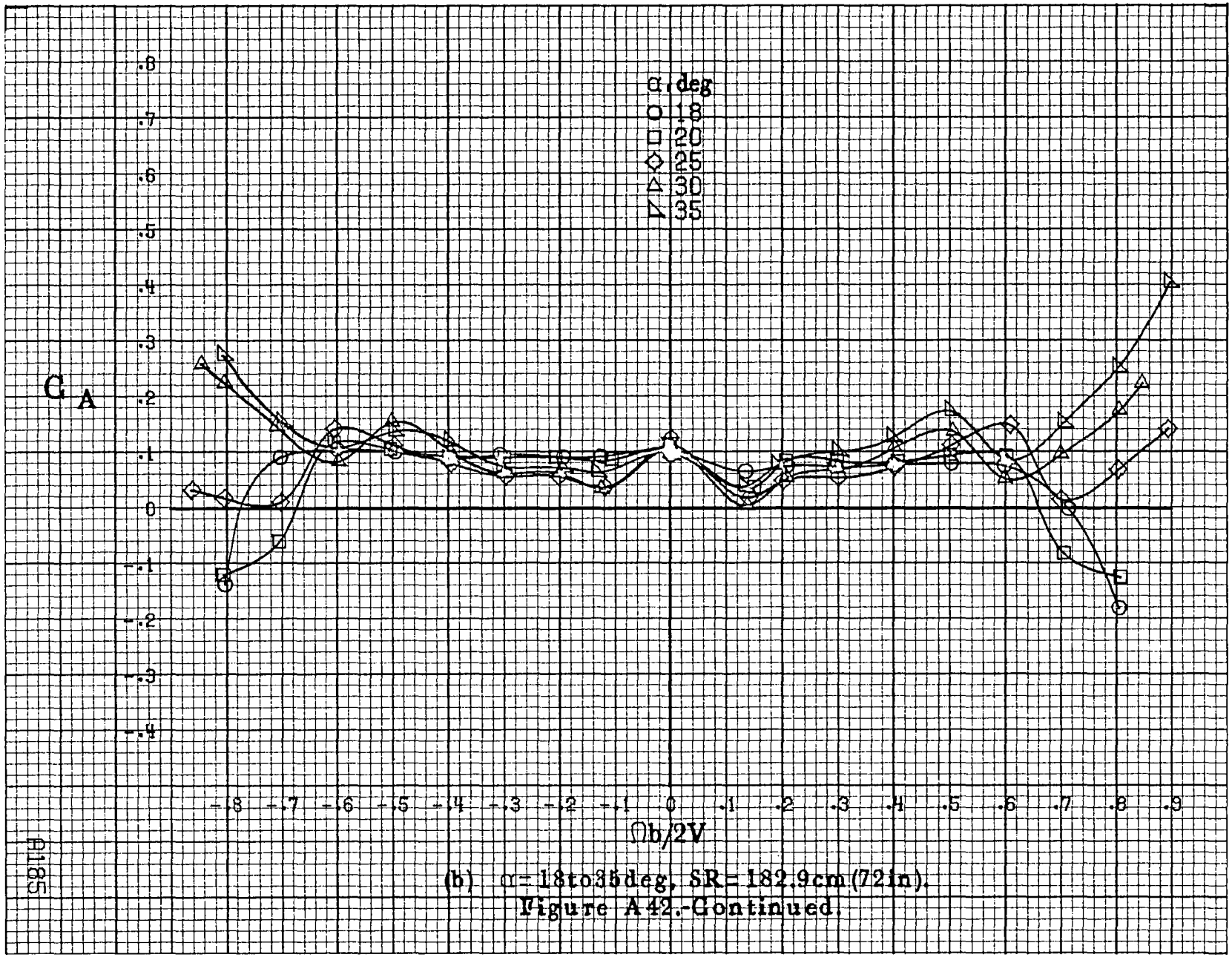

(b) $\alpha = 18$ to 35 deg, SR = 182.9 cm (72 in).

Figure A42.-Continued.

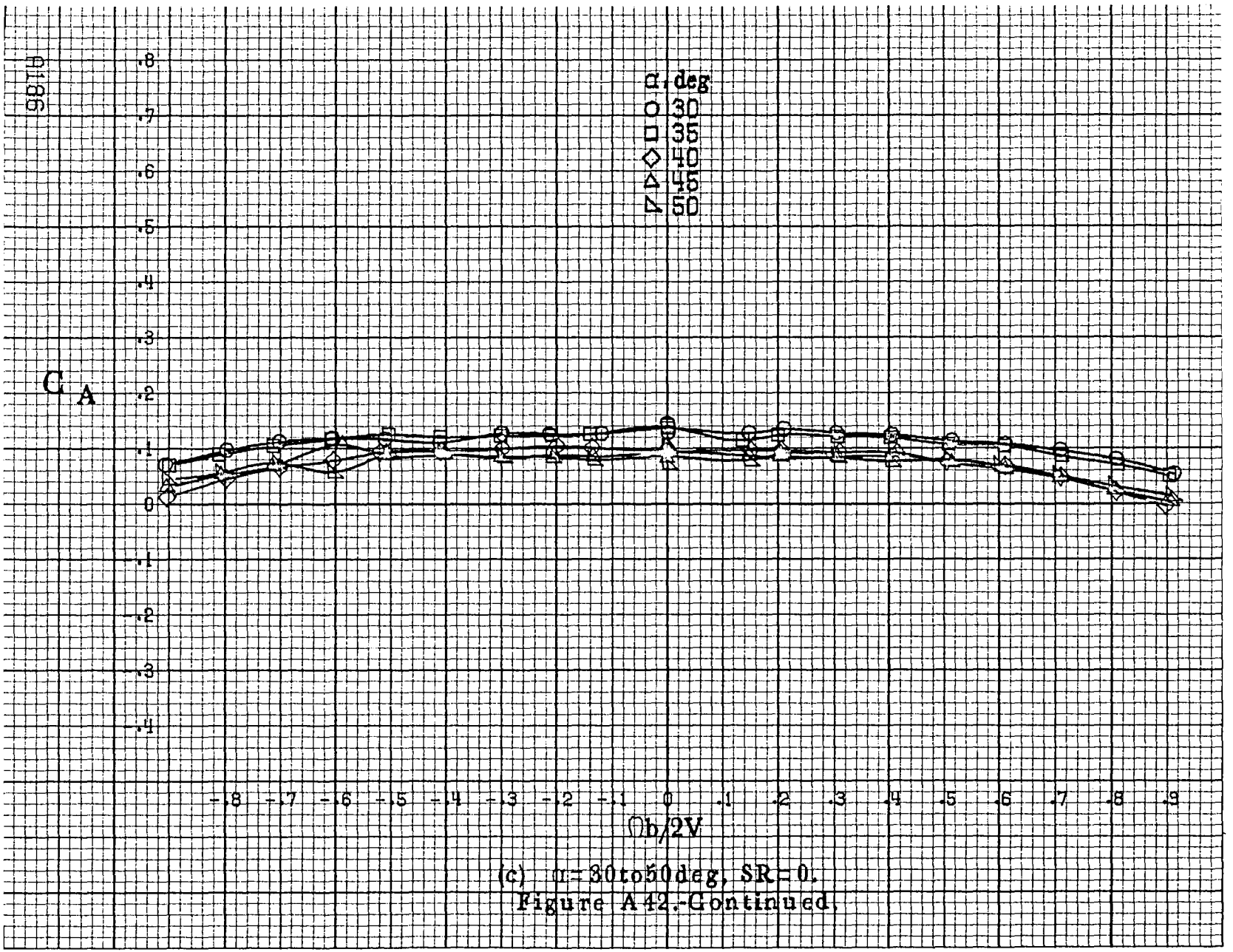

(c) α = 30 to 50 deg, SR = 0.

Figure A42.-Continued.

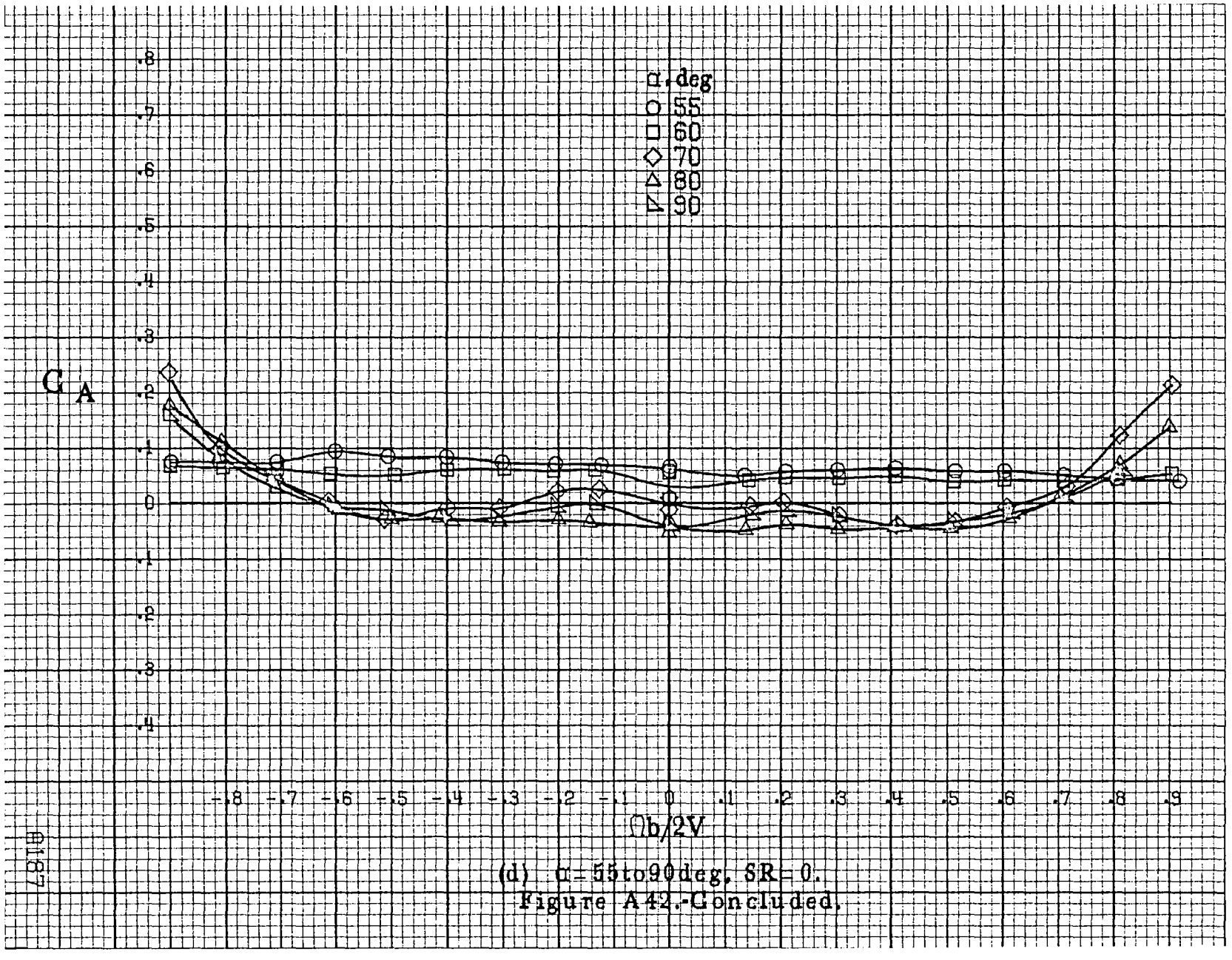

(d) α = 55 to 90 deg, δR = 0.

Figure A42.-Concluded.

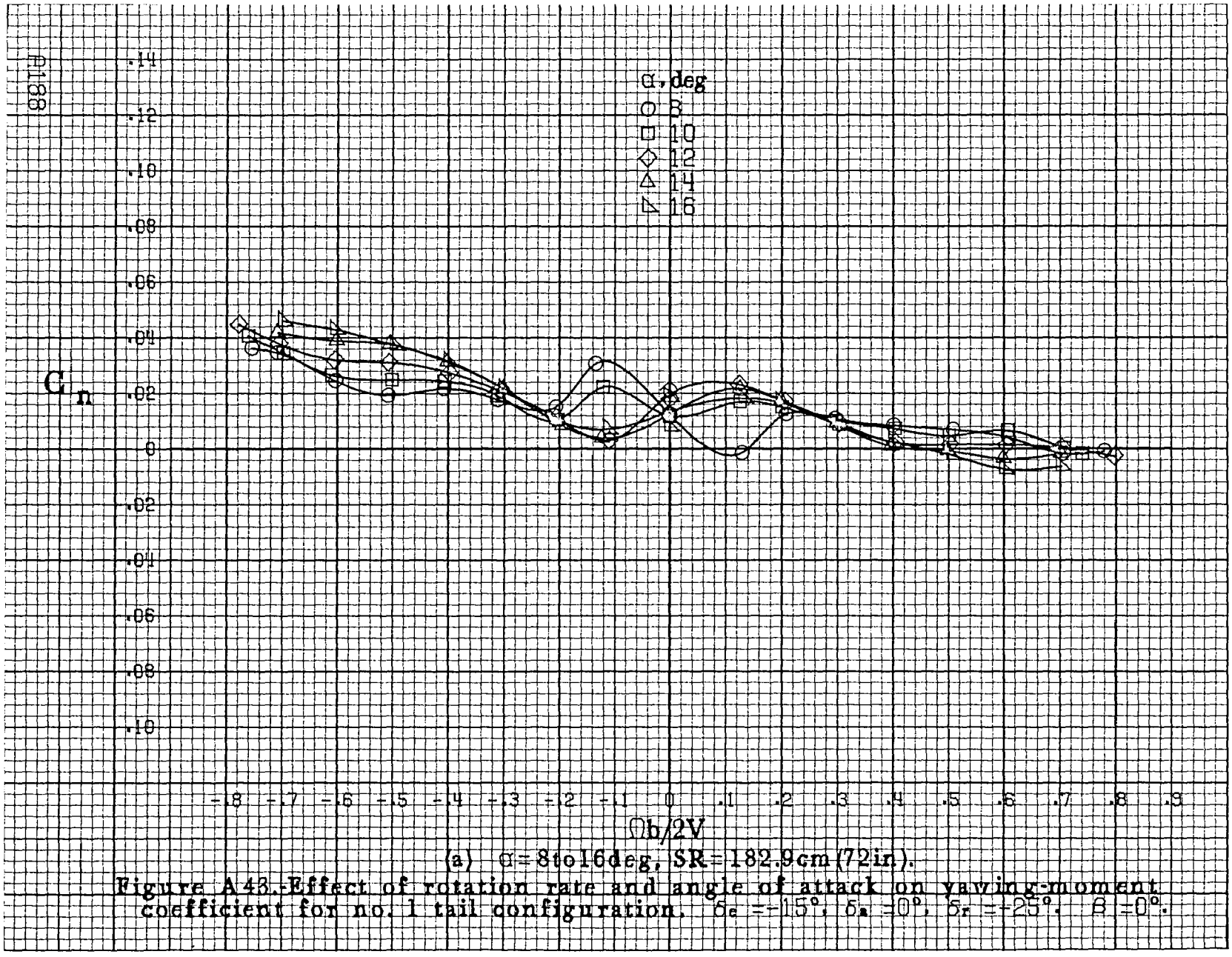

(a) α = 8 to 16 deg, SR = 182.9 cm (72 in.).

Figure A43.-Effect of rotation rate and angle of attack on yawing-moment coefficient for no. 1 tail configuration. $\delta_e = -15°$, $\delta_a = 0°$, $\delta_r = -25°$, $\beta = 0°$.

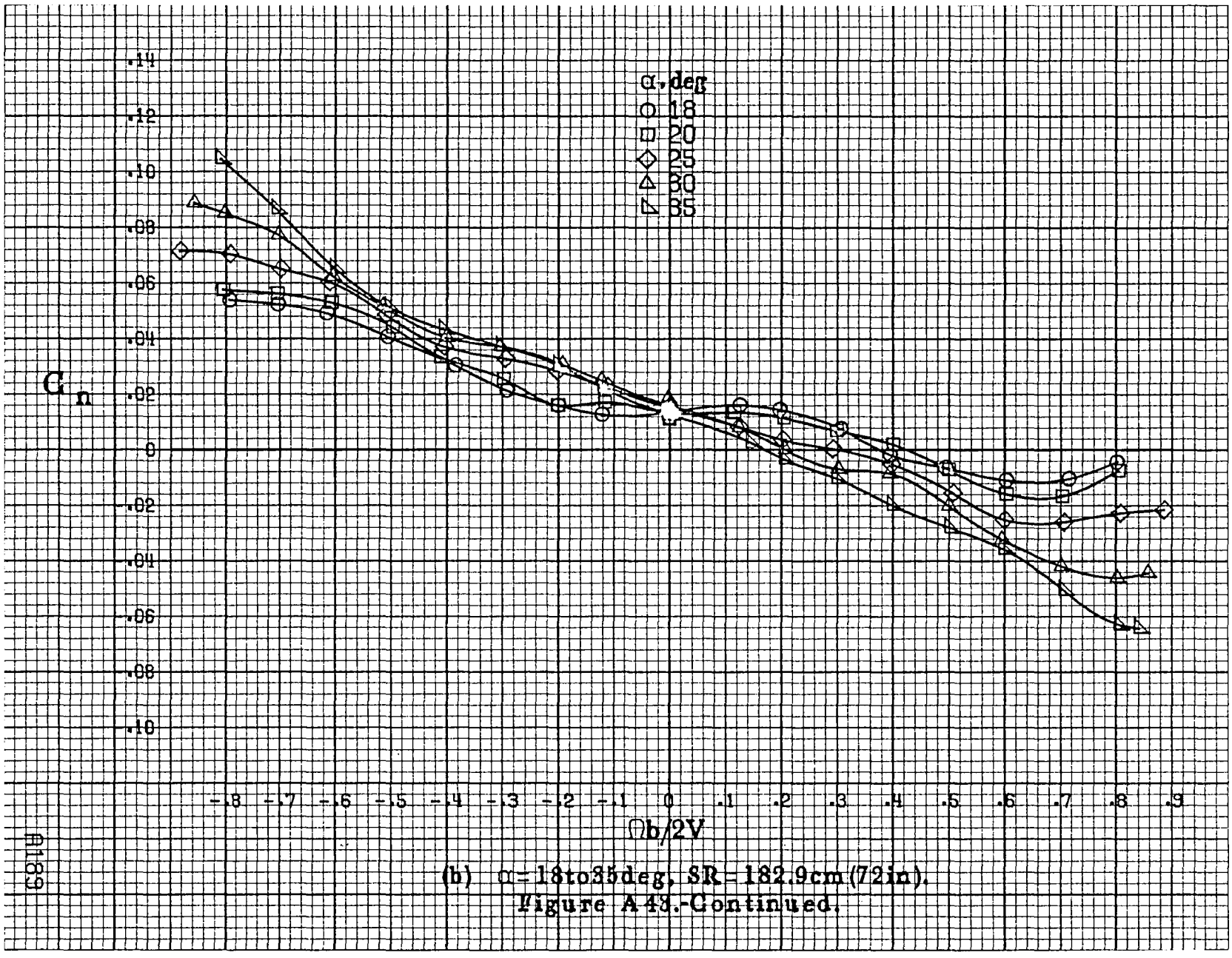

(b) α = 18 to 35 deg, SR = 182.9 cm (72 in).

Figure A43.-Continued.

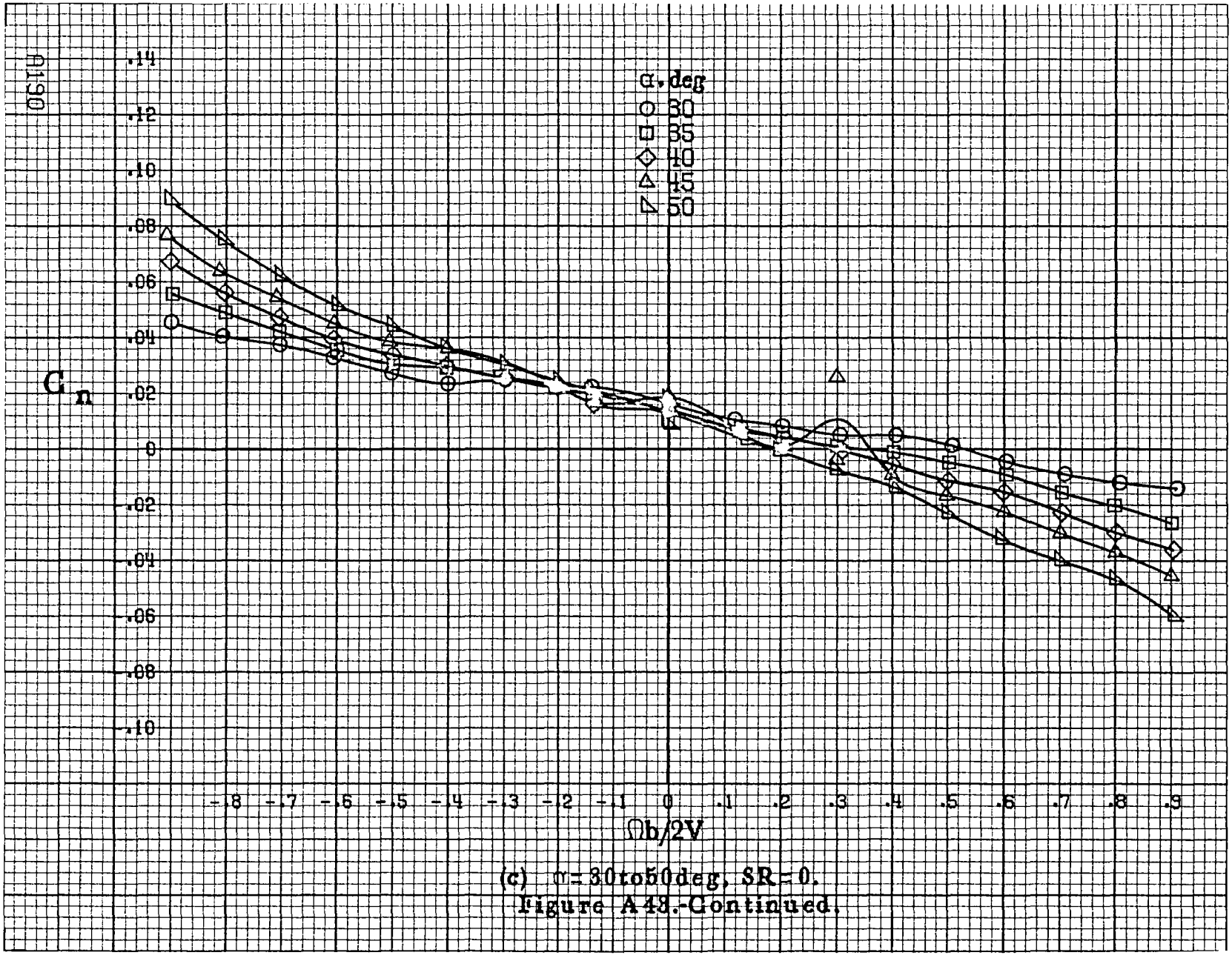

(c) $\alpha = 30$ to 50 deg, SR = 0.

Figure A48.-Continued.

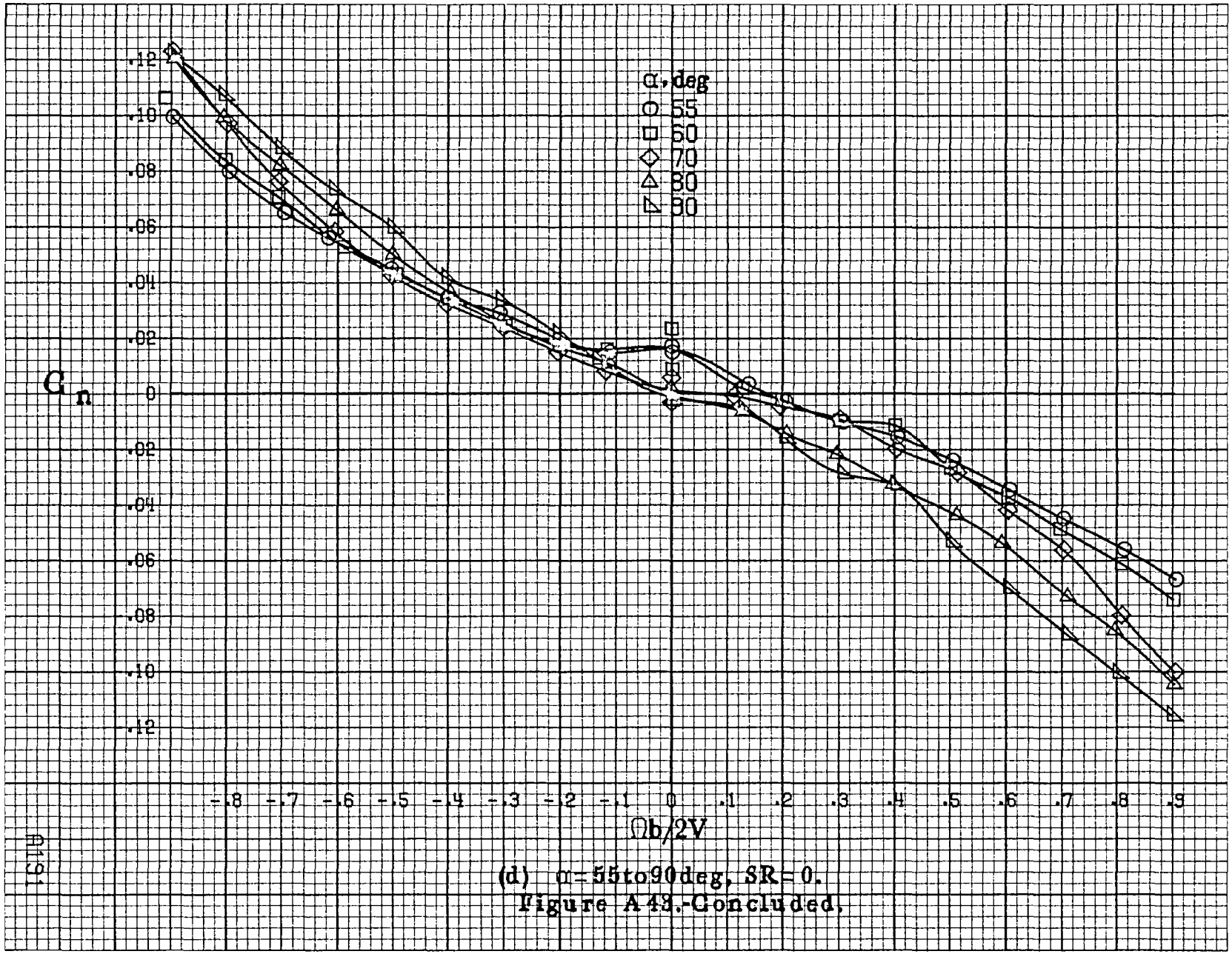

(d) $\alpha = 55$ to 90 deg, $SR = 0$.

Figure A43.-Concluded.

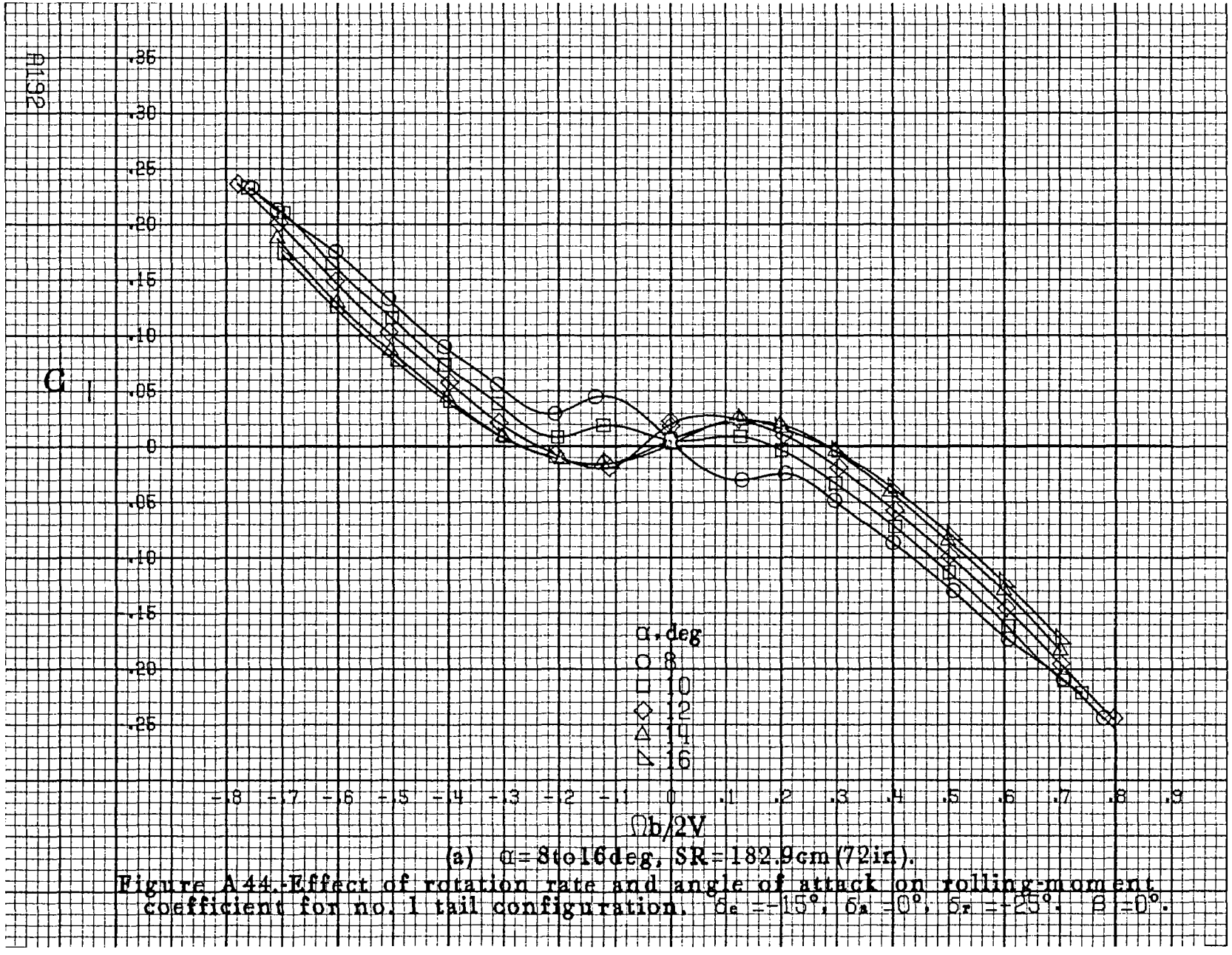

(a) α = 8 to 16 deg, SR = 182.9 cm (72 in.).

Figure A44.-Effect of rotation rate and angle of attack on rolling-moment coefficient for no. 1 tail configuration. $\delta_e = -15°$, $\delta_a = 0°$, $\delta_r = +25°$, $\beta = 0°$.

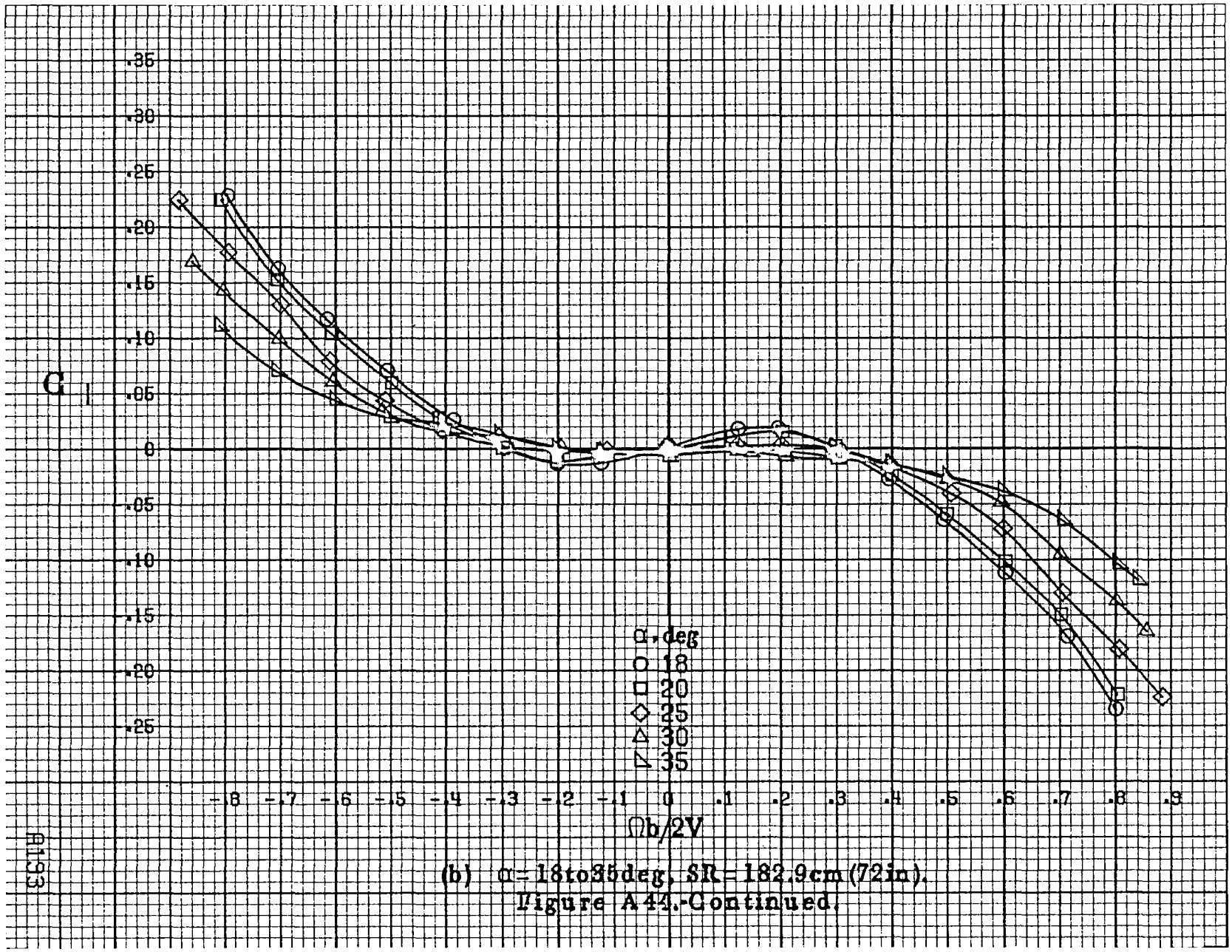

(b) α = 18 to 35 deg, SR = 182.9 cm (72 in).

Figure A44.-Continued.

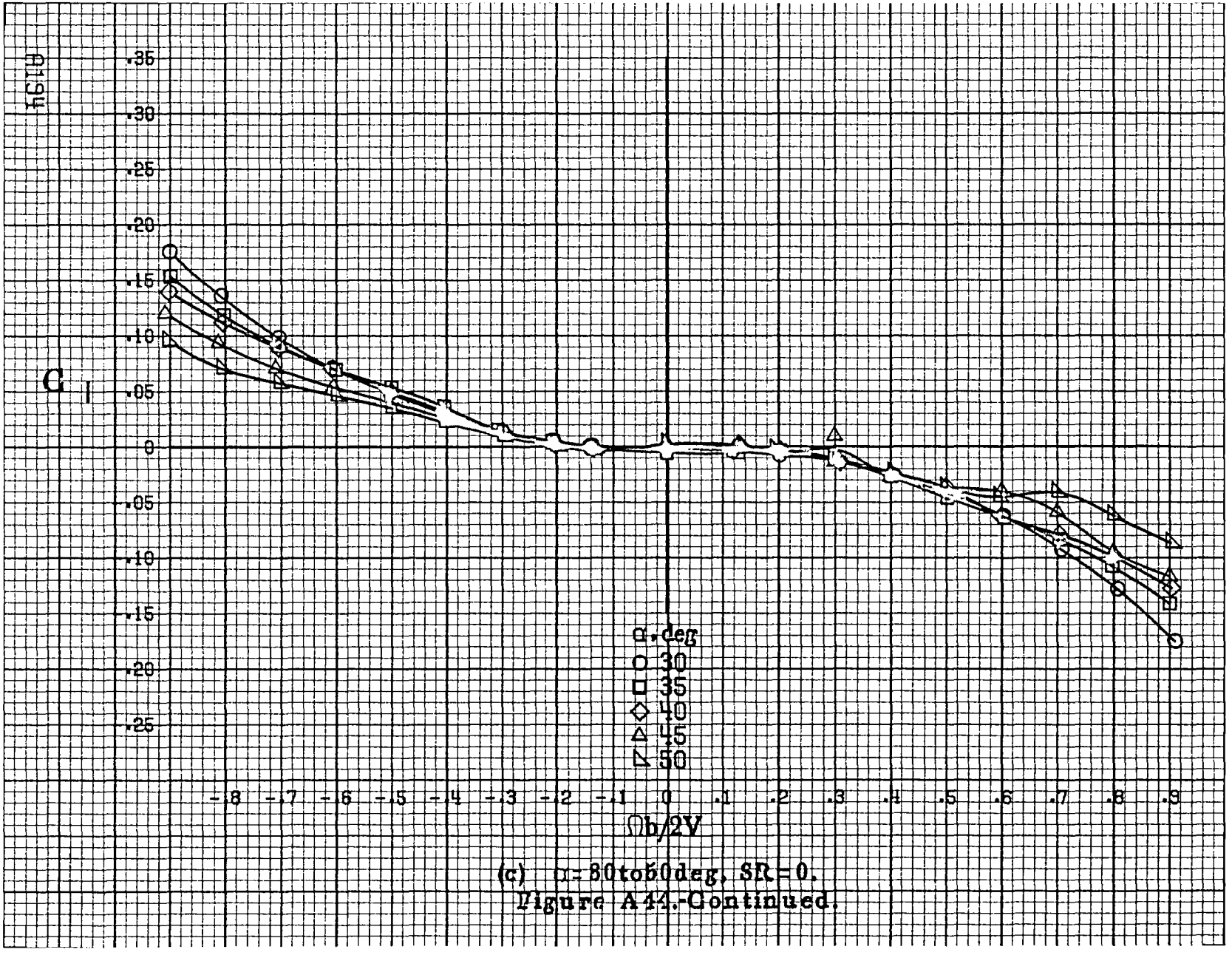

(c) $\alpha = 30$ to 60 deg, $SR = 0$.

Figure A44.-Continued.

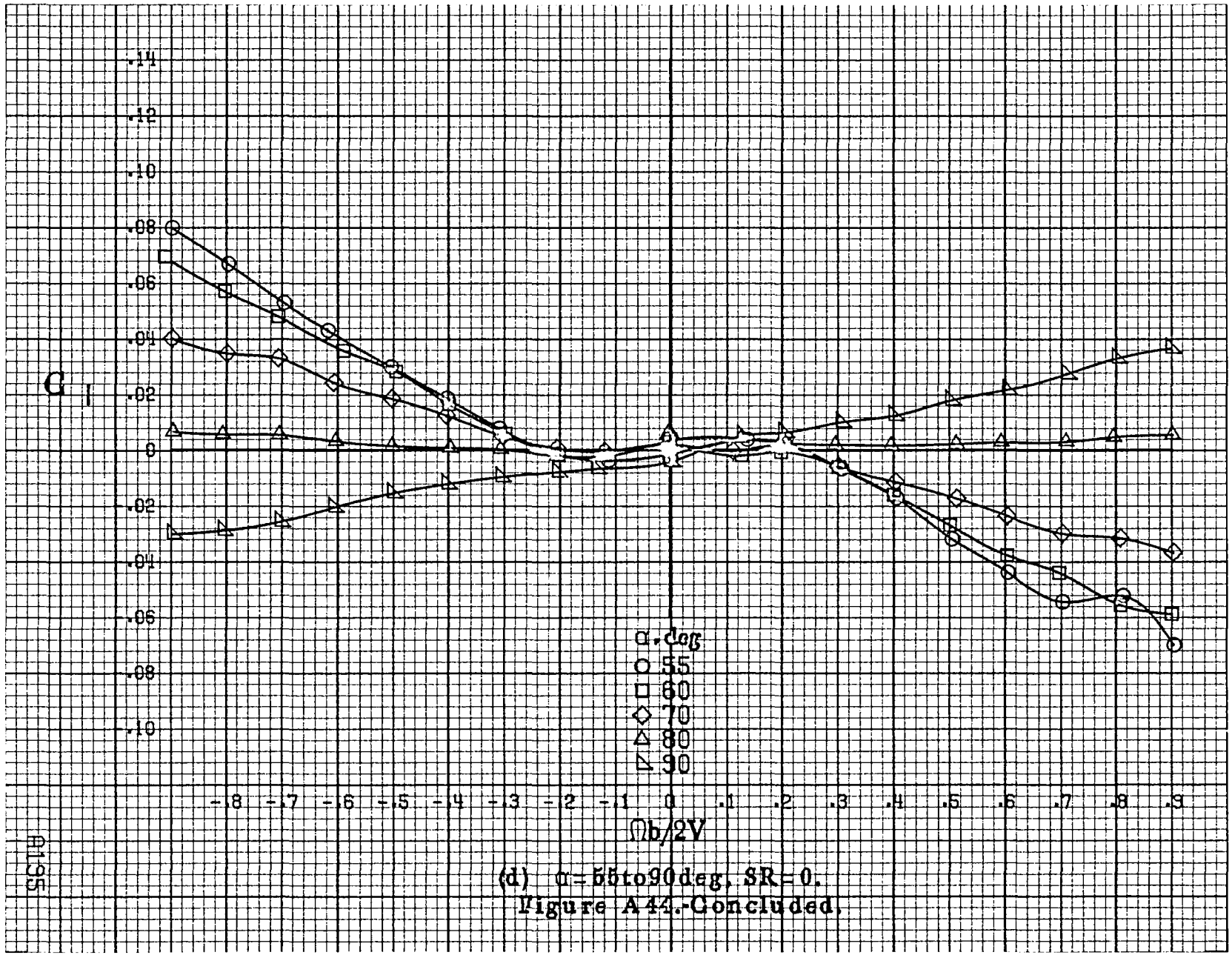

(d) α = 55 to 90 deg, SR = 0.

Figure A44.-Concluded.

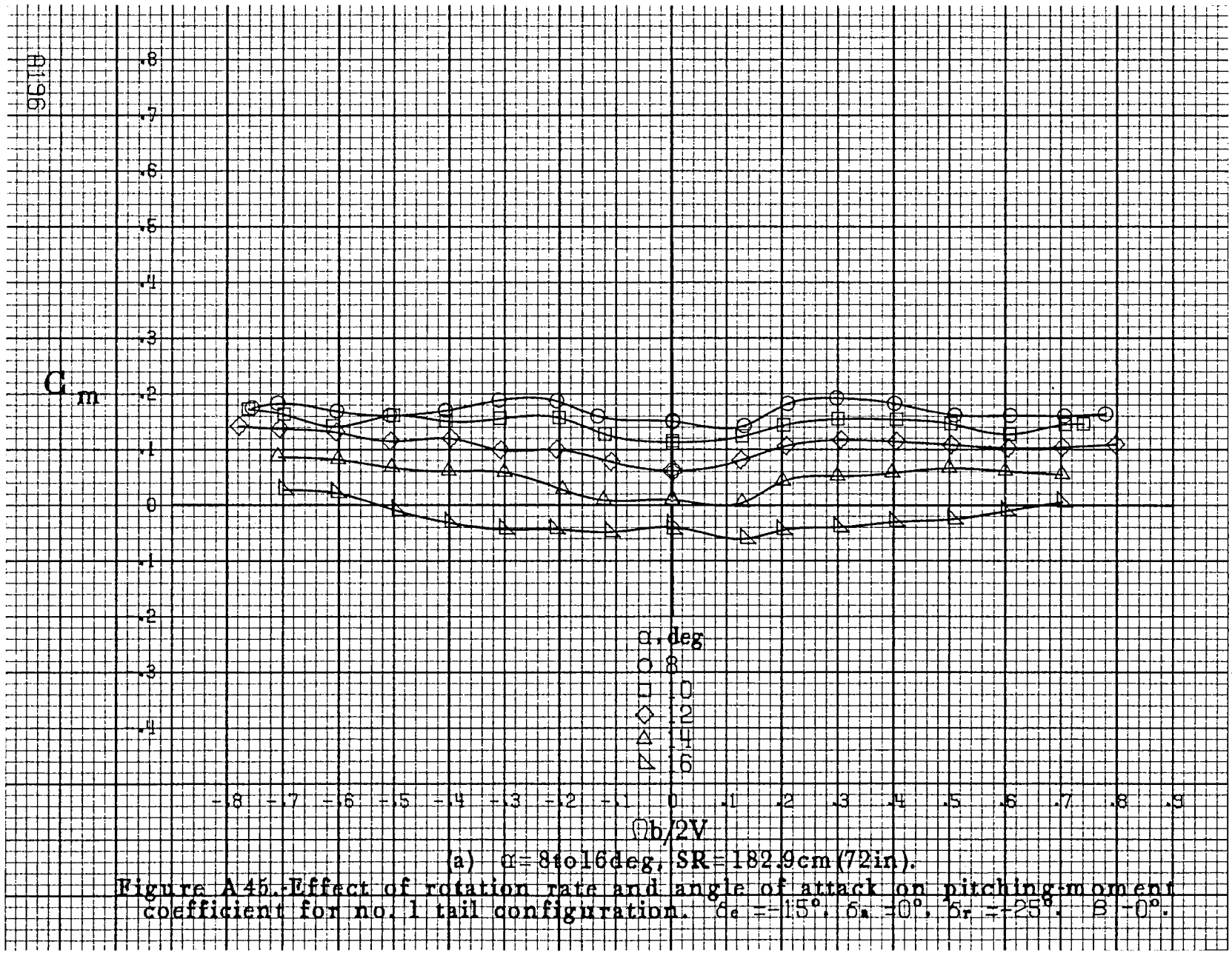

(a) $\alpha = 8$ to 16 deg, SR = 182.9 cm (72 in).

Figure A45.- Effect of rotation rate and angle of attack on pitching-moment coefficient for no. 1 tail configuration. $\delta_e = -15°$, $\delta_a = 0°$, $\delta_r = -25°$, $\beta = 0°$.

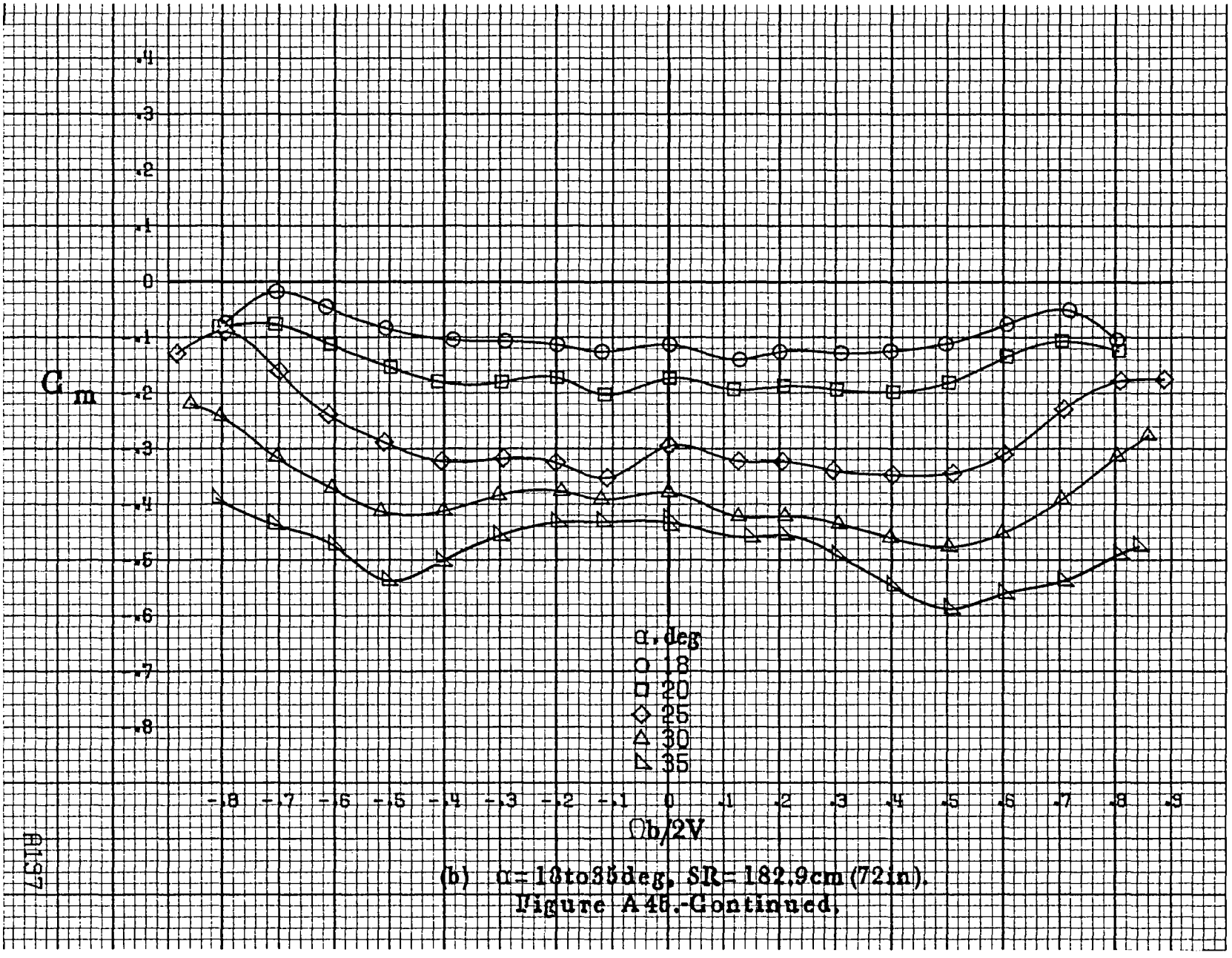

(b) α = 18 to 35 deg, SR = 182.9 cm (72 in).

Figure A45.-Continued.

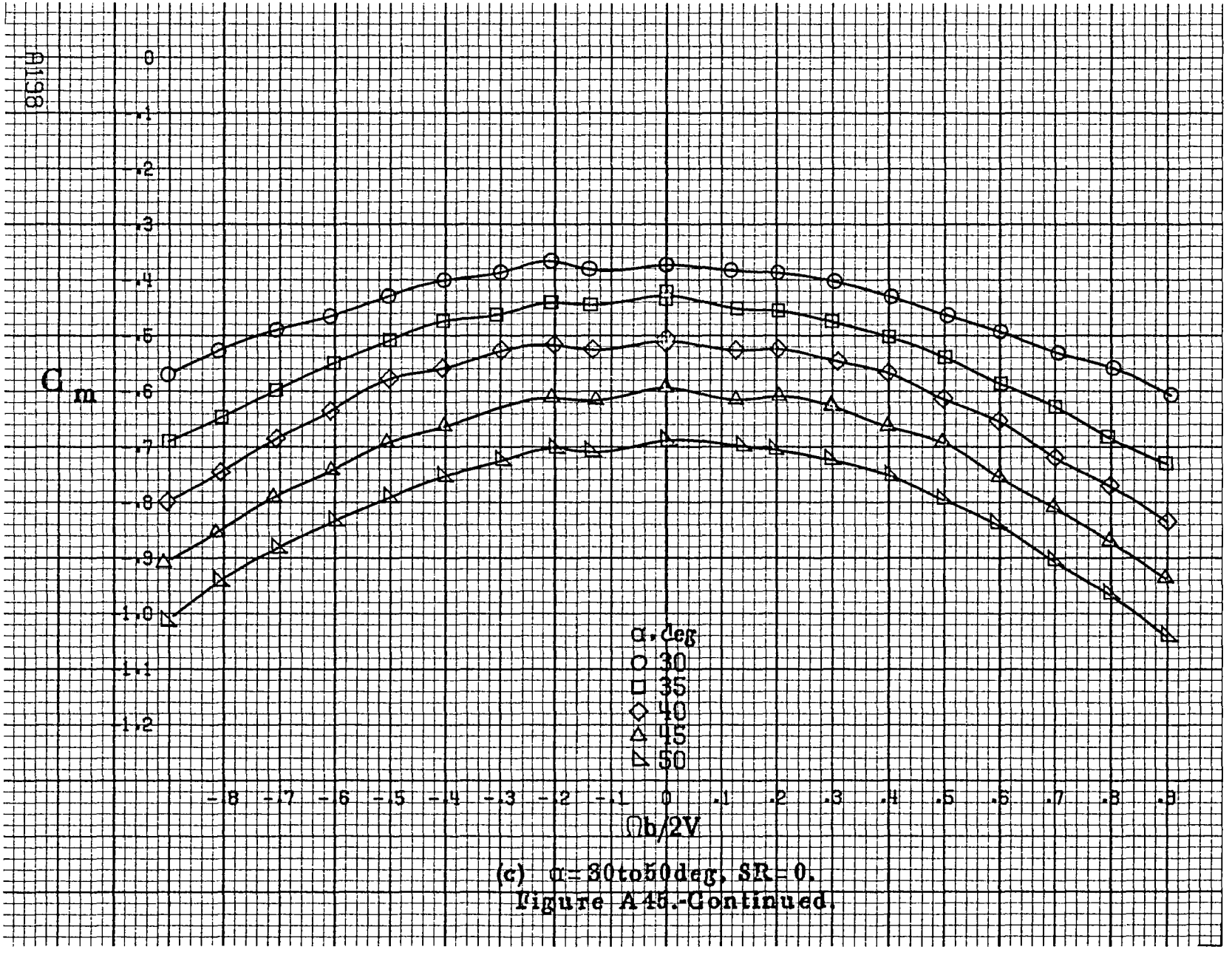

(c) α = 30 to 50 deg, SR = 0.

Figure A 45.-Continued.

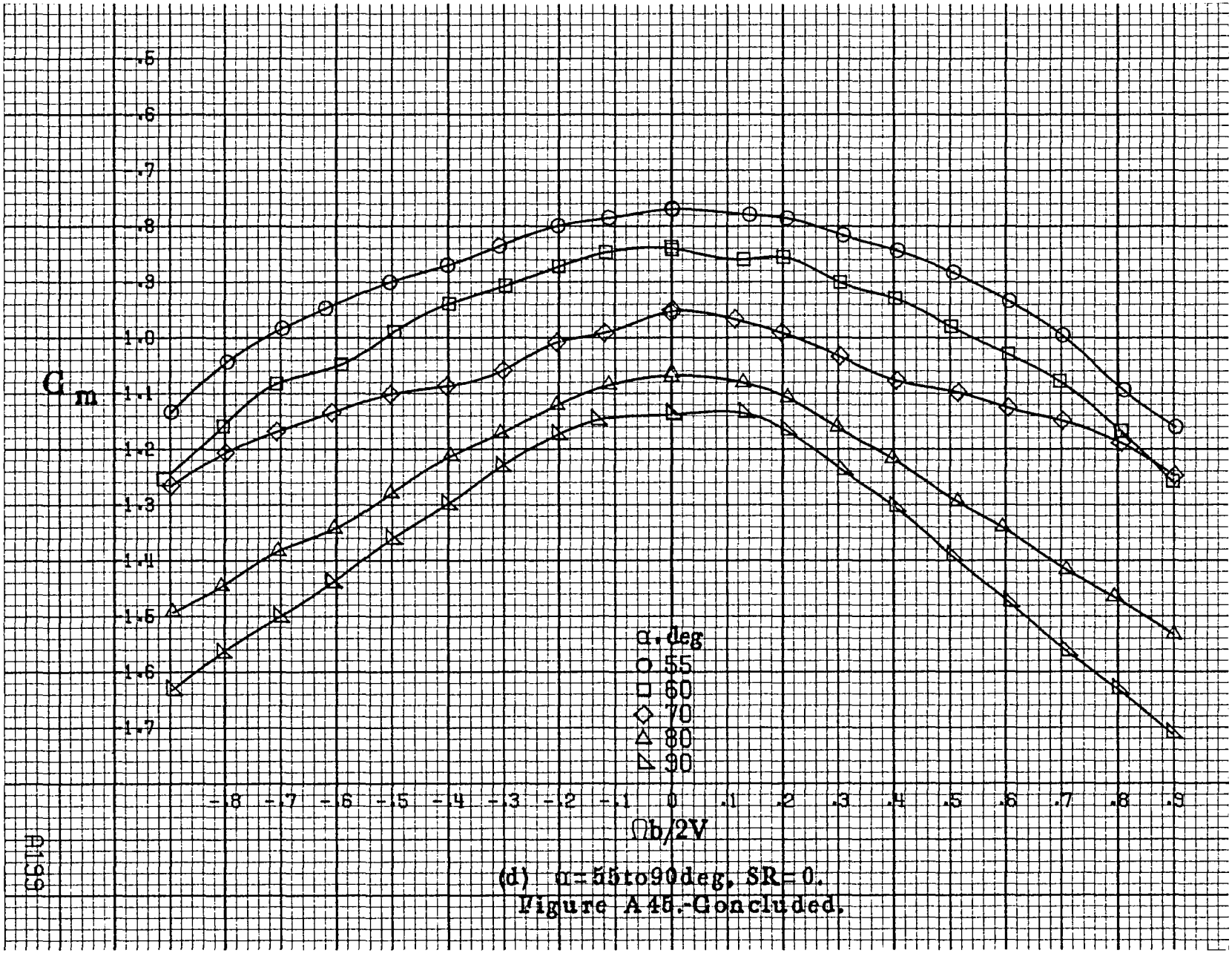

(d) α=55to90deg, SR=0.

Figure A45.-Concluded.

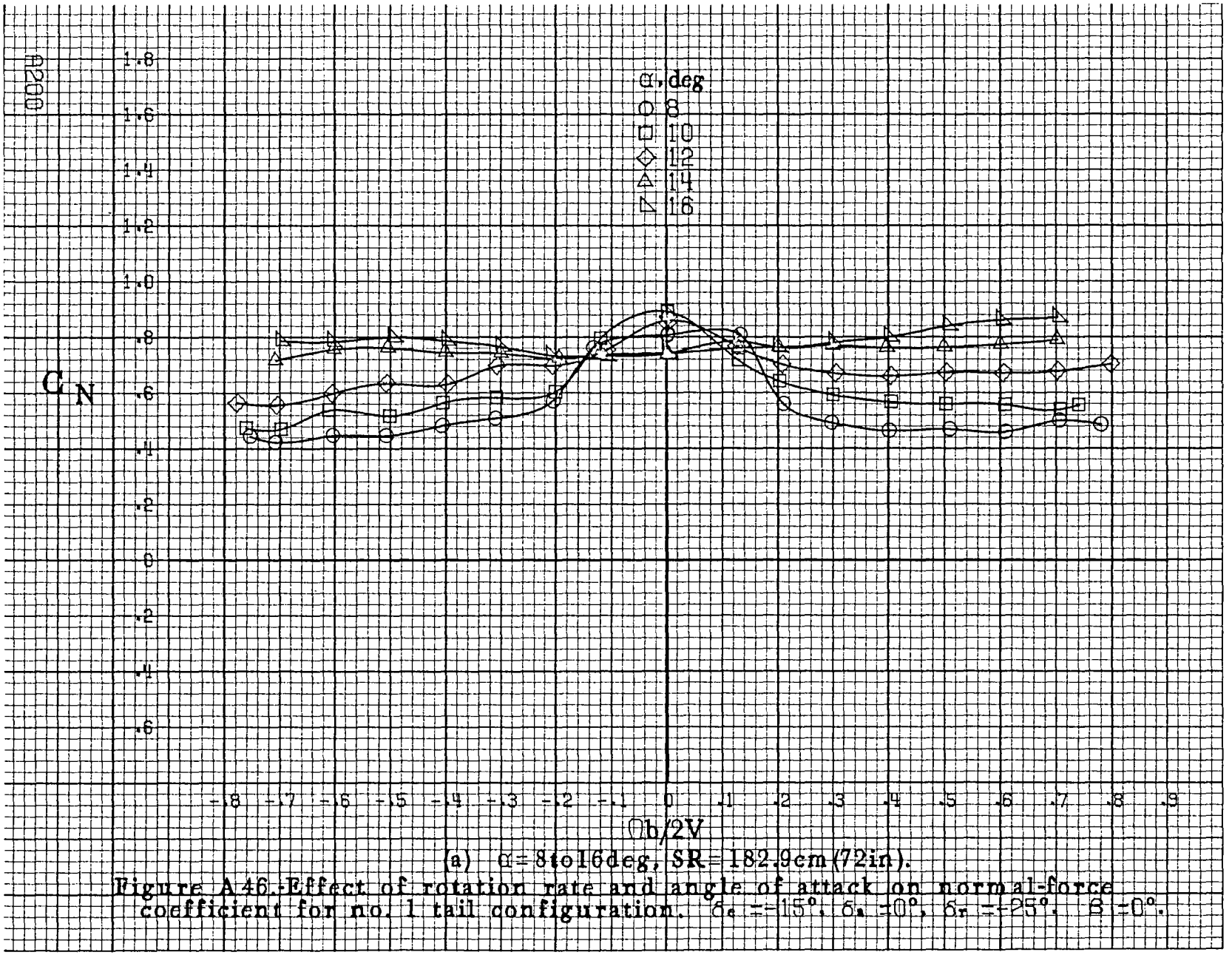

(a) $\alpha = 8$ to 16 deg, SR = 182.9 cm (72 in).

Figure A46.-Effect of rotation rate and angle of attack on normal-force coefficient for no. 1 tail configuration. $\delta_e = -15°$, $\delta_a = 0°$, $\delta_r = -25°$, $\beta = 0°$.

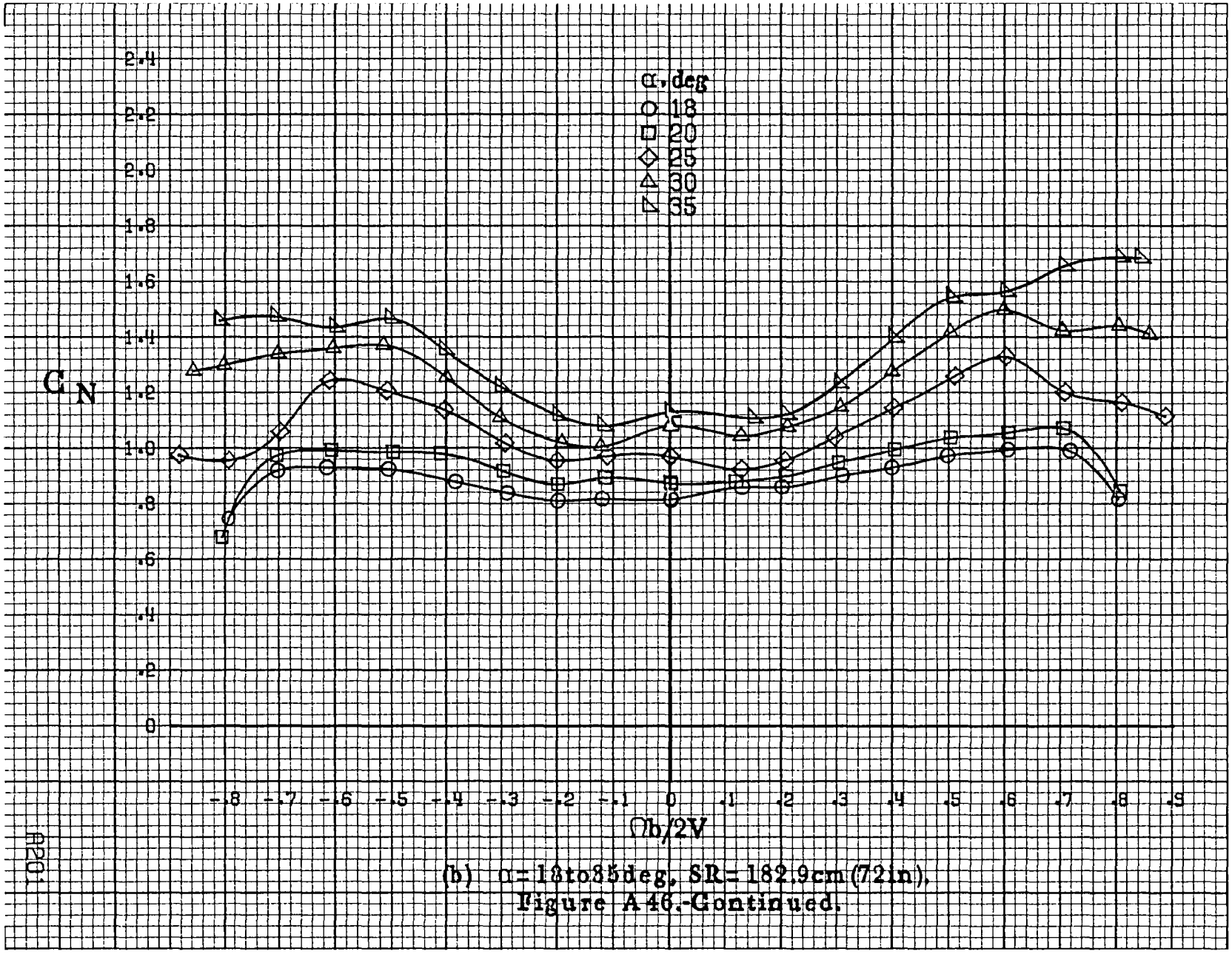

R201

(b) α = 18 to 35 deg, SR = 182.9 cm (72 in).

Figure A46.-Continued.

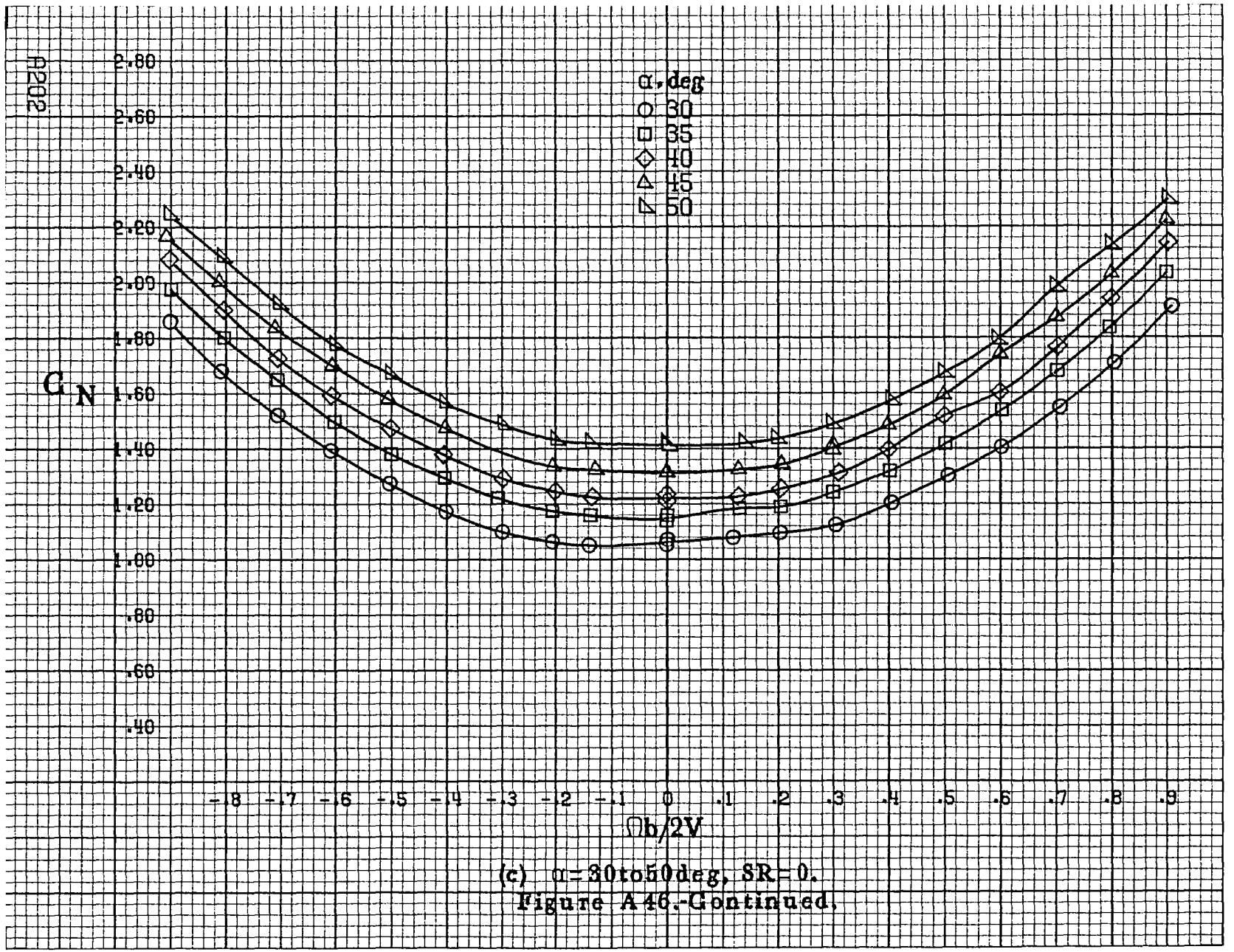

(c) α=30to50deg, SR=0.

Figure A46.-Continued.

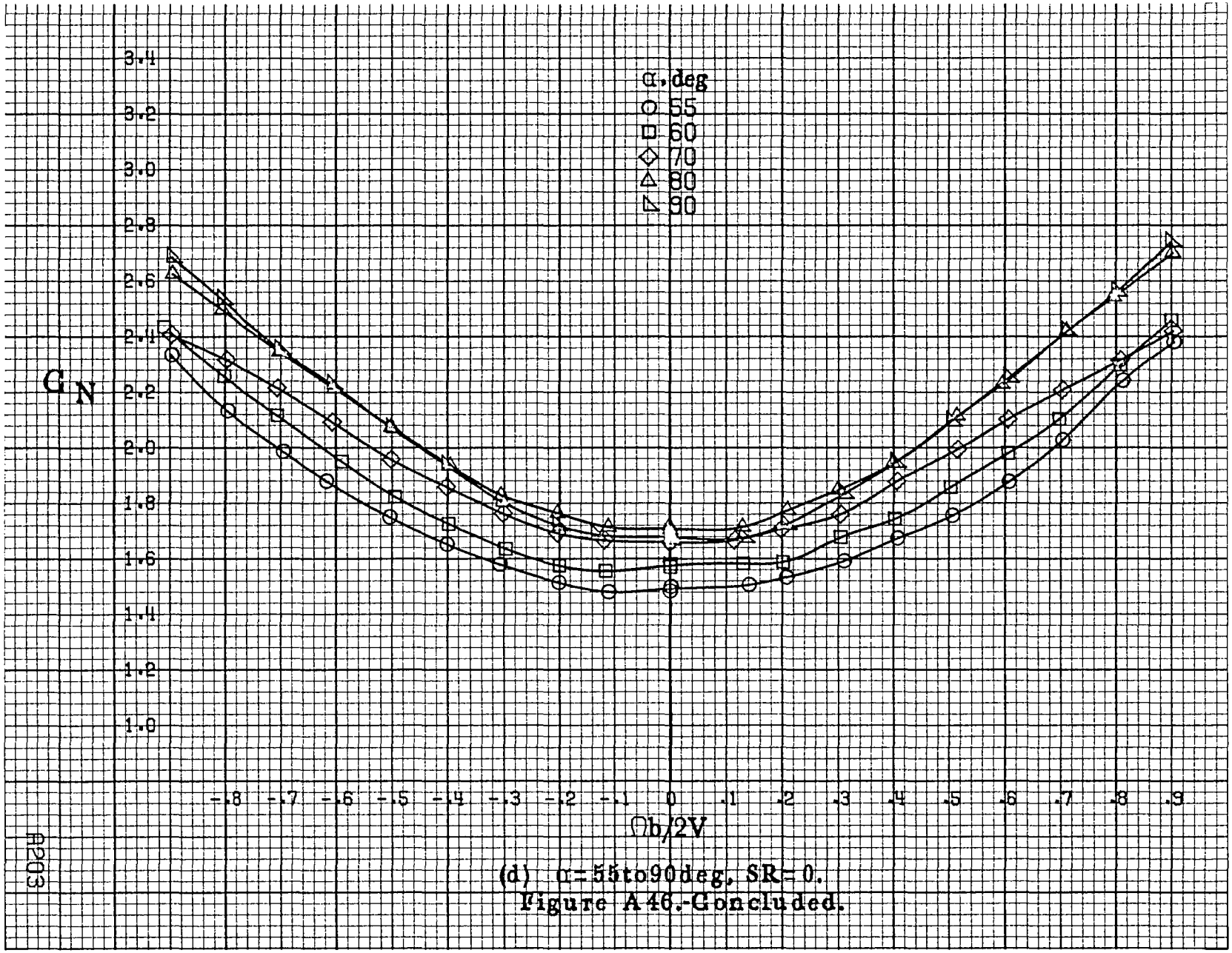

(d) $\alpha = 55$ to 90 deg, SR = 0.

Figure A46.-Concluded.

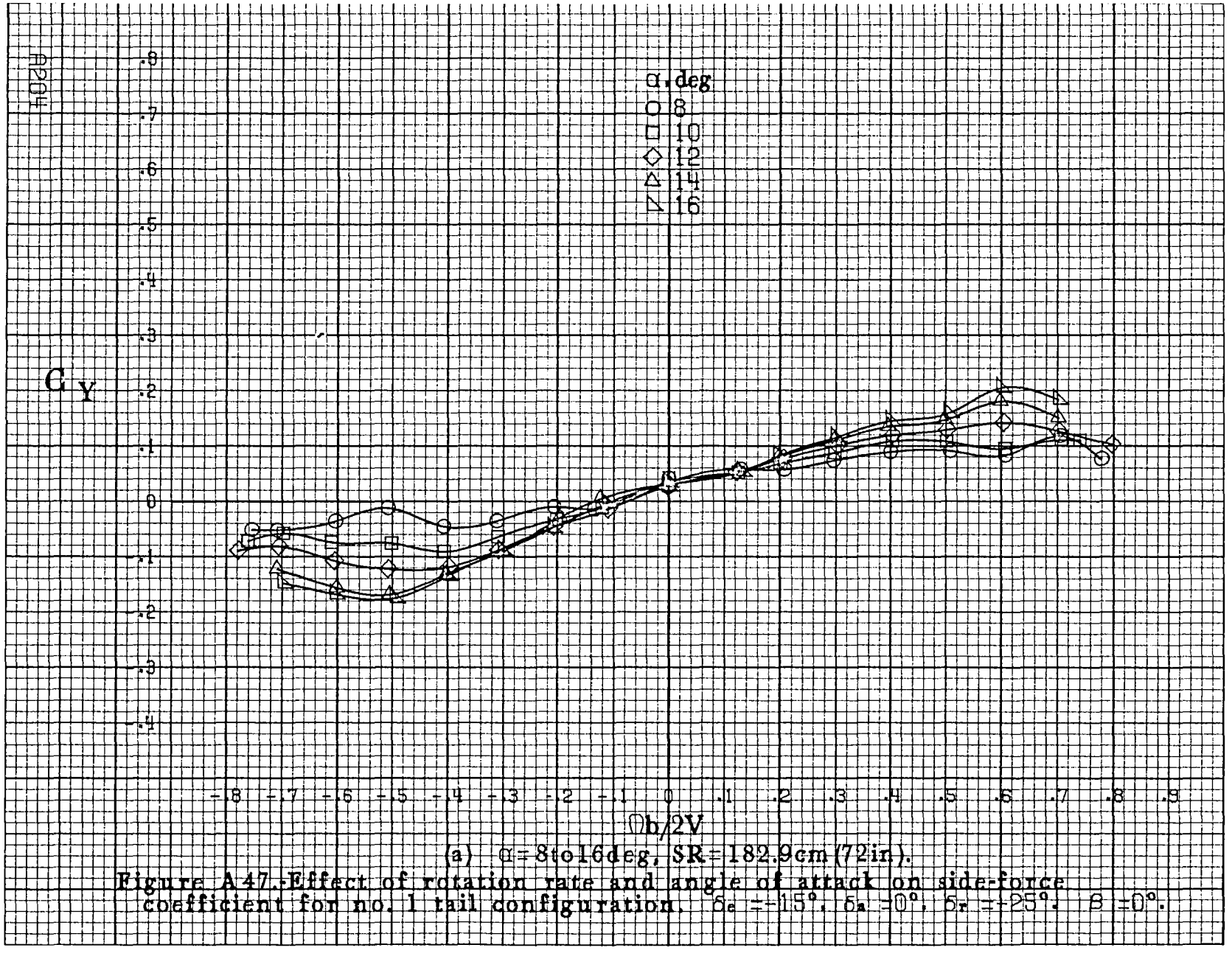

(a) α = 8 to 16 deg, SR = 182.9 cm (72 in.).

Figure A47.-Effect of rotation rate and angle of attack on side-force coefficient for no. 1 tail configuration. $\delta_e = -15°$, $\delta_a = 0°$, $\delta_r = +25°$, $\beta = 0°$.

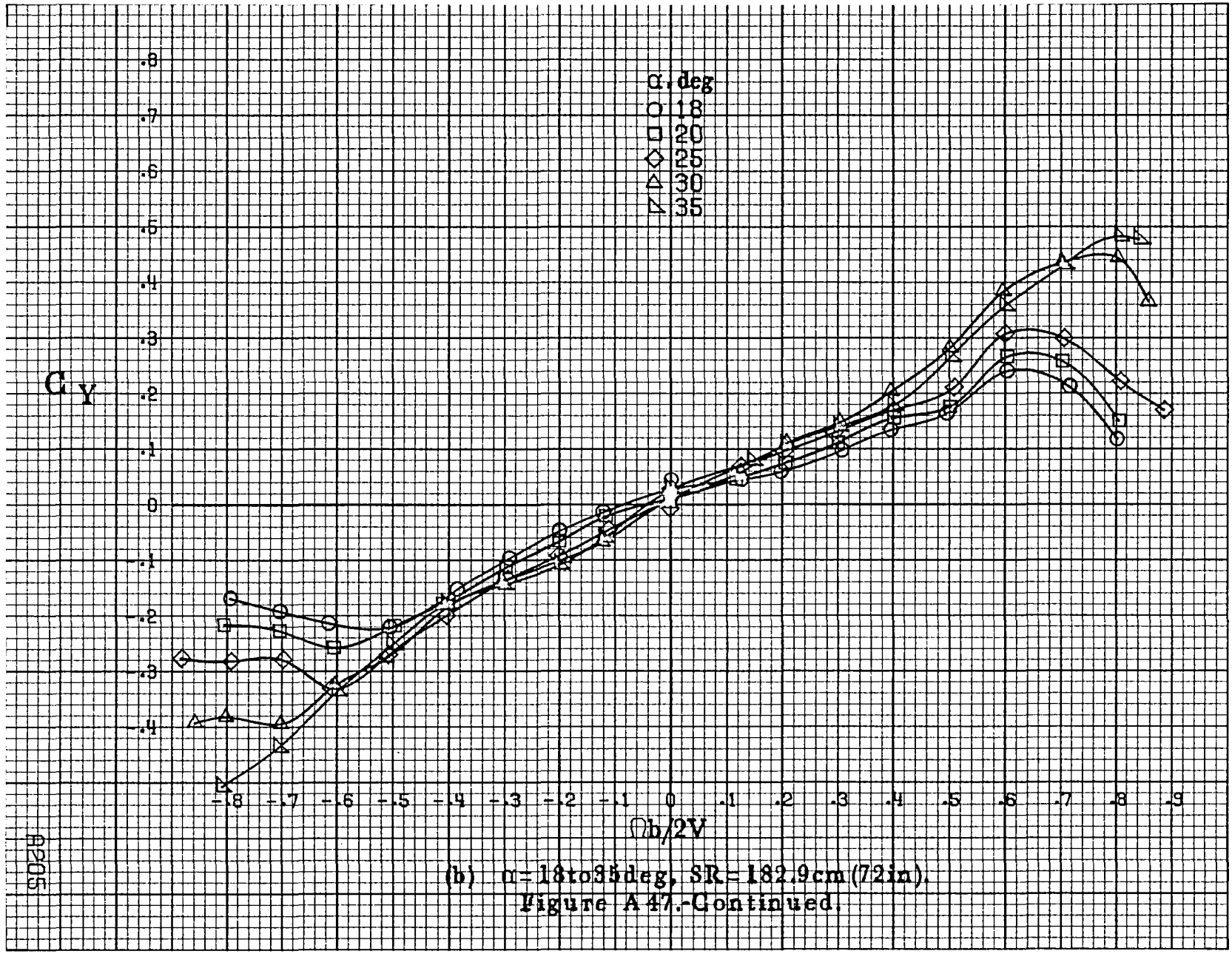

(b) α = 18 to 35 deg, SR = 182.9 cm (72 in).

Figure A47.-Continued.

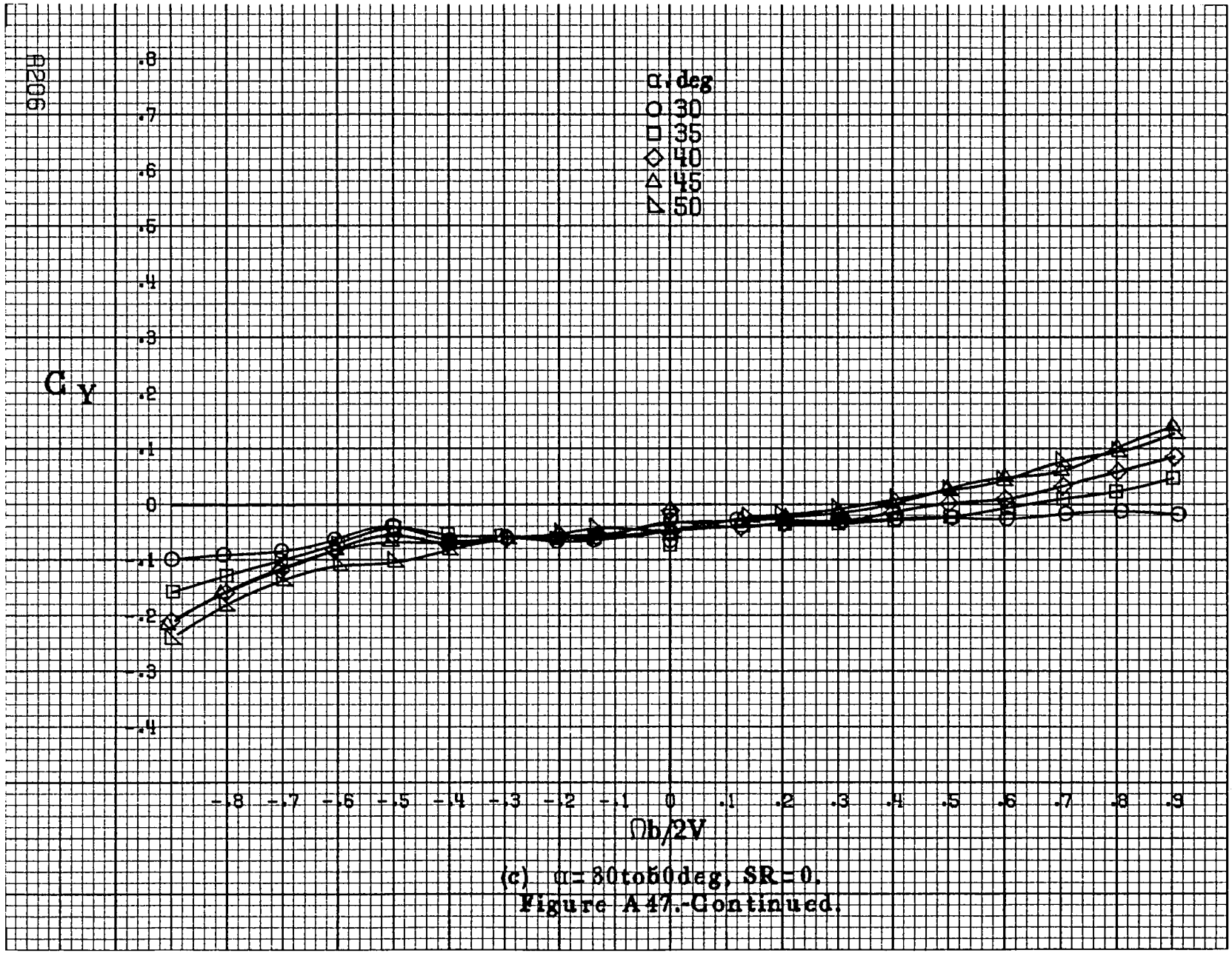

(c) α = 30 to 60 deg, SR = 0.

Figure A47.-Continued.

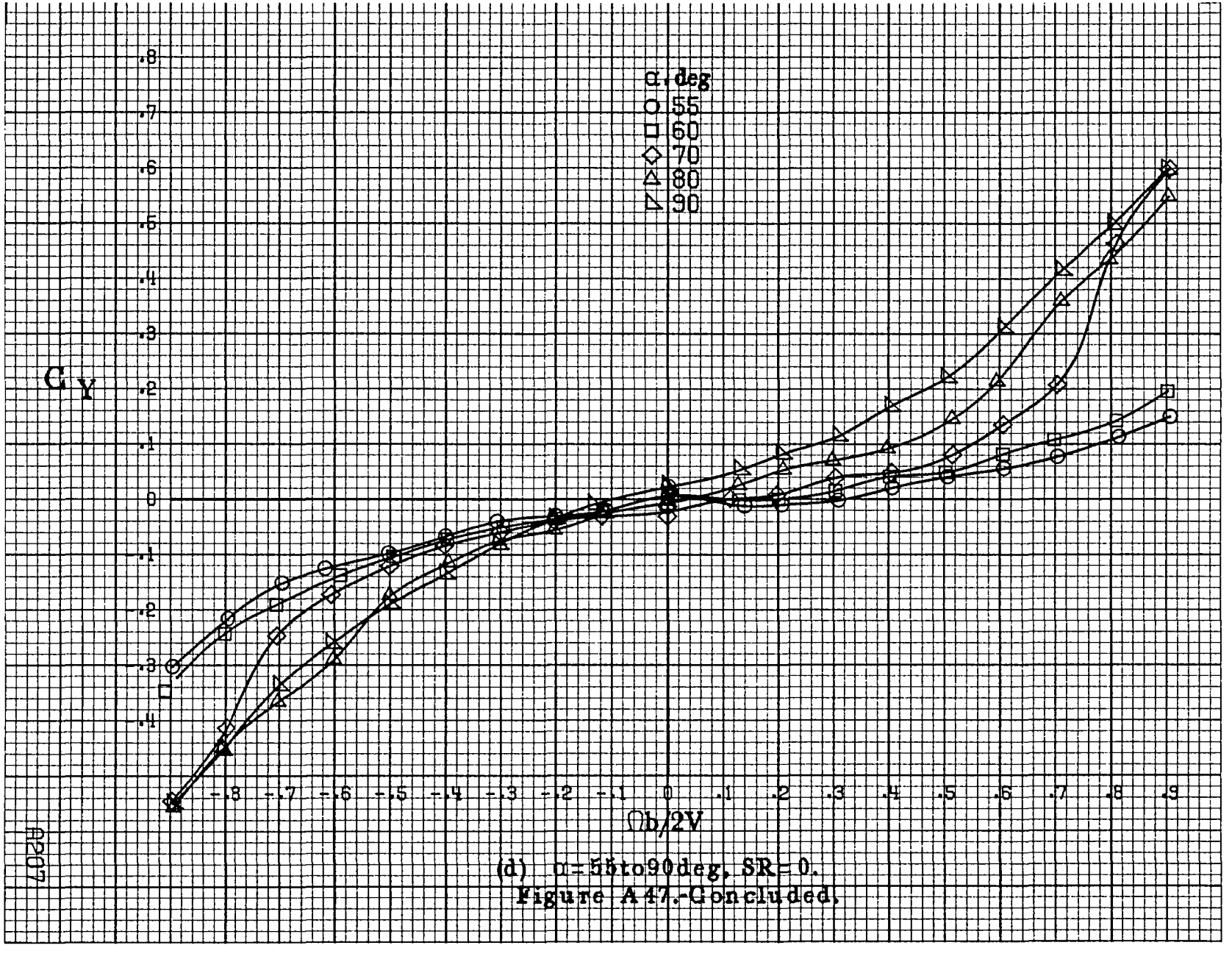

(d) $\alpha = 55$ to 90 deg, SR = 0.

Figure A47.-Concluded.

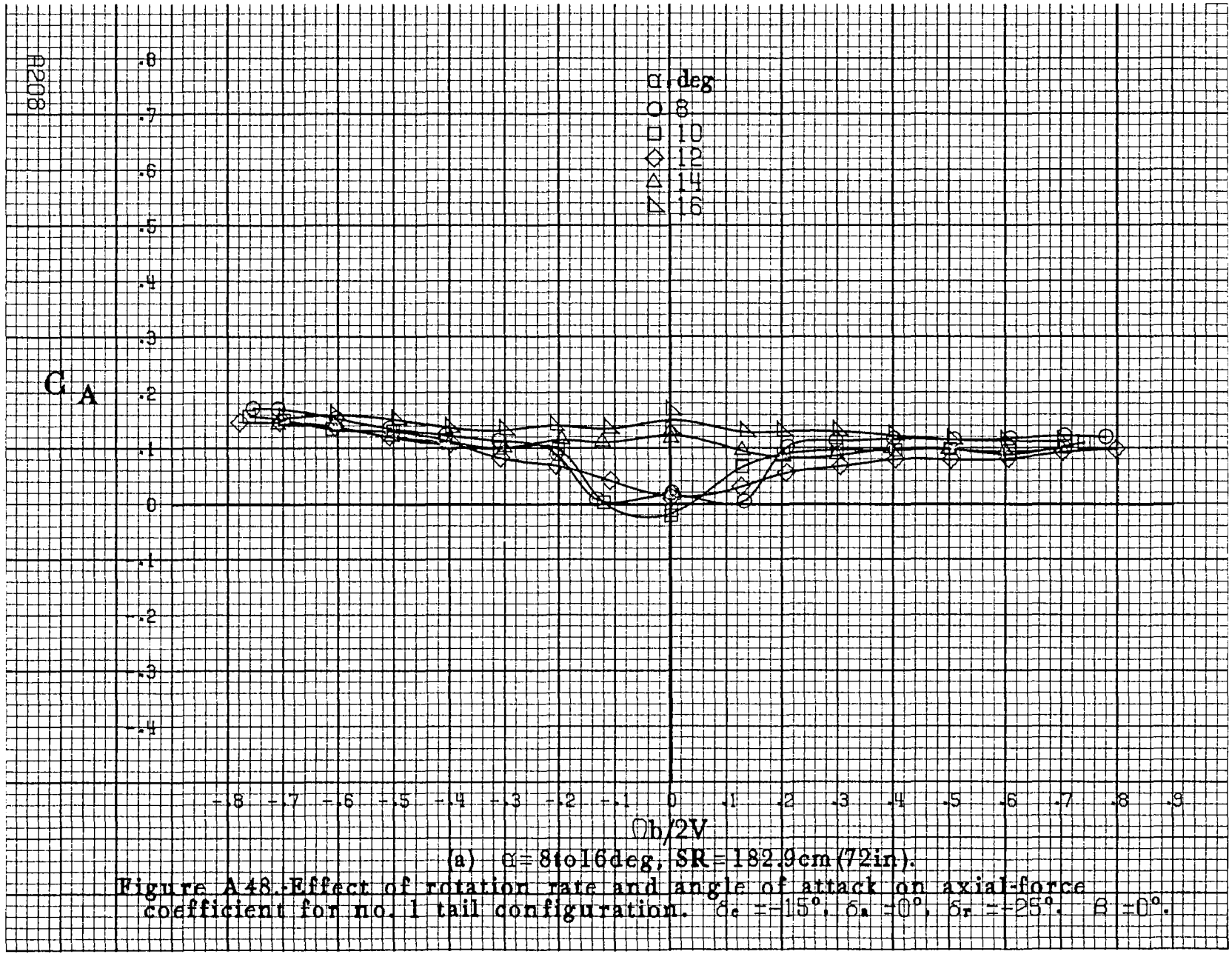

(a) $\alpha = 8$ to 16 deg, SR = 182.9 cm (72 in.).

Figure A48.-Effect of rotation rate and angle of attack on axial-force coefficient for no. 1 tail configuration. $\delta_e = -15°$, $\delta_a = 0°$, $\delta_r = -25°$, $\beta = 0°$.

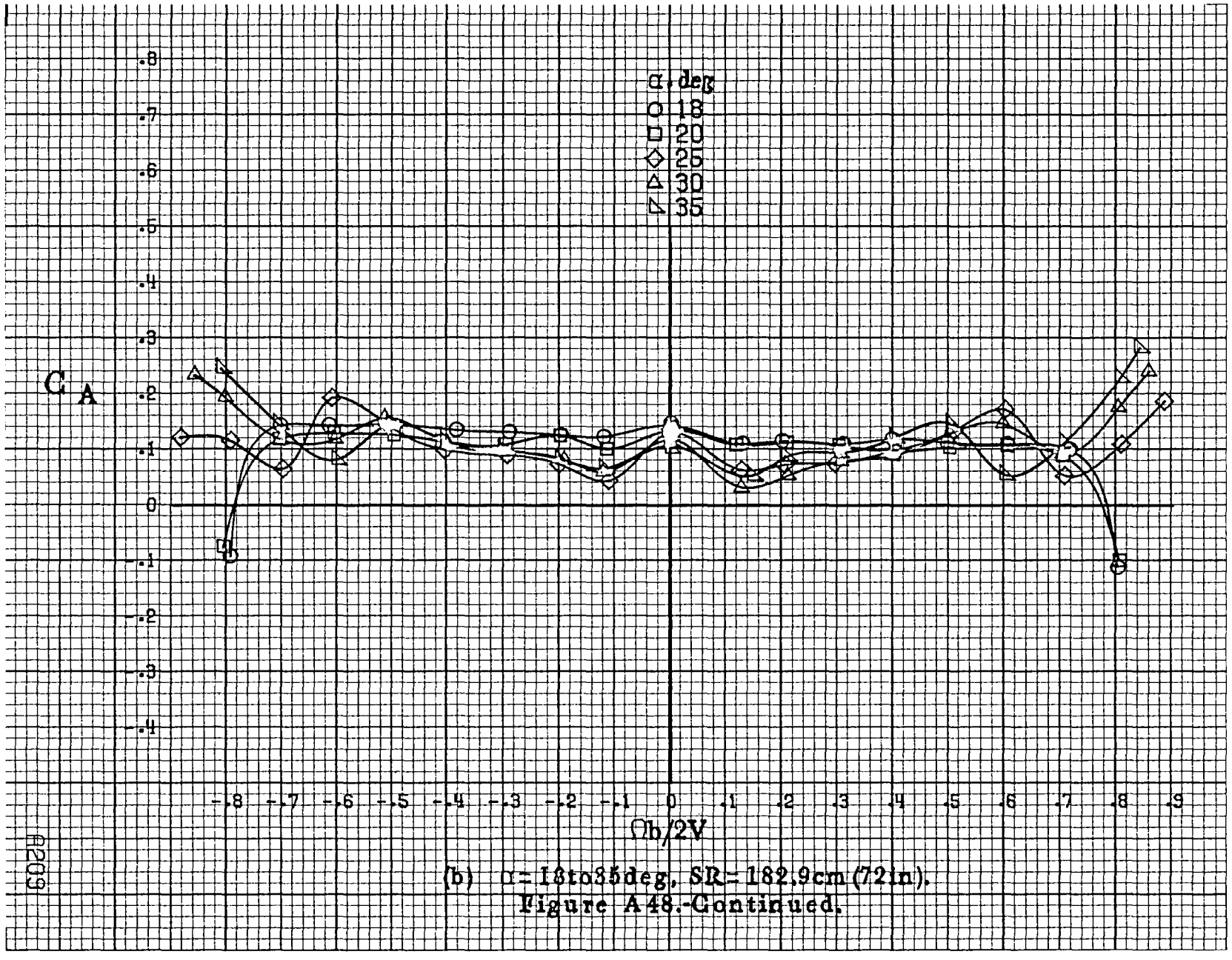

R209

(b) α = 18 to 35 deg, SR = 182.9 cm (72 in).

Figure A48.-Continued.

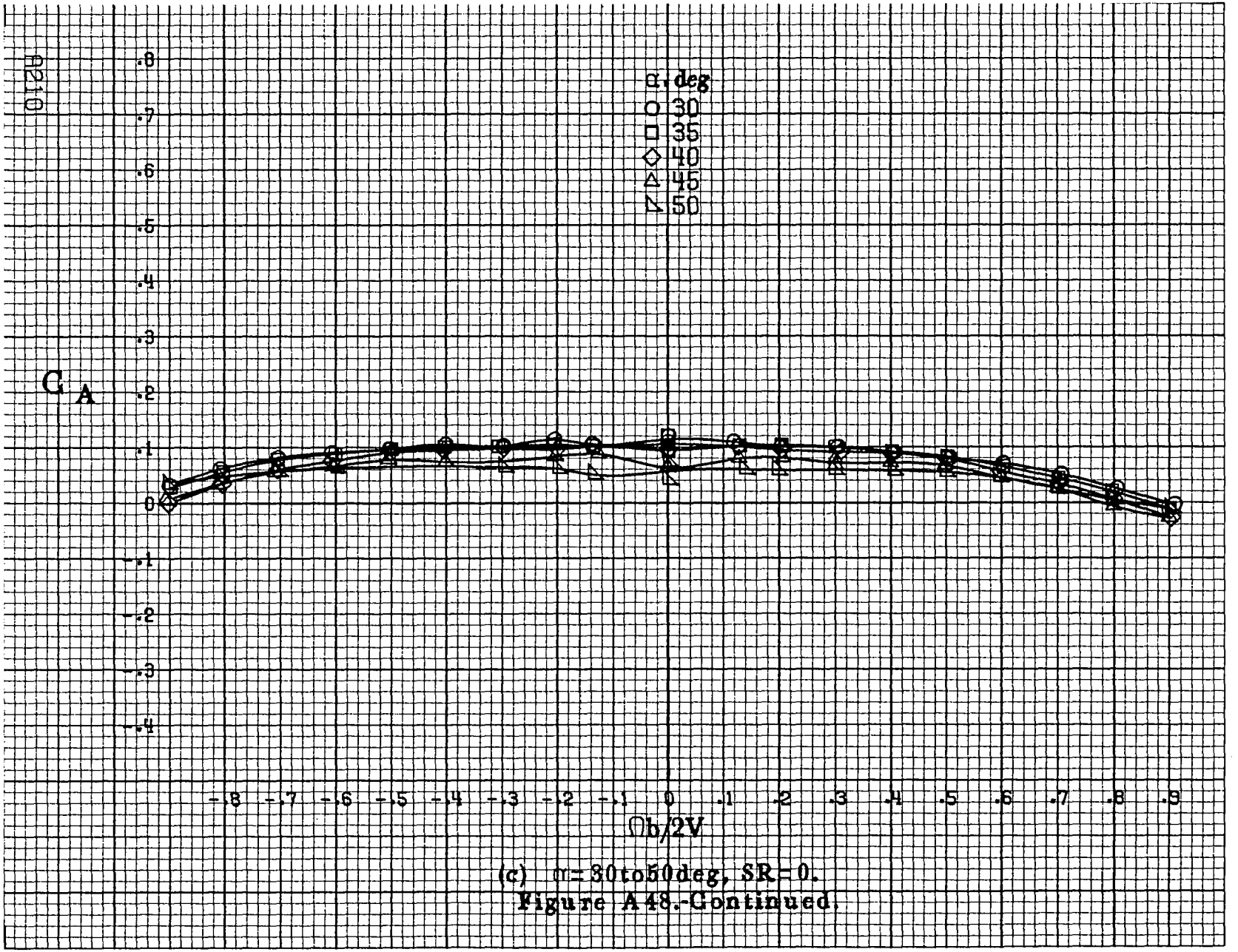

(c) $\alpha = 30$ to 50 deg, SR = 0.

Figure A48.-Continued.

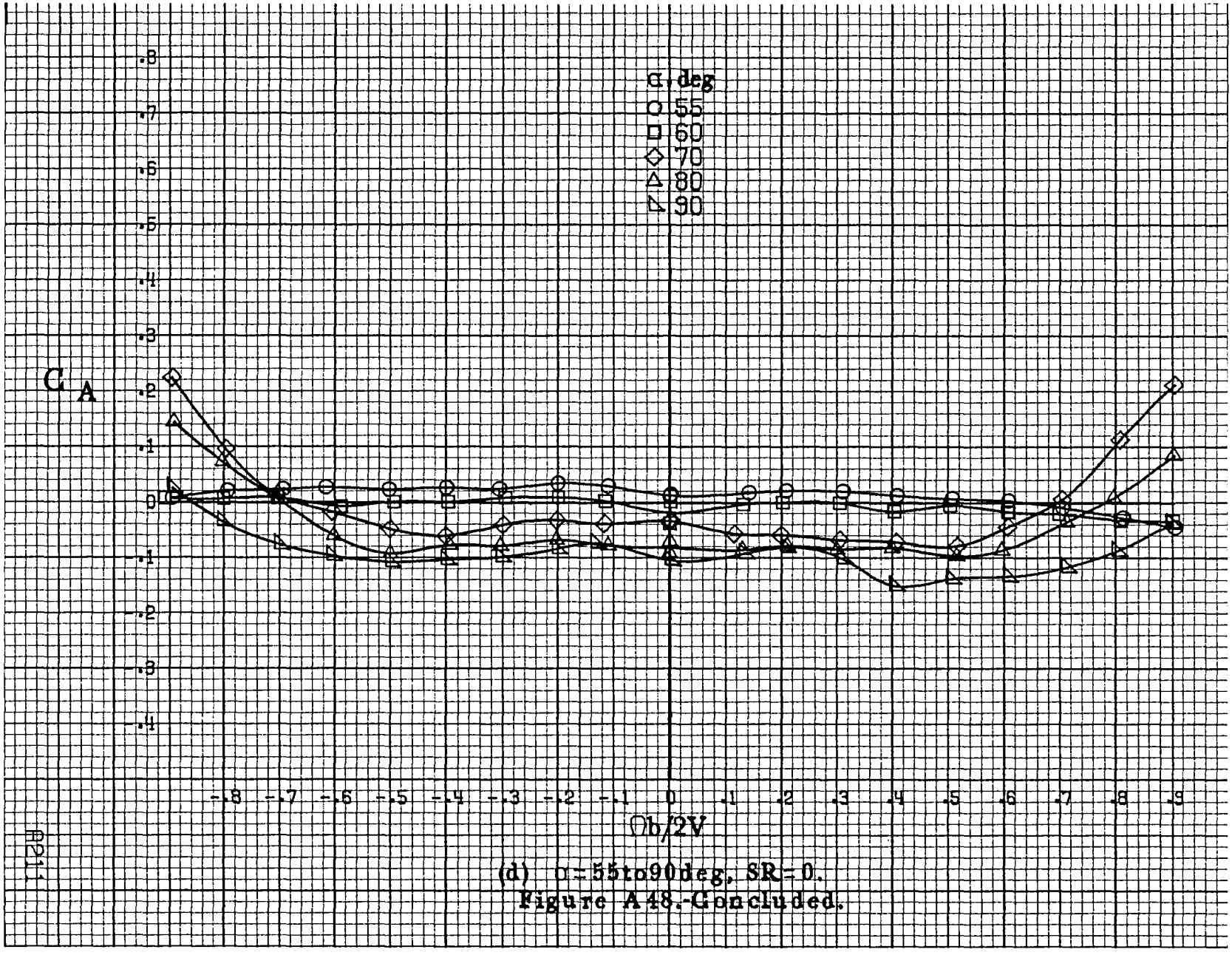

(d) α = 55 to 90 deg, SR = 0.

Figure A48.-Concluded.

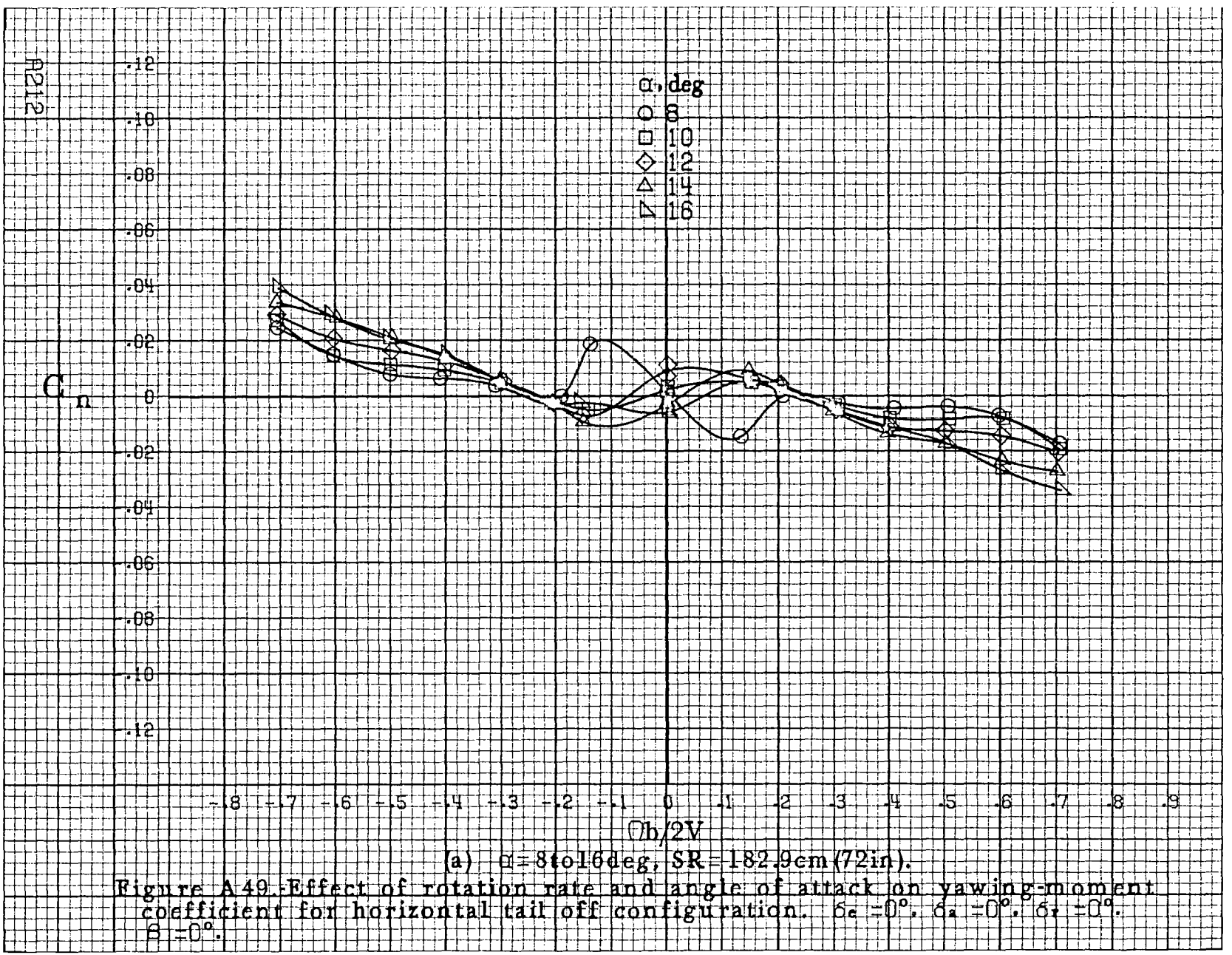

(a) $\alpha = 8$ to 16 deg, SR = 182.9 cm (72 in).

Figure A49.-Effect of rotation rate and angle of attack on yawing-moment coefficient for horizontal tail off configuration. $\delta_e = 0°$, $\delta_a = 0°$, $\delta_r = 0°$, $\beta = 0°$.

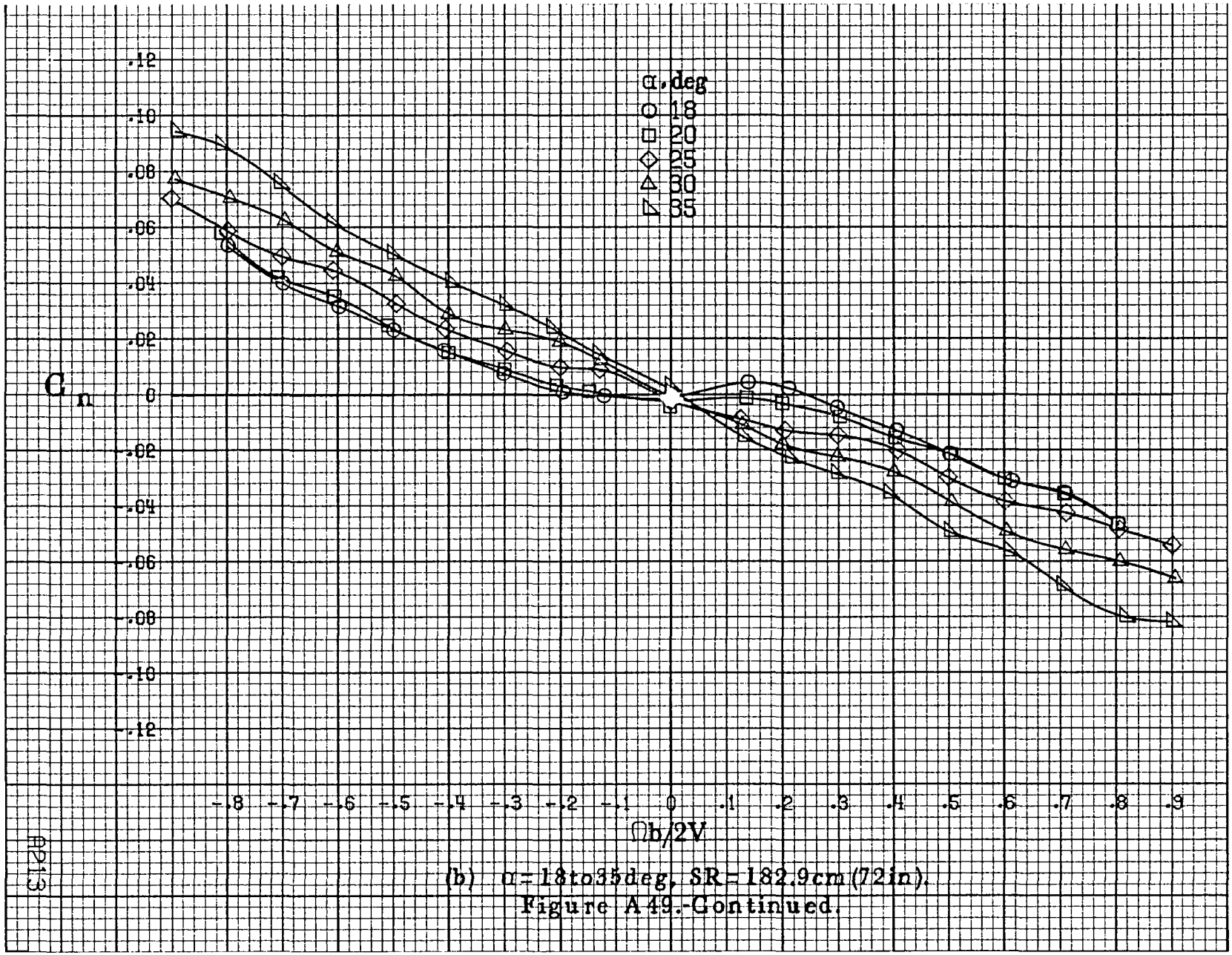

(b) $\alpha = 18$ to 35 deg, SR = 182.9 cm (72 in).

Figure A49.-Continued.

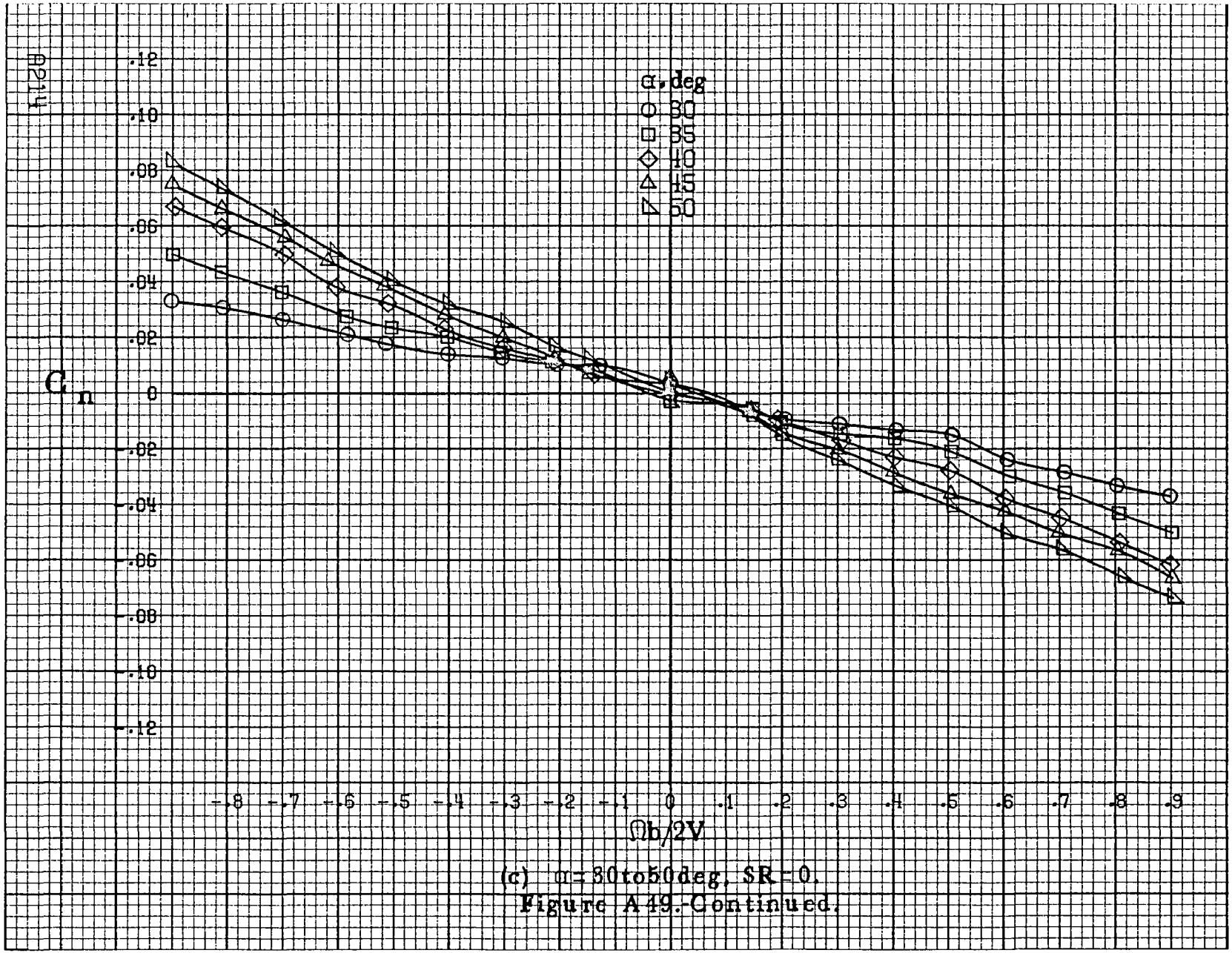

(c) $\alpha = 30$ to 50 deg, $SR = 0$.

Figure A49.-Continued.

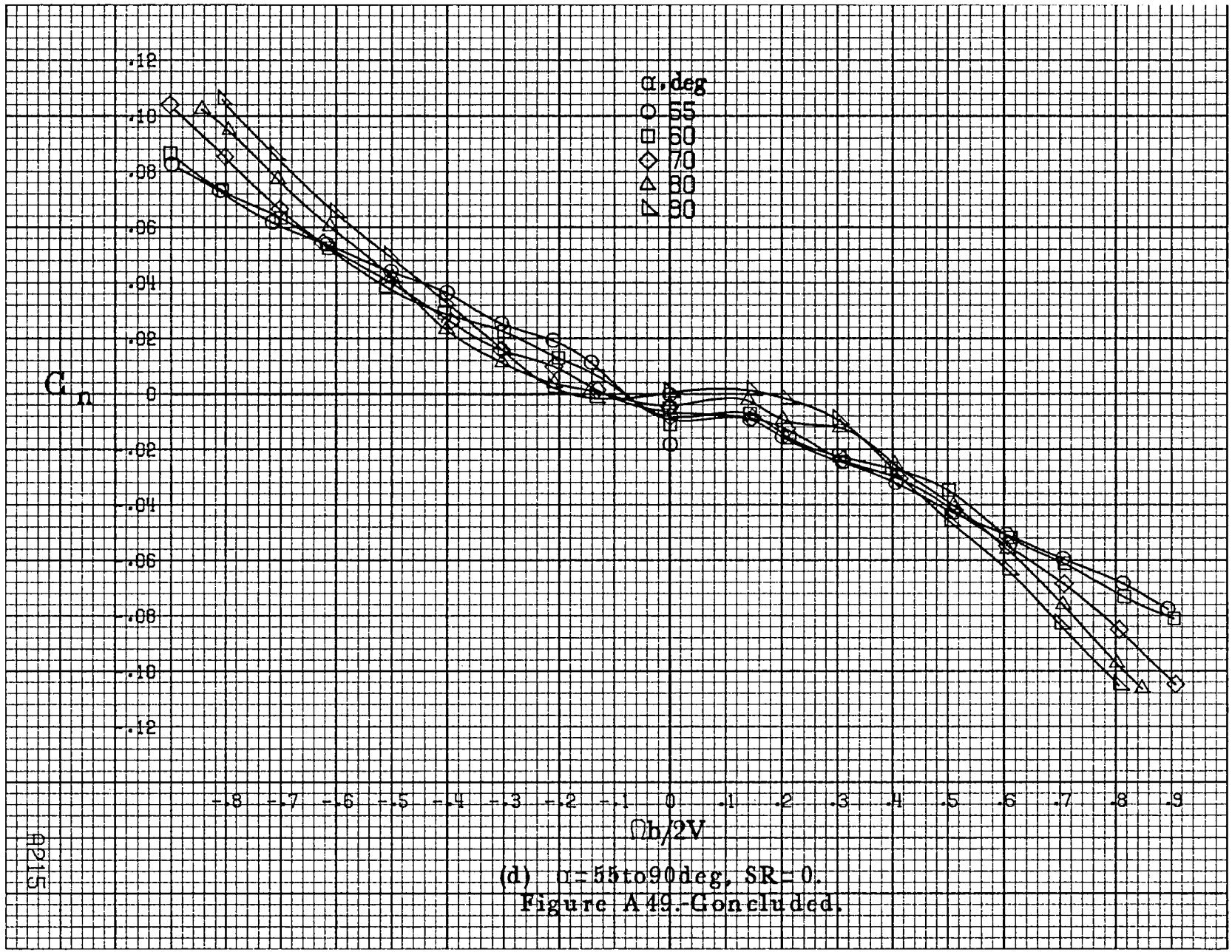

D-215

(d) α = 55 to 90 deg, SR = 0.

Figure A49.-Concluded.

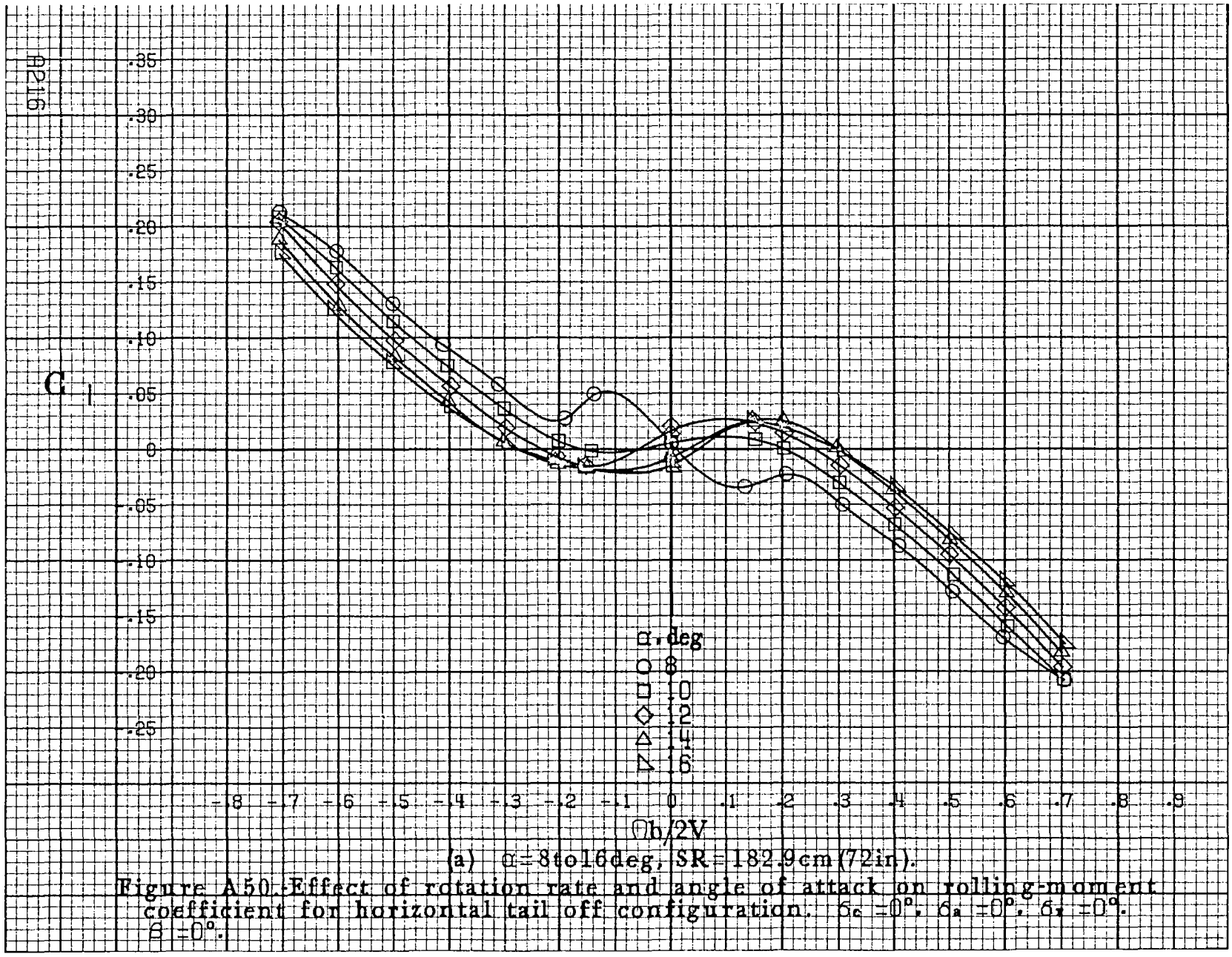

(a) $\alpha = 8$ to 16 deg, SR = 182.9 cm (72 in.).

Figure A50.-Effect of rotation rate and angle of attack on rolling-moment coefficient for horizontal tail off configuration. $\delta_e = 0°$, $\delta_a = 0°$, $\delta_r = 0°$, $\beta = 0°$.

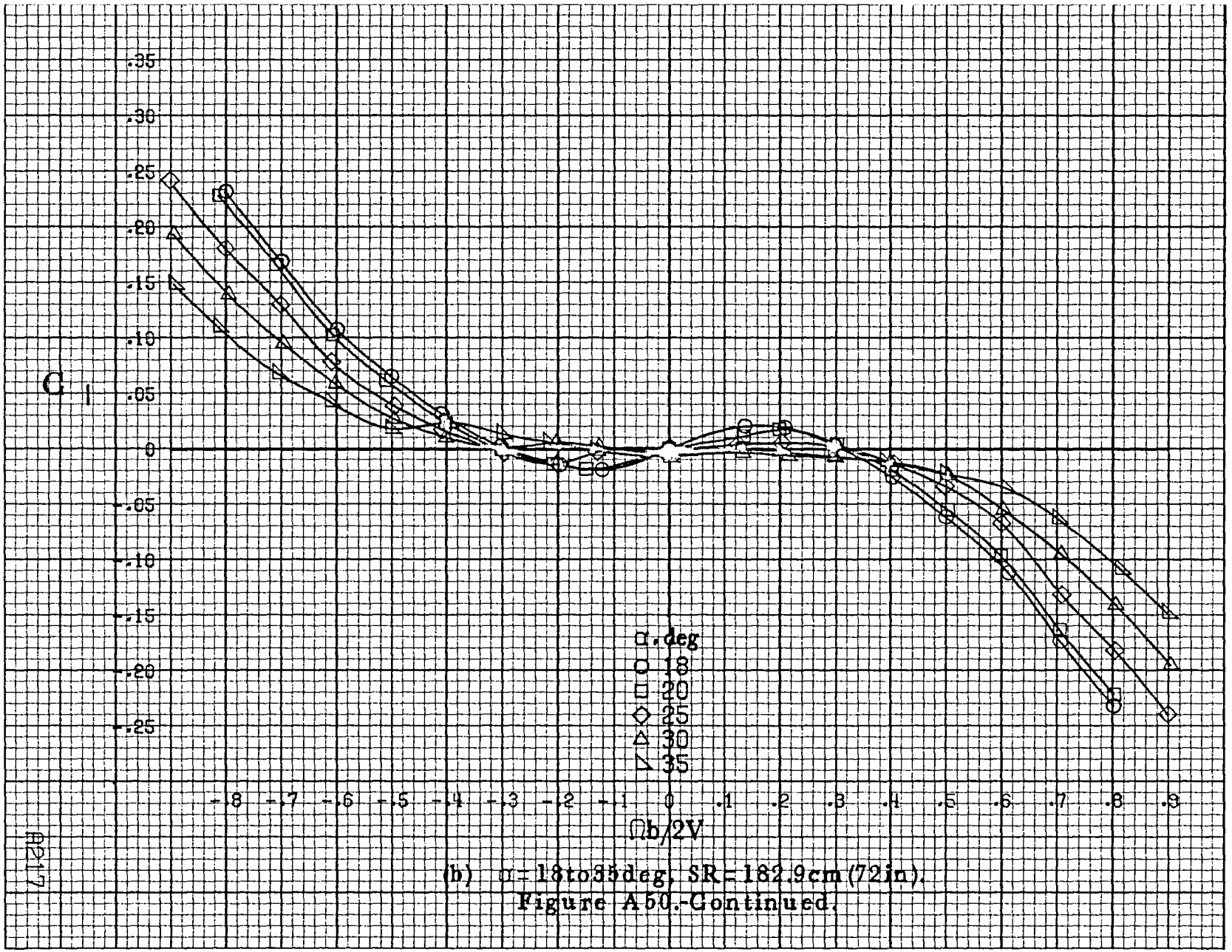

B217

(b) α = 18 to 35 deg, SR = 182.9 cm (72 in).

Figure A50.-Continued.

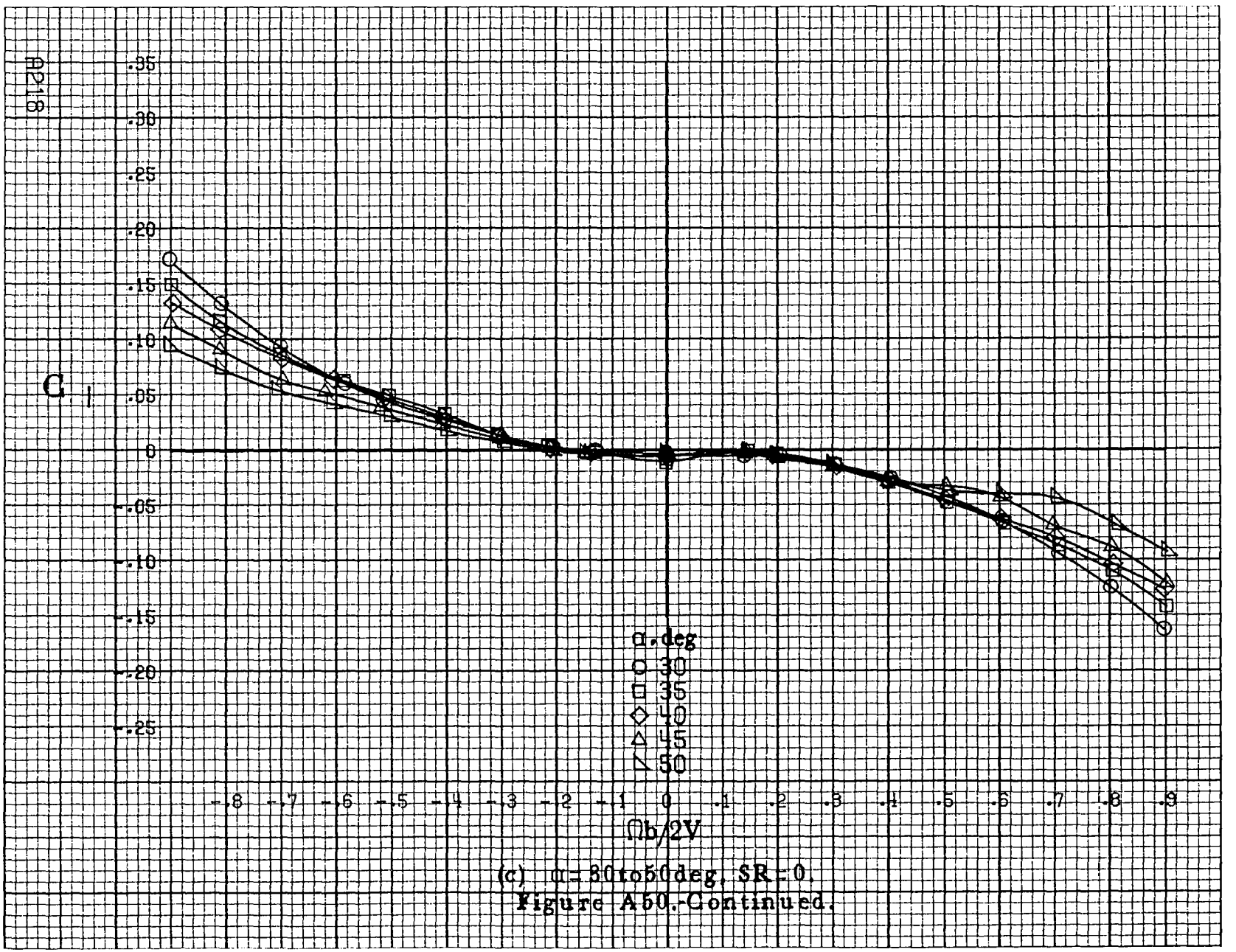

(c) α = 30 to 50 deg, SR = 0.

Figure A50.-Continued.

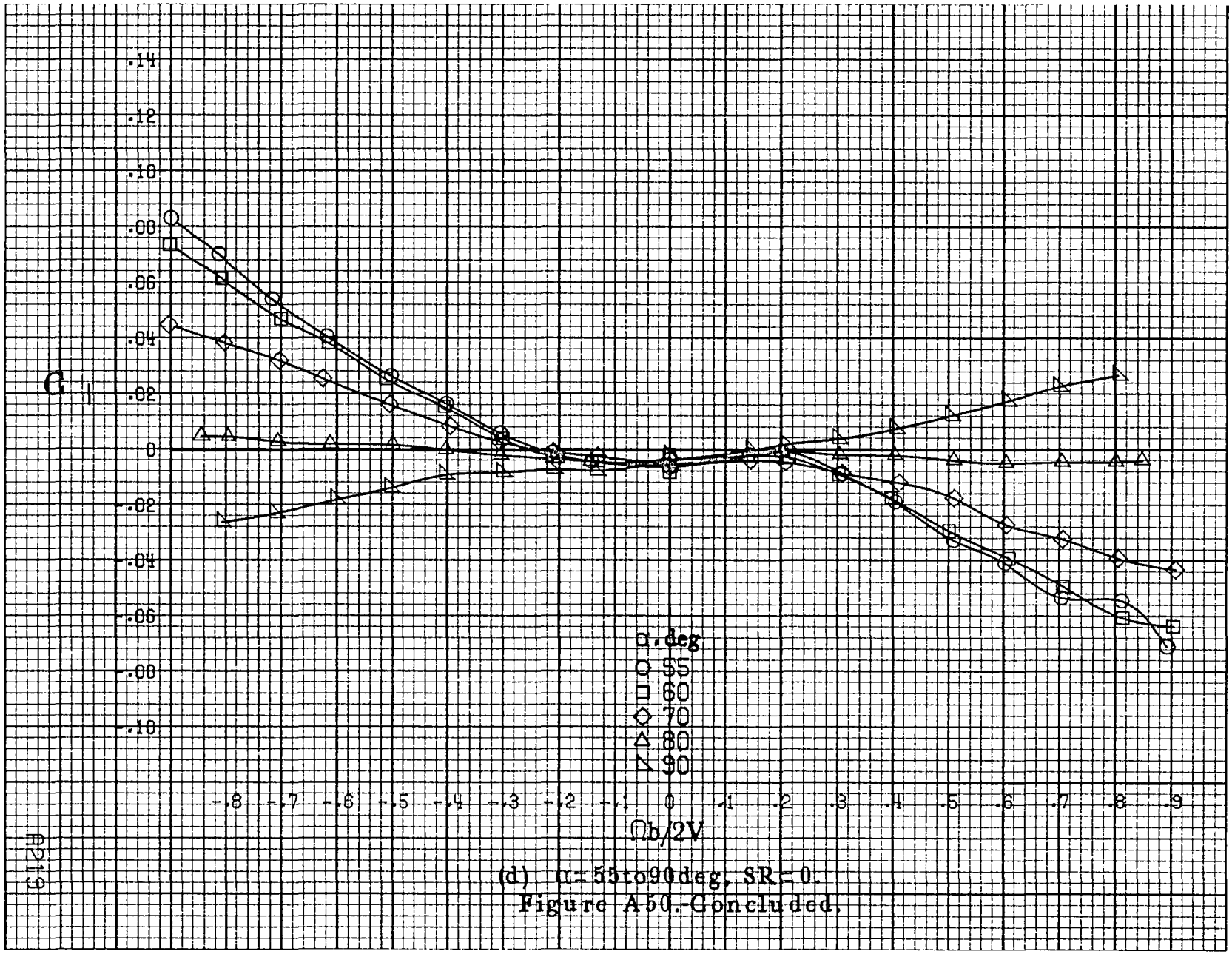

(d) α = 55 to 90 deg, SR = 0.

Figure A50.-Concluded.

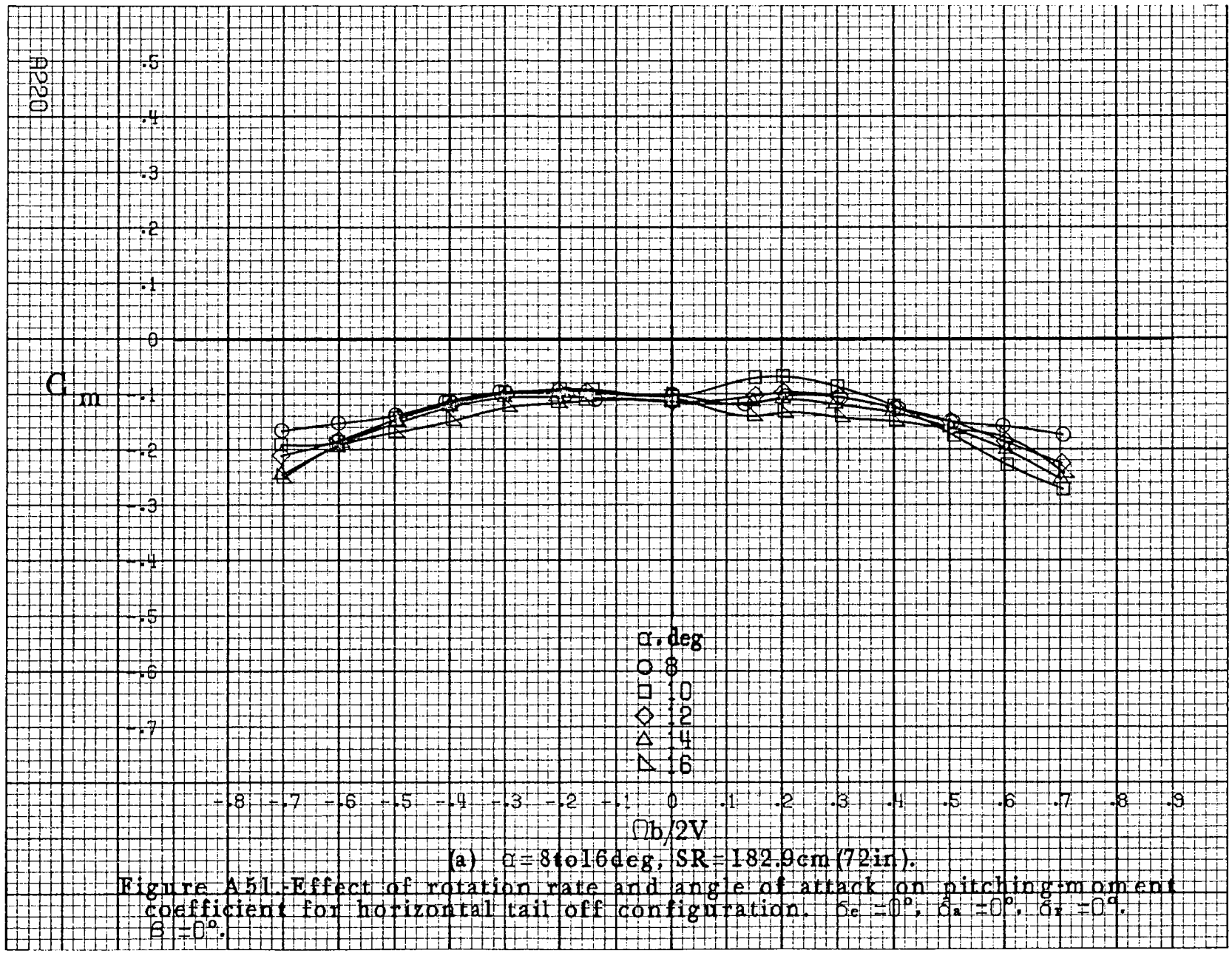

(a) $\alpha = 8$ to 16 deg, SR = 182.9 cm (72 in.).

Figure A51.-Effect of rotation rate and angle of attack on pitching-moment coefficient for horizontal tail off configuration. $\delta_e = 0°$, $\delta_a = 0°$, $\delta_r = 0°$, $\beta = 0°$.

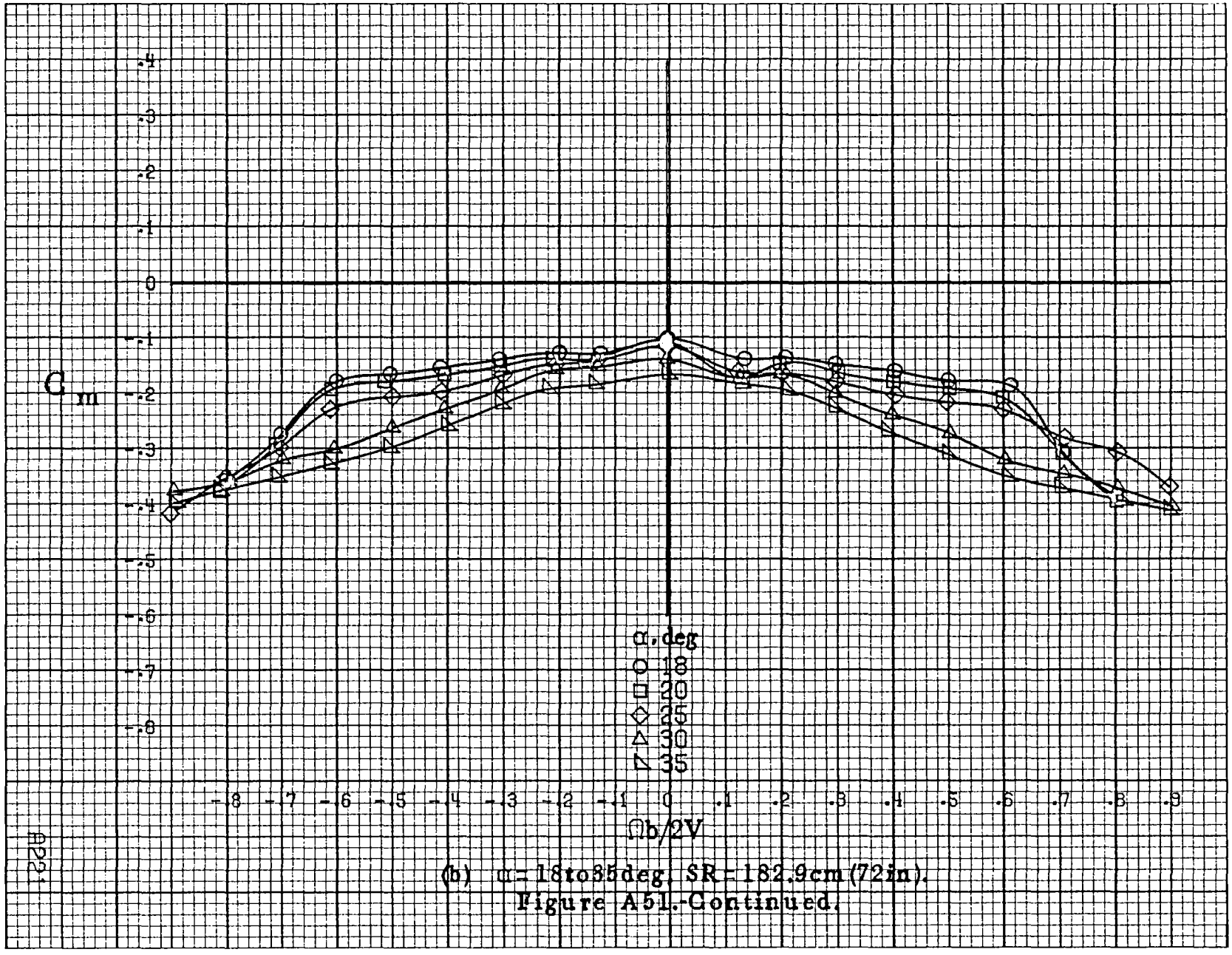

(b) α = 18 to 35 deg; SR = 182.9 cm (72 in).

Figure A51.-Continued.

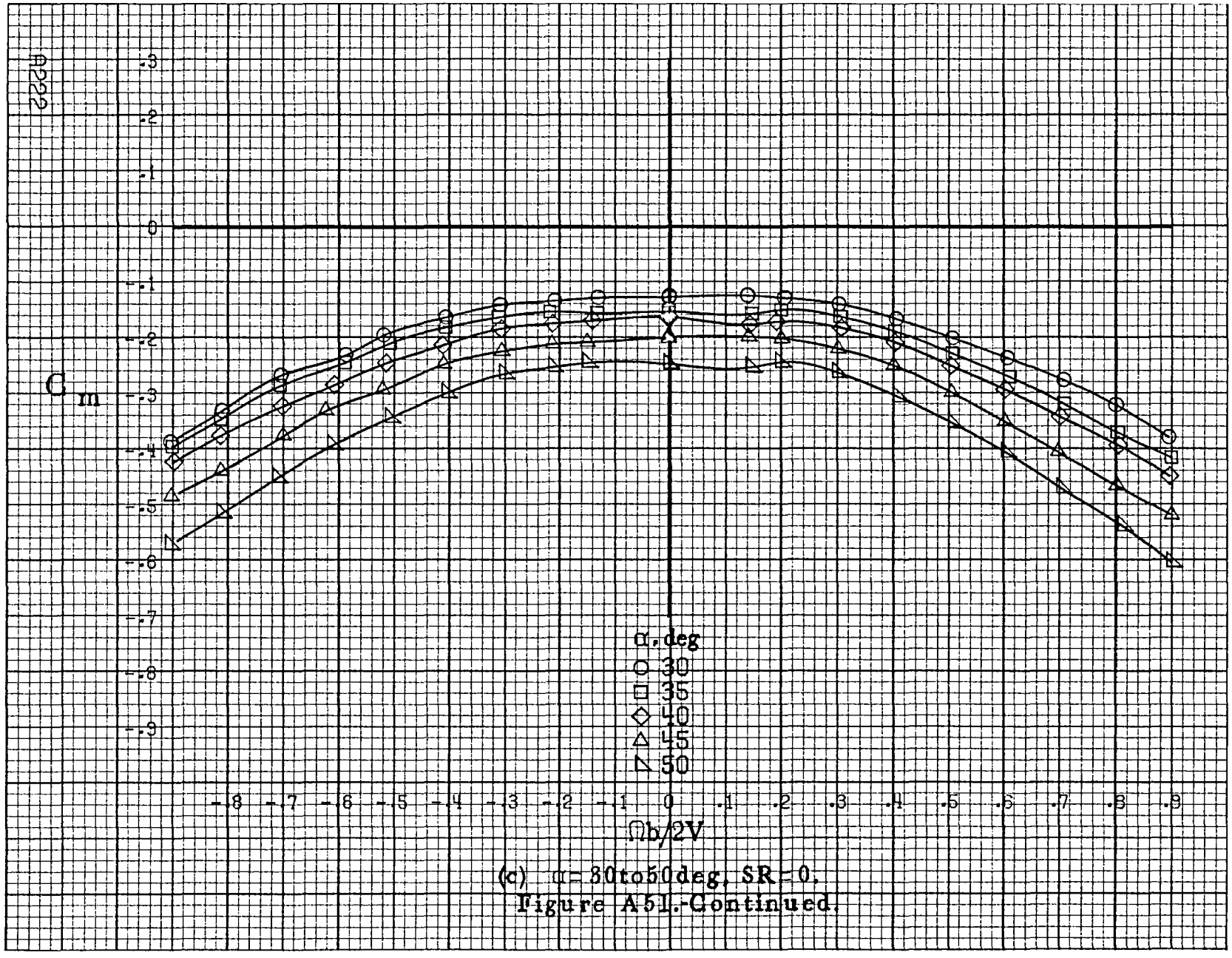

(c) $\alpha = 30$ to 50 deg, SR = 0.

Figure A51.-Continued.

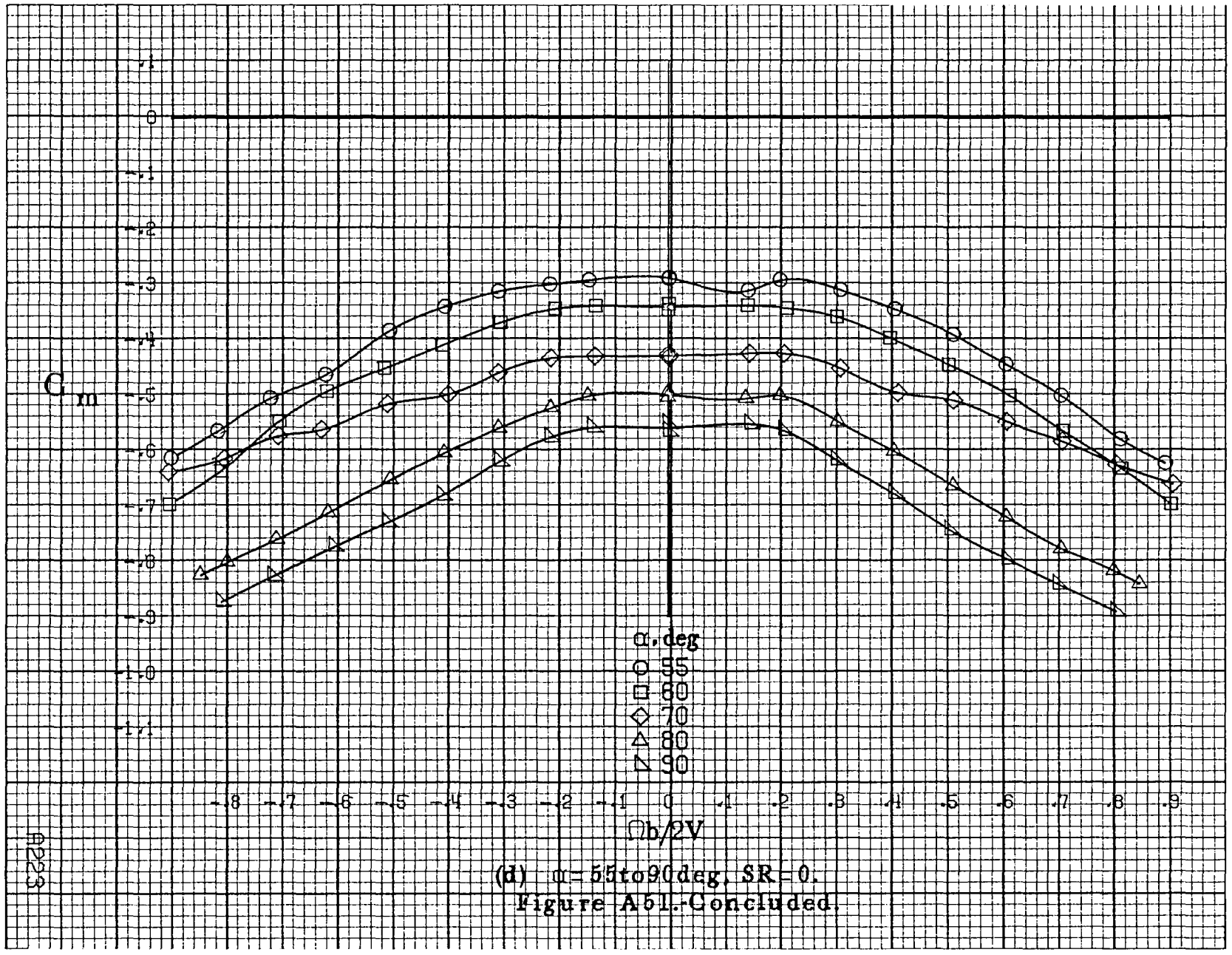

(d) $\alpha = 55$ to 90 deg, SR = 0.

Figure A51.-Concluded.

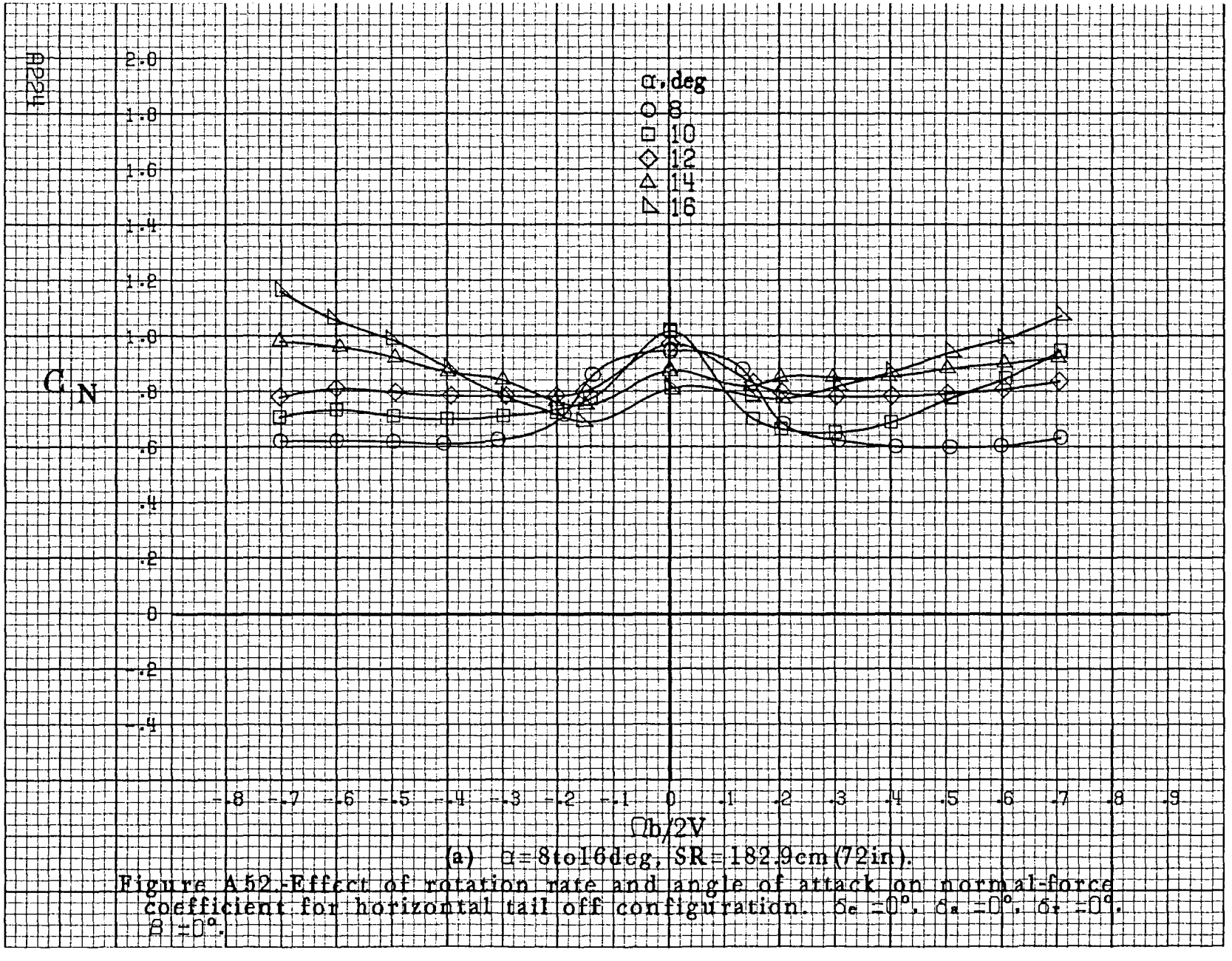

(a) $\alpha = 8$ to 16 deg, SR = 182.9 cm (72 in.).

Figure A52.-Effect of rotation rate and angle of attack on normal-force coefficient for horizontal tail off configuration. $\delta_e = 0°$, $\delta_a = 0°$, $\delta_r = 0°$, $\beta = 0°$.

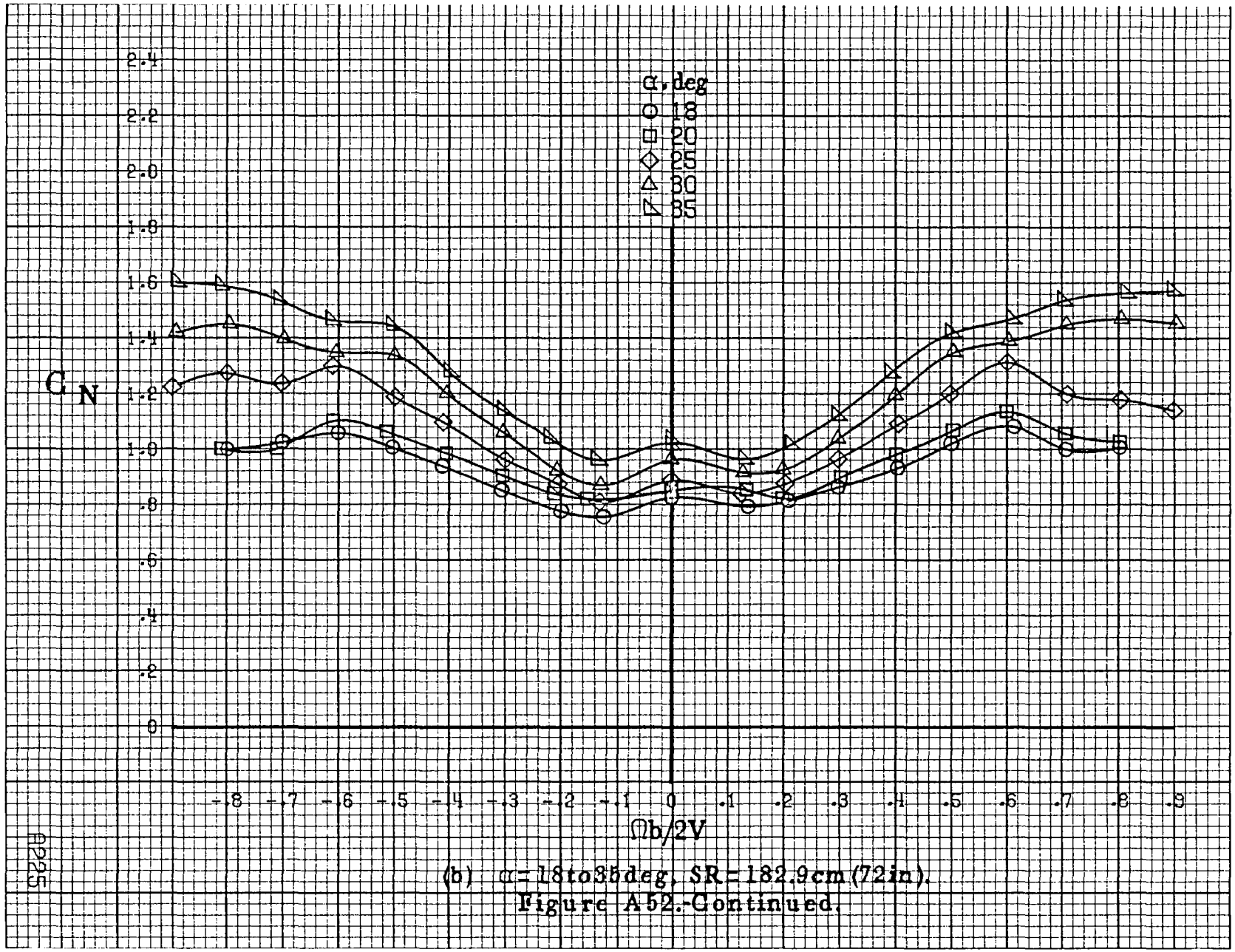

(b) $\alpha = 18$ to 35 deg, $SR = 182.9$ cm (72 in).

Figure A52.-Continued.

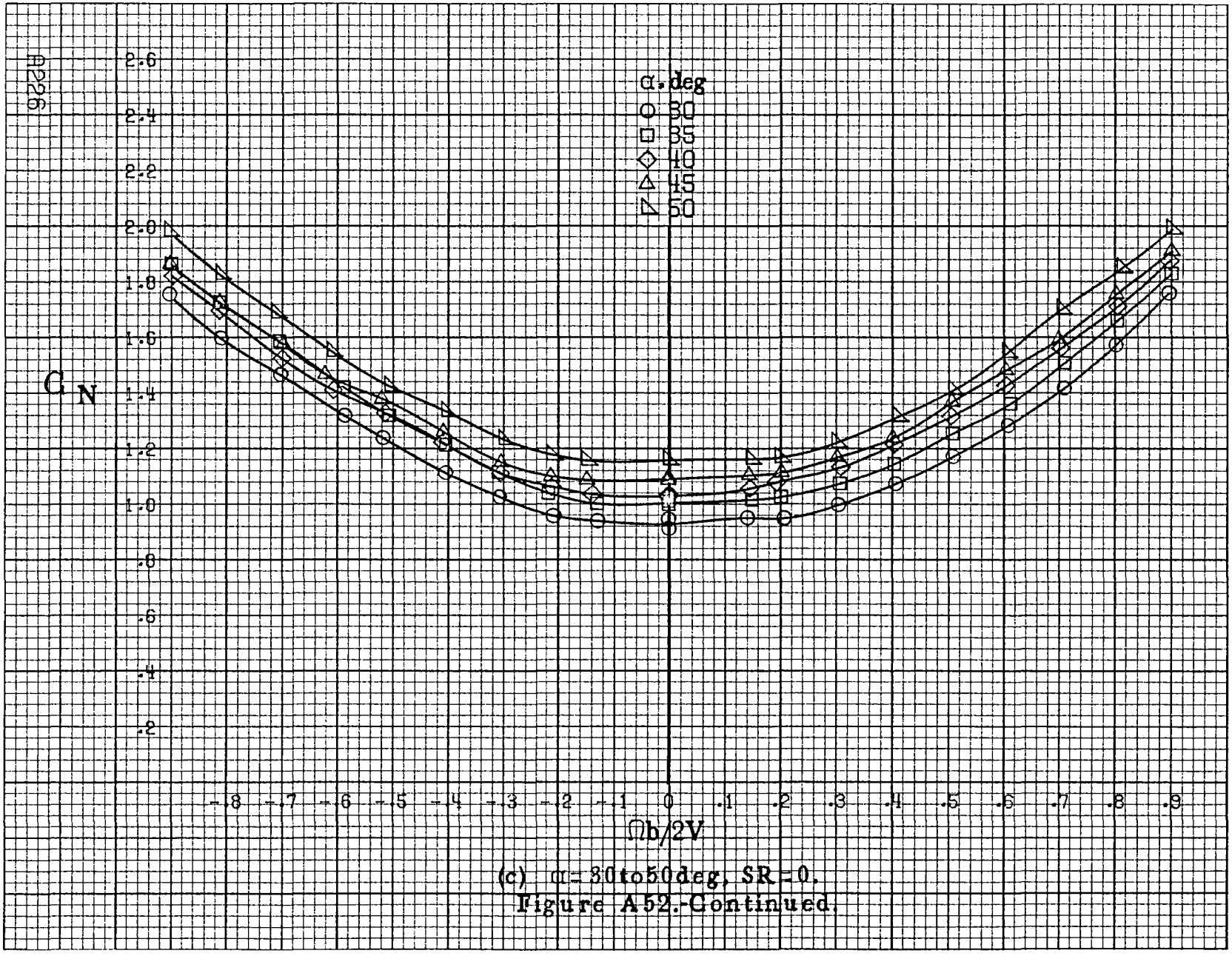

(c) α = 30 to 50 deg, SR = 0.

Figure A52.-Continued.

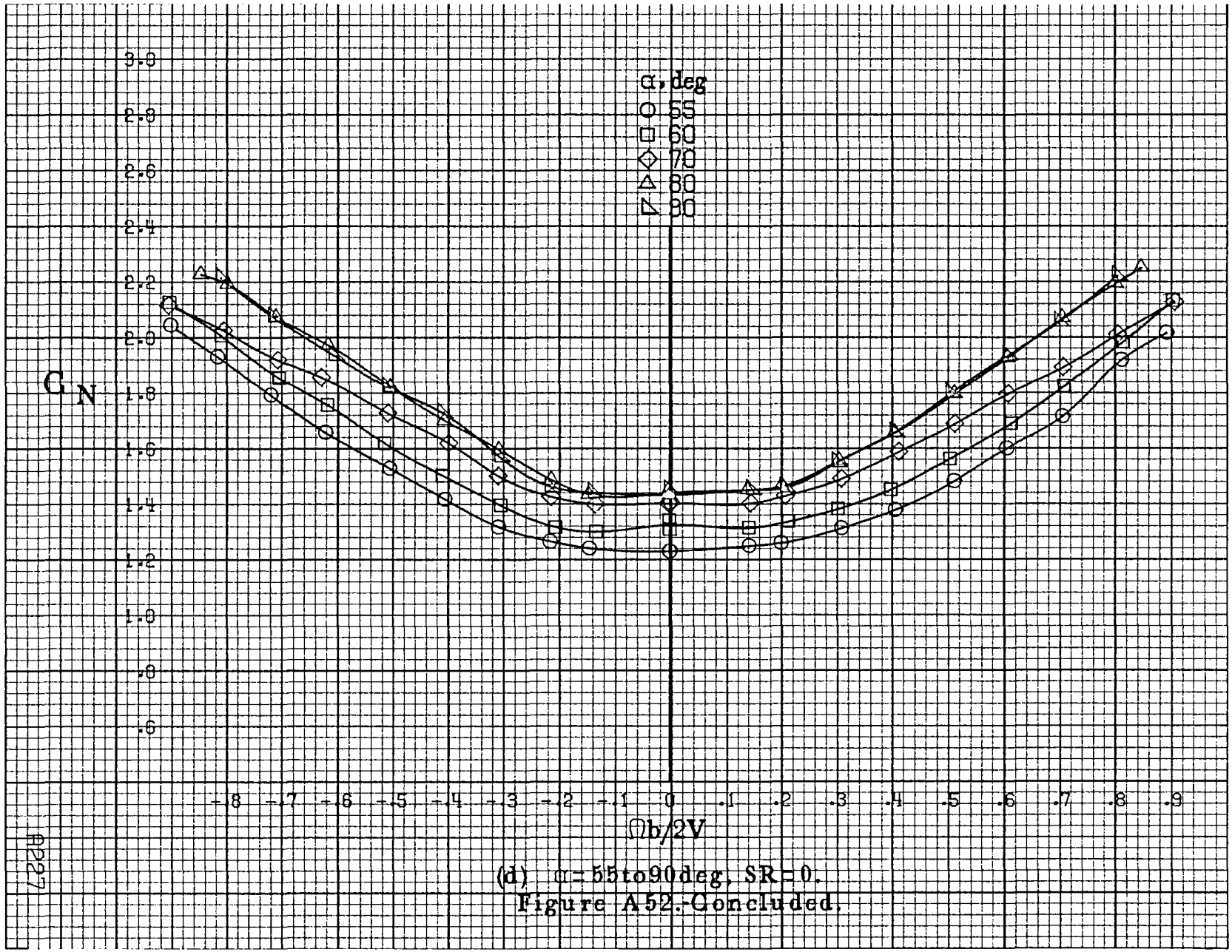

(d) α = 55 to 90 deg, SR = 0.

Figure A52.-Concluded.

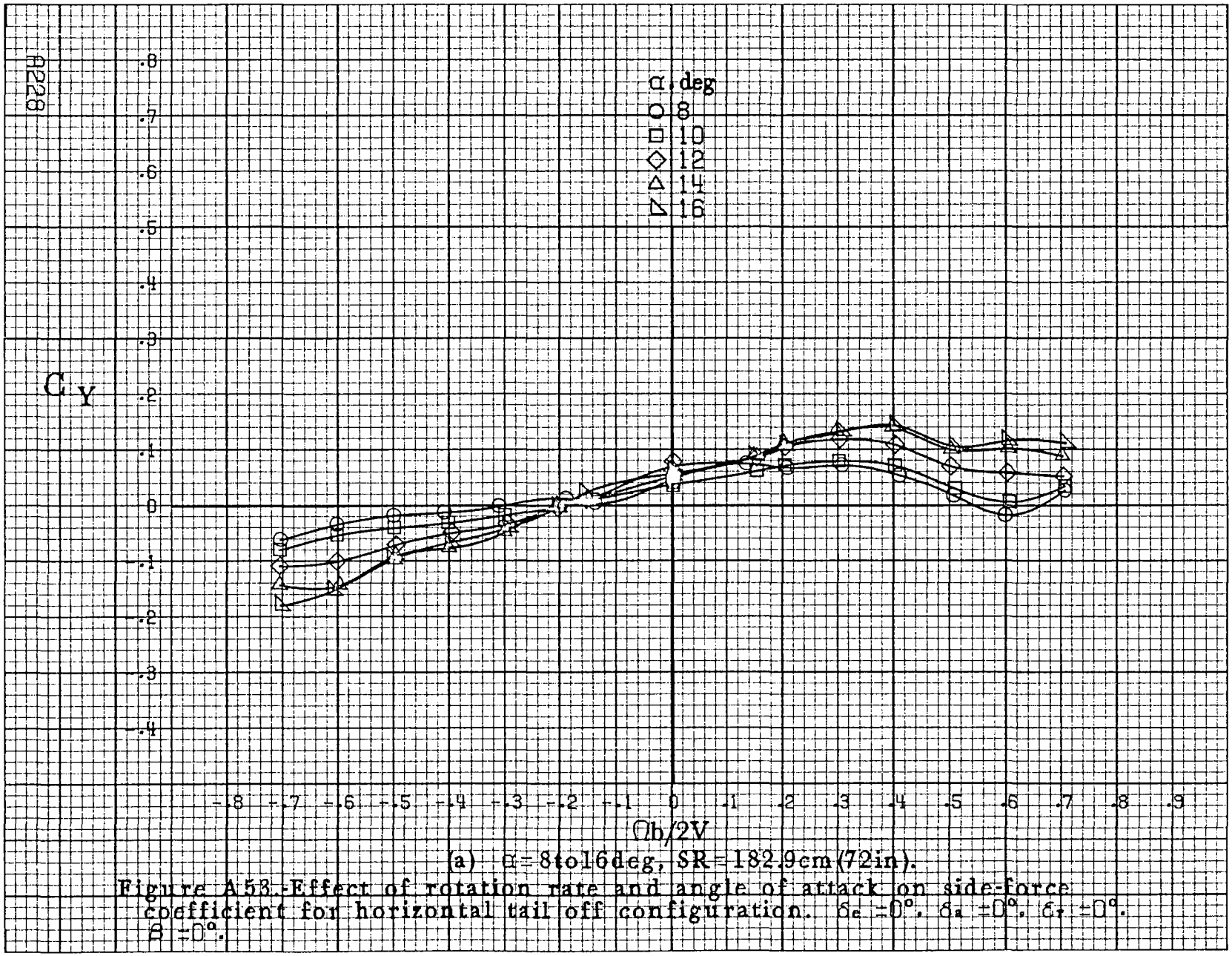

(a) $\alpha = 8$ to 16 deg, SR = 182.9 cm (72 in).

Figure A53.-Effect of rotation rate and angle of attack on side-force coefficient for horizontal tail off configuration. $\delta_e = 0°$, $\delta_a = 0°$, $\delta_r = 0°$, $\beta = 0°$.

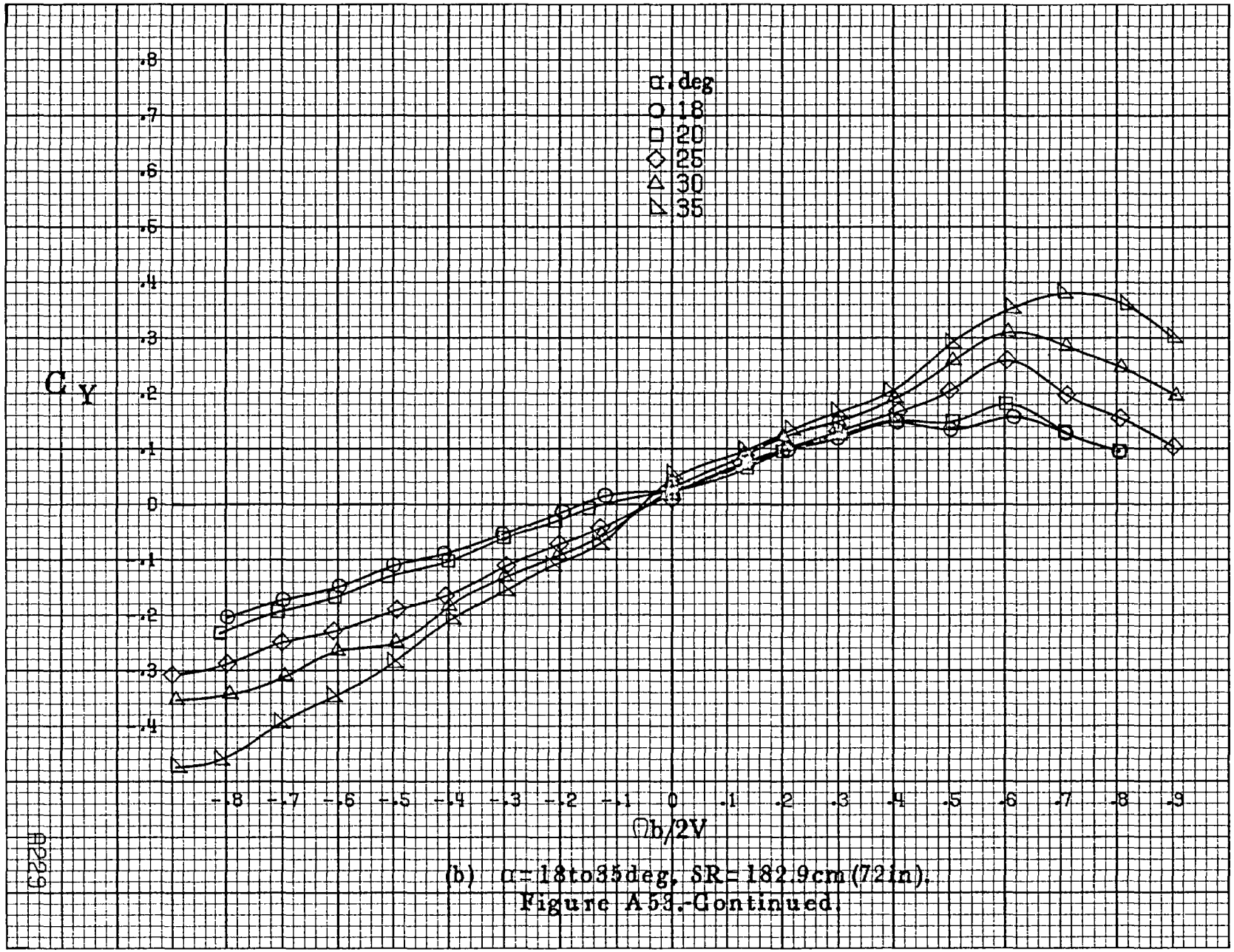

(b) $\alpha = 18$ to 35 deg, SR = 182.9 cm (72 in).

Figure A53.-Continued.

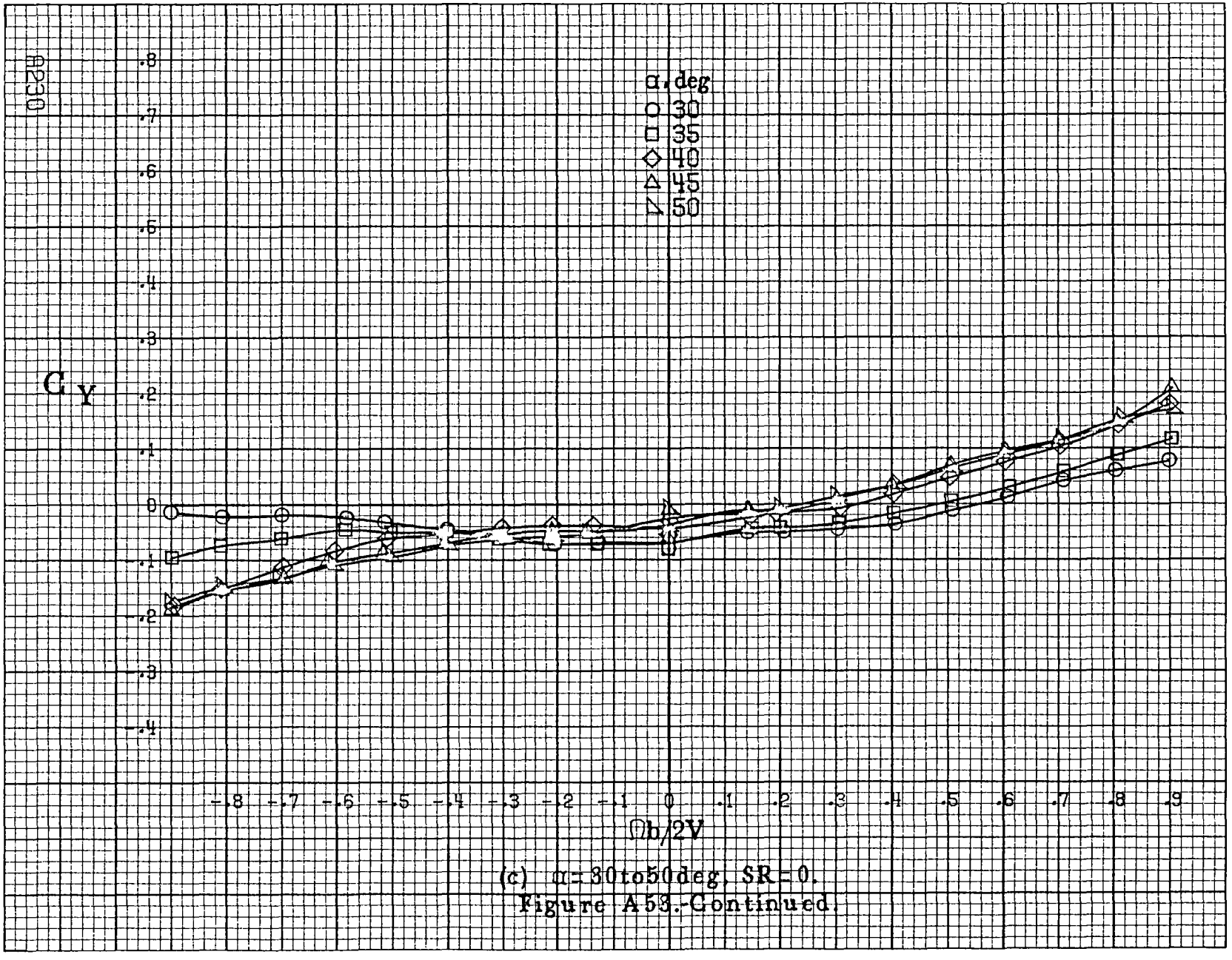

(c) α = 30 to 50 deg, SR = 0.

Figure A53.- Continued.

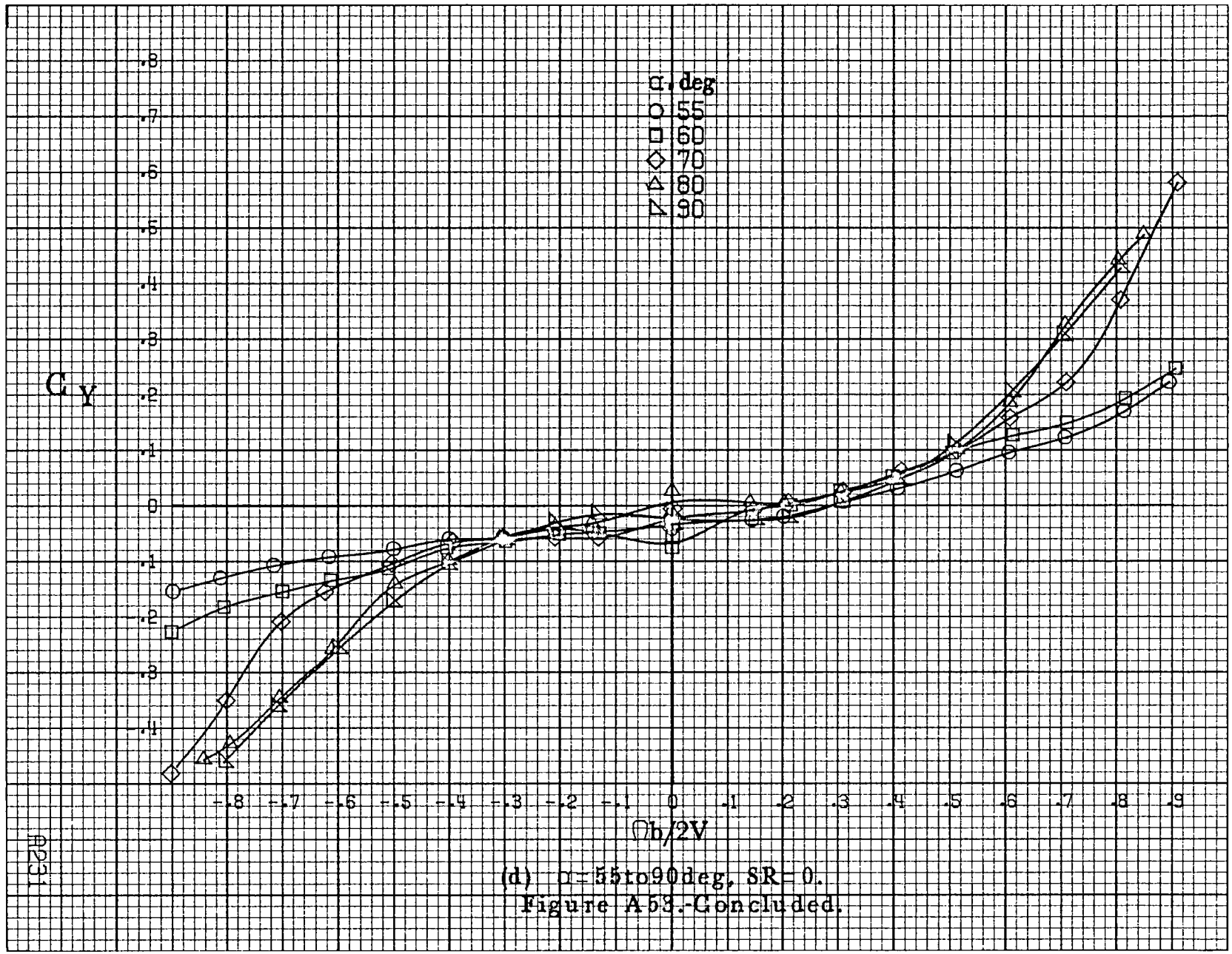

(d) α = 55 to 90 deg, SR = 0.

Figure A53.-Concluded.

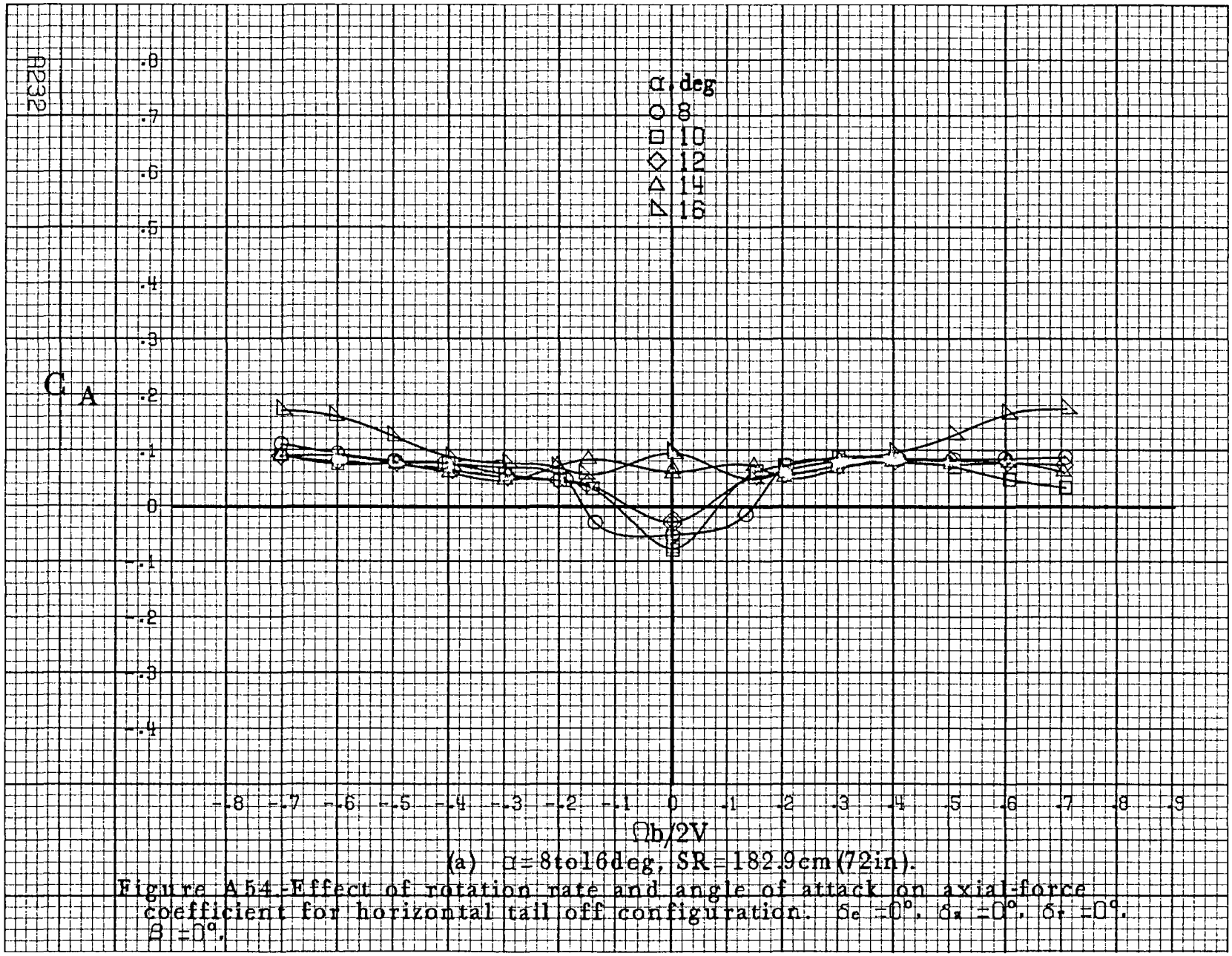

(a) α = 8 to 16 deg, SR = 182.9 cm (72 in).

Figure A54.-Effect of rotation rate and angle of attack on axial-force coefficient for horizontal tail off configuration. $\delta_e = 0°$, $\delta_a = 0°$, $\delta_r = 0°$, $\beta = 0°$.

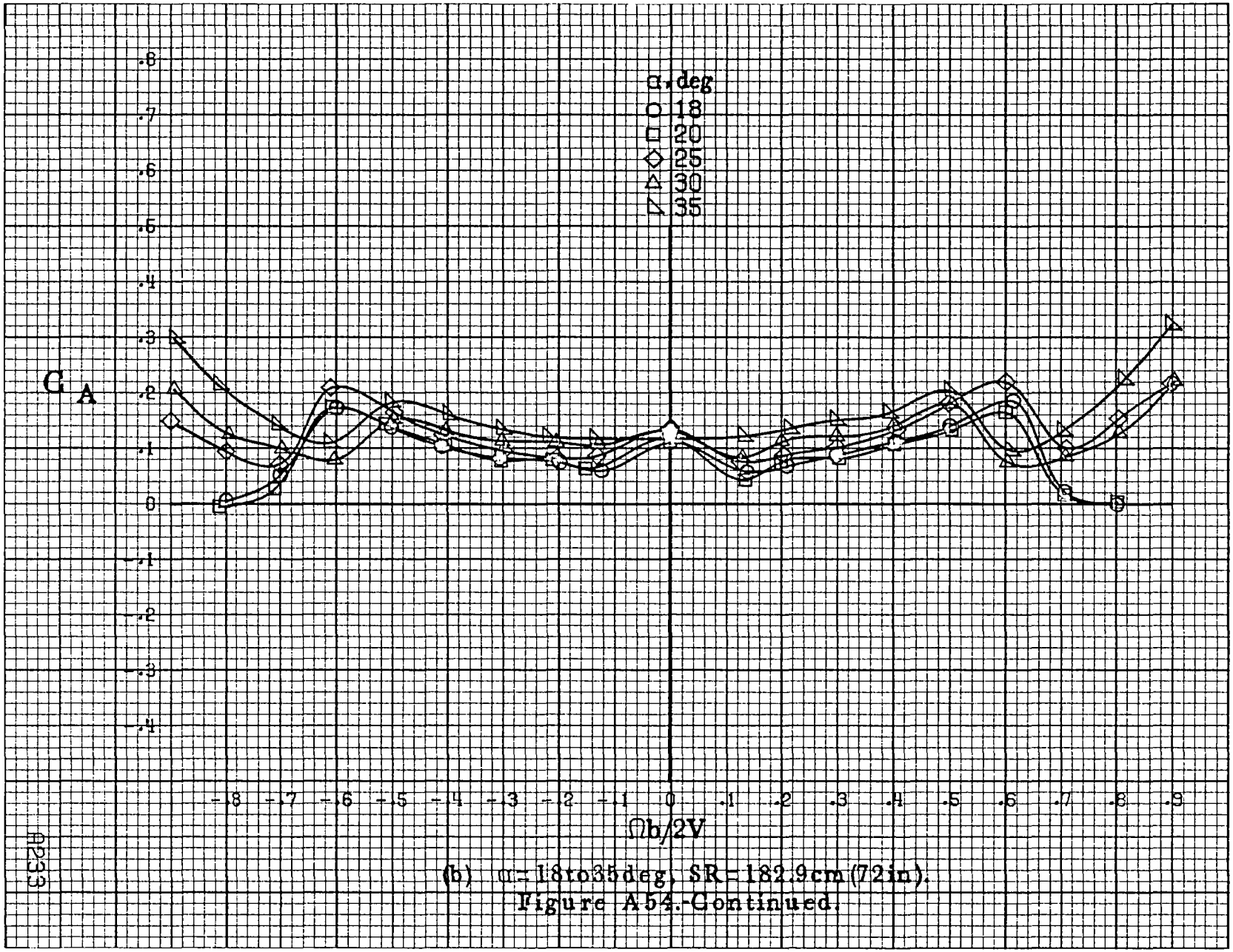

(b) α = 18 to 35 deg, SR = 182.9 cm (72 in).

Figure A54.-Continued.

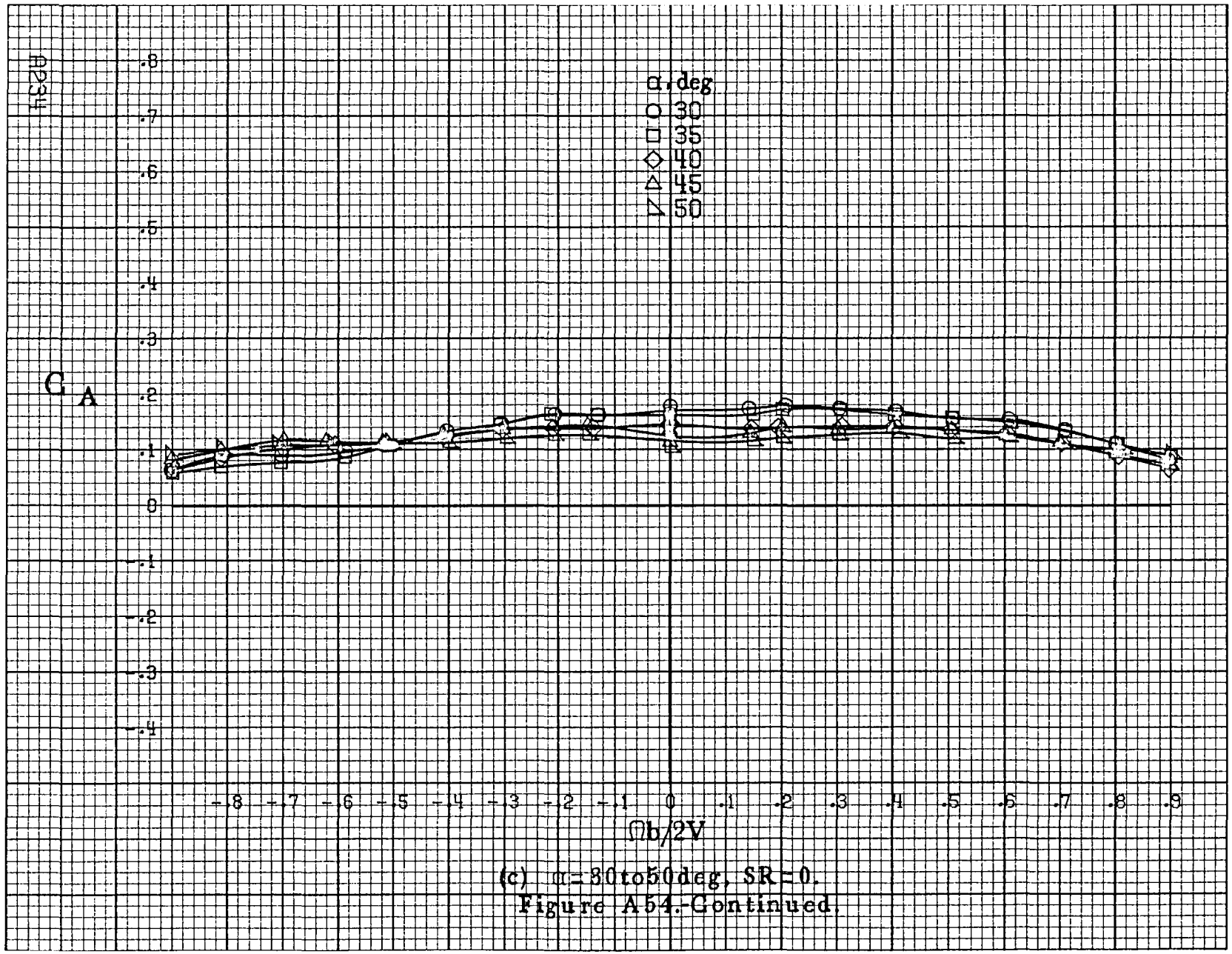

(c) α = 30 to 50 deg, SR = 0.

Figure A54.-Continued.

(d) $\alpha = 55$ to 90 deg, SR = 0.

Figure A54.-Concluded.

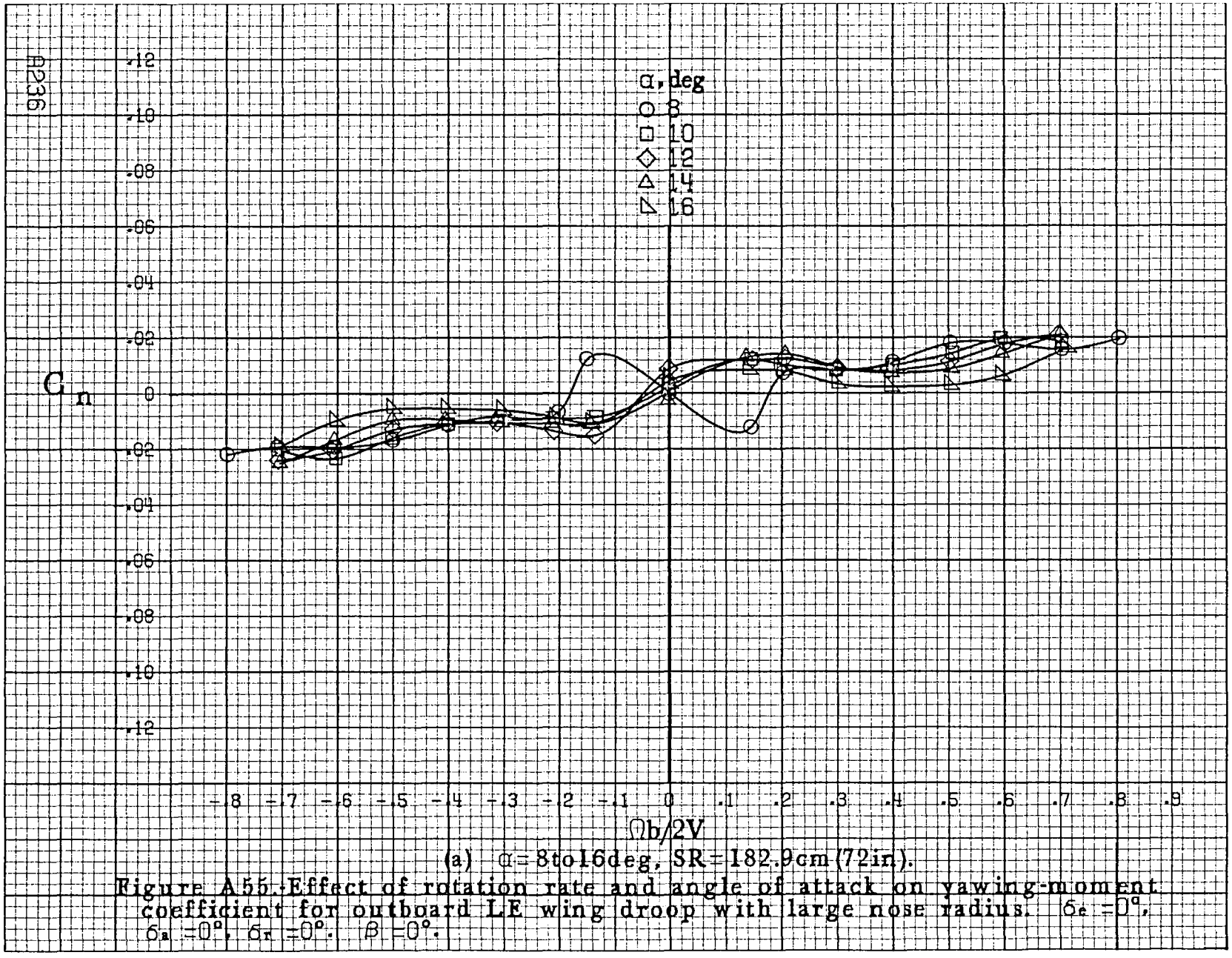

(a) $\alpha = 8$ to 16 deg, SR = 182.9 cm (72 in.).

Figure A55.-Effect of rotation rate and angle of attack on yawing-moment coefficient for outboard LE wing droop with large nose radius. $\delta_e = 0°$, $\delta_a = 0°$, $\delta_r = 0°$, $\beta = 0°$.

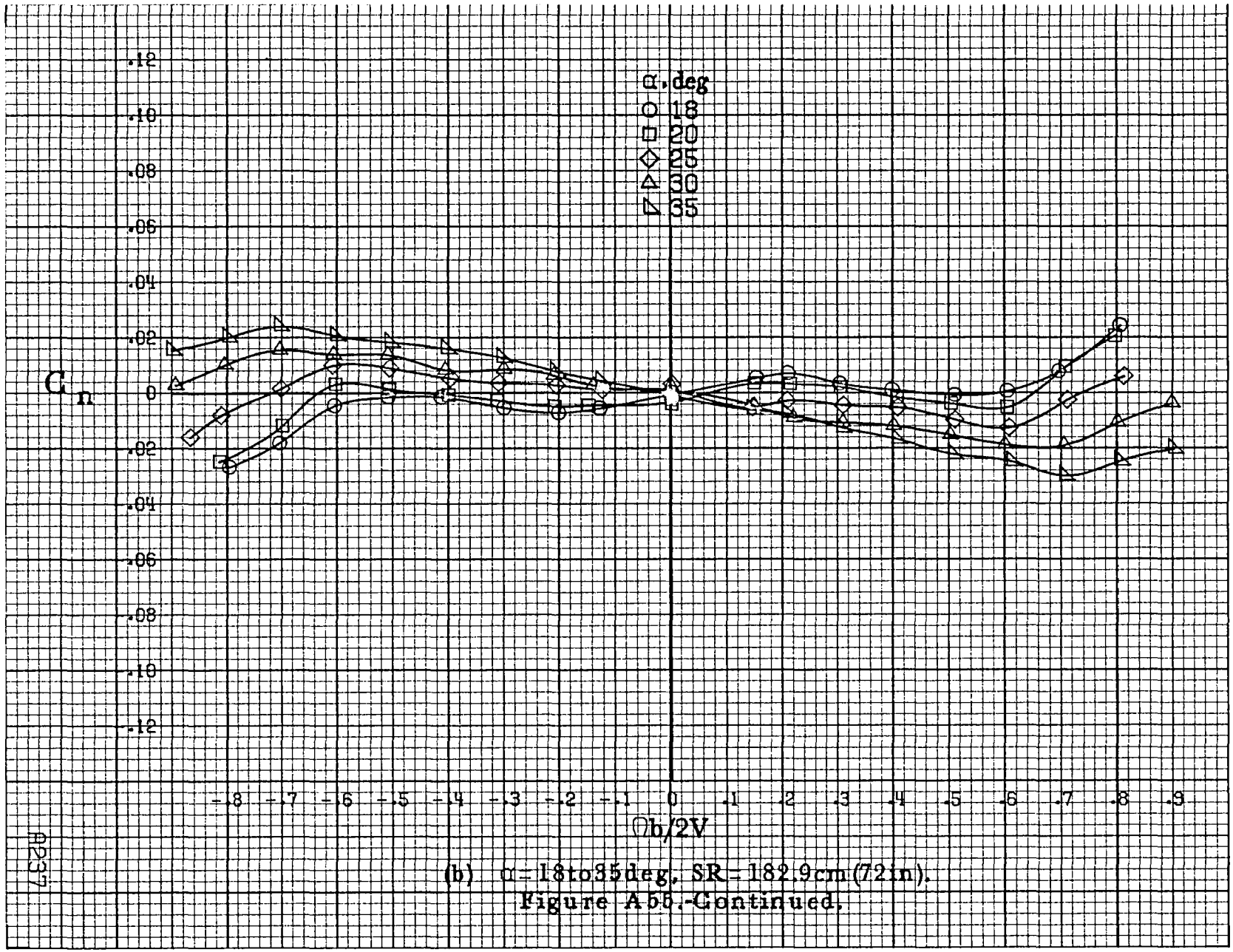

(b) α = 18 to 35 deg, SR = 182.9 cm (72 in).

Figure A55.-Continued.

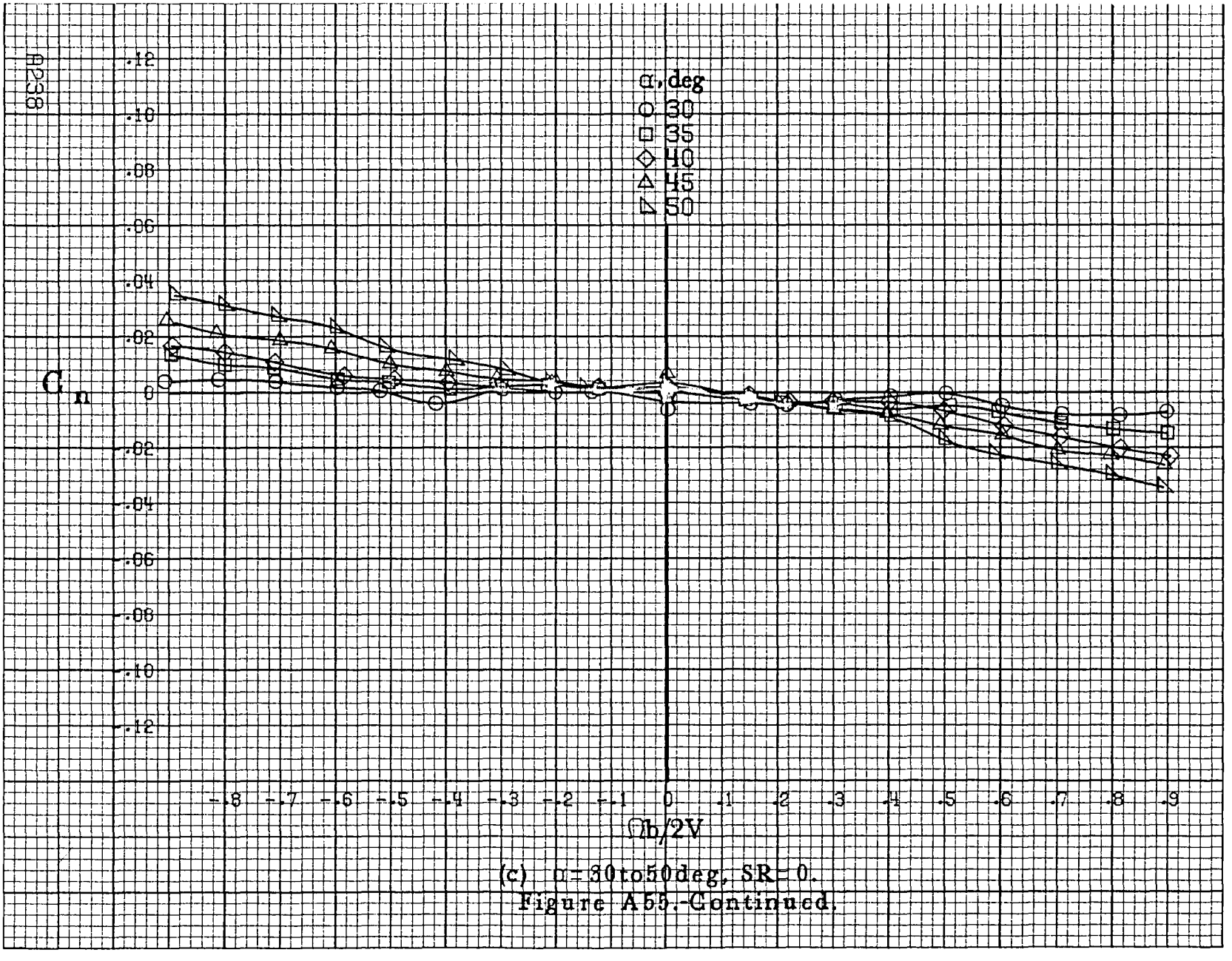

(c) α = 30 to 50 deg, SR = 0.

Figure A55.-Continued.

(d) α = 55 to 90 deg, SR = 0.

Figure A6b.-Concluded.

B239

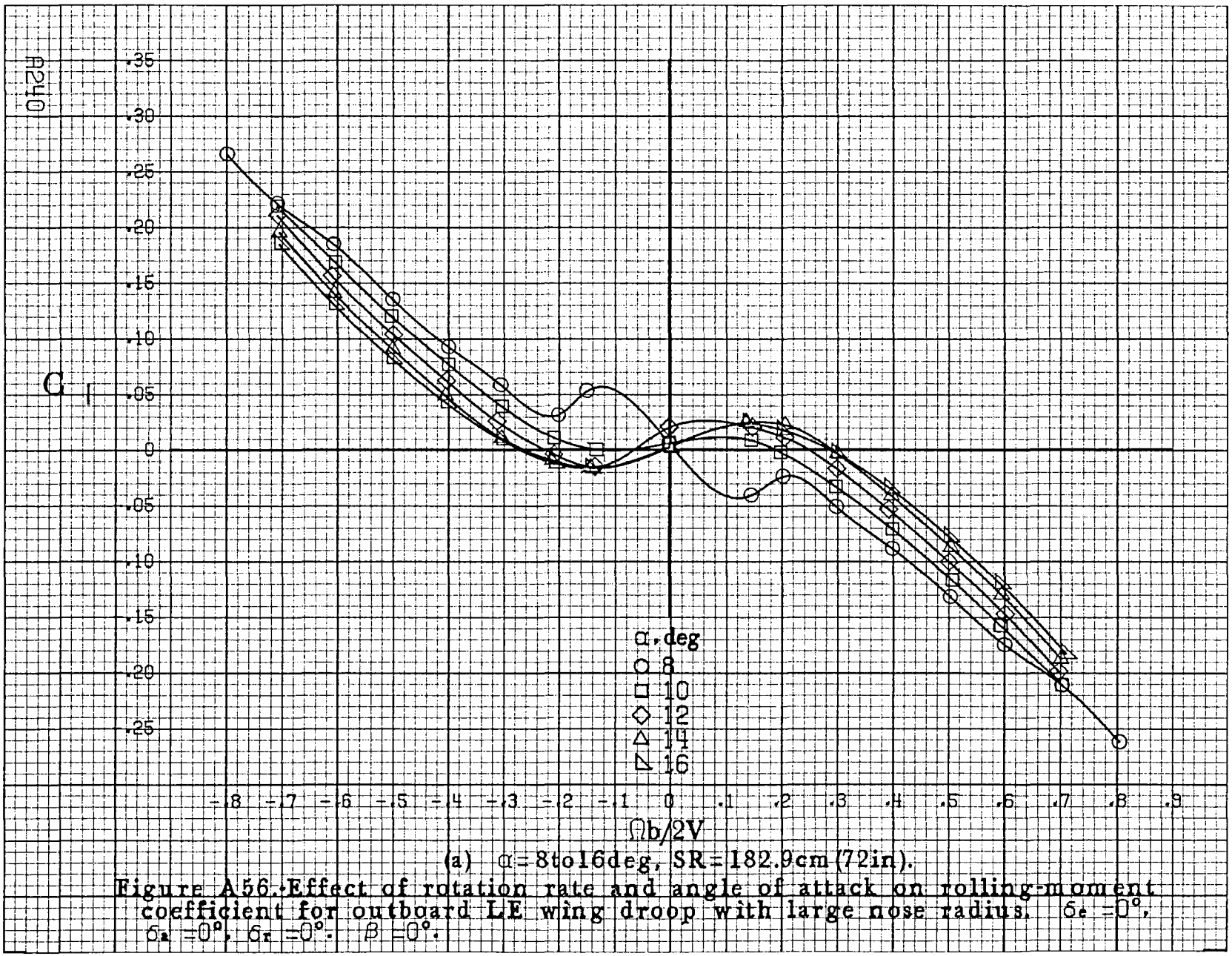

(a) $\alpha = 8$ to 16deg, SR = 182.9cm (72in).

Figure A56.-Effect of rotation rate and angle of attack on rolling-moment coefficient for outboard LE wing droop with large nose radius. $\delta_e = 0°$, $\delta_a = 0°$, $\delta_r = 0°$, $\beta = 0°$.

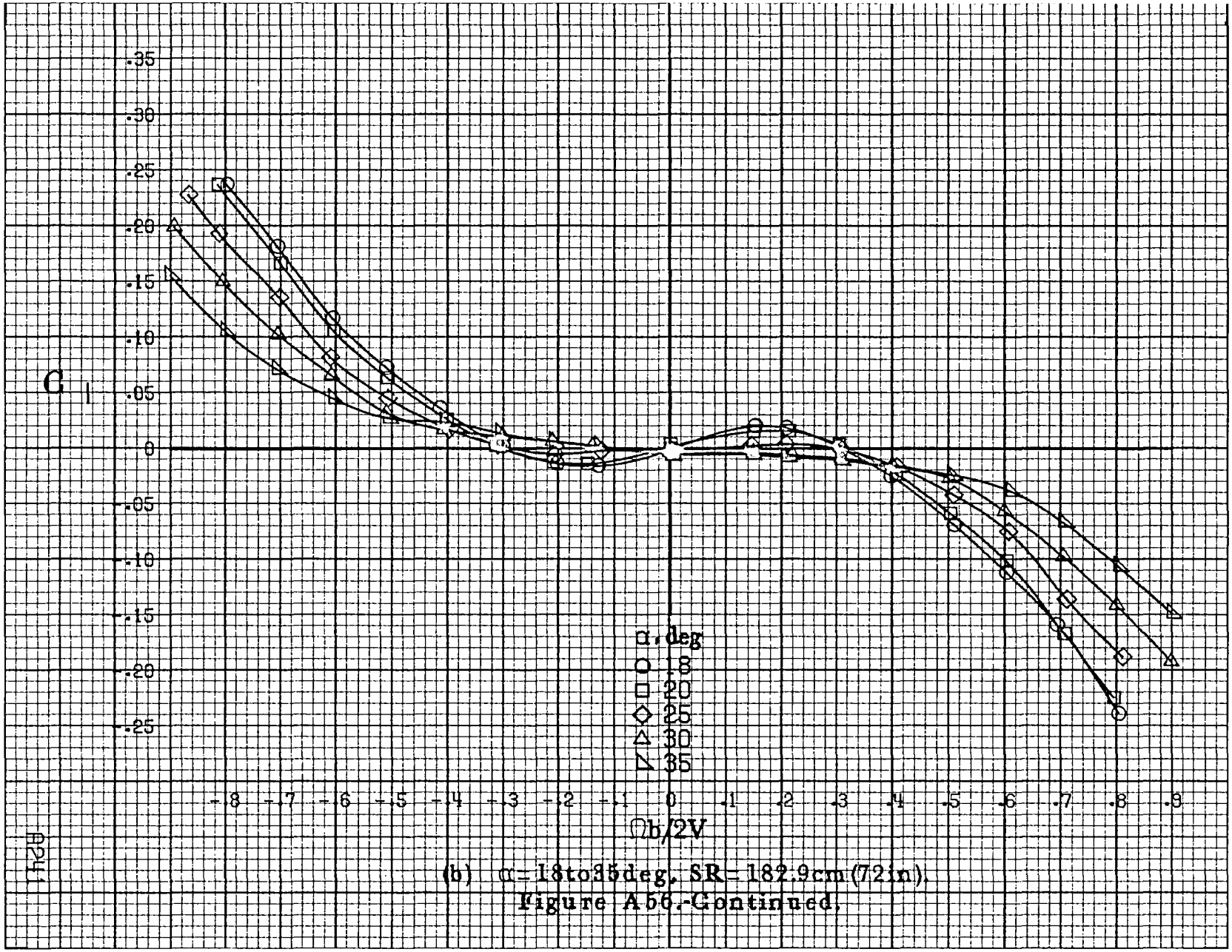

(b) α = 18 to 35 deg, SR = 182.9 cm (72 in).

Figure A56.-Continued.

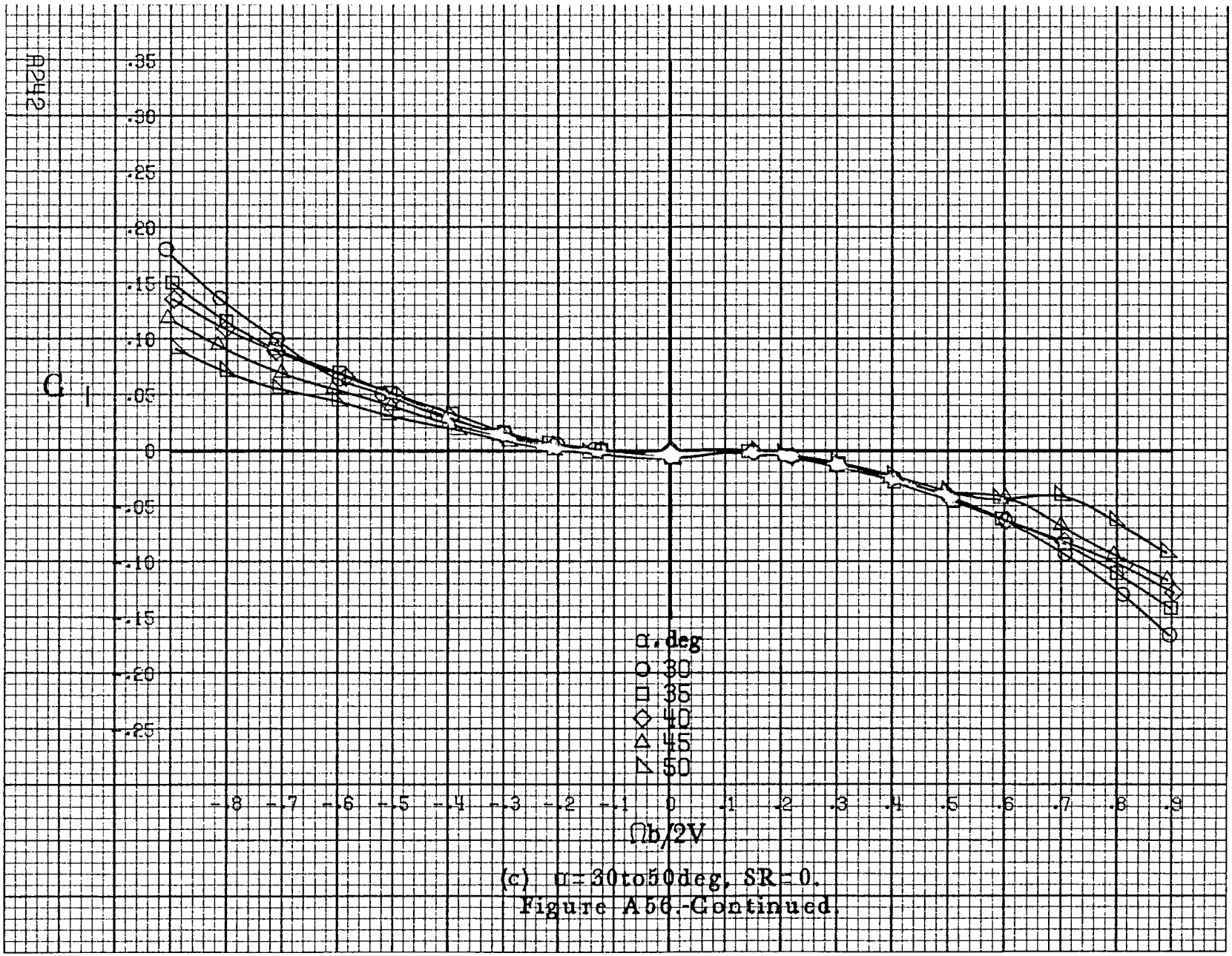

(c) $\alpha = 30$ to 50 deg, SR = 0.

Figure A56.-Continued.

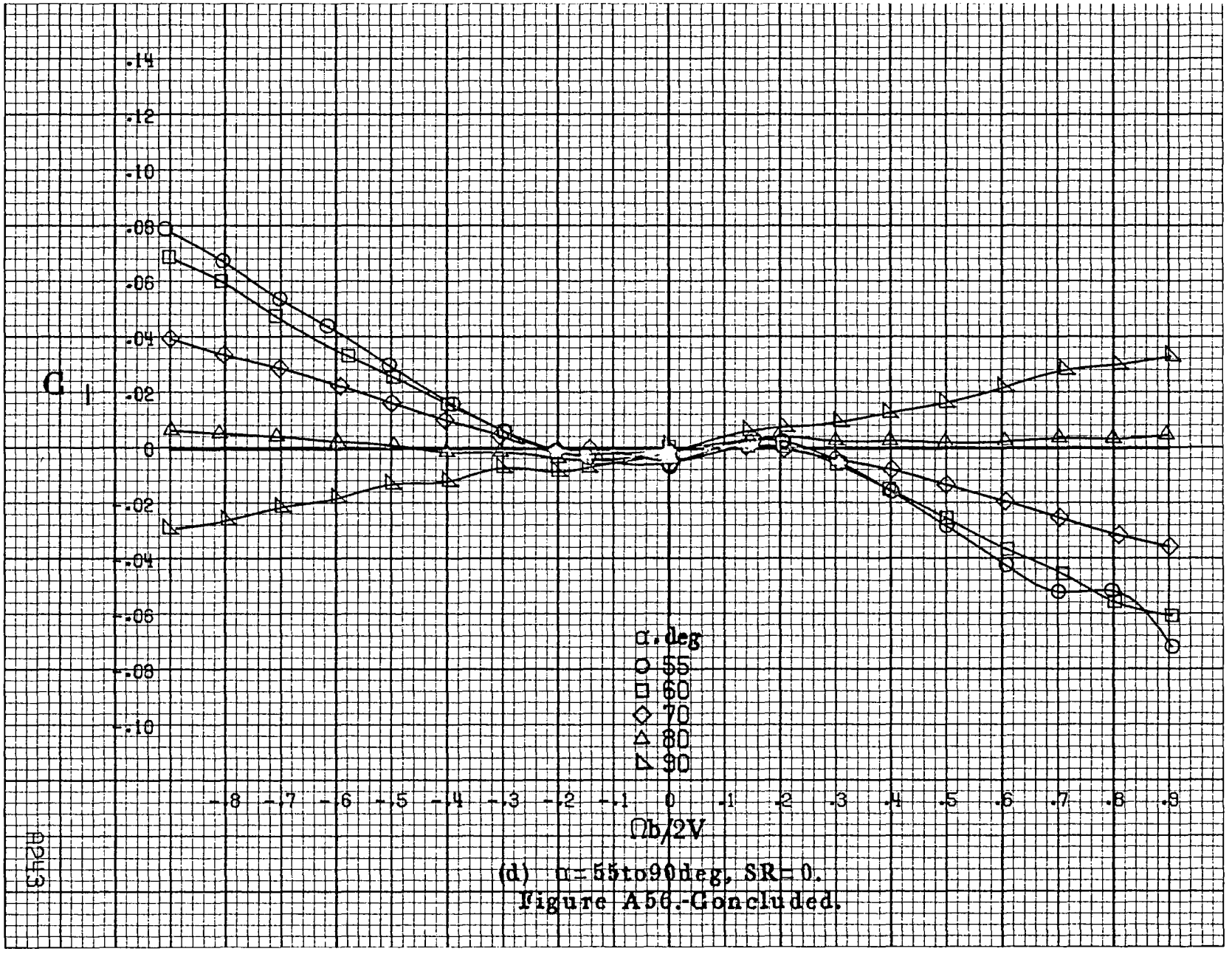

(d) $\alpha = 55$ to 90 deg, SR = 0.

Figure A56.-Concluded.

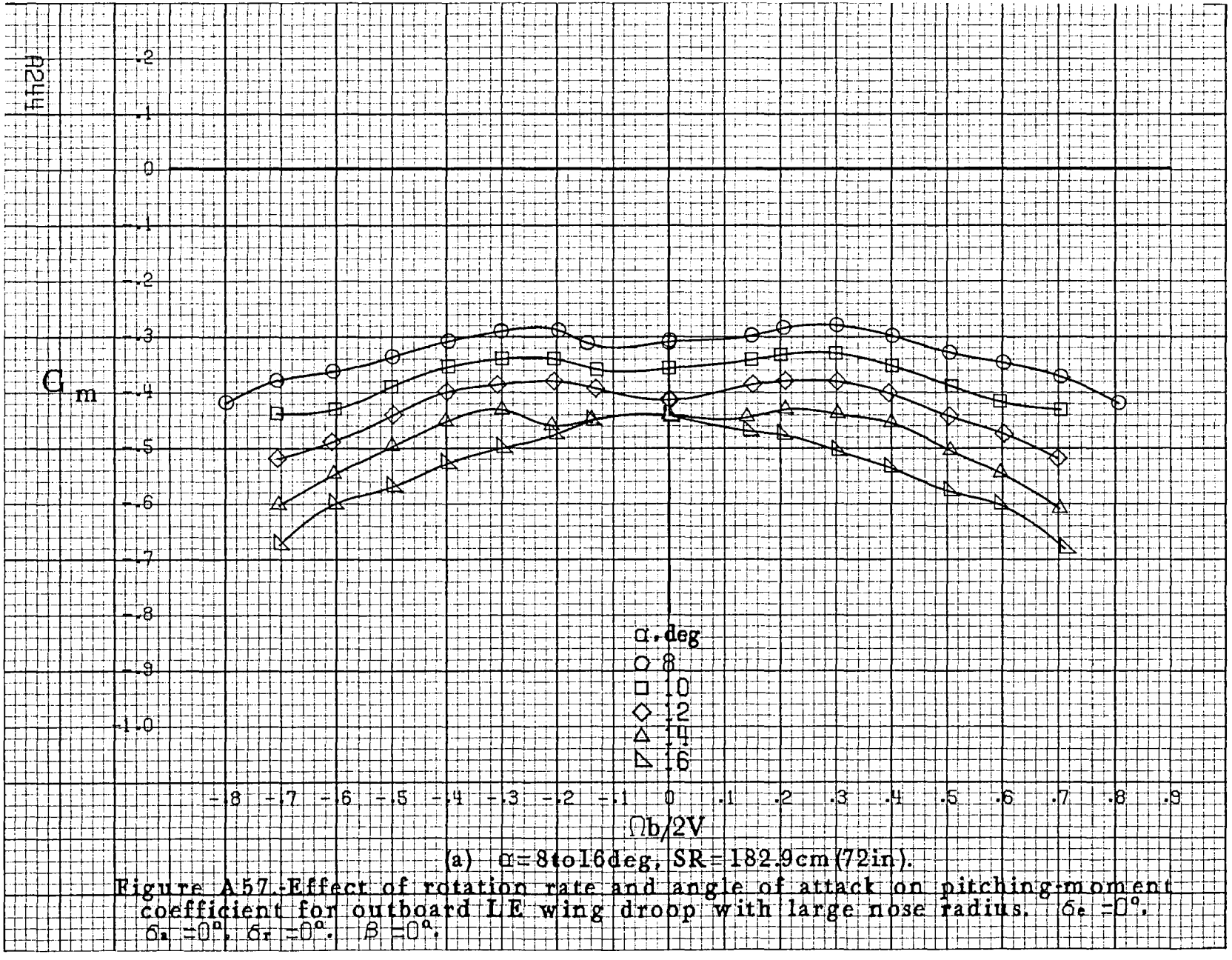

(a) α = 8 to 16 deg, SR = 182.9 cm (72 in).

Figure A57.-Effect of rotation rate and angle of attack on pitching-moment coefficient for outboard LE wing droop with large nose radius. $\delta_e = 0°$, $\delta_a = 0°$, $\delta_r = 0°$, $\beta = 0°$.

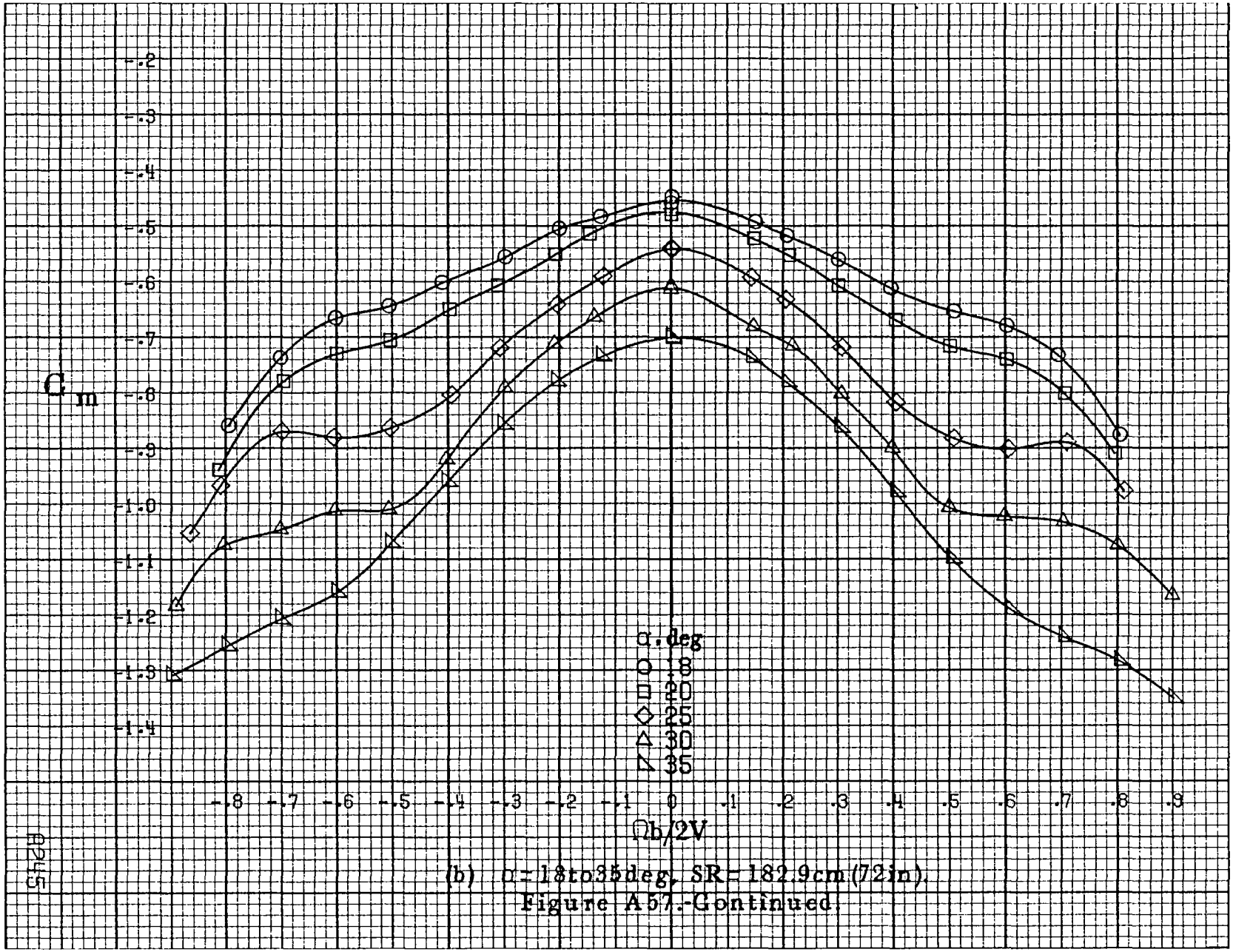

(b) α = 18 to 35 deg, SR = 182.9 cm (72 in).

Figure A57.- Continued.

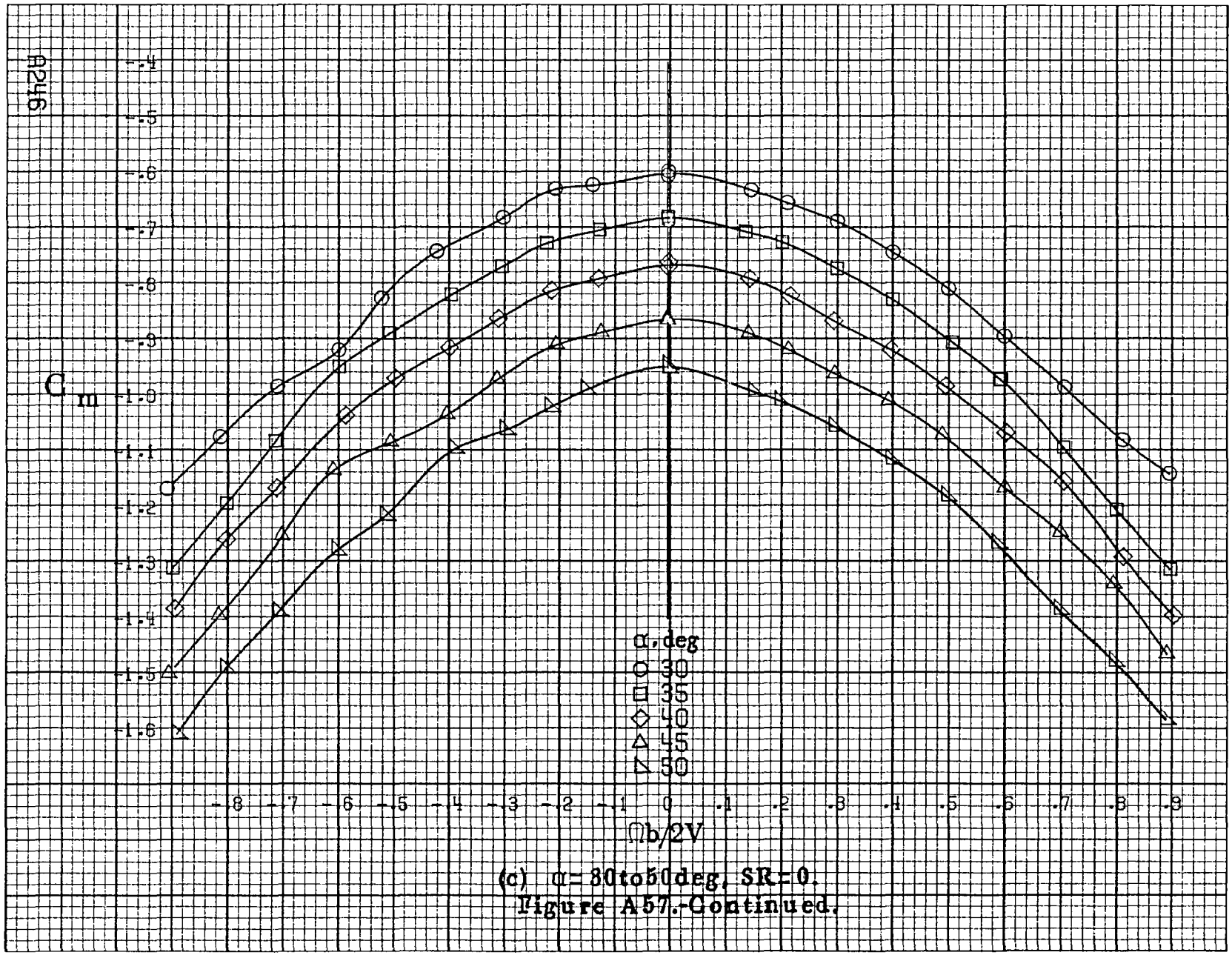

(c) α= 30to50deg, SR=0.

Figure A57.-Continued.

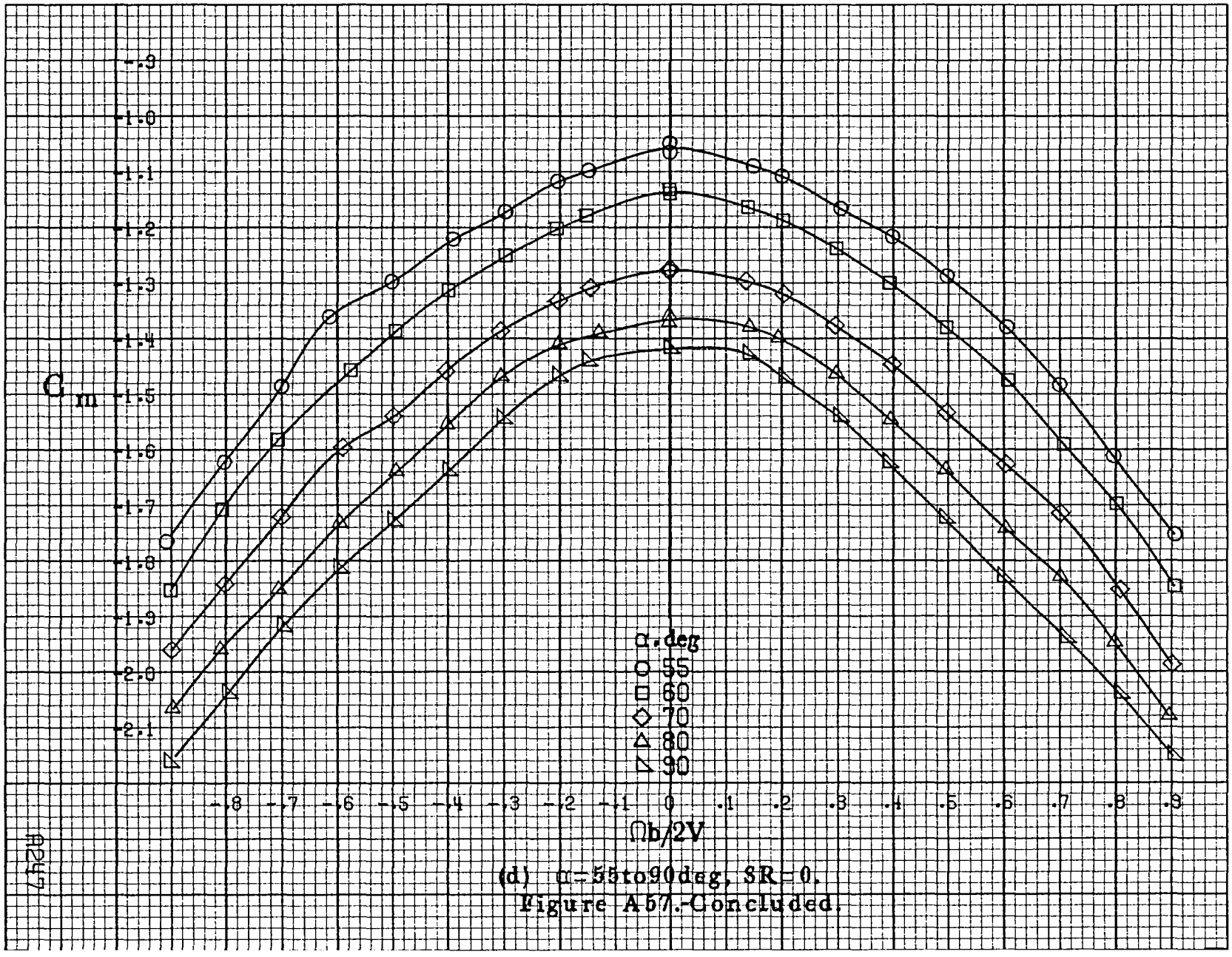

(d) α=55to90deg, SR=0.

Figure A57.-Concluded.

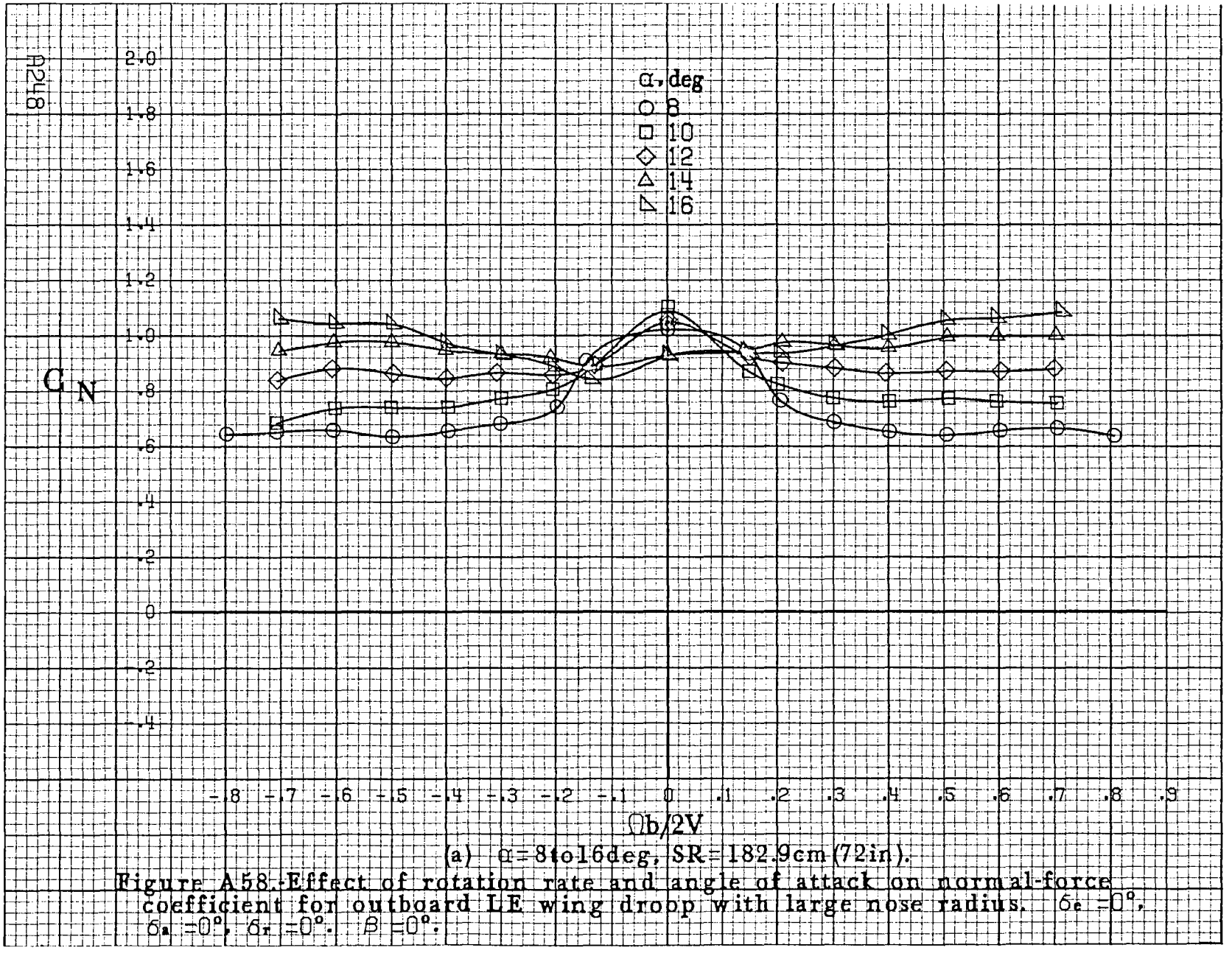

(a) $\alpha = 8$ to 16deg, SR = 182.9cm (72in).

Figure A58.-Effect of rotation rate and angle of attack on normal-force coefficient for outboard LE wing droop with large nose radius. $\delta_e = 0°$, $\delta_a = 0°$, $\delta_r = 0°$. $\beta = 0°$.

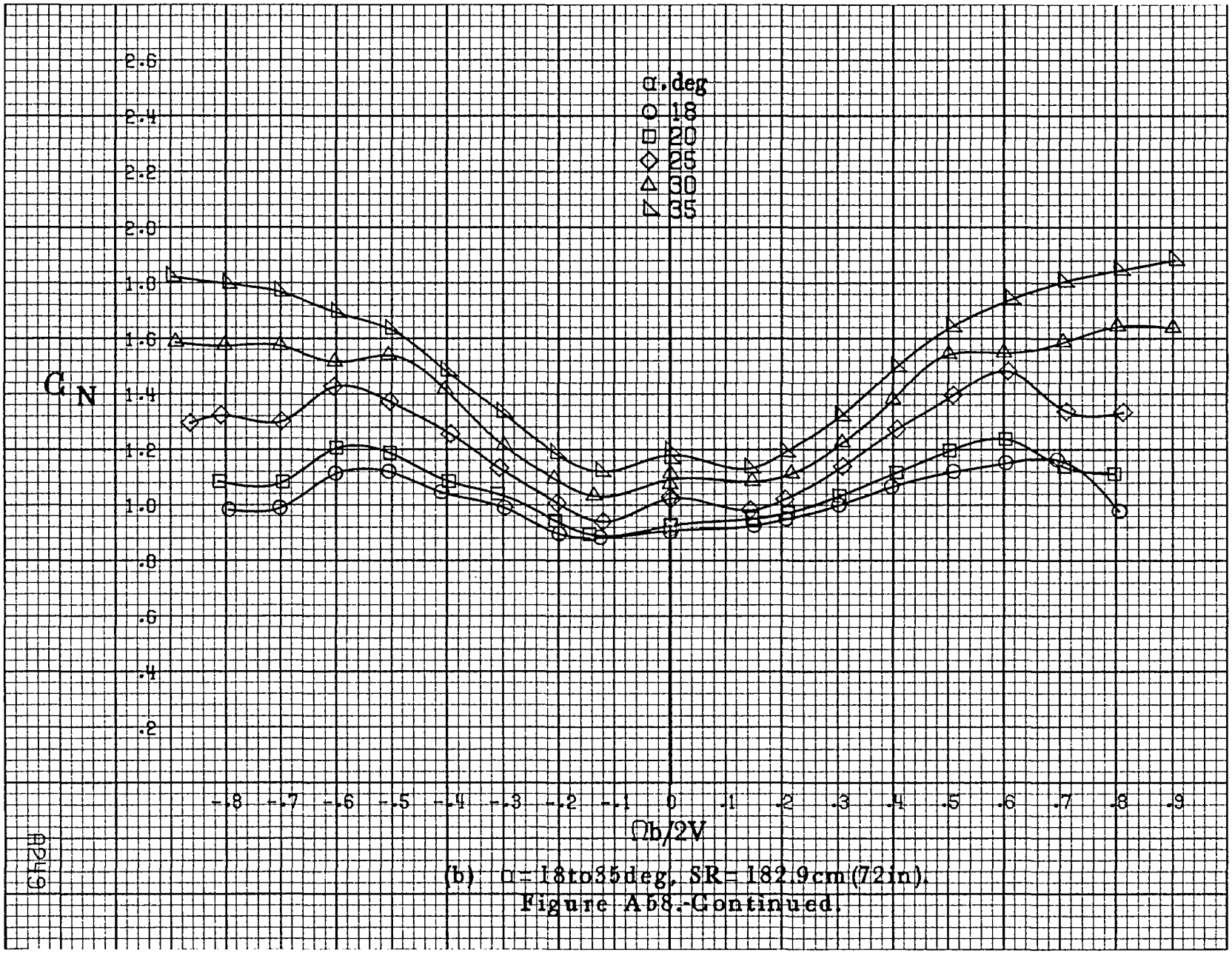

(b) α = 18 to 35 deg, SR = 182.9 cm (72 in).

Figure A68.-Continued.

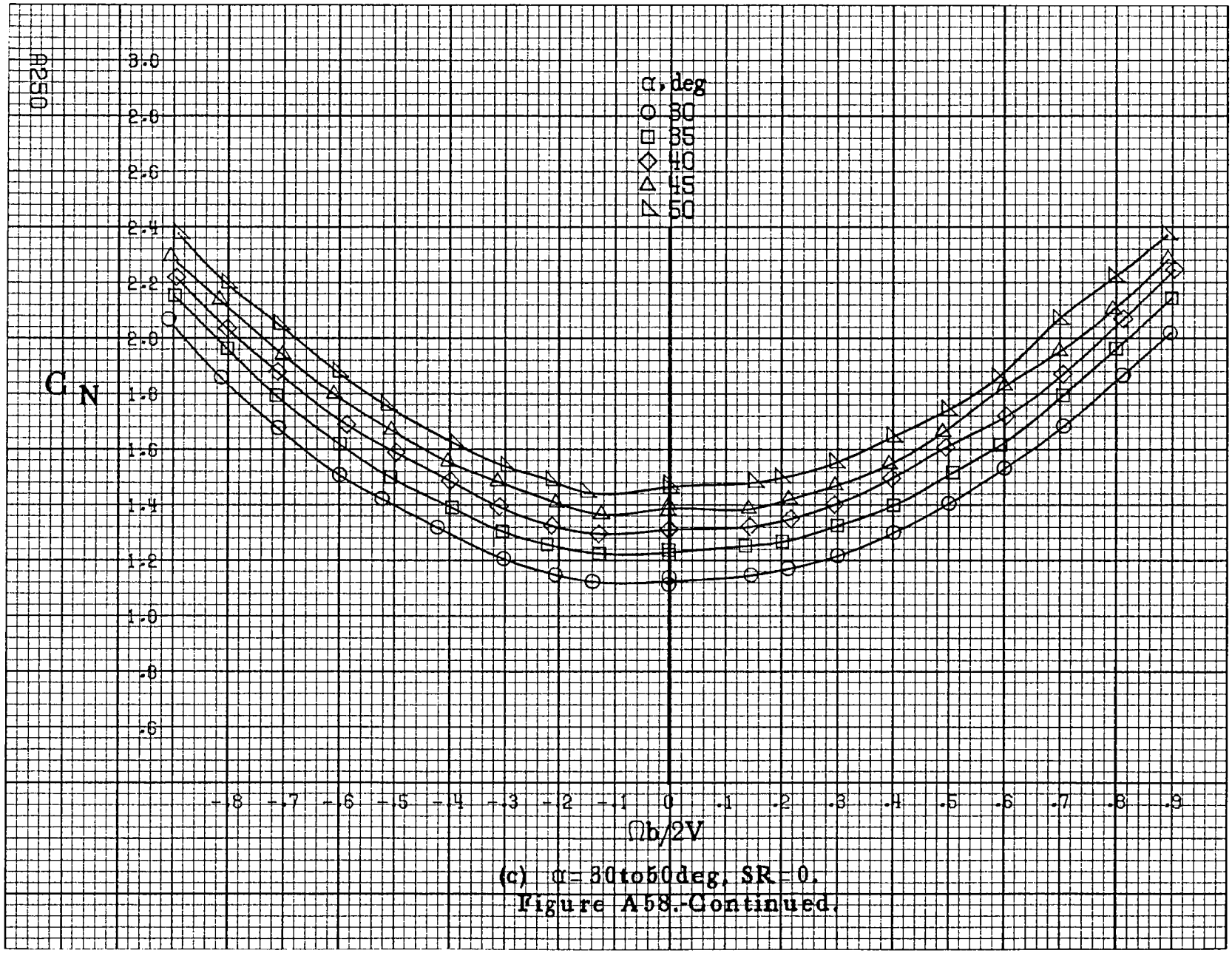

(c) α = 30 to 60 deg, SR = 0.

Figure A58.-Continued.

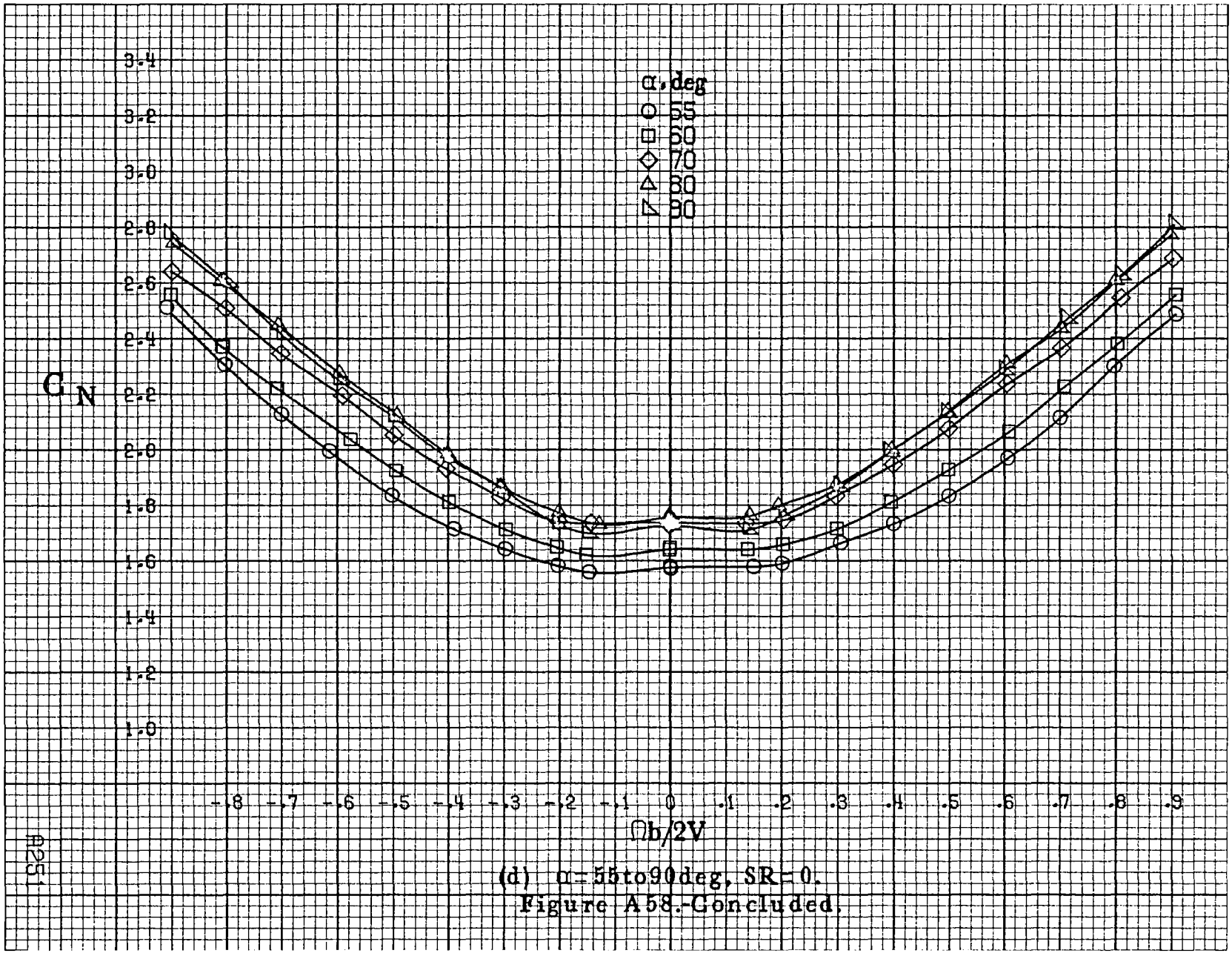

(d) α = 55 to 90 deg, SR = 0.

Figure A58.-Concluded.

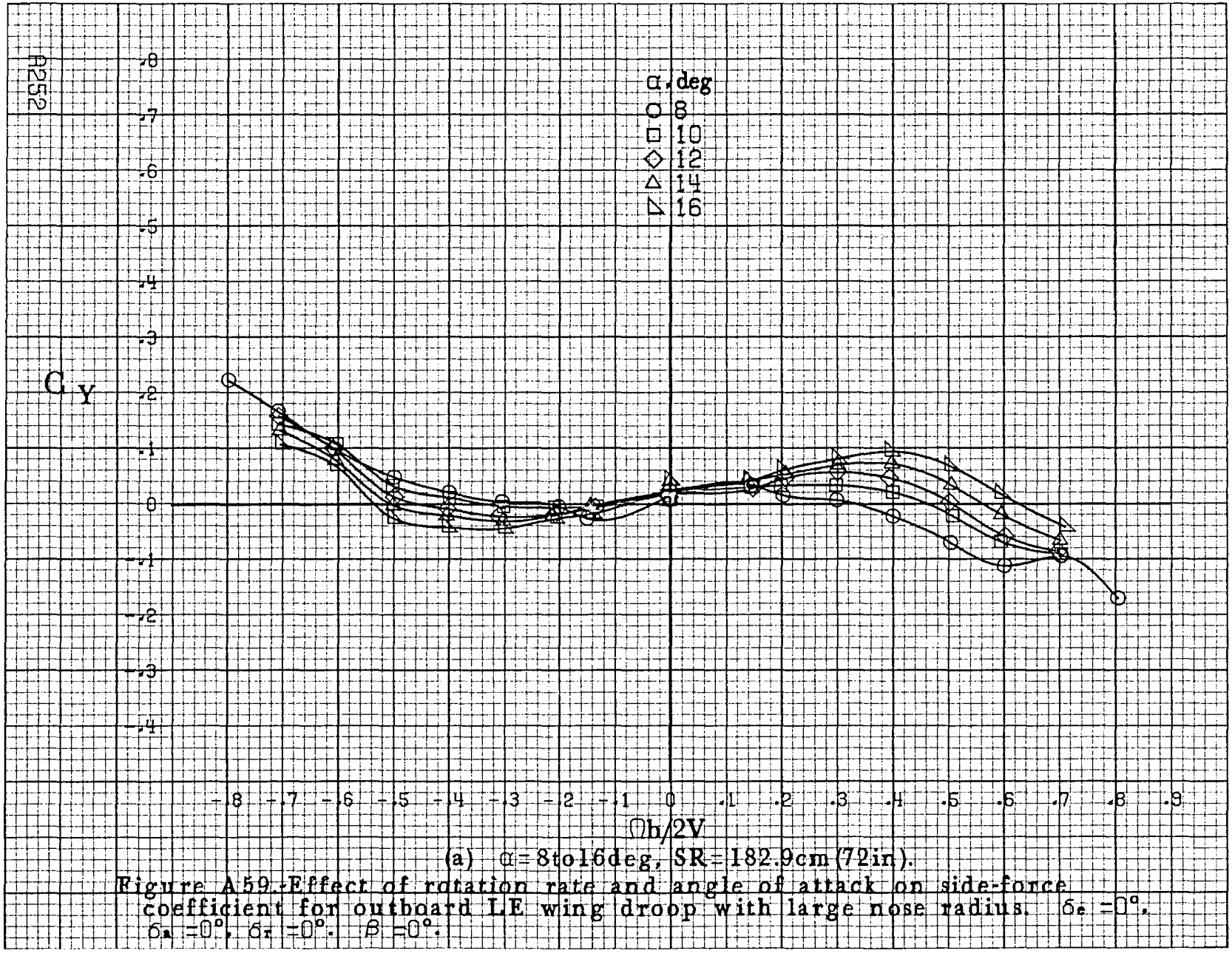

(a) $\alpha = 8$ to 16 deg, SR = 182.9 cm (72 in.).

Figure A59.-Effect of rotation rate and angle of attack on side-force coefficient for outboard LE wing droop with large nose radius. $\delta_e = 0°$, $\delta_a = 0°$, $\delta_r = 0°$, $\beta = 0°$.

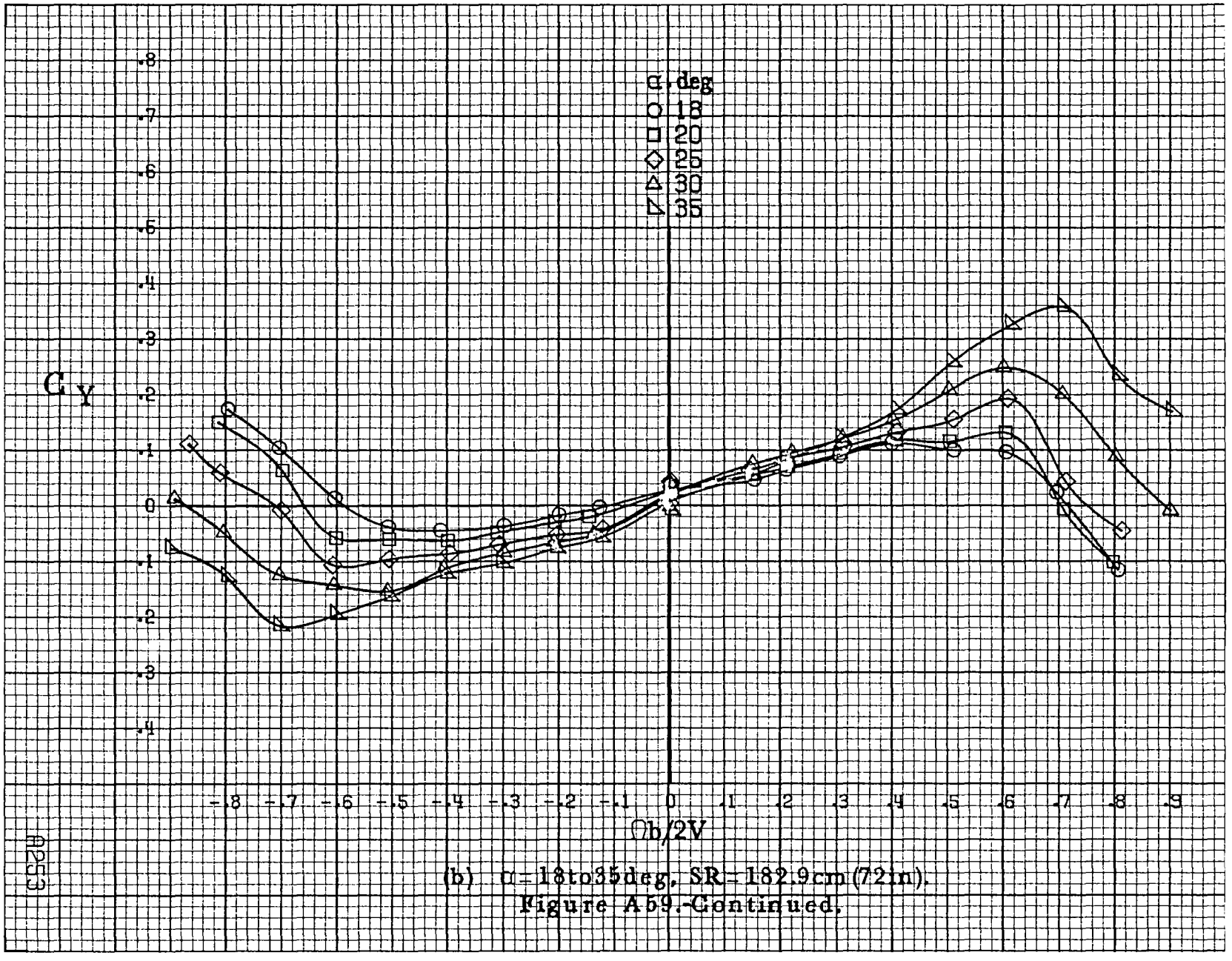

(b) $\alpha = 18$ to 35 deg, SR = 182.9 cm (72 in).

Figure A59.-Continued.

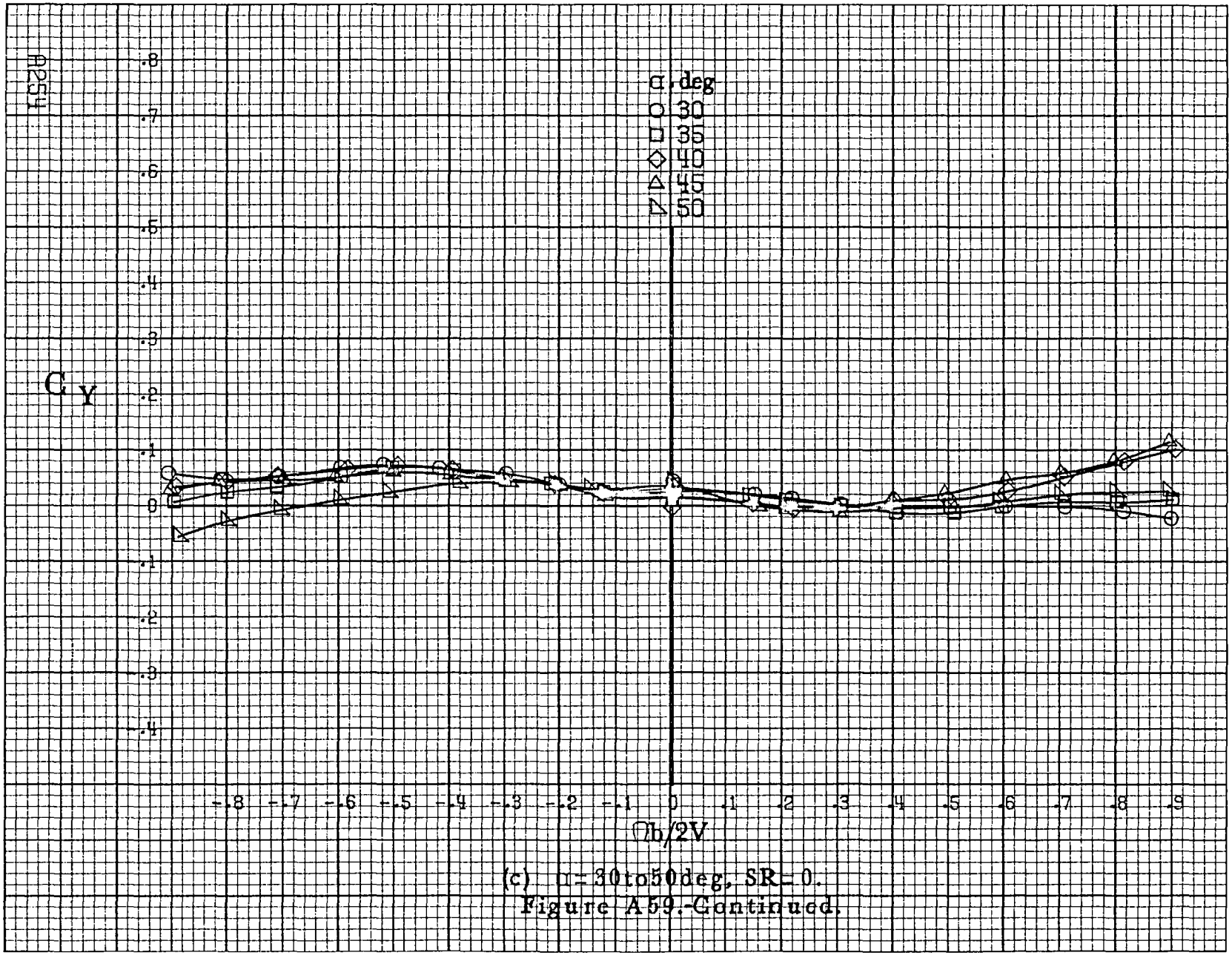

(c) $\alpha = 30$ to 50 deg, SR = 0.

Figure A59.-Continued.

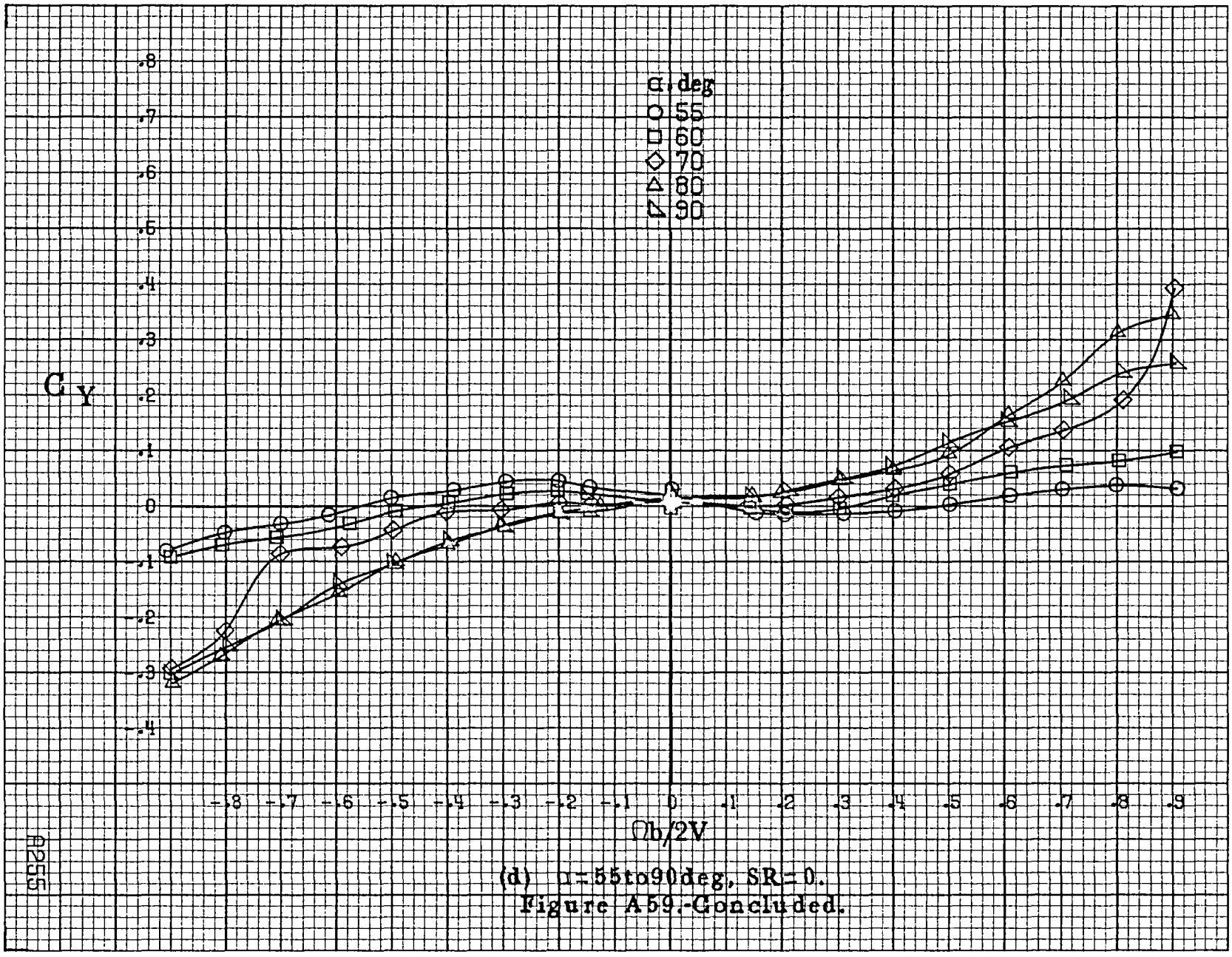

(d) α=55to90deg, SR=0.

Figure A59.-Concluded.

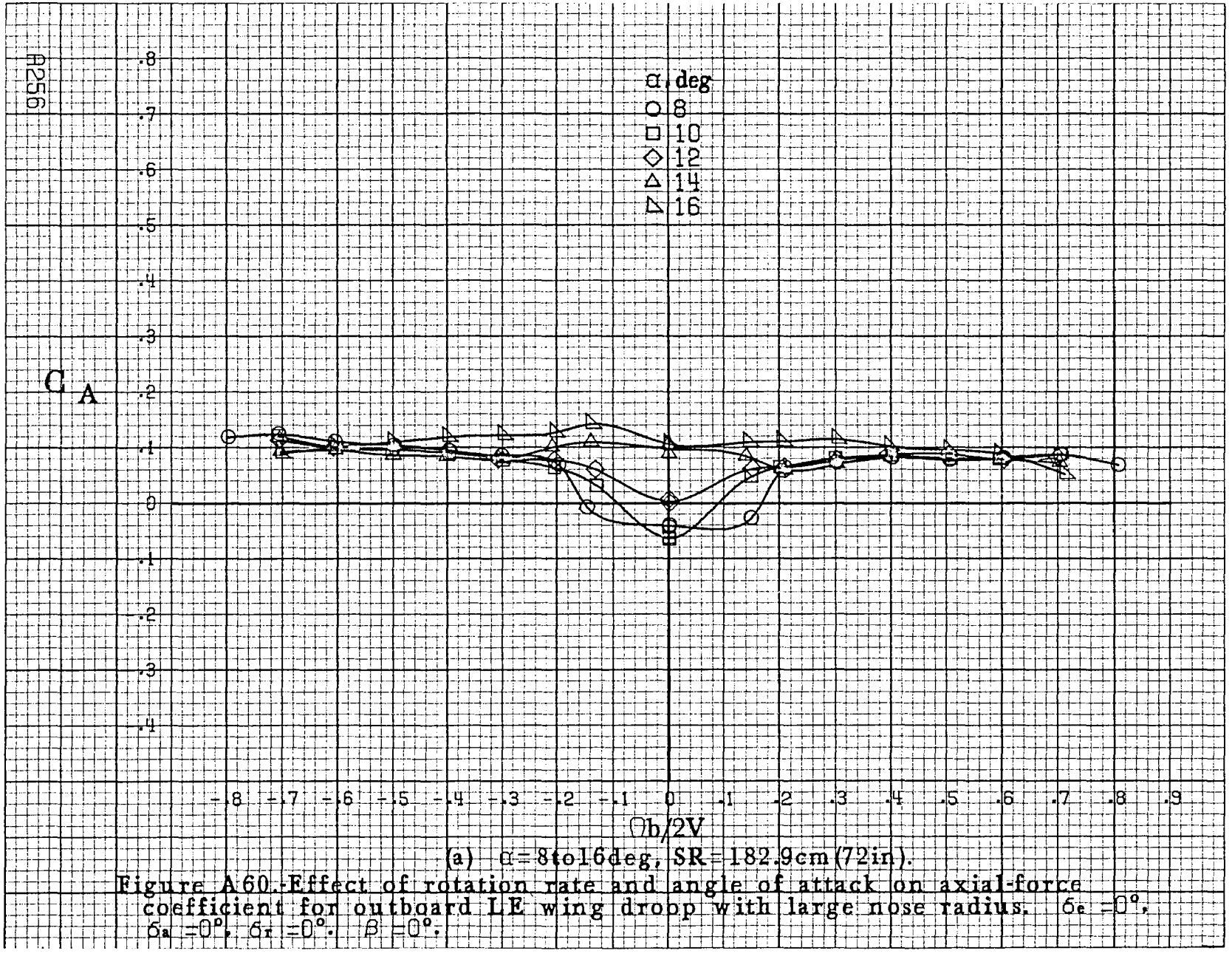

(a) α = 8 to 16 deg, SR = 182.9 cm (72 in.).

Figure A60.-Effect of rotation rate and angle of attack on axial-force coefficient for outboard LE wing droop with large nose radius. $\delta_e = 0°$, $\delta_a = 0°$, $\delta_r = 0°$. $\beta = 0°$.

B257

(b) n = 18 to 35 deg, SR = 182.9 cm (72 in).

Figure A60.-Continued.

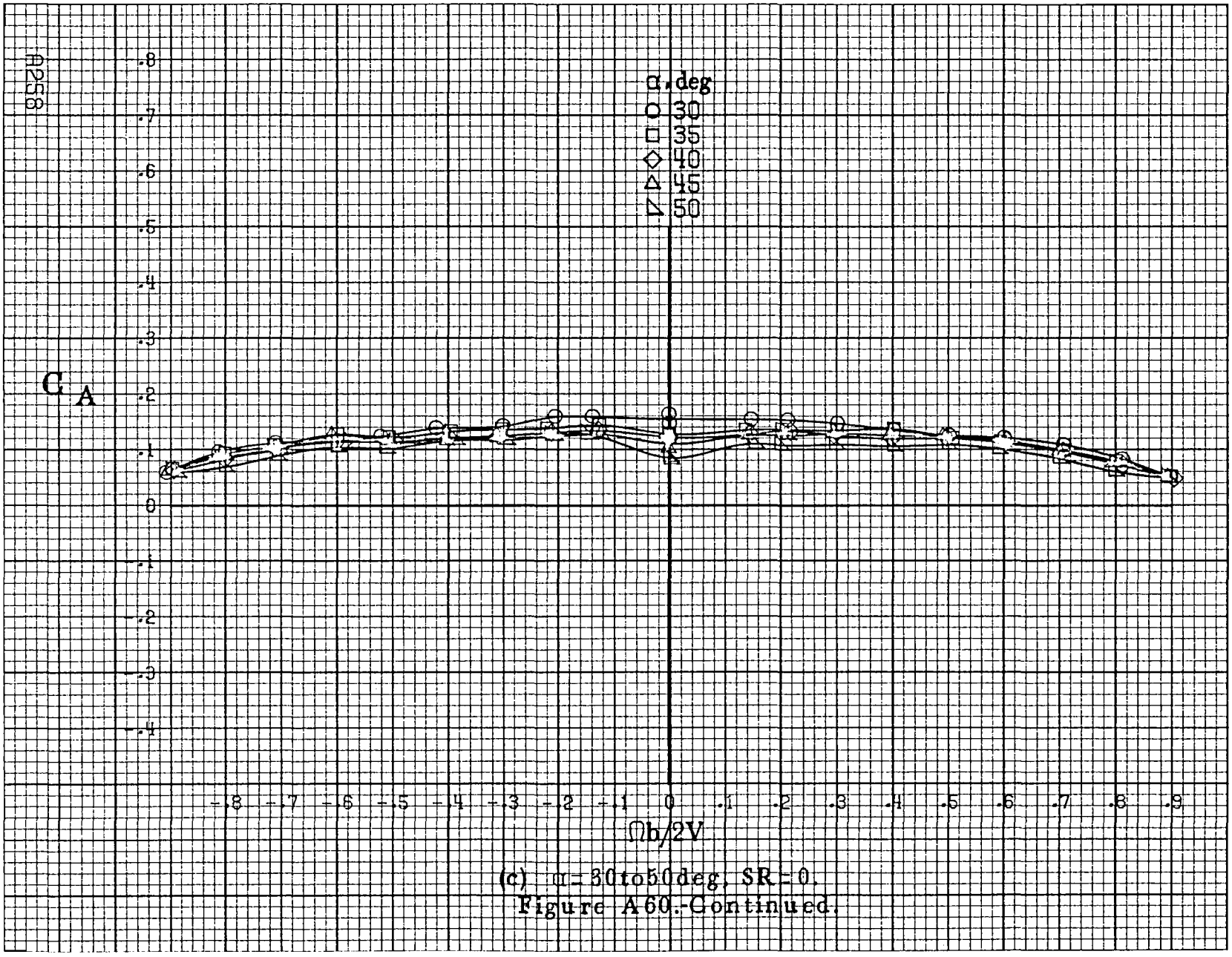

(c) α = 30 to 50 deg, SR = 0.

Figure A60.-Continued.

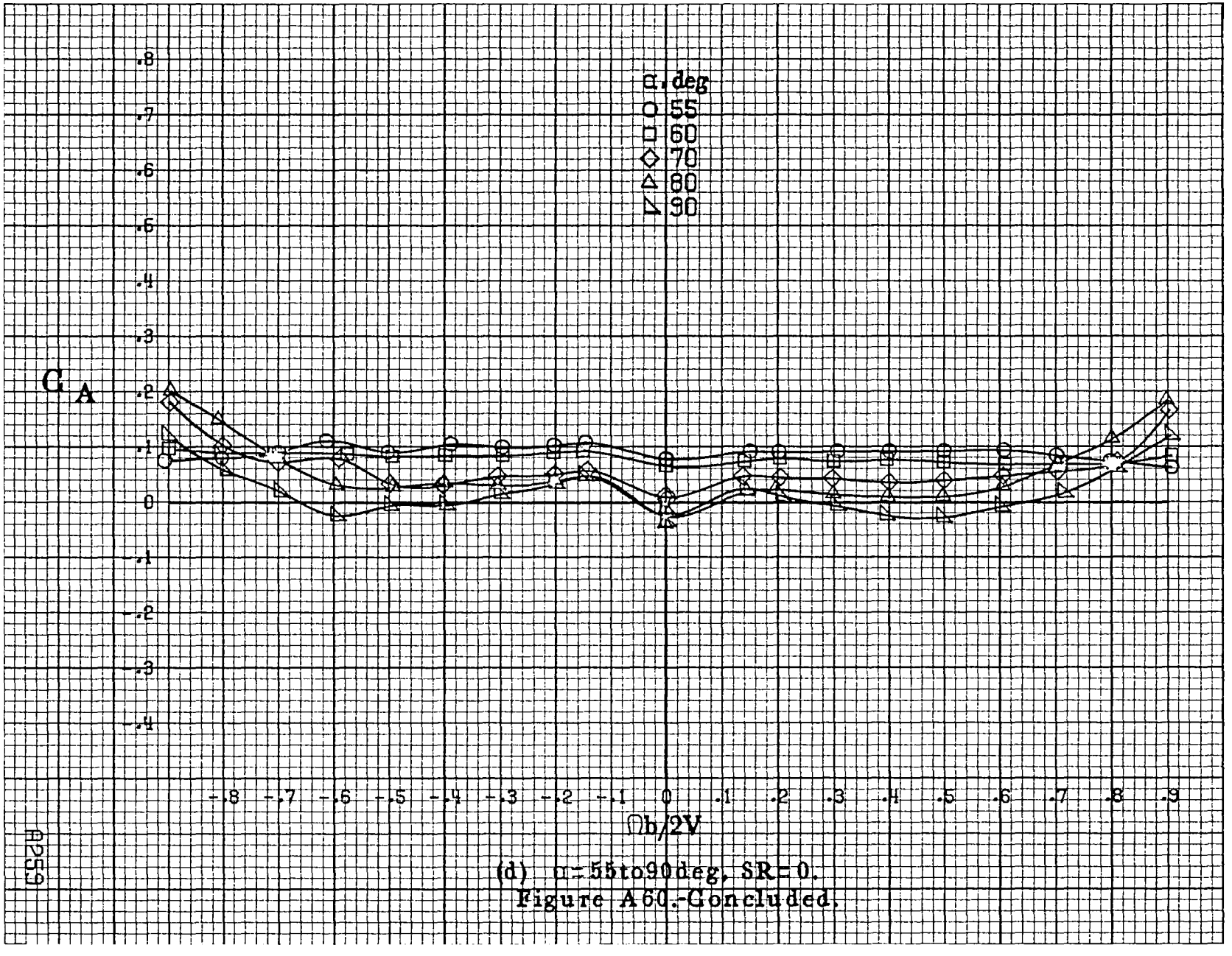

(d) α=55to90deg, SR=0.

Figure A60.-Concluded.

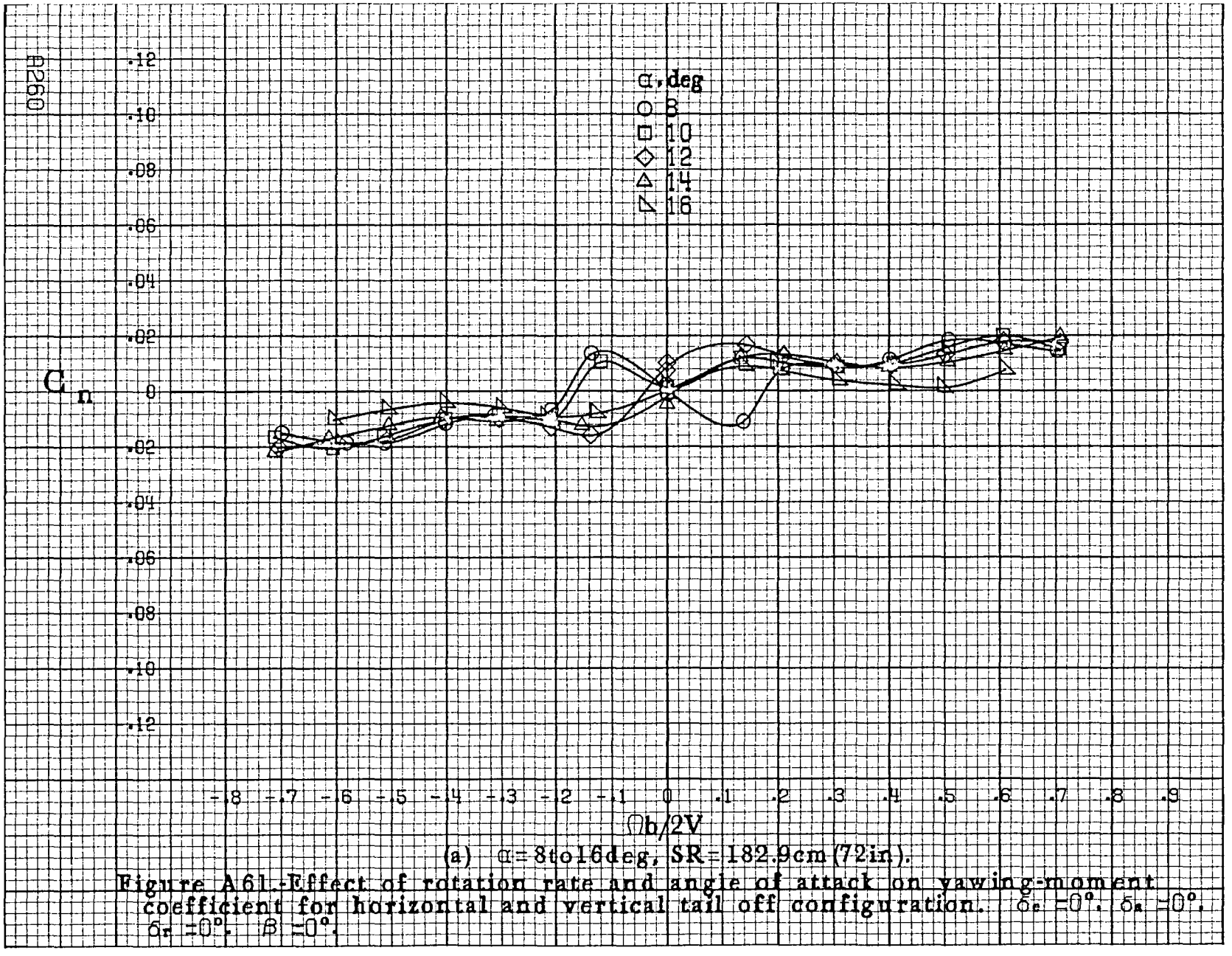

(a) α = 8 to 16 deg, SR = 182.9 cm (72 in.).

Figure A61.-Effect of rotation rate and angle of attack on yawing-moment coefficient for horizontal and vertical tail off configuration. $\delta_e = 0°$, $\delta_a = 0°$, $\delta_r = 0°$, $\beta = 0°$.

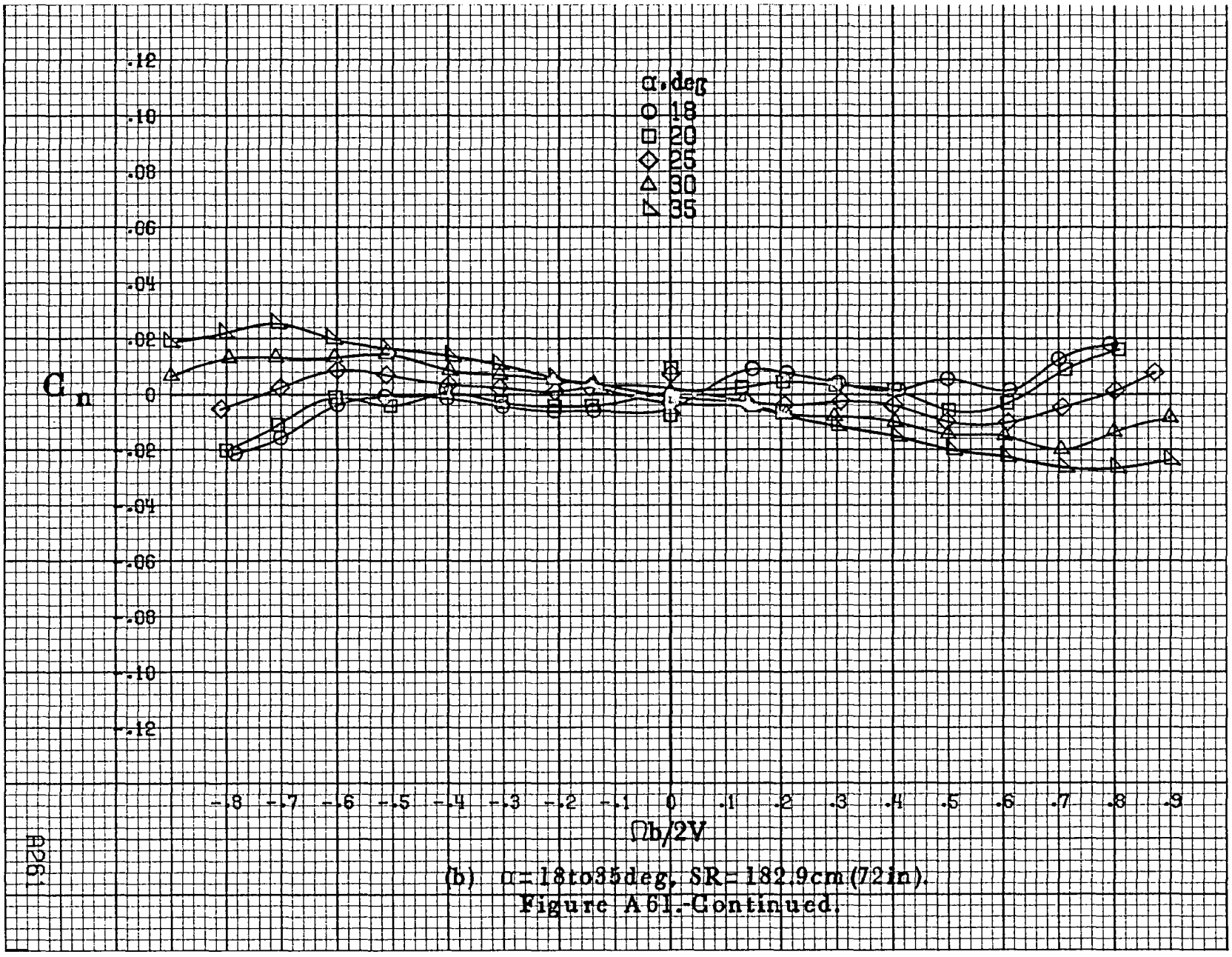

(b) $\alpha = 18$ to 35 deg, $SR = 182.9$ cm (72 in).

Figure A61.-Continued.

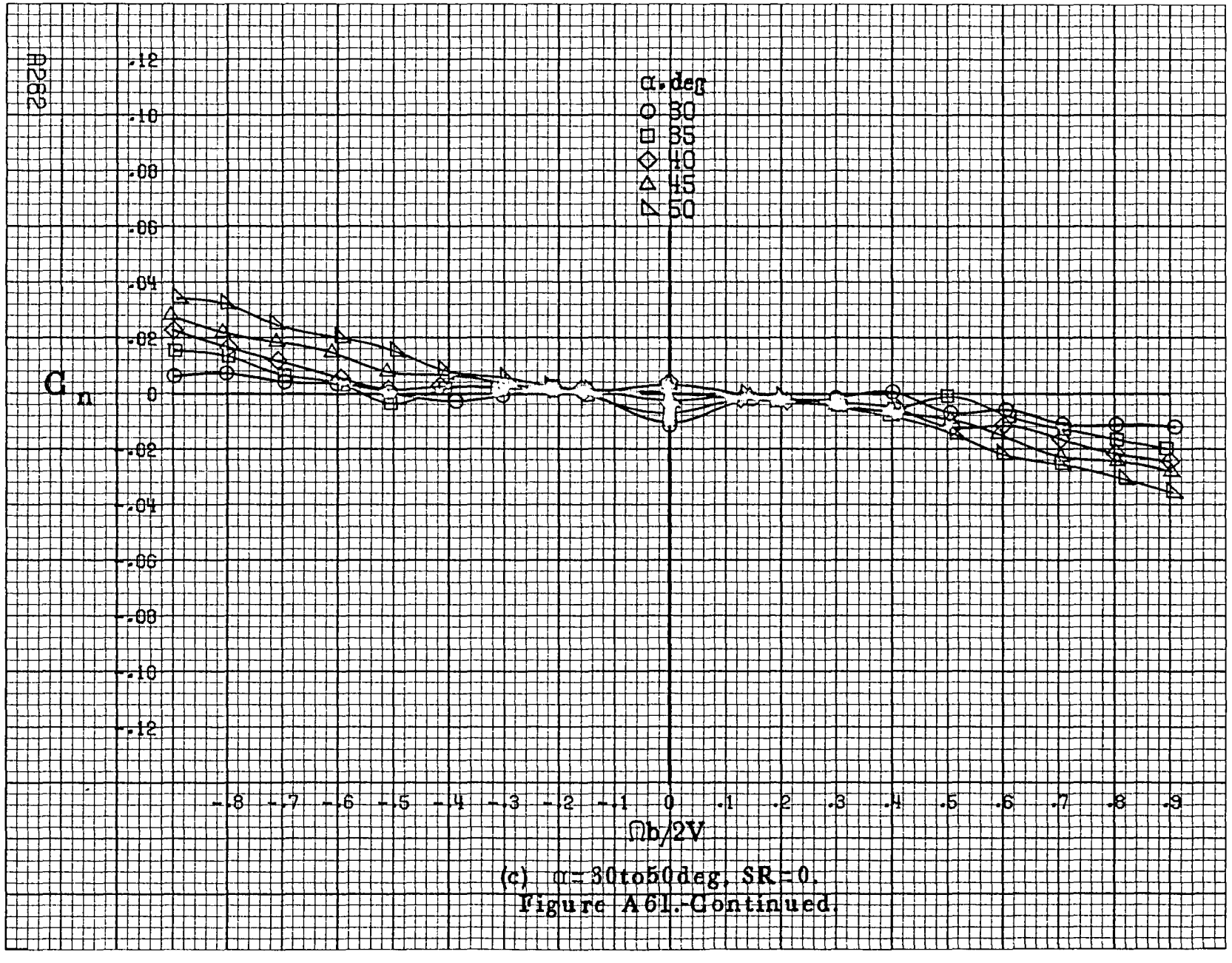

(c) α = 30 to 50 deg, SR = 0.

Figure A61.-Continued.

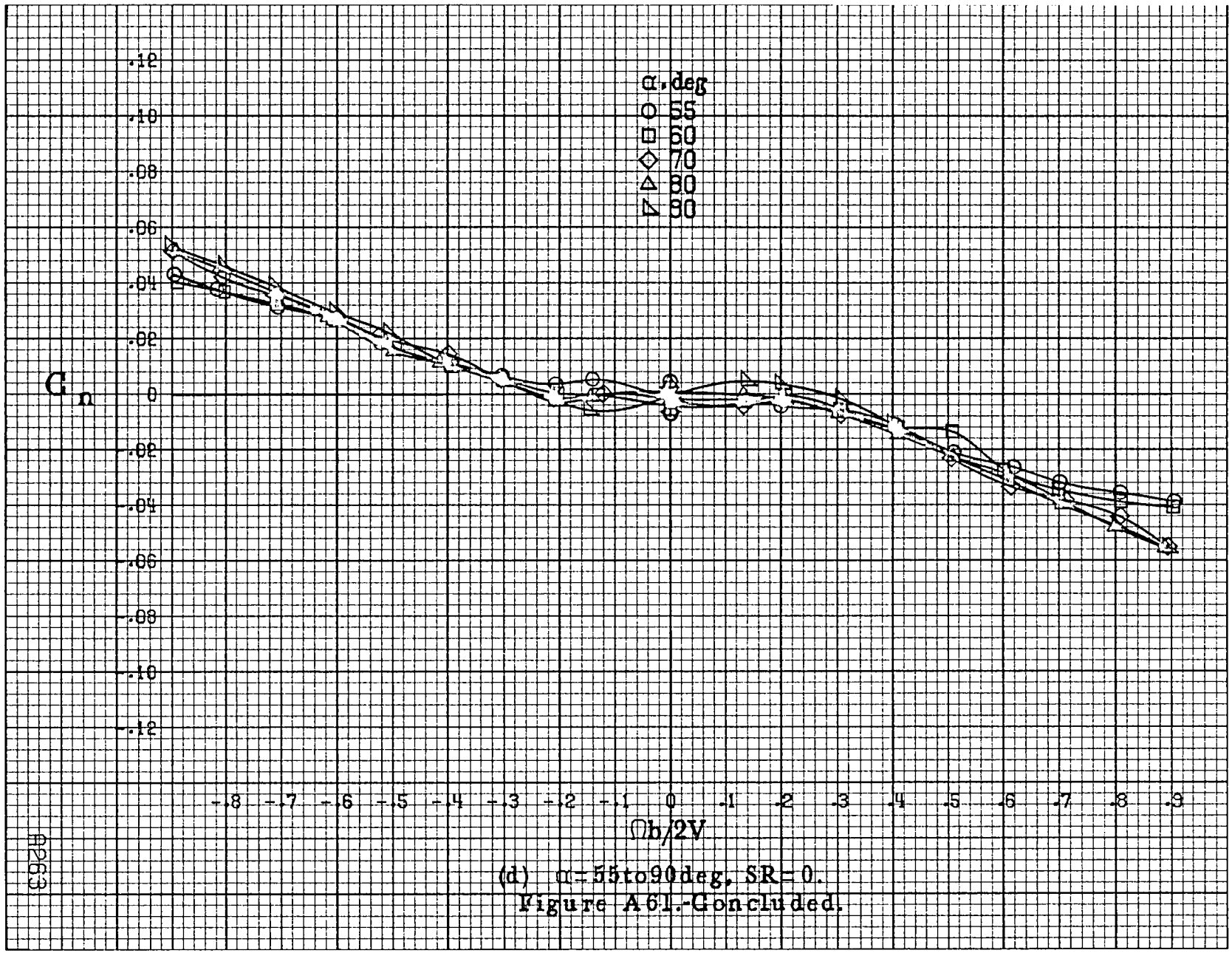

(d) $\alpha = 55$ to 90 deg, SR = 0.

Figure A61.-Concluded.

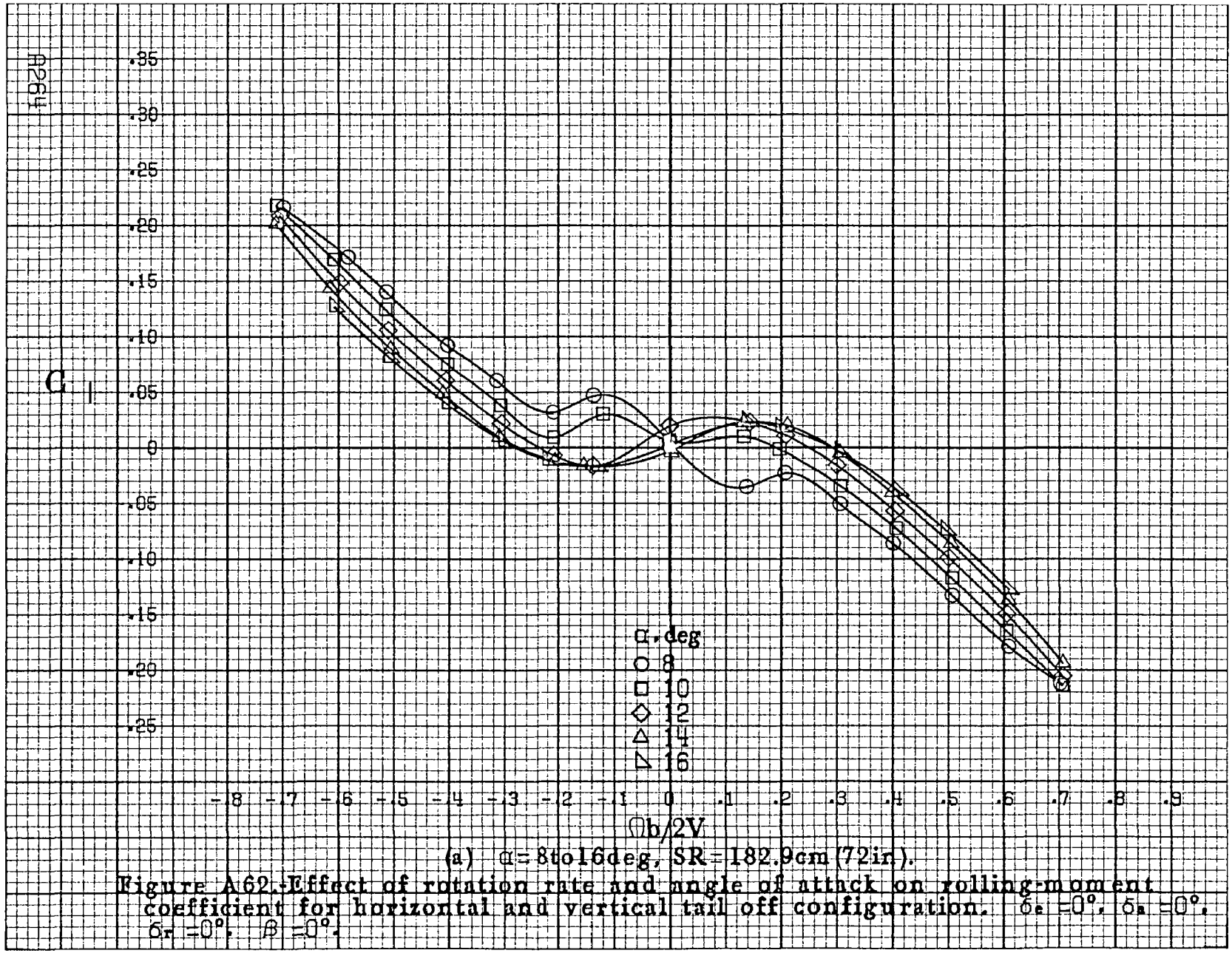

(a) α = 8 to 16 deg, SR = 182.9 cm (72 in.).

Figure A62.- Effect of rotation rate and angle of attack on rolling-moment coefficient for horizontal and vertical tail off configuration. $\delta_e = 0°$, $\delta_a = 0°$, $\delta_r = 0°$, $\beta = 0°$.

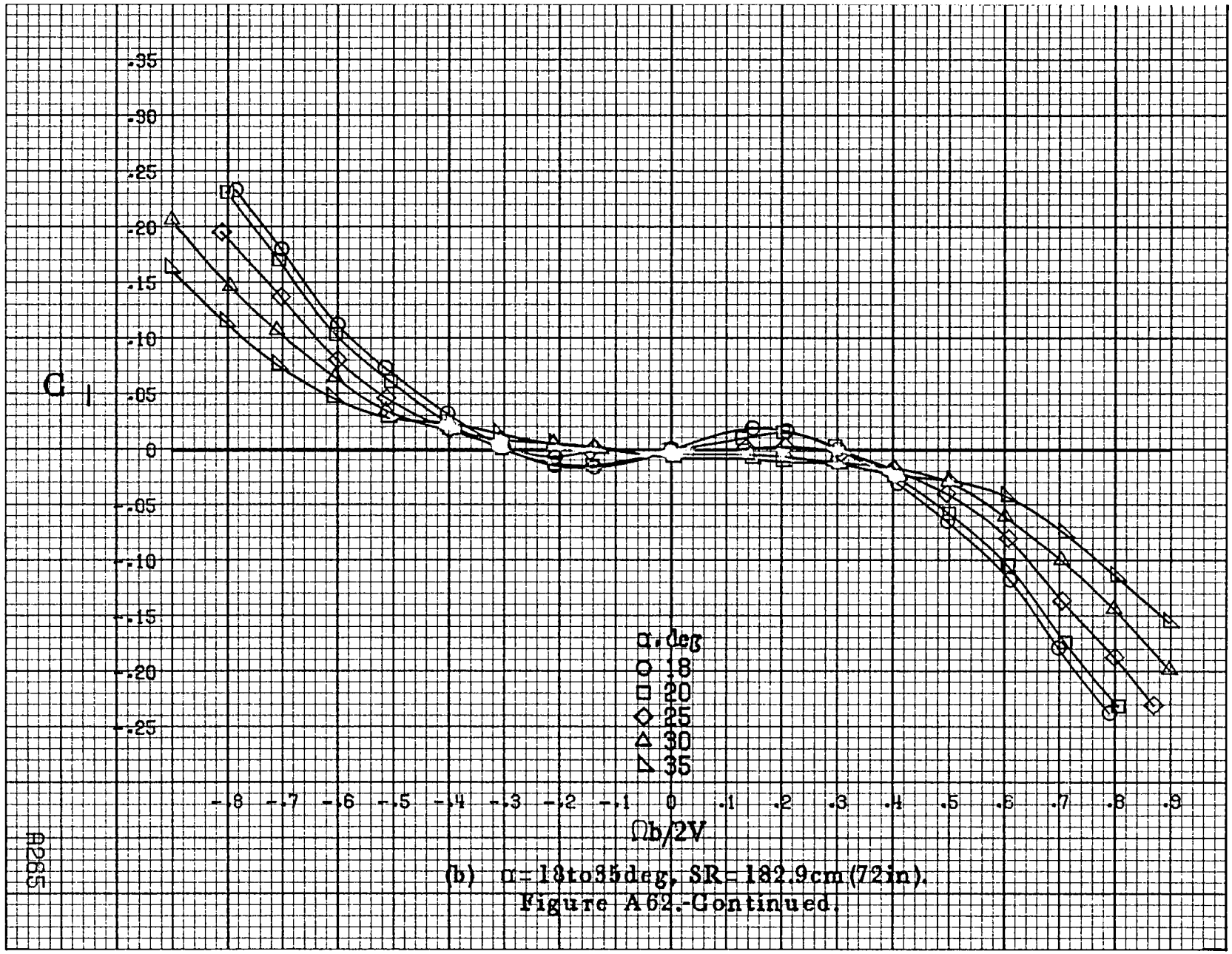

(b) α = 18 to 35 deg, SR = 182.9 cm (72 in).

Figure A62.-Continued.

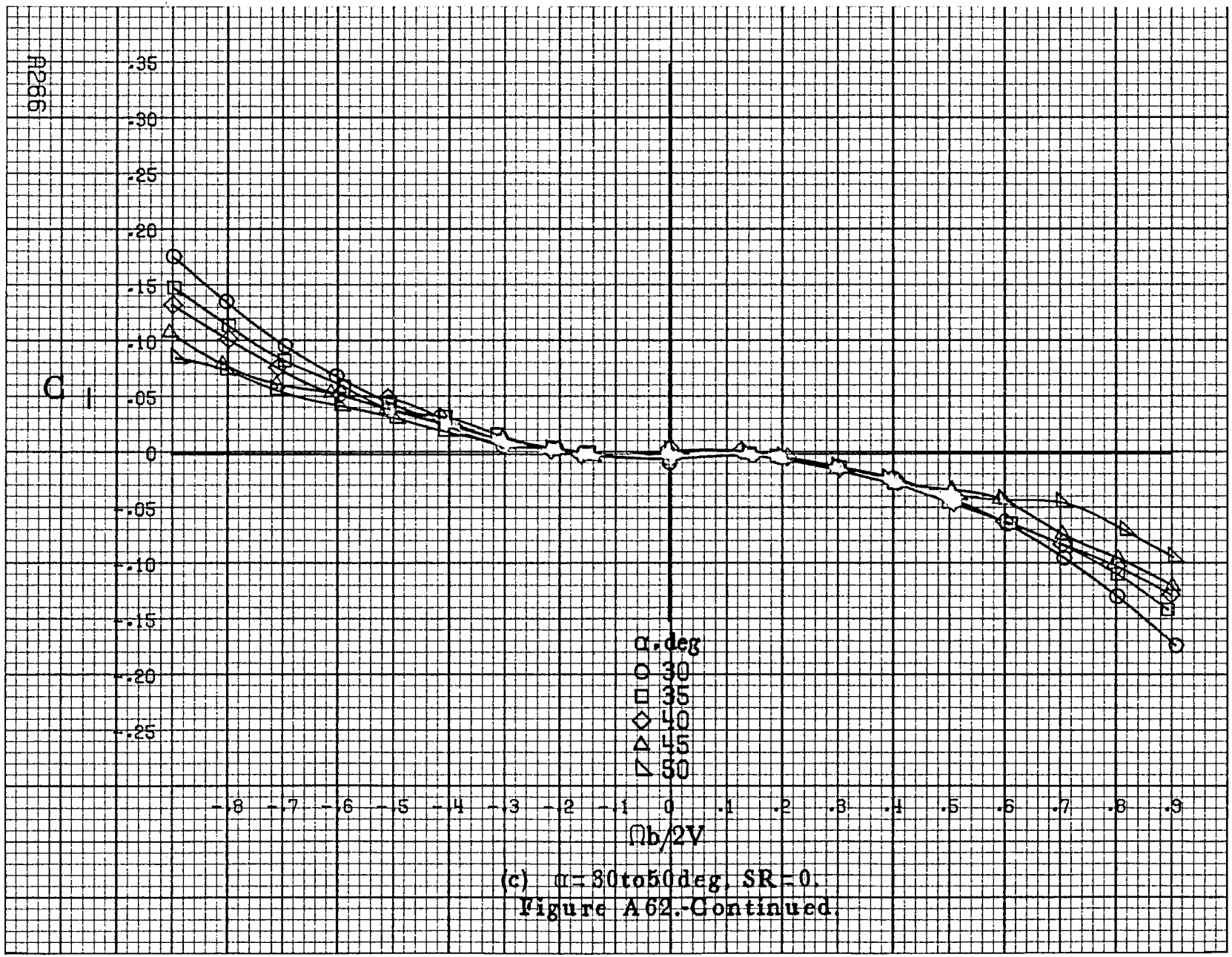

(c) $\alpha = 30$ to 50 deg, SR = 0.

Figure A62.-Continued.

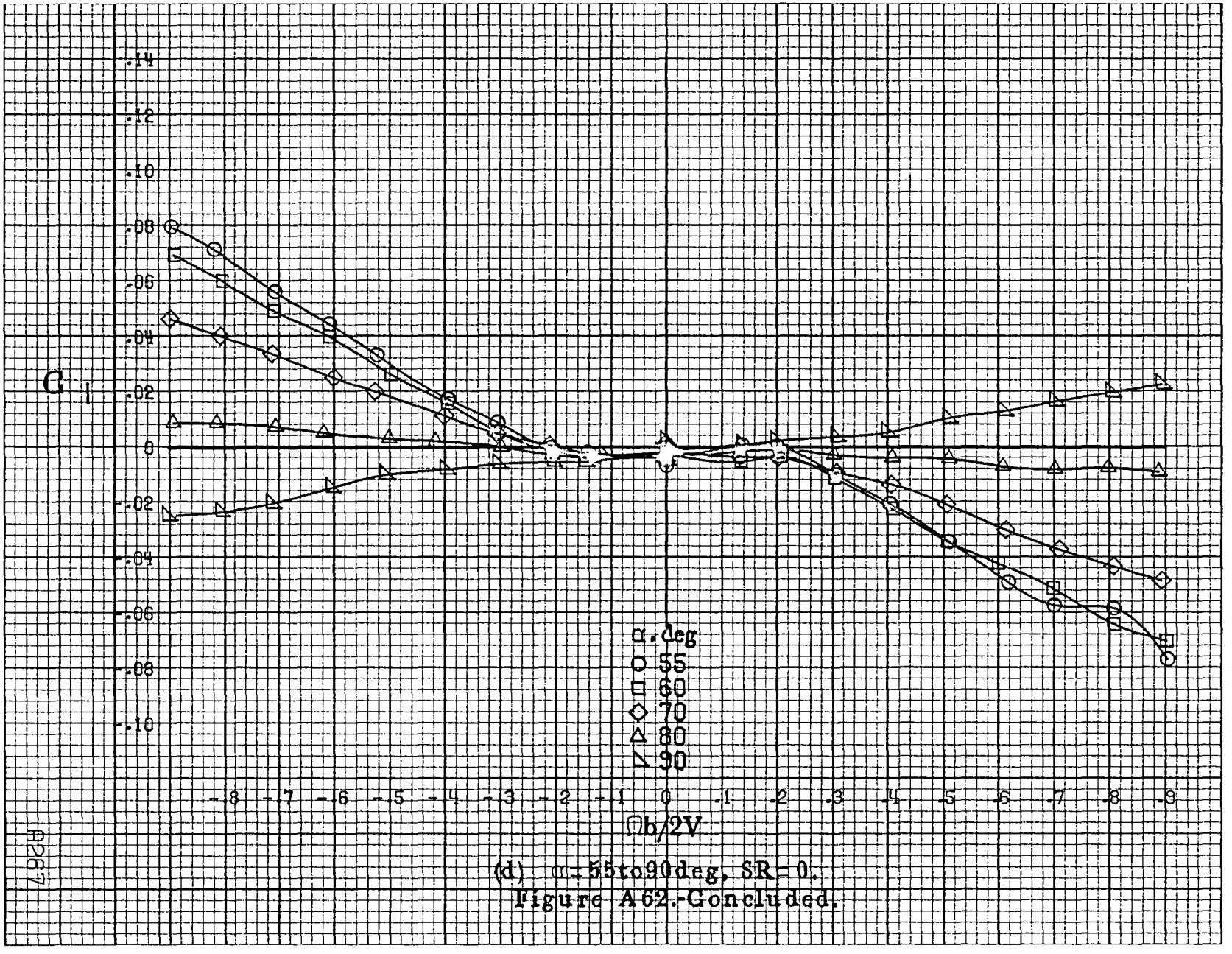

(d) $\alpha = 55$ to 90 deg, SR = 0.

Figure A62.-Concluded.

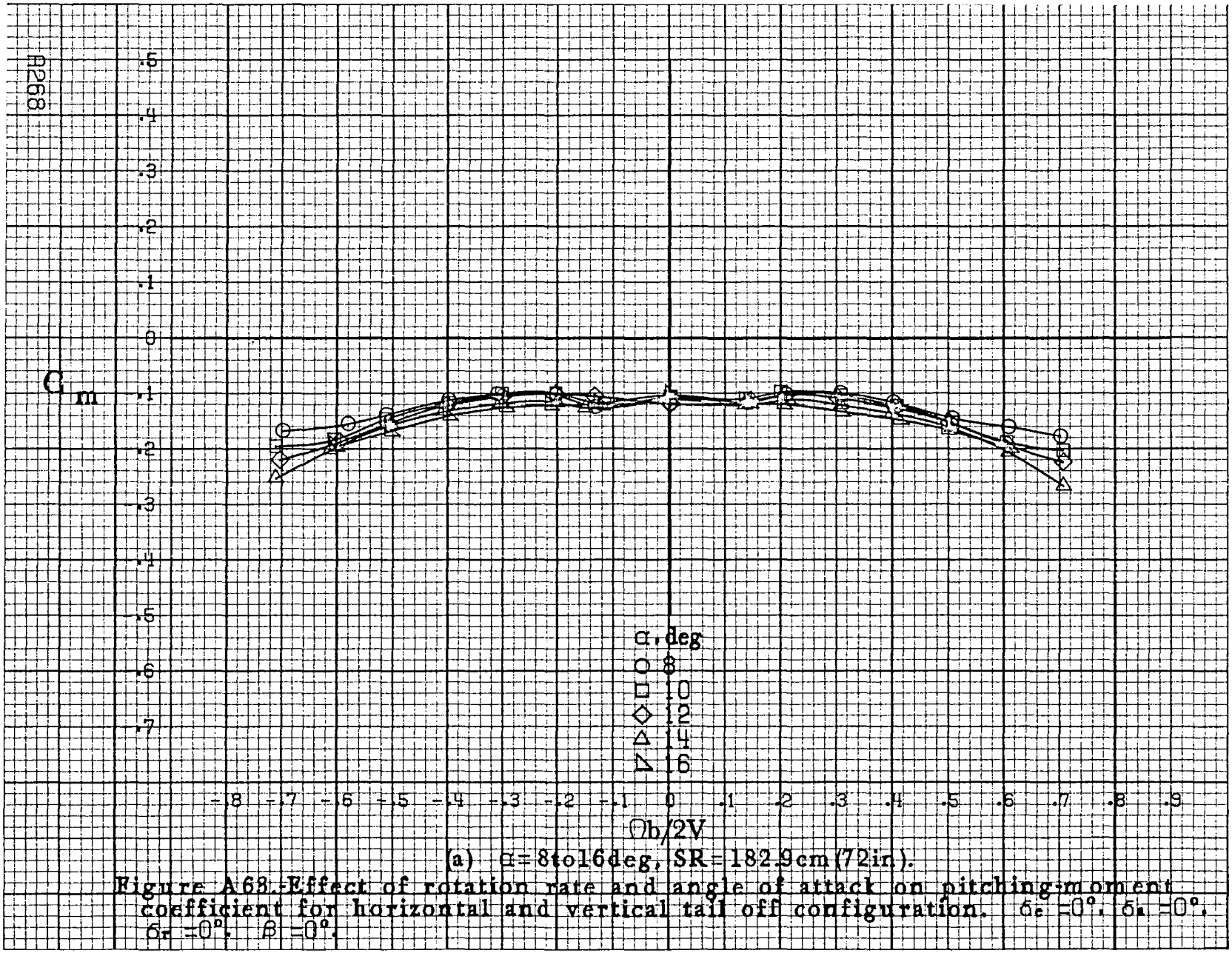

(a) α=8to16deg, SR=182.9cm(72in).

Figure A63.-Effect of rotation rate and angle of attack on pitching-moment coefficient for horizontal and vertical tail off configuration. δ_e =0°, δ_a =0°, δ_r =0°, β =0°.

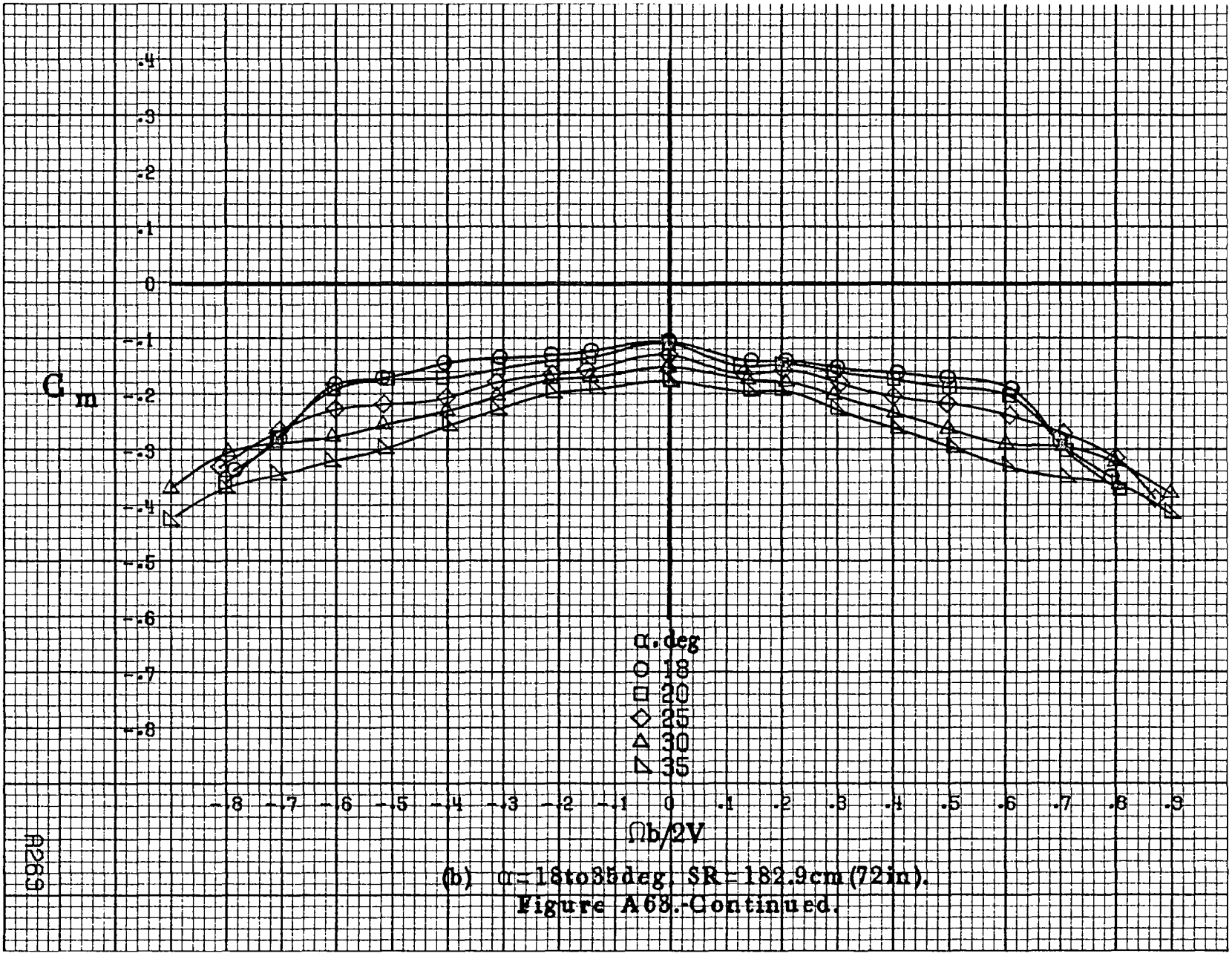

(b) α = 18 to 35 deg; SR = 182.9 cm (72 in).

Figure A68.-Continued.

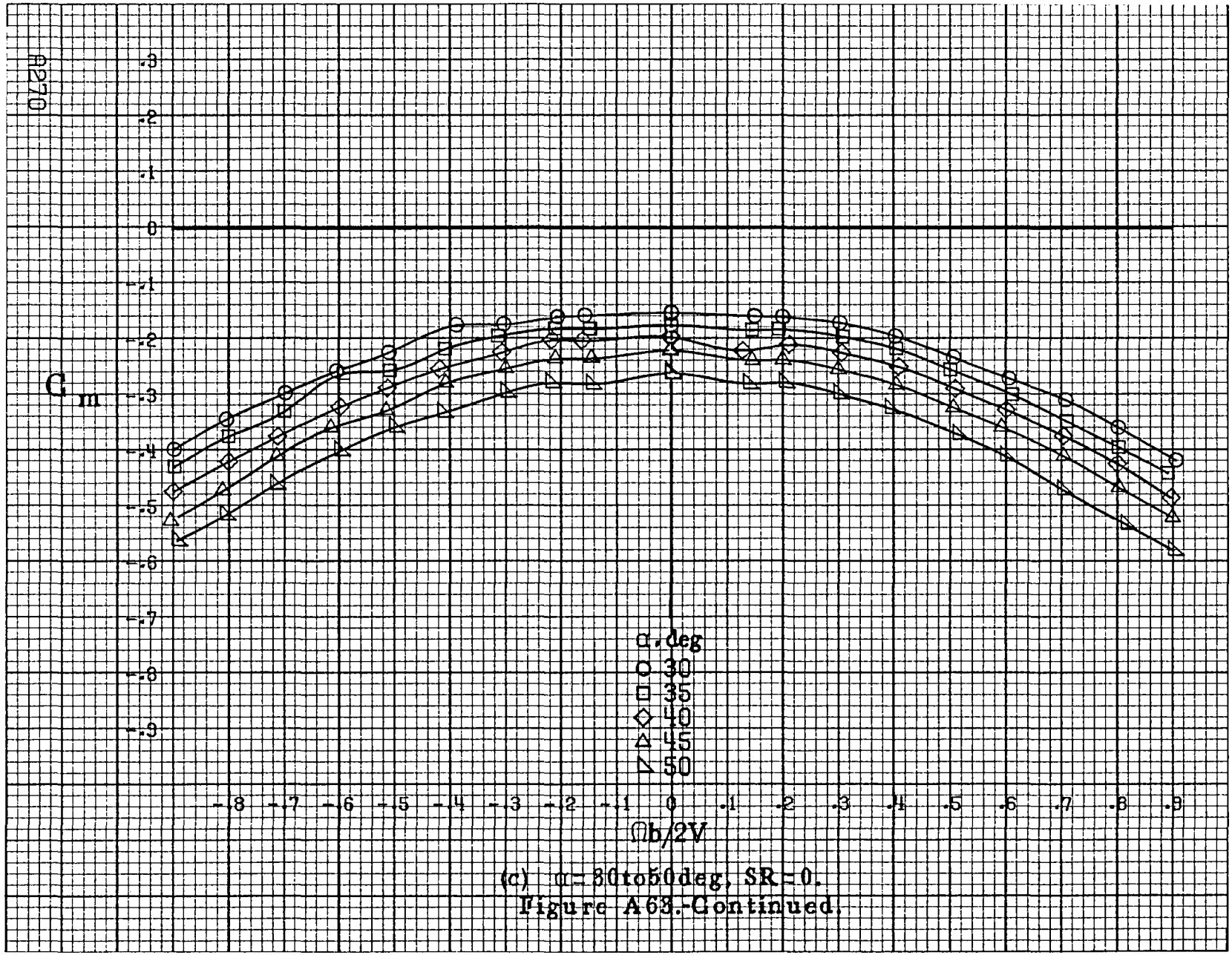

(c) $\alpha = 30$ to 50 deg, SR = 0.

Figure A63.-Continued.

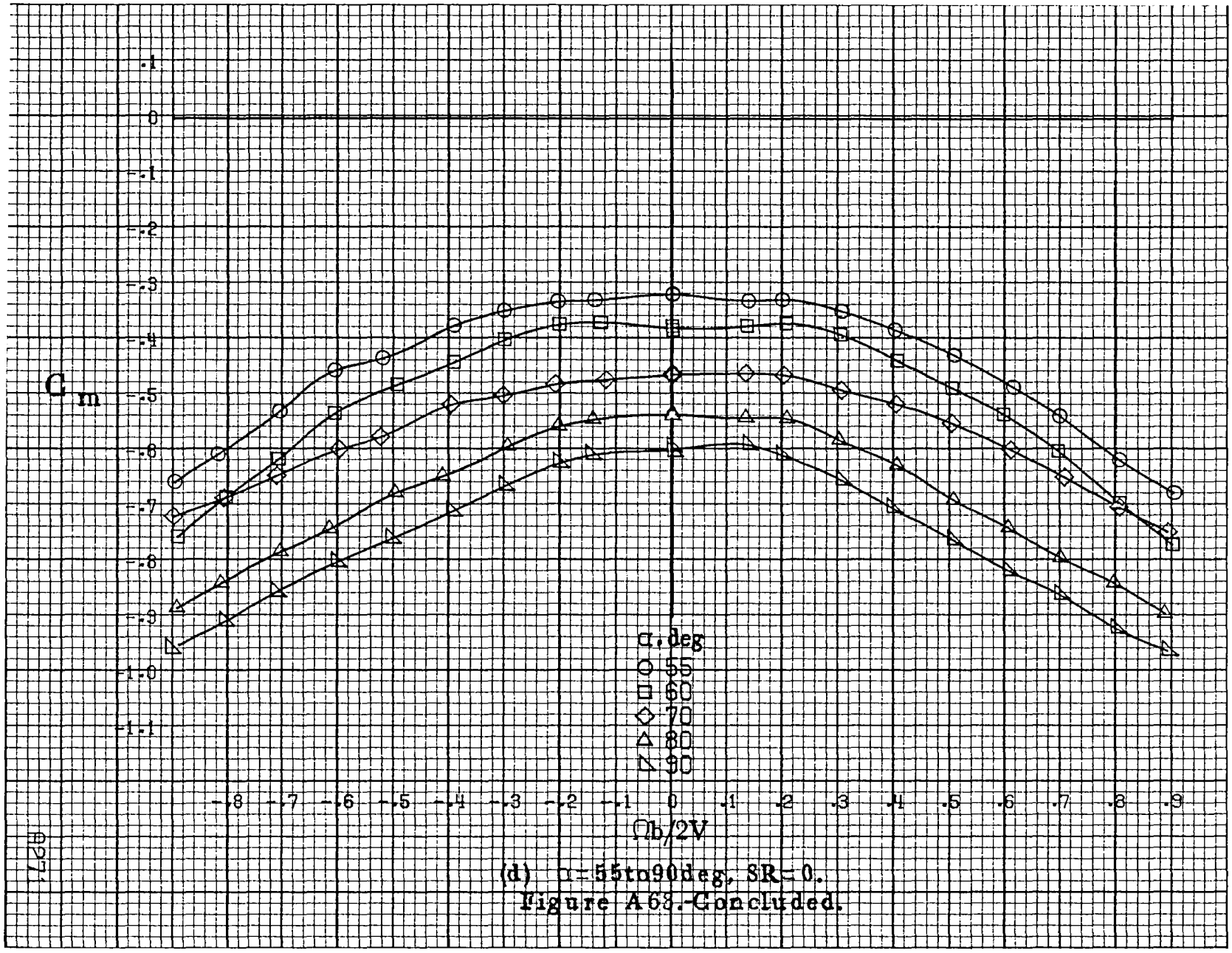

(d) $\alpha = 55$ to 90 deg, $\delta R = 0$.

Figure A68.-Concluded.

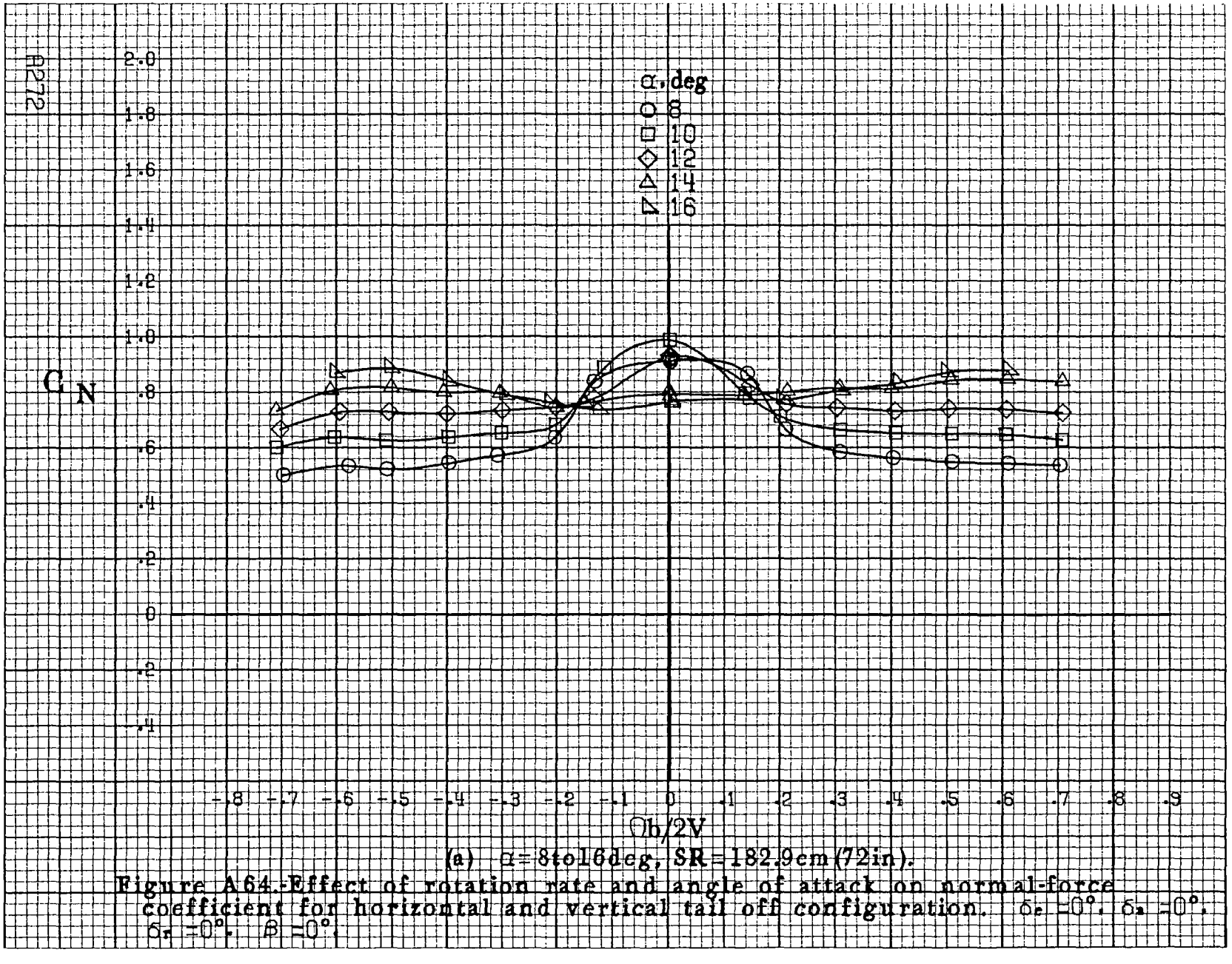

(a) $\alpha = 8$ to 16 deg, $SR = 182.9$ cm (72 in).

Figure A64.-Effect of rotation rate and angle of attack on normal-force coefficient for horizontal and vertical tail off configuration. $\delta_e = 0°$, $\delta_a = 0°$, $\delta_r = 0°$, $\beta = 0°$.

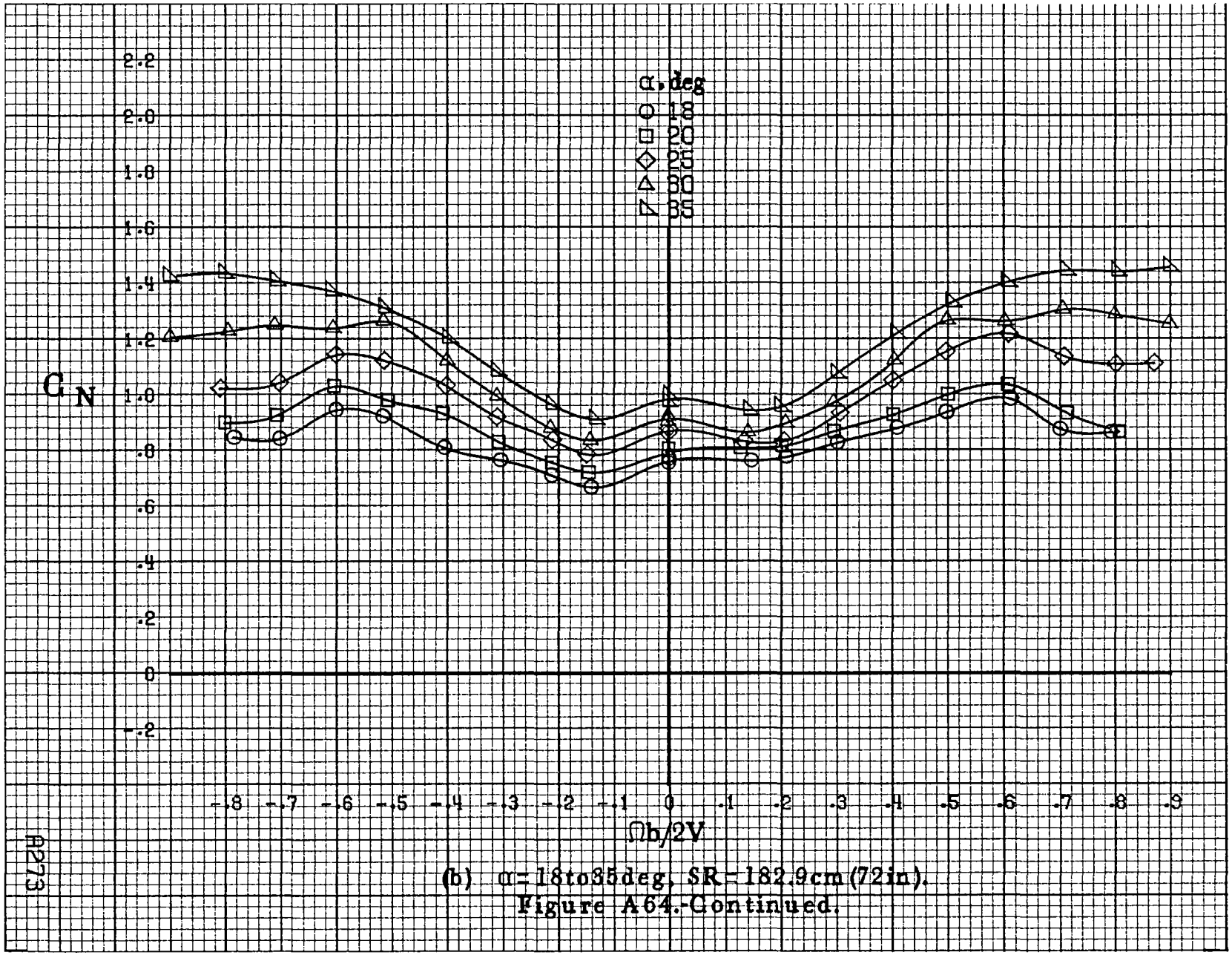

(b) α = 18 to 35 deg, SR = 182.9 cm (72 in).

Figure A64.-Continued.

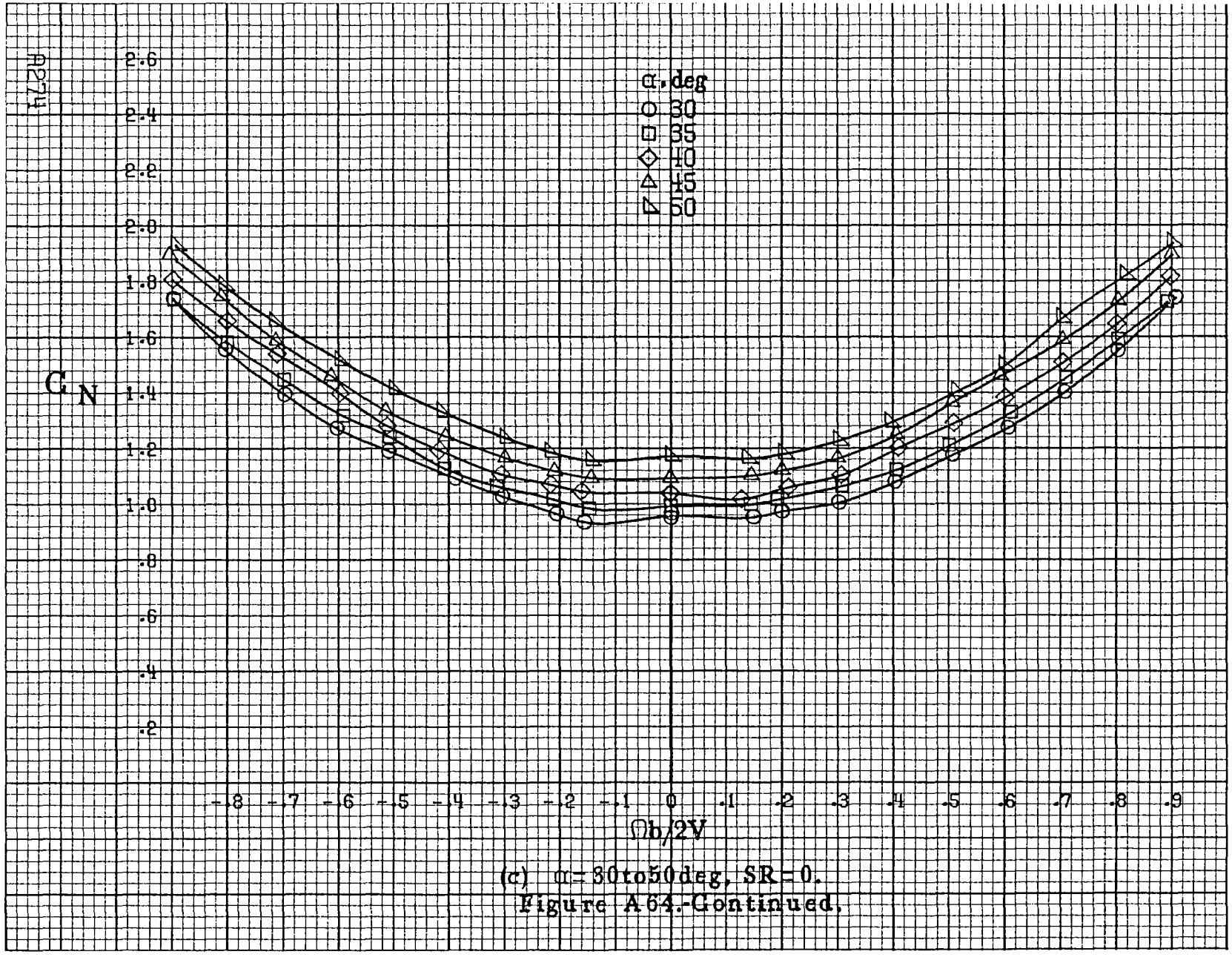

(c) α = 30 to 50 deg, SR = 0.

Figure A64.-Continued.

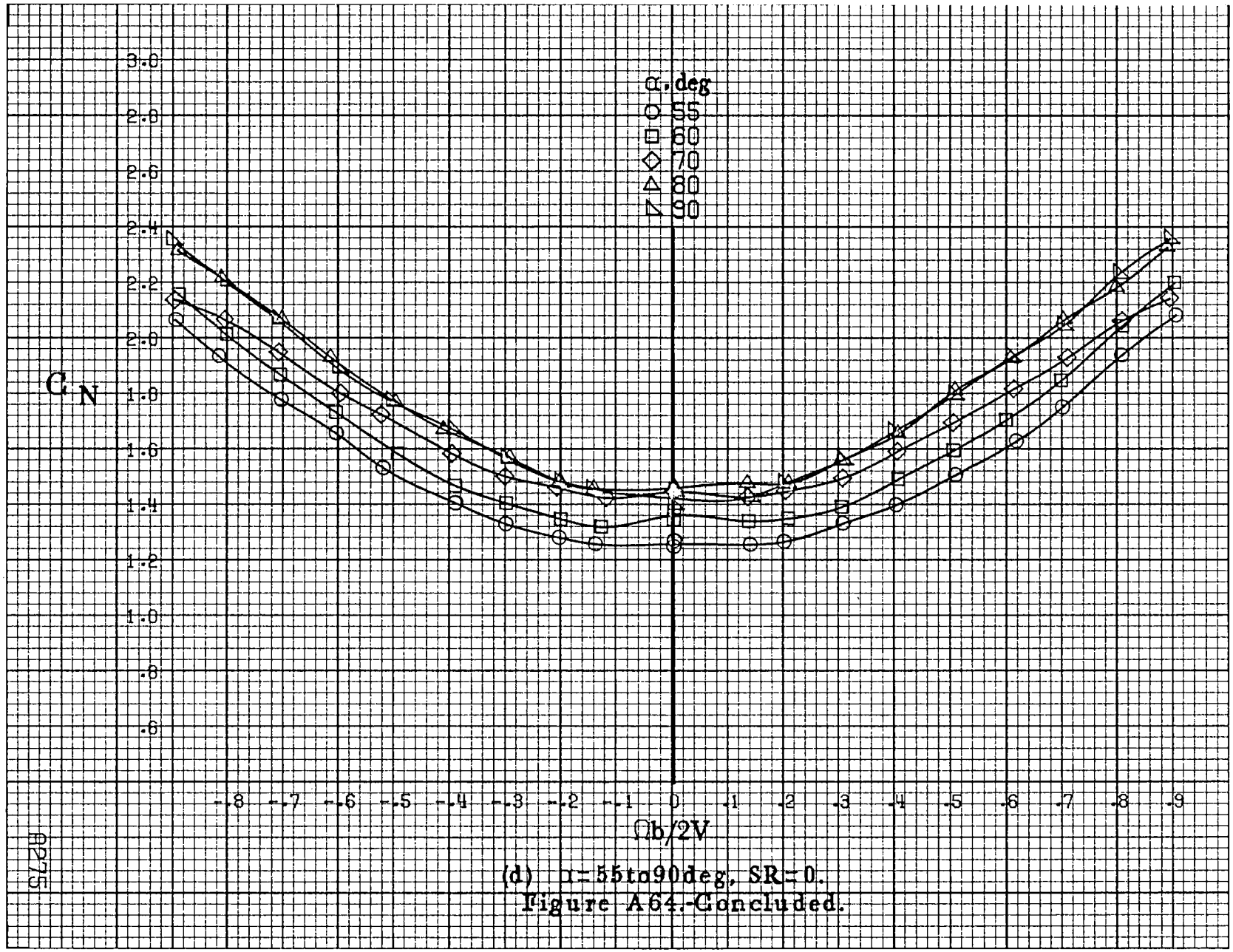

(d) α=55to90deg, SR=0.

Figure A64.-Concluded.

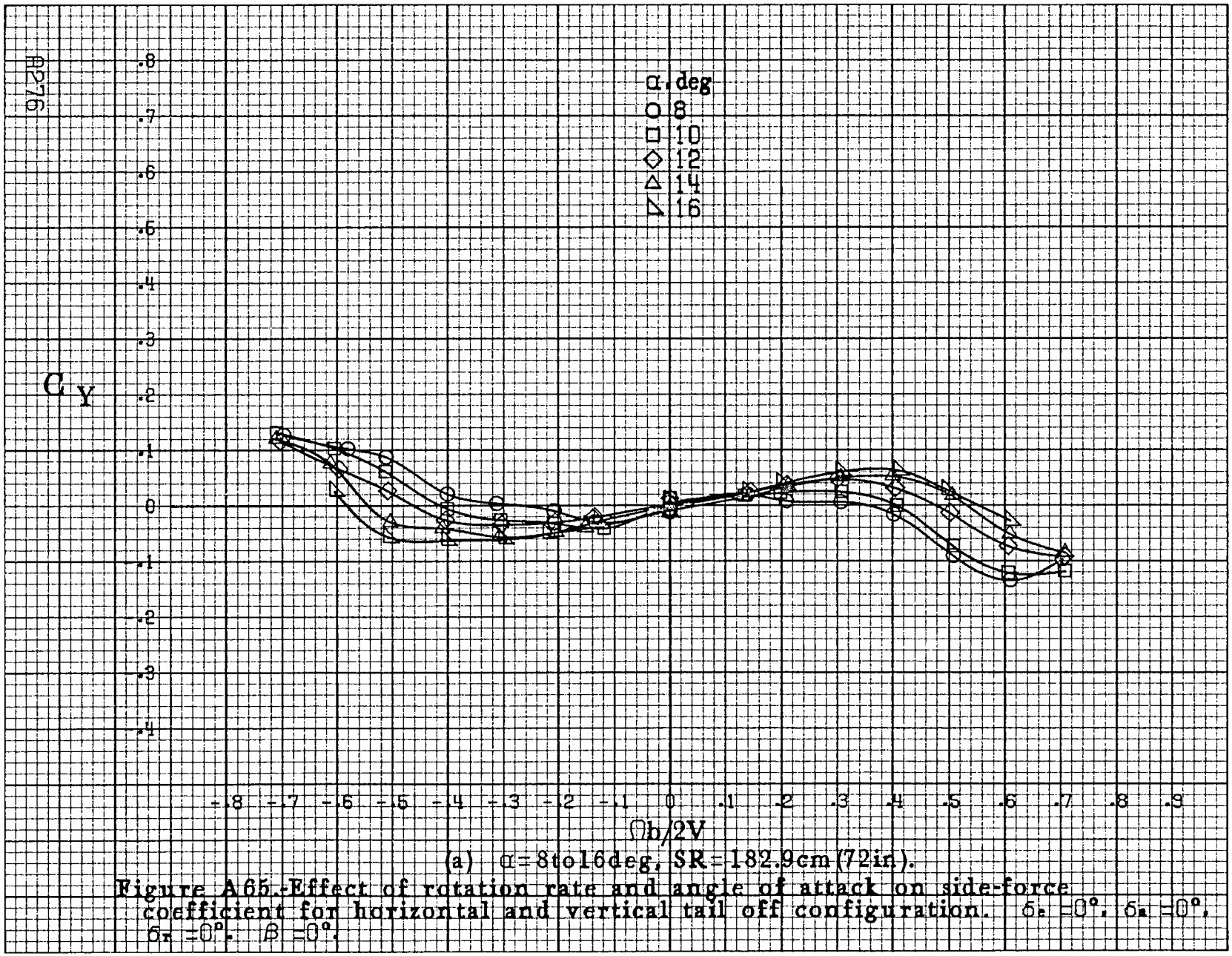

(a) α=8to16deg, SR=182.9cm(72in).

Figure A65.-Effect of rotation rate and angle of attack on side-force coefficient for horizontal and vertical tail off configuration. $\delta_a = 0°$, $\delta_s = 0°$, $\delta_r = 0°$, $\beta = 0°$.

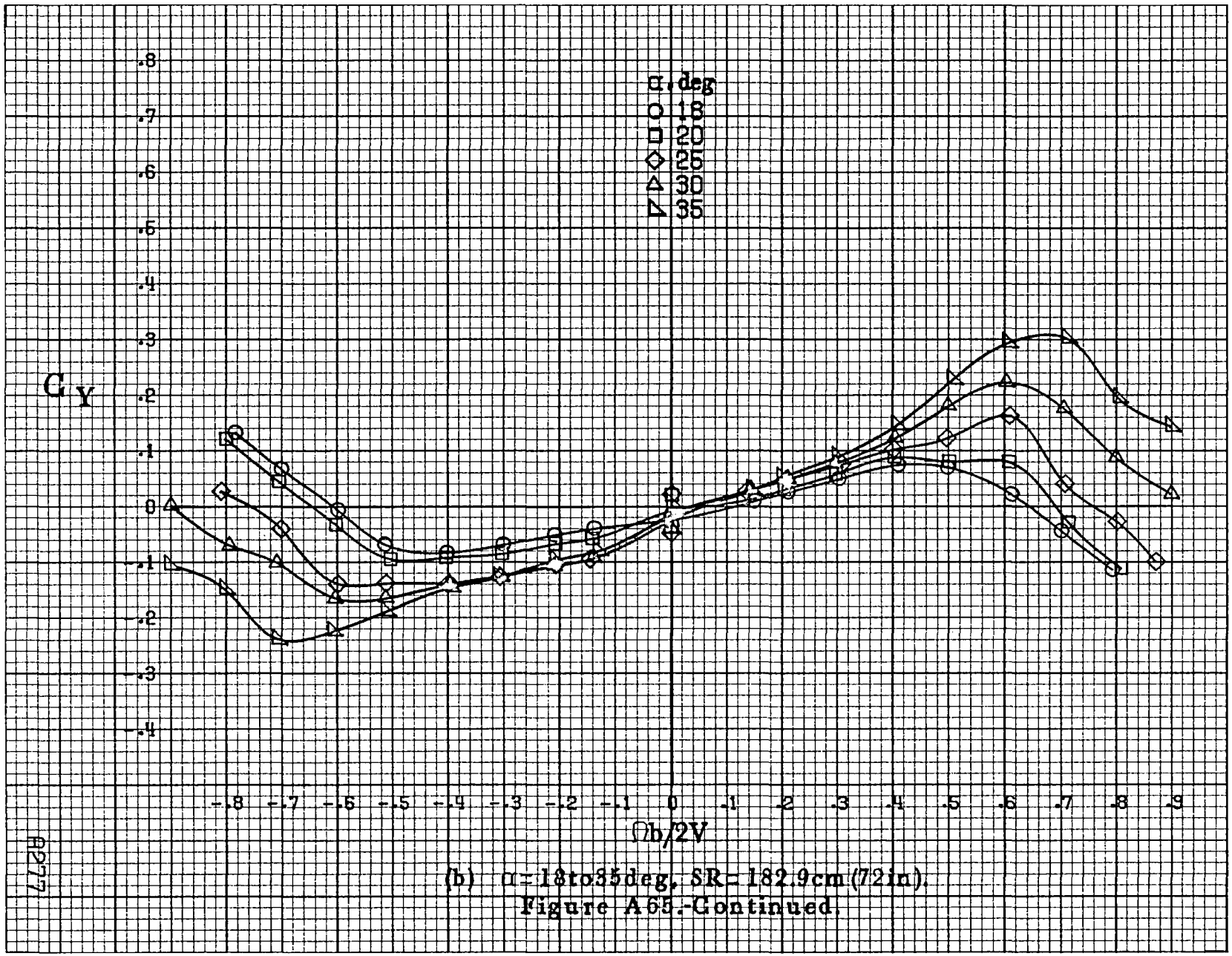

(b) α = 18 to 35 deg, SR = 182.9 cm (72 in).

Figure A65.-Continued.

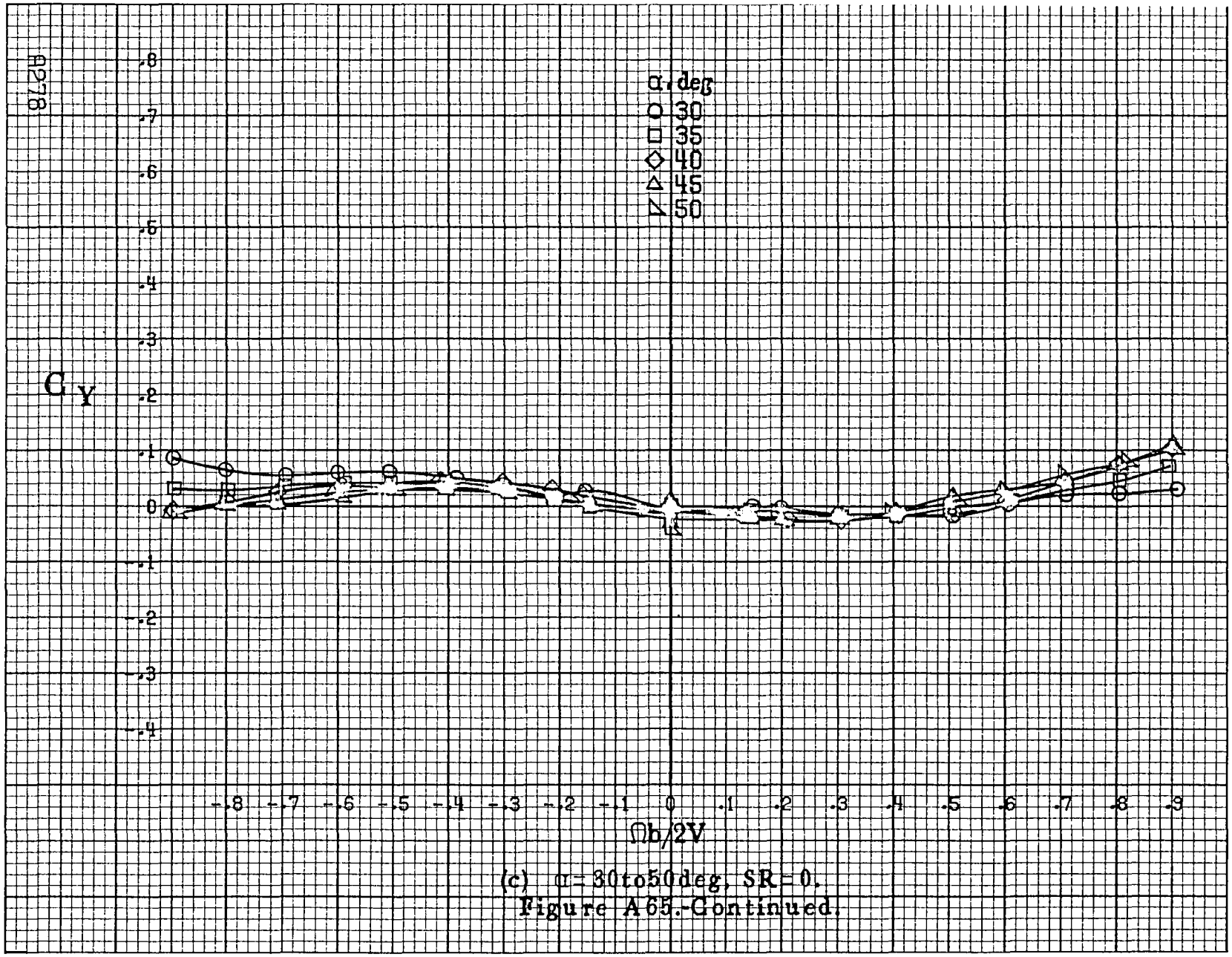

(c) $\alpha = 30$ to 50 deg, SR = 0.

Figure A65.-Continued.

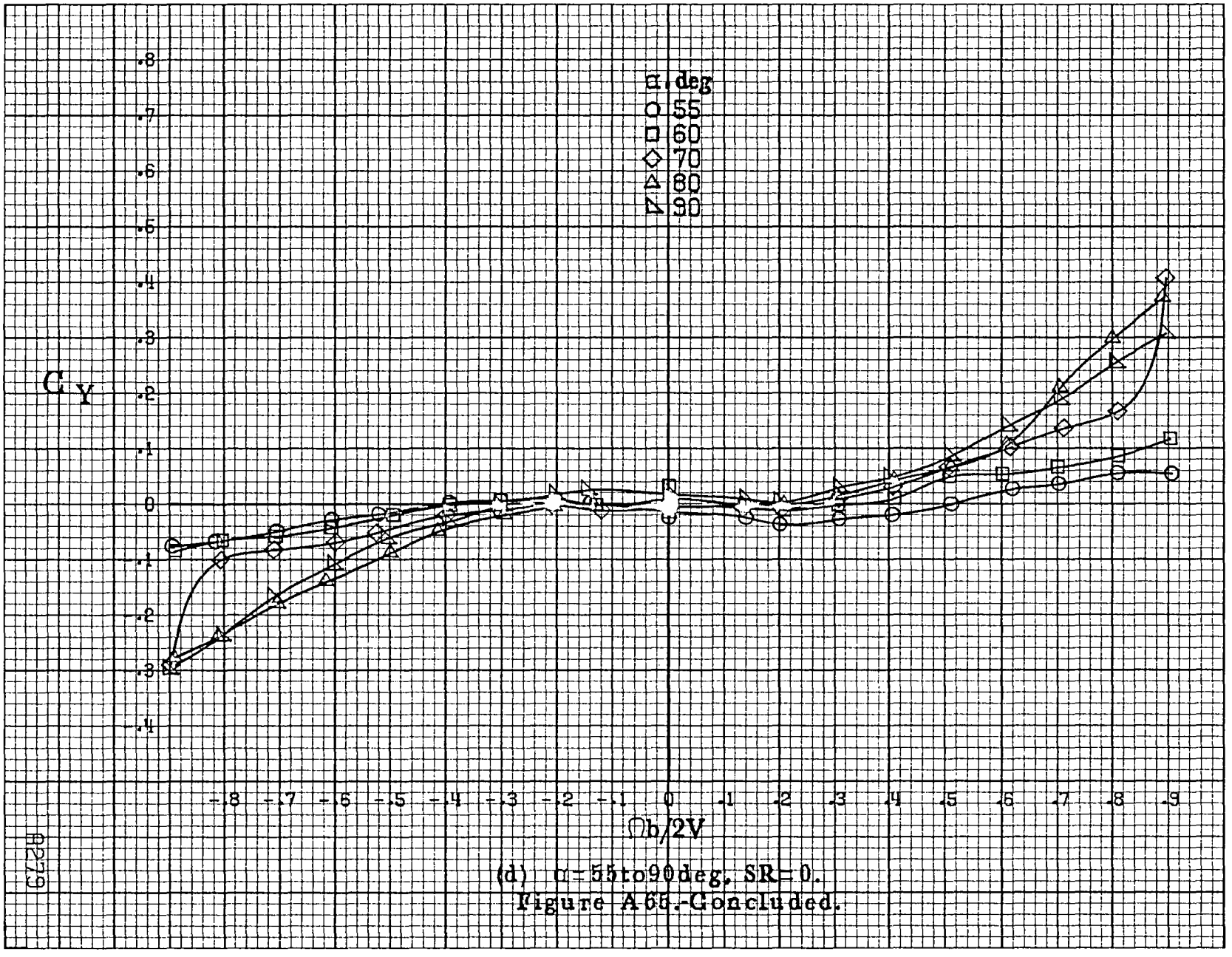

(d) $\alpha = 55$ to 90 deg, SR = 0.

Figure A65.-Concluded.

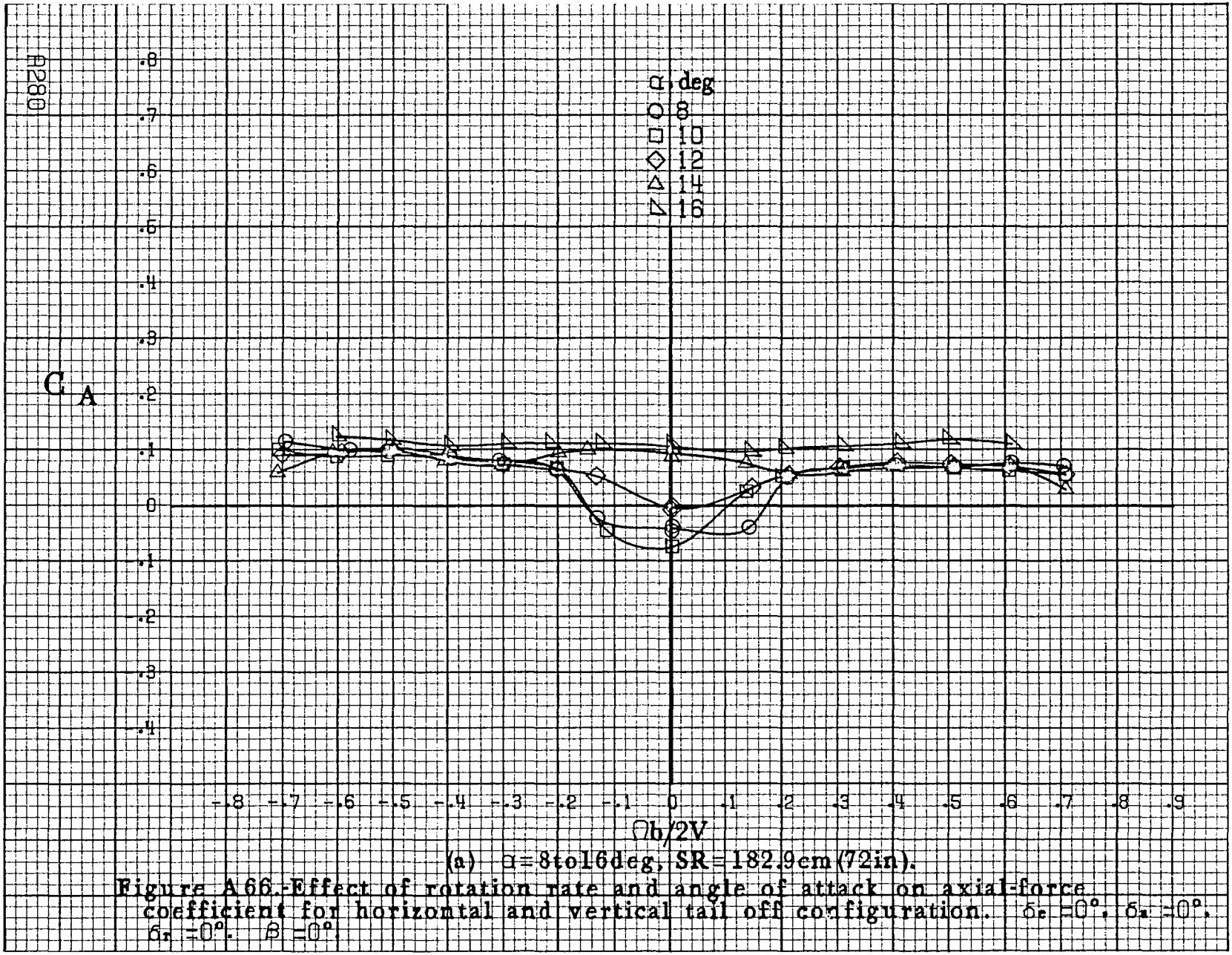

(a) $\alpha = 8$ to 16 deg, SR = 182.9 cm (72 in).

Figure A66.-Effect of rotation rate and angle of attack on axial-force coefficient for horizontal and vertical tail off configuration. $\delta_e = 0°$, $\delta_a = 0°$, $\delta_r = 0°$, $\beta = 0°$.

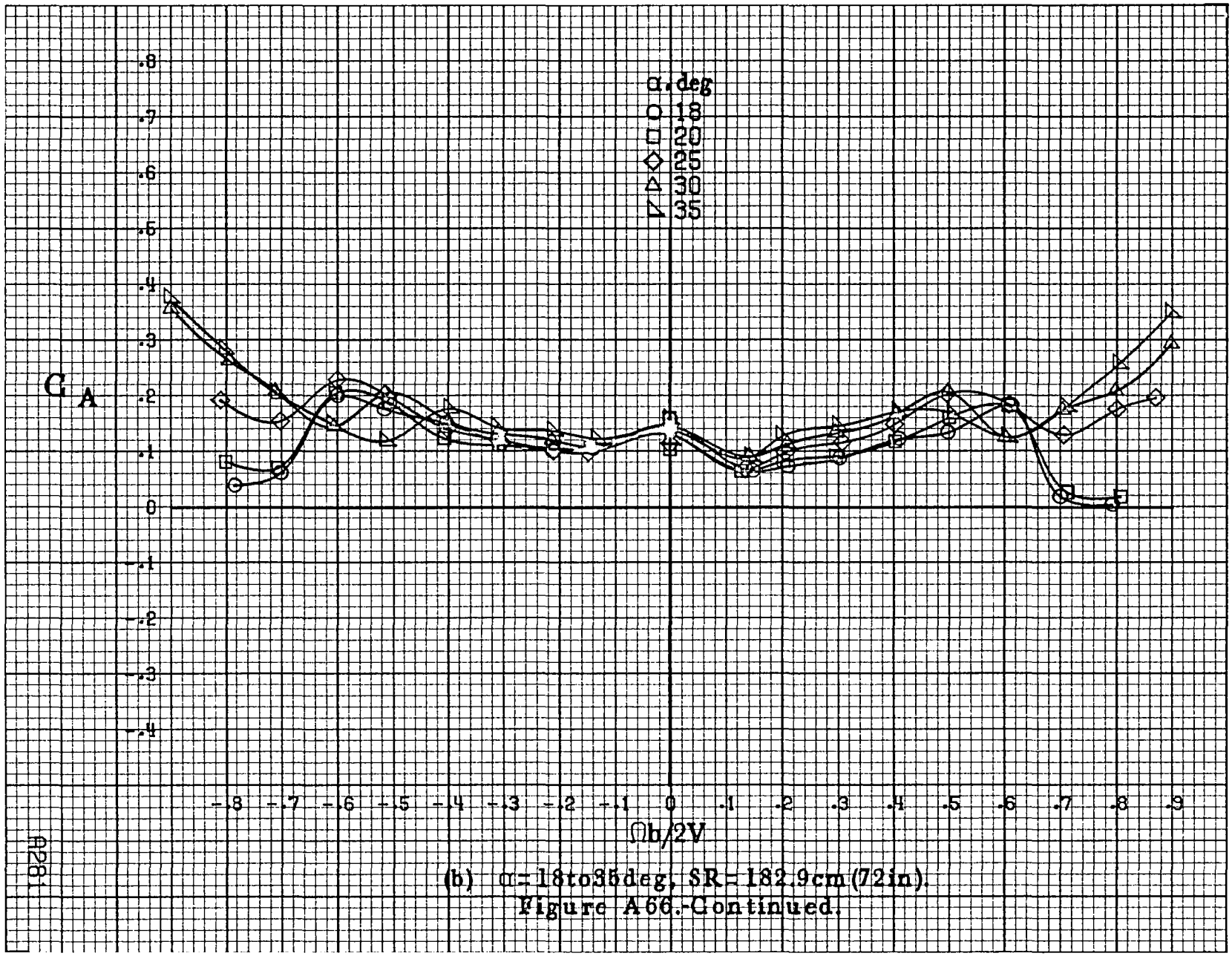

(b) α = 18 to 35 deg; SR = 182.9 cm (72 in).

Figure A66.-Continued.

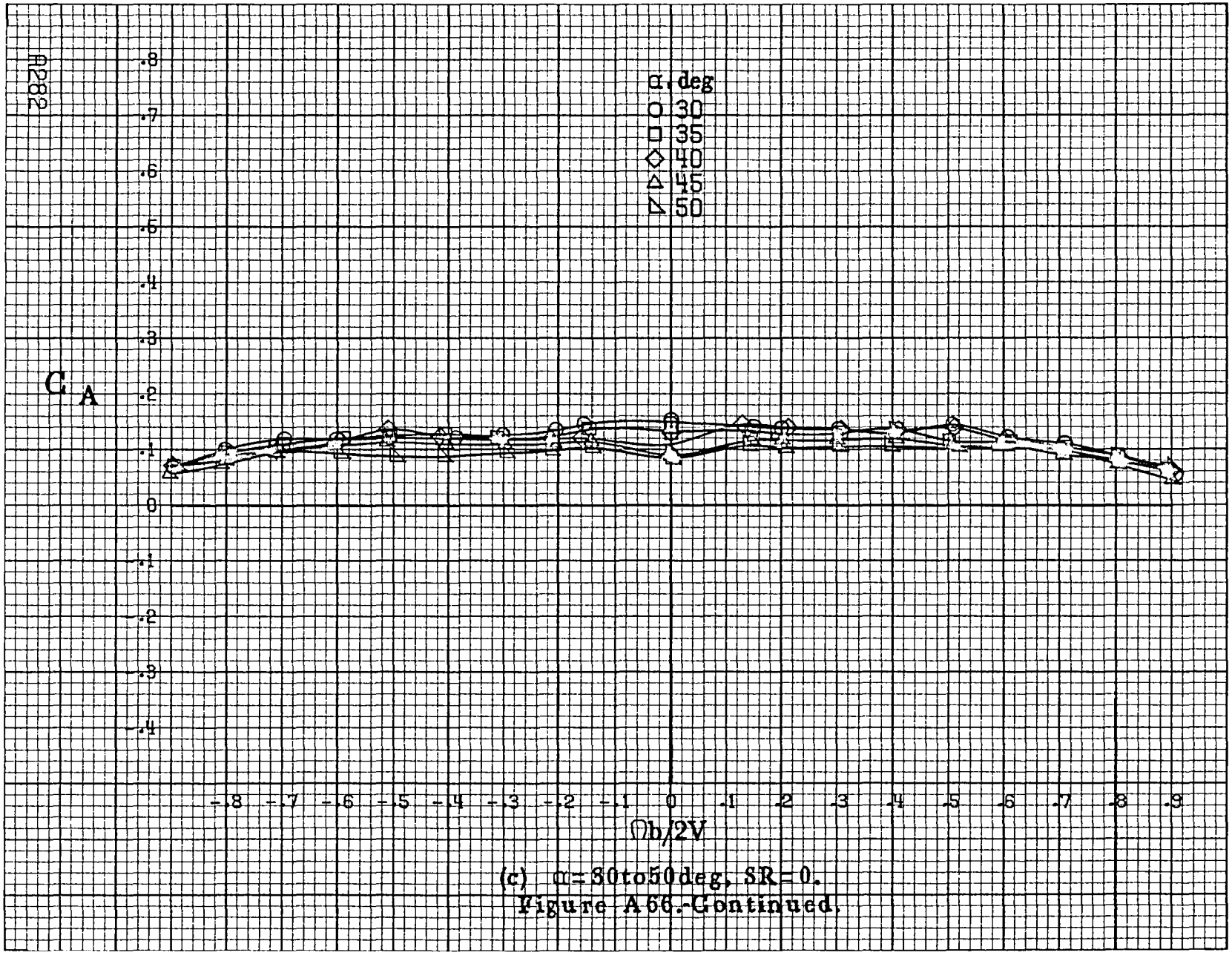

(c) $\alpha = 30$ to 50 deg, SR = 0.

Figure A66.-Continued.

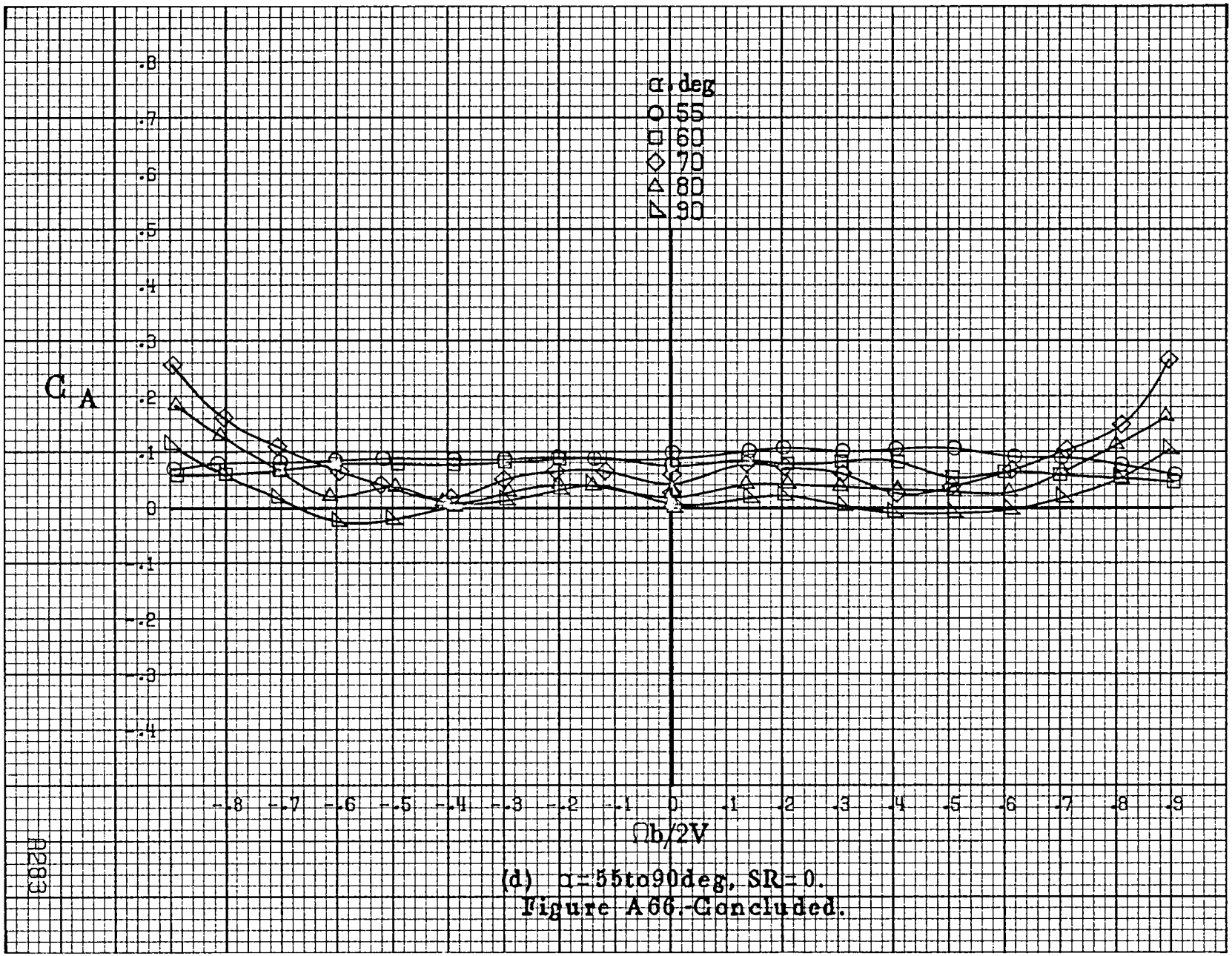

(d) α=55to90deg, SR=0.

Figure A66.-Concluded.

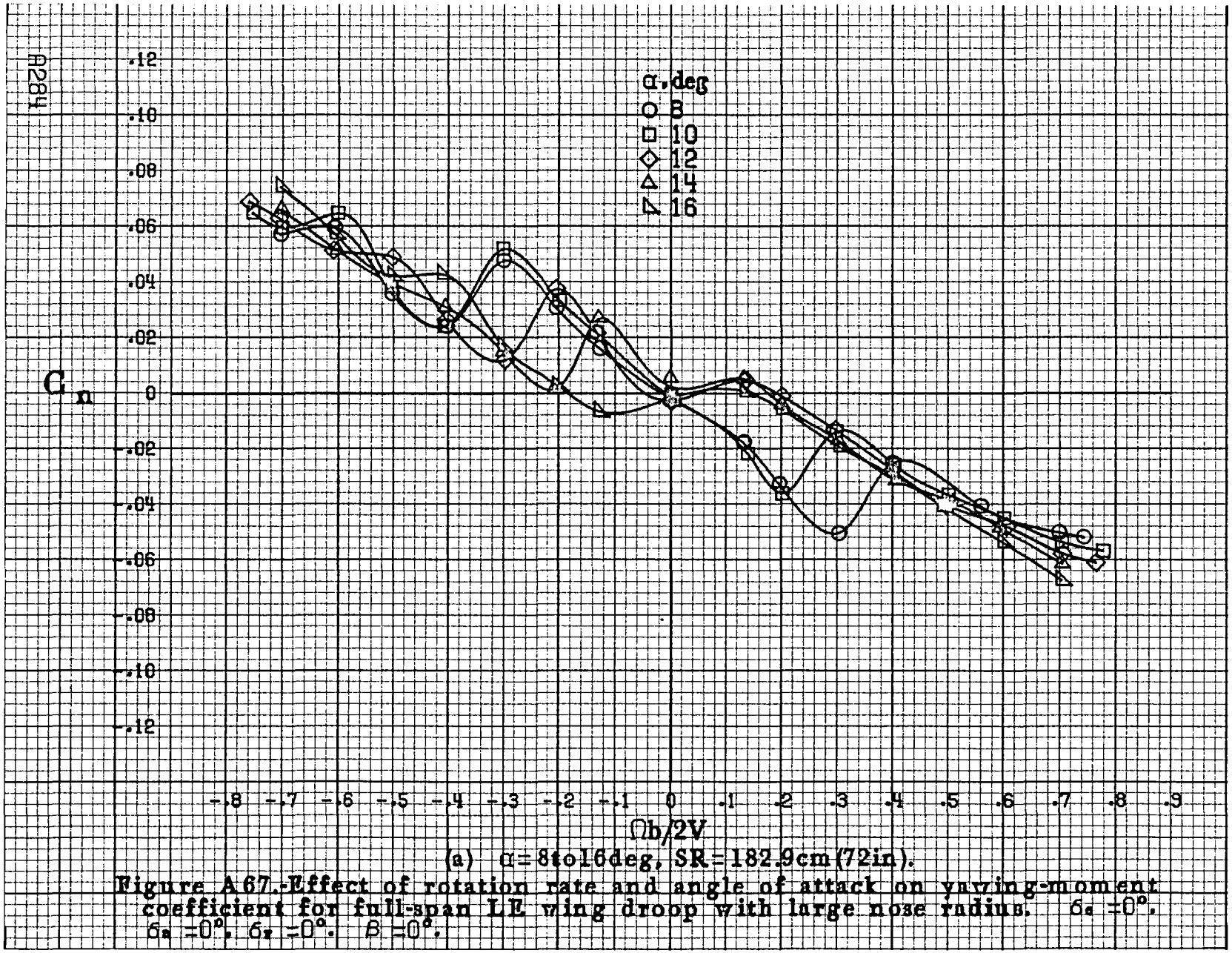

(a) $\alpha = 8$ to 16 deg, SR = 182.9 cm (72 in.).

Figure A67.-Effect of rotation rate and angle of attack on yawing-moment coefficient for full-span LE wing droop with large nose radius. $\delta_e = 0°$, $\delta_a = 0°$, $\delta_r = 0°$, $\beta = 0°$.

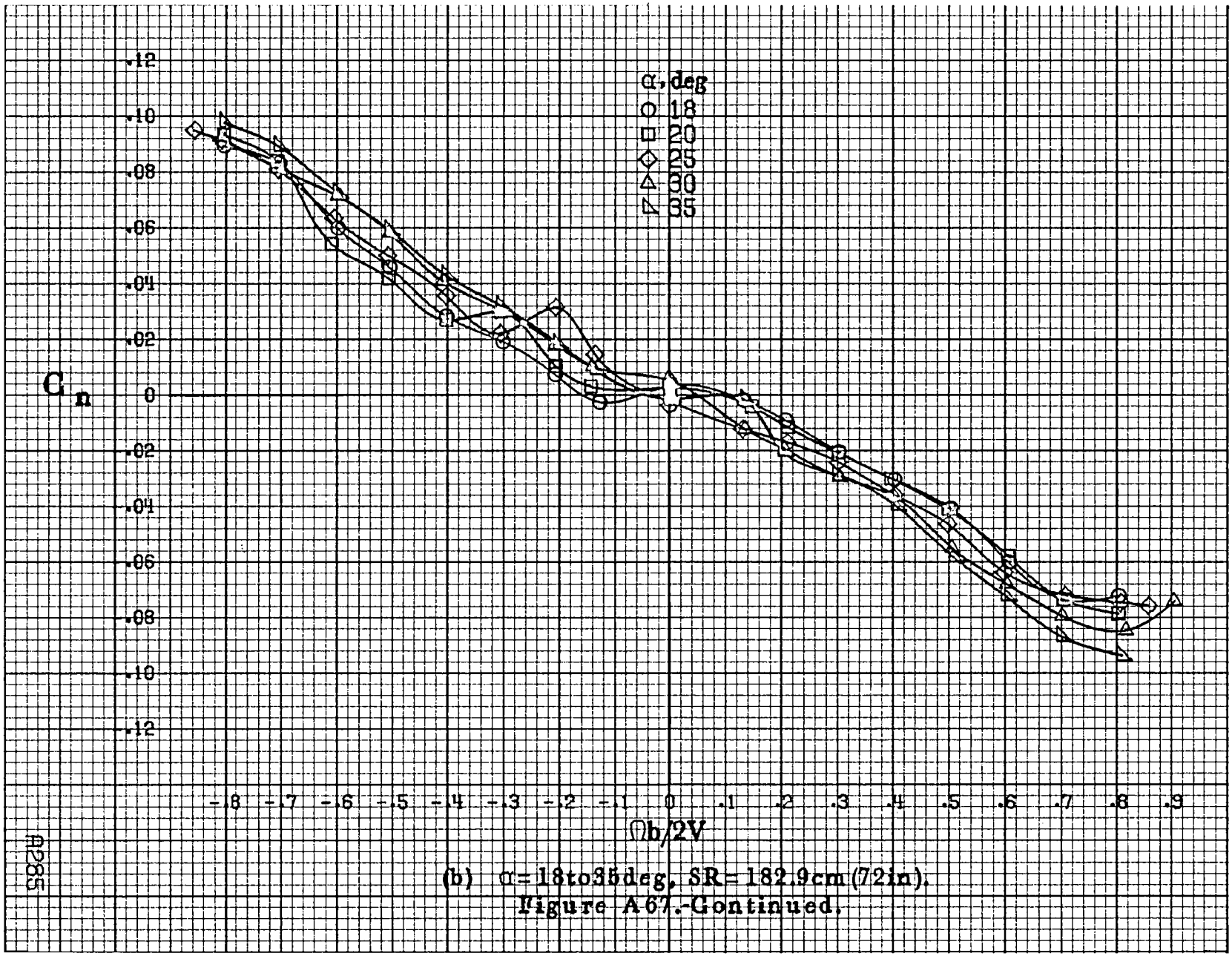

(b) α = 18 to 35 deg, SR = 182.9 cm (72 in).

Figure A67.-Continued.

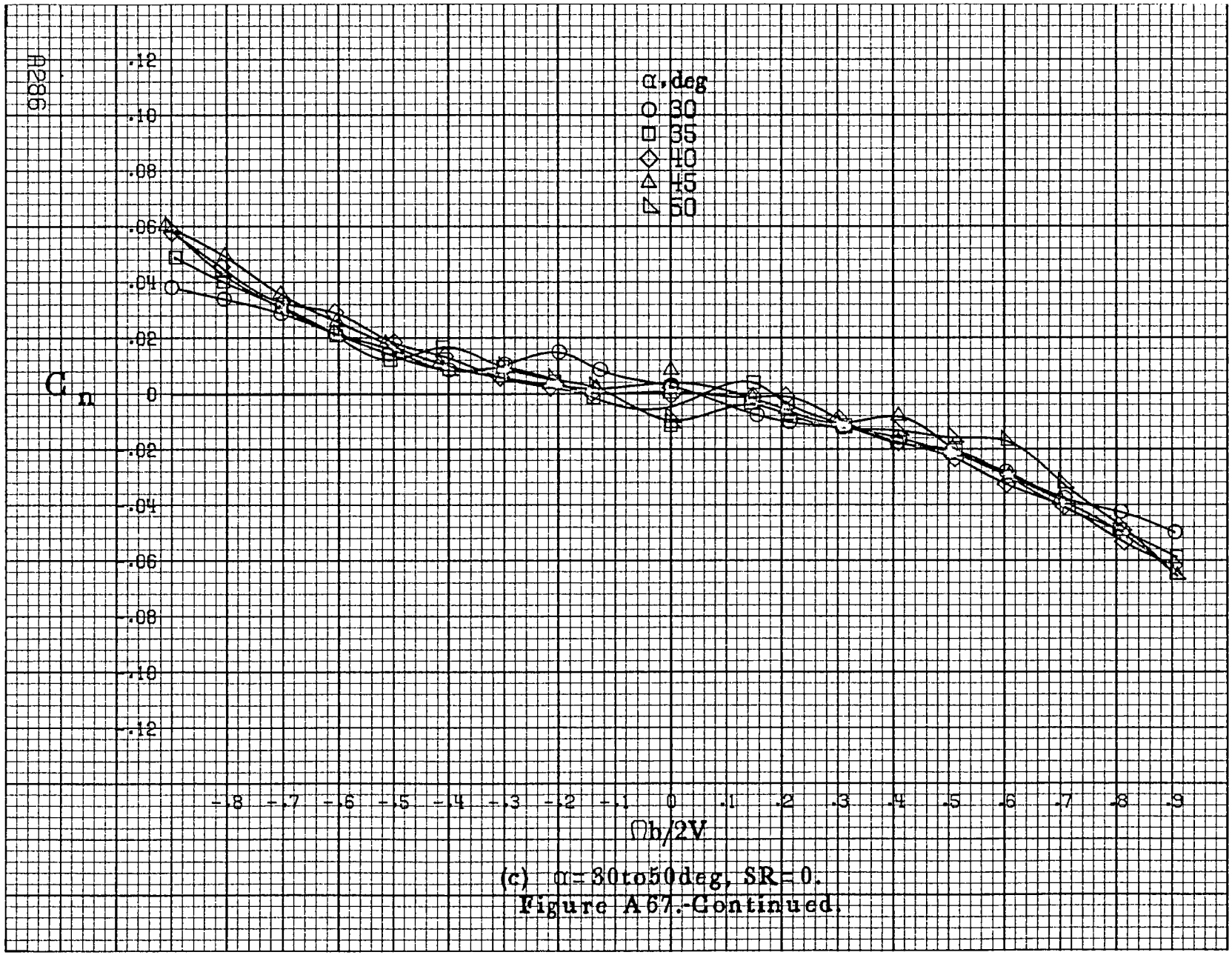

(c) α = 30 to 50 deg, SR = 0.

Figure A67.-Continued.

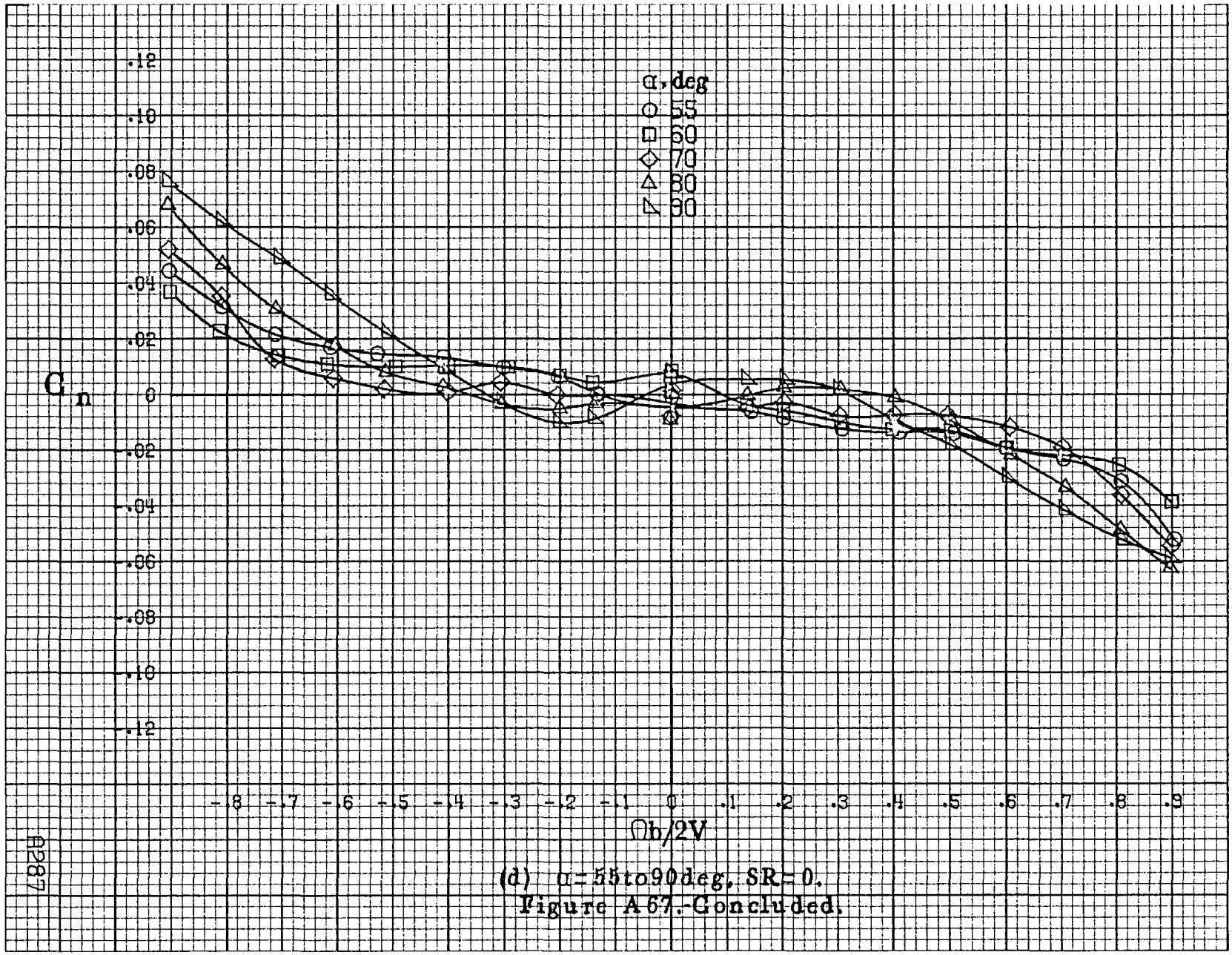

(d) $\alpha = 55$ to 90 deg, SR = 0.

Figure A67.-Concluded.

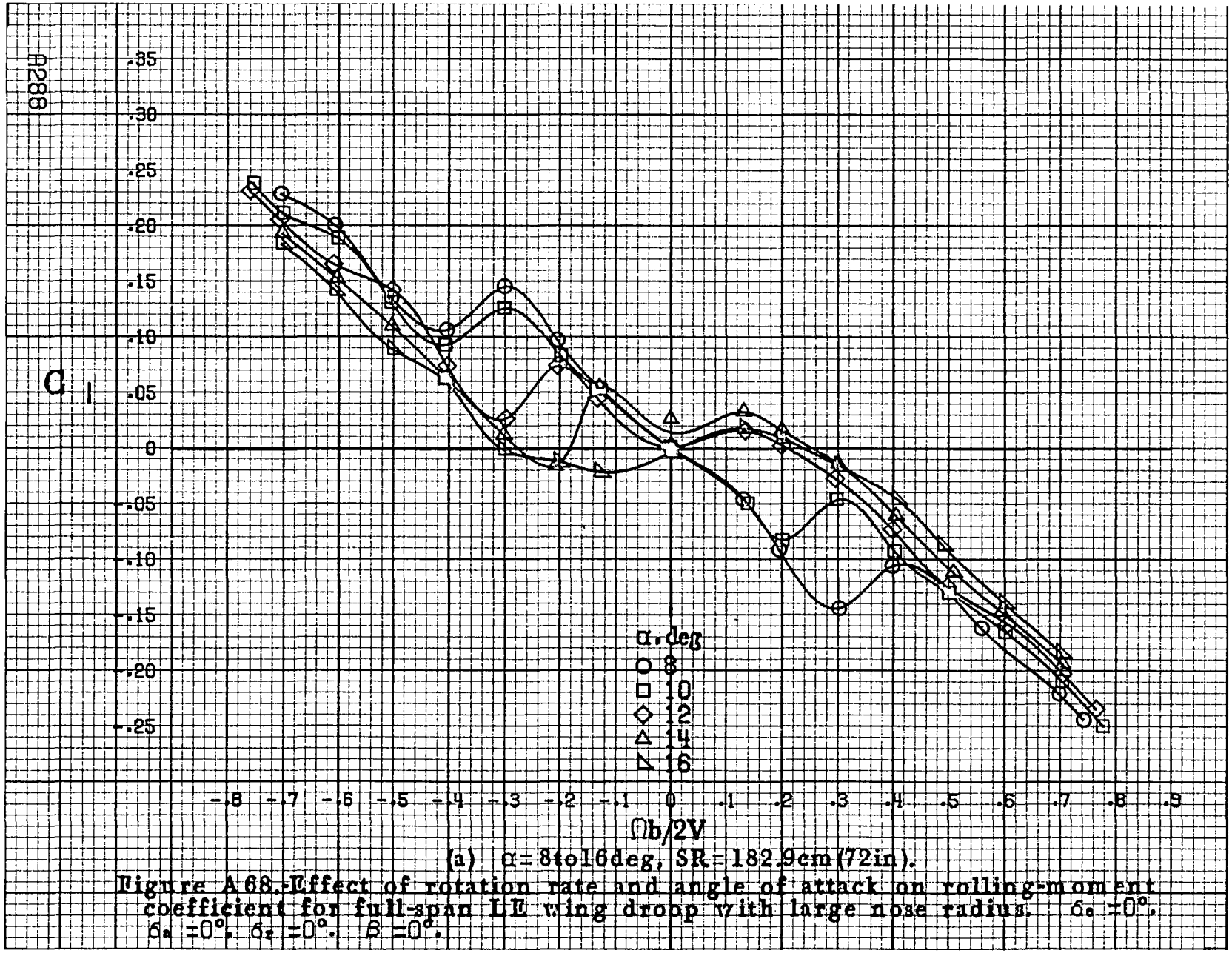

(a) α=8to16deg, SR=182.9cm(72in).

Figure A68.-Effect of rotation rate and angle of attack on rolling-moment coefficient for full-span LE wing droop with large nose radius. $\delta_a = 0°$, $\delta_s = 0°$, $\delta_r = 0°$, $\beta = 0°$.

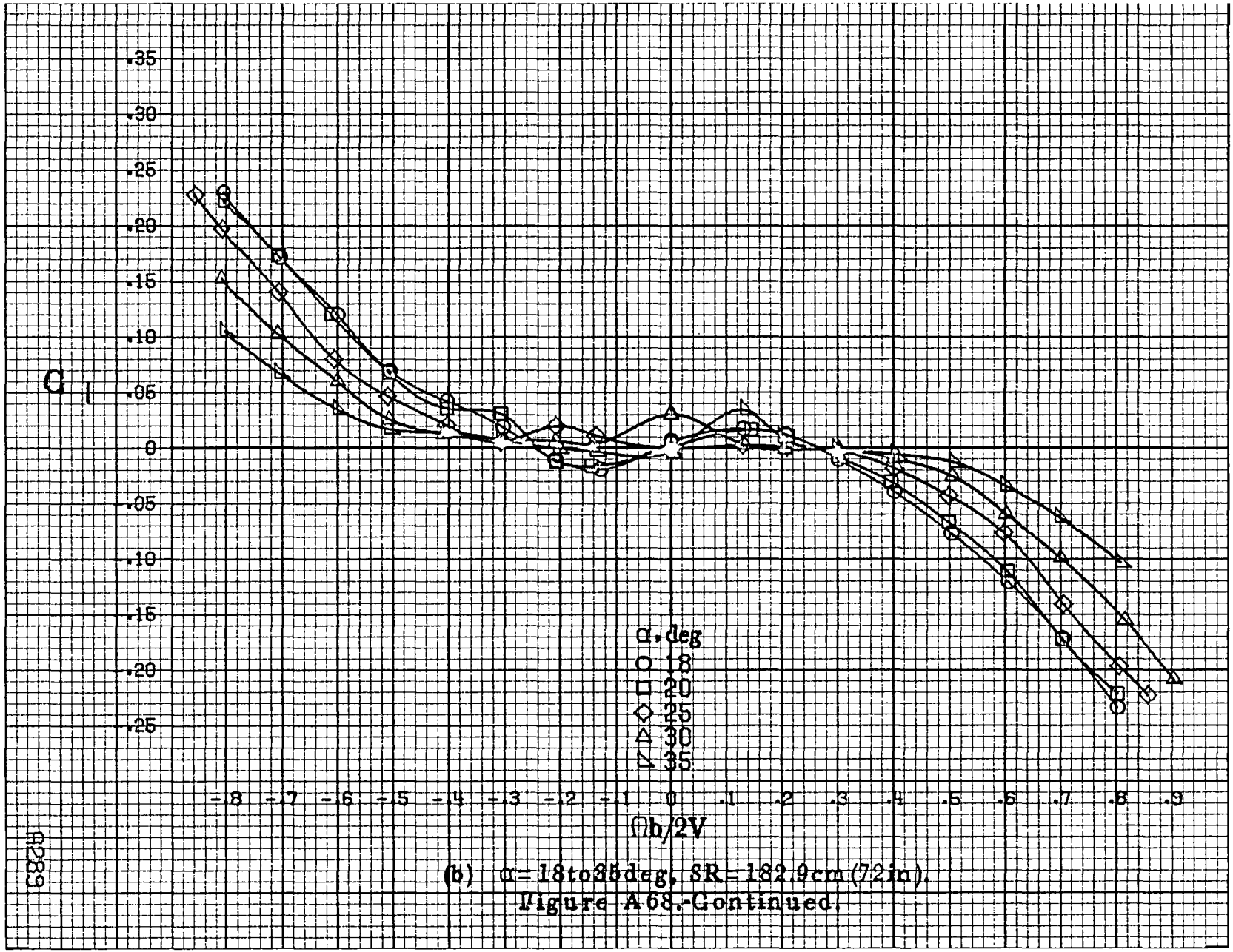

(b) α = 18 to 35 deg, SR = 182.9 cm (72 in).

Figure A68.-Continued.

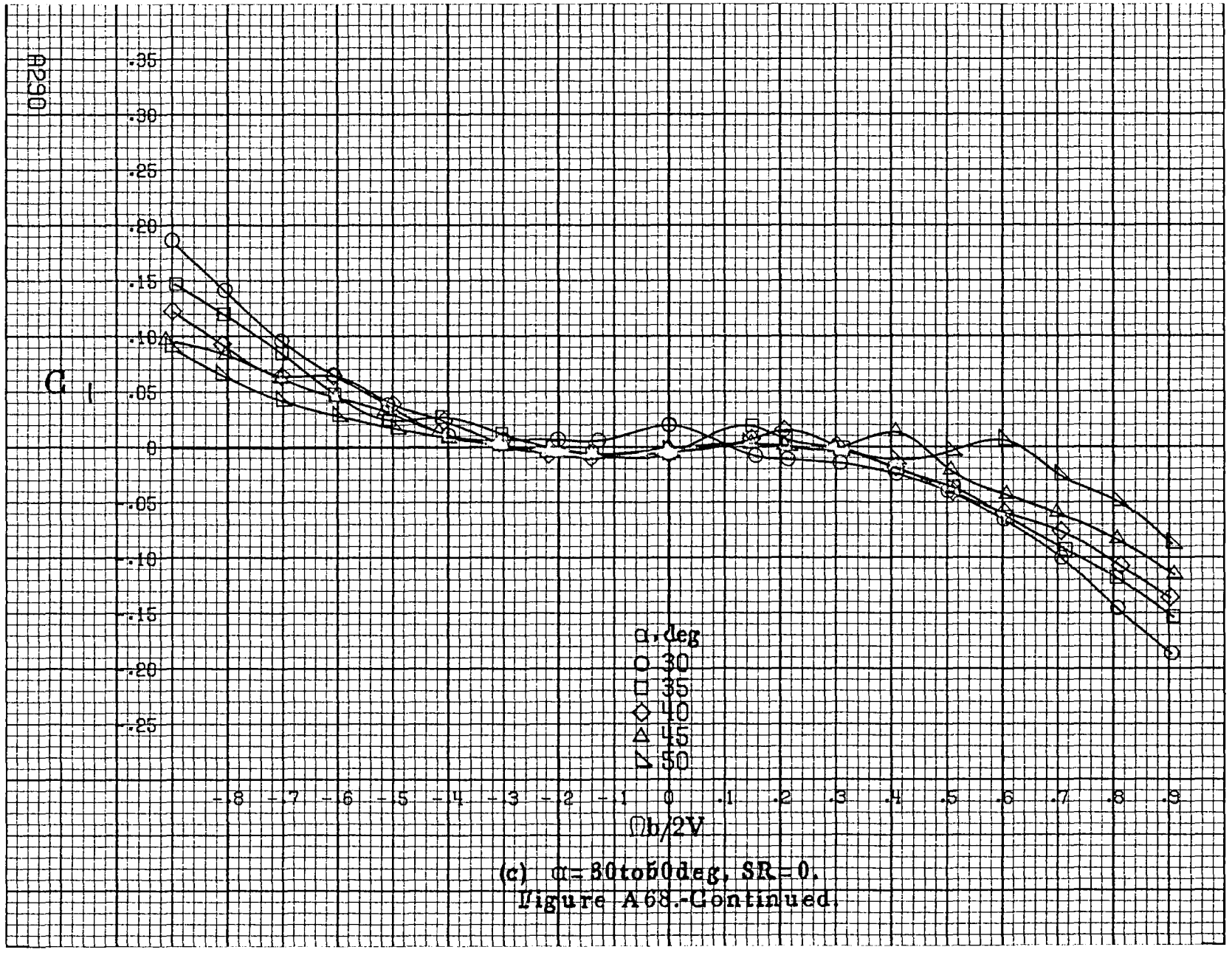

(c) $\alpha = 30$ to 60 deg, $SR = 0$.

Figure A68.-Continued.

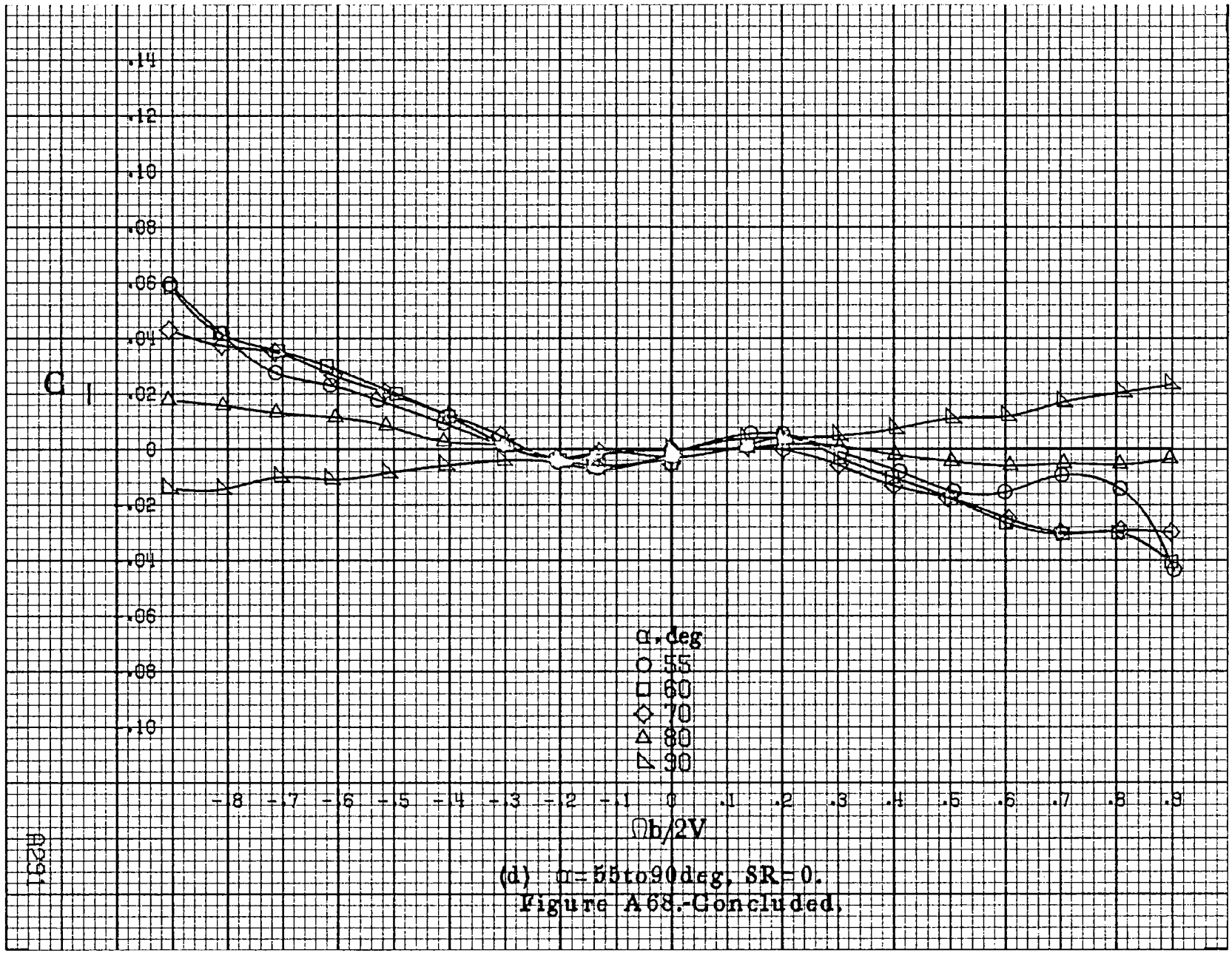

(d) α = 55 to 90 deg, SR = 0.

Figure A68.-Concluded.

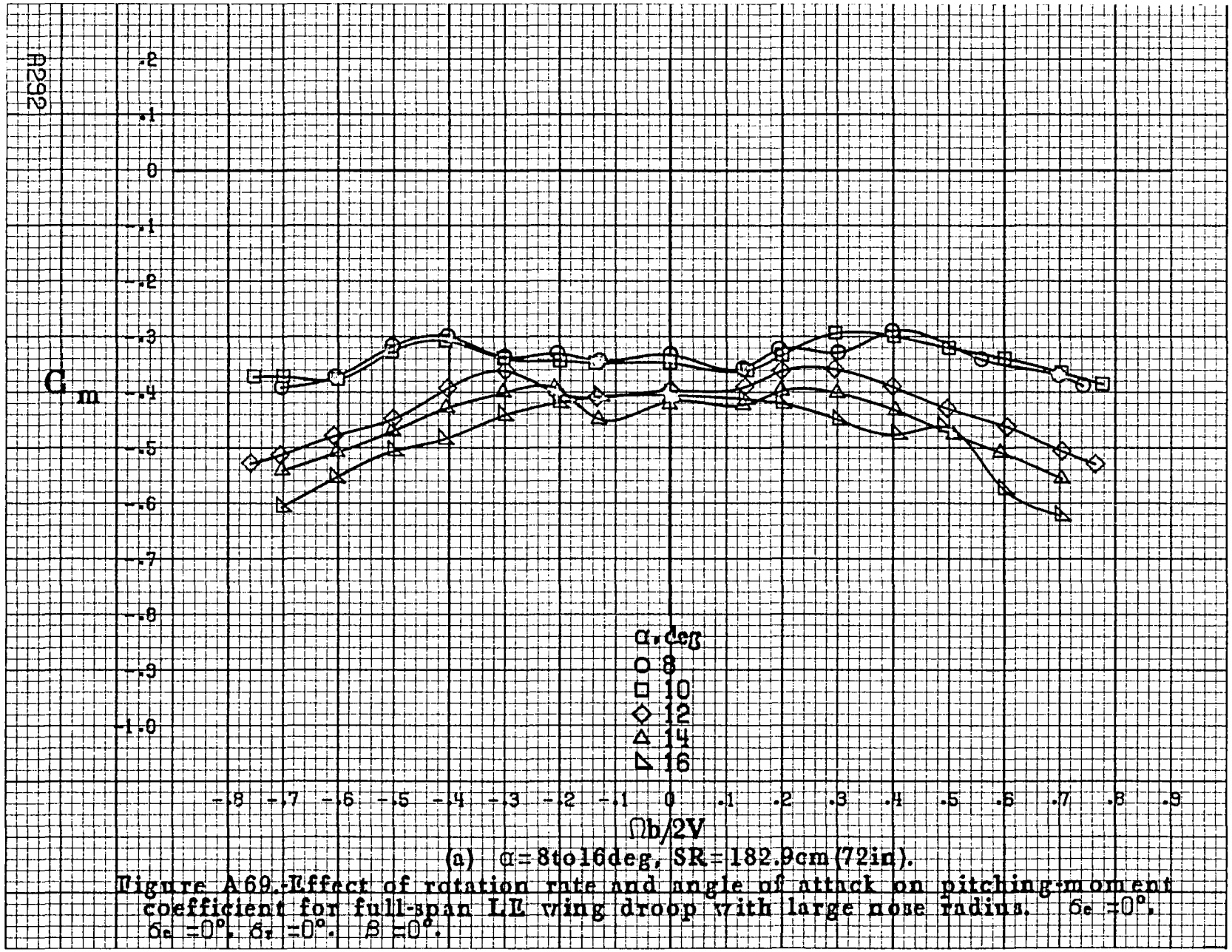

(a) α = 8 to 16 deg, SR = 182.9 cm (72 in).

Figure A69.-Effect of rotation rate and angle of attack on pitching-moment coefficient for full-span LE wing droop with large nose radius. $\delta_e = 0°$, $\delta_a = 0°$, $\delta_r = 0°$, $\beta = 0°$.

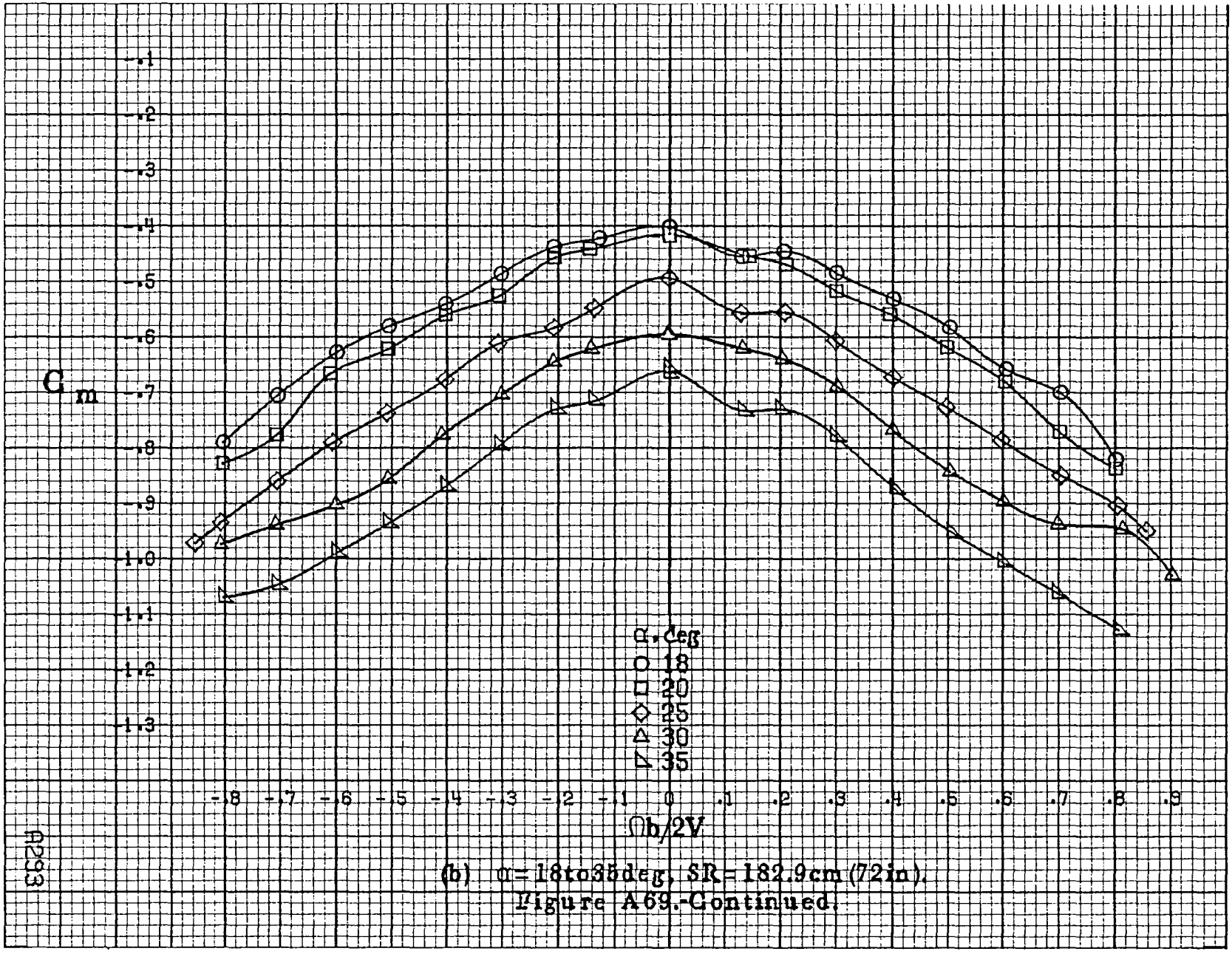

(b) $\alpha = 18$ to 35 deg, SR = 182.9 cm (72 in).

Figure A69.-Continued.

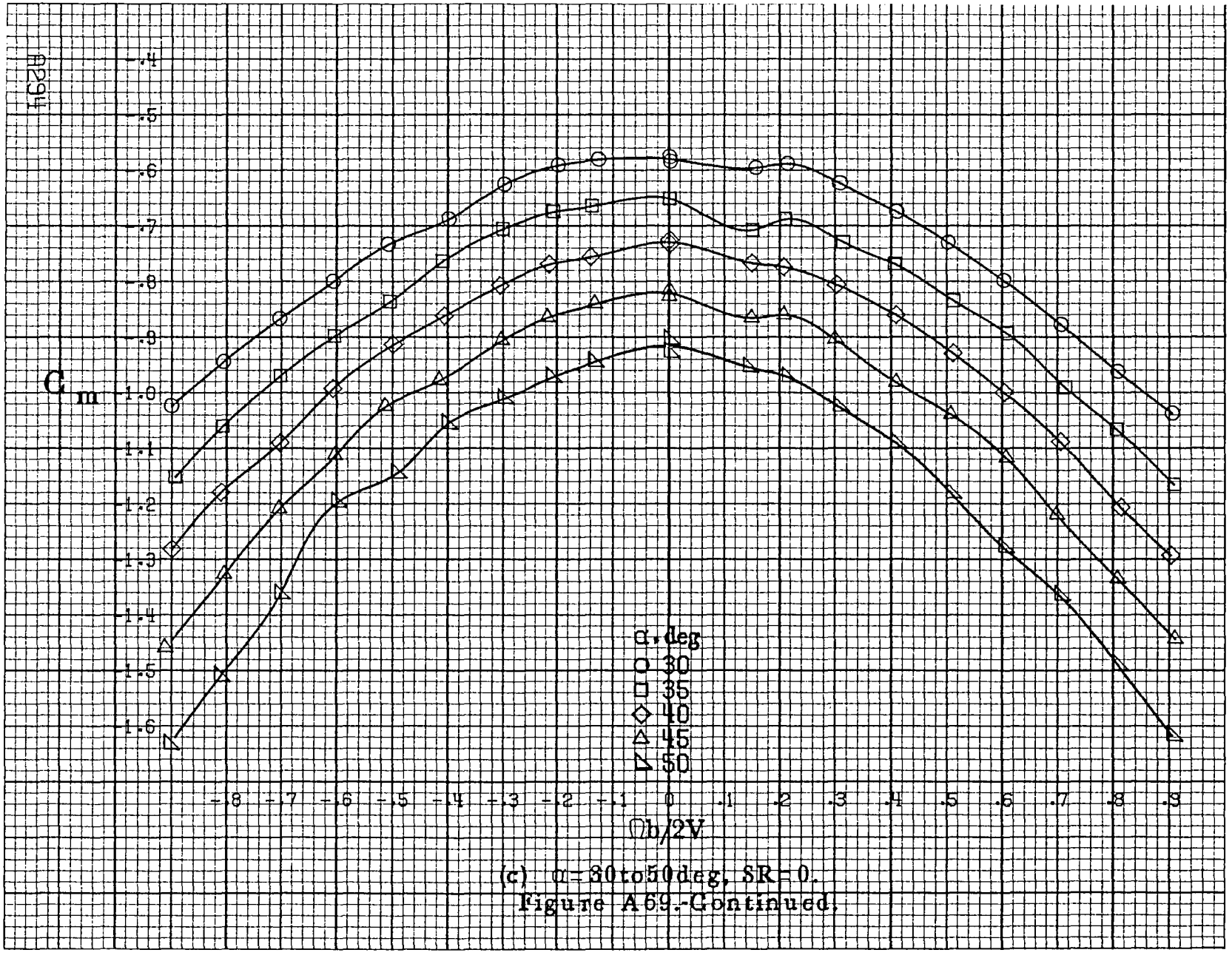

(c) $\alpha = 30$ to 50 deg, SR = 0.

Figure A69.-Continued.

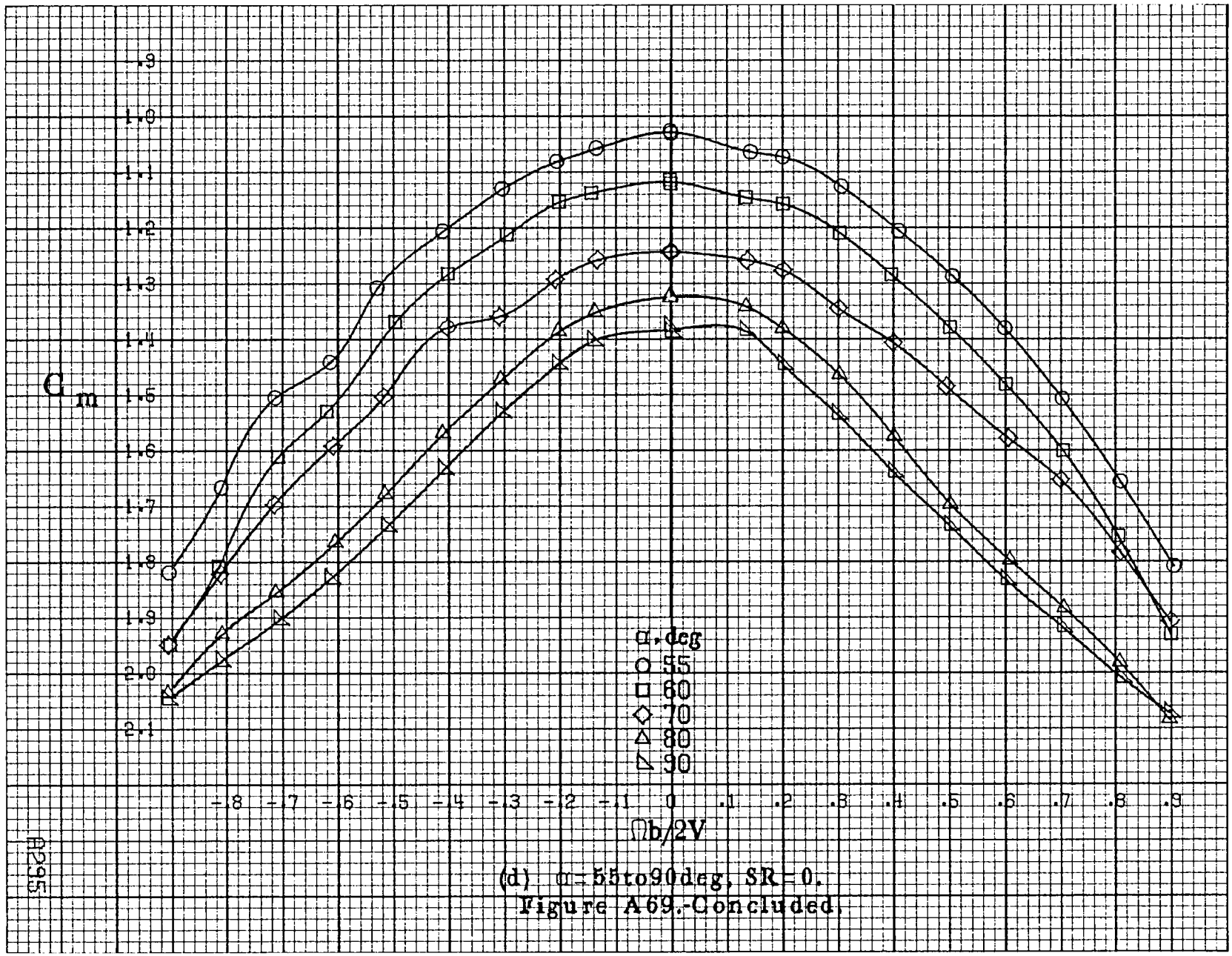

(d) $\alpha = 55$ to 90 deg; SR = 0.

Figure A69.-Concluded.

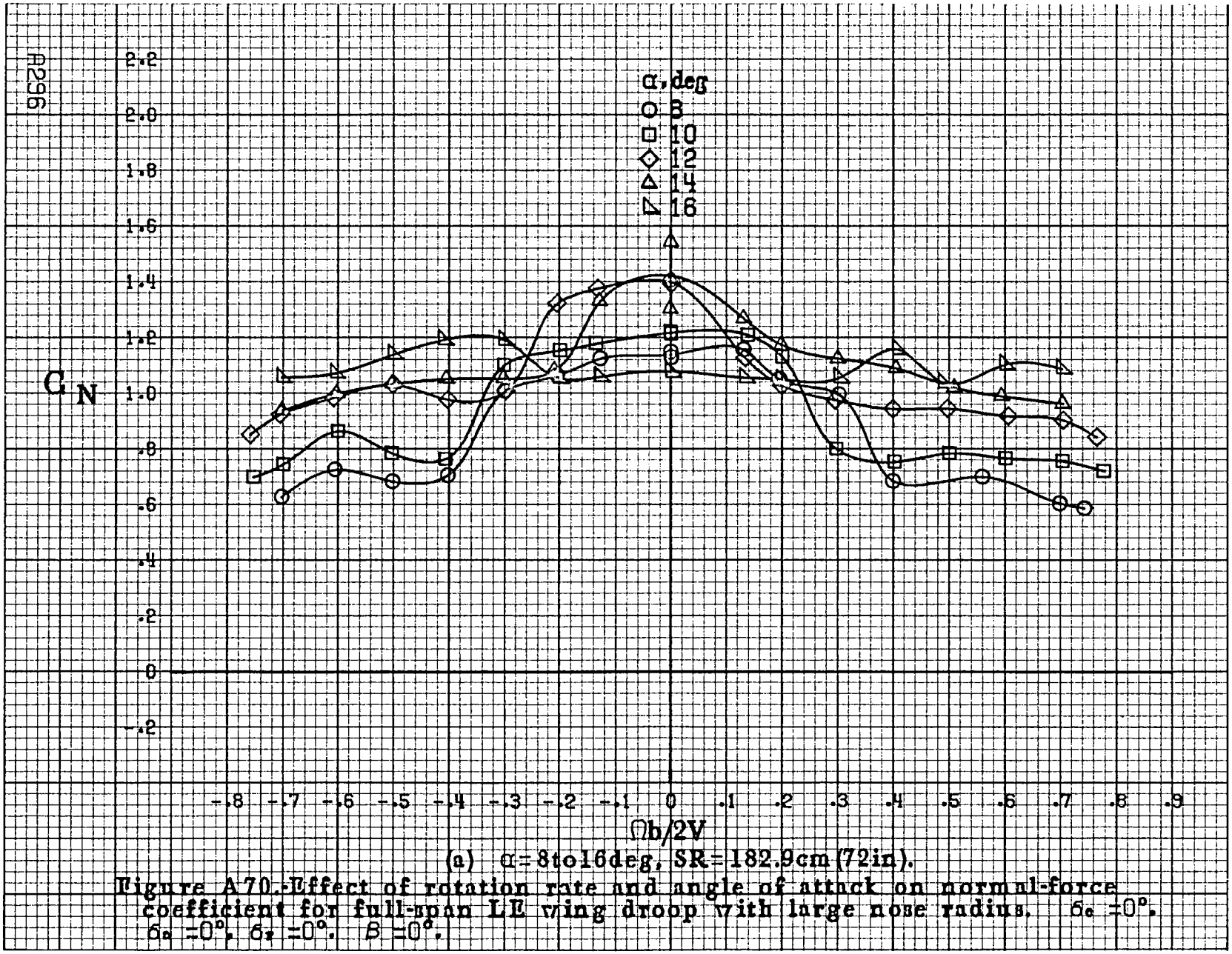

(a) α = 8 to 16 deg, SR = 182.9 cm (72 in).

Figure A70.- Effect of rotation rate and angle of attack on normal-force coefficient for full-span LE wing droop with large nose radius. $\delta_e = 0°$, $\delta_a = 0°$, $\delta_r = 0°$, $\beta = 0°$.

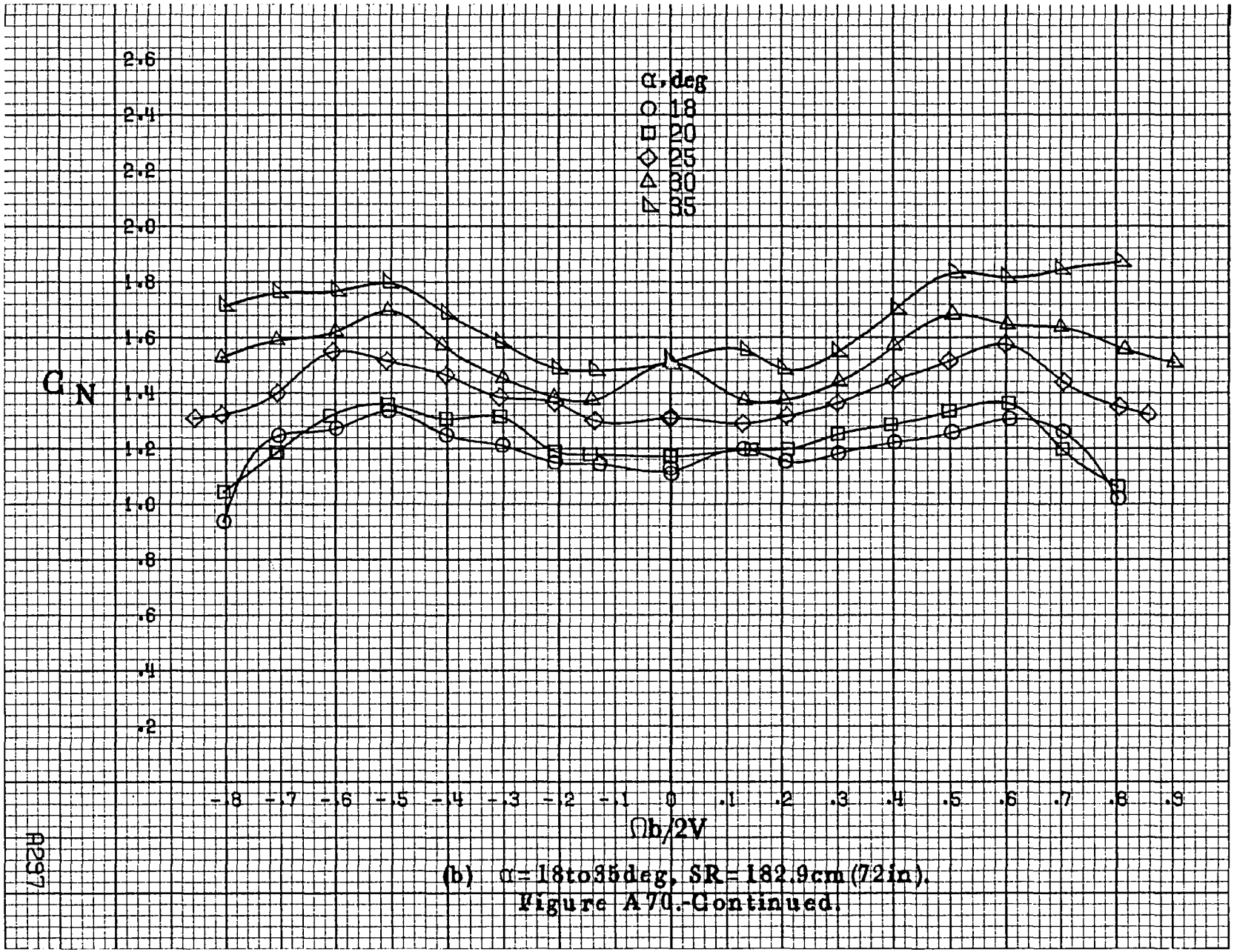

(b) $\alpha = 18$ to 35 deg, SR = 182.9 cm (72 in).

Figure A70.-Continued.

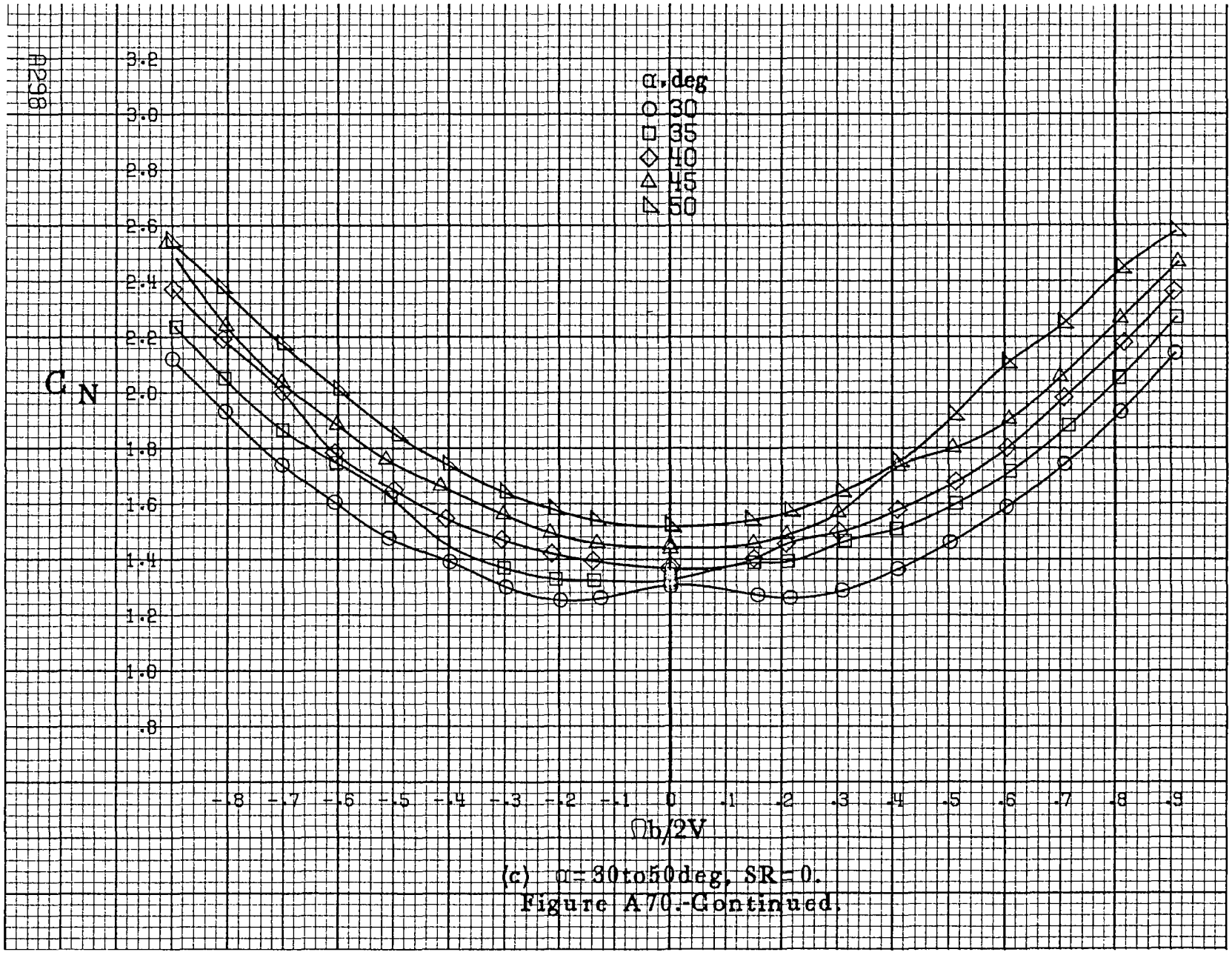

(c) α = 30 to 50 deg, SR = 0.

Figure A70.-Continued.

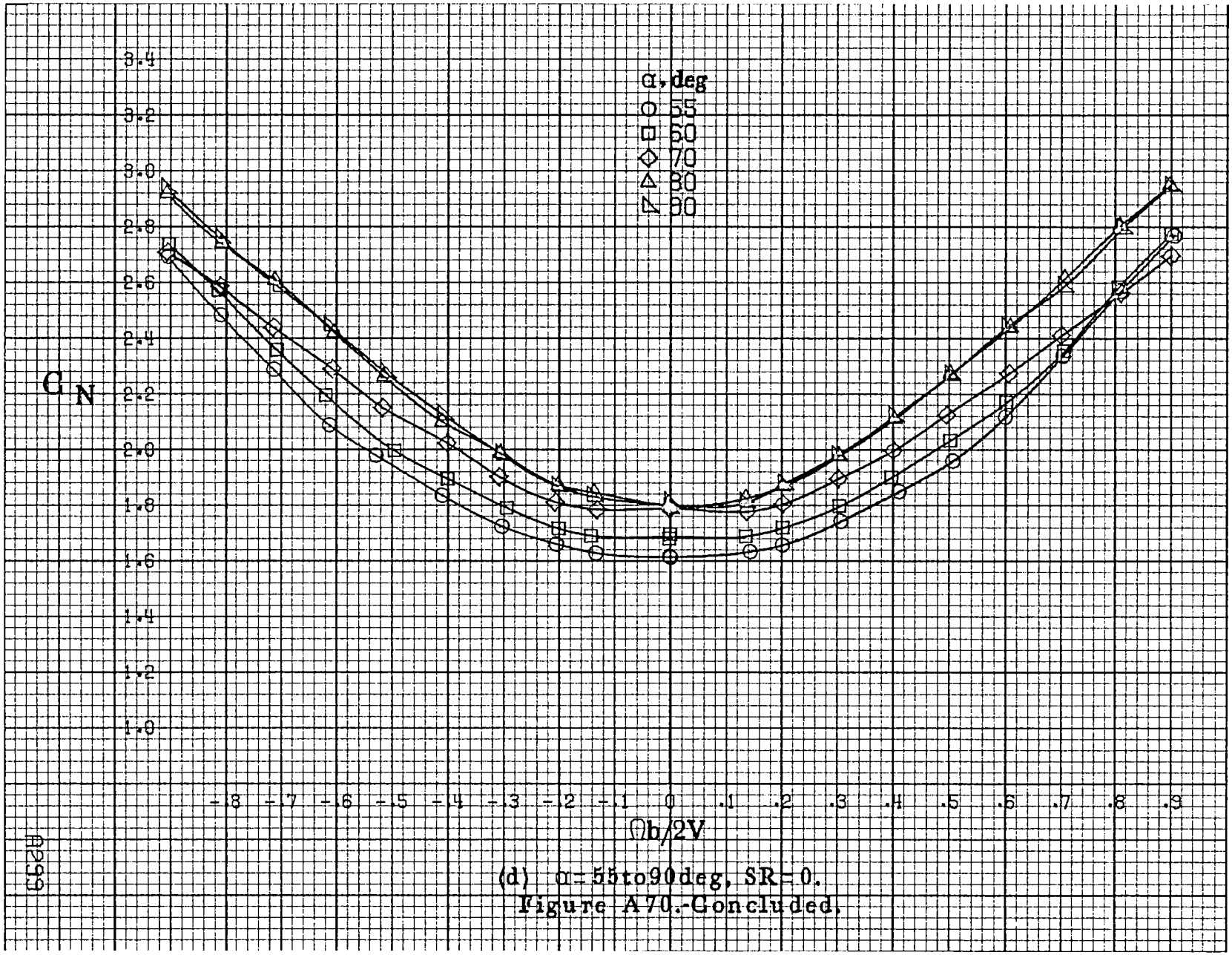

(d) α = 55 to 90 deg, SR = 0.

Figure A70.-Concluded.

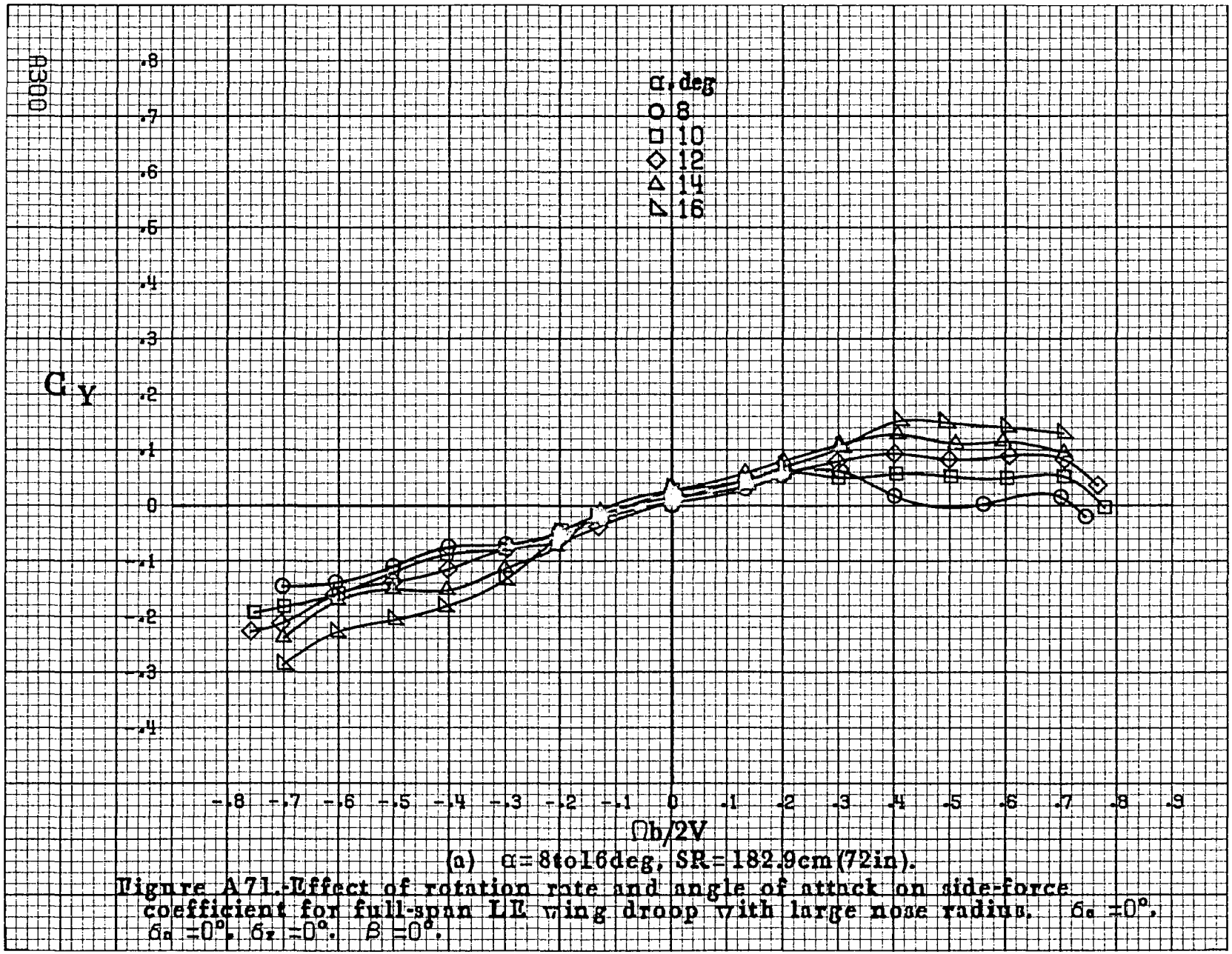

(a) $\alpha = 8$ to 16 deg, SR = 182.9 cm (72 in).

Figure A71.-Effect of rotation rate and angle of attack on side-force coefficient for full-span LE wing droop with large nose radius. $\delta_a = 0°$, $\delta_a = 0°$, $\delta_r = 0°$, $\beta = 0°$.

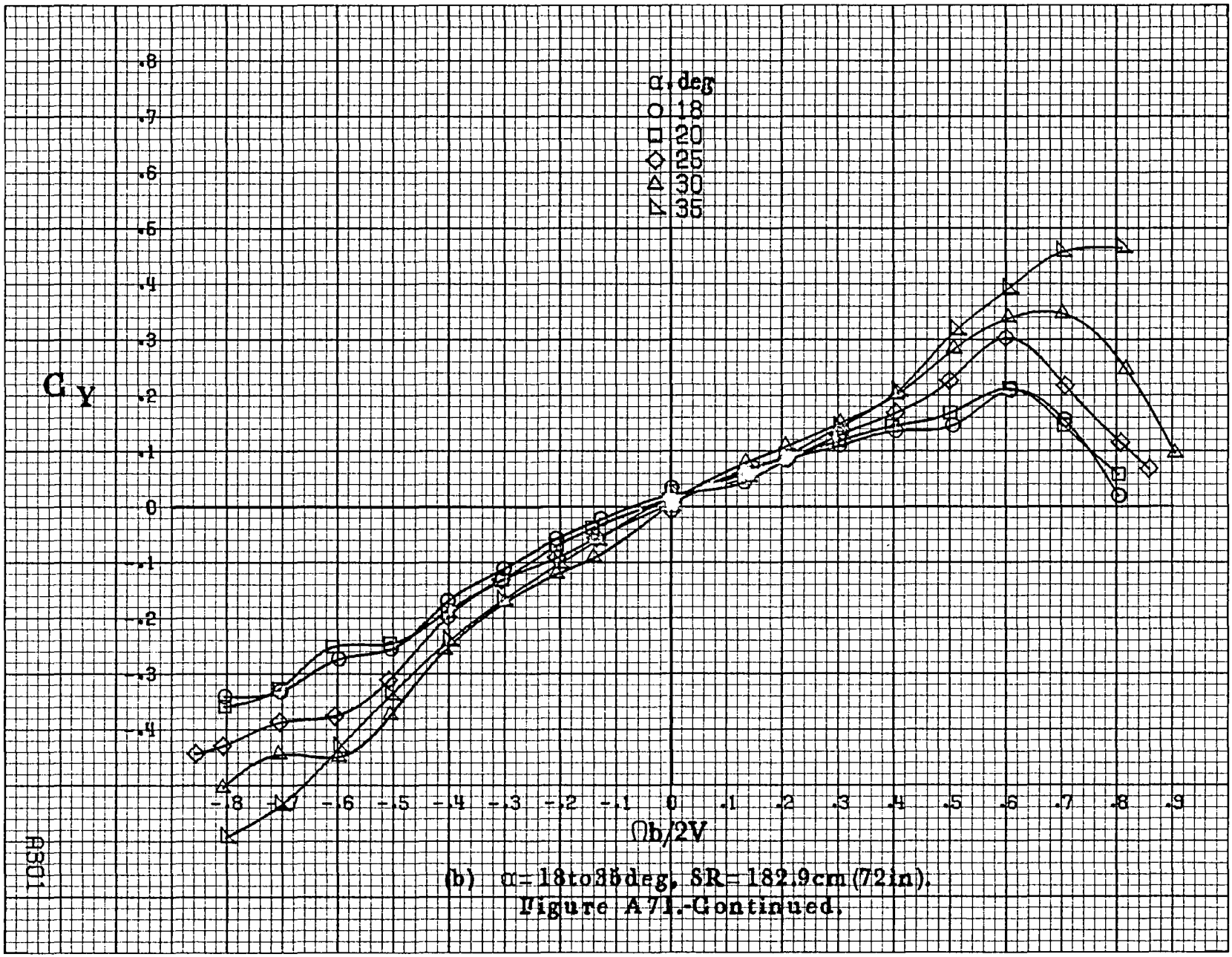

(b) $\alpha = 18$ to 35 deg, $\delta R = 182.9$ cm (72 in).

Figure A71.-Continued.

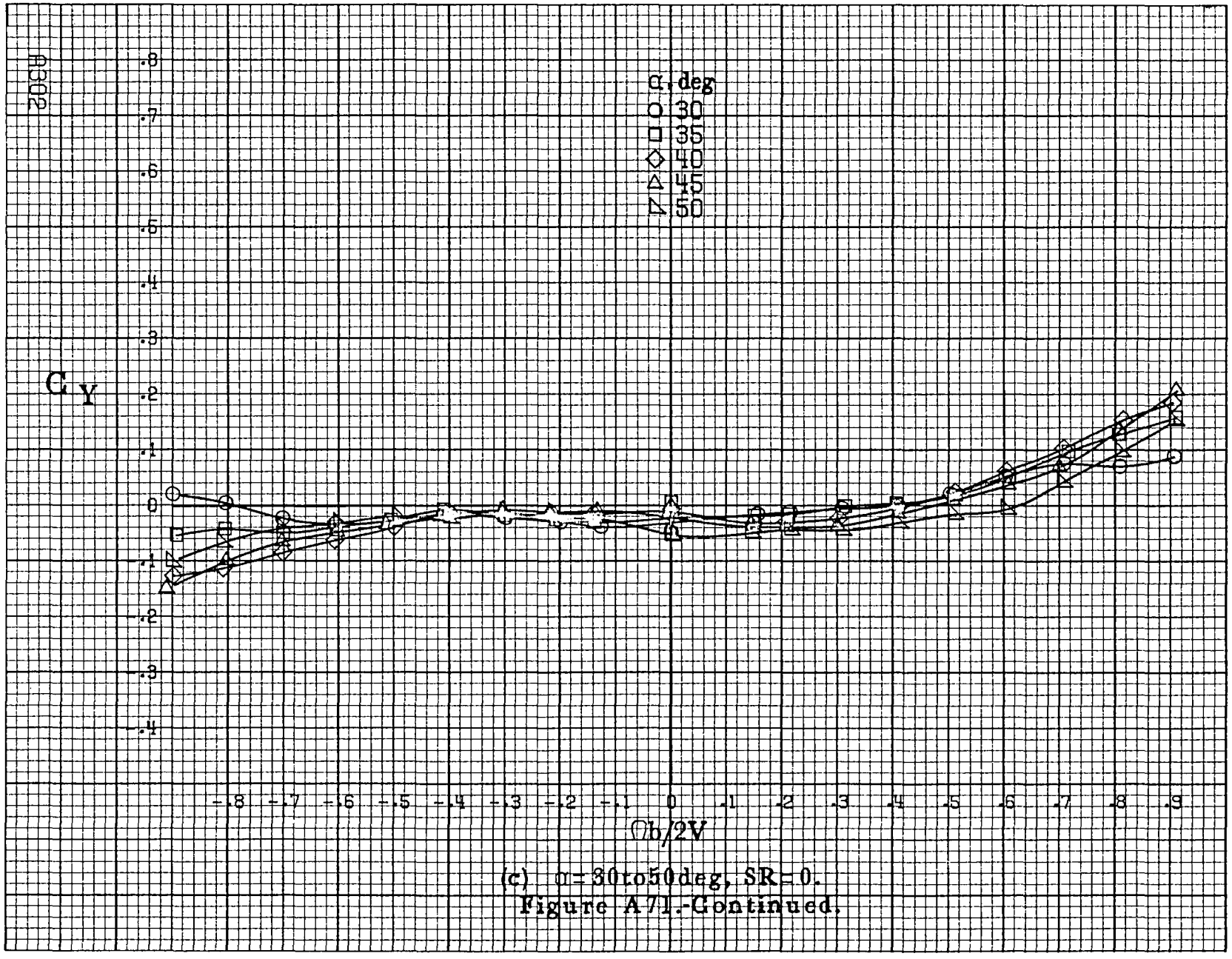

(c) α = 30 to 50 deg, SR = 0.

Figure A71.-Continued.

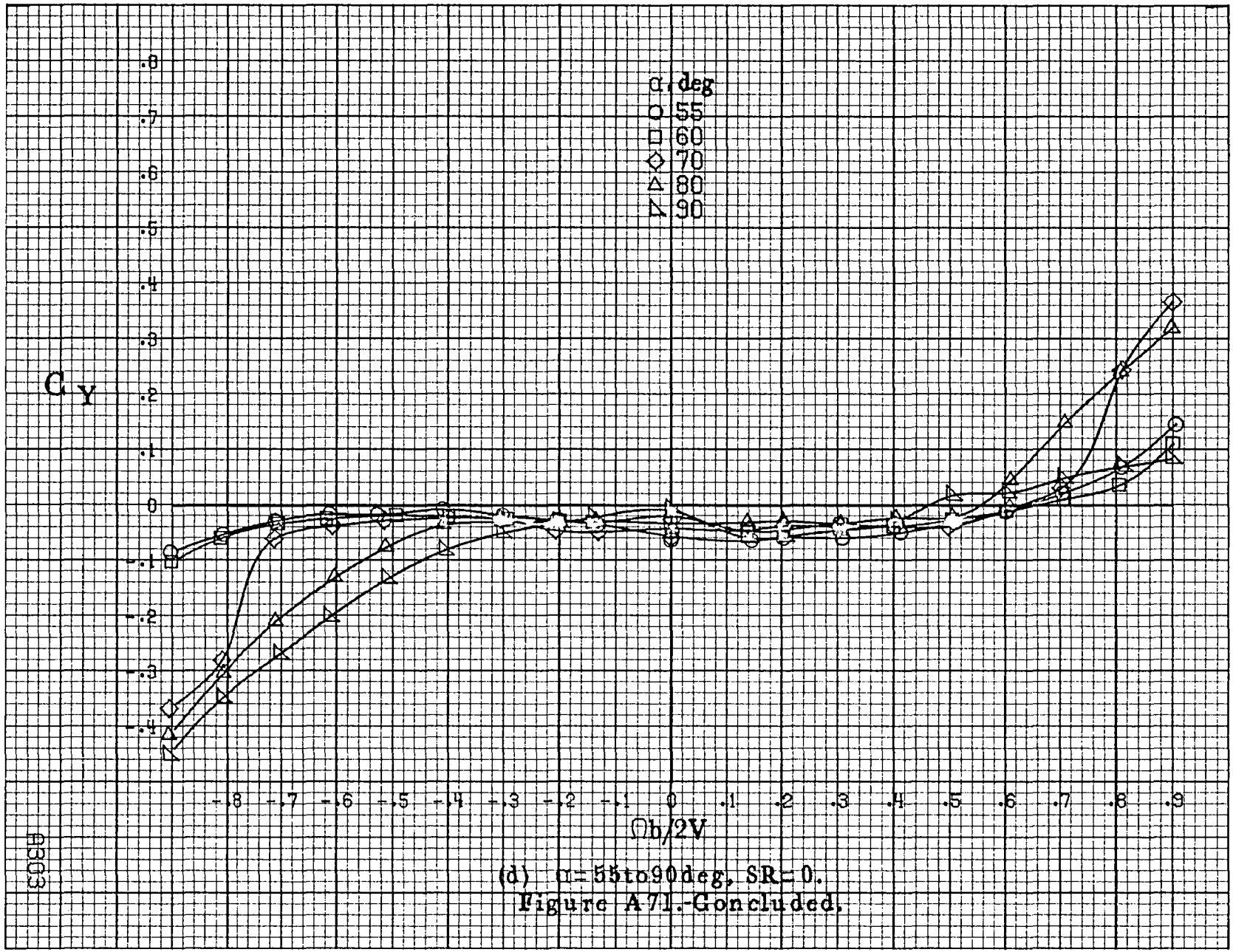

(d) $\alpha = 55$ to 90 deg, SR = 0.

Figure A71.-Concluded.

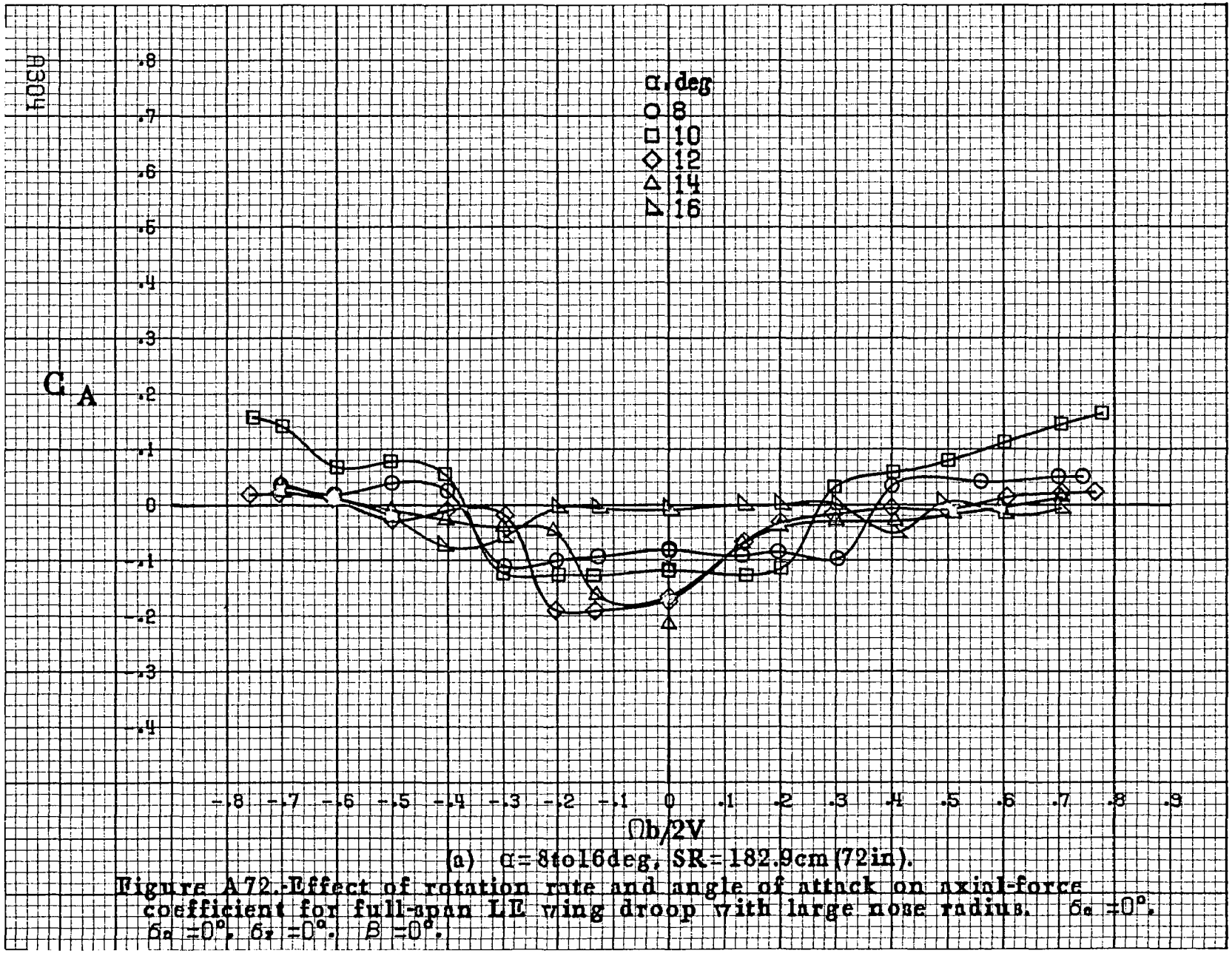

(a) α = 8 to 16 deg, SR = 182.9 cm (72 in).

Figure A72.-Effect of rotation rate and angle of attack on axial-force coefficient for full-span LE wing droop with large nose radius. $\delta_a = 0°$, $\delta_e = 0°$, $\delta_r = 0°$, $\beta = 0°$.

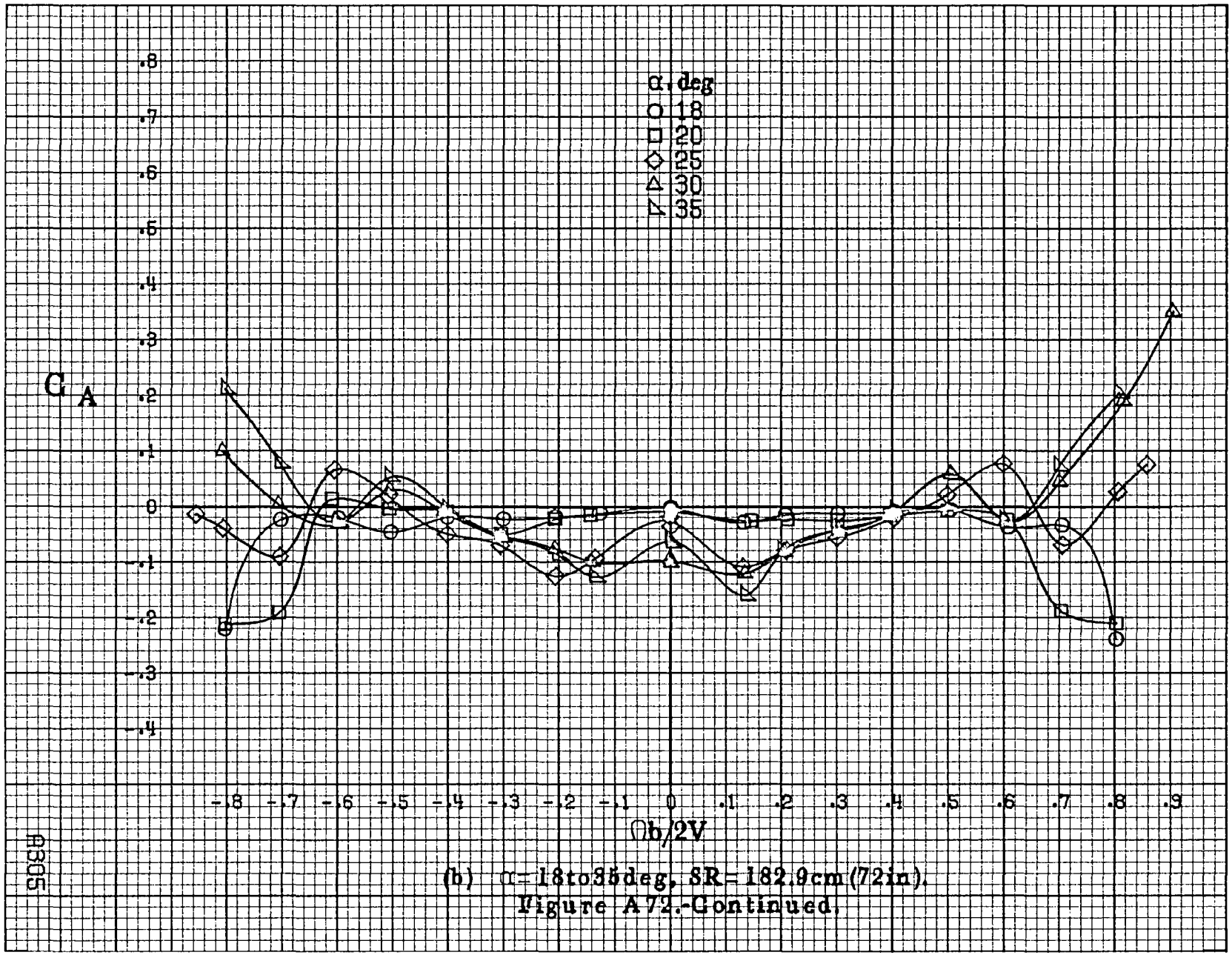

(b) α = 18 to 35 deg, S_R = 182.9 cm (72 in).

Figure A72.-Continued.

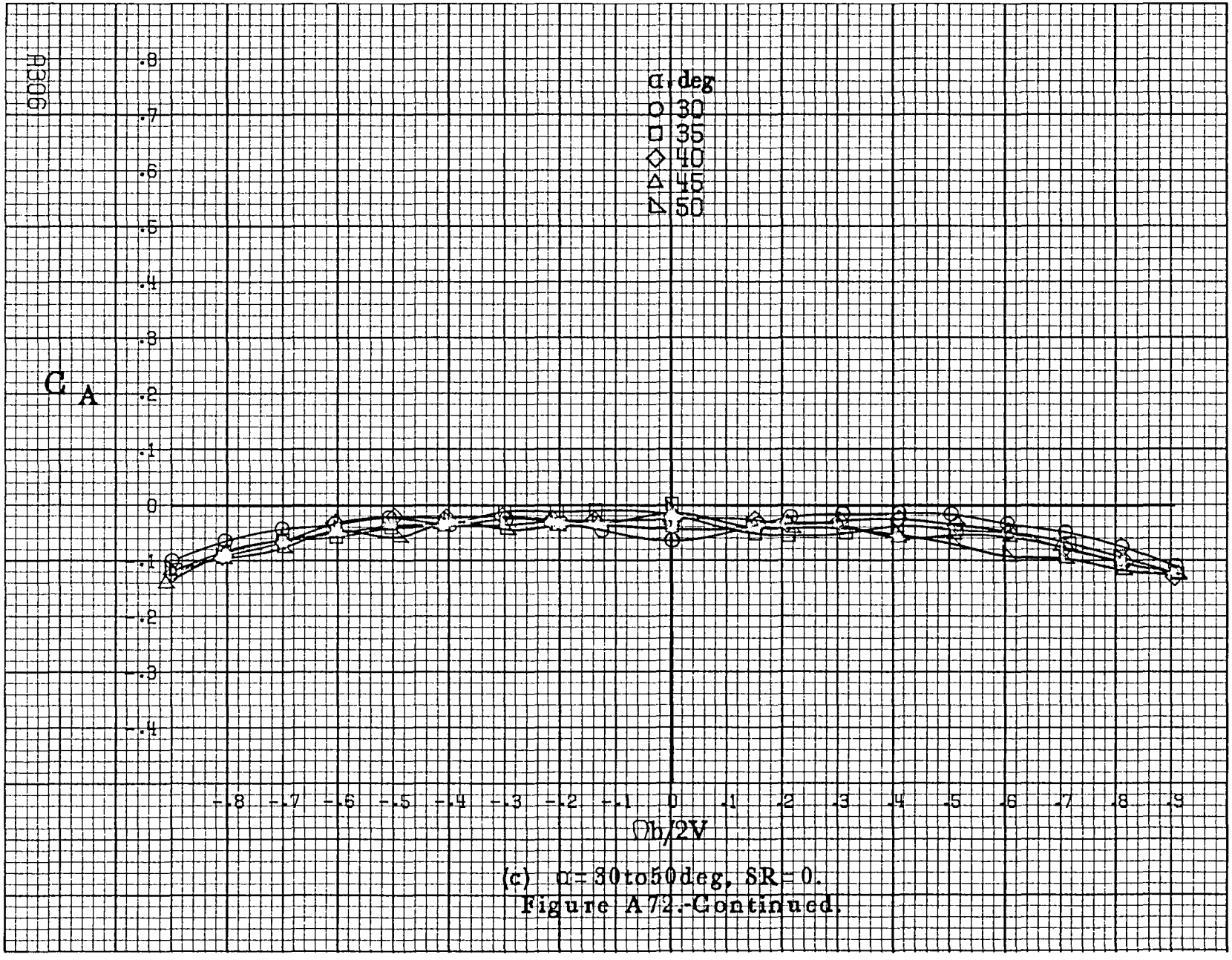

(c) α = 30 to 50 deg, SR = 0.

Figure A72.-Continued.

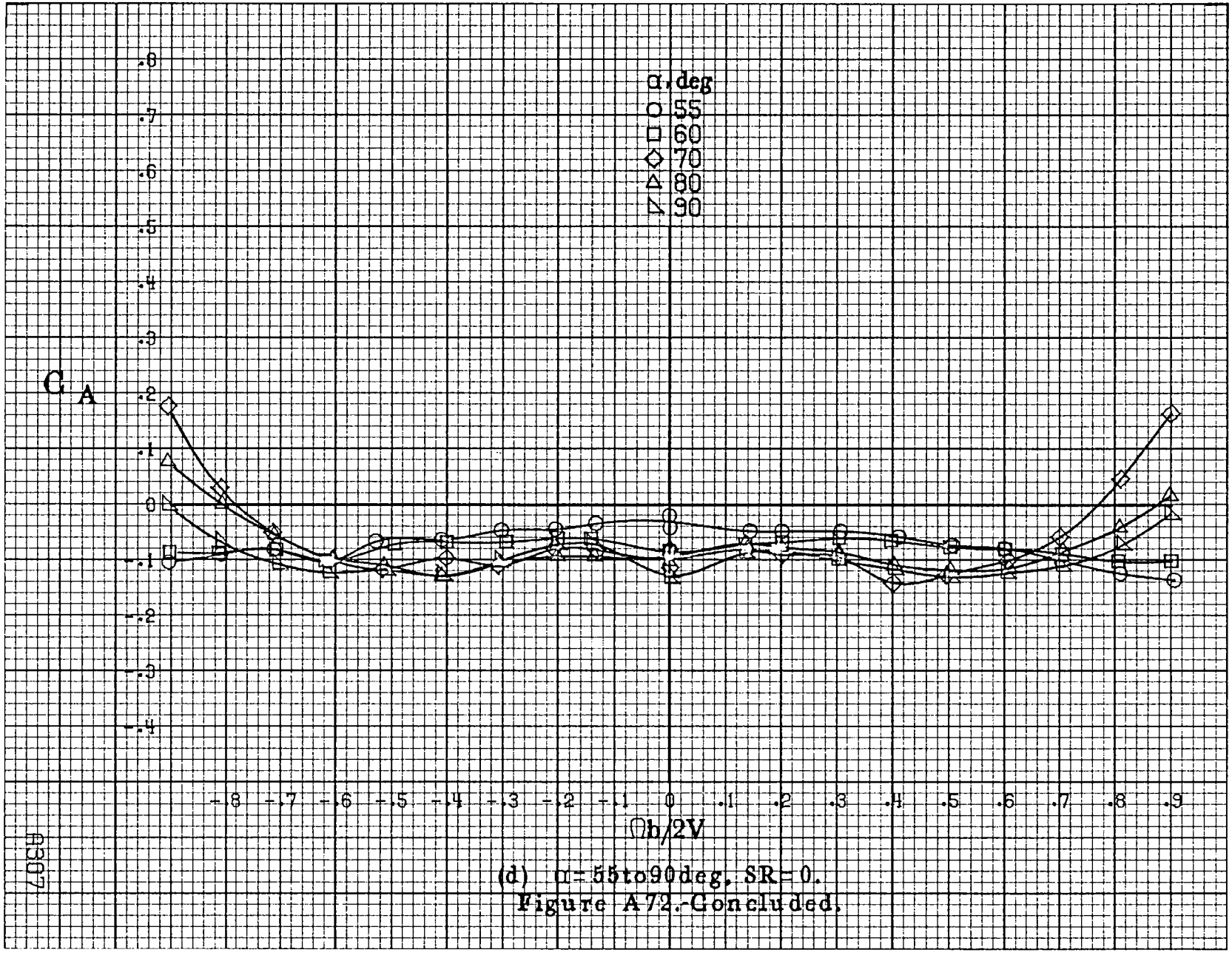

(d) $\alpha = 55$ to 90 deg, SR = 0.

Figure A72.-Concluded.

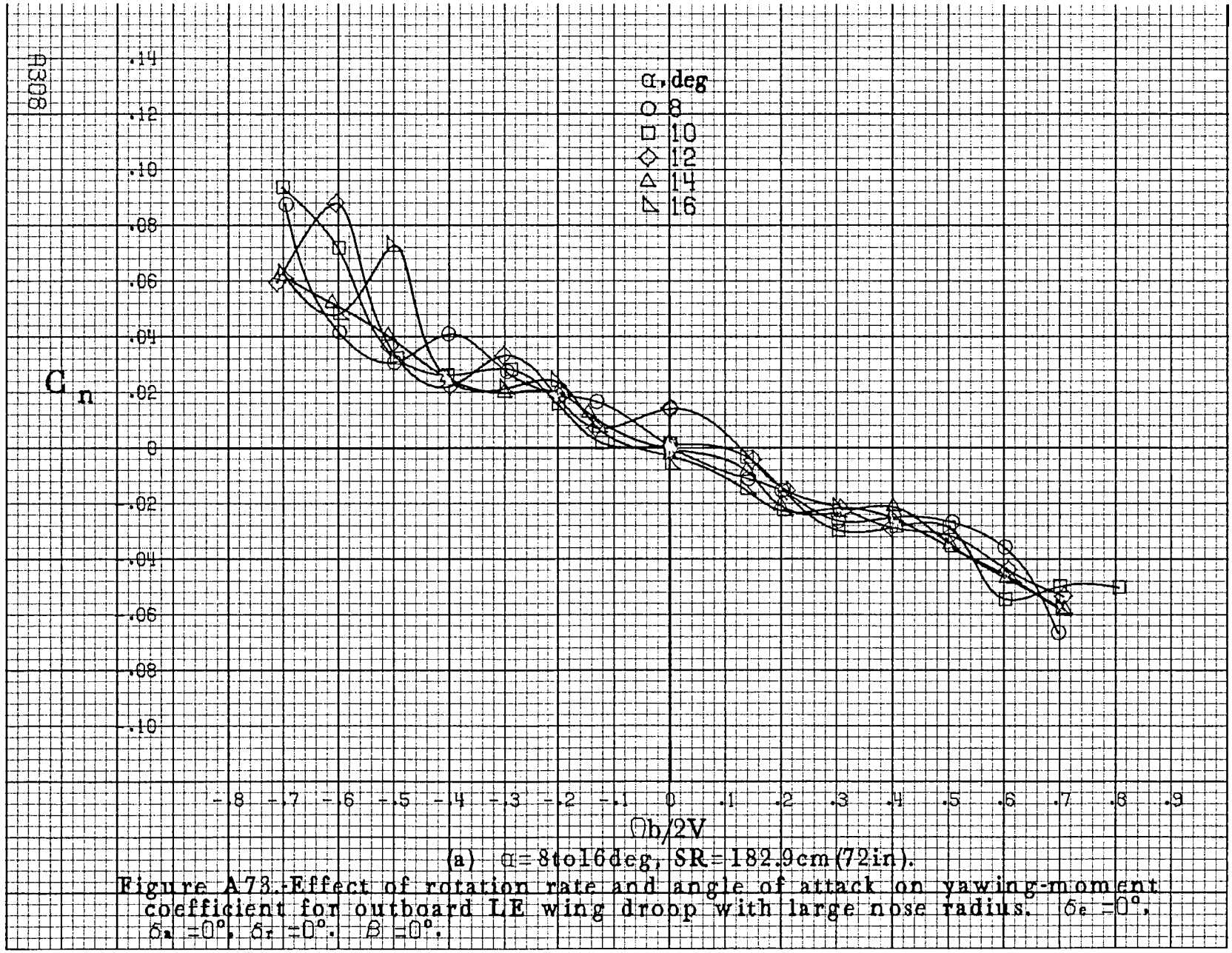

(a) $\alpha = 8$ to 16 deg, SR = 182.9 cm (72 in.).

Figure A73.-Effect of rotation rate and angle of attack on yawing-moment coefficient for outboard LE wing droop with large nose radius. $\delta_e = 0°$, $\delta_a = 0°$, $\delta_r = 0°$, $\beta = 0°$.

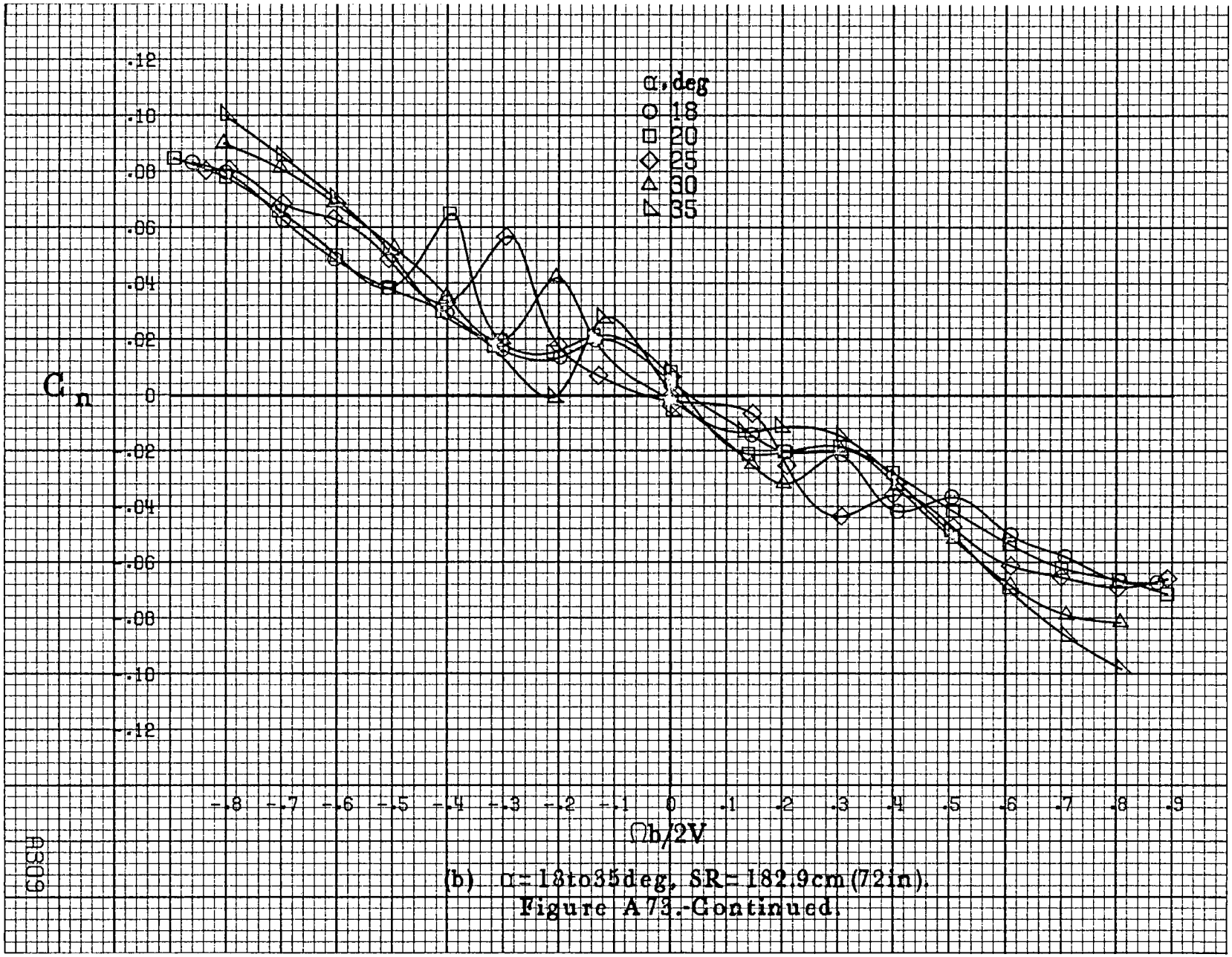

(b) α = 18 to 35 deg, SR = 182.9 cm (72 in).

Figure A73.-Continued.

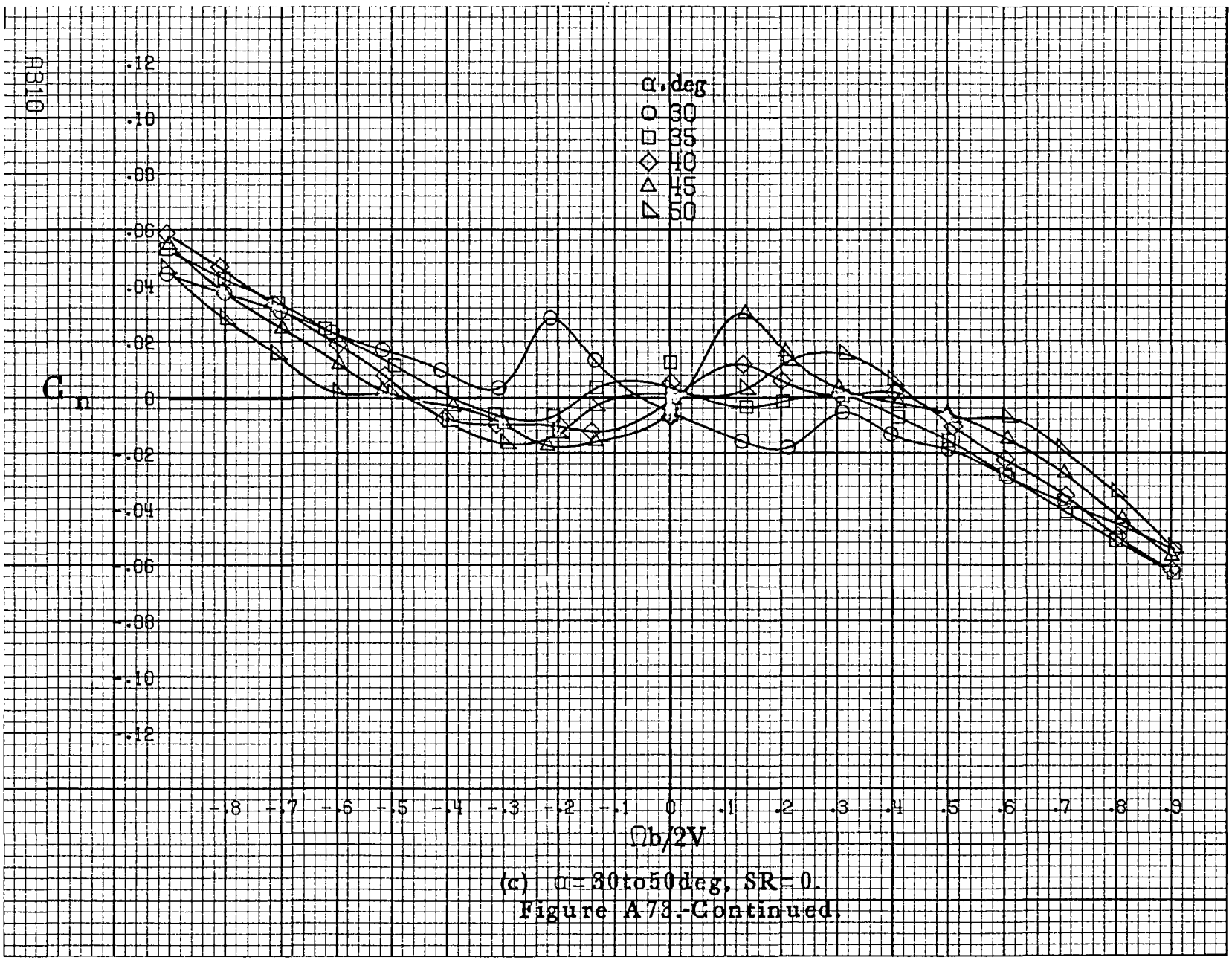

(c) $\alpha = 30$ to 50 deg, SR = 0.

Figure A73.-Continued.

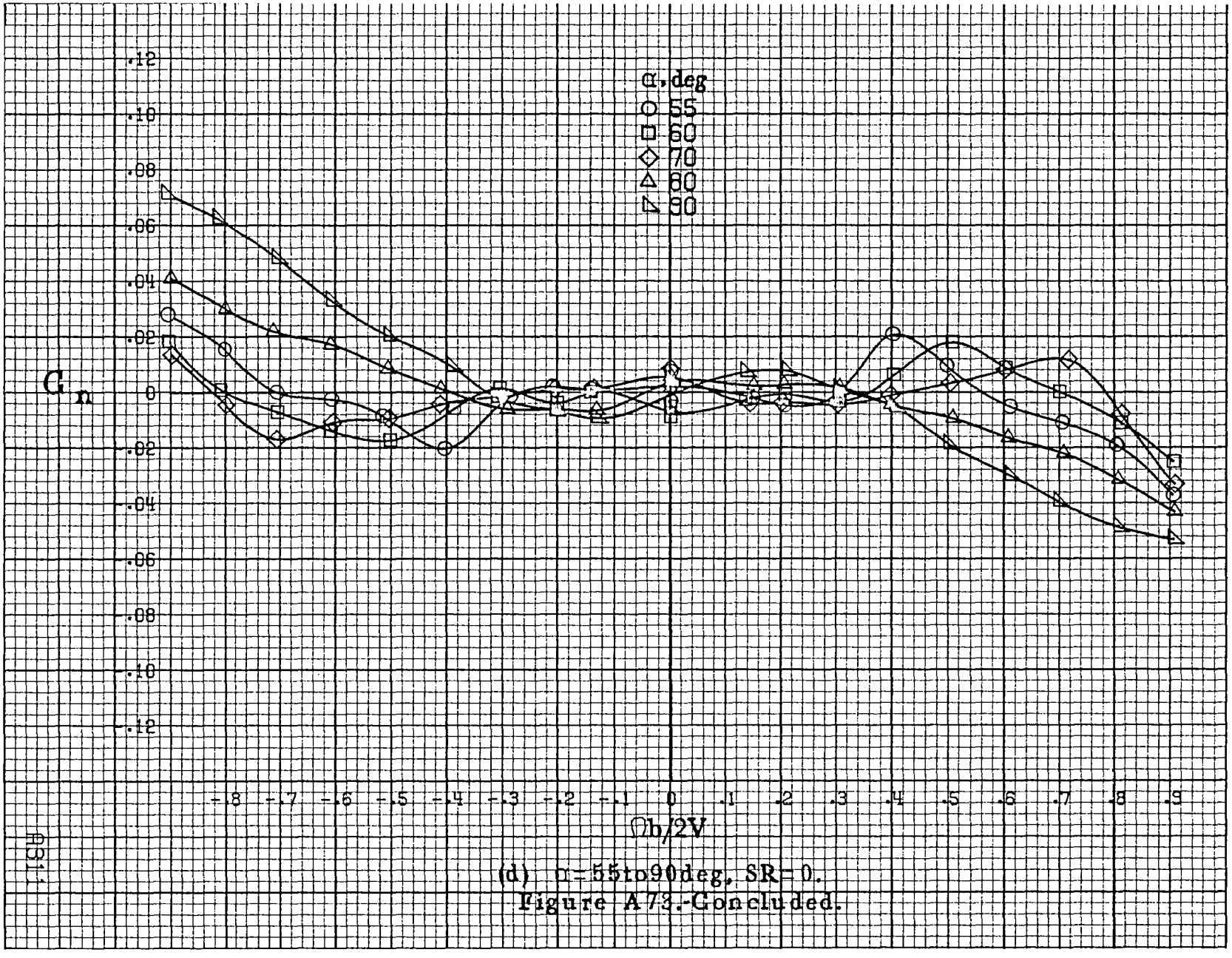

(d) α = 55 to 90 deg, SR = 0.

Figure A73.- Concluded.

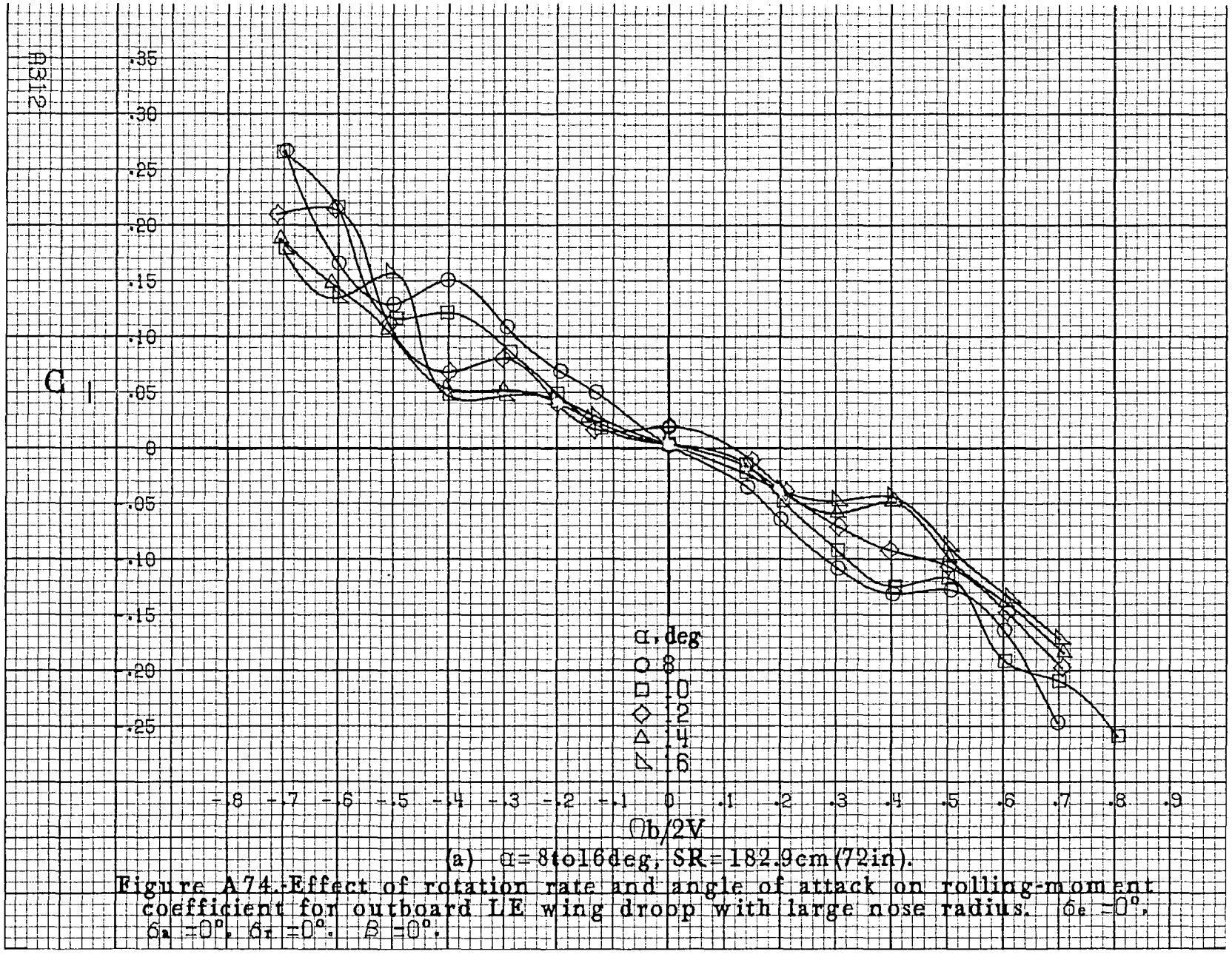

(a) $\alpha = 8$ to 16 deg, SR = 182.9 cm (72 in).

Figure A74.-Effect of rotation rate and angle of attack on rolling-moment coefficient for outboard LE wing droop with large nose radius. $\delta_e = 0°$, $\delta_a = 0°$, $\delta_r = 0°$, $\beta = 0°$.

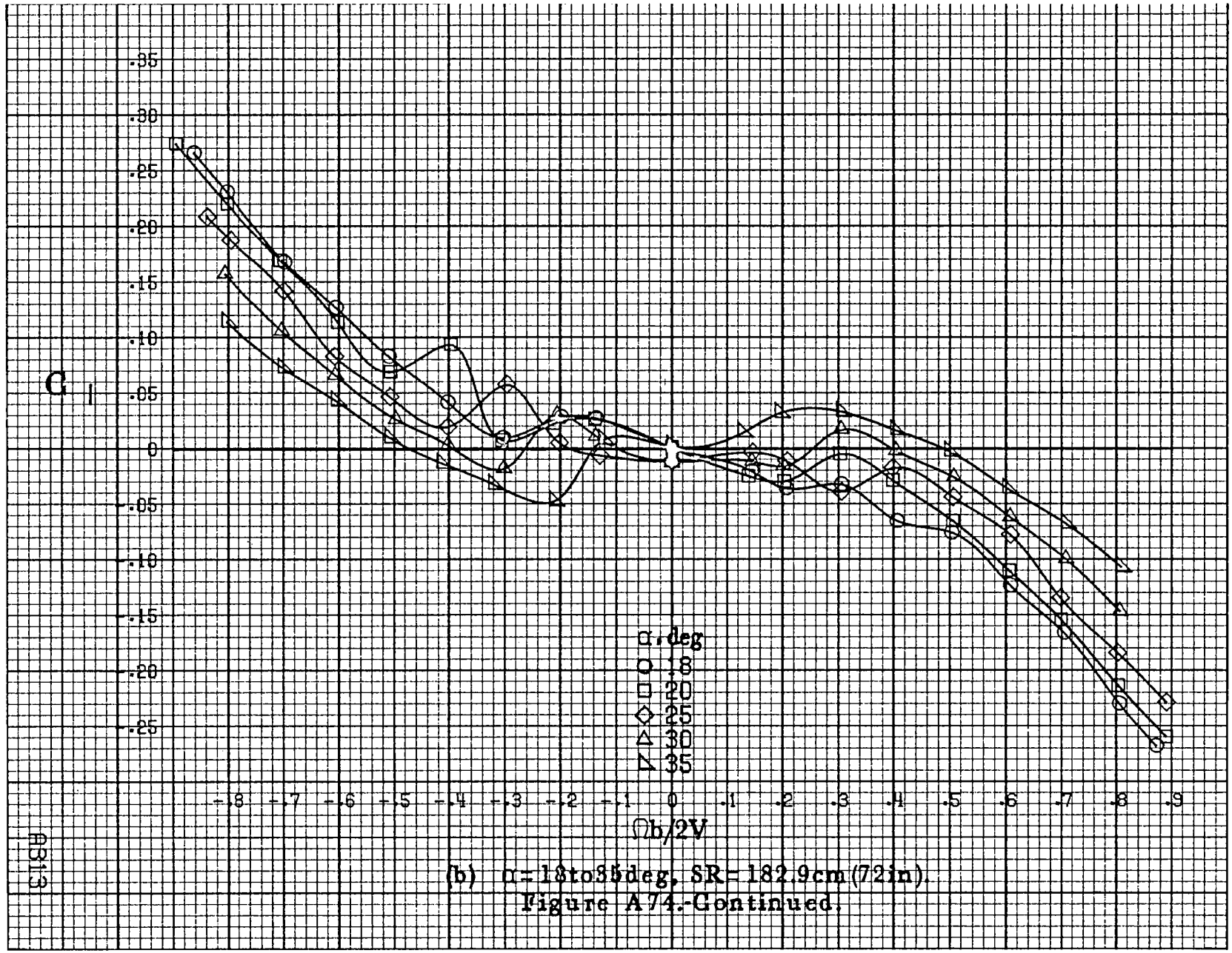

(b) α = 18 to 35 deg, SR = 182.9 cm (72 in).

Figure A74.-Continued.

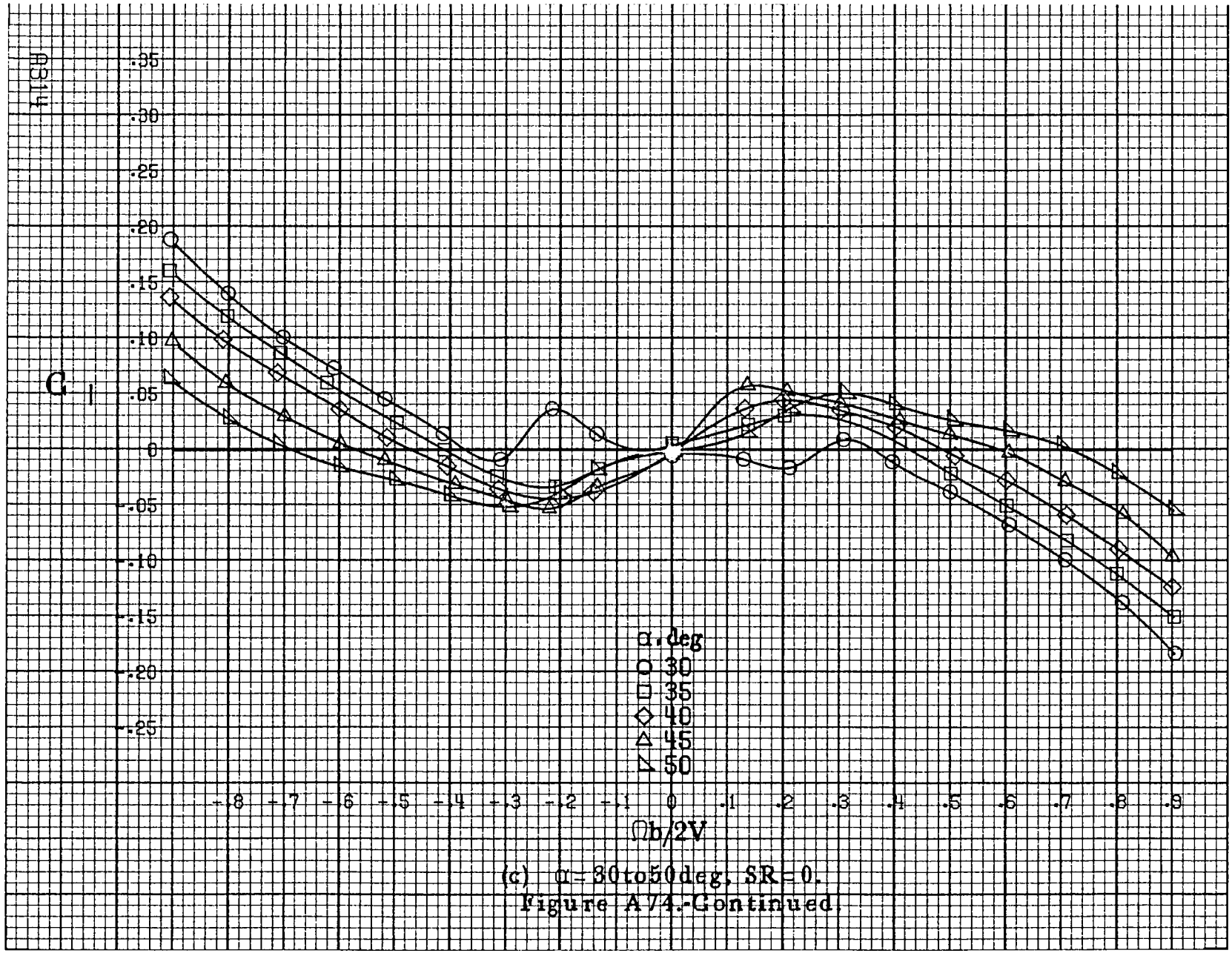

(c) $\alpha = 30$ to 50 deg, SR = 0.

Figure A74.-Continued.

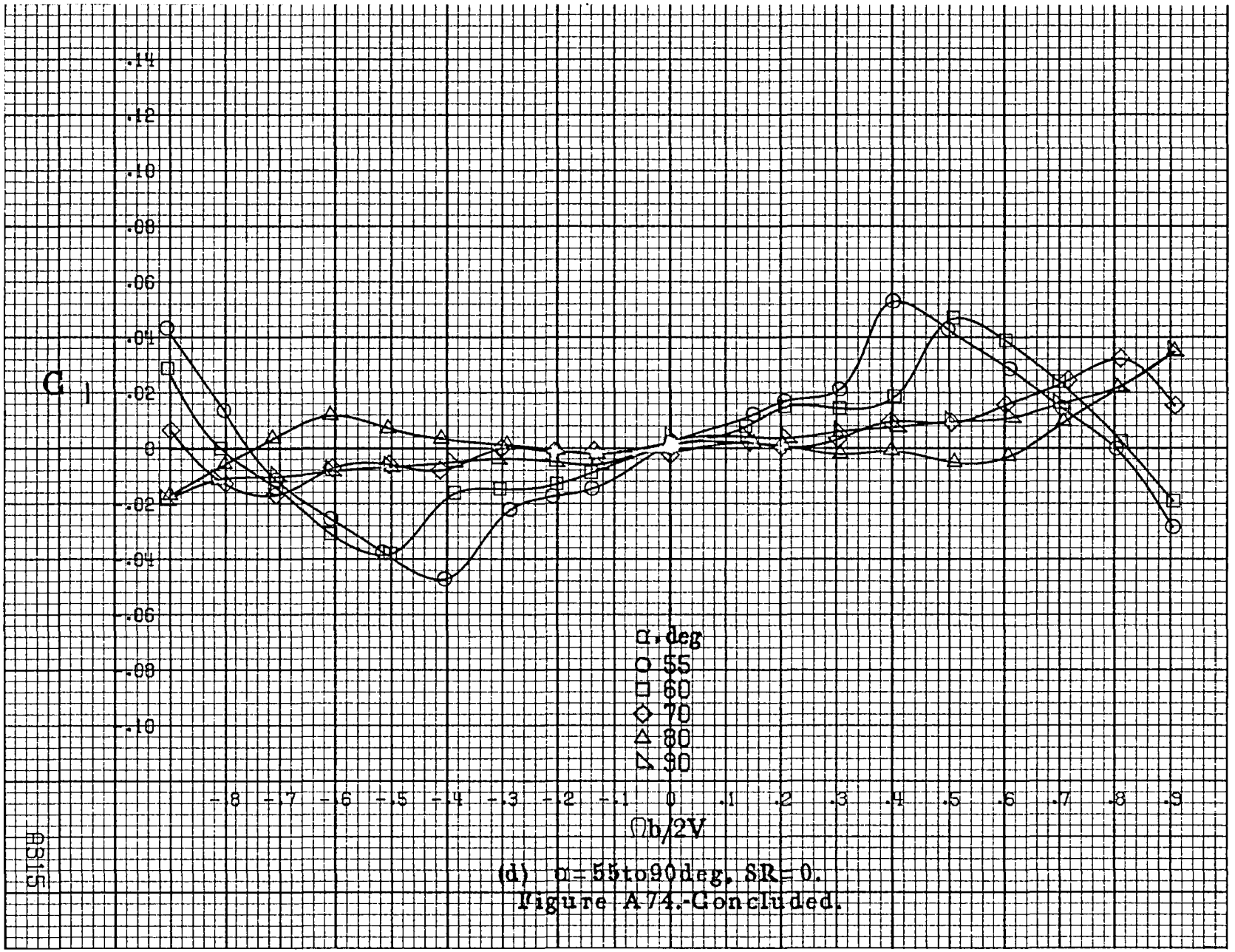

(d) α = 55 to 90 deg, SR = 0.

Figure A74.-Concluded.

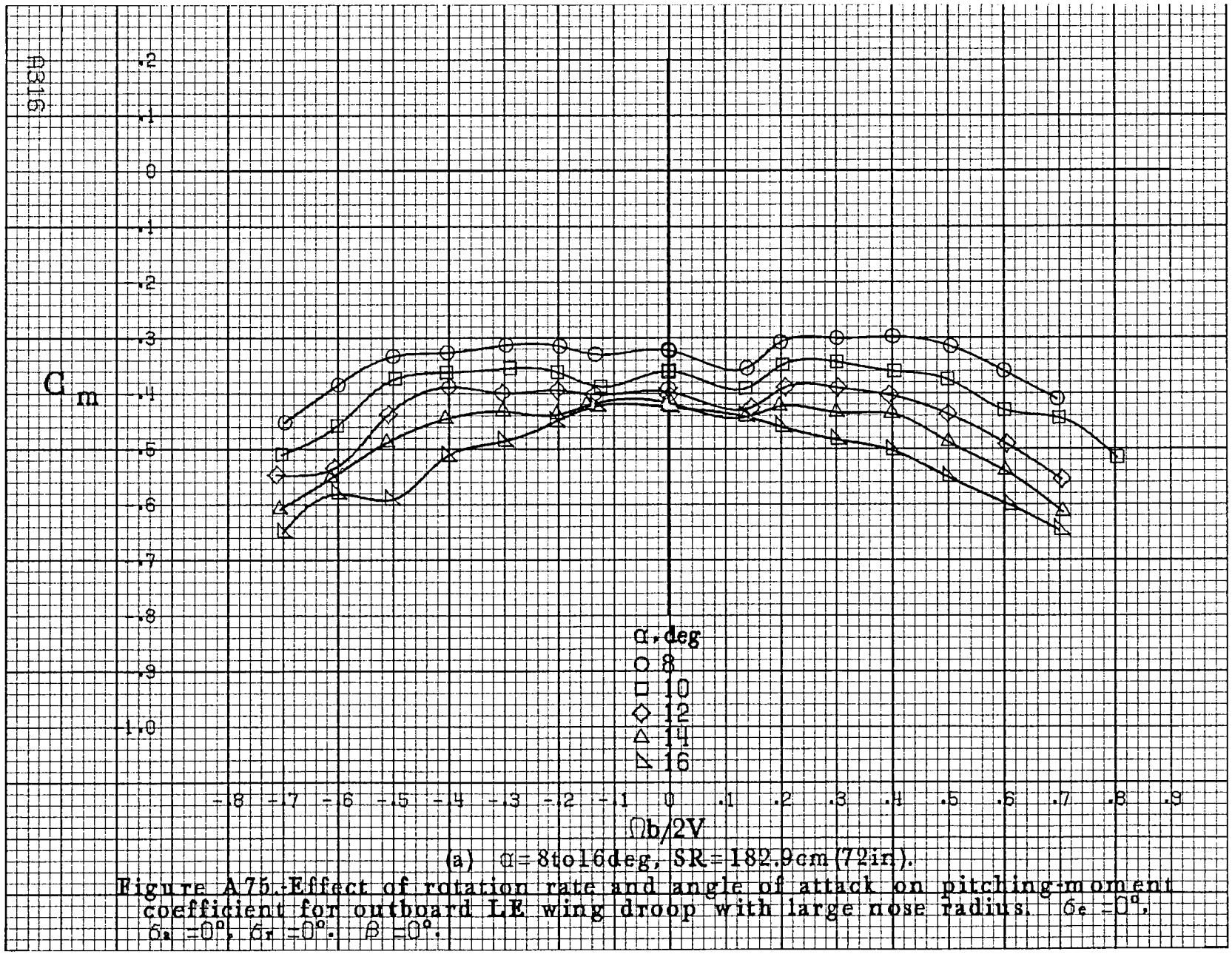

(a) α = 8to16deg, SR = 182.9cm (72in).

Figure A75.-Effect of rotation rate and angle of attack on pitching-moment coefficient for outboard LE wing droop with large nose radius. $\delta_e = 0°$, $\delta_a = 0°$, $\delta_r = 0°$, $\beta = 0°$.

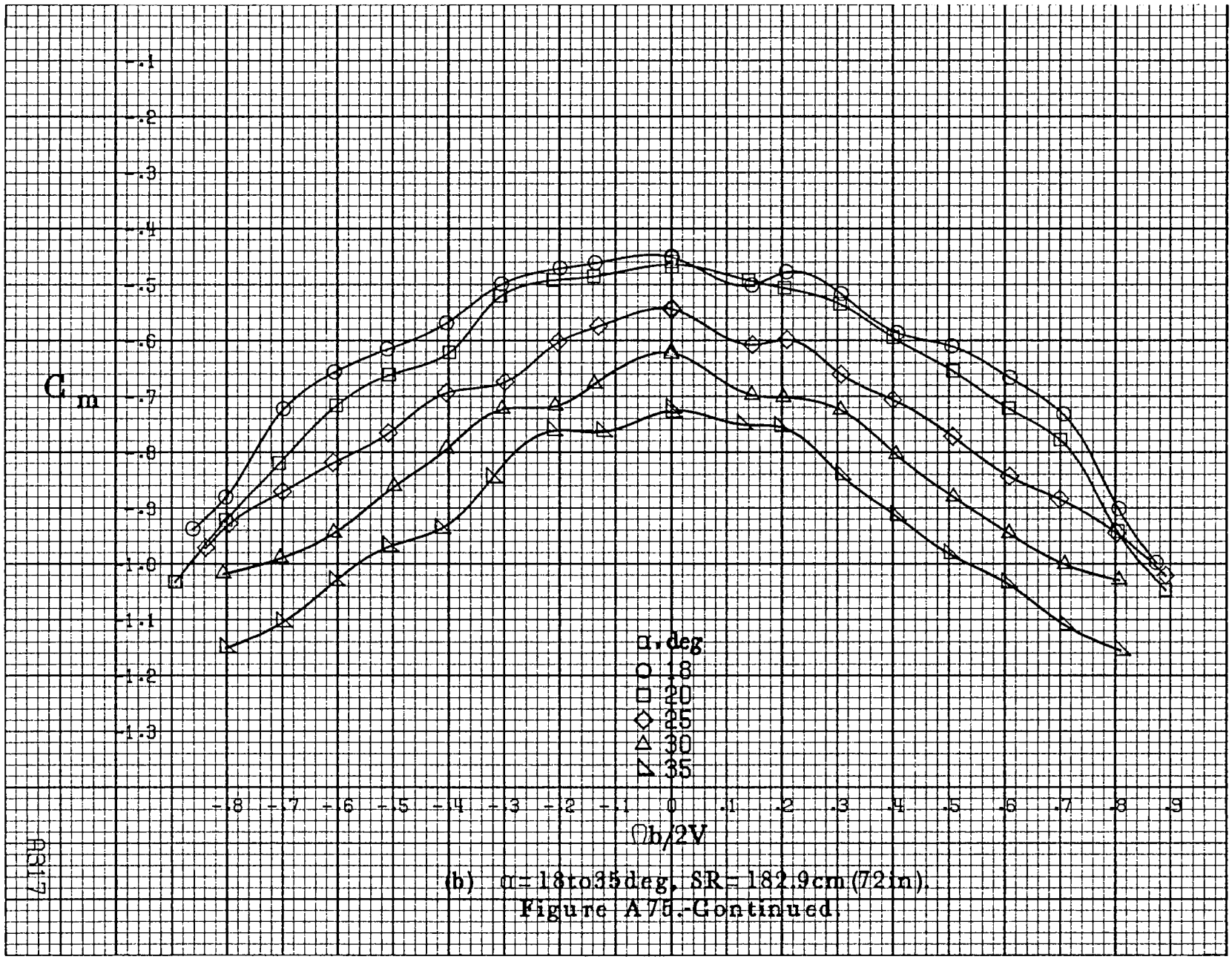

(b) α = 18 to 35 deg, SR = 182.9 cm (72 in).

Figure A75.-Continued.

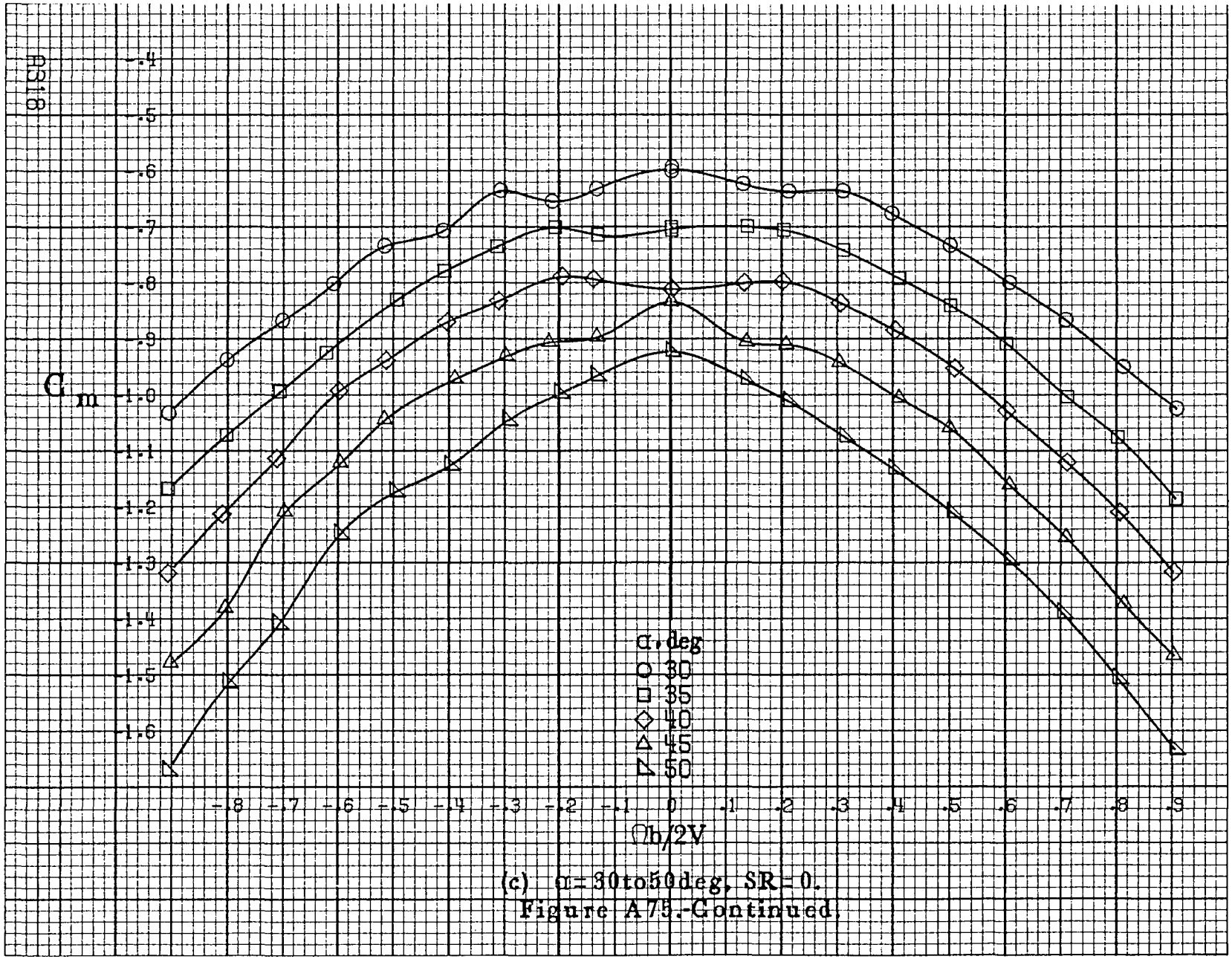

(c) α = 30 to 50 deg, SR = 0.

Figure A75.-Continued.

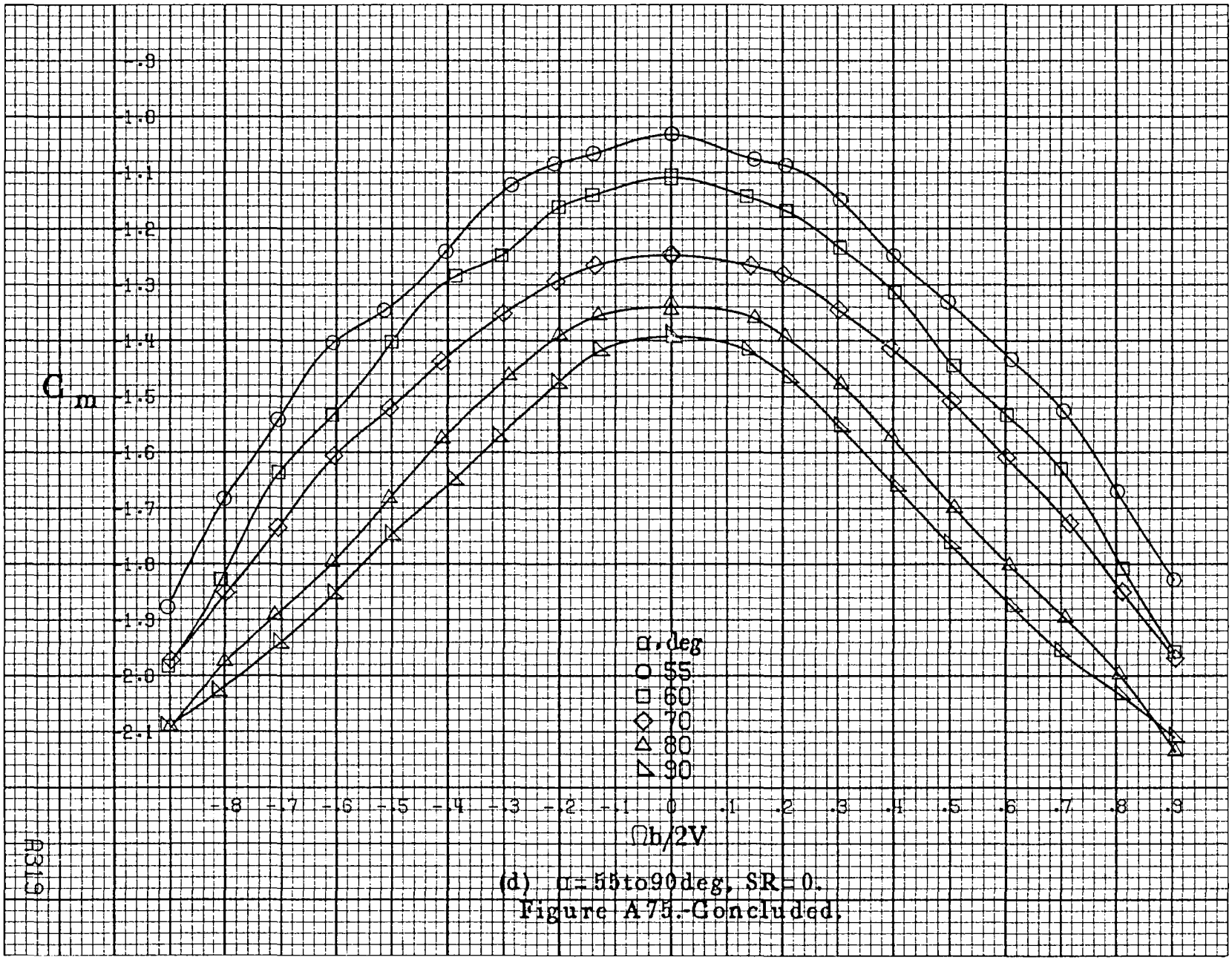

(d) α = 55 to 90 deg, SR = 0.

Figure A75.-Concluded.

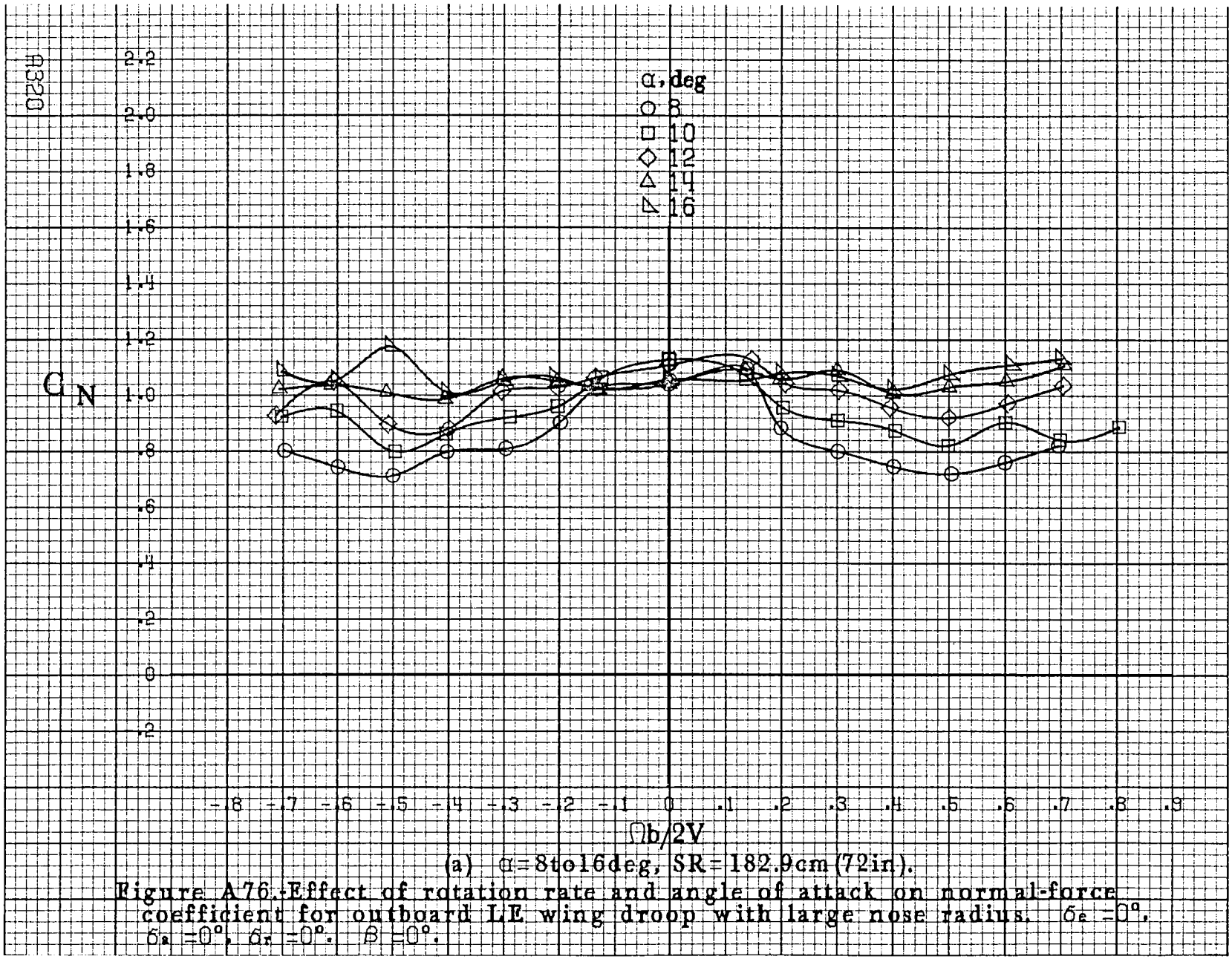

(a) $\alpha = 8$ to 16 deg, SR = 182.9 cm (72 in).

Figure A76.-Effect of rotation rate and angle of attack on normal-force coefficient for outboard LE wing droop with large nose radius. $\delta_e = 0°$, $\delta_a = 0°$, $\delta_r = 0°$, $\beta = 0°$.

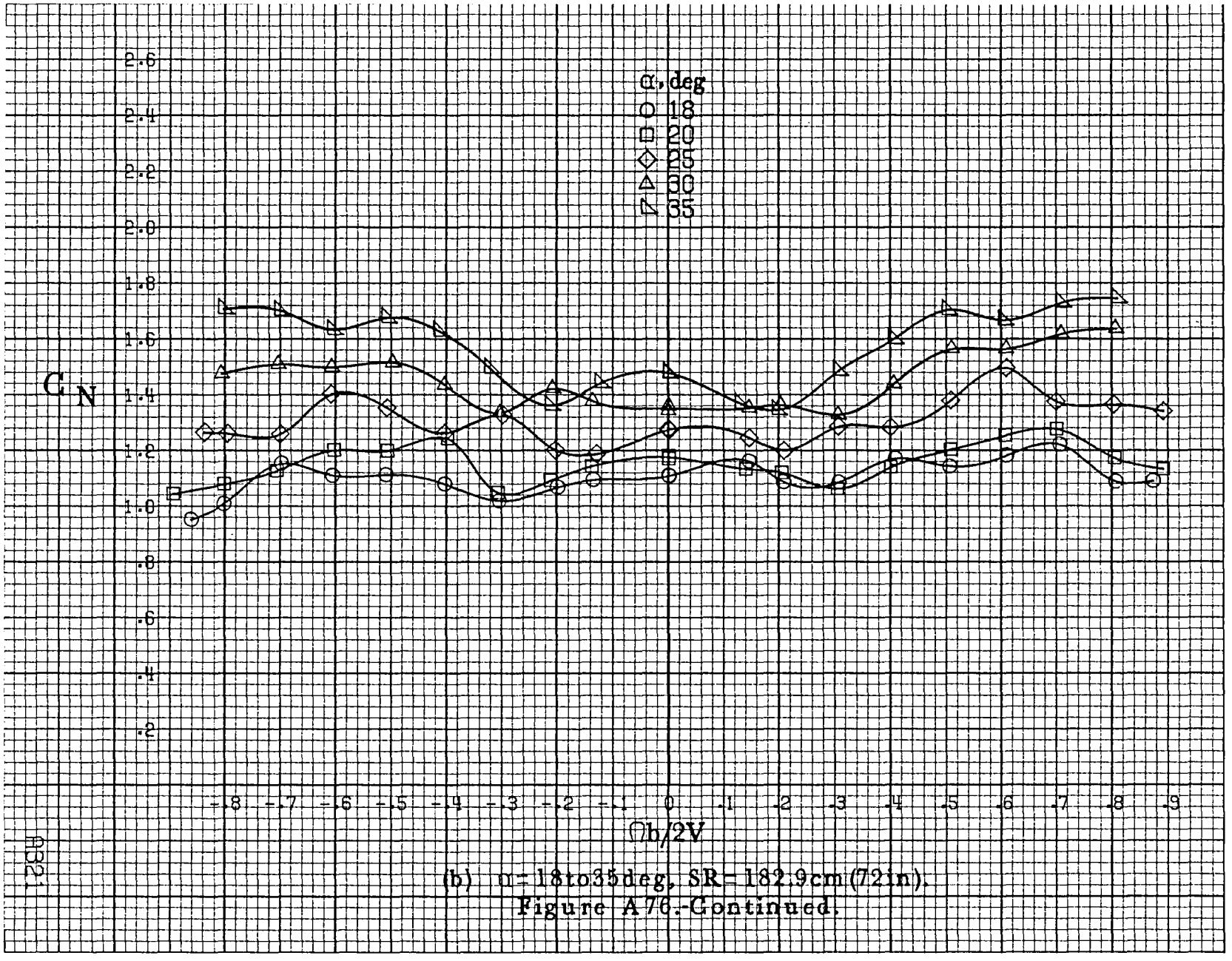

(b) $\alpha = 18$ to 35 deg, SR = 182.9 cm (72 in).

Figure A76.-Continued.

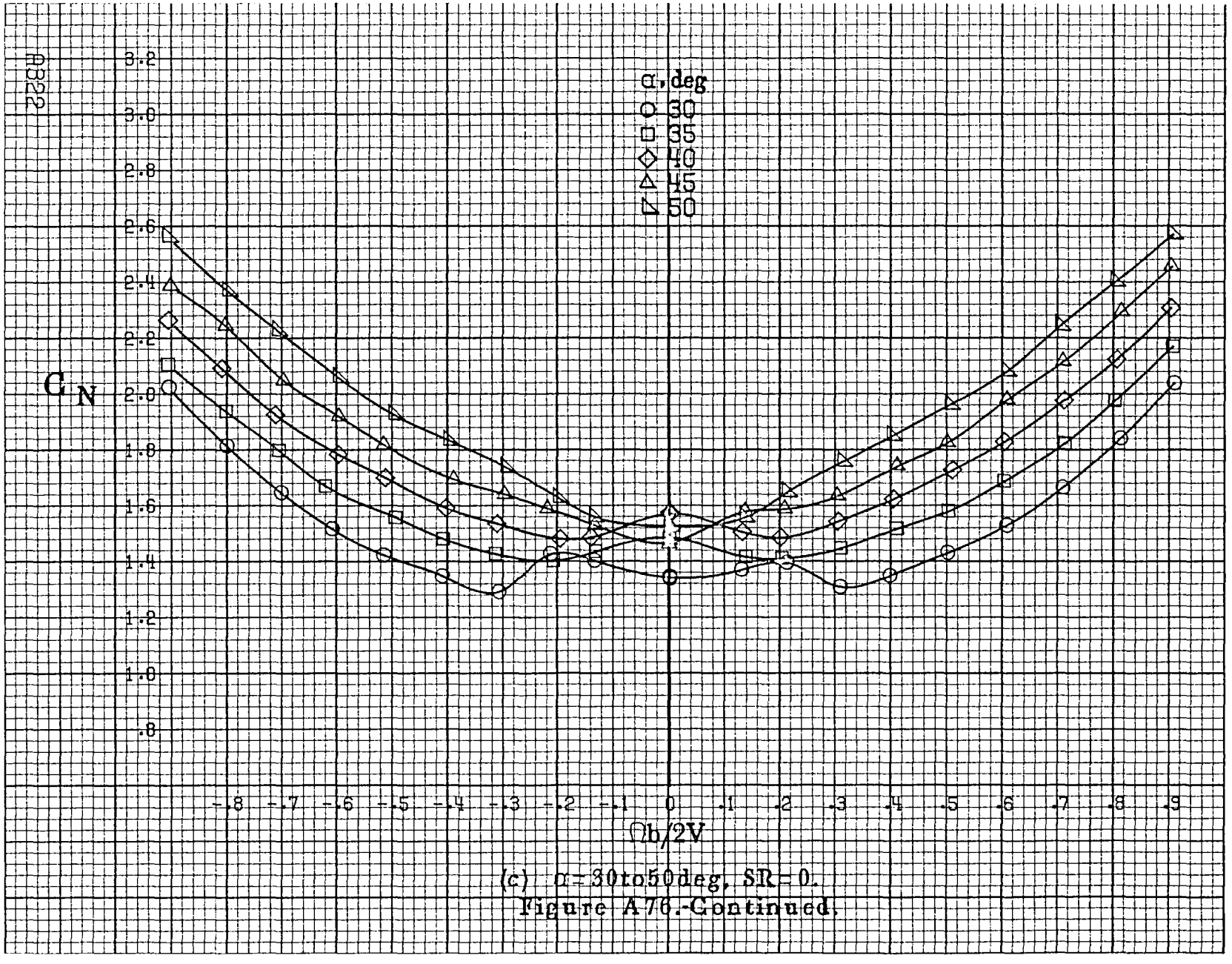

(c) $\alpha = 30$ to 50 deg, SR = 0.

Figure A76.-Continued.

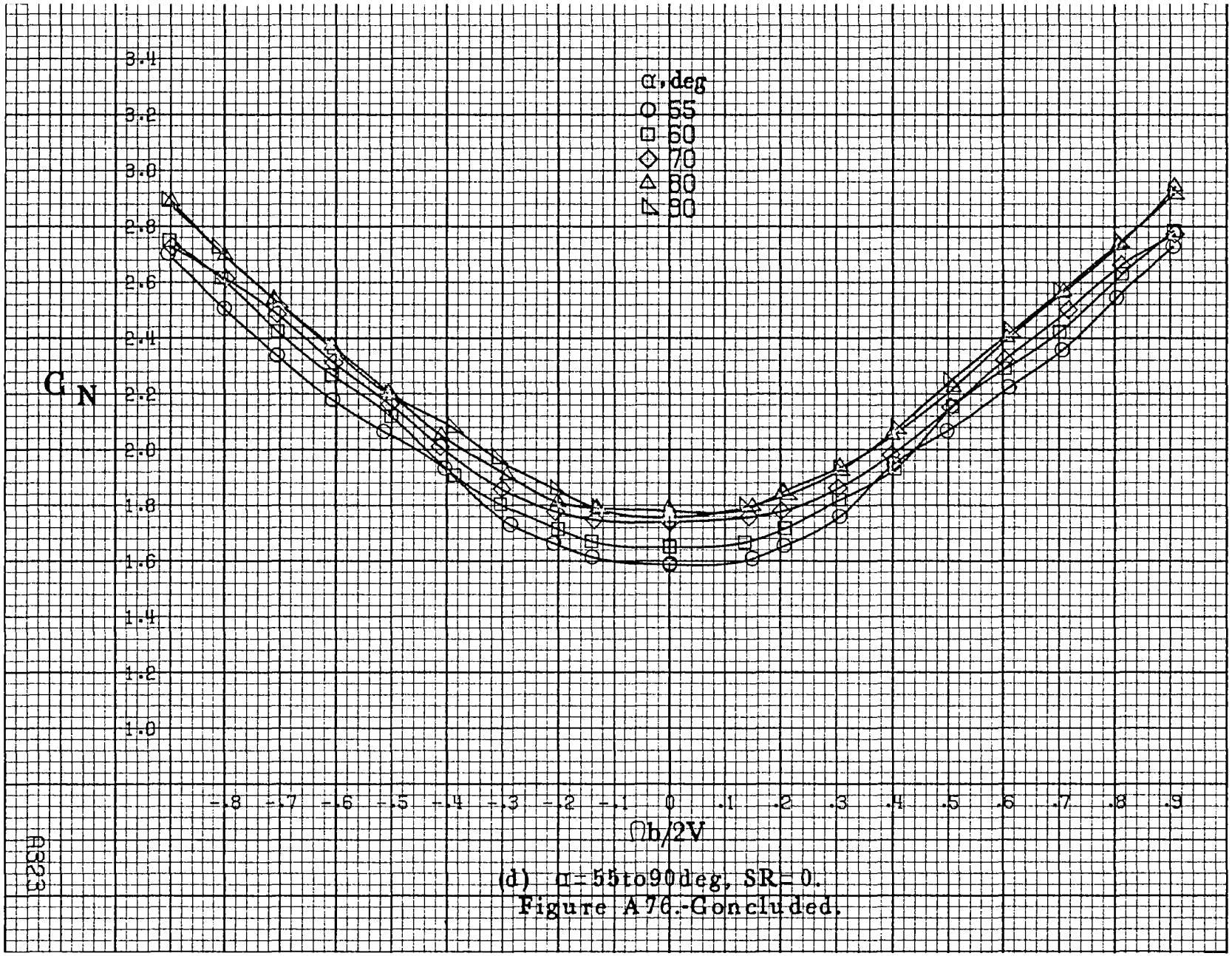

(d) α = 55 to 90 deg, SR = 0.

Figure A76.- Concluded.

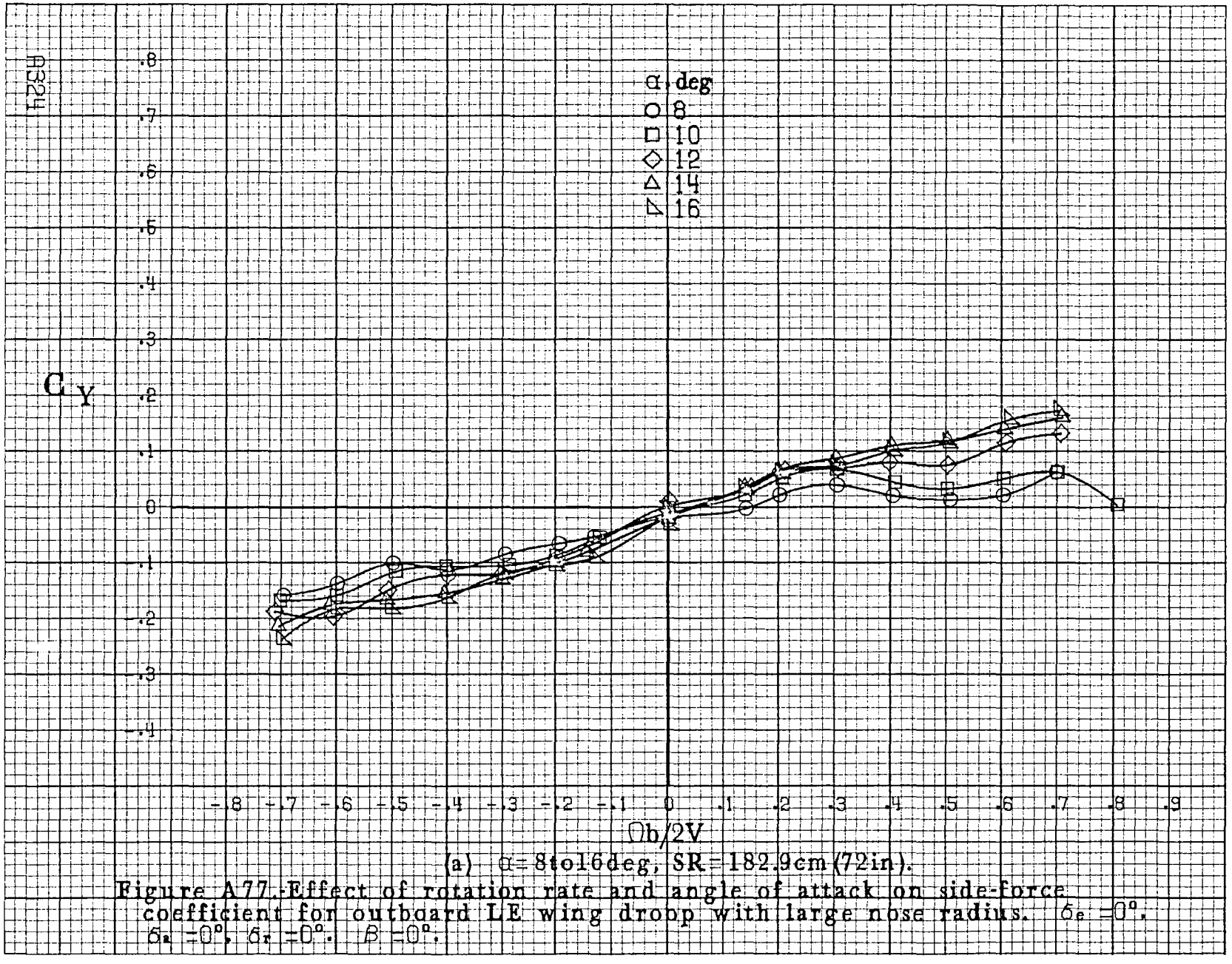

(a) α = 8 to 16 deg, SR = 182.9 cm (72 in).

Figure A77.- Effect of rotation rate and angle of attack on side-force coefficient for outboard LE wing droop with large nose radius. $\delta_e = 0°$, $\delta_a = 0°$, $\delta_r = 0°$, $\beta = 0°$.

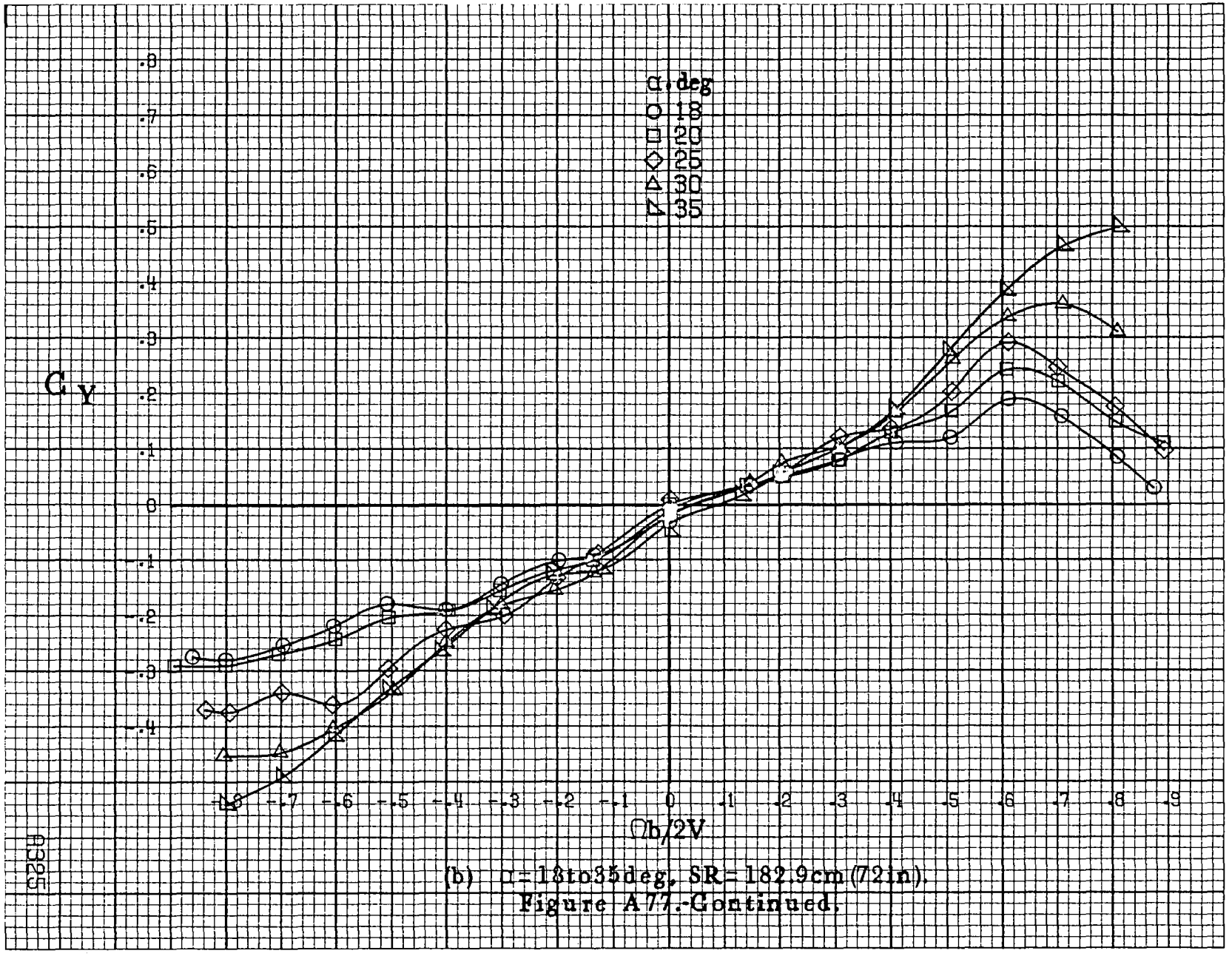

(b) α = 18 to 35 deg, SR = 182.9 cm (72 in).

Figure A77.-Continued.

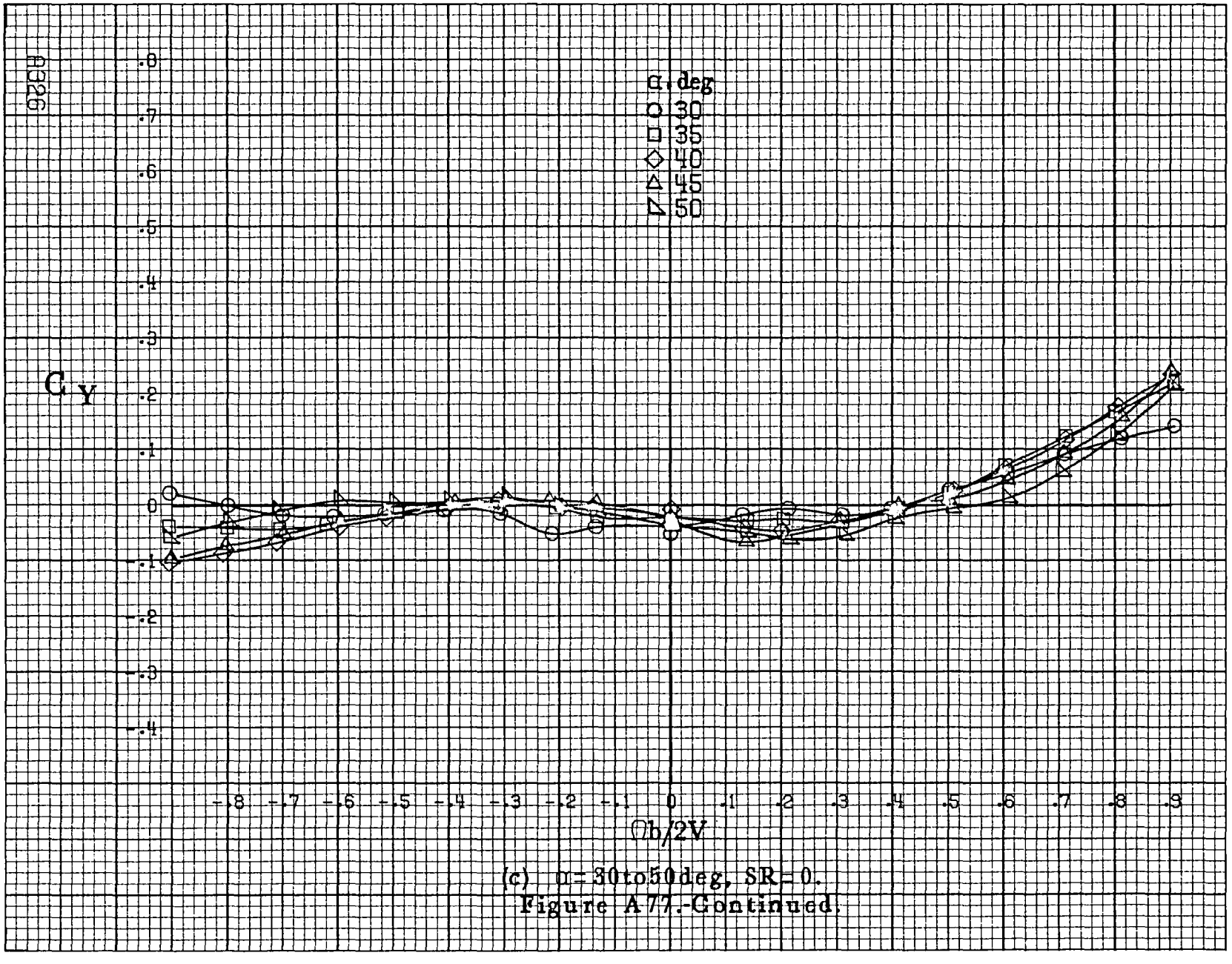

(c) α = 30 to 50 deg, SR = 0.

Figure A77.-Continued.

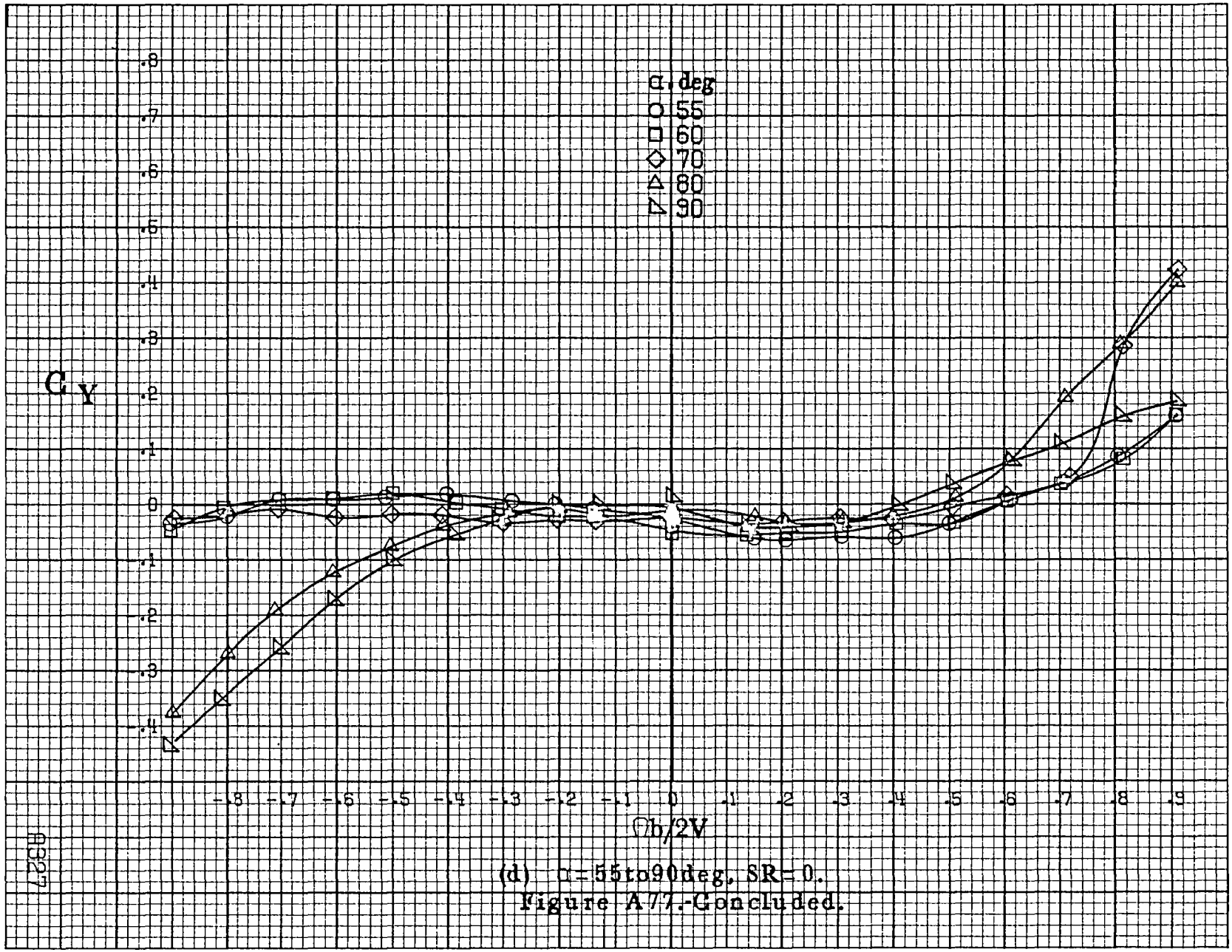

(d) α = 55 to 90 deg, SR = 0.

Figure A77.-Concluded.

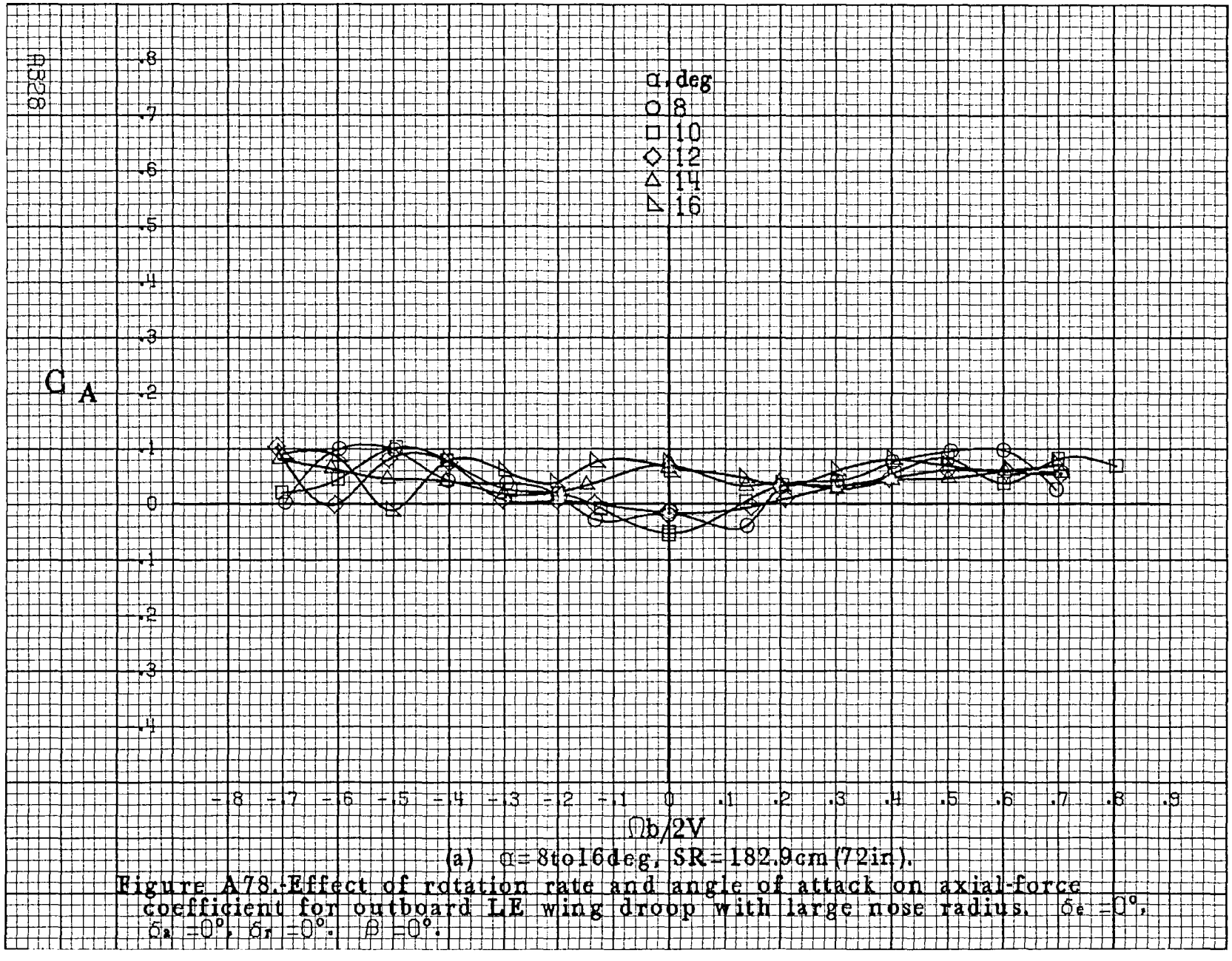

(a) α = 8 to 16 deg, SR = 182.9 cm (72 in.).

Figure A78.-Effect of rotation rate and angle of attack on axial-force coefficient for outboard LE wing droop with large nose radius. $\delta_e = 0°$, $\delta_a = 0°$, $\delta_r = 0°$, $\beta = 0°$.

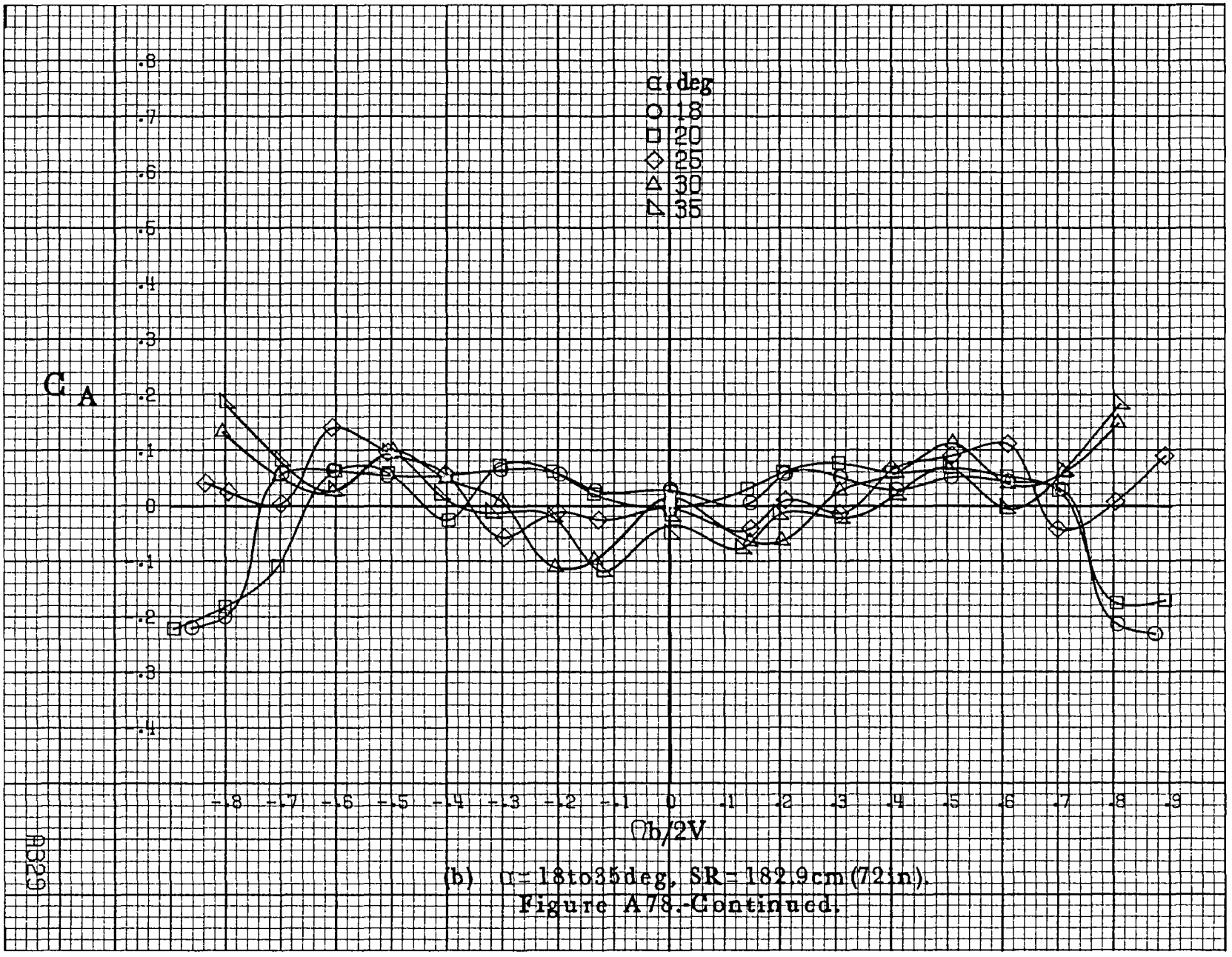

(b) α= 18to35deg, SR= 182.9cm (72in).

Figure A78.-Continued.

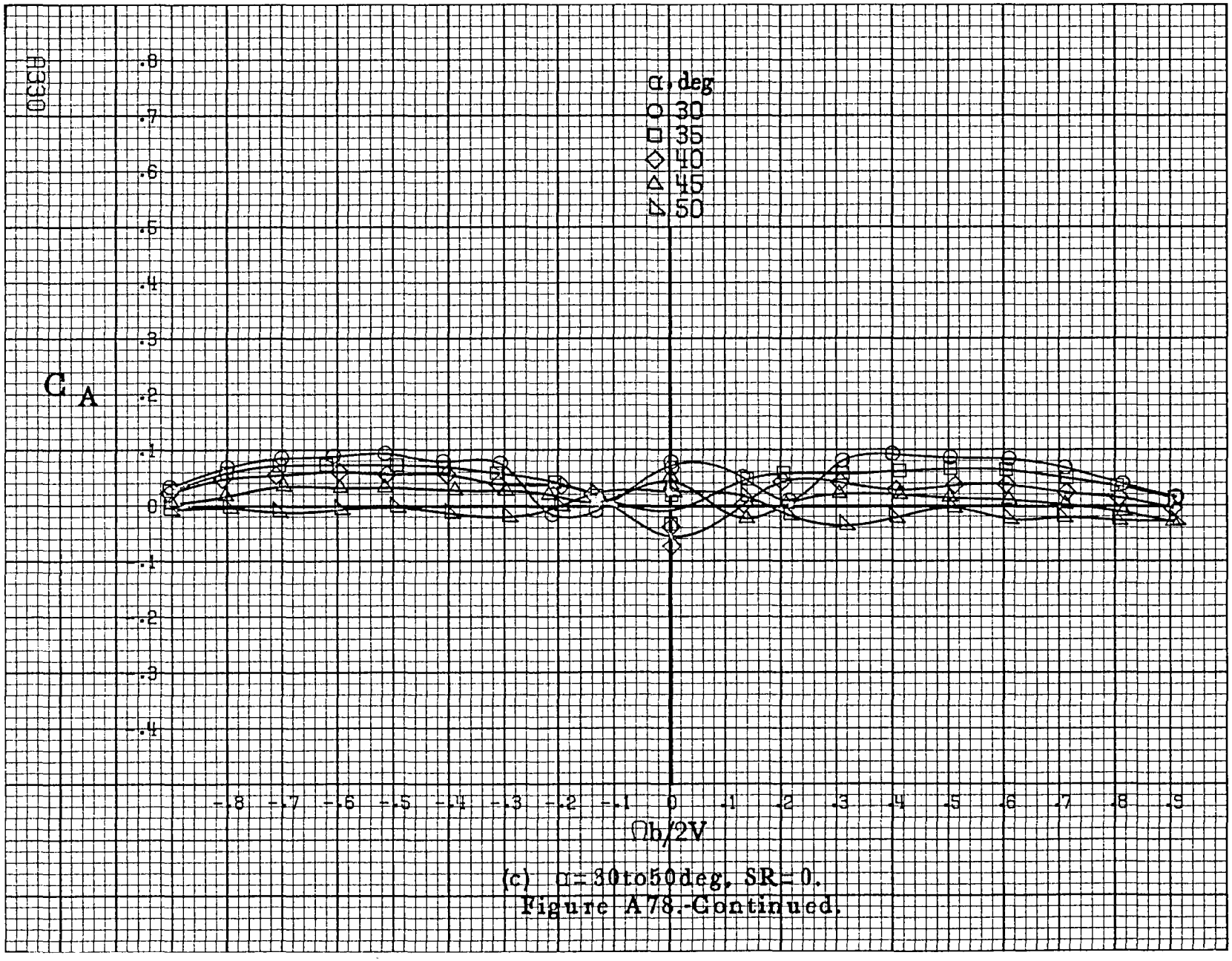

(c) $\alpha = 30$ to 50 deg, SR = 0.

Figure A78.-Continued.

(d) α = 55 to 90 deg, SR = 0.

Figure A78.-Concluded.

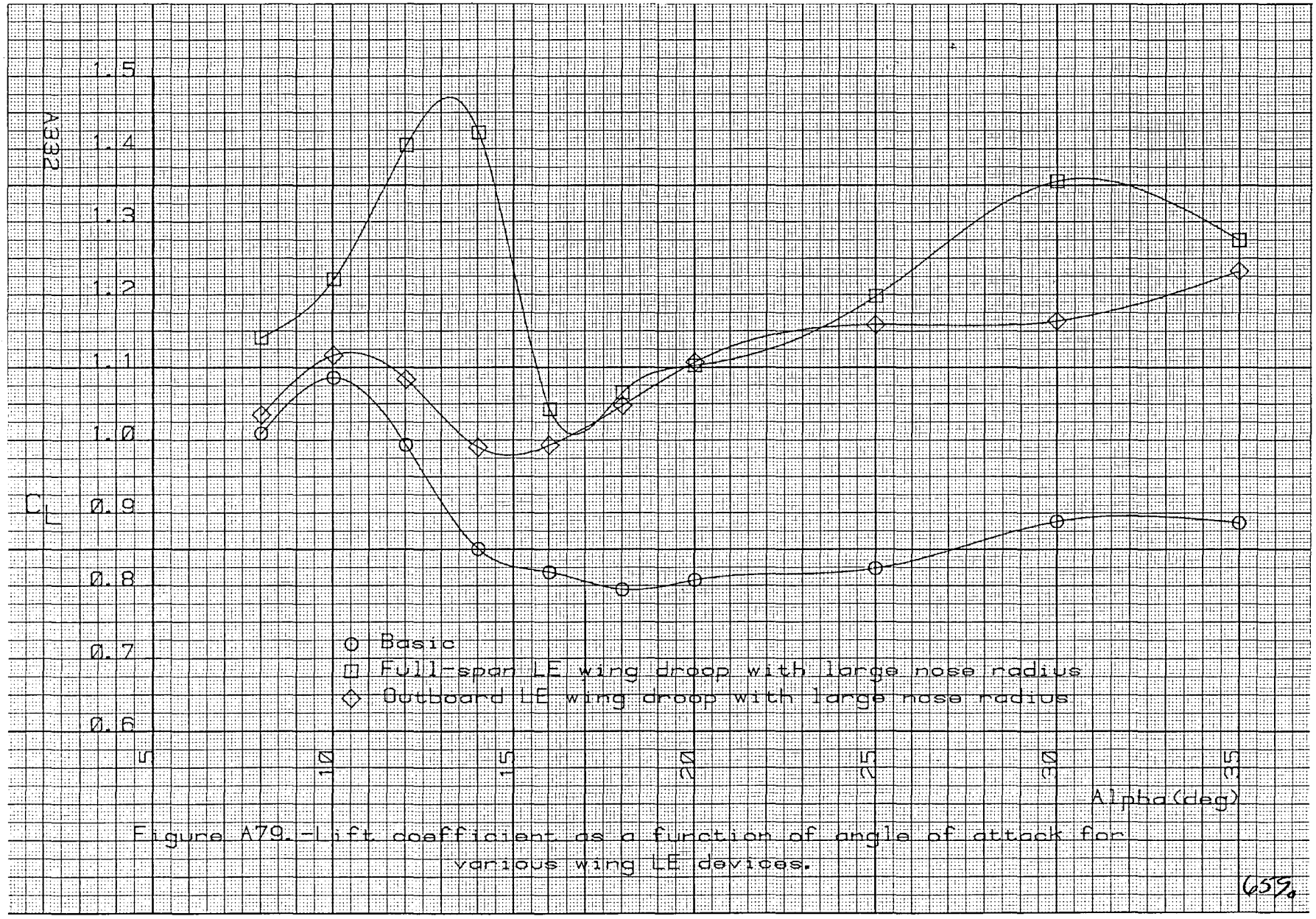

Figure A79.-Lift coefficient as a function of angle of attack for various wing LE devices.

1. Report No.	2. Government Accession No.	3. Recipient's Catalog No.
NASA CR-3201		

4. Title and Subtitle	5. Report Date
Rotary Balance Data for a Typical Single-Engine General Aviation Design for an Angle-of-Attack Range of 8° to 90°. II - High-Wing Model C.	October 1980
	6. Performing Organization Code

7. Author(s)	8. Performing Organization Report No.
Randy S. Hultberg Julio Chu Waldo L. Dickens	

9. Performing Organization Name and Address	10. Work Unit No.
Bihrle Applied Research, Inc. 400 Jericho Turnpike Jericho, New York 11753	505-10-13-06
	11. Contract or Grant No.
	NAS1-14849, Task 35

12. Sponsoring Agency Name and Address	13. Type of Report and Period Covered
National Aeronautics and Space Administration Washington, DC 20546	Contractor Report
	14. Sponsoring Agency Code

15. Supplementary Notes

Langley Technical Monitor: James S. Bowman, Jr.

Topical report

16. Abstract

Aerodynamic characteristics obtained in a helical flow environment utilizing a rotary balance located in the Langley spin tunnel are presented in plotted form for a 1/6-scale, single-engine, high-wing, general aviation model (model C). The configurations tested included the basic airplane and control deflections, wing leading edge devices, tail designs, and airplane components. Data are presented without analysis for an angle-of-attack range of 8° to 90° and clockwise and counter-clockwise rotations covering an $\frac{\Omega b}{2V}$ range from 0 to .9.

17. Key Words (Suggested by Author(s))	18. Distribution Statement
General Aviation Spinning Rotary Balance High angle-of-attack wind tunnel data	Unclassified - Unlimited Subject Category 02

19. Security Classif. (of this report)	20. Security Classif. (of this page)	21. No. of Pages	22. Price
Unclassified	Unclassified	349	A15

For sale by the National Technical Information Service, Springfield, Virginia 22161

NASA-Langley, 1980

National Aeronautics and
Space Administration

Washington, D.C.
20546

Official Business
Penalty for Private Use, $300

SPECIAL FOURTH CLASS MAIL
BOOK

Postage and Fees Paid
National Aeronautics and
Space Administration
NASA-451

NASA

POSTMASTER: If Undeliverable (Section 158
Postal Manual) Do Not Return